UNIVERSITY OF STRATHCLYDE

Faculty of Engineering

Department of Biomedical Engineering

DOCTORATE DISSERTATION

PhD Biomedical Engineering

4D CT BASED ANALYSIS OF KNEE KINEMATICS

By

Andre Attard

Supervised by Dr Phil Riches

A dissertation submitted in fulfilment of the requirements of the award of a

Doctor of Philosophy of the University of Strathclyde

July 2020
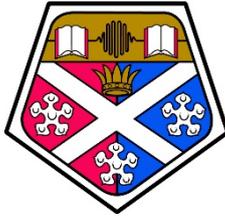
UNIVERSITY OF STRATHCLYDE

DEPARTMENT OF BIOMEDICAL ENGINEERING

DECLARATION

This thesis is the result of the author's original research. It has been composed by the author and has not been previously submitted for examination, which has led to the award of a degree.

_____   _____Andre Attard_____

Signature of Student   Name of Student

_____6th July 2020_____

Date

ACKNOWLEDGMENTS

ABSTRACT

Introduction: Total Knee Arthroplasty, which is the last resort of treatment for osteoarthritis, is aimed at restoring the functional anatomy of the knee. Despite the recent improvements in surgical techniques, limited range of motion, postoperative instability and malalignment still hinder the restoration of the knee's original function. Bearing in mind that stability, range of motion and alignment are all directly correlated with the kinematics of the knee, then focus should be given to understanding the underlying knee mechanics to be able to restore the native kinematics. Contemporarily, routine clinical practice still relies on 2-dimensional standing X-rays to diagnose the underlying knee pathology, which is limited in terms of accurately assessing the essential knee kinematics. **Aims:** Utilise the innovative 4D CT scanners to capture the articulation of healthy and replaced knees. Develop a bespoke proof-of-concept software which utilises the 4D CT data and extracts three principal kinematic outcome measures. Extract the kinematics of ten participants and analyse the data to address two low-powered pilot studies. **Methods:** A 4D CT scanning protocol was developed to record a flexion-extension exercise dynamically. The bespoke software, developed in MATLAB, extracted the three principal kinematic outcome measures for the ten participants who were scanned. The extracted kinematic data for the control participants was analysed to identify the applicable range of motion for specific flexion-extension axes of the knee, via the determination of kinematic crosstalk. The patient data was used to analyse the mobility of fixed-bearing and mobile-bearing implants. **Results:** The software successfully extracted the six-degrees-of-freedom kinematics, performed a contact point analysis and identified the axial centre of rotation of both healthy and replaced knees. The control data identified the Trans Epicondylar Axis as being applicable for the Extension (-5º to 10º of flexion) and Transition (10º to 30º of flexion) phases of flexion while the Geometric Centre Axis being applicable for the Flexion phase (30º to 120º of flexion). The participant data did not identify any variation in the level of mobility between the fixed-bearing and mobile-bearing knees. **Conclusion:** The feasibility of the developed kinematic analysis software was proven as a viable alternative, via its implementation on the healthy and replaced knees. The kinematic crosstalk of specific flexion-extension axes was shown to vary depending on the flexion angle. Mobile-bearing knees do not provide patients with extra mobility over their fixed-bearing counterparts.

PUBLICATIONS AND PRESENTATIONS

Publications

- **Attard Andre**, Tawy Gwenllian, Simons Michiel, Riches Philip, Rowe Philip, Biant Leela. (2019). **Health costs and efficiencies of patient-specific and single-use instrumentation in total knee arthroplasty: a randomised controlled trial.** BMJ Open Quality. 8. e000493. 10.1136/bmjoq-2018-000493.

Posters and Presentations

- **Attard Andre**, Rowe Philip, Riches Philip. (2020). **4D CT Based Analysis of Knee Kinematics.** Presented at the CAMS-Knee Opensim Workshop. (Zurich).

- **Attard Andre**, Rowe Philip, Riches Philip. (2018). **4D CT Based Analysis of Knee Kinematics.** Presented at the IMechE Engineering of the Knee Conference. (London).

- **Attard Andre**, Simons Michiel R., Tawy Gwenllian, Rowe Philip, Riches Philip, Biant Leela. (2018). **Health Economics Of Patient-Specific and Single-Use Instrumentation In Total Knee Arthroplasty.** Presented at the 19th EFFORT Congress (Barcelona).

- **Attard Andre**, Rowe Philip, Riches Philip. (2017). **4D CT Based Analysis of Knee Kinematics.** Presented at the European Society of Biomechanics Conference. (Seville).

- **Attard Andre**, Rowe Philip, Murphy J. Andrew. (2015). **A comparison of human walking using a conventional gait laboratory and the MOTEK Medical Computer Assisted Rehabilitation Environment (CAREN).** Presented at the International Society of Biomechanics Conference (Glasgow).

- Simons Michiel, Perrins Michael, **Attard Andre**, Marshall Helen, Semple Scott, Cooper Annette, Biant Leela, Beek Edwin, Roberts Neil. (2017). The Effect of Muscle Loading on Muscle Stiffness. Presented at 1st International MRE Conference (Berlin).

TABLE OF CONTENTS

LIST OF FIGURES

LIST OF TABLES

LIST OF ABBREVIATIONS

Acronym	Definition
3D	Three-dimensional
4D	Four-Dimensional (3D + time)
ACL	Anterior Cruciate Ligament
AHF	Anterior Horn Facet
AIDR	Adaptive Integrated Dose Reduction
AP	Anteroposterior
APA	Anteroposterior Axis
cED	Cumulative Euclidean Distance
cVSV	Cumulative Vertical Shift Value
CAOS	Computer-Aided Orthopaedic Surgery
CCS	Cartesian Coordinate System
CD	Compression-Distraction
COR	Transverse (or Axial) Centre of Rotation
CP	Contact Point(s)
CR	Cruciate Retaining
CRIC	Clinical Research Imaging Centre
CS	Coordinate System
CT	Computed Tomography
DCM	Direction Cosine Matrix
DICOM	Digital Imaging and Communication in Medicine
DOF	Degrees of Freedom
ECA	Extension Condylar Axis
ED	Euclidean Distance
EF	Extension Facet
EFC	Extension Facet Centre
FB	Fixed Bearing
FBP	Filtered Back Projection
FCA	Flexion Condylar Axis
FCM	Fuzzy C-Means
FE	Flexion-Extension
FEA	Flexion-Extension Axis
FF	Flexion Facet
FFA	Functional Flexion-Extension Axis

Acronym	Definition
FFC	Flexion Facet Centre
FPJ	Forward Projection
GCA	Geometric Centre Axis
GCP	Good Clinical Practice
GCS	Global Coordinate System
GUI	Graphical User Interface
HU	Hounsfield Units
ICP	Iterative Closest Point
ICR	Instantaneous Centre of Rotation
IE	Internal-External
IEA	Internal-External Axis
ISB	International Society of Biomechanics
JCS	Joint Coordinate System
LCC	Lateral Condyle Centre
LCL	Lateral Collateral Ligament
LCS	Local Coordinate System
MAD	Median Absolute Deviations
MAR	Metal Artefact Reduction
MATLAB	MAThematical LABoratory
MB	Mobile Bearing
MCC	Medial Condyle Centre
MCL	Medial Collateral Ligament
MDCT	Multi-Detector Computed Tomography
ME	Medial Epicondyle
ML	MedioLateral
MRE	Magnetic Resonance Elastography
MRI	Magnetic Resonance Imaging
MS	MicroSoft
MSCT	Multi-Slice Computed Tomography
NHS	National Health Service
NRMSE	Normalised Root Mean Square Error
OA	OsteoArthritis
PACS	Picture Archiving and Communication System
PCA	Posterior Condylar Axis

Acronym	Definition
PCL	Posterior Cruciate Ligament
PCR	Posterior Cruciate Retaining
PD	ProximoDistal
PE	PolyEthylene
PFR	Posterior Femoral Rollback
PHF	Posterior Horn Facet
PS	PosteroStabilised
QEUH	Queen Elizabeth University Hospital
RCT	Randomised Control Trial
REC	Research Ethics Committee
RF	Radio Frequency
RIE	Royal Infirmary of Edinburgh
RMSE	Root Mean Square Error
ROI	Region Of Interest
ROM	Range Of Motion
RSA	Radio Stereometric Analysis
SD	Standard Deviation
SEMAR	Single Energy Metal Artefact Reduction
SKM	Strathclyde Knee Modelling (software)
SSCT	Single Slice Computed Tomography
STC	Standardisation and Terminology Committee
STL	Stereo Lithography or Standard Tesselation Language
SVD	Singular Value Decomposition
TAF	Tibial Articular Facet
TEA	Trans Epicondylar Axis
TF	TibioFemoral
TKA	Total Knee Arthroplasty
TKR	Total Knee Replacement
TM	Transformation Matrix
UC	Ultra Congruent (Fixed)
UCR	Ultra Congruent Rotating (Mobile)
UI	User Interface
VSV	Vertical Shift Value
w.r.t	With Respect To

ANATOMICAL PLANES

Coronal	Divides the body into anterior and posterior portions
Frontal	Synonymous to the coronal plane
Horizontal	Divides the body into equivalent superior (proximal) and inferior (distal) portions
Median	Divides the body into equivalent left and right portions
Midsagittal	Synonymous to the Median plane
Sagittal	Divides the body into left and right portions, which are not necessarily equivalent.
Transverse	Synonymous to the Horizontal plane.
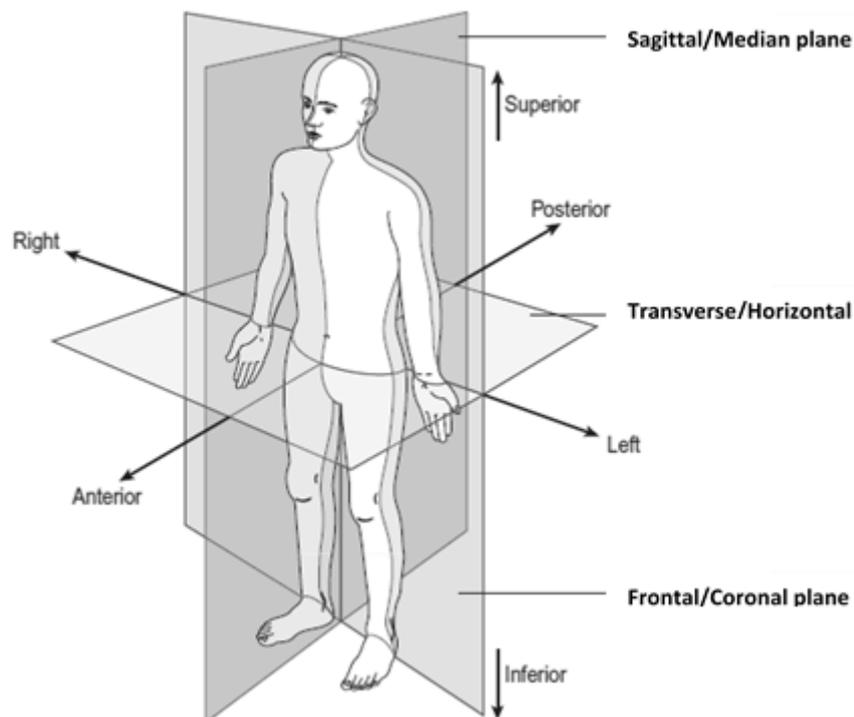
Anatomical Planes
The human body in the anatomical position, with the three reference planes and six fundamental directions. (Whittle, 2012)

1 INTRODUCTION

1.1 RESEARCH BACKGROUND & JUSTIFICATION

The knee joint has evolved over millions of years, into a highly efficient and robust articulation system linking the two longest bones in the human body, the femur and the tibia. When under compression, being akin to an inverted double pendulum, it is inherently unstable. Thus, its beauty lies in the ability of the gross anatomy and motor control systems to provide stability both in bipedal standing and in locomotion. Its ingenious construct caters for the demanding strenuous environment the knee endures on a daily basis, such as absorbing and cushioning the locomotory forces generated in the lower limbs. Additionally, it also maintains movement in all six-degree-of-freedom (DOF), while providing mobility, stability and support during both dynamic and static activities. It supports forces exceeding five times the body weight during weight-bearing activities, while also functioning effortlessly when bearing the cyclic loads experienced during mobility. The geometric and anatomical complexity of the knee along with its functional requirements, such as cyclic loading of an ageing knee, growth disturbances with consequent deformities, injuries, sports and inflammatory diseases, may lead to osteoarthritis (OA), a degenerative disease that worsens with time.

OA presents the clinician and patients alike with significant challenges in terms of reconstruction, rehabilitation and return to full function. While significant steps have been achieved in ways of treating the knee, knee arthroplasty still does not match the gains attained with hip arthroplasty. This is mainly attributed to the challenging compromise of allowing the replaced knee the native six DOF while retaining the native ligament stability of the knee in order to optimise the knee kinematics.

The knee is the most OA affected weight-bearing joint (Hunt *et al.*, 2008), affecting approximately 10% of the population aged over 50 years, such that knee OA is found in twice as many patients as hip OA (Dieppe, 2000). The population of UK citizens over the age of 65 years is predicted to increase by 53% from 2001 to 2031, leading to a likely increase in the number of people who have chronic illnesses (Majeed and Aylin, 2005). This growth in life expectancy and ageing populations are expected to make OA the fourth leading cause of disability by the end of year 2020 (Woolf and Pfleger, 2003). Along with the ever-ageing population, the number of Total Knee Arthroplasty (TKA) surgeries performed on younger patients (less than 65 years old) is projected to grow by approximately 17 times by 2030, over the figures of 2006 (Kurtz *et al.*, 2009).

Furthermore, it is predicted that by 2030 TKA occurrences in the UK are expecting an increase of 117%, over the figures in 2012 (Patel *et al.*, 2015). Financially, OA in the UK presented a total annual cost (counting direct, indirect and Quality of Life costs) of £30.7 billion in 2008 (Oxford Economics, 2010), which amounts to more than the government spent on transport and environmental protection combined.

Recent improvements in surgical techniques, such as patient-specific cutting blocks and Computer-Aided Orthopaedic Surgery (CAOS), offer patients a long-lasting and reliable surgical procedure, contributing to improved function and pain relief of the knee. These improvements result in nearly 90% patient satisfaction rates for TKA, as reported in recent studies (Gergely *et al.*, 2017). Even with high patient satisfaction rates, TKA may not be achieving its primary goal of pain relief and improvement of joint function (Robertsson *et al.*, 2000; Noble *et al.*, 2006; Wylde *et al.*, 2008). Limited range-of-motion, postoperative instability and malalignment still hinder normal knee function, even amongst patients who have a well-functioning TKA (Noble *et al.*, 2005).

Instability and stiffness of the knee are the second and third causes of early failure, while infection takes precedence (Sharkey *et al.*, 2014). Bearing in mind that stability, range of motion and alignment are all directly correlated to the kinematics of the knee, then one should focus on continually striving towards restoring the native kinematics, in order to ultimately restore the knee's original function, leading to a higher incidence of patient satisfaction.

In order to diagnose and rehabilitate patients with OA, the current clinical practice relies on 2-dimensional (2D) mediolateral (ML) and anteroposterior (AP) standing X-rays to visualise the anatomy of the knee. While this traditional method of analysis and diagnosis is standard operating procedure throughout institutions worldwide due to its accessibility, convenience and reliability, it is limited in terms of accurately assessing the essential kinematics of the patients' knees, being a static measure. Considering the aforementioned, the fact remains that at the present time, orthopaedic surgeons have minimal tools and resources which can accurately evaluate the patient's kinematics pre- and post-operatively on a routine basis.

The purpose behind this thesis is to create a supplementary tool for assessing patient-specific knee kinematics, which works alongside the conventional X-ray method, using a state-of-the-art spatiotemporal (4-dimensional or 4D) method which will provide the

clinician with accurate and essential clinical results. Currently, the foremost medical imaging methods for observing the spatiotemporal kinematics of the knee joint is to use either video-fluoroscopy, radio stereometric analysis (RSA) or ex-vivo dynamic simulators. These techniques are sophisticated, not fully three-dimensional, have a limited frame rate and/or involve a high radiation dose to the patient. Furthermore, the equipment is not widely available in clinical sites and requires specialist installation and operation. On the other hand, the innovative Computed Tomography (CT) techniques have become commonplace in clinical practice. CT (and MRI) were voted as the most valuable medical innovations in the last 30 years by physicians on the front lines of patient care (Fuchs and Sox, 2001).

In this thesis, the innovative technique of 4D CT is utilised to capture the articulation of both healthy and replaced knees. The primary aim of this thesis is to develop a novel methodology and implement it in a proof of concept software. The bespoke software processes the raw data from the 4D CT scanner and subsequently evaluates and extracts the knee kinematics for both healthy and replaced knees. The extracted kinematic profile can be provided to orthopaedic surgeons or clinicians to assist them in reliably diagnosing, managing and rehabilitating OA patients pre- and post-operatively with a more patient-specific approach.

To our knowledge, this is the first time that 4D-CT is being utilised to capture and analyse knee kinematics for both healthy and replaced knees.

In addition to the primary aim, which proved to be a substantial endeavour in and of itself, in this thesis, secondary and tertiary aims will be addressed. These two aims, which are intended to act as pilot studies for the proof of concept software, build on the current knowledge base to address two research questions which are still being incessantly discussed in the literature with no consensus yet being reached.

The first research question (secondary aim) concerns replaced knee kinematics. During TKA, a polyethylene (PE) insert is added between the femoral and tibial components to provide a bearing surface between them. These bearings can be of the fixed bearing (FB) or mobile bearing (MB) type. For the FB implants, the PE insert is locked to the tibial plate. MB implants allow planar rotation about the vertical axis of the tibia, such that the dual-surface articulation promotes a more natural articulation between the femoral and tibial components. Theoretically, this should allow for the dissipation of knee moments and shear forces to the soft tissues surrounding the knee in a manner

similar to the healthy knee (Callaghan *et al.*, 2000). Despite the theoretical benefits to the MB design, many are yet to be substantiated, and many authors have documented no improvement in outcomes compared to FB designs (Post *et al.*, 2010; Jacobs *et al.*, 2012; Mahoney *et al.*, 2012). Given the inconclusive research to date, in this thesis, it is being asked whether mobile-bearing knee implants provide additional mobility in comparison to their fixed bearing counterparts.

The second research question (tertiary aim) concerns the identification of the anatomical flexion-extension axis (FEA), or axes (FEAs), of the knee. It is known that the knee kinematics can be described by a six DOF system, which constitutes of three rotations and three translations around a knee-specific Coordinate System (CS). To quantify knee kinematics in an experimental setting, there needs to be a clear understanding of how to correctly position the anatomical local CS axes, in a repeatable and reliable manner. If the axes of a local CS are not defined according to the anatomical (also referred to as functional, natural or optimal) axis around which the knee actually rotates, then the reported data will be misleading. Axes misplacement results in the phenomenon known as kinematic crosstalk. Kinematic crosstalk occurs since rotations and translations occurring around a misplaced axis will describe rotations, and translations, occurring around, or along, another axis, thus reporting misleading results. Although there is ample research aimed at identifying the functional FEA of the knee (which will be reviewed in Chapter 2), a conclusive consensus has not yet been reached. Therefore, in this thesis, a number of pre-defined FEAs and a functionally-extracted axis will be implemented in order to understand the kinematic crosstalk that these axes exhibit as a function of their flexion angle.

1.2   THESIS STRUCTURE

1.2.1 CHAPTER 1: INTRODUCTION

In the first chapter, a brief explanation of the research background and justification is provided. A rationale is given for the development of the proof of concept kinematic analysis software developed for this thesis, along with a brief outline of inconsistencies found in the literature and the corresponding research questions being addressed in the practical aspect of this thesis, with the aim of adding to the current knowledge base. While the aims of this thesis are briefly mentioned in this chapter, these will be further defined along with their respective objectives in Chapter 3 of this thesis following the review of theory and literature.

1.2.2 CHAPTER 2: THEORY AND LITERATURE REVIEW

Chapter 2 provides additional context to perceive and appreciate the degree of intricacy with which the articulation of the knee has been studied to date. Also, this chapter will guide the reader through the workflow which is required to analyse knee kinematics, starting from the raw data to the extraction of the kinematics of the captured articulation. Initially, an overview of the functional anatomy of the native knee is given, which will act as the basis upon which the remaining text in this chapter builds. Subsequently, medical imaging techniques that exist for capturing the spatiotemporal articulation of the knee are outlined, focusing on the 4D CT imaging technique, which is utilised in the practical aspect of this thesis. This is followed by an overview of existing segmentation techniques used for extracting the morphology of the knee following imaging, focusing on the segmentation technique implemented in the bespoke software.

The "theoretical" kinematics of the native and replaced knees are consequently defined, in order to establish the baseline kinematics which are to be expected from such knees. Here it should be noted that the term "theoretical" is used loosely, in the sense that the kinematics of the knee cannot be defined by any specific set of profiles since each individual knee is known to have its own kinematic profile. Therefore, "theoretical" kinematics are chosen based on the agreement shown by other researchers on certain proposed theories which are supported by robust research methodologies. With regards to the kinematics of replaced knees, the emphasis is given to Ultra-Congruent Fixed and Mobile bearing knees, since these were the implants that were used in the practical aspect of this thesis. Additionally, a concise review of two additional kinematic outcome measures which are used in literature, namely, contact point analyses and the axial centre of rotation, is also provided.

Finally, the last section is focused entirely on the quantification of knee kinematics. An in-depth review of literature is presented to address the current state of affairs on the choice of the surrogate axes for the anatomical axes of the knee. This section is concluded with a review of the prominent kinematic mathematical models, again giving emphasis to the kinematics mathematical model that was implemented in the practical aspect of this thesis.

1.2.3 CHAPTER 3: RESEARCH AIMS AND OBJECTIVES

This brief chapter is self-explanatory. Definitions of the aims and their respective objectives are given in light of the reviewed literature in the previous chapter.

1.2.4 CHAPTER 4: METHODOLOGY

This chapter will be comprised of two sections. Initially, the planning and execution of the data collection aspect are presented. This includes the process of participant recruitment and the development of the scanning protocol, which was implemented during the 4D CT process to capture the articulation of the knees involved in this study. Secondarily, the processing of the raw data is outlined by reviewing the developed proof of concept software. The developed methodology for extracting the kinematics of the imaged knees is described by explaining the function of each consecutive module which collectively aggregate into the kinematic analysis software.

1.2.5 CHAPTER 5: RESULTS

In this chapter, the 4D CT data that was collected and processed using the bespoke software is presented and discussed. Given that this study was not a clinical trial, recruitment was opportunistic. Thus, no clear groups of volunteers are evident. Additionally, the aim of 4D CT is to provide patient-specific kinematic detail. Therefore, for these two reasons, the results section details the case-studies of the volunteers. First, the kinematic control data collected, which is composed entirely of healthy knees, is analysed to understand the effects of kinematic crosstalk that each identified FEA displayed. The discussion of the control kinematic data is aimed at addressing the second research question that is concerned with the kinematic crosstalk that is displayed by the different FEAs (which is effectively the third aim of this thesis).

Second, the kinematic patient data collected, which is composed of replaced and arthritic knees, is presented and discussed. The analysis of the replaced knees is used to determine if MB implants display signs of increased mobility in comparison to their FB counterparts. The discussion of the patient kinematic data is aimed at addressing the first research question (or secondary aim of this thesis), which is concerned with the mobility of MB implants. It should be noted that the analysis of arthritic knees is beyond the scope of this thesis and will, therefore, be only presented but not comprehensively discussed.

1.2.6 CHAPTER 6: DISCUSSION & CONCLUSIONS

Following the discussion of the results in a case-by-case approach, this chapter will conclude with an overarching discussion which aims to collate all the kinematic results and discuss any inter-participant trends that were noted. The achievements of the research aims defined in chapter 3 are assessed in light of the work presented in this thesis, including the collected results and the reviewed literature.

Furthermore, the conclusions derived from the work presented in this thesis are summarised in this chapter, focusing on the level of achievement of the research aims. Lastly, this chapter highlights the scope of future work in the same research area, with the aim of building on the work achieved in this study.

2 THEORY AND LITERATURE REVIEW

2.1 INTRODUCTION

The knee joint is the largest and most complex joint in the human body. It is responsible for various complex movements which we use during locomotion and day-to-day activities. A team of researchers stressed the complexity of the knees' articulation by stating that:

> *"The human knee joint is probably one of the most complicated joint structures from a kinematics point of view, and certainly more complex than any technical joint design known"* - (Berme, Engin and Correia da Silva, 1985).

This chapter is aimed at providing sufficient context to the reader to perceive and appreciate the intricacy with which the articulation of the knee is studied. Also, this chapter will guide the reader through the workflow which is required to go from the raw data collected during the imaging of the articulation of the knee to the extraction of the kinematics of the said articulation.

The first section will set out the foundation for the subsequent sections, by starting with a concise introduction to the functional anatomy of the knee, which is the basis upon which the remaining text in this chapter builds. This section will explain the principal anatomical features which define the way that the knee articulates.

The second section presents a review of the medical imaging techniques, which are available for capturing the dynamic movement of the knee. Imaging of the knee is the first step in the aforementioned workflow of measuring the kinematics of the knee. A brief overview of the current and emerging technologies are discussed and differentiated. This is followed by an overview of segmentation techniques in the field of medical imaging. Segmentation represents the second step in the workflow for extracting the kinematic of the knee. The preferred method for delineating the different tissues in the captured volume is discussed in preparation for its implementation in the practical aspect of this thesis.

With an understanding of the methodology involved in capturing, delineating and visualising the movement of the knee, the third section then introduces the theory of the kinematics of the knee to explain the complex cyclic articulation occurring within the knee. The six DOF kinematics, being the principal kinematic outcome measure of this study, are approached by looking at the medial and lateral aspect of a healthy knee

and understanding the articulation that is occurring at the chondral level of the knee from hyper-extension through to hyper-flexion. In addition to the six DOF kinematics, the reader is provided with a brief overview of two additional kinematic outcome measures, the tibiofemoral contact points and the axial centre-of-rotation, which are referenced in the literature as supporting measures to supplement the six DOF kinematics. These kinematics outcome measures will be implemented in the developed kinematic analysis software to give the user or clinician an additional perspective to be able to formulate a more comprehensive understanding of the complex articulation of the knee.

Subsequently, the fourth section delves in the kinematics of the replaced knee. In this thesis, the emphasis is given to Ultra-Congruent Fixed and Mobile-Bearing type implants, which are the implants that are being used in the practical aspect of this study. The knee implant designs are principally explained from a mechanical perspective, followed by an overview of the literature investigating the kinematics of patients with such implants. The way that the kinematics of the replaced knee vary from those of the healthy knee is highlighted in order to give the reader an understanding of the limitations and benefits of such implants. This is intended to assist the reader in appreciating the results obtained and discussed later in this thesis.

Up to this stage, the reader is cognisant of the complexity of the kinematics of the healthy and replaced knees. The fifth section deals with the process of going from the aforementioned segmented data (second step in the workflow) and manipulating it to be able to quantify the kinematics of the knee (third step). An in-depth review of the available literature examines the way knee kinematic studies evolved, from the time of analysing the morphology of the knee using ink and paper to the current state of the art 4-dimensional studies of knee kinematics. Through this review of literature, the reader is made aware of the controversy and numerous interpretations that exist in the analysis of knee kinematics, mainly with respect to the choice of the principal axes of the knee and their relative location to the morphology of the knee. The knowledge gained from this review of literature serves as the foundation for the development of the methodology of the kinematic analysis software which was developed to process the raw medical imaging data, and subsequently extract the kinematic data that will be presented in the results section of this thesis.

2.2 THE FUNCTIONAL ANATOMY OF THE NATIVE KNEE

In this section, an understanding of the functional anatomy of the knee joint will be presented to the reader as a basis for the subsequent section reviewing the kinematics of the native knee. This will allow the reader to appreciate how the underlying kinematics relate to the geometry and anatomy of the knee. Also, it will give the reader a better foundation to understand the effect that a prosthetic implant has on the kinematics of the replaced knee after reconstructing an arthritic knee. This theory is presented in its elementary form in order to establish a good foundation for more complex theory and literature thereon.

2.2.1 RIGID-BODY STRUCTURES

The bone morphology of the knee is known to be largely asymmetrical, hence creating the complex kinematics which are still debated in literature until the present day (Eckhoff *et al.*, 2005). The correlation between functional anatomy and kinematics leads to linear and angular relationships which need to be implemented in the design of prosthetic replacements in order to re-create the original functionality of a native knee, a paradigm which is still far from perfect at the present day in terms of restoration of the native kinematics.

2.2.1.1 ARTICULATIONS

The morphological characteristics of the distal femur have been a source of both historical and contemporary interest (Weber and Weber, 1837; Fick, 1877; Mensch and Amstutz, 1975; Yoshioka, Siu and Cooke, 1987b; Hollister *et al.*, 1993; Iwaki, Pinskerova and Freeman, 2000; Eckhoff *et al.*, 2001). From a superficial point of view, the knee has three main rigid-body structures (Figure 1A). The femur is the longest and heaviest bone in the human body. Proximally the femoral head articulates with the pelvis's acetabulum, and distally the femoral condyles articulate with the tibial condyles. Similarly, the tibia articulates proximally with the distal condyles of the femur (and with the fibula – interface not visible in Figure 1), while distally, it articulates with the fibula and the talus bone, forming the proximal part of the ankle joint complex. Furthermore, the patella, which is both formed and resides within the quadriceps femoris tendon (Figure 1A), provides a fulcrum point which pushes the tendon as far out as possible during knee extension. This increases its moment arm, thus increasing the power that the knee extensor group generates at the patellar ligament

insertion point in the proximal tibia. The patella also serves as a stabilising structure that reduces frictional forces placed on the femoral condyles.

The knee joint exhibits two distinct articulations (Figure 1B). The primary articulation, which is the focus of this thesis since it dictates the key knee kinematics, is the tibiofemoral articulation. This articulation, as the name dictates, occurs between the femur and the tibia, and become apparent at the medial and lateral compartments of the knee. A knee compartment is defined as the area where one femoral condyle contacts the corresponding tibial condyle throughout the knee's range of motion (ROM). The secondary patellofemoral articulation occurs between the posterior surface of the patella and the trochlear groove on the anterior surface of the distal femur (Jones, 2018b).
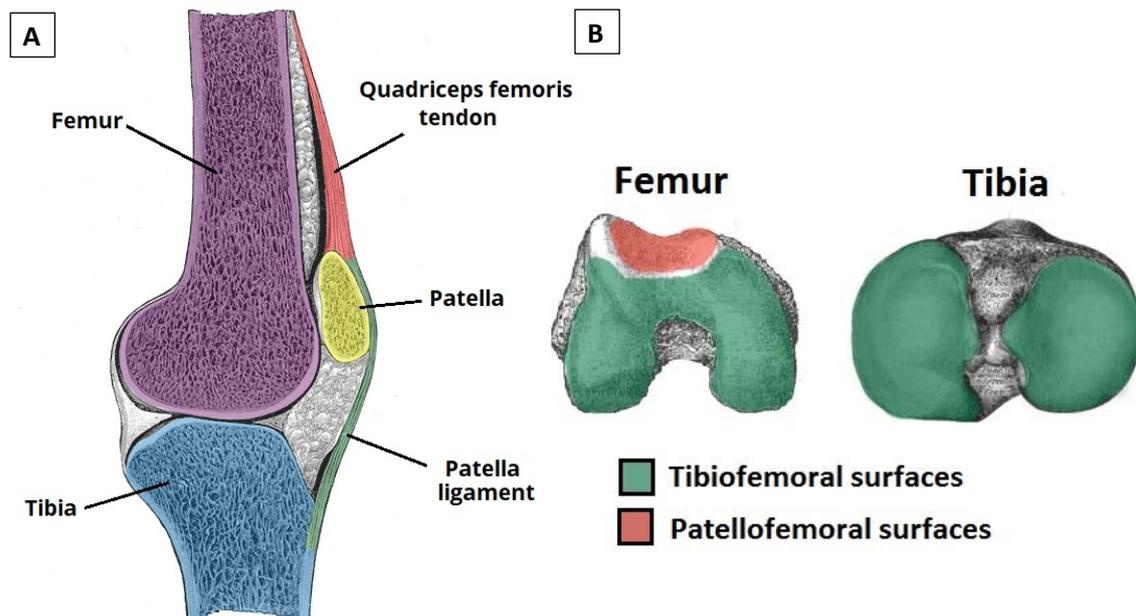
Figure 1: Bone anatomy of the knee (Jones, 2018b).

A: The three main rigid-body structures of the knee.
B: The contact surfaces of the knee, i.e. the corresponding tibiofemoral surfaces (green) and the patellofemoral surface (red).

2.2.1.2   MORPHOLOGY

Morphologically the distal femur bears two rounded articular surfaces, the condyles, which project posteriorly beyond the femoral shaft in a J-shaped fashion (Figure 1A). The medial condyle is larger than the lateral condyle due to the fact that medially the knee has to bear a larger weight since the centre of mass of the human body lies medial to the knee (for both single and double-legged stance). On the other hand, the lateral condyle is more prominent anterolaterally, in order to help prevent the natural lateral

movement of the patella, avoiding dislocation. In its neutral position, the femur is not vertical in the coronal plane, but it rather converges towards the midsagittal plane distally meeting the vertical tibia at an angle between 5˚ and 12˚ valgus relative to the tibia. The larger medial condyle compensates for the valgus angle between the femur and the tibia, such that the femoral condyles make contact with the vertical tibia evenly. The sides of the condyles each bear a projection on the non-articular areas called the medial and lateral epicondyles (Figure 2A and Figure 2B). The medial epicondyle is the larger, corresponding to the size of the condyle. The epicondyles mark the origin of the corresponding collateral ligaments. Finally, the intercondylar fossa (Figure 2A) is a depression located on the posterior surface of the femur, containing two facets, for the attachment of the cruciate ligaments (Jones, 2018b).
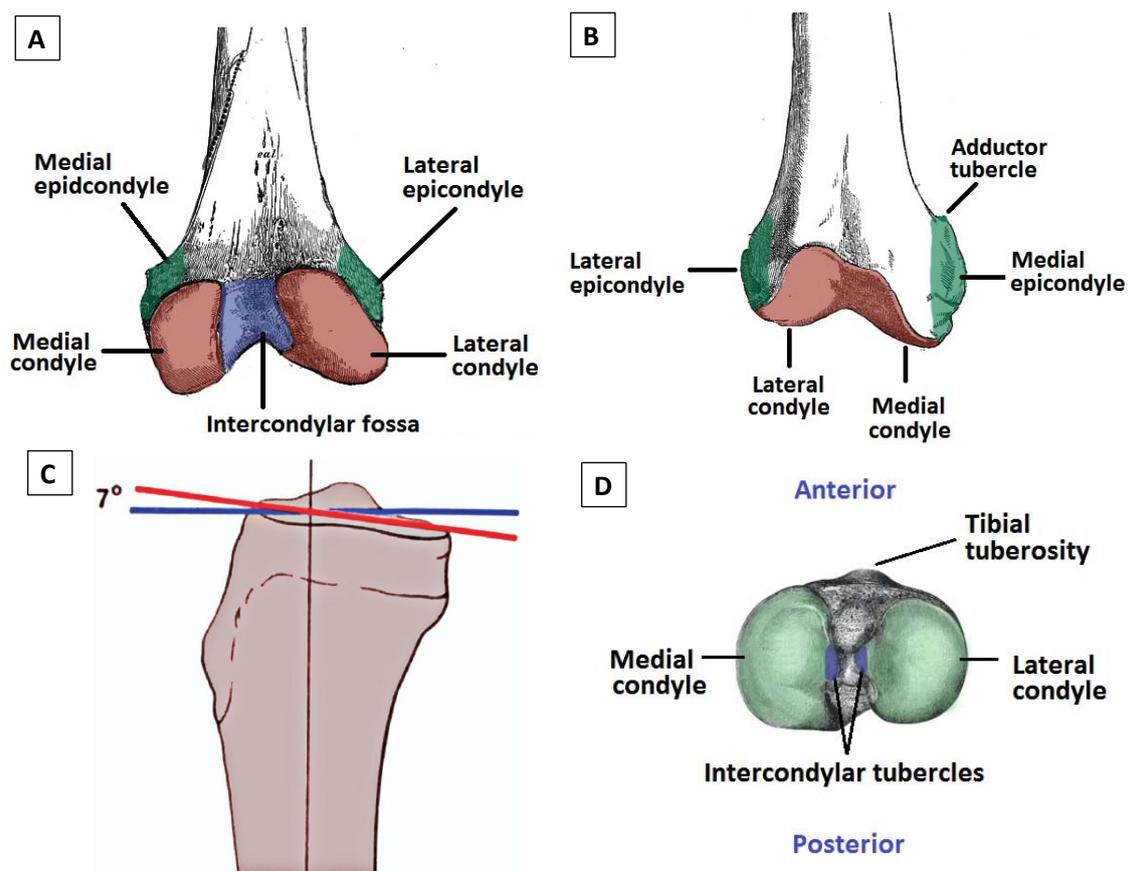
Figure 2: Knee morphology

A: A posterior view of the distal end of the femur (Jones, 2018).
B: An anterior view of the distal end of the femur (Jones, 2018).
C: A sagittal view of the tibia showing the tibial slope (Hohmann and Bryant, 2007)
D: A Superior view of the proximal end of the tibia (Jones, 2017).

The proximal tibia is oval-shaped in the transverse (or axial) plane and projects posteriorly, similar to the femoral condyles, in order to increase the surface area for weight-bearing. The medial tibial surface is sloped posteriorly (Figure 2C) at an angle of around 7° (varies depending on population group) while the lateral side is roughly flat. The proximal tibia contains two surfaces covered with articular cartilage, the medial and lateral plateaus, which articulate with the corresponding femoral condyles (Figure 2D). The lateral tibial plateau is slightly convex and smaller than the contralateral concave medial plateau. The plateaus are separated by the intercondylar tubercles, which correspond with the insertion points of the cruciate ligaments. The tibial intercondylar tubercles fit into the aforementioned femoral intercondylar fossa. Anteriorly, and slightly inferior to the plateaus lies the tibial tuberosity (Figure 2C and Figure 2D), which is a bony prominence where the patellar ligament attaches to the tibia. Finally, the plateaus are covered by the menisci, which will be discussed in more detail in the subsequent paragraphs.

2.2.2 SOFT-TISSUE STRUCTURES

While the bone morphology determines the principal articulations of the knee, it is important to have a basic understanding of the supporting accessory structures which assist the articulation of the knee, mainly in terms of stability and support. The major soft-tissue structures which are directly implicated in the complex articulation of the knee will be outlined to give the reader the required knowledge to understand the forthcoming kinematic description.

2.2.2.1   LUBRICATION SYSTEM

The soft tissue sleeve of the knee is comprised of skin, fat, muscles, ligaments, tendons, cartilage, menisci, a network of blood and nutrient vessels, nerves and the synovial capsule (Figure 3B). At all locations where the bones make contact with each other during articulation, i.e. both femoral and tibial condyles, the trochlear groove and the posterior surface of the patella, are lined with articular cartilage. The surface of articular cartilage is slick and smooth to reduce friction during movement. Under normal physiological loads, the articular cartilage does not touch one another because of a thin film of synovial fluid. The synovial fluid lies within the synovial capsule's joint cavity space (Figure 3B) keeping the bones from making contact. The thin film, which amounts to only 3mL in volume in a normal knee, has a high viscosity, having the
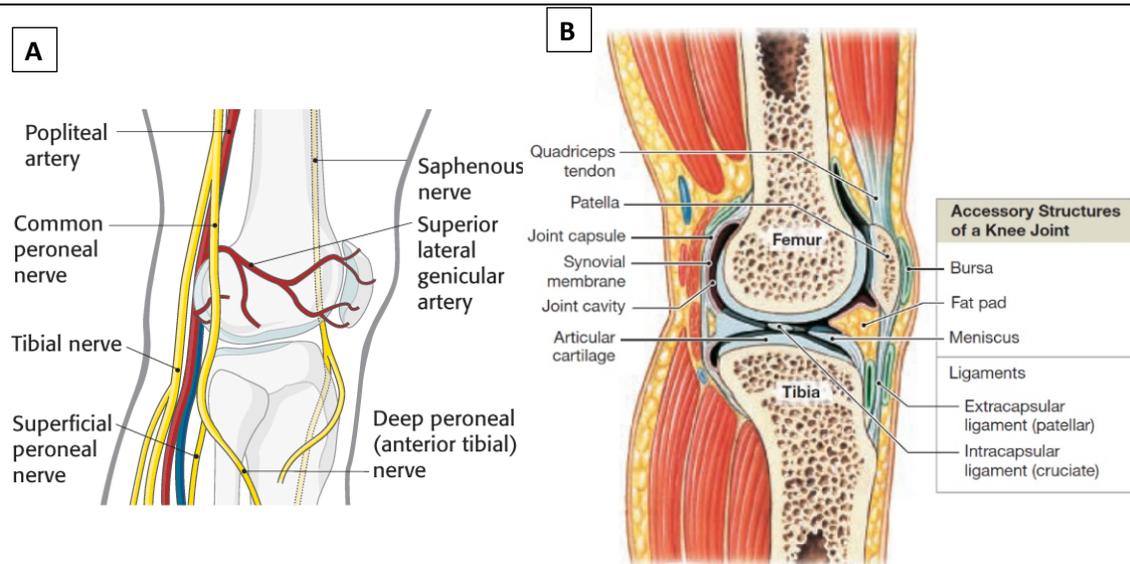
Figure 3: Accessory structures of the knee.

A: A diagram illustrating the location of the primary neurovascular structures of the knee (AO foundation, 2008)

B: A sagittal section of the knee joint showing the soft-tissue accessory structures of the knee (Martini, Nath and Bartholomew, 2018).

consistency of egg yolk. It has three primary functions, namely providing lubrication in order to further minimise friction within the joint, assisting nutrient distribution and waste disposal to the avascular articular cartilages and absorbing shock loads since under sudden impacts the liquid is compressed, increasing its already high viscosity (Martini, Nath and Bartholomew, 2018).

The skin, fat, synovial capsule and the network of blood and nutrient vessels provide protection and nutritional support to the knee. The location of the vessels and nerves around the knee is beyond the scope of this dissertation and will not be discussed, although it should be appreciated that the vessels and the nerves pass along the posterior aspect of the knee while branching medially and laterally (Figure 3A). This allows for surgically exposing the knee from the anterior aspect with minimal risk of damaging neurovascular structures.

2.2.2.2   MENISCI

The knee menisci have a primary role throughout the entire ROM of the knee's articulation, playing a secondary role in knee kinematics. There are two menisci, one for each compartment of the knee. They are fibrocartilaginous structures which were marvellously biomechanically engineered through evolution to perform specific integral tasks in the knee joint. They are C-shaped (Figure 4A) and attach at both anteroposterior (AP) ends to the intercondylar area of the tibia.
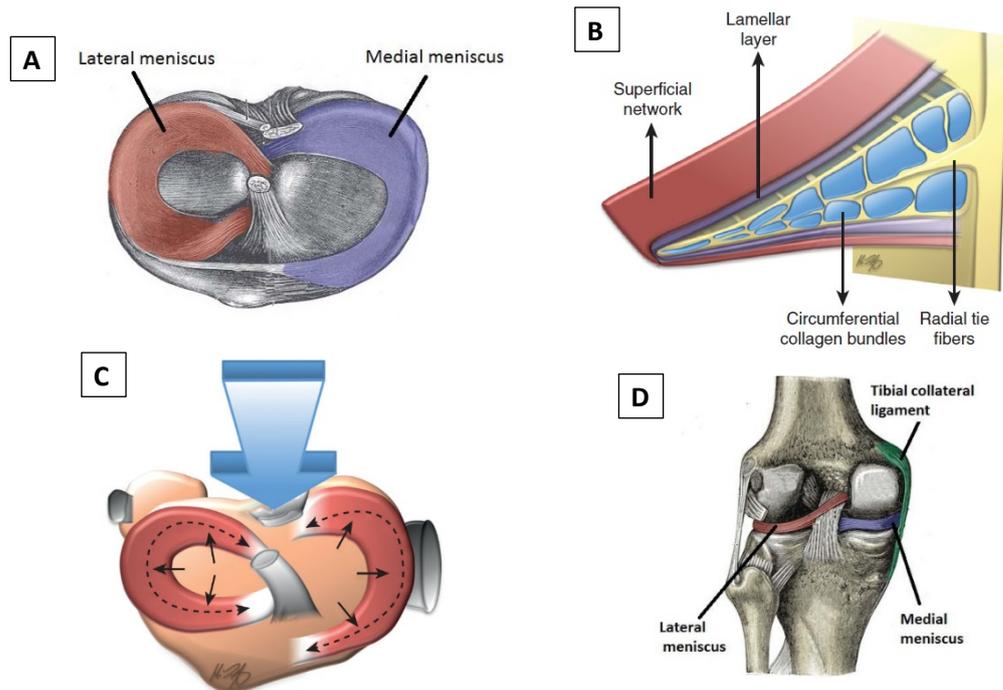
Figure 4: The menisci of the knee joint.

A: A superior view of the tibial bone, outlining the medial and lateral menisci (Jones, 2018b).
B: The micro-structure of the meniscus, showing the three distinct layers of the network of collagen fibres.
(1) The random collagen fibres on the superficial layer which receive the external compressive forces, (2)
the deeper lamellar layer, and (3) the central (deepest) layer constituted by the circumferential and the
radial (or tie) fibres which are responsible for the absorption of the tensile stresses (Scott, 2018).
C: A representation of the normal biomechanics of the meniscus. Hoop stresses (black arrows) are
generated as axial forces (blue arrow) are converted into tensile stresses (dashed arrows) along the
circumferential fibres of the meniscus (Scott, 2018).
D: A posterior view of the knee joint, showing the deep soft-tissue anatomy. Note the close relationship
of the medial meniscus and the medial collateral ligament (Jones, 2018b).

Primarily, they convert the high compressive forces that are transferred axially through

the knee into tensile stresses (in the form of hoop stresses). These tensile stresses are

absorbed by the circumferential and radial fibres on the exterior loop of the menisci

(Figure 4B). The compressive axial forces from the femur and tibia during knee loading

are received at the surface of the meniscus, where a random collagen fibrillar network

exists. This random network is capable of receiving multi-directional forces, and

distributing them into the circumferential and radial fibres (Figure 4C) which absorb

the loads by resisting the tensile stress with the assistance of the pulling force from the

anterior and posterior insertion ligaments at each end of the meniscus. To put the

menisci's load absorption capabilities into perspective, it was reported that in full

extension the medial meniscus absorbs approximately 50% of the load, while the lateral

meniscus absorbs approximately 30% of the load (Walker and Erkiuan, 1975). While

this force dissipation mechanism is utilised as a shock absorber in the knee, the menisci

also increase the surface area of contact between the femur and the tibia. In order to

avoid having direct contact between the femoral and tibial condyles, the menisci's shape developed to match the contours of the condyles as the femur changes position, thus deepening the articular surface. This leads to a larger surface area of contact, therefore, reducing the chance of having points of high-stress concentrations. Additionally, this has the benefit of further dissipating forces, while also increasing the stability of the knee joint.

The medial and lateral menisci are asymmetrical in shape and function. The medial meniscus has a larger radius of curvature than its lateral counterpart since it needs to accommodate the larger medial femoral condyle. Furthermore, the medial meniscus is attached laterally to the Medial (tibial) Collateral Ligament (MCL) constraining its AP movement (Figure 4D), while the lateral meniscus is allowed a higher degree of movement since it is not constrained to the Lateral (fibular) Collateral Ligament (LCL). This freedom of movement is imperative in maintaining stability during hyper-flexion, as will be explained in sections 2.4.1.4 and 2.4.2.3.

2.2.2.3   LIGAMENTS

Complete dislocation of the knee is very rare, thanks to seven major ligaments which passively strengthen and stabilise it during different stages of its articulation.

1.   The anterior surface of the knee is supported by the patellar ligament, the quadriceps femoris tendon and two ligamentous bands known as the patellar retinaculae (Figure 5A). The quadriceps tendon, which is responsible for knee extension upon muscle contraction, passes over the anterior surface of the joint and wraps the patella. The patellar ligament is a continuation of the quadriceps tendon distal to the patella, attaching itself to the tibial tuberosity. The patellar ligament is assisted both medially and laterally by the patellar retinaculae for extra strength.

2,3.   Posterior stabilisation is offered via the two popliteal ligaments which extend between the femur condyles and the heads of the tibia and fibula (Figure 5B).

4,5.   In between the femur and the tibia lie the Anterior and Posterior Cruciate Ligaments (ACL and PCL respectively) which connect the two bones together. The 'anterior' and 'posterior' terms refer to the sites of origin of these ligaments on the tibia. The term cruciate refers to the way the two ligaments cross each other as they proceed to their insertion points in the femur (Figure 5C and Figure 5D). The ACL's primary function is to prevent anterior dislocation of the tibia with respect to the femur.
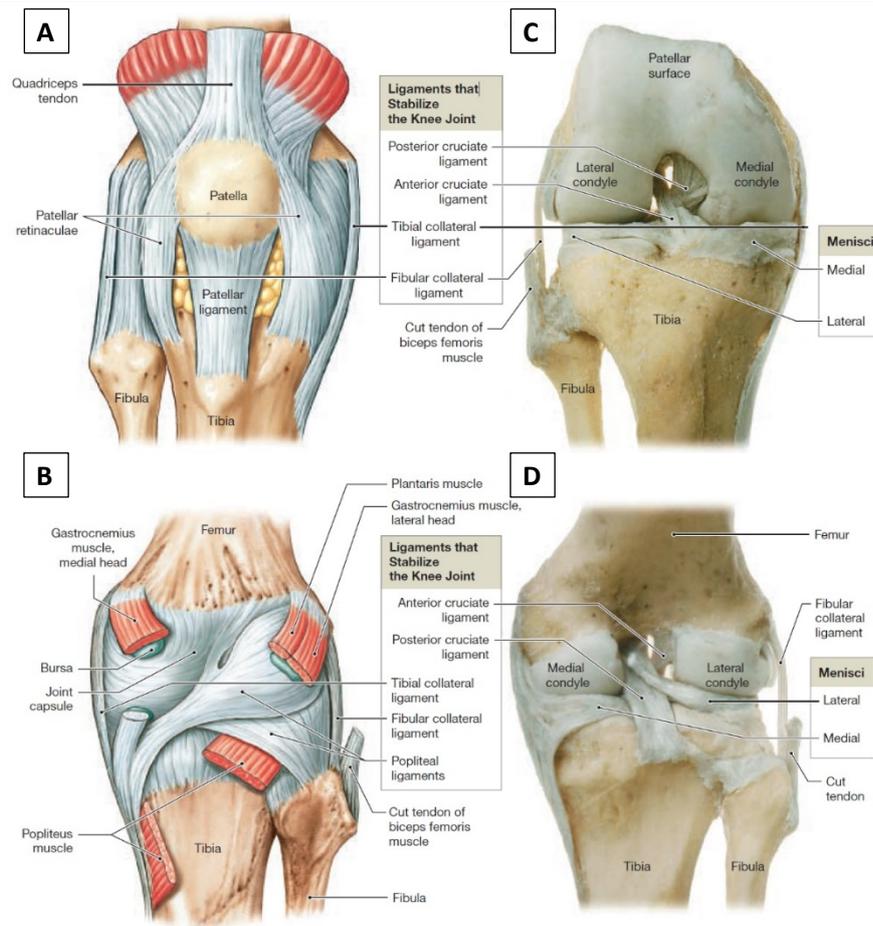
Figure 5: Superficial and deep anatomical views of the knee (Martini, Nath and Bartholomew, 2018)

A: Superficial layer of the extended knee, viewed anteriorly.
B: Superficial layer of the extended knee, viewed posteriorly.
C: Deep tissue layer of the flexed knee, viewed anteriorly.
D: Deep tissue layer of the extended knee, viewed posteriorly.

Secondarily, it acts as a stabiliser against the internal rotation of the tibia. It originates from the anterior intercondylar region of the tibia, blending with the anterior attachment of the medial meniscus. It ascends posteriorly and attaches to the posterior region of the intercondylar fossa. The PCLs primary function is to prevent posterior dislocation of the tibia with respect to the femur. Secondarily, it acts as a stabiliser against the external rotation of the tibia. It originates from the posterior aspect of the intercondylar region of the tibia and ascends anteriorly attaching to the anteromedial femoral condyle. These ligaments are crucial in maintaining alignment during articulation of the knee.

Each of the cruciate ligaments contains functionally different fibre groups. One fibre bundle is always taut, while numerous others are taut in intermediate or extreme positions. The bulk of the fibres of the ACL is taut in maximal extension, while that of the PCL is taut in the intermediate positions and in maximal flexion. Fibres taut in extreme positions serve as restraints, such that during hyperextension, the ACL

restrains forward translation of its tibial attachment, while the PCL interacts with other structures to prevent the posterior opening of the joint. The inverse situation occurs in hyperflexion. Cruciate fibres are dissimilar in length and angular arrangement so that, they can adapt their length to different movement scenarios which will require varying restraints.

6,7.   The collateral ligaments (Figure 5) are two strap-like ligaments which offer mediolateral (ML) stability to the knee. The MCL (also referred to as the tibial collateral ligament), which is wide and flat in cross-section, reinforces the medial surface of the knee joint. Proximally, it inserts in the medial epicondyle of the femur, while distally it attaches to the medial condyle of the tibia. The LCL (also referred to as the fibular collateral ligament), which is thinner and rounder in cross-section, reinforces the lateral side of the knee joint. It attaches proximally to the lateral epicondyle of the femur, while distally it attaches to a depression on the lateral surface of the fibular head. The collateral ligaments are only taut at full extension, the position at which they offer the most stability to the joint. Finally, it should be pointed out that these ligaments also assist the knee in rotational stability since they counteract excessive internal or external rotation.

2.2.2.4   MUSCLES

The muscle-tendon components make up a significant component of the functional anatomy of the knee. There are four major movements that are powered by the active muscular contractions:

1. Flexion: The flexion mechanism of the knee lies posterior to the thigh (Figure 6A and Figure 6C), specifically the hamstrings group, comprised of the lateral hamstring (biceps femoris), the medial hamstring (sartorius, gracilis, semitendinosus and semimembranosus). Additionally, the popliteus muscle is also a flexor muscle whose function mainly lies in the first few degrees of flexion. When the knee is in the locked (fully-extended) position, the popliteus muscle, often referred to as the "key", unlocks the knee by laterally rotating the femur on the tibia, thus allowing the remaining flexor muscles to take-over and initiate knee flexion.

2. Extension: The extensor mechanism of the knee lie on the anterior to the thigh, specifically the quadriceps group. This quadriceps group is made up of the rectus femoris, vastus lateralis, vastus intermedius and vastus medialis (Figure 6B and

Figure 6C), inserting into the tibial tuberosity via the aforementioned patellar ligament.

3. External (lateral) rotation: The biceps femoris (lateral hamstring) also has the responsibility of externally rotating the tibia relative to the femur.

4. Internal (medial) rotation: The aforementioned medial hamstring muscles and the popliteus muscle rotate the tibia internally relative to the femur.
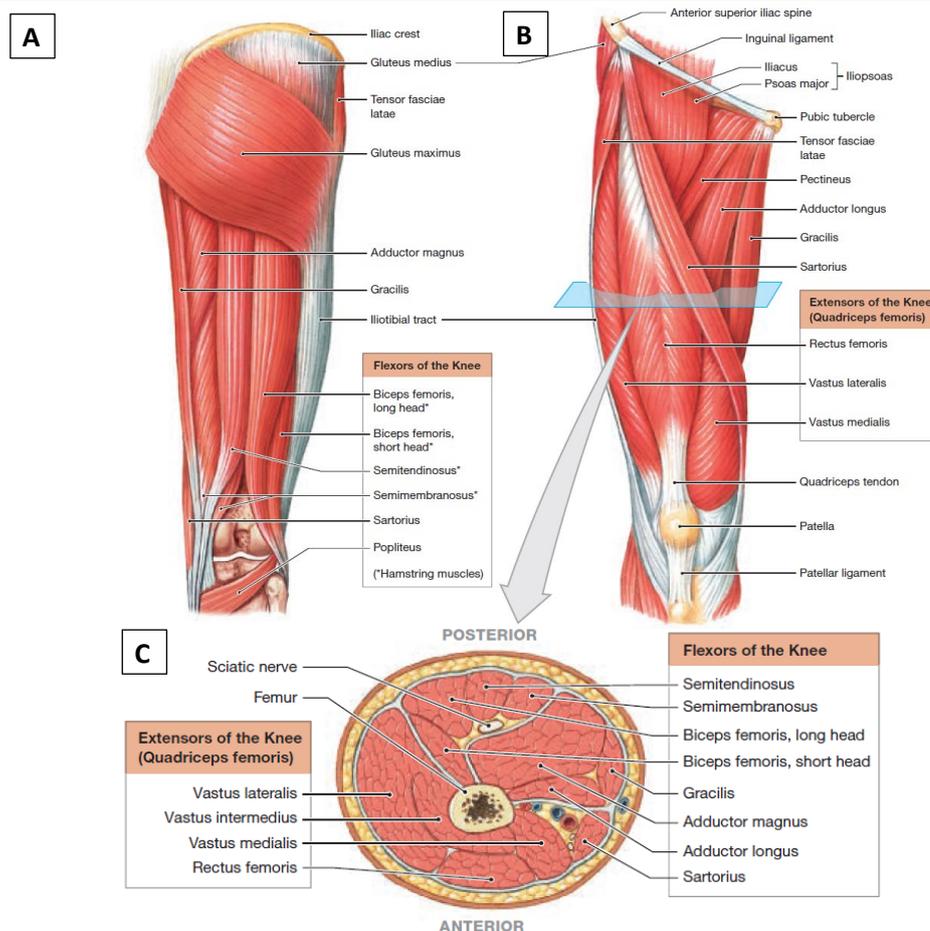
Figure 6: Muscles that articulate the knee (Martini, Nath and Bartholomew, 2018).

A: Posterior view of the thigh muscles, showing the location (including origin and insertion points) of the knee flexor muscle group (the hamstring muscles).
B: Anterior view of the thigh muscles, showing the location (including origin and insertion points) of the knee extensor muscle group (the quadriceps muscles).
C: A cross-sectional view of the thigh muscles outlining the position of the muscles.

It should be noted that external and internal rotation of the knee is only allowed when the knee is in the flexed position. In the extended position, the rotation will occur at the hip joint.

During TKA, the balancing of these muscles is crucial in determining the performance of the implant. Improper balancing of these soft-tissues will lead to imbalanced loads on the contact surfaces of the knee, such that accelerated wear may result as a result of these unbalanced loads (Bellemans, Ries and Victor, 2005).

2.3   VISUALISING DYNAMIC KNEE JOINT MOTION

In knee arthroplasty, medical imaging is used extensively to assist surgeons in visualising a patient's knee during diagnosis, treatment, pre-operative planning, intra-operative execution, postoperative evaluation and revision planning. While imaging technologies have advanced significantly, most routine practices are still restricted to static 2D radiographs. While these static images are enough for providing the orthopaedic surgeon with a tool to evaluate the joint space, and the balancing and alignment of the native or replaced knee, these images provide considerably limited kinematic information which is necessary to perform a more comprehensive diagnosis of the patients' knees. Orthopaedic imaging has nowadays developed considerably, such that for roughly the same amount of radiation which the patient receives for a 2D bilateral lower-limb x-ray radiograph (average typical effective dose per procedure of 0.05 ± 0.05 mSv - UNSCEAR, 2000), a more advanced dynamic scan can be performed using enhanced imaging modalities (average typical effective dose per procedure of 0.05 ± 0.06 mSv - Gondim Teixeira *et al.*, 2015), giving the surgeon the possibility of quantitatively assessing the dynamic knee kinematics. This gives the surgeons, and clinicians alike, a much more comprehensive kinematic understanding of the native or rehabilitated knee being studied. Section 2.3.1 describes the available imaging technologies which are capable of acquiring multiple 3D images over time, thus allowing for a 4-dimensional (4D) analysis of the patient's kinematics.

Capturing the dynamic motion of the knee over time is only the tip of the iceberg in the workflow of quantifying the dynamic knee joint motion. Following the acquisition of the dynamic motion of the knee, the acquired 4D data needs to be visualised in 3D virtual space. The first step towards visualising the 3D morphology of the scanned knee is to utilise segmentation techniques to delineate the anatomy of interest from the rest of the tissues in the captured volume. This allows the anatomy of interest to be virtually modelled on its own in preparation for further manipulation which is required to quantify the dynamic motion of the knee. Segmentation techniques are briefly introduced in section 2.3.2, focusing on the methods used later in this thesis.

2.3.1 MEDICAL IMAGING FOR KINEMATIC STUDIES

Medical imaging has come a long way. Historically, a broad range of techniques has been employed to perform kinematic analyses, from the early elegant work of descriptive anatomists to the more recent computationally sophisticated in-vivo 3D dynamic systems. As technology progressed, cadaver ex-vivo simulators, optoelectronic stereophotogrammetry, single and bi-plane radiogrammetry and video fluoroscopy were also being utilised for knee kinematic studies.

Nowadays, volumetric (3D) imaging systems, namely computed tomography, or CT, and magnetic resonance imaging, or MRI, have become commonplace in clinical practice due to their ability to capture 3D volumetric images with relative ease. Most of the current 3D imaging systems found in hospitals today are generally limited to static imaging protocols. This is the case since up until a few years ago technology did not allow for recording continuous dynamic motion due to technical limitations such as limited detector width and temporal resolution which impeded the quality and sharpness of the volumetric images being produced. Thus, if a continuous dynamic scan was attempted, the resulting images would be affected by motion artefacts created by the patient's voluntary and/or involuntary movements, while giving patients a relatively high radiation dose (Pan, 2005).

4D medical imaging has been recently developed with the aim of overcoming these motion artefacts, which result when using the current 3D volumetric imaging systems. Thanks to the accelerated image acquisition, improved image quality and diversified imaging techniques which allow for correcting motion artefacts, nowadays clinicians can visualise dynamic organs, such as the heart and lungs with high quality and fidelity. 4D medical systems have been initially developed for cardio and pulmonary tumour identification since tumour motion is critical for the radiation oncologist to delineate the target tumour. Recently, interest in the potential of using this technology for other medical uses has started to gain traction.

Currently, most volumetric-based kinematic analyses are performed using either bi-plane video fluoroscopy or CT and MRI (both utilising static-image protocols). While alternative methods to capture the dynamic motion of the knee exist, and some are commonly utilised, these methods are not considered to offer comprehensive and reliable kinematic data due to the following reasons:

- Optoelectronic stereophotogrammetry. Two methods exist to record motion using this method. Skin-mounted retro-reflective marker-based motion tracking is unable to accurately represent the motion of the underlying bone due to skin deformation and displacement which causes marker movement with respect to the underlying bone (also known as soft tissue artefacts) (Kadaba, Ramakrishnan and Wootten, 1990; Cappozzo, 1991; Fuller *et al.*, 1997; Lucchetti *et al.*, 1998; Lu and O'Connor, 1999). Bone or skeletal pins, which are also used to measure skeletal movement, were responsible until recently, for some of the most realistic quantitative data in biomechanics but are very invasive and to a certain extent unethical, thus having limited applications for human studies.

- Single plane radiogrammetry or video fluoroscopy. Single-plane systems only provide 2D images, which is not sufficient for recording and subsequently analysing motion in 3D. Two of these systems are used in conjunction with each other to record bi-planar, or stereo, images of the same point-of-interest, thus allowing for the analysis of motion in 3D (You *et al.*, 2001). These systems will be explained in more detail in section 2.3.1.1.

- Cadaver ex-vivo simulators. While these systems are very practical in nature since they allow for fully instrumented experiments, they have several drawbacks which impede their use. Firstly, the tissue being analysed has different mechanical properties than in-vivo, thus the data obtained using such systems always leave certain doubt with respect to its implication on real in-vivo mechanics (Varadarajan *et al.*, 2009). Secondly, such equipment is costly to create, validate and maintain, and would generally have a sole specific use, thus making it very cost-intensive.

Given the choice of medical imaging techniques which currently exist and the emerging 4D imaging techniques, choosing the best technique to utilise for a given study, depends on the nature of the specific research question, the acceptable level of invasiveness, the required accuracy, and the available resources. A brief outline of the principal medical imaging modalities used for dynamic kinematic analysis is given in the following sections, with the aim of identifying the best method for the dynamic analysis of healthy and replaced knees.

2.3.1.1   BI PLANAR VIDEO FLUOROSCOPY

Video-fluoroscopy is essentially a continuous X-ray image usually displayed directly on a monitor for the clinician to observe the tissue of interest in real-time. Fluoroscopy is routinely used in a wide variety of clinical examinations and procedures such as:

- Gastrointestinal tract surgeries, where a barium enema is used as a contrast agent to create a clear silhouette of the patient's colon, which assists the surgeon in identifying abnormalities.

- Coronary artery bypass surgeries to direct the movement of the catheters and stents through blood arteries/vessels.

- Angiograms to visualise blood vessels during surgical interventions.

In order to analyse motion, the 3D position and orientation (also referred to as the *pose* of a body in 3D space) of the body being analysed needs to be defined. Single-plane video fluoroscopy produces a single 2D image which refreshes every time the patient is given a radiation dose. However, a single 2D perspective is not enough for defining the 3D pose of the body being recorded since the 3D pose of the knee cannot be extracted from a single 2D image. In order to be able to perform a proper 3D kinematic analyses of skeletal motion, biplanar video fluoroscopy must be utilised.

Biplanar video fluoroscopy captures two 2D images from two different perspectives whose relative locations in 3D space are known. For biplanar videofluoroscopy to successfully recreate the pose of the knee being recorded, apart from the biplanar 2D fluoroscopic images, a digitally reconstructed 3D model of the knee is required. These 3D models are usually obtained using static MRI or CT (Figure 7A), which allows for clear delineation of the osseous tissue, thus resulting in an accurate morphological digital reconstruction. Following the acquisition of the sequence of biplanar 2D images (Figure 7B) and the reconstruction of the 3D morphology, the 3D model can be mapped onto a pair of time-matched 2D images to locate the pose of the knee at the instance the images were captured. The mapping process consists of using a series of calculations to scale the distance between the object being recorded and the X-ray sources to allow for correct magnification, and then a normalised contour matching algorithm is used to align the 3D model onto the 2 perpendicular 2D images until the silhouette of the 3D model matches the outline of the bones in both the 2D images (refer to Figure 7C and D) (Dennis *et al.*, 1996; Stiehl *et al.*, 1997). When this is applied to all the fluoroscopic
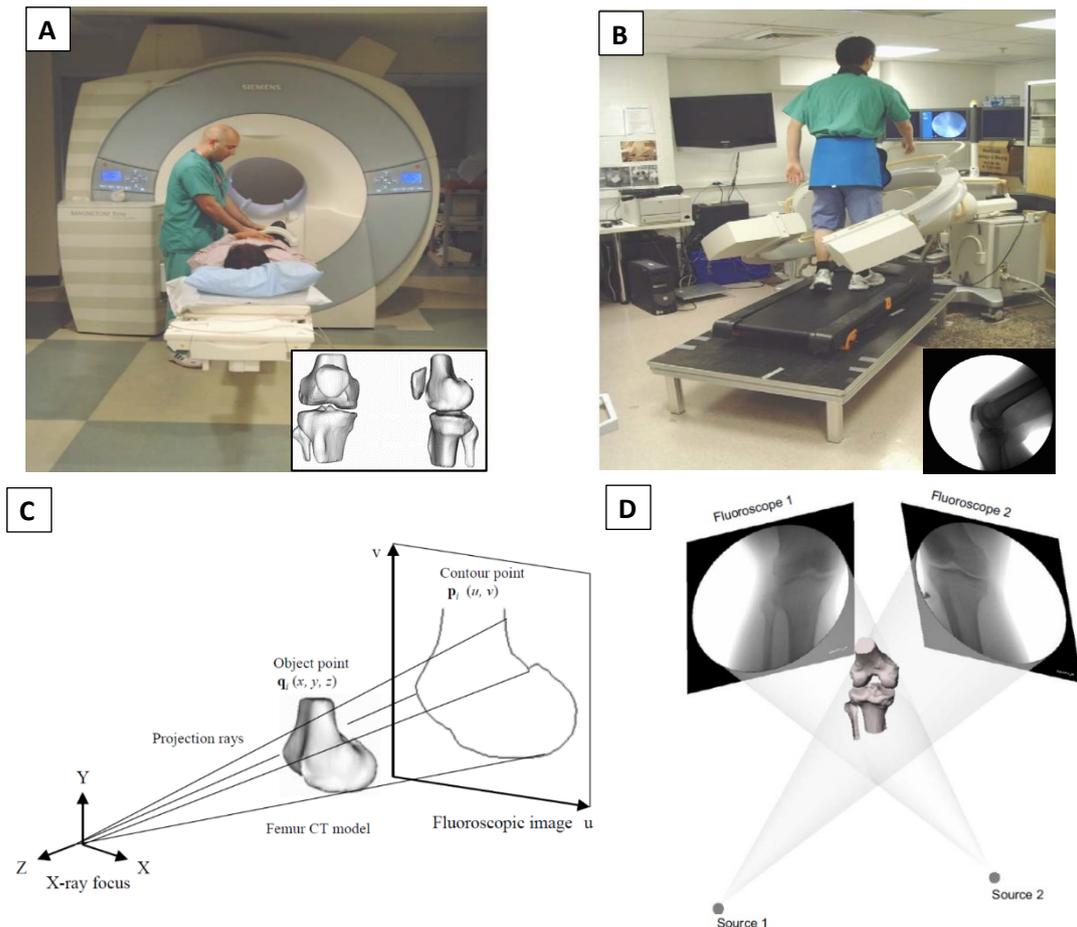
Figure 7: Bi-planar fluoroscopy setup for the kinematic analysis of the knee (Yamazaki et al., 2007; Kozanek et al., 2009)

A: MRI being used for the reconstruction of the 3D model (shown bottom-left);
B: The Fluoroscopic setup used to capture the dynamic motion (typical fluoroscopic image shown in the bottom-left);
C: Pose estimation of the model onto a single 2D fluoroscopic image;
D: The location of the knee is calculated by matching the contours of the 3D-model onto the two 2D fluoroscopic images to obtain the pose of the bones for each individual frame.

timeframes, the movement of the recorded knee can be digitally reconstructed (Kozanek *et al.*, 2009). Following the digital mapping of the knee, the six DOF kinematics of the recorded knee can then be calculated by embedding a joint coordinate system (explained in depth in section 2.6.3).

Biplanar video fluoroscopic systems have become widespread in the field of biomechanics since they can capture weight-bearing kinematics, are relatively accurate, allow for scanning of metallic implants and use a non-invasive approach when compared to the systems discussed so far. Nonetheless, such systems are limited to research laboratories, and it is highly unlikely that these systems will be part of routine clinical equipment in the near future. Additionally, they have limitations due to the long setup and processing time to capture the data, the high-level of radiation doses (an

effective dose of 0.125mSv for a typical 20-second scan - Li, Wuerz and DeFrate, 2004) which the patient is exposed to, tedious positioning of the joint during the scans which might lead to sub-consciously altered movement and issues arising from errors in the mapping process which reduce the fidelity of the process in acquiring the exact pose of the objects being recorded. Furthermore, rapid bone movement encountered during typical dynamic studies causes significant motion blur further obscuring the edges of the 2D images and thus negatively impacting the mapping process.

2.3.1.2 MAGNETIC RESONANCE IMAGING (MRI)

MRI is based on the re-emission of an absorbed radio frequency (RF) while the patient is lying in a magnetic field, with field strengths of 0.3 to 3 tesla. When the patient's tissues are subjected to this strong magnetic field, protons align themselves with respect to the field. In this steady-state, an RF pulse is applied, which excites the magnetised protons in the field. After application of this pulse, a receiver coil 'listens' for an emitted RF signal that is generated as these excited protons relax or return to equilibrium. This signal, with the help of localising gradient fields and Fourier transformation, creates the MRI image (Maravi *et al.*, 2015).

MRI is particularly useful for the evaluation of soft tissues and fluids since these materials contain water molecules containing hydrogen (which houses only one single proton), which respond to the RF pulses when present in a strong magnetic field. Soft-tissues and tissues with elevated water content display a high degree of proton movement, thus producing very detailed images. Therefore tissues with elevated water content produce the clearest and brightest images. Contrarywise, tissues containing a an elevated percentage of collagen or hydroxyapatite, the main component of osseous and fibrous connective tissues (such as ligaments and tendons), produce no or very low signal, thus appearing black due to their dense nature and their low water content which leads to low resonance to the RF signal (Wilson, 2011). MRI images can be further discretised by their weighting, which represents the timing and sequence of the radio pulse, specifically the Repetition Time (TR) which is the time spent between successive RF pulses applied to the same slice, and the Time to Echo (TE) which is the time between the emission of the RF pulse and the receipt of the echo signal. By varying these two time-based metrics, two types of MRI images can be obtained, T1 and T2 weighted images. T1-weighted images use short TE (14 msec) and TR (500 msec) times (Preston, 2006), which result in images which highlight fat tissue within the body
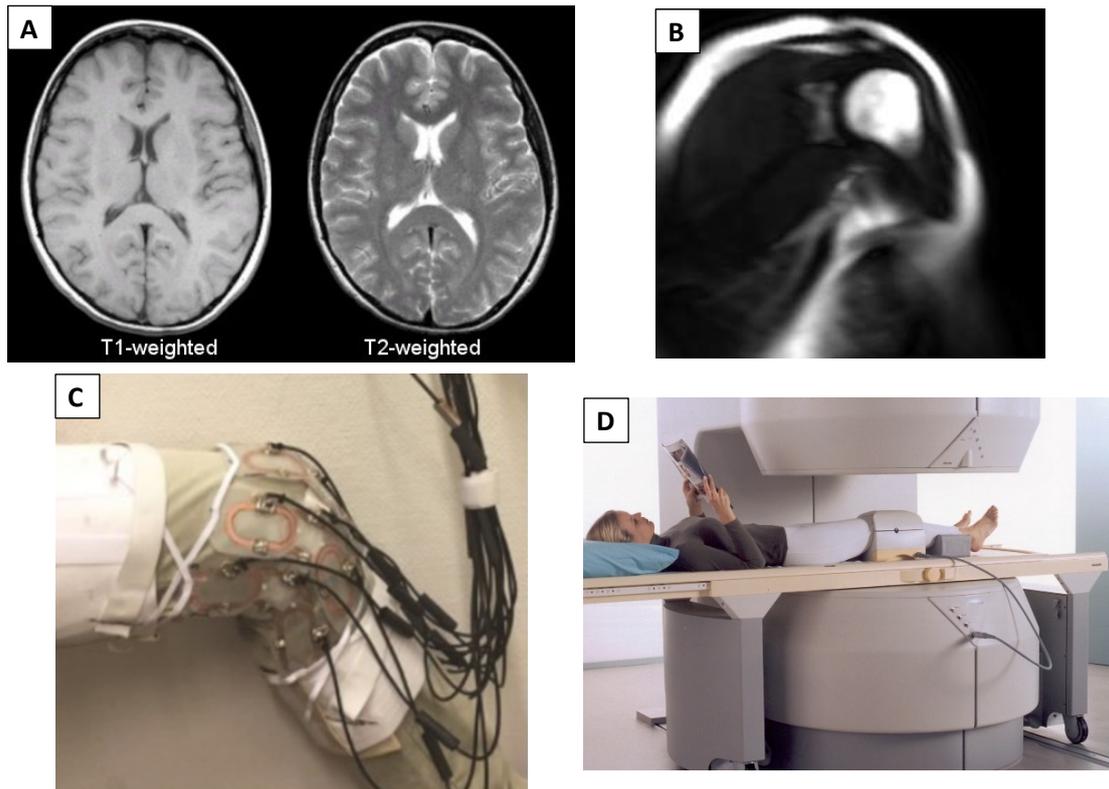
Figure 8: Dynamic MRI modalities

A: Comparison of T1 and T2 images (Preston, 2006)
B: The resulting coarse image obtained when scanning with real-time MRI using high acquisition speed (Pierrart *et al.*, 2014).
C: The knee specific RF coil with increased receiving elements, used to achieve accelerated data acquisition through parallel imaging (Mazzoli *et al.*, 2017);
D: A typical open-bore scanner, utilising two big flat magnets (Doral Medical Imaging, 2006).

(Figure 8A – left). T2-weighted images use long TE (90 msec) and TR (4000 msec) times (Preston, 2006), which result in images which highlight both fat and tissues with high water content within the body (Figure 8A – right). Nonetheless, both alternatives limit the visibility of bone tissue, rendering the resulting images inappropriate for the delineation of bones.

MRI is routinely used for the analysis of the knee pathologies, mostly for the evaluation of meniscal and Anterior Cruciate Ligament (ACL) injuries (Mink, Levy and Crues, 2014; Robertson *et al.*, 2014). Nearly all of the current clinical MRI approaches used for the evaluation of the lower extremities are acquired in a static and unloaded configuration. Conventional MRI is usually performed while the subject lies motionless in the scanner, producing static anatomical images. While these static images are sufficient for diagnostic purposes, they fail to depict problems that are only revealed during the complex orchestrated interaction of bone and soft tissue structures, when the joints and muscles move to perform daily functional activities. Until nowadays, purely

dynamic MRI is still hindered by clinical acceptance and technical challenges to implement it as a routine application due to lack of clinical validation studies. A number of papers (Patel *et al.*, 2004; D'Entremont *et al.*, 2014; Yao *et al.*, 2014) have used quasi-static approaches using MRI to analyse kinematics, where static images acquired at different joint positions are often played in a loop, suggesting the idea of joint motion. While this quasi-static method presents less technological challenges related to MRI acquisition, it is appealing for more sophisticated approaches. It has been shown that kinematic parameters, such as tibial abduction, internal rotation and anterior translations were different during dynamic tasks as compared to a series of static positions (D'Entremont *et al.*, 2013).

Purely dynamic MRI imaging is still in its infancy due to technological limitations. Dynamic imaging can be performed using two main approaches, real-time or in a segmented, or triggered, fashion, often referred to as Cine (kinematic) MRI. Real-time imaging does not require any additional sensors or other hardware, which are otherwise required for triggering the scanner to activate at particular instants in time, and it can be performed with a temporal resolution (time to capture one volumetric frame) as high as 20 msec (Uecker *et al.*, 2010). However, this high acquisition speed comes at the expense of limited coverage and limited spatial resolution, such that the resolution will be very coarse (Figure 8B), limiting the quality and thus the use of the collected data (Pierrart *et al.*, 2014). The issue of low image quality can be attempted to be surpassed by performing imaging registration of a 3D high-resolution volume, but this process is prone to further errors (Gilles *et al.*, 2005). On the other hand, Cine MRI uses multiple motion cycles, which must be performed in an identical fashion, to create a single motion cycle. This method offers higher bone tracking accuracy, with studies reporting an error of only 0.5 mm (Kaiser *et al.*, 2016). The major limitation for this method is that it heavily relies on the motion task being repeatable and performed precisely in the same way during each repetition. If this is not achieved, the resulting data suffers from blurring, streaking and ghosting, which hinders the subsequent data analysis. This limits the patient population to healthy subjects having no pain or difficulties in performing the motion task. New advanced image acceleration techniques could potentially lead to faster data acquisition that will allow for fewer repetitions for Cine MRI, or ideally allow for real-time 3D imaging with higher resolutions than the current systems (Mazzoli *et al.*, 2017). This accelerated data acquisition is achieved through parallel

imaging, where the RF coil receiver elements are increased to capture more data. However, implementing such RF coil arrays (Figure 8C) would be cumbersome for the patients while also limiting the ROM of the patient and considerably increasing costs to purchase or manufacture such additional equipment.

The potential of MRI lies in the fact that in comparison to other available imaging techniques (such as X-rays and CT scanners) there's no risk of exposing the patient to ionising radiation. On the other hand, due to factors such as the degree of proton movement and the strong magnetic fields on the tissues being scanned, when scanning patients with certain metallic implants, such as stainless steel and cobalt-chrome, distortions in the magnetic field occur, producing intense image artefacts which degrade the image quality of the surrounding tissues (Waldman and Campbell, 2011). Additionally, MRI utilises a very narrow bore (typically up to 60 cm) which limits movement to the bare minimum, while also potentially being claustrophobic for certain patients. Open-bore scanners utilising two big flat magnets instead of a fixed gantry are available in hospitals (Figure 8D) but these systems' maximum field strength typically only reaches 1 Tesla, which leads to limited image resolution and higher errors in bone tracking for the analysis of bone kinematics (Draper *et al.*, 2008). Finally, considering that conventional static MRI is known for being a very expensive and time-consuming investigation compared to other methods such as X-Ray and CT, then it is only reasonable to assume that dynamic MRI will be more expensive and time-consuming when it gets developed for clinical therapy.

2.3.1.3   4D COMPUTED TOMOGRAPHY (CT)

Since the discovery of CT in the 1970s, diagnostic decision making has been revolutionised (Esses *et al.*, 2004; Mettler *et al.*, 2008). CT is responsible for better surgeries, better diagnosis and treatment of cancer, better treatment of major trauma and post-injury, stroke and cardiac conditions (Randen *et al.*, 2008; Hricak *et al.*, 2011). CT is also responsible for decreasing the need for emergency surgery from 13% to 5% and has made exploratory surgical procedures significantly less prevalent. Furthermore, CT has also shown to have decreased the proportion of patients requiring inpatient admissions (Rosen *et al.*, 2000, 2003). Each year, technological advances in CT have made it a yet more appealing modality due to the ever-increasing spatial resolution and decreasing temporal resolution, being managed while considerably reducing the radiation doses (Power *et al.*, 2016).

Conventional static 3D CT scanning forms the basis for capturing dynamic motion using the revolutionary 4D CT systems. 3D CT is a technique whereby an X-ray source rotates around the anatomical region of interest while a detector, which always faces the X-ray source, measures the attenuation of the X-ray beams passing through the slice of the anatomical region. The detectors used in CT are scintillation crystals, composed of gadolinium oxysulfide that generates small flashes of light (scintillations) when the X-ray interacts with the crystals. Subsequently, a photodiode converts the light scintillations into an electronic signal which is further amplified before it is recorded. While the method of X-ray transmission and detection remains the same in the current generation of CT systems, the coverage of the anatomy of interest has gone through five generations of development to address issues of high radiation doses, slow scan times and low spatial resolutions.

The first generation of CT scanners defined the fundamental methodology for mapping the internal structure of the anatomical area being analysed, which is still the foundation of fifth-generation scanners used nowadays. The first-generation scanners were designed to scan the subjects in 2D axial slices. Using a single X-ray tube and detector, first, the subject is scanned by linearly translating transversely across the subject capturing the first view, and then rotating the setup by 1 degree axially and repeating the translational scan to capture the second view (Figure 9A). This translate-rotate motion is repeated until all 180 views are scanned and recorded, which generally requires around 5-6 minutes to complete one single slice of anatomy. In order to reconstruct the internal anatomy, the scanned slice is virtually broken down into a matrix of 3D voxels (rectangular boxes) of tissue (refer to Figure 9B). By translating and rotating the X-ray source around the region of interest, the detector receives the attenuated x-ray beam signal from multiple known angles. By a process called back-projection, which takes into account the sums of the different attenuation values from all the different angles, the attenuation values of individual voxels can be deduced (Figure 9C). By using this method of back-projection on all voxels of the matrix forming the slice of anatomy being scanned, the image of the slice of internal anatomy can be reconstructed. This method of CT scanning was the basis of first-generation CT scanners.

The attenuation values deduced using the back-projection method are expressed in Hounsfield Units (HU), after the inventor of CT, Godfrey Hounsfield (Ghonge, 2013).
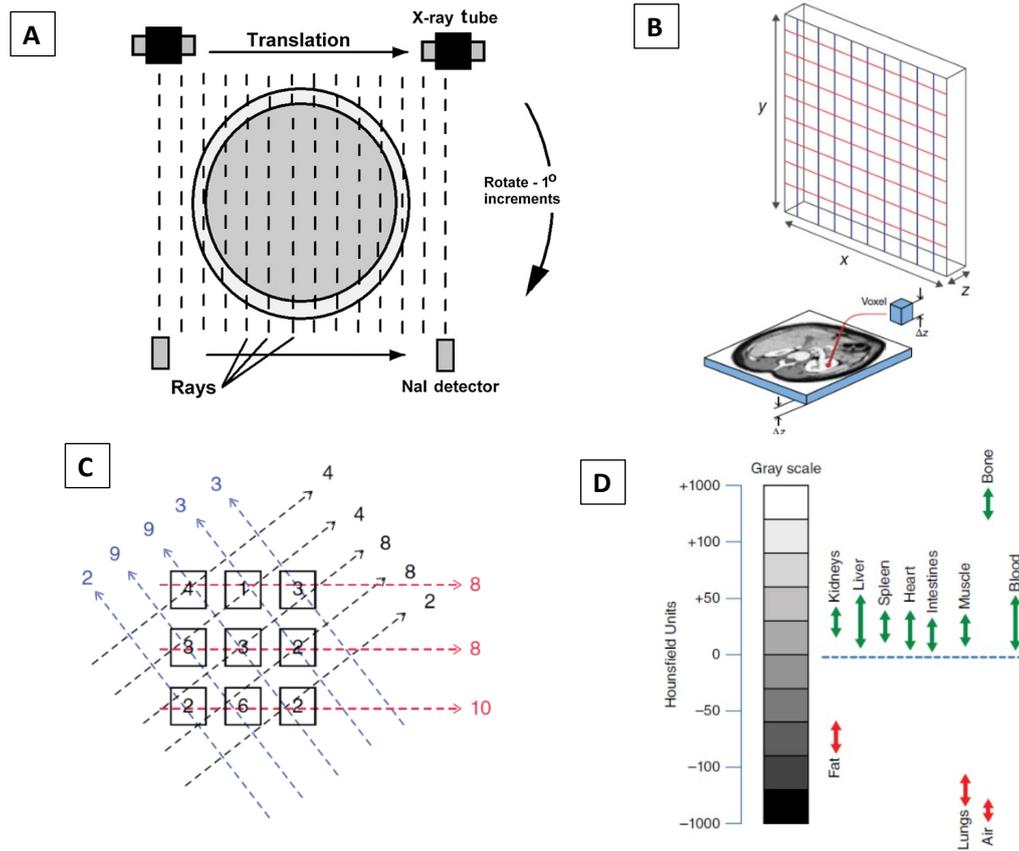
Figure 9: Computed Tomography basics (Goldman, 2007; Reilly and M., 2019)

A: First generation scanners took readings at several points during their initial translation motion of the tube and detector. This first pass was known as the first view. Subsequently, the tube and detector were rotated by one degree, and the translational motion was repeated, capturing a second view. This was repeated 180 times to scan the whole region.

B: The attenuation measurements collected following a complete CT scan rotation are reconstructed to form a 3D image of the patient which can be read in slices at any location and orientation (axial, sagittal and coronal). Each slice is made up of a 2D plane of voxels (VOlumetric piXELS) which would be coloured depending on the attenuation value collected during the scan.

C: The attenuation value of each voxel is calculated by a process called *back-projection,* which takes into consideration the *sum* and *angle* of all the X-rays passing through the voxel during a single scan.

D: The HU scale describes the attenuation of the X-ray by a tissue compared to the attenuation of water.

The values are depicted on the reconstructed images by a grey intensity scale which represents the density of the tissue within the voxel, where a voxel of an HU of 0 (zero) represents the attenuation by a voxel composed entirely of water. Similarly, for a voxel of air, in which there is almost no attenuation of the X-ray, the voxel HU would be -1000, which is represented by black. In anatomy, HU values usually range from -100 for adipose (fat) tissue to +20 to +50 for soft tissues, while bone, which is much denser has an HU close to +1000 (Figure 9D), represented by white. The way that anatomy is represented by HU brings to light the reason why CT scanners are preferred for imaging bones and denser tissues, such as cartilages, ligaments and tendons, as they can be easier to differentiate since they use a more specific range of the Hounsfield scale. Conversely,

soft tissues share a very small range of the scale, thus making it much more difficult to delineate soft tissues on a CT scan (Reilly and M., 2019).

With every generation of scanners, the scanning became faster, giving less radiation to the patients while increasing the spatial resolution of the acquired images. Second generation CT scanners introduced several innovations which are now standard in all CT systems. These included a table moving axially through the gantry, gantry angulation, laser indication to better position the patient to 'slice' at the ideal location and a Fourier-based reconstruction algorithm. Apart from these improvements, the number of rays and detectors were increased to three to reduce scan times. The rays were fanned out by one degree, such that in one translational scan, the scanner could collect data for three rotational steps (Figure 10A). This reduced translational scans three-fold, thus reducing scanning to around 2 minutes. Second-generation scanners kept increasing the number of rays and detectors, thus increasing the scan coverage and quality to the point that body scans could be performed within a breath-hold for most patients. Further speed improvements were limited by the mechanical complexity of the rotate-translate geometry, which brought about the next generation of scanners.

Third generation scanners overcame the limitations which existed with the rotate-translate systems by scrapping the translation motion and moving onto smoother and simpler pure rotational motion. The X-ray beam was widened into a fan beam encompassing the entire patient width while having an array of detectors to read the attenuation of the beam (Figure 10B). The X-ray tube and detector were rigidly linked together, such that they rotated together as one unit. The third-generation scanners had reduced the scan time to around 5 seconds. These were followed by fourth-generation CT scanners, whose design incorporated a large stationary ring of detectors, with the X-ray tube alone rotating around the patient (Figure 10C). This method allowed for better sampling of the collected data, since each individual detector was capable of collecting all the X-Rays emitted from the tube, rather than a single one. This generation allowed for higher quality images, with fewer image artefacts thanks to the increased sampling, while also reducing the scan times to one second. Drawbacks of the fourth generation CT scanners was X-Ray scatter, which was not an issue in the previous generations but had emerged in this generation due to its geometrical design which did not allow for the installation of scatter-absorbing septa used in previous generations. Furthermore, both the third and fourth generations suffered from long temporal
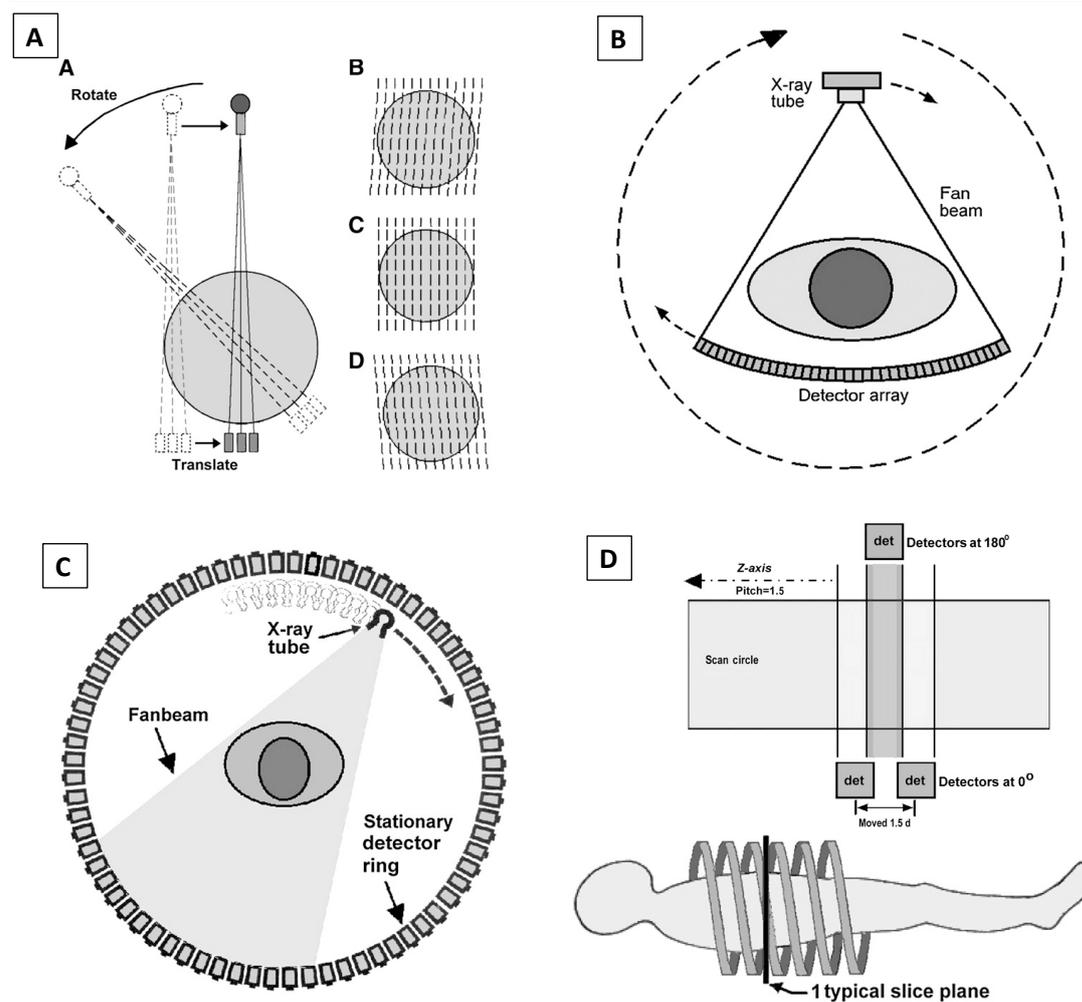
Figure 10: Development of CT scanner detectors (Goldman, 2007)

A: Second-generation data collection consisted of multiple beams with a corresponding number of detectors which acquired multiple views during a single translational scan. This reduced the scan time by a factor of 1/(number of detectors);

B: Third-generation design was overhauled to eliminate the translational motion which was creating several issues of vibrations due to the complexity of numerous moving parts. The wide detector was capable of capturing the entire width of the slice instantly, thus only requiring the tube-detector complex to undergo one single rotational motion in order to capture all the required views;

C: Fourth-generation scan geometry consisted of a fixed detector ring with a rotating tube internally. Later design moved the tube outside a smaller fixed ring, which required the ring to tilt out of the way of the X-ray as the tube swept by;

D: Helical CT scanning allows for continuous scanning by moving the patient table smoothly through the gantry, and data is collected by the rotating detectors. For reconstructing helical CT data, sample spacing and interpolation had to be introduced, whereby data from adjacent slices is used to interpolate areas which the scanner missed due to the inherent way of a helical path.

resolution due to long inter-scan delays. After each 360° rotation, the cables which connected the rotary components to the rest of the gantry required the rotation to stop and reverse direction in order to avoid excessive twisting of the cables. This resulted in a temporal resolution of 8-10 seconds, of which only 1-2 seconds were spent acquiring data. These long delays were eliminated by the introduction of slip rings, which allowed the rotating components to rotate continuously while allowing electrical power and data

to be transmitted via a drum with grooves along which electrical contact brushes slid. While slip rings allow for the complete elimination of inter-scan delays, there was still time being wasted in moving the table to the next slice position. This was overcome by the revolutionary helical scanning method, whereby constant rotation allowed for continuous data acquisition as the patient is smoothly moved through the gantry (Figure 10D). Helical scanning had a significant impact since it allowed for rapid scans of entire anatomical regions, such that it became the de facto standard of care for body CT.

While helical scanning was turning out to be a great method in terms of temporal resolution, the X-ray tubes were heating up a lot following helical scanning due to the lengthy, non-stop scanning. While developing X-ray tubes with higher heat capacity seemed the most logical way of solving this heating issue, there was another technology emerging in parallel to this. So far only Single-Slice detectors were used in CT (SSCT) systems, which consisted of single, long elements along the z-direction. Multi-Slice CT (MSCT) consisted of multiplying the number of detectors in the z-direction (Figure 11A) to reduce the number of rotations required to cover the desired anatomy, thus reducing heat generation at the tube level. It should be noted that MSCT is only applicable to third-generation scanners due to limitations of the design of the fourth-generation scanners.

At the early days of MSCT, the number of rows of elements was determined by the processing power, which was available at the time, since the scanner was required to process all the data coming from the detectors during one rotation in 0.5 seconds. For a 16-row MSCT, the processor was required to perform an equivalent of 26 million computations per second, which for the late 90s was beyond the technology of the time. Therefore, the first MSCT scanners limited simultaneous data acquisition to 4-slices, or 4 parallel data channels. By 2002 16-slice scanners were available, which broke through the submillimetre mark. 64-slice MSCT scanners were later introduced in 2005. 128 and 256-slice MSCT scanners started emerging in the late 2000s bringing along with them the advent of dynamic 3D, or 4D CT scanners.

Increasing the number of slices not only reduced the number of rotations the tube and detectors required to perform in the gantry, thus reducing heat generation, but it also decreased scanning times, thus reducing radiation doses. On the other hand, with the amount of research and development being invested on detector technology, the spatial resolution also increased drastically, reaching the limit of 0.5mm which presented
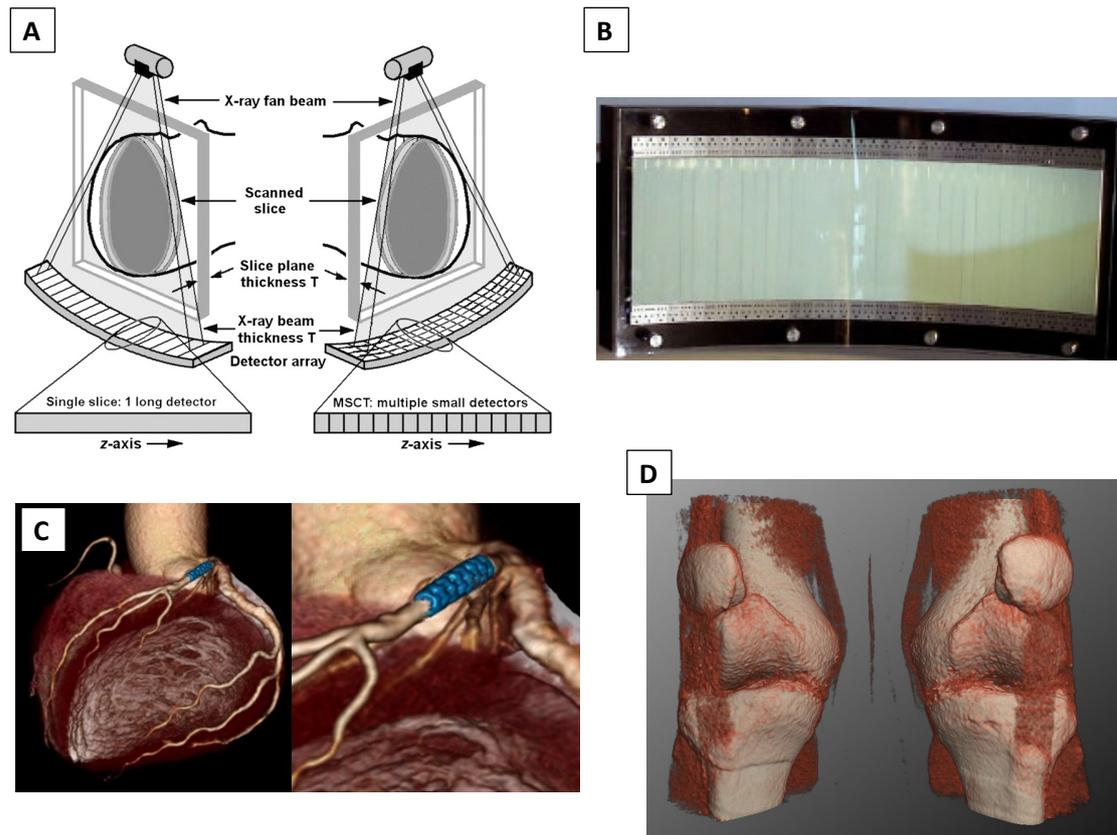
Figure 11: Multi-Slice and Dynamic CT scanners

A: Single-Slice CT detectors (SSCT - left) containing single, long detectors in the z-direction, while MSCT detectors(right) contain multiple rows of small detector elements in the z-direction (Goldman, 2007);

B: The detectors used in 4D CT are 16cm wide composed of a 320-slice detector capable of scanning the whole heart in one cycle (Toshiba Medical Systems, 2008);

C: A reconstruction of a 3D volumetric heart during the diastolic phase of the heartbeat cycle, clearly demonstrating a LAD (Left Anterior Descending artery) stent. This was acquired during one single rotation of a dynamic scanner (Toshiba Medical Systems, 2008);

D: A reconstruction of a knee during full extension using a dynamic CT scanner. In order to study the joint movement patterns, dynamic scanners can be used. These allow for the diagnosis of certain pathologies, such as the patellar dislocation occurring in this patient when reaching full extension (Nguyen *et al.*, 2016).

another limitation whereby detectors smaller than 0.5mm were producing lower quality images thus presenting diminishing returns. Once the heating issue was surpassed, cardiac, and to a certain extent, pulmonary, MSCT was driving the state-of-the-art technology. Cardiac CT so far had been a difficult hurdle because of its demanding performance requirement from the CT system. To scan the heart in a motionless state, there is a 175-millisecond time-window (for a heart beating at 60 beats per minute) during which the heart lays motionless (occurs at approximately 65% - 75% of the R-R interval of the heartbeat cycle). Due to these requirements, CT developers started pushing for yet wider detectors and increased gantry speeds, to be able to scan the whole heart in one rotation. 4D CT scanners were developed as a result of this drive due to

cardiac CT. These scanners have 320-slice detectors with 896 detectors per row, giving a spatial resolution of 0.5 mm x 0.5 mm and coverage of 160mm (Figure 11B and Figure 11D). Due to the wide coverage in the Z-direction, the scanners are designed to scan with and without helical scanning, depending on the radiologist requirements to scan anatomy longer than 160mm. These features allowed for capturing whole volumes of anatomy with very high resolutions and low cycle times (Figure 11C and Figure 11D). When not using helical scanning, these scanners are capable of recording dynamically. In dynamic scanning mode, the CT scanner is able to record the entire heart (or organs falling within that field-of-view) for complete functional diagnosis, either continuously during a specific pre-defined interval (minimum of 0.275 seconds per scan, 3.64Hz) or intermittently in certain time intervals (Endo *et al.*, 2003). Intermittent scanning can be gated with electrocardiograms to capture specific phases of the cardiac cycle. Compared to MSCT scanners, dynamic scanners reduce radiation exposure by 80%, only requiring a dose of 0.4mSv dose per scan (Toshiba Medical Systems, 2008). This is due to "Low-dose" scanning modes in which the tubes' currents and voltages are adapted dynamically to achieve the best images using the smallest possible radiation doses. Furthermore, by eliminating helical scanning altogether, this has intrinsically eliminated the requirement of over-sampling since interpolation of data is not required, thus dramatically reducing the radiation dose (Lee and Chhem, 2010; McCollough *et al.*, 2012).

Artefacts

Motion and metal artefacts are the most common and/or problematic artefacts encountered during conventional (static) CT-based kinematic analysis. Motion artefacts are caused by the rapid movement of the imaged anatomy during scanning, resulting in blurring and "double images" since the scanner would have ultimately captured the anatomy in more than one single position during a single scan. In comparison to 3D scanners, dynamic scanners significantly reduce the risk of motion artefacts due to the high scanning speeds, which are capable of essentially taking static shots of a moving target. While these artefacts are inherent to dynamic CT due to the imposed motion of the patient being recorded, if the patient is trained to control the movement being performed, by moving at a constant "slow" speed, these artefacts can be controlled. To be reliable and reproducible, stabilisation of adjacent body parts is essential to allow a single movement in one plane of the space to be performed (Moore *et al.*, 2015). For

optimal image quality, the motion has to be smooth and controlled. Excessive motions artefacts appear as ghosting and linear streaks, while they are frequently located over 5cm of the fulcrum of motion (where linear and angular speeds are the highest). Movement control, along with the increased scanner temporal velocity is sufficient to keep motion artefacts to a minimum (Tay *et al.*, 2007).

On the other hand, metal artefacts occur when the scanner has metallic objects in its field-of-view. Metal leads to starburst-shaped bright and dark streaking in the CT images which obscure the underlying image content, thus rendering accurate bone segmentation challenging. Metallic materials highly attenuate the emitted X-rays, causing artefacts due to the phenomenon of "photon starvation" and "beam hardening" along the path of the X-ray which alters the HU resulting values (Kidoh *et al.*, 2014). Several studies have been performed to reduce the metal artefact from CT images. These mainly involve manipulating X-Ray energies, such as the dual-energy acquisition techniques (Bamberg *et al.*, 2011), high energy X-rays (De Marzi *et al.*, 2013; Paudel *et al.*, 2014), and image processing methods, namely, iterative reconstruction techniques (De Man *et al.*, 2000; Meyer *et al.*, 2012), or interpolation of metallic objects (Kalender, Hebel and Ebersberger, 1987; Zhao *et al.*, 2002; Mehranian *et al.*, 2013).

In this text, the focus will be given to Single Energy Metal Artefact Reduction (SEMAR), which is the Metal Artefact Reduction (MAR) technique that comes with the 4D CT Toshiba Aquilion ONE™ scanner used for the practical aspect of this thesis. SEMAR works on the raw data collected from the scanner, thus allowing it to be applied to the data after acquisition, facilitating its implementation into the clinical workflow (Miki *et al.*, 2016). SEMAR is a combination of iterative reconstruction techniques and interpolation techniques since it uses an algorithm that applies linear interpolation to the raw data between subsequent forward and back projections. This has been clearly explained by Gondim Teixeira *et al.*, 2014, as follows (refer to Figure 12 for a visualisation of the process explained below):

Step 1. Segmentation of the metallic parts is performed using a simple fixed threshold or automatic threshold approach on the iteratively reconstructed original image (first-pass image).

Step 2. The resulting image is forward reprojected to find the metal trace in the sinogram. The metal trace sinogram is subtracted from the full sinogram.

Step 3. Linear interpolation is performed on the "metal-removed" sinogram by identifying the neighbouring measurements.

Step 4. The interpolated sinogram is reconstructed to create the second-pass image.

Step 5. Segmentation of the second-pass image is performed on the interpolation-corrected image in order to classify the remaining tissues into various classes.

Step 6. Forward reprojection of the classified image is again performed, and the resulting sinogram is linearly integrated to the interpolated raw data.

Step 7. Blending of the original sinogram with the forward reprojection (sinogram) of the tissue-classified image on the metal trace using a linear baseline shift approach.

Step 8. Reconstruction of the resulting sinogram (third-pass image);

Step 9. Blending of the reconstructed image with the metal image to obtain the final image.
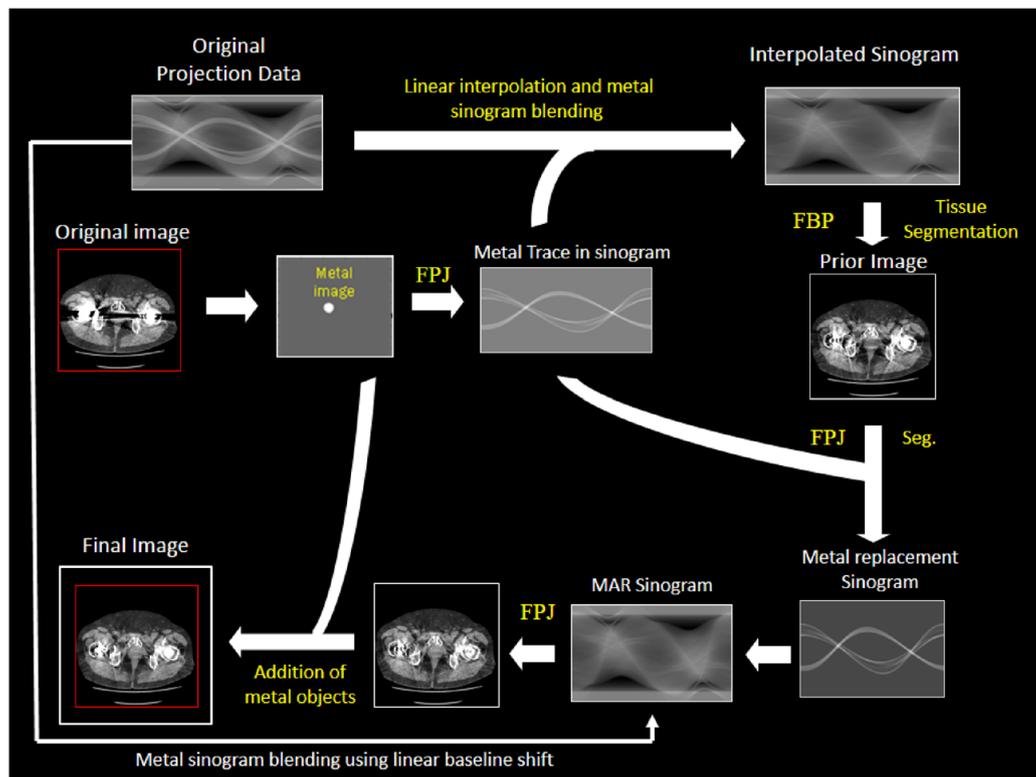
Figure 12: A visual representation of the SEMAR algorithm (Gondim Teixeira *et al.*, 2014).

A workflow of the SEMAR technique, demonstrating the multiple steps of the MAR algorithm used. FPJ = Forward projection; FBP = filtered back projection; Seg = segmentation of metallic artefacts in the image domain.

While the SEMAR algorithm is very computationally intensive, its accuracy and reduction in patient dose (over dual-energy acquisition and high energy X-ray techniques) is favoured, thus being the preferred choice. The improvement of image

quality using projection-based algorithms for MAR in patients with metallic implants is well supported in the literature (Kalender, Hebel and Ebersberger, 1987; Brook *et al.*, 2012; Morsbach *et al.*, 2013).

2.3.1.4 IMAGING MODALITY FOR THE KNEE

As mentioned earlier, given the choice of medical imaging techniques which currently exist and the emerging 4D imaging techniques, choosing the best technique to utilise for a given study, depends on the nature of the specific research question, the acceptable level of invasiveness, the required accuracy, and the available resources. Provided that this study is aiming to investigate the kinematic differences which exist between healthy and replaced knees during a dynamic flexion-extension exercise, the primary requirement is to be able to record dynamically. Another imperative requirement is the possibility of recording metallic implants with the best artefact reduction possible. Also, since we are concerned about the movement of the bones, the imaging technology which is needed will preferably have a wide dynamic range for calcified (or osseous) tissue since this will result in more detailed images of bones and calcified tissue, rather than soft-tissue. Finally, given the resources available for this study, a relatively cheap imaging technology was required in order to be able to record as many participants as feasibly possible.

Given the aforementioned requirements, Dynamic or 4D CT proves to be the preferred choice for imaging the dynamic movement of the healthy and replaced knees. Apart from ticking the above requirements, this modality has the significant advantage that it can be performed within minutes, is relatively cheap and is widely available in hospitals and clinical settings worldwide, allowing physicians to rapidly confirm or exclude a diagnosis with improved convictions.

2.3.2 SEGMENTATION TECHNIQUES

In this section, the reader will be introduced to the subsequent step following data acquisition from the preferred imaging technique. The raw data collected from the scanner is outputted as a 3D matrix composed of voxels, whose values correspond to the HU of the scanned tissue. Segmentation is the process of partitioning a volumetric image into different segments, which, in the case of medical images, would typically correspond to different tissue classes such as ligaments, bone and muscles. The different tissues are visualised on these medical images as numerous voxels in different

shades of grey intensity values (represented by the aforementioned HUs). Segmentation can be performed either manually or in an automated fashion. Manual delineation of tissues in 3D images can be very tedious and time-consuming and usually is not feasible in clinical practice. Automated analysis of the collected data is the only way to overcome manual segmentation. While many automated techniques exist, it goes beyond the scope of this thesis to discuss all of them (Haralick and Shapiro, 1985; Pal and Pal, 1993; Zhang, 1996; Sun, Teo and Zhang, 2006; Gonzalez, Woods and Masters, 2009; Aly, Bin Deris and Zaki, 2011; Deserno, 2011; Narkhede, 2013; H. Shaikh, Panbude and Joshi, 2014). One should bear in mind that while automated algorithms do a good job at outlining the tissue of interest, manual intervention is often still required to correct errors. In this section, the segmentation techniques utilised in this thesis will be introduced to the reader, with the aim of explaining their underlying function while outlining their limitations and advantages.

2.3.2.1 THRESHOLDING

Segmentation is defined as the partitioning of an image into non-overlapping, constituent regions which are homogeneous with respect to some characteristic such as intensity or texture (Gonzalez, Woods and Masters, 2009). If the domain of the image is given by I, then the segmentation problem is to determine the sets $S_k \sum I$ whose summation is the entire image I (refer to Figure 13). Thus, the sets that make up a segmentation must satisfy:
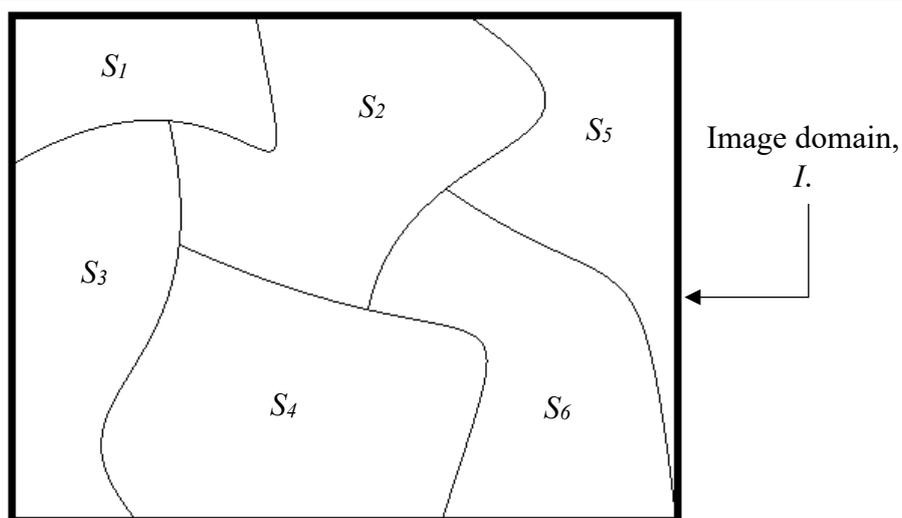
Figure 13: A pictorial explanation of the notion of segmentation of medical images (author's rendition).

All medical images, I, are made up of a number of sets, S_k, which make up the whole image, yet they do not intersect each other and are all connected (touching).

$$I = \sum_{k-1}^{K} S_k \qquad \text{①}$$

Ideally, a segmentation method detects which sets correspond to distinct anatomical structures in the image. Determining the sets, S_k, is called pixel classification and the sets themselves are called classes. Pixel classification, rather than conventional segmentation, is often desirable in medical images, particularly when disconnected regions belonging to the same tissue class exist and need to be identified, such as in our case of bones in the knee joint. For the case of medical images, the value of K can be assumed to be known, since prior knowledge of the local anatomy allows us to categorise which tissues exist in the area being investigated, such as the knee joint, where we know the exact number of different tissues we expect to find.

Thresholding approaches segment scalar volumes by creating binary partitioning of the voxel intensities. A thresholding procedure generally identifies the histogram of the scalar volume and determines the intensity values for the region of interest, called thresholds, which represent the separate classes being investigated (Figure 14). The segmentation is then performed by grouping all voxels falling within a specific threshold into one class, and all the other pixels into another class.

For any pixel $j \in I$, the thresholding function considers the pixel to be a part of the object if the intensity of the pixel falls within its threshold limits. This can be mathematically represented as follows:

$$f(j) = \begin{cases} 1, & if \ T_{Min} \leq I(j) \leq T_{Max} \\ 0, & otherwise \end{cases} \qquad \text{②}$$

Thresholding is a straightforward yet often effective method for segmenting images whose structures have contrasting intensities. Although thresholding is generally performed manually, automated methods do exist (Sankur, 2004). In complex images, thresholding is often used as an initial step in a sequence of image processing operations. Its main limitations are that it only generates two different classes (unless multi-thresholding techniques are used), thus not taking into account the spatial characteristics of the image making it sensitive to artefacts such as noise and intensity inhomogeneity. These artefacts corrupt the histogram of the image, making it harder to
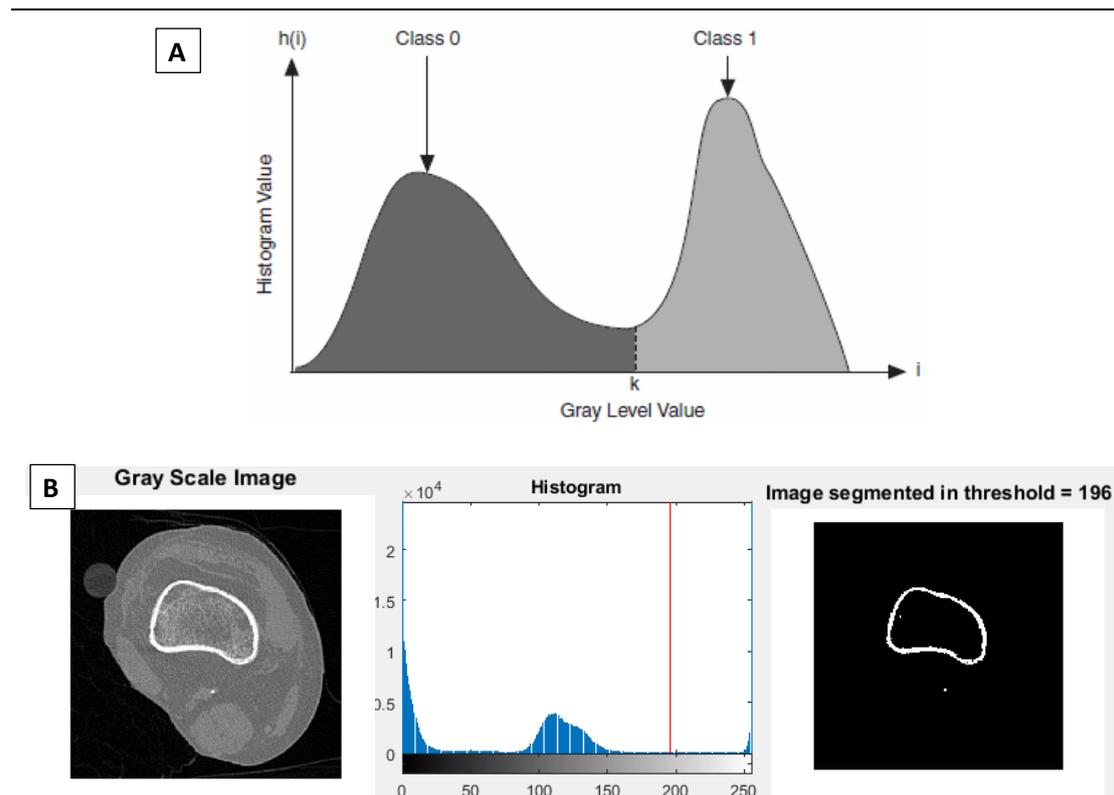
Figure 14: Thresholding using grayscale intensity histogram (author's images).

A: The grey level values are used to separate the different classes in the image.
B: This image shows how a raw axial slice of the thigh, can be observed using a grayscale intensity histogram. The threshold values are chosen based on the peaks which are visible on the histogram. When the threshold is determined and applied to the raw image the resulting binary image is produced showing the segmented bone.

locate the threshold values. Thresholding on its own is not suggested for segmenting the knee due to the high similarity in the intensities (densities) of bone, cartilage and ligaments. These will not create distinguished peaks and troughs on the intensity histogram, making it hard to delineate such structures appropriately (Deserno, 2011).

A notable limitation of manual thresholding is soft segmentation. Soft segmentations occur when two different classes overlap on an image. With the ever-increasing spatial resolution of medical imaging, this is frequently encountered because of the partial volume effects, where multiple classes (or tissues) contribute to a single voxel, resulting in a blurring of the intensities across the boundaries of these tissues. With reference to Figure 15, it can be noted that in a realistic scenario, it is difficult to determine the boundaries of the two objects precisely. Using conventional thresholding methods would force the pixel to be either inside or outside of one of the objects. On the other hand, alternate methods exist which retain more information from the original image since they allow for uncertainties in object boundaries.
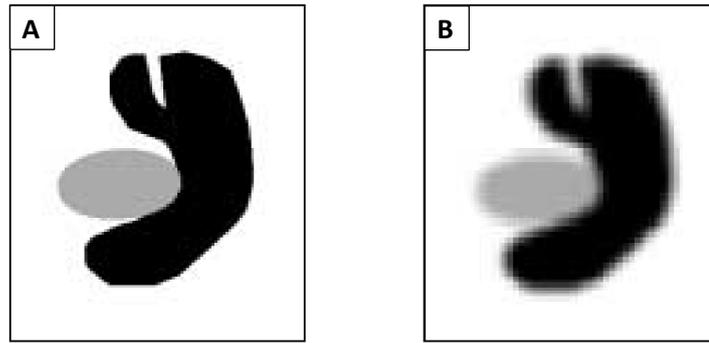
Figure 15: An illustration of the partial volume effect (Dzung, Chenyang and Prince, 1998).

A: An image in the ideal world.
B: A realistic scanned image which is affected by the partial volume effect.

This is performed in voxel classification techniques by creating what is known as a set characteristic function. This is simply a function which indicates whether a voxel is inside or outside of its corresponding set. For a location $j \in I$, the characteristic function $\chi_k(j)$ of the set S_k is defined as:

$$\chi_k(j) = \begin{cases} 1, & if\ j \in S_k \\ 0, & otherwise \end{cases} \qquad (3)$$

Characteristic functions can be generalised by membership functions (Deserno, 2011), whose only difference is that they need not be binary-valued. The value of a membership function $m_k(j)$ can be interpreted as to how class k contributes to the location j. Therefore, when membership values are unity for some value of j and k, then the class k is the only contributing class at the location j. Conversely, when membership values are between zero and unity for two or more classes, then those classes are overlapping.

Membership functions are implemented and derived using fuzzy clustering and classifier algorithms (Pham and Prince, 1999; Udupa and Saha, 2003). Implementing these algorithms allows for clustering (or classifying) all the partial volume fractions which then allows the soft segmentations to be easily converted to hard segmentations by assigning a voxel to the class with the highest membership value.

2.3.2.2   FUZZY C-MEANS (FCM) IMAGE SEGMENTATION

The Fuzzy C-Means algorithm (FCM) is one of the best known and most widely used fuzzy clustering algorithms. FCM is an unsupervised (automated) classification segmentation method which is sub-categorised as a clustering method. Clustering is a process of assigning voxels with similar HUs to the same class and dissimilar voxels to different classes (Han, Kamber and Pei, 2012). Members within a cluster (or class) exhibit similar characteristics than the members of other clusters. The clustering process is usually based on a proximity measure and in the case of medical images on the HU of the voxel and its neighbouring voxel HUs. Generally, there are two main clustering approaches: hard clustering (crisp clustering) and soft clustering (fuzzy clustering). Fuzzy clustering provides a useful method to cluster voxels whose boundaries between clusters cannot be clearly defined since some voxels may belong to more than one cluster (Hung and Yang, 2001).

The degree of belongingness plays a vital role in Fuzzy Clustering and provides the required flexibility to determine the correct cluster during soft segmentation (Sandhya and Kumar, 2017). The algorithm initialises by either automatically identifying the number of classes that exist (usually using the histogram) or else the user defines the number of classes that exist, and the algorithm subsequently clusters the voxels into the predefined number of classes. Clustering is mainly used when classes are known in advance (Kauffmann *et al.*, 2003), such as in the case of knee images, since the number of different classes (tissues) which exist are known. A similarity criterion is defined amongst the voxels, and then they are clustered according to their similarity co-efficient. This method of grouping is based on the principle of maximising the inter- and intra-class similarity. In order to calculate the degree-of-similarity, the algorithm utilises membership functions to give a value of the varying levels of "greyness" that each voxel has, based on the knowledge of its surrounding voxels (Hung and Yang, 2001). The algorithm identifies the similarity that each individual voxel has to all clusters with membership values between 0 and 1. When all voxels are mapped, then the soft segmentation can be converted to a hard segmentation by assigning each voxel to the cluster with the highest membership value.

Mathematically, the algorithm (for the application of medical images) aims to minimise the following objective function:

$$J_m = \sum_{k=1}^{N} \sum_{i=1}^{c} u_{ik}^m (x_k - \mu_i)^2 \qquad \qquad \text{(4)}$$

where: u_{ik} is the membership value of voxel x_k with respect to cluster c_i;
m is the fuzzy weight exponent (must be greater than unity);
μ_i is the centre of cluster i;

The variable u_{ik}^m is defined as follows:

$$u_{ik}^m = \frac{1}{\sum_{j=1}^{c} \left(\frac{|x_k - c_i|}{|x_k - c_j|} \right)^{\frac{2}{m-1}}} \qquad \qquad \text{(5)}$$

Where: $1 \leq k \leq N$;
$1 \leq i \leq c$;

It can be noted that u_{ik}, is inversely proportional to the distance from the voxel x_k to the cluster centre. Also, the parameter m, also referred to as the fuzzy weight exponent, defines the level of cluster fuzziness (i.e. the weight of each voxel). A value of m close to unity gives a cluster solution which is increasingly similar to the solution of hard clustering, while a value of m close to infinity leads to complete fuzziness between groups. Finally, the centroid of a cluster is defined as the mean of all the points which belong to the said cluster, weighted by their membership value (u_{ik}):

$$C_j = \frac{\sum_{k=1}^{N} u_{ik}^m x_k}{\sum_{k=1}^{N} u_{ik}^m} \qquad \qquad \text{(6)}$$

Where: C_j is the centroid of cluster j;

Therefore, in order to compute FCM, the number of clusters and a fuzzy weight exponent have to be predetermined. Once these are inputted, the algorithm initialises by using the histogram of image intensities to determine the initialisation coefficients (i.e. determining the first cluster centroids based on histogram peaks). Then the algorithm will iterate until either the maximum (predetermined) number of iterations are reached, or else when the algorithm converges (i.e. J_m does not change beyond a predefined difference between one iteration and the next). When the algorithm converges, the membership values of each voxel are used to assign each voxel to an individual label (cluster), which identifies a different tissue (Pal and Pal, 1993; Udupa and Saha, 2003).

2.3.3 SYNOPSIS

In this section, the first two steps in the workflow of extracting the kinematics of the captured articulation of the knee were reviewed (refer to sections 1.2, 2.1 and 4.2 for an overview of the workflow). Initially, the current medical imaging modalities were reviewed, and 4D CT was determined as an ideal imaging modality for the dynamic analysis of healthy and replaced knees. Subsequently, the preferred segmentation methods, namely manual thresholding and Fuzzy C-Means, were defined.

The subsequent step in the workflow is to isolate and virtually model, the individual, delineated bones and embed a six DOF anatomical Coordinate System (CS) into each individual bone (in all recorded frames). In order to accurately implement a coordinate system into the extracted models, a clear understanding of the work done by previous researchers and clinicians on the matter is necessary. In the subsequent sections, the relevant theory and literature are reviewed in order to allow the reader to appreciate the analysis of the kinematics of the native knee. This is aimed at giving the reader a clear picture of the entire workflow of the study of the kinematics of the knee, in preparation for the analysis of the raw data which was collected and analysed for this study.

2.4 THEORY OF NATIVE KNEE KINEMATICS

In this section, the reader will be introduced to the way the knee articulates as a result of the coaction of both bone morphology and the passive and active restraints of the soft-tissue sleeve. First, an insight into the theory of the relative tibiofemoral (TF) movement from hyper-extension through to hyper-flexion will be explained. This will give the reader a clear understanding of how the functional anatomy of the native knee functions in unison to achieve the complex articulation which occurs throughout the ROM of the knee. This section will also introduce the reader to kinematic outcome measures used in the practical aspect of this thesis, namely the Tibial Axial Plots, Contact Point plots and the Axial Centre-of-Rotation of the knee.

One of the major challenges in TKA is the successful restoration of the native knee biomechanics in the replaced knee. Biomechanics remains a major challenge due to the complex TF kinematics of the native knee, which can be fully described by a six DOF movement along a set of perpendicular axes (Figure 16). While the six DOF motion of the knee will be discussed in detail in section 2.6.2, they are introduced below in Table 1 and Table 2 below.

Table 1: The three rotational degrees-of-freedom of the knee.

Anatomical rotation	Anatomical plane	Range of Motion (Sheldon, 1994)
Flexion – Extension	Sagittal	From -5˚ up to 165˚
Internal – External	Transverse (Axial)	Up to 25˚ to 30˚ during flexion
Varus – valgus (Adduction – Abduction)	Coronal	6˚ to 8˚ in extension.

Table 2: The three linear degrees-of-freedom of the knee.

Anatomical translation	Range of Motion (Sheldon, 1994)
Mediolateral (ML)	1 to 2mm
Compression – Distraction (CD)	2 to 5mm (compression)
Anteroposterior (AP)	5 to 10 mm

The asymmetrical morphology of the medial and lateral compartments of the knee, the varying passive ligamentous restraints of the knee and the action of the muscles contribute to the compound movements of the knee, such as the screw-home mechanism in terminal extension, and the apparent and true femoral roll-back during flexion. While articulation is allowed in all 6 DOF, the three major DOF are flexion-extension and internal-external rotation, along with the anteroposterior translation. For this reason, knee kinematics are characterised by the coupled internal tibial rotation and anteroposterior roll-sliding translation with progressing flexion (Bull and Amis, 1998). On the other hand, the remaining three DOF, namely varus-valgus rotations and mediolateral and proximodistal translations are minimal, relative to the three major DOF, and vary depending on subjective morphology.
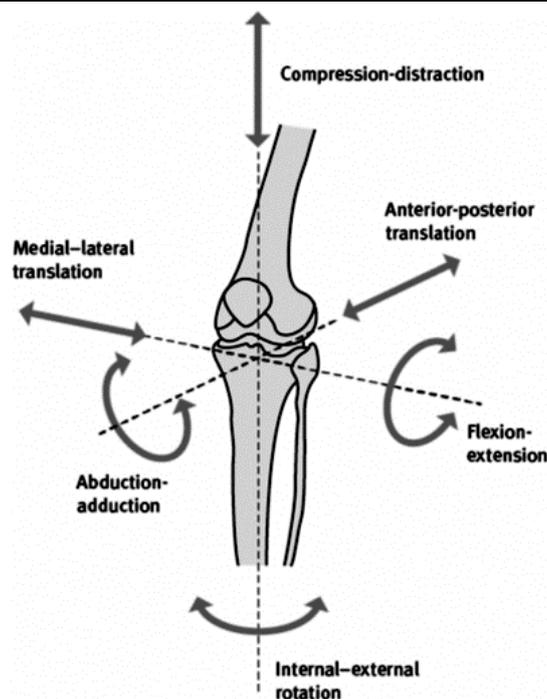
Figure 16: The six DOF of the knee (Shenoy, Pastides and Nathwani, 2013).

The articulation of the knee will be outlined by explaining the way the knee responds to the articular geometry of the medial and lateral compartments from hyper-extension to hyper-flexion (the full ROM of the knee). In November 2000, in the British Journal of Bone and Joint Surgery, the international research team of Freeman, a pioneer in the analysis of knee kinematics and the development of TKA, published a number of articles (Hill *et al.*, 2000; Iwaki, Pinskerova and Freeman, 2000; Karrholm, Brandsson and Freeman, 2000; Nakagawa *et al.*, 2000) describing the kinematic motion of the loaded and unloaded healthy knee by using MRI. The same research team issued three further articles in 2004, 2005 and 2009, which supported their theory of knee kinematics (Pinskerova *et al.*, 2004, 2009; Freeman and Pinskerova, 2005).

As a result of this research, knee kinematic theory has seen a fundamental revision of the concept of the axes of motion of the knee. These articles will be reviewed here in order to give the reader a thorough understanding of the knee's articulation in preparation for the review of literature of kinematics thereafter (specifically in section 2.6). It should be noted that the presented dimensions in the following text vary depending on the size of the knee, but the ratios of the measurements remain approximately constant regardless of the size of the knee. Furthermore, the angles (°) and lengths (mm) are given as averages of the respective study populations.
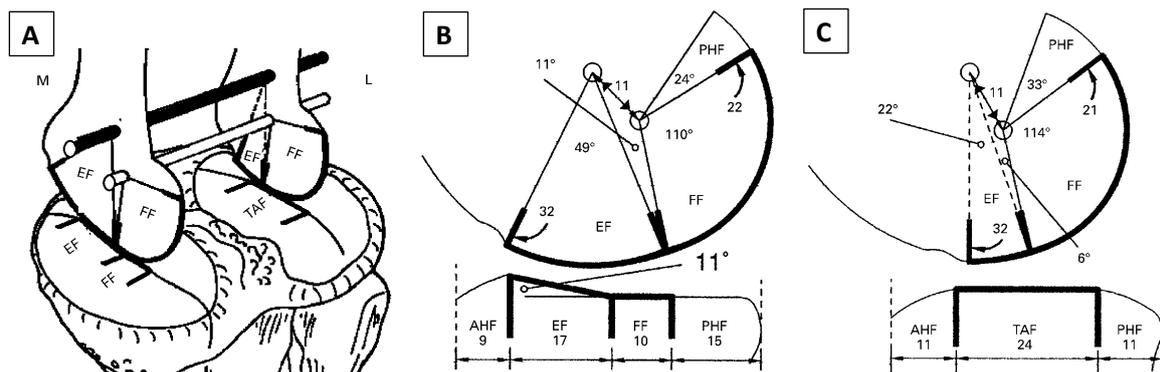
Figure 17: Geometry of the condyles of the knee (Iwaki, Pinskerova and Freeman, 2000).

An analytical diagram of the relations between the circular arcs of the medial and lateral femoral condyles and the corresponding tibial condyles.

A: An orthographic illustration of the geometry of the condyles of the knee. The two axes connecting the femoral condyles mediolaterally represent the centre of the extension (black) and flexion (white) facet arcs respectively. Refer to text for further information.
B: A sagittal cross-section of the medial compartment showing the dimensions of the identified facets.
C: Same as Figure 17B but this time representing the lateral compartment of the knee.

The femoral condyles articulate solely with their corresponding tibial condyles by way of rotating and sliding. The femoral condyles are composed, in the sagittal section, of the arcs of two circles (Figure 17):

- An anterior circle also referred to as the extension facet (EF), and

- The posterior circle also referred to as the flexion facet (FF)

Due to the asymmetry of the medial and lateral compartments, the medial and lateral articulations will be introduced separately, and then this will be followed by an overview of how both compartments move in unison. The ROM of the knee will be sub-divided into four phases, as follows:

1. Extension Phase: -5˚ (termed hyper-extension) to 10˚

2. Transition Phase: 10˚ to 30˚

3. Flexion Phase: 30˚ to 120˚

4. Hyper-Flexion: 120˚ to 160˚ (termed full-flexion).

2.4.1 THE MEDIAL COMPARTMENT

2.4.1.1 EXTENSION PHASE

The medial femoral condyle's EF forms a circular arc of approximately 27mm, while the EF of the medial tibial plateau is on average 17mm in length and slopes upwards by an average 11˚ relative to the posterior horizontal surface (Iwaki, Pinskerova and Freeman, 2000). Furthermore, the anterior extremity of the medial tibial condyle contains the Anterior Horn Facet (AHF), where the tibial surface slopes downwards to make space for the anterior horn of the medial meniscus in full extension. During extension, the anterior horn of the meniscus sits in the corresponding recess in the femur (Figure 17B), which provides additional support and stability to the medial compartment while in this position.

From hyper-extension (-5˚) to 10˚ of flexion, the medial femoral condyle rotates around the Extension Facet Centre (EFC – the centre of the EF arc – refer to Figure 18A). During this ROM the femoral EF is in constant contact with the tibial EF. The EFC does not move relative to the tibia, resulting in pure TF sliding motion (Weber and Weber, 1837; Kurosawa et al., 1985; Iwaki, Pinskerova and Freeman, 2000).
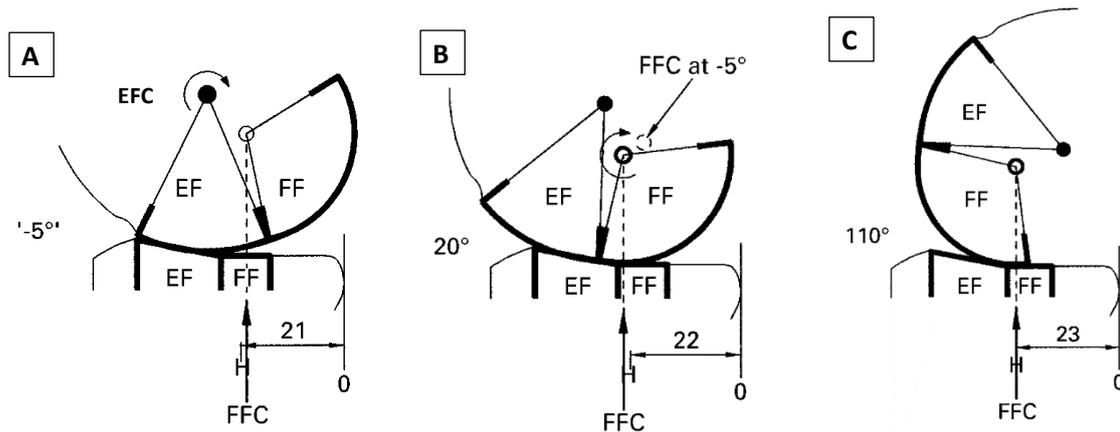
Figure 18: The geometry of the medial compartment at three instances during the ROM of the knee (Iwaki, Pinskerova and Freeman, 2000)

| **A**: At full extension (-5˚) | **B**: At early-flexion (20˚) | **C**: At late-flexion (110˚) |

2.4.1.2 TRANSITION PHASE

Between 10˚ and 30˚ of flexion the medial TF contact shifts from the EF to the FF. The femoral arcs of the EF and FF do not form a tangent at their transition point, producing a 'kink angle' of 11˚ between the adjacent radii. At the tibial surface, contact with the femur transitions from the posterior part of the EF to the anterior part of the horizontal surface of the FF, which is 10mm in length, at around 20˚± 10˚ of flexion (Figure 18B). Although the medial femoral condyle does not exhibit AP motion during this ROM, the condyle does 'rock' when it transitions from the EFC to the FFC. This phenomenon was first noted by Weber and Weber (Weber and Weber, 1837) and was named 'rocking' by Steindler (Steindler, 1955).

2.4.1.3 FLEXION PHASE

From 30˚ to approximately 120˚ of flexion the femoral condyle FF, forming a circular arc of 110˚, contacts the tibial condyle at the FF, with the FFC constantly laying above the contact area (Figure 18C). The FFC does not move vertically with respect to the tibia, showing that rotation is occurring purely around the FFC. The FFC does move forward slightly, by around 2mm between 110˚ and 120˚, but does not move during the rest of the ROM. This results in a pure TF sliding motion on the medial compartment.

2.4.1.4 HYPER-FLEXION PHASE

At the femoral condyle, posterior to the FF lies the Posterior Horn Facet (PHF), which exhibits an arc of 24˚. The femoral PHF interacts exclusively with the tibial PHF which is 15mm in length and on it lies the posterior horn of the medial meniscus. During the

ROM of hyper-flexion, the medial femoral condyle moves posteriorly by 8mm with respect to the tibia. As the femur moves posteriorly, it exhibits pure rotation as it rolls up on to the posterior horn of the medial meniscus. At 140˚ the femur moves up on to the posterior horn of the medial meniscus, which is correlated to the resistance to flexion experienced from this point onwards through to 160˚ when it completely limits flexion. Furthermore, the fixed meniscus on the medial slide not only limits flexion but also prevents the medial femoral condyle from moving posteriorly beyond 10mm from the posterior tibial cortex. For this reason, the importance of the menisci in the knee is further amplified.

2.4.2 THE LATERAL COMPARTMENT

2.4.2.1 EXTENSION PHASE

Similar to the medial condyle, the lateral femoral condyle is circular posteriorly but exhibits a smaller radius than its contralateral counterpart. The EF of the lateral femoral condyle is much smaller, with an average angle of 24˚. It should be noted that, based on literature, there are cases where the EF is absent such that the lateral condyle is of a single radius curvature (Iwaki, Pinskerova and Freeman, 2000).   In fact,   the corresponding lateral tibial condyle is composed of a single articular surface, termed the Tibial Articular Facet (TAF). Anterior to the TAF, the surface slopes downwards onto the AHF to accommodate the anterior horn of the lateral meniscus in extension. Similar to the contralateral condyle, during extension, the anterior horn of the meniscus sits in the corresponding recess in the femur to provide further stability (Figure 17C).

During the extension phase, the EF (or the FF in the absence of an EF) is in contact with the TAF (Figure 19A). During extension, the FFC moves distally by 1mm, representing rotation around the EFC, although this is not always the case, since the EF may be absent. Furthermore, the femoral condyle moves 2mm posteriorly in the first 15˚ of flexion, showing that sliding is the chief mode of motion during this phase.

2.4.2.2 TRANSITION & FLEXION PHASE

For the lateral compartment, the transition and flexion phases will be discussed together since the motion from 10˚ to 120˚ is consistent. The lateral FF exhibits a smaller circular radius in comparison to the medial posterior circular FF. During these two phases, the femoral FF is in contact with the TAF from 10˚ through to 90˚ (Figure 19B), after which the femoral FF contact starts transitioning onto the tibial PHF (Figure 19C). Over the

arc of 10° to 120° the FFC moves posteriorly by 17mm relative to the tibia by a ratio of rolling and sliding of 1.7:1 (Hill *et al.*, 2000). In comparison to the medial AP translation, the lateral compartment clearly displays a larger posterior displacement which directly correlates to the internal tibial rotation that is known to occur throughout the full ROM of the knee.
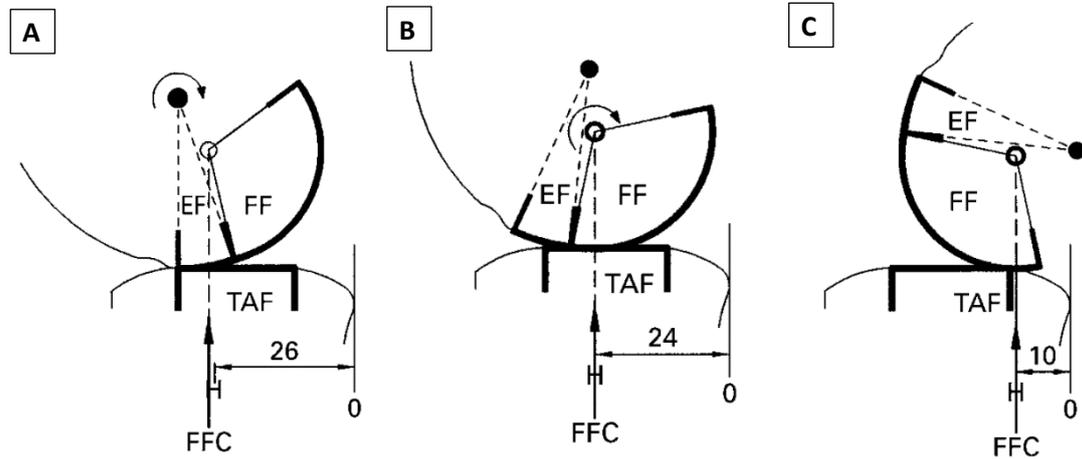
Figure 19: The geometry of the lateral compartment at three instances during the ROM of the knee (Iwaki, Pinskerova and Freeman, 2000)

| **A:** At full extension (-5°) | **B:** At early-flexion (20°) | **C:** At late-flexion (110°) |

2.4.2.3 HYPER-FLEXION PHASE

Laterally, during the ROM of this phase, the femur continues to move posteriorly by a further 5mm. In comparison to the contralateral side, the amount of posterior translation is close enough to show little to no TF axial rotation between 120° and 160°. Although the femoral FF (flexion facet) transitions onto the tibial PHF during the termination of the flexion phase, it is important to note that while this transition continues until 160° of flexion, the lateral femoral condyle still contacts the tibial bone by approximately 1mm anterior to the posterior tibial cortex, thus pushing the lateral meniscus posteriorly to make contact. At 160° the femoral FFC is 2mm distal to its position during mid-flexion (Iwaki, Pinskerova and Freeman, 2000). The coronal asymmetry that is exhibited between the contralateral condyles (i.e. medial femoral condyle lifted on the meniscal horn and lateral condyle touching bone 2mm distal to mid-flexion position) equates to a tibial position of 3° valgus and 30° tibial internal rotation when compared to its hyper-extended position.

2.4.3 OUTLINE OF KEY KNEE MOVEMENTS

Table 3 is aimed at summarising and collating the movements occurring in the medial and lateral compartments during the four phases, outlining the most important features.

Table 3: A summary of the data given about the movement exhibited by the knee in the medial and lateral compartments of the knee.

Range of Motion		Medial Compartment	Lateral Compartment
Extension Phase Range: -5˚to 10˚	Centre of Rotation	EFC	EFC
	Contact Facet	EF with EF	EF (or FF if absent) with TAF
	Motion	Sliding	Sliding
	Relative Movement	No movement	Femur 2mm posterior
Transition Phase Range: 10˚to 30˚	Centre of Rotation:	FFC	FFC
	Contact Facet:	FF with FF	FF with TAF
	Motion:	Sliding	1.7:1 (Rolling:Sliding)
	Relative Movement:	No Movement	Femur 2mm posterior
Flexion Phase Range: 30˚to 120˚	Centre of Rotation:	FFC	FFC
	Contact Facet:	FF to FF	FF with TAF
	Motion:	Sliding	1.7:1 (Rolling:Sliding)
	Relative Movement:	No movement except for 2mm posterior in last 10˚	Femur 15mm posterior
Hype-flexion phase Range: 120˚to 160˚	Centre of Rotation:	FFC	FFC
	Contact Facet:	PHF to PHF	PHF to PHF (with 1mm contact on FF)
	Motion:	Rolling	Rolling
	Relative Movement:	Femur 8mm posterior	Femur 5mm posterior

As a result of the asymmetry of the medial and lateral compartments, the TF joint experiences varying levels of axial rotations as a function of flexion. In order to better understand this compound movement occurring at the chondral level of the TF interface, reference is made to the Tibial Axial Plots in Figure 20 which portray the relative movement experienced in both compartments into a single diagram. In these Tibial Axial Plots, the tibial plateau is overlaid with projections of the medial and lateral FFCs and EFCs, which are represented by the black circles on the corresponding tibial plateaus. The EFCs are connected by dotted lines which represent the black axis connecting the EFCs in Figure 18A, while the solid lines represent the white axis

connecting the FFCs. These "imaginary" axes represent the FEAs (flexion-extension axes) of the knee during the corresponding phases of flexion. Since more FEAs will be introduced, compared and discussed in this thesis, the FEAs defined by the international research team of Freeman (Hill *et al.*, 2000; Iwaki, Pinskerova and Freeman, 2000; Nakagawa *et al.*, 2000; Pinskerova *et al.*, 2004; Freeman and Pinskerova, 2005) will be defined as follows in order to be able to differentiate amongst the different FEAs later on in this text:

- Extension Condylar Axis (ECA): An axis connecting the EFCs (dotted lines in the Tibial Axial Plots - Figure 20).

- Flexion Condylar Axis (FCA): An axis connecting the FFCs (represented by the solid lines in the Tibial Axial Plots - Figure 20).
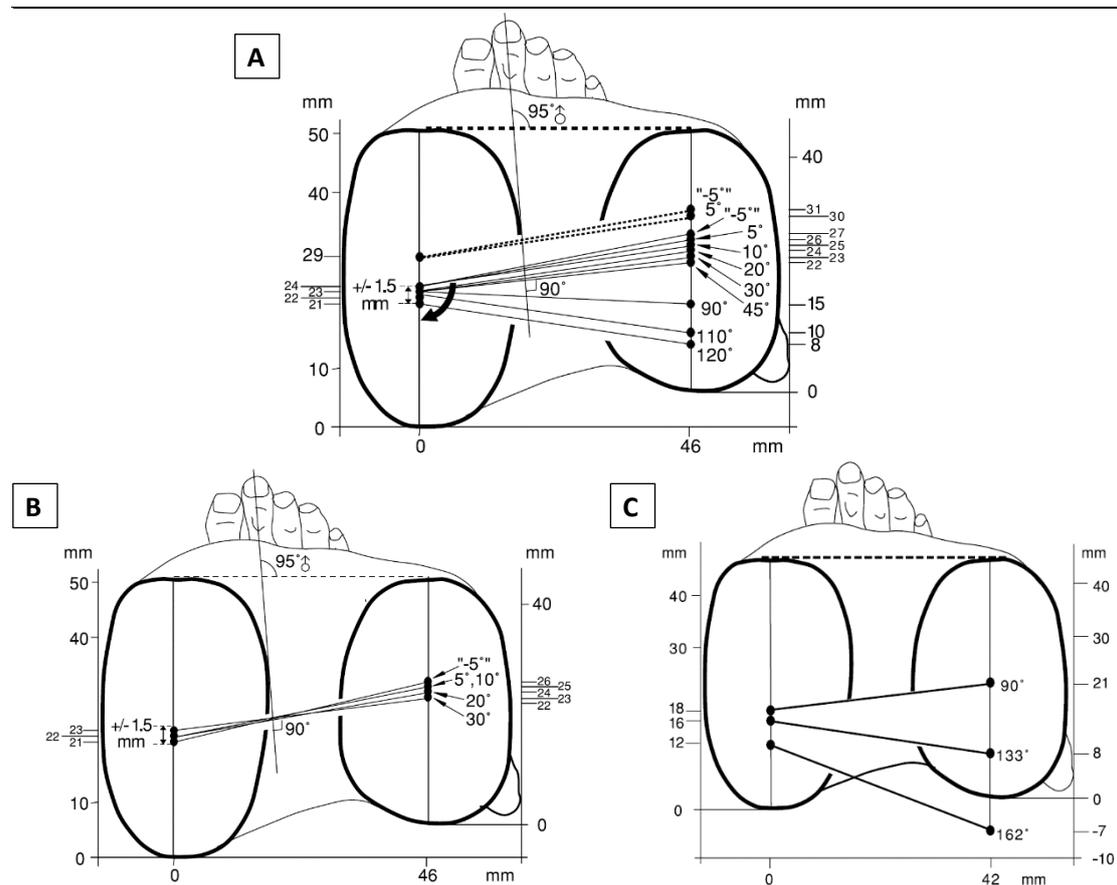
Figure 20: Tibial Axial Plots of the tibial condyle overlaid with projections of the imaginary axis connecting the medial and lateral EFCs and FFCs (white rod in Figure 17A).

A: A representation of the position of the EFCs and FFCs from -5˚ to 120˚ of flexion. Refer to the text for context. (Iwaki, Pinskerova and Freeman, 2000)
B: An illustration of the unadjusted positions of the FFCs from -5˚ to 30˚. Refer to the text for context. (Iwaki, Pinskerova and Freeman, 2000).
C: An illustration of the position of the FFCs at 90˚, 133˚ (full active flexion) and 162˚ (full passive flexion). Refer to the text for context. (Nakagawa *et al.*, 2000)

At each flexion increment, the ECAs and the FCAs represent the AP location of the corresponding EFCs and/or FFCs with respect to a static tibia. Measurements are taken with respect to the posterior cortex of the corresponding tibial plateau. It is important to note that the projected ECAs and FCAs shown in the Tibial Axial Plots represent the relative location of the corresponding facet centres and not the TF contact points between the tibia and femur. Contact point profiles will be discussed in section 2.4.4 below.

Recall that during the extension phase, the individual knee compartments rotate around the EFCs. The ECA, represented by the dotted lines, during the extension phase shows that the tibia is externally rotated at full-extension with respect to the femur. This external rotation, along with the fact that the EFC exhibits a larger radius than the FFC, results in tightening of primarily both the collateral ligaments and secondarily the ACL while wedging the meniscus between the tibia and femur. In this position, the knee joint is essentially locked, resulting in a very stable position which is termed the screw-home mechanism. With the joint locked, a person can stand for prolonged periods without using, and hence tiring-out, the muscles that extend the knee. Unlocking the knee joint requires muscular contractions from the popliteus muscle that internally rotates the tibia or externally rotates the femur (depending on the status of the kinematic chain[1] during the initial stages of flexion), thus unlocking the knee (Last, 1950). An internal tibial rotation of 5° can be noted between the increments of -5° and 5° in Figure 20A, representing the unlocking of the knee as the knee initiates flexion. This internal tibial rotation occurs as the EFC location on the lateral compartment translates slightly posteriorly while the medial EFC shows no signs of movement with respect to the medial tibial condyle (i.e. sliding).

---

[1] A **kinematic chain** is combination of links (bones in our case) and (anatomical) joints assembled in series to form a complex motor system. A kinematic chain may be open or closed. In a closed kinematic chain, the terminal links in the system are fixed in space, presenting a reduction in the DOF of the system such that when one link moves all the other links will move in a manner as to accommodate the reduction in DOF being imposed by the fixed links. Conversely, in an open kinematic chain the terminal end of the distal segment is free in space. This results in the distal end possessing a higher DOF than the proximal counterparts such that these distal segments can achieve a larger variety of movements.

In view of the specific case given in this text, in an open-chain scenario, that is, the distal end (i.e. the tibia) is free in space (i.e. the foot is not making contact with the ground) during the initial stages of flexion, then the popliteus muscle will internally rotate the tibia while the femur is static. Contrariwise, in a closed-chain scenario, both the femur and tibia perform a degree of internal and external rotation respectively, since both links are experiencing a reduction in their DOF.

Additionally, it should be noted that in the Tibial Axial Plots in Figure 20A the -5˚ and 5˚ increments, which correspond to the ECA, are also plotted for the FCA. This is performed in order to represent the full ROM of the knee using a single FEA, which makes it easier to visualise the relative AP translation occurring within the knee. In order to implement this, allowance must be made for the 'apparent translation' of the FFCs during the extension phase. It is known that from -5˚ through to 10˚ the FFCs both move distally and anteriorly by about 2mm as a consequence of rotation around the EFCs (this movement is known as kinematic crosstalk – explained further down in section 2.6.2). Therefore the FCA profiles for the -5˚ and 5˚ increments in Figure 20A are adjusted to compensate for this movement. Their unadjusted position is displayed in Figure 20B for comparison. This technique of portraying the relative motion of the TF interface by utilising Tibial Axial Plots has been utilised by several researchers in their studies of the kinematics of the knee (Yoshioka *et al.*, 1989; Hill *et al.*, 2000; Karrholm, Brandsson and Freeman, 2000).

In summary, the work by Freeman *et al.* (Hill *et al.*, 2000; Iwaki, Pinskerova and Freeman, 2000; Karrholm, Brandsson and Freeman, 2000; Nakagawa *et al.*, 2000; Pinskerova *et al.*, 2004) have shown that the femur exclusively rotates around the ECA between -5˚ and 10˚ of flexion (or during the Extension phase). Subsequently, from 30˚ through to hyper-flexion (or during the Flexion phase) the femur rotates exclusively around the FCA. Between 10˚ and 30˚ of flexion (or the Transition phase) the femur transitions from the ECA to the FCA, creating the 'rocking' of the femur. This translates the femur's rotational centre posteriorly by roughly 4 mm as a result of the femur switching its axes of flexion from the EFC to the FFC. This can be noted in Figure 20A by comparing the locations (and the respective distance) of the ECAs and the corresponding -5˚ and 5˚ FCA profiles.

Taking the FCA as the axis of reference, it can be noted that between -5˚ and 120˚ the tibia internally (or femur externally) rotates by a significant 20˚. The first 5˚ of axial rotation occurs between -5˚ and 5˚, during the unlocking of the knee, while the remaining 15˚ occur in the remainder of the flexion through to 120˚. Of these 15˚, the tibia marginally rotates between 5˚ and 45˚ as the femur lies in a quasi-perpendicular state in relation to the long axis of the foot (Figure 20A and Figure 20B). The majority of the internal tibial (external femoral) rotation occurs between 45˚ and 120˚, especially after 60˚.

Finally, during the hyper-flexion phase (Figure 20C), between the flexion angles of 120° and 160°, we notice the phenomenon of femoral roll-back. In these last 40° of flexion, both compartments move posteriorly in order to allow the femur to rotate further before impingement occurs. It should be noted that active flexion allows up to around 120° of flexion, while passive flexion achieves a further 40° of flexion (Nakagawa *et al.*, 2000). In contrast to the static position of the medial FFC from -5° through to 120°, the FCA experiences a further 5mm posterior translation, medially, during hyper-flexion. At around 140° the femur's medial PHF rolls onto the posterior horn of the medial meniscus, compressing it between the tibia and the femur. The meniscal horn starts resisting flexion from this point through to 160° when it restricts any further posterior movement on the medial side. Laterally, between the flexion angles of 120° and 160°, the lateral FFC moves 21mm posteriorly, thus further increasing the magnitude of the internal tibial rotation. At terminal passive flexion (160°) the lateral femoral condyle loses all contact with the tibia, such that the femur becomes posteriorly subluxated (dislocated). This happens due to the fact that the lateral meniscus allows more posterior translation to occur, in contrast with its contralateral counterpart which terminates posterior translation 10mm from the posterior tibial cortex. In terminal flexion, the position of the tibia with respect to the femur equates to 3° valgus and 30° internal rotation compared to its hyperextended position.

In light of the functional anatomy discussed in section 2.2.2.3, the cruciate and collateral ligaments are known to have a crucial role in maintaining stability throughout the flexion cycle. The MCL is taut in hyperextension and late flexion while allowing a higher degree of mobility in between the two extremes (Figure 21). In conjunction with the constrained medial meniscus, the tension on the MCL supports the aforementioned restricted motion of the medial compartment. Laterally, the LCL is taut in hyperextension and relaxed throughout flexion, allowing a much greater degree of posterior translation in the lateral compartment, which in conjunction with the constrained medial compartment generates the axial rotation. On the other hand, the ACL is taut in extension, serving as a check against both hyper-extension and internal and external rotation in this locked position. The PCL is relaxed in extension but starts tightening with flexion, becoming taut in terminal flexion. This ligament serves as a check against posterior instability in a flexed knee.

In conclusion, the medial femoral condyle predominantly slides on the corresponding tibial condyle, while demonstrating minor translation during later stages of flexion. In contrast, the lateral condyle rolls and slides posteriorly on the tibial plateau, demonstrating larger posterior translations. This leads to the coupled internal rotation of the tibia during flexion.
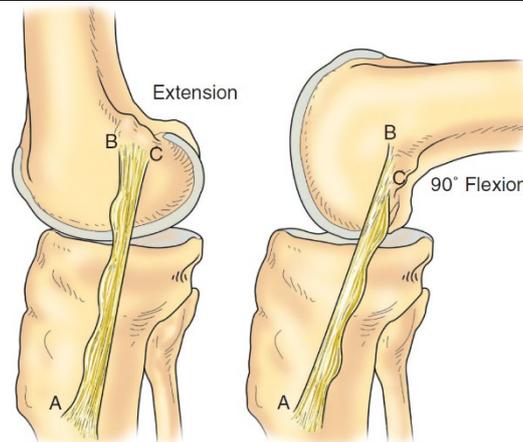
Figure 21: Diagram of the MCL's mechanism with flexion and extension of the knee (Scott, 2018).
During extension point C, the posterior aspect of the MCL, moves superiorly, thus tightening the posterior aspect of the ligament. Conversely, during flexion point B moves superiorly, tightening the anterior border.

2.4.4 TIBIOFEMORAL CONTACT POINTS

In this section, the reader will be introduced to the TF contact point (CP) plots, in particular how they can be interpreted and how these plots can provide clinicians with an additional perspective into the articulation of the knee when used in conjunction with the Tibial Axial Plots (Figure 20). It should be noted that the term "contact point" refers to the centroid of the area making contact between the tibial plateau and the corresponding femoral condyle.

While Tibial Axial Plots are capable of describing the relative location of the TF complex, the TF CP plots do not, since CPs are not fixed locations on the femur or the tibia and therefore cannot be used to measure the relative positions of the two bones directly. This occurs due to the asymmetrical morphology of the condylar contact regions in the knee. If the femoral condyles were perfect circles and the tibial plateau was flat (from a sagittal perspective), then the contact points would reflect the relative position of the bones. Using the analogy of the wheel of a car (the femoral condyle) moving on a flat road (the tibial plateau), then if the knee had the aforementioned geometry the CP would lie on a line perpendicular to the road passing through the centre of the wheel, but in reality, this is not the case. In the knee, the anterior sagittal section

of the femoral condyle is of a larger radius than the posterior condyle, while the tibial plateau is not entirely flat, displaying an inclined anterior section with an angle of roughly 11° (Iwaki, Pinskerova and Freeman, 2000). These "irregular" morphological features of the knee "uncouple" the movement of the CPs from the movement of the condylar axes.

The discrepancies that exist between the TF contact profiles and the ECA and FCA profiles (in Tibial Axial Plots) have been presented and explained by the same international team of Freeman (Pinskerova *et al.*, 2004) whose work has been presented earlier in this section. In their research paper, they studied the relationship between the movement of the TF contact points and the movement of the femoral condyles from full-extension through to 120° of flexion, the arc under active muscular control, in cadaver, living weight-bearing and non-weight-bearing knees. Their aim was to provide further clarification on the articulation of the knee and thus resolve the controversy arising from kinematic descriptions of the knee based on the condyles as against those based on the contact profiles. In Pinskerova's study, the contact points were defined as
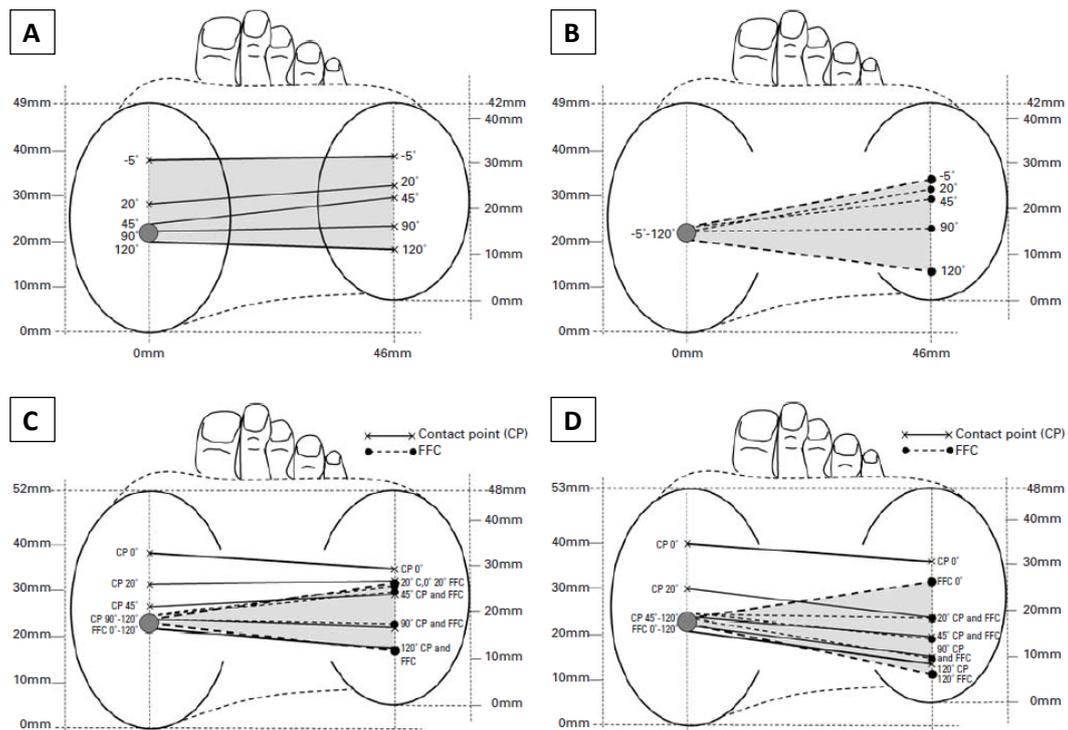
Figure 22: Tibial Axial Plots with overlaid Contact Point profiles (Pinskerova et al., 2004)
A: CPs for cadaver knees (N=6);
B: FCA projections on a Tibial Axial Plot for the same cohort of cadaver knees;
C: Non-weight-bearing living knees (N=5);
D: Weight-bearing living knees (N=5);

the locations where the subchondral plates of the femur and tibia most closely approach each other.

Medially, in all three groups being investigated, the FCA, ECA and CP profiles displayed no significant difference at any flexion angle. The CPs were located anterior to their FCA and ECA counterparts during the Extension and Transition phases of flexion. The CPs displaced posteriorly by about 15 mm with increasing flexion from -5º to 30º of flexion (the range of flexion during which the ECA is the acting FEA). The CPs during this range of flexion were noted to always lie below the EFC, on a line perpendicular to the articulating tibial surface (that is, the inclined anterior tibial surface – refer to Figure 23A). As the knees transitioned to the Flexion phase (that is, rotation occurring around the FCA), the CPs lied directly below the FCA (specifically, the corresponding FFC of the medial condyle), again occurring perpendicular to the tibial surface. The CPs and FCA profiles showed agreement from 45º to 120º of flexion.

Laterally, the FCA and CP profiles moved posteriorly in all three groups by about 17 mm from 0º to 120º of flexion. Similar to the medial compartment, the CPs were located anterior to the corresponding FCA locations during the Extension Phase (-5º to 10º of flexion), but not to the same extent as on the medial side. The cadaver and non-weight-bearing knees showed similar profiles throughout the recorded ROM, while the weight-bearing group displayed larger posterior translation in both the FCA and CP profiles during early flexion phases (20º and 45º of flexion) and then approximated the non-weight-bearing profiles from 90º of flexion onwards. In contrast to the medial
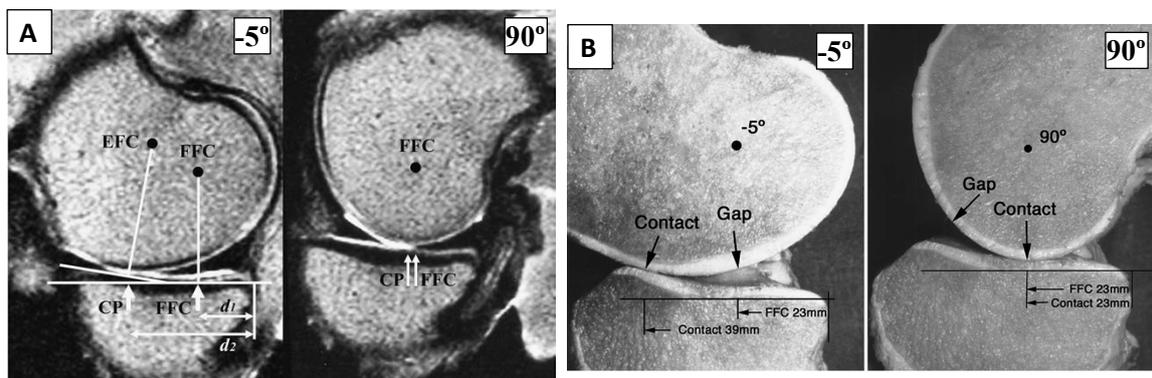
Figure 23: MRI images of the medial and lateral condyles at hyper-extension (-5º) and 90º flexion (Pinskerova et al., 2004)

A: Sagittal MRI scan of the medial condyle at -5º (left) and 90º (right) of flexion overlaid with markings identifying the CP and FFC location on the tibial plateau for both cases.
B: Sagittal MRI scan of the medial compartment at -5º (left) and 90º (right) of flexion displaying the movement of the CPs but not the condyle.

compartment, the CPs and FCA profiles showed agreement from 20º to 120º of flexion, which reflects the larger effective FF on the lateral compartment in comparison to the relatively smaller FF on the medial side.

Taking into consideration both compartments, it can be noted, how the CP profiles remained approximately parallel throughout flexion while moving posteriorly by about 20 mm throughout the recorded ROM. Conversely, the FCA profiles showed clear signs of rotation around the centre of the medial condyle, which reflects the external femoral rotation known to occur with increasing flexion.

Following the presentation of these results, it can be clearly noted that there exists a discrepancy between the CP profiles and the FCA profiles, especially medially towards extension. This discrepancy can be explained by again referring to the analogy mentioned earlier. Medially, as the knee extends from 120º to 30º of flexion, that is, during the Flexion phase, as the TF FFs are in contact (Figure 24A - left), the circular posterior femoral condyle rotates on the corresponding flat posterior tibial surface, such that the FFC lies vertically above the CP. As the knee reaches the 30º flexion mark, the contact transitions to the medial TF EF composed of the anterior femoral condyle and the anterior tibial surface. Due to the larger radius of the anterior femoral condyle and the inclined tibial surface of the EF, the CP starts to shifts anteriorly relative to the location of the FFC (Figure 24B – left). As extension progresses towards hyper-extension (10º to -5º) rotation is exclusively around the ECA, which leads to the FF losing contact such that the knee 'opens' posteriorly (Figure 23B left) due to the CP (fulcrum point) now having moved anteriorly and slightly proximal. As a result of the inclined anterior tibial facet, although the CP now lies anterior to both the locations of the EFC and FFC, the CP and EFC are still perpendicular to each other. The analogy here still applies if the inclined tibial surface and the larger anterior condyle are taken into account.

Laterally, the femoral condyle is known to have a constant circular sagittal profile from 120º to 10º and contacts an essentially flat tibial surface. Thus, as a result of the morphology of the lateral compartment, the CP lies vertically below the lateral FFC through the effective ROM of the lateral FCA (Figure 22C and D; Figure 24A and B - right). As the lateral compartment moves beyond the 10º flexion mark, the anterior femoral condyle rotates downwards, following the convex sagittal profile of the lateral tibial plateau. Due to the larger radius of the anterior femoral condyle, seemingly

appearing to be almost flat, it rolls over the anterior edge of the tibial surface, thus moving the CP anterior to the location of the lateral FFC (Figure 24C – right).
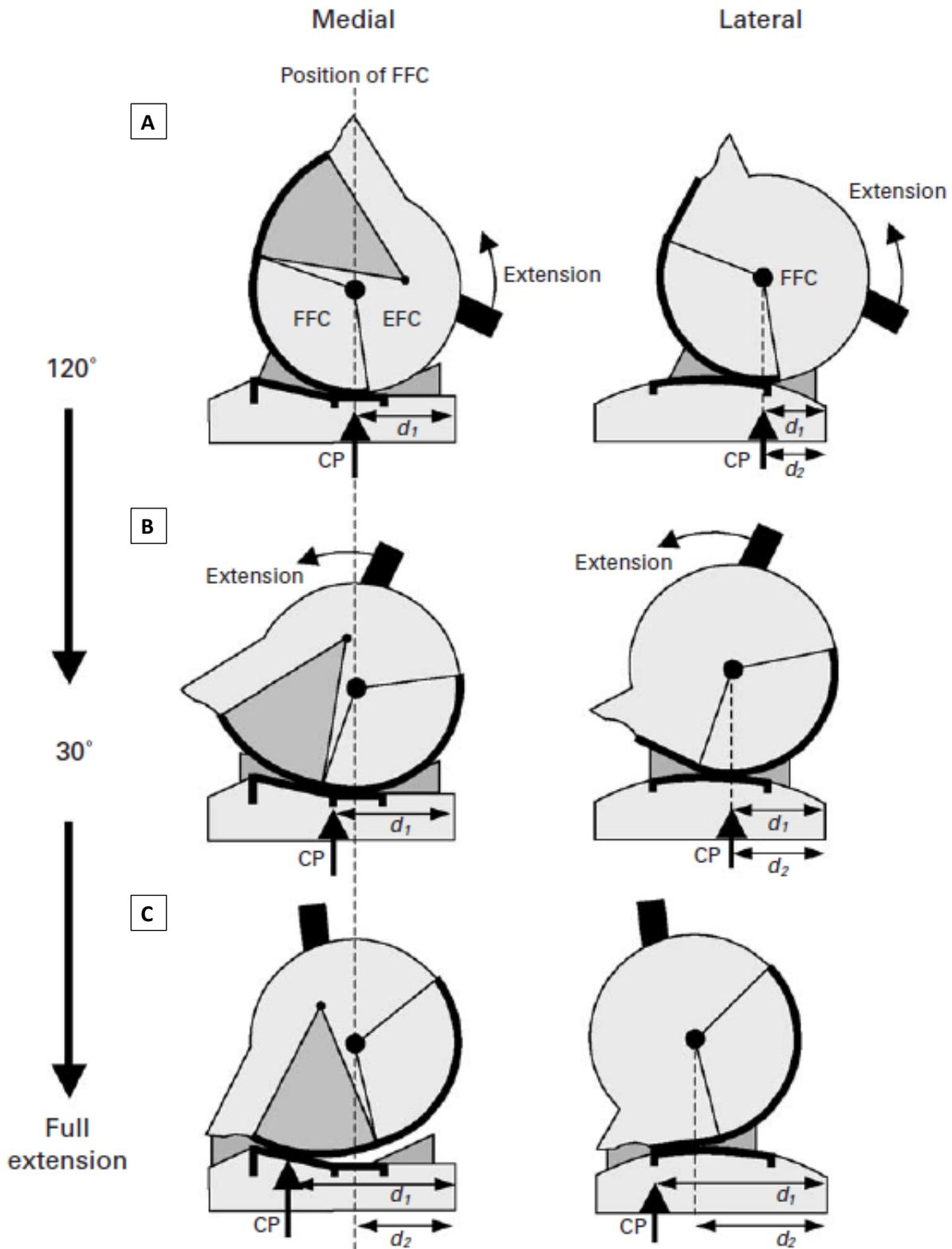
Figure 24: An overview of the TF movement occurring in both compartments (Pinskerova et al., 2004)

In summary, it has been shown that the discrepancy that exists between CP profiles and the ECA and FCA profiles is due to the differences that exist in the morphology between the anterior and posterior surfaces of the TF complex. The author finally points out that when describing the movement of the knee, it is imperative that care must be taken to define what is being investigated, whether it is the CPs or the condylar profiles since the two move differently. While presenting the CP profiles on their own does not explain the movement of the knee, presenting the condylar profiles on their own is sufficient for analysing the relative movement of the tibia and femur. If the Tibial Axial Plots (containing condylar profiles) are used in conjunction with the CP profiles, a more comprehensive understanding of the functional anatomy and the directly-linked kinematics of the knee can be appreciated.

2.4.5 AXIAL CENTRE-OF-ROTATION

So far it has been shown that a unique combination of the principal three DOF of the knee, that is, FE rotation, AP translation and IE rotation, occurs within the knee depending on the activity which is driving the movement (such as squat, gait, lunge, etc.). While the Tibial Axial Plots including the CP profiles can be used as a comprehensive tool to understand the articulation of the knee over a range of flexion, another metric can be additionally incorporated into them in order to encapsulate the movement into a single metric. This is known as the Axial (or transverse) Centre-of-Rotation (COR), which represents the motion of the medial and lateral condyles of the femur relative to the proximal tibia.
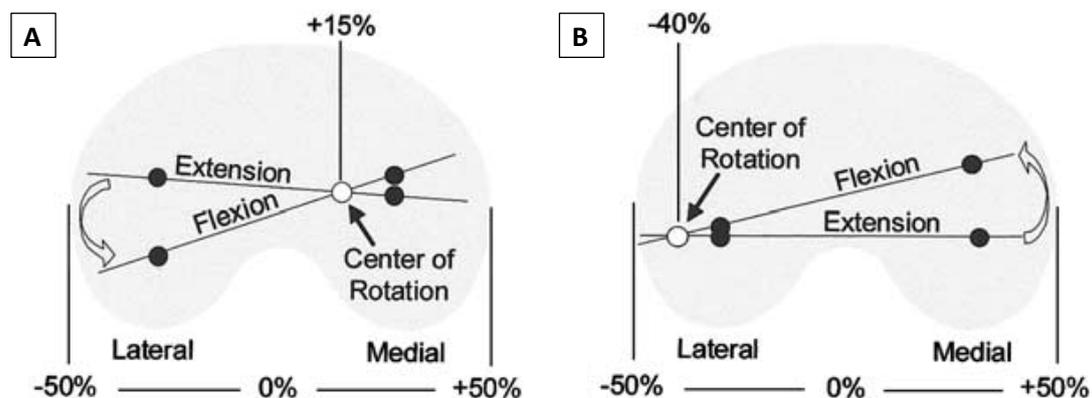
Figure 25: The axial Centre-of-Rotation (COR) of the knee (Banks and Hodge, 2004)

A: An example of a Tibial Axial Plot showing two instances of a FEA having an axial COR which lies in the medial compartment of the knee.
B: An example of a Tibial Axial Plot showing two instances of a FEA having an axial COR which lies in the lateral compartment of the knee.

The axial COR was first defined by Banks and Hodge in 2004 (Figure 25), as a parameter to simply describe TF translations using a single metric. While keeping in mind that on its own it does not provide full kinematic detail of the motion being analysed, the idea behind using this metric was to permit intuitive comparisons between different types of knees (such as healthy, arthritic and different designs of replaced knees).

In order to identify the axial COR, the parametric line equations of the projected FEAs on the Tibial Axial Plots in terms of the Tibial CS are first identified. The average COR is subsequently calculated by solving the least-squares system of equations of the projected lines, such that the location of the COR for the entire ROM is obtained in terms of the AP (y-axis) and ML (x-axis) distance from the origin of the tibial CS.

If the axial COR is located in the medial compartment of the knee (that is, on the medial tibial plateau), then the lateral condyle tends to move posteriorly as the femur externally rotates with flexion, which reflects a deep-knee bend movement of a healthy knee. Contrariwise, if the axial COR is located in the lateral compartment, then the medial condyle tends to move forward with flexion. The axial COR is found to predominantly lie in the lateral compartment during the swing phase of normal gait (Koo and Andriacchi, 2008). There is also the chance of obtaining extreme axial COR values which indicate that there is almost pure AP translation (that is, no IE rotation) occurring during the movement being analysed, resulting in an axial COR which lies far out on one of the extremities of the tibial plateaus.

In the context of this study, this metric is not being introduced to compare the articulation occurring during different activities, since we will only be using one type of movement, a knee-bend. This metric is being introduced and will be implemented into the Kinematic Analysis Suite since it is useful in identifying marginal differences in the articulation, specifically IE rotation, occurring within different designs of knee replacements (Banks and Hodge, 2004; Koo and Andriacchi, 2008).

2.5 THE REPLACED KNEE

In this section, the reader will be provided with an understanding of the pathology of the degenerating knee due to Osteoarthritis and the treatment methods that are provided before opting for TKA. The different alignment techniques which are implemented during TKA to achieve proper alignment are briefly discussed with the aim of

highlighting the correlation between implant alignment and the ensuing postoperative knee kinematics. This will allow the reader to appreciate how the surgical technique used in TKA factors into the patients' kinematics and is another area which is not yet fully understood. Finally, the discussion is shifted onto the different implant designs and their effect on the kinematics of the knee. Focus is given to the Ultra-Congruent Fixed-Bearing, and Mobile-Bearing implant designs since these will be the knee implants which will be used in the practical aspect of this thesis. The benefits and limitations of these implants will be reviewed in light of the kinematics, which are reported in the literature.

2.5.1 OSTEOARTHRITIS

Osteoarthritis (OA) is the most common form of arthritis in the UK, with the highest occurrence in the age group of 65-74 years old (Woolf and Pfleger, 2003). The prevalence of OA in the knee joint is relatively high, at 30% of the pensionable UK population (Zhai *et al.*, 2007). OA, which is known as 'degenerative arthritis' since it occurs as a result of excessive 'wear-and-tear' of the affected joint, is a chronic disease causing pain and dysfunction (Figure 26). This wear-and-tear occurs due to the constant interaction between two moving surfaces.

In a healthy joint, the cartilage covering the contacting ends of the bones, allows them to glide over one another in a frictionless joint movement. OA is a metabolically active and dynamic process where the destruction and repair can be triggered by various biochemical and mechanical factors (Dieppe, 2000). One of the signs of OA is through a radiological investigation where cartilage can be seen to be thinned, and as a result, the joint space is reduced. A primary sign of OA is the increase in water content of the cartilage. This alters the quality and quantity of the proteoglycan matrix of the cartilage, leading to fibrillation of the cartilage, loss of cartilage substances, osteophyte formation and an increase in bone density below the affected cartilage. Chondrocytes which make part of the aforementioned proteoglycan matrix in cartilages are involved in repairing the cartilage, however, with the ageing human body, the equilibrium of breakdown and repair of cartilage is not balanced in articular diseases such as OA. Through the repetitive use of the knee joint over years of going through cyclic repetitions of the same movements, the joint will starts showing signs of irritation and inflammation of the cartilage, leading to pain and swelling. Eventually, the cartilage will begin to degenerate by chipping and also showing signs of fatigue when cracks start forming on

the surface of these anatomical features. As the disease progresses, the protective cartilage also starts to roughen up (Moskowitz, 1984). The body compensates for these alterations in the physiology by causing the outer edges of the bone to thicken, forming an 'outgrowth' known as osteophytes or bone spurs, leading to a change in the shape of the underlying bone (Figure 26). While both TF and patellofemoral joints of the knee can be affected by OA, this thesis will only focus on TF OA.
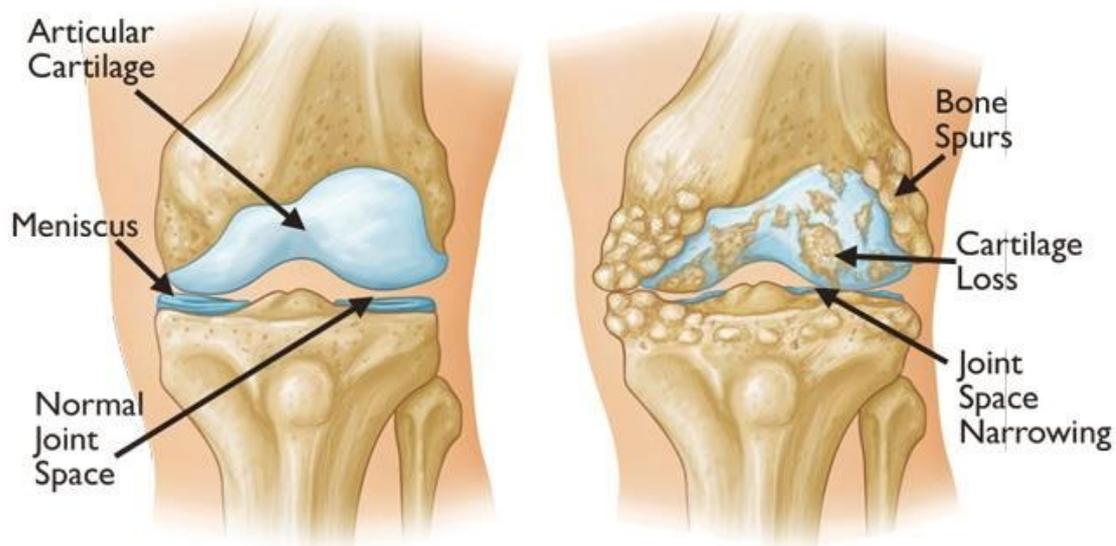
Figure 26: The degeneration of the healthy knee as a result of OA (American Academy of Orthopaedic Surgeons, 2014).

When a patient shows symptoms of OA and reports pain, stiffness, swelling and decreased ROM, a series of preliminary treatments are first suggested to control the pain and try to slow the progression of the disease. The first methods of treatment are:

- Maintain, and if possible increase, activity and mobility

- Weight-loss for over-weight patients, to decrease the excessive stresses on the joint

- Pain management using pain killers

- Anti-inflammatory medication if the joint is swollen, hot and inflamed.

- Physiotherapy exercises to manage the pain and increase the ROM

- Other orthotic devices can be proposed, such as shoe wedges and cushioned shoes to reduce the load on the affected joint.

If the pain and swelling persist following any, or a combination, of the above treatments, then the only remaining options are to follow surgical options for the management of OA. Again, there are various surgical options for knee OA, which are dependent on the stage of arthritis and the affected compartments (e.g. medial or lateral). These surgical treatments include:

- Knee arthroscopy – performed when loose fragments of worn-out cartilage form within the knee. During arthroscopy, these fragments are 'washed out' of the knee.

- Osteotomy – realign the lower limb mechanical axes in order to shift the weight-bearing forces and thus unload the worn-out side of the joint, preventing abnormal localised stresses on specific compartments of the knee. This is mostly performed on young, active patients who are not yet considered to be candidates for more invasive procedures.

- Uni-compartmental knee replacement – Preformed when arthritis is confined to a single compartment. This surgery removes less bone, leading to less soft-tissue disruption, which in turn leads to faster recovery times and is claimed to improve the patients' functional outcome (Harwin, 2003).

- Total Knee Arthroplasty (TKA) – This is left as a last-resort treatment since it is the most invasive of all treatments. It is only performed on severe cases of OA. This involves the replacement of the entire articular surfaces of the femur and tibia (and sometimes the patella). When successful, this treatment provides noticeable pain relief and functional improvement in the majority of patients with severe knee OA.

2.5.2 TOTAL KNEE ARTHROPLASTY

Total Knee Arthroplasty (TKA), or Total Knee Replacement (TKR), is an effective method of alleviating pain, correcting substantial deformities and restoring mobility in patients with advanced OA. It is only considered at the end-stage of the disease process. During the surgery, special instrumentation is used to measure the correct thickness and angulation of the required bone cuts so as to remove the thinnest layer of the damaged surface of the femur and tibia. The removed bone is then replaced by a prosthesis following an alignment process.

It is imperative to understand the principals of the surgical technique, as a perfectly designed prosthesis implanted with incorrect alignment would lead to problems. A number of factors play a part in the success of a TKA:

- Surgeon and surgical technique

    o The level of the surgeons' experience

    o Level of technological intervention – this improves the accuracy of implant positioning and alignment while reducing the effect of human-error (e.g. Patient-Specific instrumentation and/or Computer Assisted Orthopaedic Surgeries (CAOS))

- Prosthesis design

    o Mobile or Fixed bearing prosthesis

    o Cruciate retaining or sacrificing prosthesis

    o High or low congruent designs

    o Principal implant axes have to be matched to the cuts performed during surgery.

Proper alignment of the knee is one of the most influential factors in determining the long-term outcomes after TKA (Barrett *et al.*, 2011). Malalignment results in increased mechanical, and shear stresses placed on the bearing surfaces and the bone-implant interfaces (D'Lima *et al.*, 2001; D'Lima, Chen and Colwell, 2001; Sikorski, 2008). Furthermore, proper alignment aids to balance the forces transmitted through the soft-tissue structures, which are crucial for the sustainable functioning of the joint. Poorly aligned TKAs result in decreased implant survivorship, increased polyethylene wear, poor functional outcomes and early implant failure through component loosening. (Cherian *et al.*, 2014).

Knee alignment is a relative, three-dimensional concept that was originally defined in order to allow surgeons to compare pathological knee alignment to that of a 'normal' knee. This allows for better patient diagnosis and also, the assessment of the alignment of the patients' knee to 'normal' is performed pre-operatively in TKA in order to allow for proper surgical preparation, thus confidently correcting the existing deformities of the patient's knee. This allows the surgeon to implant a well-aligned prosthesis with good ligament balance, which is considered a pre-requisite in TKA.

Conventionally, surgeons referred to one of the two alignment techniques which were employed in TKA, namely the mechanical (also referred to as the classical) technique and the anatomical technique. These two alignment methods are ingrained in TKA practice and have been understood for a long time and are not really a source of controversy (Kapandji, 1971; Moreland, Bassett and Hanker, 1987). Nonetheless, recent studies have started to question if the conventional methods of classical and anatomical alignment are actually responsible for the relatively high rate of failures in TKA. This is not because these conventional methods of alignment are incorrect, but it is being reasoned that the way these alignment axes are being referenced to the 'normal' knee alignment, targeting all TKA outcomes to match the alignment of a 'normal' knee is incorrect. This is supported by the fact that studies are concluding that a 'normal' knee is not so common after all, such that aiming to restore 'normal' knee alignment is resulting in implant failures rather than improved function and longevity of the implant (Cherian *et al.*, 2014).

It should be noted that referencing a 'normal' knee should be considered with caution. This is due to the fact that a normal knee, in reality, is a rare occurrence. Clinicians and researchers alike have calculated the variations that exist in large populations and averaged them to identify a standard knee model with which can be utilised as a base-line, or reference, model in terms of joint alignment. This represents one of the most debated issues in the field of TKA since the main aim of alignment techniques is to achieve neutral alignment of the knee when in reality studies have shown that neutral alignment is very rarely seen in healthy non-arthritic patients. Studies revealed that only 2.2% of patients had a neutral alignment (Hsu *et al.*, 1990) while 32% of men and 17% of women had varus knees which exceeded the normal alignment by 3˚ (Victor, Van Doninck, Labey, Innocenti, *et al.*, 2009)(Bellemans *et al.*, 2012), which exceeds the boundaries of normal alignment allowed during TKA. Therefore, restoration of adequate function and good long-term prosthesis survivorship following TKA is hard to achieve unless the patient's pre-arthritic alignment is taken into consideration.

Recently, the novel kinematic alignment technique started gaining traction as a better alternative to the former two methods. This technique is not based relative to the 'normal' knee alignment, but it uses the patients' anatomy along with three-dimensional functional information to create a patient-specific alignment. The kinematic alignment technique was developed following the classical research by Hollister *et al.* in 1993 on the kinematics of the knee, which will be introduced and discussed in section 2.6.2.1.

Kinematic alignment in TKA is based on matching the functional kinematic axes about which the knee rotates with the primary axis of the femoral and tibial components. In contrast to the mechanical and anatomical axes, these axes are intended to mimic the dynamic motions of the knee. Kinematically aligned knees have shown significantly better results in terms of functional outcome scores and the actual function of the replaced knee, including contact mechanics (Hsu *et al.*, 1990). Furthermore, kinematically aligned knees have shorter operating and recovery times and earlier return to daily routines (Karuppal, 2016).

Nonetheless, given the benefits of the kinematic alignment technique, few authors have evaluated the role of kinematic alignment in improving the outcomes following total knee arthroplasty. Larger studies are needed to appropriately define which alignment method will result in the optimal outcomes for patients after TKA. The fact remains that the kinematics of the replaced knee will always be directly impacted by the alignment technique used by the surgeon intra-operatively. While alignment plays an integral role in defining the kinematics of a replaced knee, the majority of the kinematics are defined by the implant design which plays a significant role in the resulting kinematics (Essner *et al.*, 2011). While, several different implant designs exist in the ever-growing market, in this thesis, the focus will be on ultra-congruent fixed and mobile bearings, since the kinematics of these kinds of implants will be assessed later on in this thesis.

2.5.3 ULTRA-CONGRUENT FIXED AND MOBILE BEARING IMPLANTS

The goal of all TKA implant designs is to provide stability, longevity and restore knee biomechanics as close as possible to the natural knee (Hirschmann and Becker, 2015). The standard primary TKA implant is comprised of a cemented Cobalt-Chrome femoral component, a polyethylene tibial liner and a titanium or Cobalt-Chrome tibial baseplate (Figure 27A - right). Several design variants of TKA implants exist, each one having its own advantages and disadvantages.

As discussed in section 2.2.2.3, the cruciate ligaments are crucial in preventing anteroposterior dislocation, controlling the internal and external rotation of the knee while also maintaining alignment during flexion. While the importance of the ACL is well recognised, to this point, no bi-cruciate retaining prosthesis has achieved general acceptance, and as a result, the ACL is generally resected (Nowakowski, 2006). Bi-cruciate retaining knee implants are considered to be technically difficult to implant,
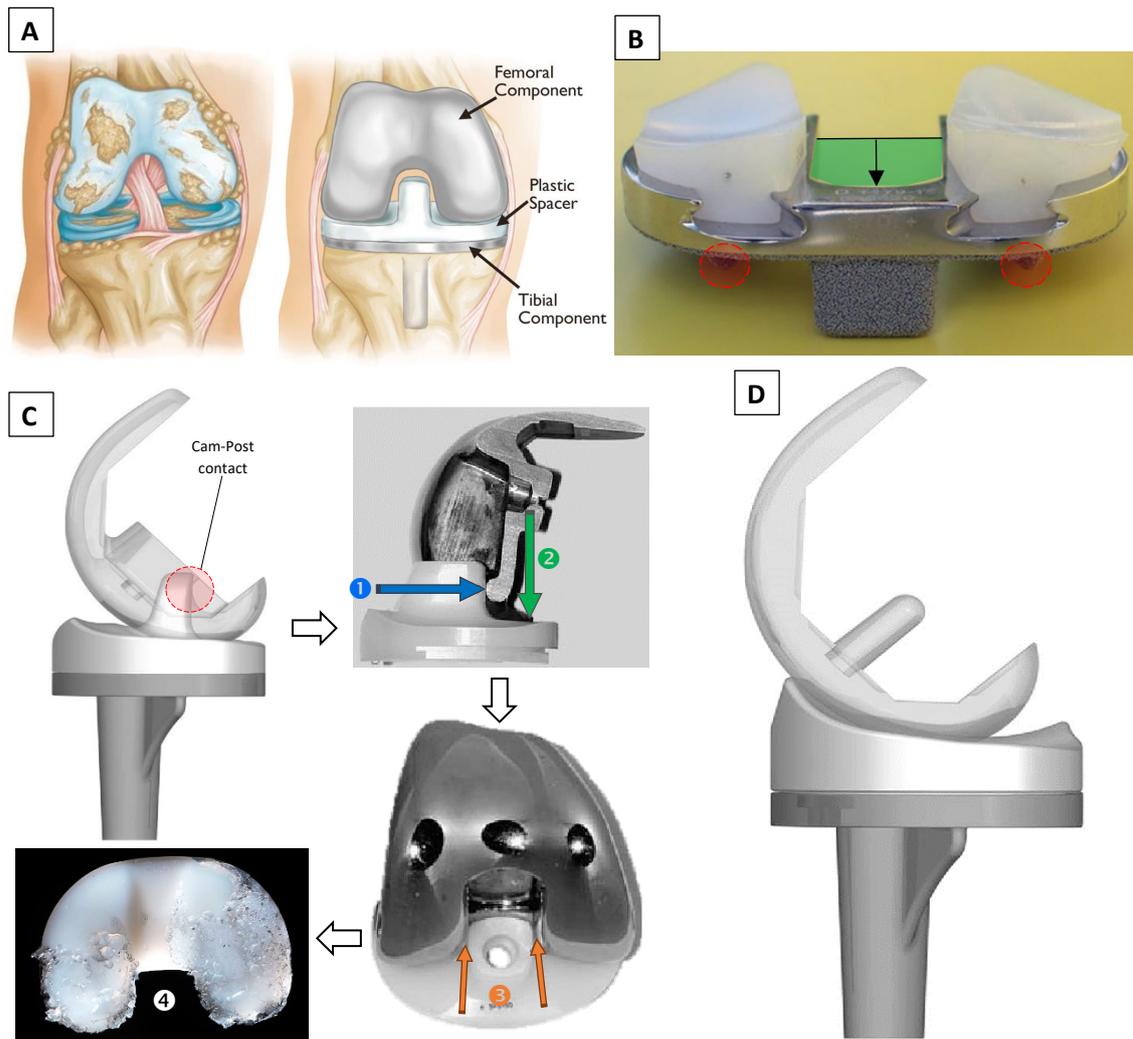
Figure 27: TKA prosthesis designs: CR, PS and UC.

A: The three primary components of a TKA prosthesis are the Cobalt-Chrome Femoral components, the polyethylene tibial insert and the titanium or cobalt-chrome tibial tray (Manner, 2016).

B: A modified CR prosthesis, in which the recess for the PCL is extended anteriorly to allow for ACL retention. Due to the enlarged recess (shown in green), the implant bridge anteriorly becomes prone to failure due to torsion loading in this region. In addition, the short anchoring elements (highlighted in red) cannot prevent increased implant loosening due to the lack of a central stem. (Hirschmann and Becker, 2015)

C: In a PS design, the function of the PCL in mimicked by including a vertical post in the centre of the tibial insert and a cam, or crossbar, in between the posterior femoral condyles which prevent paradoxical anterior motion with increasing flexion and in turn assisting with femoral roll-back. The pitfall of this design comes to light when the cam engages with the tibial post. At this moment the cam-post acts as a lever (❶), transferring the entire force to the posterior femoral condyles which are in contact with the posterior edge of the tibial insert (❷). This results in excessive wear as seen in ❹. Frictional wear also occurs on the sides of the tibial post (❸) upon internal and external rotation of the knee which leads to abrasion between the metallic femoral implant and the PE tibial insert (Hirschmann and Becker, 2015).

D: A typical Ultra-Congruent knee implant, showing the deep-dished tibial insert design. The Anterior lip of the tibial insert is elevated in order to restrict paradoxical anterior femoral gliding. In comparison to the PS implant, this kind of prosthesis provides high congruency throughout the entire ROM of the knee, thus avoiding peak contact stresses occurring at the tibia insert surface (Lützner *et al.*, 2017).

and also, in order to retain the ACL, the design has to allow for an extended PCL recess anteriorly and also replace the central stem with two smaller anchoring elements superior to each compartment (Figure 27B). The extended PCL recess results in a relatively narrow anterior bridge (connecting the medial and lateral tibial plateau) which is prone to failure due to the relatively large torsion loading that occurs in the region connecting the medial and tibial plateaus. Furthermore, the short anchoring elements which replace the larger central tibial stem, are not sufficient to prevent implant loosening (Figure 27B). As a result of these modified design features, fixation is not as good as that found in traditional Posterior Cruciate Retaining (PCR) prosthesis (Hamelynck and Stiehl, 2002).

Conversely, the PCL is considered to be one of the primary stabilisers of the knee joint (Harner *et al.*, 1995). Its retention following TKA has a direct impact on knee stability, kinematics, proprioception, and it may also reduce the shear forces occurring on the tibia. Nonetheless, retaining the PCL has shown to be challenging to achieve due to the difficulty in obtaining proper balancing. Appropriate tension of the PCL requires the restoration of the anatomical joint line, the shape of the femoral condyles and the correct posterior slope of the tibia. If the PCL is too lax, it will lose its purpose and function and if it is too tight, then it could limit flexion and will result in higher contact pressures and edge loading (Jacobs, Clement and Wymenga, 2005). Considering the risks involved with retaining the cruciate ligaments, the posterior stabilized (PS) implants were developed in order to overcome these limitations (Maruyama *et al.*, 2004).

The PS design is a cruciate-sacrificing design, allowing for the tibial plate to cover the entire tibial plateau. The principal design change occurs at the tibial insert, where a post-cam mechanism is introduced to increase the ROM by reproducing the physiological Posterior Femoral Rollback (PFR), which is typically performed by the PCL. The PS design simplifies the issue of soft tissue balancing and joint stabilisation but has shown to produce less physiological kinematics (Colizza, Insall and Scuderi, 1995; Fantozzi *et al.*, 2006; Argenson *et al.*, 2012). In literature, similar outcomes and kinematics were reported for cruciate-retaining and PS prosthesis (Li *et al.*, 2014; Sando *et al.*, 2015). While PS implants guarantee posterior stability of the implant, it has been shown that this results in more stresses on the insert (refer to the text of Figure 27C) leading to a higher risk of polyethylene wear at the level of the cam-mechanism (Maniar, 2006).

Additionally, it was noted that the fixed tibial insert was constraining the knee excessively leading to excessive stresses at the bone-implant interface. Therefore in order to circumvent these issues related to polyethylene wear different implant designs were developed, which focused on increasing implant conformity while reducing stresses transmitted to the bone-implant interface (Carothers *et al.*, 2011). Mobile-bearing (MB) inserts were developed in order to minimise shear stresses and the resulting polyethylene wear at the TF interface, thus providing less constraint on internal and external rotation for a more physiological motion of the implant while also indirectly correcting small tibial rotational misalignment which might occur surgically (Buechel and Pappas, 1986; Ranawat *et al.*, 2004). From a design perspective:

- Fixed bearing (FB) inserts consist of a polyethylene tibial insert which is locked within the tibial tray (Figure 28A), and

- Mobile bearing (MB) knees, consist of a tibial insert which is allowed to rotate, and in some instances also translate anteroposteriorly (AP), relative to the fixed tibial baseplate (Figure 28A and B).

While MB inserts were hypothesised to circumvent the issues of wear and dislocation due to high stresses generated at the interface between the femoral component and the fixed tibial insert, no differences in clinical outcomes and survivorship were found between FB and MB implants (Van der Bracht *et al.*, 2010; Jacobs *et al.*, 2012; Bistolfi *et al.*, 2013). Both FB and MB designs showed excellent survival rates of up to 95% in 10-year follow up studies (Ranawat, Luessenhop and Rodriguez, 1997; Buechel *et al.*, 2001; Huang *et al.*, 2003; Callaghan *et al.*, 2010). Conversely, MB implants were found to increase polyethylene wear due to the movement occurring at the tibial component and insert interface (backside wear). The issue of wear of the tibial insert was due to the high contact stresses which were occurring since the point of contact between the femoral component, and the tibial insert was very small, therefore resulting in large contact stresses at these contact point areas (this was further enhanced when used in conjunction with the PS feature). For this reason, ultra-congruent (UC) inserts were recently developed in an attempt to distribute these contact stresses at the TF interface, thus reducing the wear. UC inserts replaced the post-cam mechanism with a higher anterior wall and a deep-dish through (Figure 27D). The higher anterior wall theoretically acts as a replacement to the post-cam mechanism since it should prevent the paradoxical anterior subluxation of the femoral condyles with increased flexion

(Hofmann *et al.*, 2000; Laskin *et al.*, 2000), while the deeper through should increase the contact surface area, therefore, avoiding contact stress peaks and providing better stress forces distribution and also assuring stability of the knee (Figure 28D).
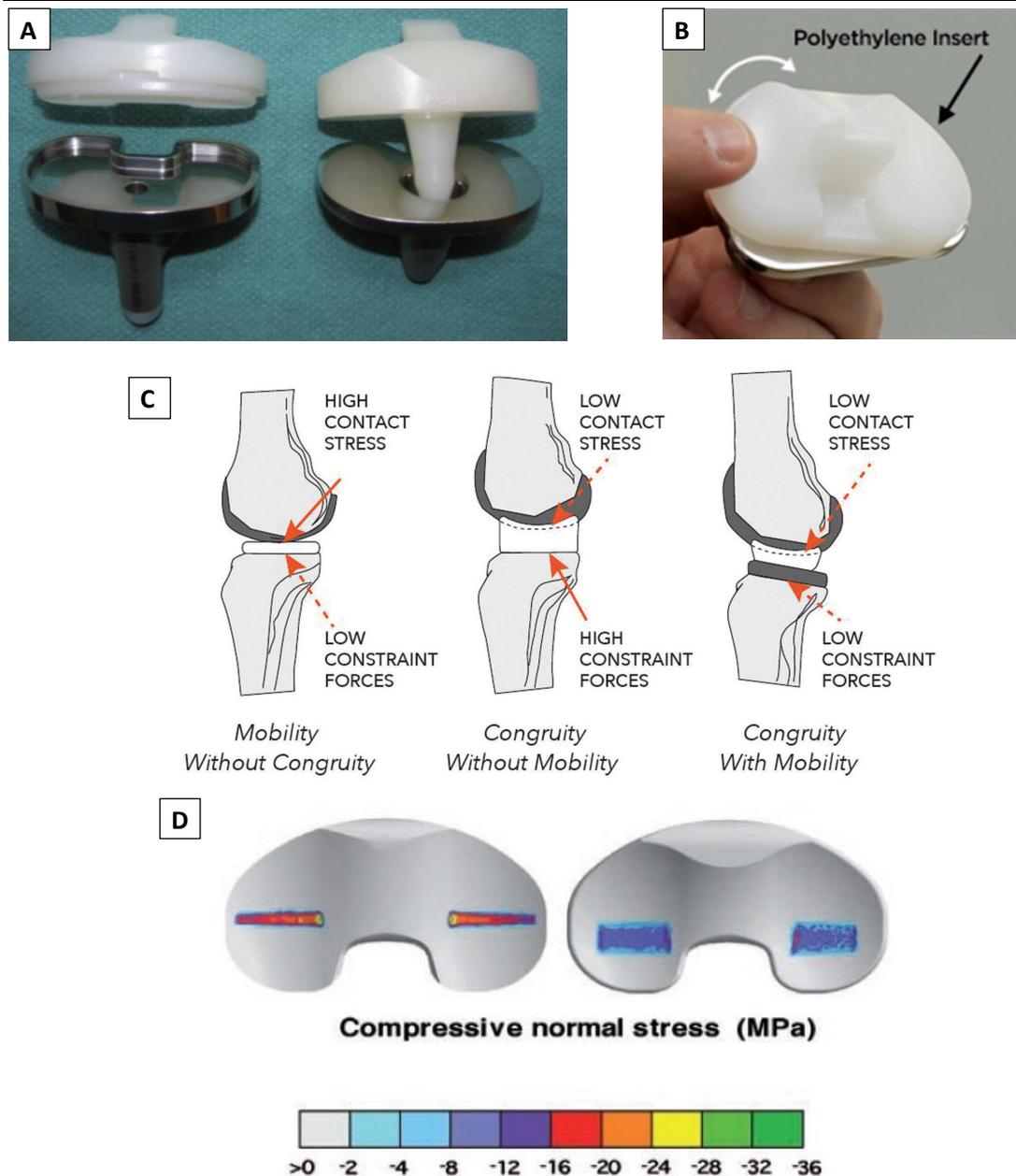
Figure 28: TKA prosthesis design: FB, MB and Congruency of the implant components.

A: Fixed-bearing (left) and mobile-bearing (right) designs. The fixed tibial liner fits tightly within the recess in the tibial base plate in order to restrict any sort of rotation or translation of the tibial liner with respect to the base plate. The mobile bearing liner has a stem which extends into the tibial baseplate to allow for stable rotation under load. (Post *et al.*, 2010)
B: A mobile-bearing design highlighting the rotating tibial liner on a tibial component.
C: Visualisation of the relation between bearing configuration, articulation stress and interface forces (Buechel and Pappas, 1989)
D: Surface contact stresses and related contact areas at 15º flexion and a 2600N axial load for a flat (left) and an ultra-congruent (right) tibial insert (Grupp *et al.*, 2009).

FB inserts with UC bearing surfaces were the first to be introduced. These designs provided low contact stresses due to high congruency, which allowed for better force dissipation at the TF interface. On the other hand, the high conforming bearing surfaces in conjunction with FB design produced high torque at the bone-implant interface due to the reduced freedom of movement at the contacting surfaces. This high torque, in turn, gets transferred to the bone-implant interface resulting in cement failure leading to early component loosening (Blunn *et al.*, 1997). In FB prosthesis, achieving low contact stress articulation along with low torque, cannot be realised due to its design limitation (Callaghan *et al.*, 2000). FB implants were ultimately known for two major causes of late failure (Huang, Liau and Cheng, 2007):

- Implant loosening when using the UC inserts, and

- High polyethylene wear when using non-UC inserts (PS models)

UC MB inserts were introduced with the aim of eliminating the aforementioned issues which were being faced with FB inserts. The UC MB insert is capable of achieving both congruency and mobility at the TF bearing surface (Figure 28C). This allows for low contact stresses and low constraint forces to be simultaneously achieved, therefore improving wear resistance and, theoretically, minimising implant loosening (Callaghan *et al.*, 2000).

To the author's knowledge, there are no papers directly comparing the kinematics of UC FB and UC MB implants. This limited amount of research on UC implants is reflected in a study performed in 2016 which reported that 50% of surgeons in the USA used PS implants while 42% used CR implants, therefore having only a subset of the remaining 8% of surgeons using UC implants (amongst other designs) in TKA (Vaishya, Agarwal and Vijay, 2016). The only identified literature which focused on UC inserts compared one of the two variants of UC inserts (FB or MB) with either PS or CR implants. Therefore, a short review of literature pertaining to the comparison of the kinematics of these type of inserts versus CR or PS will follow.

The most important degrees-of-freedom (DOF) when assessing the level of mobility of knee implants are the anteroposterior translation and axial rotation. In normal healthy knees, the anteroposterior translation and axial rotation with increasing flexion have already been adequately defined in section 2.4. In summary, the medial femoral condyle predominantly slides and rotates, demonstrating minor AP translation during flexion.

In contrast, the lateral condyle rolls and glides posteriorly on the tibial plateau with progressing flexion. The contrasting kinematic behaviour in the medial and lateral compartments lead to the coupled internal rotation of the tibia in relation to the femur during flexion (Freeman and Pinskerova, 2005). In a study by Dennis *et al.* (2003), whereby they looked at the AP translation of the medial and lateral condyle of 10 healthy knees, they noted that all 10 subjects experienced posterior motion of the lateral condyle throughout the entire ROM (from full extension to 90º of flexion). Nine out of the ten healthy knees showed the posterior motion of the medial condyle. On average, the lateral condylar motion was -19.2 mm (-5.8 to -31.6 mm; SD, 8.4) and medial condylar motion was -3.4 mm (3.3 to -11.8 mm; SD, 4.6) in the posterior direction. These values agree with those stated by the international team of Freeman. Also, all knees experienced posterior motion in both condyles through the entire ROM (Figure 29A).

Patients having fixed-bearing implants showed a relatively small amount (4.8 mm) of PFR in the lateral compartment during the first 60º of flexion, followed by a paradoxical anterior femoral translation from 60º to 90º of flexion (Stiehl *et al.*, 1997). In the study by Dennis *et al.* (2003), where they assessed the AP movement of 136 PCL-retaining and 163 PS fixed-bearing knees, they noted that in both knee modalities the resulting AP movement was significantly smaller in magnitude from that of the natural knee (Figure 29B and C). The PCL-retaining knees experienced -1.6 mm (-6.4 to 4.7 mm; SD, 3.4) of posterior motion on the lateral condyle, and 1mm (-4.3 to 6.1 mm; SD, 3.5) of anterior motion on the medial condyle (Figure 29B). On the other hand, the PS fixed-bearing knees experienced an average of -3.7 mm (-9.6 to 1.5 mm; SD, 3.3) posterior motion on the lateral compartment and -1.0 mm (-5.6 to 3.1 mm; SD, 2.7) posterior motion in the medial compartment (Figure 29C).

When compared with normal knees, FB knees tend to exhibit paradoxical anterior femoral sliding with increasing flexion. This paradoxical motion is normally noted in PCL-retaining and PS models. On the other hand, patients having PCL sacrificing UC MB implants showed 3.3 mm of PFR on the lateral condyle from 0-90º of flexion followed by anterior translation with further flexion, resulting in the TF contact points remaining near the middle of the articular surface of the tibial component (Callaghan *et al.*, 2000). Daniilidis *et al.*, 2012, compared non-UC and UC fixed CR implants and noted that UC tibial inserts improved AP stability (minimising the anterior paradoxical

motion), but also mentioned that physiological kinematics were far from restored when using UC inserts or fixed variants. Another study which compared fixed bearing UC and PS inserts concluded that they both resulted in similar kinematic patterns, showing a reduction in the rotation of the femur for both cases (Dennis *et al.*, 2005).
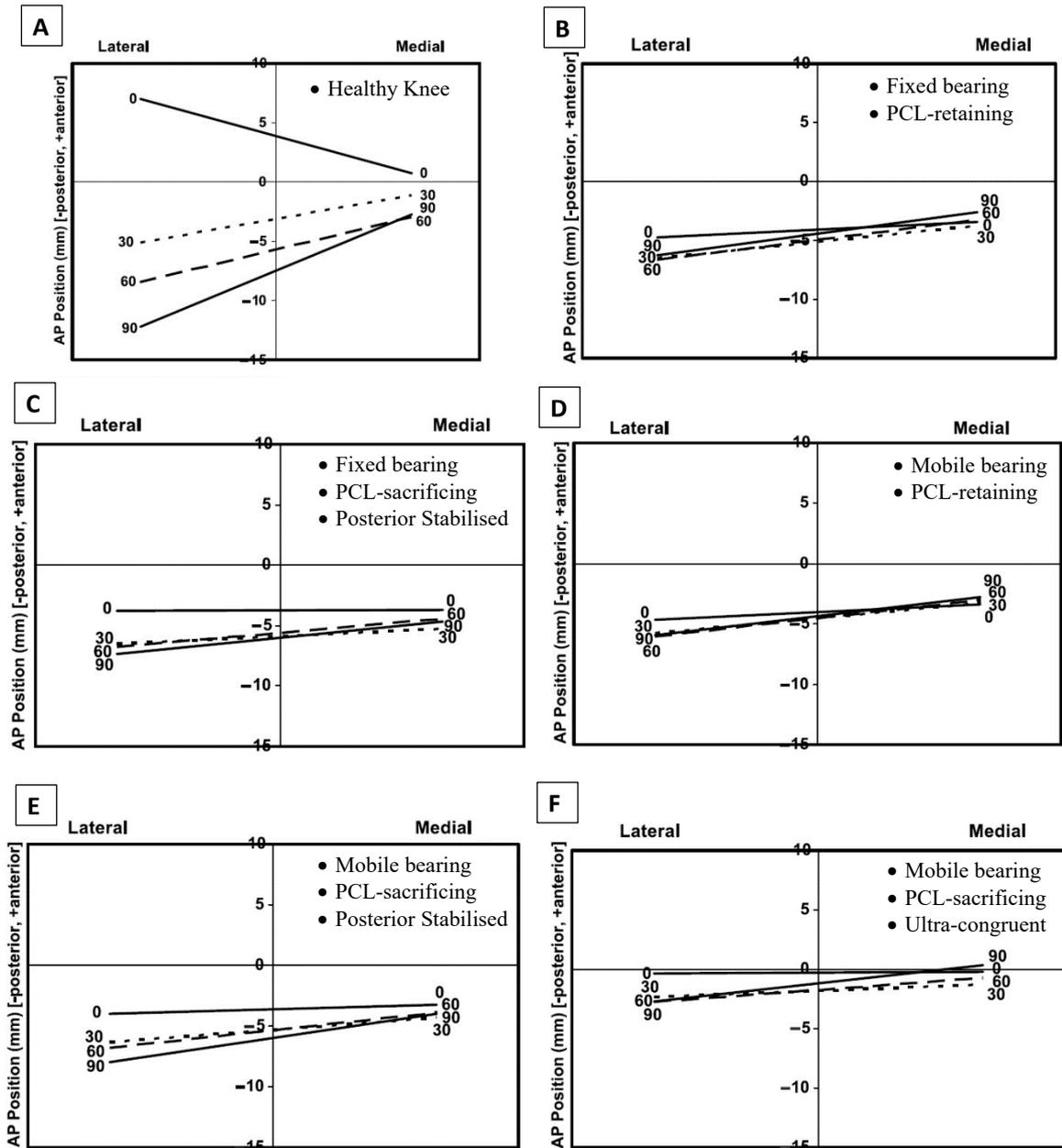
Figure 29: Average medial and lateral condyle contact positions during a deep knee bend (0-90º flexion) (Dennis et al., 2003)

A: The average AP movement of 10 healthy knees.
B: The average AP movement of 136 PCL-retaining fixed-bearing knees.
C: The average AP movement of 163 PS fixed-bearing knees.
D: The average AP movement of 69 PCL-retaining mobile-bearing knees.
E: The average AP movement of 103 PS mobile-bearing knees.
F: The average AP movement of 59 PCL-sacrificing mobile-bearing knees.

The characteristic paradoxical anterior sliding of the femoral component on the tibial insert is commonly noted in most traditional TKA designs and is also known as the concept of mid-flexion instability. This results in the patients feeling stability in their replaced knee at full-extension and beyond 90º of flexion, but experience instability between these two positions. This phenomenon, as reported above, is commonly noted in PCL-retaining and PS implants (Schmidt *et al.*, 2003). For PCL-retaining designs this instability occurs since the PCL is made up of several layers of fibres which are continually shifting their load amongst them, becoming taut and loose as flexion progresses (refer to section 2.2.2.3). When a section of the PCL becomes loose, this in turn results in loss of control, and stability, at the tibiofemoral interface thus allowing the femoral condyle to slip forward resulting in the paradoxical anterior movement. On the other hand, while PS designs experienced the largest AP movement on the medial side following cam-post engagement (beyond 60º of flexion), apparently, at cam-post engagement, the medial condyle experiences the greatest shear forces and translates anteriorly as the lateral condyle levers posteriorly.

Patients having MB designs show similar AP movements to those noted in FB designs. In the study of Dennis *et al.* (2003), three types of MB designs were assessed, namely PCL-retaining, PS and UC designs. The average AP translation experienced by the 69 PCL-retaining MB knees that were studied were, -1.3 mm (-7.1 to 5.2 mm; SD, 3.5) posterior movement at the lateral condyle and 0.4 mm (-6.8 to 5.9 mm; SD, 3.8) anterior movement at the medial condyle (Figure 29D). The similarity in the values between the FB and MB PCL-retaining designs is already apparent. The average AP translation experienced by the 103 PS MB knees that were studied were, -3.8 mm (0.9 to -9.0 mm; SD, 2.9) posterior motion of the lateral condyle and -0.7 mm (4.2 to -5.7 mm; SD, 3.0) posterior motion for the medial condyle (Figure 29E). Again, the similarity in both FB and MB PS knees is apparent in the values obtained for both knees. Finally, the average AP translation experienced by the 59 UC (PCL-sacrificing) MB knees that were studied were, -2.1 mm (-8.8 to 1.5 mm; SD, 2.8) posterior motion for the lateral condyle and 0.3 mm (-4.1 to 3.8 mm; SD, 0.3) anterior motion for the medial condyle (Figure 29F). This data for UC MB knees aligns with the data reported by Bellemans, Ries and Victor (2005), who reported that the lateral condyle moved posteriorly by an average 3.3 mm with 90º of flexion. They have also noted that in 40% of their cases, some anterior

paradoxical movement was noted, which agrees with the results reported by Dennis *et al.* (2003).

While a few studies are published about UC inserts, the few that exist mostly focus on Patient-Reported-Outcome-Measures, or PROMs (Goebel and Schultz, 2012; Hakki *et al.*, 2013), rather than the investigation of the kinematics of these implant variants. Reviewing the limited literature on FB and MB using UC, PCL-retaining and PS inserts, it was noted that high variations are reported with respect to PFR and AP kinematic patterns with no consensus being reached amongst the researchers on the implant design of choice. One conclusion that most researchers agreed upon was that normal knee kinematics are considered as a far cry when compared to the kinematics achieved using the knee implant designs which were investigated in this thesis (UC FB and UC MB). Furthermore, the kinematic differences between FB and MB knees are of minimal clinical significance. In the authors' opinion, the majority of the difference in the resulting knee kinematics are dependent on whether the insert is PCL-retaining and PCL-sacrificing (PS or UC), as noted in the results reported by Dennis *et al.* It appears that the potential to achieve more normal kinematics would involve a prosthetic design which incorporated congruency with guided motion. Ideally, the design features of an MB knee prosthesis would incorporate full conformity with the ability to translate posteriorly and externally rotate the femur with flexion. Because of the absence of functioning cruciate ligaments in TKA, this rotation and translation would somehow need to be driven by a design feature that does not interfere with congruency. It should be noted that the aforementioned does not take into consideration the novel medially-pivoted knee inserts and uni- and bi-condylar (i.e. two uni-condylar implants, thus maintaining both cruciate ligaments) prosthesis whose kinematics are beyond the scope of this thesis.

2.6   QUANTIFICATION OF KNEE KINEMATICS

In the last century, owing to the continuous exponential advancement in computer modelling technology, a paradigm shift has occurred in the approach taken to quantify knee kinematics. So far, in this text, the relative movement of the knee from the perspective of the functional anatomy has been elucidated. Performing an analysis like the one performed by Freeman's team (Iwaki, Pinskerova and Freeman, 2000 - section 2.4) to explain the relative movement of the knee requires an intricate analysis of the contours of the knee which is very demanding and time-consuming, making it impracticable on larger-scale studies. Furthermore, such a method does not allow for extracting the six DOF kinematics. In this chapter, the reader is taken through a series of discussions which build chronologically upon one another to offer a clear and logical understanding, backed by theory and scientific literature, of the way that scientists have developed their understanding of how to capture and analyse the intricate articulation of the knee on a milli-scale, that is, with millimetre accuracy. The knowledge learnt following this review of literature along with the pit-falls which will be pointed out will then be used to design a robust mathematical model which will then be implemented in the kinematic analysis software in the practical aspect of this thesis, to calculate the 4-dimensional kinematics of the human knee.

After capturing the dynamic movement of the knee and visualising the 4-dimensional articulation of the knee (discussed earlier in section 2.3), the theory of rigid-body kinematics is invoked to quantify the pose (position and orientation) of each bone in virtual space. Rigid-body kinematics employs local (or anatomic) coordinate systems (CSs) which are placed in specific anatomical locations within the femur and the tibia. These CSs allows engineers to extract the relative pose of the TF complex for every time-step (or frame) in a relatively simplistic manner. The theory of rigid-body kinematics will be introduced to the reader in section 2.6.1.

To confidently embed the CS in each of the rigid bodies (in our case these being the femur and tibia), the three axes of both anatomical CSs must be well defined so that accurate and repeatable results can be obtained between studies. Embedding a well-defined CS in the femur and the tibia is a very challenging feat, primarily due to the complex relative articulations that exist in the TF joint, which make it hard to identify the natural (also referred to as optimal or functional) axes around which the coupled rotational articulation occurs. Secondarily, the intra-patient knee morphological

variation is remarkably high, making it even harder to identify a standardised model which applies to all patients (Mahfouz *et al.*, 2012). An agreement amongst involved professionals that is surgeons, clinicians and engineers must be reached to have a standardised model which can be reliably used to compare reported results amongst studies with varying patient populations. Although the literature is converging towards an agreement on the definitions of the functional axes of the knee, at present, such a model is yet to be standardised. Technological advancement in medical imaging is opening new avenues, such as the emerging statistical atlas-based morphological variation models. This technology is focused on building models which take into account the statistical anatomical variations that exist in patient anatomy. Using such a morphological model will allow the standardised model (having all functional axes embedded accurately within it) to be morphed into patient-specific models thus accurately compensating for the variations that exist in the patients' anatomy while avoiding human-error when identifying anatomical regions-of-interest (ROIs).

In section 2.6.2, the principal axes of knee joint motion are discussed, with the aim of giving the reader a clear idea of the current definitions of these anatomical axes, as agreed upon in the literature. It should be noted that when discussing knee axes, one can either refer to the axes around which the DOF of the knee act (one single non-orthogonal CS), or else reference could be made to the local CSs of each bone, that is the orthogonal unit vectors of the femur and tibia (two separate CSs which are used to define the aforementioned DOF system). In section 2.6.2, the focus will be initially given to the DOF system, since the majority of the rotation within the knee occurs around these axes. Understanding the amount of kinematic crosstalk displayed by each proposed axes would assist in being able to define the kinematics of the knee accurately. The focus will be given to the principal rotational DoFs of the knee, which are the Flexion-Extension Axis (FEA) located in the femur and the Internal-External (rotation) Axis (IEA) located in the tibia. The review of the literature on these two axes will be outlined in a chronological order to be able to appreciate how and why different FEA and IEA emerged in the literature. Through the reviewed studies, preference will be given to specific axes based on published results. These axes will be modelled into the aforementioned mathematical model to be able to investigate further how the kinematics of the knee vary depending on which surrogate axes is used. The third, and final, rotational DOF that is Varus-Valgus rotation, and the three translations will be

defined in section 2.6.3.3, where the remaining local anatomical axes embedded within each bone, which are used to define the pose of the bones in space, will be defined. This would conclude the definitions of all axes used in the mathematical model implemented in this study.

Having the local CSs confidently defined and embedded in the femur and tibia, the next step is to choose a mathematical model which is capable of quantifying the six DOF kinematics of the relative movement occurring between subsequent captured frames. In the field of biomechanics, three primary methods are used to explain the kinematic behaviour of anatomical rigid-bodies (Incavo, Beynnon and Coughlin, 2005):

1. The instantaneous centre of rotation model (Reuleaux method),

2. The helical-axis model (twist axis, screw axis or axis of rotation), and

3. The Joint Coordinate System model (two-axis or coupled rotations model).

The former two models will be briefly explained in section 2.6.3 to explain the limitation imposed by such models. The latter model, which is the model that will be implemented in this thesis, has been utilised by numerous in-vitro and in-vivo studies since its conception (Hollister *et al.*, 1993; Piazza and Cavanagh, 2000; Most *et al.*, 2004; Eckhoff *et al.*, 2005; Yin *et al.*, 2015). The Joint Coordinate System (JCS) model has been developed specifically to facilitate communication between biomechanical engineers and clinicians. The JCS is ultimately a special case of defining the motion of a rigid body in 3D space using Euler angles. The application of this model to the knee was published in a ground-breaking paper by Edward Grood and Fred Suntay (Grood and Suntay, 1983). The JCS has been since applied to all the major joints in the human body and standardised by the International Society of Biomechanics (ISB) as the mathematical model to be used for kinematic studies of human joints (Wu *et al.*, 2002). The JCS has proved to be adequate for a comprehensive understanding of knee kinematics while not compromising accuracy and allowing for reporting results in clinically meaningful terms and anatomical planes.

To sum up, the upcoming discussion will have the following format. Section 2.6.1 presents a concise introduction to rigid-body kinematics to familiarise the reader with the mathematics which will be referred to in the subsequent sections. Sections 2.6.2 will define the current definition of the two principal rotational axes of the knee around which the coupled rotational articulation of the TF joint occurs. A chronological

overview of the prominent studies performed on the identification of these axes will be presented. Section 2.6.3 will discuss the three mathematical models briefly, concluding with the JCS model. This will conclude the review of the literature on the definition of the mathematical model of the knee utilised in the software of this study.

2.6.1 RIGID-BODY KINEMATICS

The concept of a rigid-body in mechanics is defined as a system of particles, that act as one unit, which does not deform under the influence of external forces, or simply that the deformation is negligible. The etymology of 'kinematics' is Greek, originating from "κίνημα", pronounced *kinema,* which means motion, thus kinematics being "the study of motion". Therefore, rigid-body kinematics is the study of the position and orientation of a rigid-body in 3-dimensional space over time (essentially time being the 4th dimension), without taking into consideration the forces acting on the body(-ies) in question. In the knee, the rigid-bodies are the bones, in our case these being the femur and the tibia.

The first step in analysing the kinematics of two relatively moving rigid-bodies is to have a clear description of the <u>position</u> and <u>orientation</u> (also referred to as the pose), and their changes over time. In order to determine the pose of a rigid-body, a *Local Coordinate Systems* (LCS) is embedded within the rigid-bodies being analysed. An LCS on its own is not sufficient to determine the pose, but this needs to be accompanied by a *Global Coordinate System* (GCS) in a fixed position in space, which will be used to reference the position and orientation of the moving LCSs. Theoretically, there are several CSs which can be utilised depending on the problem being analysed, such as cartesian, polar or spherical CSs. For the case of the knee, a cartesian CS is used, since this provides orthogonal results, which correspond, to a certain extent, with the anatomical six DOF system of the knee in a simplistic manner which facilitates communication between engineers and clinicians alike (Grood and Suntay, 1983). Furthermore, a considerable number of researchers use cartesian CS systems to report their findings, making it a better case for the comparison of data between studies.

A cartesian coordinate system (CCS) consists of three mutually perpendicular axes which meet at a unique point, called the origin. The axes are arranged according to the right-hand rule, such as the Red-Green-Blue (corresponding to the X-Y-Z axes respectively) coloured CSs shown in Figure 30. For the case of the knee, two local (or

anatomical) coordinate systems, one embedded in the femur and one in the tibia must be defined. For the time being, the exact location of the CSs will not be defined, as these will be discussed in further detail in section 2.6.2 and 2.6.3.
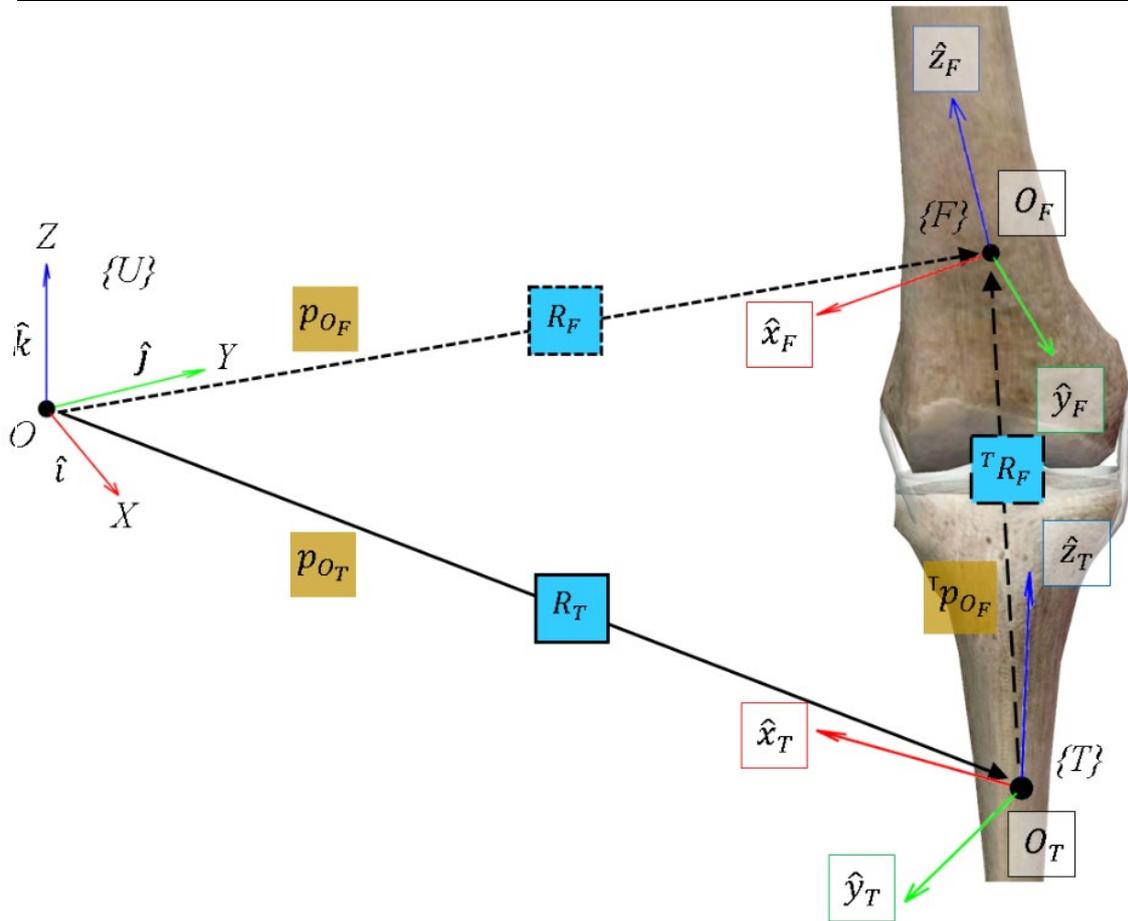
Figure 30: A generic rigid-body model of the knee for the determination of the pose (position and orientation) of the femur and tibia in space. (Author's rendition)

An illustration of the relation between the GCS, {U}, and two LCSs, {F} and {T}, embedded in the femur and tibia respectively. Refer to text for description of all shown variables.

Note: This diagram is not to scale, its only purpose is to help visualise the multiple references to the different CSs mentioned in the text.

With reference to Figure 30, let us assume that the LCS, {F}, is embedded in the femur, having an origin O_F and three perpendicular axes represented by the unit vectors $\widehat{x_F}$, $\widehat{y_F}$ and $\widehat{z_F}$ respectively. The same applies for the LCS, {T}, embedded in the tibia. Finally, the GCS, {U}, will be represented by the origin O and the unit vectors $\hat{\imath}$, $\hat{\jmath}$ and $\hat{k}$. The reader is referred to Figure 30 for a visualisation of the generalised CS model described above. With this generalised system in mind, the position of rigid-bodies F and T with respect to the GCS can be fully described by the relative position of the origins O_F and O_T with respect to O, or vice-versa. Also, the orientation of the Femur and the Tibia can be fully described by the direction of their axes (specifically the orthogonal unit

vectors making up the LCS) with respect to those of the GCS, or vice-versa. The vector and matrix manipulations required to define these mathematically will now be explained in order to provide a good foundation for this topic.

Let us assume we want to define the <u>position</u> of the femur with CS {F} in 3D space. The position of the femur can have multiple definitions. This is the case since the position of a rigid-body can be defined as expressed from any given CS. Thus, in our case, it is possible to define the position of the femur as expressed from either the LCS of the tibia or the GCS. In other words, the position of the femur changes depending from which CS it is expressed. Therefore, in order to specify which CS is being used to express the position of a rigid-body, vector notations are used when defining the position of an object in space. Let us assume that we want to define the position of the Femur as expressed in the GCS. First, two reference points, which will form the two ends of the position vector (or matrix if in matrix format), need to be defined. For simplicity, let us consider the origin of the femur LCS, O_F, and the origin of the GCS, O. With the two points defined, a position vector is drawn connecting the two points.

This position vector defines the position of the femur as expressed in the GCS as follows:

$$\overline{OO_F} = {}^{U}p_{O_F} = a\hat{\imath} + b\hat{\jmath} + c\hat{k} = [a \quad b \quad c]^T \qquad \text{(7)}$$

where, a, b and c are the corresponding X, Y and Z components of the distance from the GCS origin, O, to the LCS origin, O_F. It should be noted that when reporting the position of the femur as expressed from the GCS {U} we use the notation ${}^{U}p_{O_F}$ instead of the common vector notation $\overline{OO_F}$ for a line. The notation follows the standardised system where p_{O_F} is the position vector, and the superscript refers to the frame of expression (Huang, 2017), which can be omitted if the observation frame is the GCS, as in our case. Therefore, the right way to report the definition of the position of the femur as expressed from the GCS would simply be:

$$p_{O_F} = a\hat{\imath} + b\hat{\jmath} + c\hat{k} = [a \quad b \quad c]^T \qquad \text{(8)}$$

This system of reporting the position of a rigid-body in space is presented in Figure 30. The position vectors are referenced in the mustard-shaded boxes. The position vector

for the femur expressed in the GCS is p_{O_F}, the position vector of the tibia expressed in the GCS is p_{O_T} and the position vector of the femur expressed in the tibial LCS is $^Tp_{O_F}$.

The <u>orientation</u> of a rigid body is governed by the directions of the aforementioned unit vectors of the rigid-body in question with respect to the orthogonal unit vectors of another CS. First, let us again assume we want to determine the orientation of the femur with respect to the GCS. In order to define the orientation of the femur, the direction cosine, or the angle, of each unit vector of {F} with each unit vector of {U} needs to be determined (i.e. nine permutations). The direction cosine between two vectors in 3D space is determined by using the dot product as follows:

$$\hat{\imath} \cdot \widehat{x_F} = \cos\theta \qquad (9)$$

In equation 9, the angle θ represents the angle formed between the {U} x-axis unit vector, $\hat{\imath}$, and the {F} x-axis unit vector, $\widehat{x_F}$. Each unit vector in {F} forms three angles, one with each of the unit vectors of {U}. Therefore, the orientation of the unit vector $\widehat{x_F}$ with respect to the GCS would be composed as follows:

$$^U\widehat{x_F} = \widehat{x_F} = (\widehat{x_F} \cdot \hat{\imath})\hat{\imath} + (\widehat{x_F} \cdot \hat{\jmath})\hat{\jmath} + (\widehat{x_F} \cdot \hat{k})\hat{k} \qquad (10)$$

On the left-hand side of equation 10, $^U\widehat{x_F}$ is the notation for the vector representing the orientation of $\widehat{x_F}$ with respect to {U} and on the right-hand side, in vector format, are the three direction cosines that $\widehat{x_F}$ exhibits with the three orthogonal unit vectors of {U}. This can also be reported in matrix format as follows:

$$\widehat{x_F} = \begin{bmatrix} \widehat{x_F} \cdot \hat{\imath} \\ \widehat{x_F} \cdot \hat{\jmath} \\ \widehat{x_F} \cdot \hat{k} \end{bmatrix} \qquad (11)$$

The same can be derived for the orientation of $\widehat{y_F}$ and $\widehat{z_F}$ with respect to {U}:

$$^U\widehat{y_F} = \widehat{y_F} = (\widehat{y_F} \cdot \hat{\imath})\hat{\imath} + (\widehat{y_F} \cdot \hat{\jmath})\hat{\jmath} + (\widehat{y_F} \cdot \hat{k})\hat{k} = \begin{bmatrix} \widehat{y_F} \cdot \hat{\imath} \\ \widehat{y_F} \cdot \hat{\jmath} \\ \widehat{y_F} \cdot \hat{k} \end{bmatrix} \qquad (12)$$

$$\widehat{^U z_F} = \widehat{z_F} = \left(\widehat{z_F} \cdot \hat{k}\right)\hat{k} + \left(\widehat{z_F} \cdot \hat{j}\right)\hat{j} + \left(\widehat{z_F} \cdot \hat{k}\right)\hat{k} = \begin{bmatrix} \widehat{z_F} \cdot \hat{\imath} \\ \widehat{z_F} \cdot \hat{j} \\ \widehat{z_F} \cdot \hat{k} \end{bmatrix} \qquad (13)$$

Combining equations 11, 12 and 13, the rotation matrix, R_F, describing the orientation of the femur with respect to the GCS can be assembled as follows:

$$^U R_F = R_F = [\widehat{x_F} \quad \widehat{y_F} \quad \widehat{z_F}] \qquad (14)$$

$$R_F = \begin{bmatrix} \widehat{x_F} \cdot \hat{\imath} & \widehat{y_F} \cdot \hat{\imath} & \widehat{z_F} \cdot \hat{\imath} \\ \widehat{x_F} \cdot \hat{j} & \widehat{y_F} \cdot \hat{j} & \widehat{z_F} \cdot \hat{j} \\ \widehat{x_F} \cdot \hat{k} & \widehat{y_F} \cdot \hat{k} & \widehat{z_F} \cdot \hat{k} \end{bmatrix} \qquad (15)$$

It can be noted that the column vectors of R_F consist of the direction cosines of the axes of {F} with respect to the axes of{U}, while the row vectors consist of the direction cosines of the axes of {U} with respect to the axes of {F}. Since the matrix is composed entirely of direction cosines, R_F is also referred to as a direction cosine matrix (DCM). Furthermore, it should be noted that this kind of 3x3 matrix is an orthonormal matrix. This is because the rotation matrix obeys the following rule:

$$[R_F]^{-1} = [R_F]^T \qquad (16)$$

As a result of the above relationship, if the reverse orientation is required, i.e. {U} with respect to {F}, then all that is required is to calculate the transpose of the rotation matrix rather than having to calculate the inverse of the matrix, giving the following DCM:

$$[R_F]^{-1} = {}^F R_U = {}^F R = \begin{bmatrix} \widehat{x_F} \cdot \hat{\imath} & \widehat{x_F} \cdot \hat{j} & \widehat{x_F} \cdot \hat{k} \\ \widehat{y_F} \cdot \hat{\imath} & \widehat{y_F} \cdot \hat{j} & \widehat{y_F} \cdot \hat{k} \\ \widehat{z_F} \cdot \hat{\imath} & \widehat{z_F} \cdot \hat{j} & \widehat{z_F} \cdot \hat{k} \end{bmatrix} \qquad (17)$$

In order to determine the orientation of one LCS with another, such as in the case of determining the orientation of {F} with respect to {T}, the same procedure as above is performed, resulting in the following DCM:

$$^T R_F = \begin{bmatrix} \widehat{x_F} \cdot \widehat{x_T} & \widehat{y_F} \cdot \widehat{x_T} & \widehat{z_F} \cdot \widehat{x_T} \\ \widehat{x_F} \cdot \widehat{y_T} & \widehat{y_F} \cdot \widehat{y_T} & \widehat{z_F} \cdot \widehat{y_T} \\ \widehat{x_F} \cdot \widehat{z_T} & \widehat{y_F} \cdot \widehat{z_T} & \widehat{z_F} \cdot \widehat{z_T} \end{bmatrix} \qquad (18)$$

Again, this system of reporting the orientation of a rigid-body in space is presented in Figure 30. The orientation DCMs are referenced in the azure-shaded boxed. The orientation of the femur with respect to the GCS is R_F, the orientation of the tibia with respect to the GCS is R_T and the orientation of the femur with respect to the tibial LCS is $^T R_F$.

It should be noted that rotation matrices are not only used for determining the orientation of a rigid body in 3D space, also referred to as passive interpretation. They can also be used to rotate a rigid body's LCS onto the LCS of another rigid-body, which is referred to as active interpretation. Both techniques will be exploited in the kinematic analysis software designed for this study.

Rotation matrices, or DCM, can be combined with position matrices to form Transformation Matrices (TMs) which can be used to perform homogeneous transformations of rigid-bodies in three-dimensional space. Taking the case that we require to transform the femur (i.e. its rigid-body coordinates) from the Femur LCS {F} into the GCS {U}, the following transformation matrix, $^U T_F$, is formulated:

$$^U T_F = \begin{bmatrix} \widehat{x_F} \cdot \hat{\imath} & \widehat{y_F} \cdot \hat{\imath} & \widehat{z_F} \cdot \hat{\imath} & a \\ \widehat{x_F} \cdot \hat{\jmath} & \widehat{y_F} \cdot \hat{\jmath} & \widehat{z_F} \cdot \hat{\jmath} & b \\ \widehat{x_F} \cdot \hat{k} & \widehat{y_F} \cdot \hat{k} & \widehat{z_F} \cdot \hat{k} & c \\ 0 & 0 & 0 & 1 \end{bmatrix} \tag{19}$$

The green 3x3 sub-matrix is the rotational matrix derived in equation 15, and the orange 3x1 sub-matrix is the position matrix derived in equation 8. A square matrix is obtained by adding the row [0 0 0 1] in the bottom of the TM. With the above TM, any coordinates in {F} can be transformed (i.e. rotated and translated) into {U}. Let $^F c = \begin{bmatrix} ^F c_x & ^F c_y & ^F c_z \end{bmatrix}$ be coordinates on the femur, described in the {F} LCS. Then, in order to transform $^F c$ into {U}, the following matrix manipulation is performed:

$$\begin{bmatrix} ^U c_x \\ ^U c_y \\ ^U c_z \\ 1 \end{bmatrix} = [^U T_F] \begin{bmatrix} ^F c_x \\ ^F c_y \\ ^F c_z \\ 1 \end{bmatrix} \tag{20}$$

The resulting coordinates, $^U c = \begin{bmatrix} ^U c_x & ^U c_y & ^U c_z \end{bmatrix}$, are the transformed femur coordinates. Taking the case of transforming the entire femur, the above manipulation would translate the femur onto the GCS origin, O, and rotate the rigid-body onto the

GCS unit vectors, $[\hat{\imath} \quad \hat{\jmath} \quad \hat{k}]$, as its orthogonal axes, rather than its pre-transformed LCS unit vectors, $[\widehat{x_F} \quad \widehat{y_F} \quad \widehat{z_F}]$. It should be noted that this kind of TM is also referred to as an affine TM since it does not scale or shear the rigid-body.

The mathematical manipulations explained in this section will be referenced in the subsequent sections in order to assist the reader in better understanding the upcoming discussions on the mathematical models of the knee, namely the calculation behind the implementation of the Joint Coordinate System model (sections 2.6.3.3 and 4.2.7.3).

2.6.2 AXES OF KNEE JOINT MOTION

As explained earlier in section 2.4, knee kinematics can be described by three rotations and three translations about the three planes of knee joint motion. In clinical terminology, the three rotational displacements of the knee are defined as follows:

1. Flexion/extension: about an axis in the ML direction,

2. Internal/external rotation: about an axis along the length of the tibia, and

3. Adduction/abduction: about an axis in the AP direction.

The three translational displacements are defined with respect to (w.r.t) the tibia as follows:

1. Mediolateral shift: along the axis in the ML direction,

2. Compression-Distraction: along the axis in the proximodistal (PD) direction,

3. Anteroposterior draw: along the axis in the AP direction.

These definitions do not fully describe the motion involved until the locations of the anatomical reference axes are adequately identified. Describing the clinical rotations and translations in these general terms is not enough and thus unacceptable in a kinematic study. To quantify the knee kinematics in an experimental setting, there needs to be a clear understanding of how to correctly position the anatomical LCS axes, in a repeatable and reliable manner. If the axes of an anatomical LCS are not defined according to the anatomical axis around which the knee rotates, then the reported data will be misleading. Axes misplacement results in the phenomenon known as kinematic crosstalk. Kinematic crosstalk occurs since rotations and translations happening around a misplaced axis will describe rotations (and translations) occurring around (or along) another axis, thus reporting misleading results. An example of kinematic crosstalk is

given in section 2.4.3, whereby the FCA (Flexion Condylar Axis) is noted to display 2 mm of out-of-plane motion in the distal and anterior directions w.r.t the ECA (Extension Condylar Axis) during the Extension Phase. In this section, a review of published literature on the definitions (i.e. the position and orientation w.r.t the known anatomical regions of interest) of the axes of the knee up to the present time will be outlined.

This must be born in mind when comparing studies that were conducted under different loading conditions (in vitro) or activities (in vivo). These variations in methodologies result in dissimilarities in the reported results, which, although minute, create inconsistencies when relating them to each other. Due to the complex relative articulations that exist in the TF joint, identifying the functional (also referred to as natural or optimal) axes around which the bones articulate is subjective. The knee axes may vary depending on the activity being performed since the passive restraints of the soft-tissue sleeve, and active restraints of the muscles are activity-dependent While the adaptability of the passive and active restraints allows the knee to cater for the demanding strenuous environment which the knee endures daily, this adaptability results in functional axes which vary depending on the activity being performed (Berme, Engin and Correia da Silva, 1985; Churchill *et al.*, 1998). Also, the intra-patient knee morphological variation is remarkably high (Mahfouz *et al.*, 2012), making it even harder to identify a standardised model which applies to all patients. Due to these reasons an agreement amongst involved clinicians and engineers, on the location of the functional axes of the knee, has not yet been reached.

Due to these confounding variables, attention to detail will be given to the upcoming sub-sections, mainly regarding the FEA and to a certain extent the IEA, since these axes are responsible for the largest ROM in the knee, thus displaying the largest variability under different loading scenarios. The meticulous approach taken for these two principal axes in the following text has been well verbalised by Churchill *et al.* (1998) with the following quote from one of the key papers which will be reviewed in this section:

> *"Proper positioning of the optimal flexion and longitudinal rotation axes is critical. They are not necessarily perpendicular, nor are they aligned with the conventional anatomic planes. When the axes are located properly, all motions of the knee can be accounted for by simultaneous rotations about them."*

The remaining rotational DOF, the abduction-adduction axis, will not be discussed in detail since it is not as activity dependant as the former two axes, while also having marginal movement relative to the other two axes. The definitions of the femoral and tibial anatomical co-ordinate systems w.r.t the anatomical ROIs in the corresponding bone will be covered in section 2.6.3.3. In that section, an in-depth explanation of the kinematic knee joint mathematical model implemented in the practical aspect of this thesis will be described. The purpose of this review is to confidently identify and define the locations of the FEA and the IEA within the tibial and femoral LCSs, to understand better the kinematic data collected during the practical aspect of this thesis.

2.6.2.1   THE FLEXION-EXTENSION AXIS

Note: In this review of literature, reference is made to two different femur FEA models. For clarification purposes, the two models will be defined here:

- Singular-FEA model theory: This approach uses the assumption that the femur rotates around a single FEA from hyper-extension through to terminal flexion. This model is an over-simplification of the articulation which occurs within the knee since, as mentioned in section 2.4, the femur has been noted to rotate around two axes, the ECA and the FCA. Unfortunately, this model is the most used and referenced type of the two, probably due to its simplified approach. While simplification of a complex scenario is always preferred, one must always keep in mind the assumptions being taken when implementing such a model.

- Dual-FEA model theory: This approach follows the definitions of Freeman's team (Iwaki, Pinskerova and Freeman, 2000), where the femur is modelled to rotate around two separate FEAs. This model is the most accurate since it eliminates the effects of kinematic crosstalk, but it is not easy to implement since the effective ROM of the ECA and FCA are subjective and not easy to identify. Also, there is yet no consensus amongst researchers regarding an anatomically defined surrogate to the ECA, making it even harder to accurately locate in-situ.

The advent of the identification of the FEA of the knee

The first documentation of the morphology of the femur was performed by the Weber brothers in an anatomical study of the knee (Weber and Weber, 1837). They were the first to describe the circular contour of the posterior femoral condyles, but they did not correlate their results to the kinematics of the knee (Figure 31A). The work of the Weber brothers was dismissed for the more than a century due to numerous researchers contradicting their work, reporting that the condyles were of a helical shape rather than circular (Braune and Fischer, 1891; Zuppinger, 1904). This occurred since most researchers were analysing the knee in the true-sagittal plane sections, which showed them a skewed cross-section of the knee, resulting in elongated profiles of the condyles. Nevertheless, the circular profile of the knee was brought back to light in the 1970s when a number of researchers reported the FEA to pass through the centres of spheres fitted to the posterior femoral condyles (Smidt, 1973; Lewis and Lew, 1978). Due to the asymmetric nature of the condyles, they reported that the FEA would result in an inclined axis which would produce a coupled rotation (with the IEA) that is nowadays known to occur in the knee (also known as the compound-axis, or two-axis model of the knee).

The inadvertent push towards the singular-FEA model theory (the cTEA versus the GCA)

A prominent study by Hollister tested the theory of a fixed Functional FEA (FFA) in the femur, which is offset to the sagittal plane (Hollister *et al.*, 1993). Hollister *et al.* (1993) used an engineering tool, called the "Axis finder" on cadaver specimens to identify the FFA around which most of the articulation of the knee occurs. It was concluded that a fixed FFA exists, and is offset by 7° to the sagittal plane, while a secondary, yet independent, axis for longitudinal rotation of the knee also exists and is fixed in the tibia (detailed in section 2.6.2.2). The clear identification of the two fixed functional axes of the knee revolutionised the way knee kinematics research was heading at the time. Hollister concluded that the fixed FFA passes through the origins of the collateral ligaments (MCL and LCL) and passes superior to, but not coinciding with, the intersection of the cruciate ligaments. This relationship to the functional anatomy of the knee, supported the statement of Hollister since it is assumed that the anatomical structures of the knee evolved to support its functionality most efficiently. Having the major axis of rotation of the knee coincide with the four major ligaments of

the knee is surely not a result of coincidence but more a matter of evolution driving towards an efficient and stable movement.
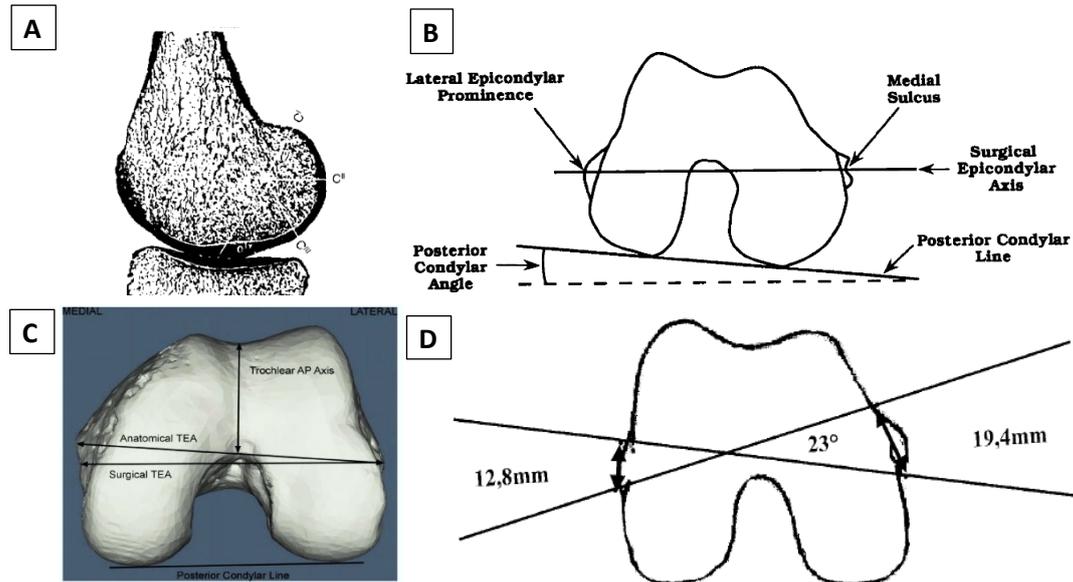
Figure 31: The surrogate axes of the FFA of the distal femur.

A: A cross-sectional image of the femoral condyles by the Weber brothers in 1837. This was obtained by cutting cadaveric specimens, coating them with ink, and pressing them on paper. They found radii C^I, C^{II} and C^{III} to be equal. (Weber and Weber, 1837).
B: A distal view of the distal femur showing the location of the surgical TEA and it's relation to the PCA. (Berger *et al.*, 1993)
C: A view of the distal femur with the rotational reference axes projected in the axial plane. Emphasis is given here to the difference in location of the sTEA (surgical) and the cTEA (anatomical). (Victor, 2009)
D: A depiction of the average measurement error for the angle variation noted when surgeons were asked to identify the cTEA intraoperatively. (Jerosch *et al.*, 2002)

Inadvertently this study was one of the first to promote the singular-FEA model theory of the femur. Considering its ground-breaking impact in the field of knee kinematics, this theory was allowed to 'reign' until the contradicting evidence-based research papers of Freeman *et al.* (2000) were published.

From a surgical perspective, the results reported by Hollister *et al.* (1993) were also in line with the current research being performed at the time on establishing a surrogate axis for surgeons to utilise intraoperatively. At the time, surgeons had three principal intra-operative techniques of identifying a surrogate axis for the FFA of the knee. The surrogate axis[2] is used to align the femoral component in the axial plane to the neutral

---

[2] To avoid confusion amongst the mentioned axes throughout this text, the principal <u>kinematic</u> surrogate axes are the cTEA, sTEA, ECA, FCA and GCA, while the <u>surgical</u> surrogate axes used for intra-operative alignment are the cTEA, sTEA, APA (Whiteside Line) and the PCL (Posterior Condylar Line). In this text focus is given to the kinematic surrogate axes. The surgical surrogate axes are only mentioned briefly for context.

rotational alignment of the native knee. Choosing the right surrogate axis is imperative since even a few degrees of rotational malalignment will result in unbalanced loads on the implant-bone interface and irregular tensions in the ligaments throughout the ROM. Rotational malalignment still accounts for an unacceptable number of failures in TKA (Victor, 2009). At the time of Hollister's study, incessant controversy existed amongst researchers and surgeons alike on the preferred choice of a surgical surrogate axis. The three principal surrogate axes were:

1. The anteroposterior axis (APA), also known as the Whiteside Line. The APA is perpendicular to a line connecting the deepest point in the sulcus of the femoral groove anteriorly and the deepest point of the intercondylar notch posteriorly (Figure 31C).
2. The Posterior Condylar Axis (PCA), which is at a tangent with the two most posterior points on the femoral condyles when the knee is at 90° of flexion (i.e. the position of the knee when the surgeon is working on the femoral cuts intra-operatively).

3. The Transepicondylar Axis (TEA), which has two variants, the clinical (or anatomical) TEA and the more recent surgical TEA. The clinical TEA (cTEA), which was first defined by Yoshioka *et al.* is formed by connecting the lateral epicondyle with the medial epicondyle (Yoshioka, Siu and Cooke, 1987a). This is termed clinical or anatomical, since these two anatomical locations are easily palpable, making it ideal for estimating the TEA of the knee in a clinical setting. The surgical TEA (sTEA), which was first defined by Berger *et al.* is found by connecting the lateral epicondyle with the centre of the sulcus of the medial epicondyle (Berger *et al.*, 1993). This is termed surgical since, at the time of its definition, the medial sulcus could only be identified intraoperatively since it lies underneath the deep soft-tissue sleeve of the knee.
Contemporarily, the medial sulcus is being also identified pre-operatively during the surgical planning stages using CT or MRI imaging. The reader is referred to Figure 31B and Figure 31C for an illustration of the relationship amongst the three surrogate axes mentioned above.
The TEA, in contrast with the PCA and the APA, has the important advantage of not being defined by the articular surfaces. If the patient's knee is deformed, which is the case in patients with osteoarthritis, condylar hydroplasia or condylar erosion, this would impede the surgeon's ability to accurately locate the PCA and the APA intra-operatively. Also, taking the case of revision surgeries, the articular surfaces are unusable, making it impossible to use the PCA and the APA for rotational alignment.

On the other hand, if the surgeon uses the TEA when working on deformed, arthritic or replaced knees, the rotational reference can still be estimated since the epicondyles are rarely symptomatic.

Studies analysing the accuracy of these surrogate axes suggested that the surgeons' ability to accurately and reproducibly identify the epicondyles is poor (Griffin *et al.*, 2000; Kinzel, Ledger and Shakespeare, 2005; Hatayama *et al.*, 2011). One notable study reported a significant variance of 22.3mm on the medial side and 13.8mm on the lateral side (Jerosch *et al.*, 2002) resulting in a rotational discrepancy of 23°, which is clinically unacceptable (refer to Figure 31D). The larger discrepancy on the medial side occurs because the medial epicondyle lies somewhere along the relatively long crescent-shaped ridge of the sulcus (Figure 32A) with no single discernible prominence, thus resulting in a large variability when identifying the medial epicondyle.
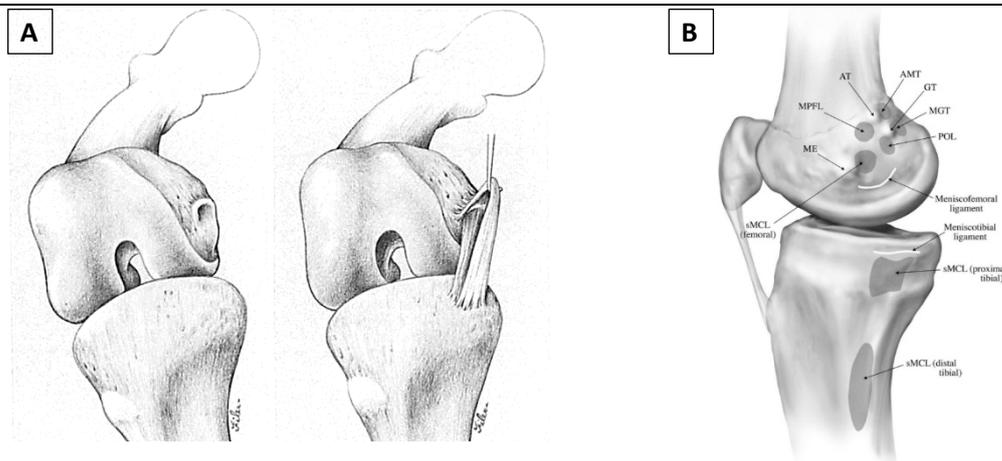
Figure 32: The sulcus of the medial epicondyle of the knee

A: An artist's depiction of the bony anatomy of the medial sulcus (left) and the crescent-shaped prominence encircling it. The apex of the medial epicondyle is located along the crescent thus the variability in identifying the epicondyle (apex). The two separate ligamentous tissue of the MCL is shown on the right, with the deep fibres of the MCL attaching in the sulcus and the superficial fibres attaching onto the crescent-shaped prominence. Refer to text for more detail. *(Berger et al., 1993)*
B: An illustration of bony landmarks and attachment sites on the medial side of the distal femur. The attachment site of the MCL (sulcus) is shown (labelled sMCL in the figure). Its location with respect to the medial epicondyle (labelled ME) can be noted. (LaPrade, 2007)

Another study evaluated the accuracy of identifying the epicondyles intraoperatively concluding that the cTEA was an unreliable landmark and should not be relied upon as the sole determinant for femoral component rotation in TKA (Katz *et al.*, 2001). The study by Katz *et al.* (2001) did not investigate the sTEA. Further studies comparing the cTEA, APA and PCA techniques noted that a range of error greater than 5° occurred in 56% of the time surgeons tried locating the cTEA, 72% for the PCA and 60% for the APA (Yau, Chiu and Tang, 2007). While such results are worrying in terms of accuracy,

the cTEA was, relatively, still the most accurate method to intraoperatively use as a reference for the FFA. Berger *et al.* defined the sTEA as being a more accurate location of the conventional cTEA when approximating the FFA (Berger *et al.*, 1993). This statement was based solely on an anatomical perspective since upon careful inspection of the MCL it was noticed that its point of origin (the deep fibres of the MCL) is

embedded within the sulcus (Figure 32A). It can be noted that the distance between the medial sulcus and the medial epicondyle (the inconsistent location on the ridge of the sulcus) is relatively small (Figure 32B), resulting in a slight angular deviation between the sTEA and cTEA (Figure 31C). Taking into consideration that minor malrotation of 1-4° will result in lateral patellar tracking and other unbalanced tissue loads (Victor, 2009), the angle between the two variants of the TEA will have a considerable effect on the kinematics of the knee, and thus should not be underestimated.

Returning to Hollister's statement that the FFA is a line located at the origins of the collateral ligaments, the sTEA would, therefore, from an anatomical perspective, be a better approximation of the FFA. Studies investigating the kinematic effect of these two TEA variants on the knee kinematics will be revisited below in order to follow the chronological order of developments in the identification of the FFA.

While Hollister's study provided vital information on the biomechanics of the knee, it was still questioned in some aspects by other researchers (Bull and Amis, 1998). The major drawbacks of her study were the Axis Finder, which modelled the knee as a 3 DOF system without considering the translations involved during knee motion, and the fact that the experiments were performed on an unloaded knee. Thus, Churchill *et al.* performed an in-vivo study whose purpose was to verify and build on the data collected by Hollister (Churchill *et al.*, 1998).

The study was aimed at locating the functional axes of the knee (i.e. the FFA and IEA) this time under realistic load-bearing conditions. The author hypothesised that a compressed knee joint might tend to seat the medial femoral condyle in the sulcus of the medial tibial plateau, thus reducing its mobility. This weight-bearing effect was hypothesised to alter the location of the functional axes, leading to different kinematics. Rather than using a mechanical axis finder, the authors used a mathematical modelling technique developed by the authors themselves (Churchill *et al.*, 1996). It was called the compound hinge model, which was used to identify the functional flexion and

longitudinal rotation axes for the ROM of 5° to 90°. Secondarily, the study investigated the relationship between the identified FFA and the cTEA and the Geometric Centre Axis (GCA - coincident with the FCA defined in section 2.4). In Hollister's study, the location of the identified FFA was not referenced to any surrogate FEA (such as cTEA) but only gave quantitative descriptions of its location.

Churchill *et al.* (1998) reported that the FFA was found in all cases to pass through the posterior femoral condyles but not precisely through their centres. It was reported that the distance between the FFA and the GCA averaged 2.8 mm (± 1.2 mm) medially and 3.1 mm (± 1.8 mm) laterally. On the other hand, when comparing the FFA to the cTEA, it was reported that the medial epicondyle was 0.2 mm (± 2.4 mm) posterior and 0.14 mm (± 2.7 mm) distal from the FFA, while the average lateral epicondyle position was 0.2 mm (± 2.7 mm) posterior and 0.6 mm (± 2.9 mm) distal to the FFA. The FFA was on average at an angle of 2.9° (± 1.2°) with the cTEA. The FFA was oriented between 5° and 10° to the sagittal plane, running posteriorly and distally from medial to lateral. Also, they reported that the medial to lateral condyle ratio was on average 1.125 (± 0.023). The study concluded, based on a statistical analysis of the data collected, that there was no statistically significant difference between the FFA and the cTEA. Nonetheless, the authors concluded that two good surrogates of the FFA could be used for kinematics studies, namely the cTEA and the GCA.

Additionally, Churchill *et al.* (1998) referred to previous studies that reported a moving axis of rotation. They pointed out that previous studies which reported a moving axis of rotation are not contradictory to their study, but they suggested that these studies introduced a confounding variable in their experimental setup. Churchill *et al.* (1998) stated that if an anatomical joint has more than one major axis of rotation, such as the knee, then it is bad practice to limit the joint to rotate solely around one axis of rotation in an experimental setting. While this technique was used by several researchers (whose work is not reviewed here for this reason) to isolate and identify a single axis of rotation (Soudan, Van Audekercke and Martens, 1979; van Dijk, Huiskes and Selvik, 1979; Shiavi *et al.*, 1987a, 1987b; Jonsson, Kärrholm and Elmqvist, 1989; Blankevoort, Huiskes and de Lange, 1990), this matter was being overlooked. In essence, these experiments were simulating a closed kinematic chain scenario (refer to definition in section 2.4.3), whereby they considerably reduced the DOF of the knee. When one of the rotational axes is not allowed to move, the resulting kinematics will change such

that the axis that is allowed to rotate does not remain fixed but will move to accommodate for the reduction in the DOF of the anatomical joint. Thus, they concluded that when both axes of rotation are allowed to move freely, the axes can then be assumed to be fixed in the bone in which they reside. This train of thought was later backed by Eckhoff *et al.* (2001) in his manuscripts (discussed in the following paragraphs).

The theory advocated by Hollister *et al.* (1993) and Churchill *et al.* (1998) of a fixed singular-FEA model of the femur being composed of an axis lying between the GCA and the TEA was supported by several other researchers who performed in vivo and in vitro studies arriving at similar conclusions (Kurosawa *et al.*, 1985; Yoshioka, Siu and Cooke, 1987b; Berger *et al.*, 1993; Siu *et al.*, 1996). Nonetheless, this theory was later challenged by the manuscripts of Freeman *et al.* in 2000. With reference to section 2.4, their manuscripts stated that during active flexion the knee rotated about two fixed FEAs, namely the ECA from -5º through to 10º of flexion and the FCA (which reflects the location of the GCA) from 30º through to 120º of flexion, with a transitionary phase between 10º and 30º of flexion. This defined the dual-FEA model theory. It should be noted that the work of Hollister *et al.* (1993) and Churchill *et al.* (1998), is in no way incorrect, but is simply an attempt at simplifying our perception of knee motion by describing the movement of the femur to occur around a single fixed axis. Implementing the singular-FEA model theory can be sufficient for the analysis of knee kinematics, if and only if, the assumptions being taken when implementing such a model are known in order to be able to appropriately interpret the resulting data from such a 'simplified' model. While Freeman *et al.*'s (2000) dual-FEA model theory is still considered as the gold-standard until nowadays, implementing such a model can be tedious and demanding. For this reason, the majority of the research, bar a handful, prefer the 'simpler' singular-FEA model theory.

With that being said, the singular-FEA model is still surrounded by controversy, since researchers have not yet agreed on a surrogate axis which applies to the entire ROM. The following text will put into perspective the constant challenge which researchers are facing when trying to identify a single anatomically-defined axis which describes FE rotation throughout the entire ROM.

Following the work of Freeman *et al.* (2000), thanks to the progress of computer technology at the time, researchers started using modern computer techniques. This

allowed them to visualise the spatial motion of the knee better, thus allowing for improved 3D models of the knee and therefore more accurate kinematic analyses (Garg and Walker, 1990; Blankevoort and Huiskes, 1996; Sathasivam and Walker, 1997; Veselko, Jenko and Lipuscek, 1998; Iwaki, Pinskerova and Freeman, 2000). A prominent series of studies were performed by Eckhoff *et al.* on the correlation of the asymmetric morphological features of the distal part of the femur and the kinematics of the knee, and the relationship between the GCA and the cTEA (Eckhoff *et al.*, 2001, 2003, 2005, 2007b). In their study, they clarified various misconceptions that were being debated in the literature. The focus was to determine the cylindrical morphology of the femoral condyles and identify the relationship between the GCA and the FFA, which they tested using three different approaches on ten cadaver knees (five pairs):

1. The specimens were scanned using CT medical imaging, and their bone morphology was extracted following segmentation. For each specimen, a computer algorithm placed and enlarged a cylinder in each of the two condyles in an iterative fashion until less than 1mm of condylar bone remained outside the cylinders (Figure 33A). This resulted in two cylinders which were colinear, even though each cylinder had different diameters (medial larger than lateral).

2. A six DOF motion-analysis apparatus with realistically-simulated loads (Bach and Hull, 1995) was used to functionally align the same knee specimens and locate the FFA (Figure 33B). They reported that the FFA coincided with the colinear cylindrical axis reported in the first technique as long as the system was allowed freedom of movement in all its DOF, that is, an open kinematic chain.

3. A haptic device was used on the knee specimens to outline the surface of the condyles. When all the condyles were outlined, the point clouds obtained from the haptic device were inputted into an algorithm that fitted a cylinder to the data points of each condyle with the requisite 1mm tolerance of remaining condylar bone (Figure 33C). The cylindrical axis was located from the fitted cylinders. Again, the two cylinders had a colinear axis which defined the FEA. (This method was subsequently incorporated into the algorithm of the Stryker navigation system for identifying the FFA intra-operatively (Stryker Navigation, Kalamazoo, Michigan)).

The agreement amongst these three methods confirmed the cylindrical morphology of the femoral condyles, the collinearity of the cylinders forming a single fixed FEA around which the tibia rotated and the relationship of the cylindrical axis to the FFA.

Eckhoff *et al.* (2003) stated that the single cylindrical axis applied for flexion of the knee through the arc of 20˚ to 120˚. For the remaining extension arc, from 20˚ to hyper-extension, both Freeman *et al.* (2000) and Eckhoff *et al.* (2003) reported the knee to rotate around an axis lying anterior and proximal to the GCA, or FCA, and having a larger radius than the posterior segment (that is, the ECA).
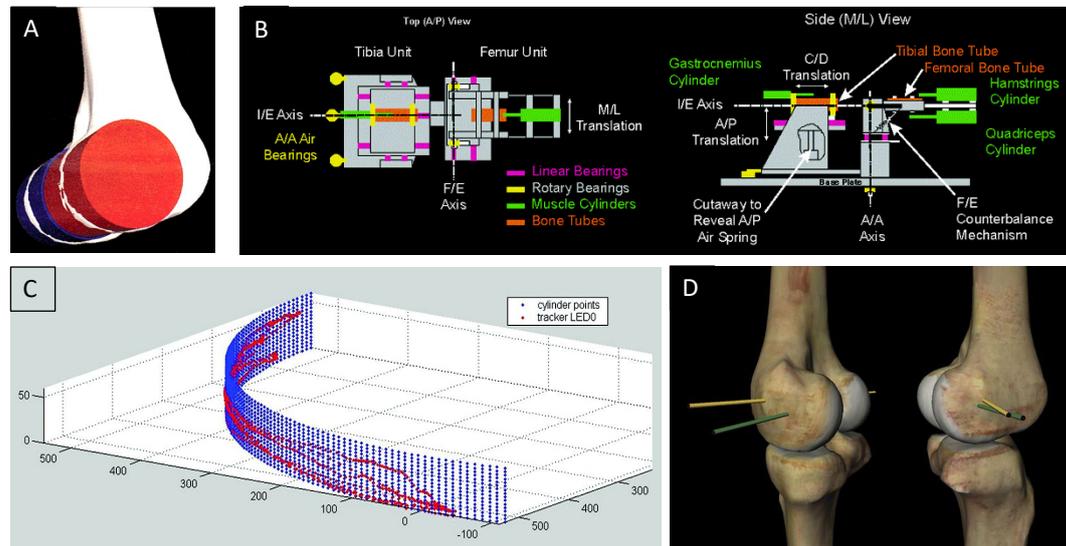
Figure 33: The three methods used to identify the GCA and the FFA of the knee

A: A demonstration of the fitted cylinders on the medial (blue) and lateral (red) condyles. The 1mm tolerance of remaining condylar bone can be noted in the reconstruction. It was demonstrated that while the medial cylinder is slightly larger than the lateral one, they still share the same cylindrical axis. (Eckhoff *et al.*, 2001)

B: Schematic illustration of the knee simulator. Top view oriented from posterior to anterior (left image) and a side view with the tibial unit on the left and the femoral unit on the right (right image). (Eckhoff *et al.*, 2001)

C: Point-cloud created by the haptic device used in surgical navigation, demonstrating the cylindrical shape of the condyles. Red points show the recorded points, and blue points represent the fitted cylinder. (Eckhoff *et al.*, 2003)

D: A 3D view of the relationship between the GCA (green) and the cTEA (yellow) as viewed from the medial (left volume) and the lateral (right volume) aspects of the knee. (Eckhoff *et al.*, 2003)

Further analysis was performed on the relationship between the GCA and the cTEA. For each specimen used in the aforementioned three approaches, the investigators automatically determined the most prominent points on the medial and lateral aspects of the femur by elongating the fitted cylinders along their axes until only a single point of bone remained (Figure 34C). These points were labelled as the epicondyles of the knee. A 3D line was drawn connecting the locations of the epicondyles in order to compute the cTEA. It is good to note that using this virtual approach in identifying the epicondyles resulted in a standard deviation of only 1mm (amongst four investigators)

which when compared to the variance reported earlier by Jerosch *et al.* (2002) of 22.3mm on the medial side and 13.8mm on the lateral side, is an exceptional improvement in accuracy. The researchers subsequently compared the relationship between the cTEA and the GCA by measuring the angle between the two axes in 2D and 3D. They projected both axes onto the traditional orthographic reference planes, namely the coronal and transverse planes and measured the angle between the projected axes in 2D (Figure 34A and Figure 34B). For the 3D relationship, they simply calculated the dot product (direction cosine) between the two axes, which reports the angle between two lines that are not coplanar (Figure 33D). The cTEA was found to be always anterior and proximal to the GCA. The coronal projections had an average divergence of 1.8˚ (range, 0.1˚ to 3.9˚), while the transverse projections had an average divergence of 2.3˚ (range, 0.2˚ to 5.2˚). In 3D it was reported that the angle between both axes was 4.6˚±1.6˚ (with a range of 1.8˚ to 11.3˚).
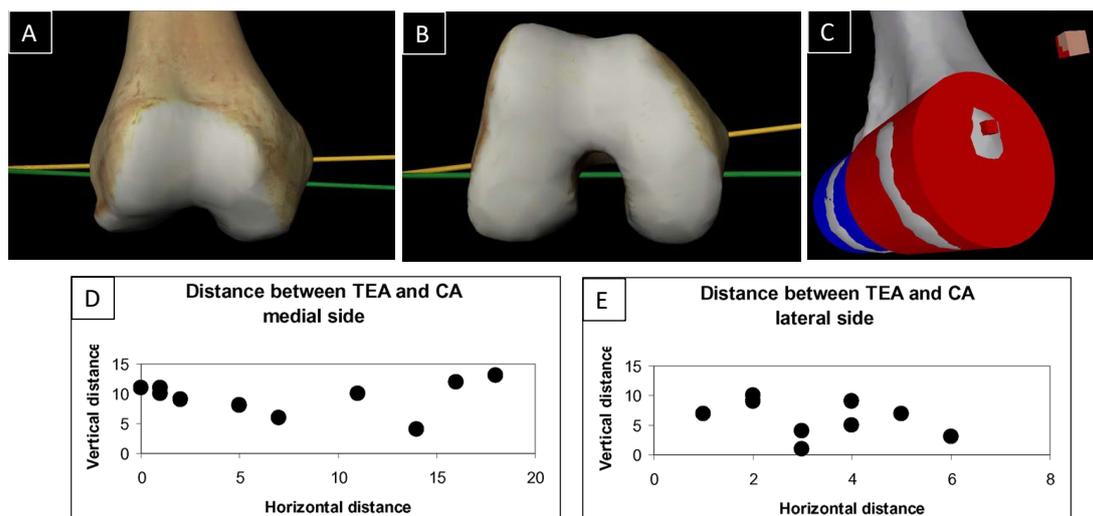
Figure 34: The GCA versus the clinical TEA (Eckhoff *et al.*, 2005)

A & B: Coronal (**A**) and transverse (**B**) view of the projected GCA (green) and cTEA (yellow).

C: An illustration of the computer-assisted epicondyle identification technique. The fitted cylinders were extended along their axis until only one point of bone remained on the side.

D & E: Scatterplot of the 10 tested specimens demonstrating the distance (in millimetres) between the cTEA and the GCA. The cylindrical axis was designated as the absolute zero (origin of plots). The distances on the medial (**D**) and lateral (**E**). The only apparent pattern is that the cTEA is always anterior and proximal to the GCA.

They concluded that the GCA and cTEA differ significantly, and the cTEA is not a good surrogate for the FFA of the knee for the flexion range of 20º to 120º. They referenced the study of Churchill *et al.* (1998), who concluded that the cTEA is a good approximation of the FFA. Eckhoff *et al.* (2005) pointed out that in Churchill's study,

whereby the cTEA was projected onto the traditional orthogonal planes to compare their angular deviation, the variation that existed in 3D space was muted by "flattening" (or projecting) the axis onto the 2D orthogonal planes. As can be noted from the results reported by Eckhoff *et al.* (2005 - above), the 3D angular deviation (average, 4.6˚ with values going up to 11.3˚) is clinically significant in contrast with the same deviations reported in 2D projections (averages, 1.8˚ and 2.3˚). This brings to light the benefits of using modern-day visualisation techniques for the evaluation of geometric and kinematic problems.

Eckhoff *et al.* (2005) further dismissed the theory that the cTEA is close-to or a good surrogate of the FFA (which in this study was being assumed to be approximated by the GCA for the ROM being used) by referring to the relatively large discrepancies that exist at the intersection of each of these axes with the condyles. They reported that when both axes are viewed from the medial and lateral aspects (Figure 34D and Figure 34E), noticeable differences can be noted, mostly for the medial side which showed up to 18mm difference. The work of Eckhoff *et al.* (2005) was later supported by the work of Lustig *et al.* who tried to fit circles to CT slices in a plane perpendicular to the cTEA with no success (Lustig *et al.*, 2008). This is yet another reason to dismiss the cTEA as a surrogate of the FFA since no relationship exists between the morphology of the TF contact area from 20º to 120º of flexion and the cTEA. The study by Lustig *et al.* (2008) will be revisited below when reviewing the literature on the relationship between the sTEA and the FFA.

The relationship of the GCA to the soft-tissue passive restraints was also examined by Eckhoff *et al.* (2005). They stated that the GCA passed through the origin of the cruciate ligaments in the intercondylar notch (Figure 2A and Figure 4D) while the cTEA passed superiorly and anteriorly through solid bone. This statement falls in line with a statement by Kapandji who suggested that the morphological shape of the condyles is determined during early development by the length and point of origin on the cruciate ligaments (Kapandji, 1970). Eckhoff *et al.* (2005) stated that since the kinematics of the knee are defined by the cruciate ligaments, which correspond to the location of the GCA, this provides more evidence that the GCA is a natural surrogate for the FFA of the knee. It was noted that Eckhoff *et al.* (2005) did not comment on the fact that the cTEA also corresponds to two major ligaments (the collateral ligaments) of the knee

which are also responsible for defining the kinematics of the knee, or how the GCA relates to the collateral ligaments.

On further inspection of the data that was collected in this study, it was noted that the plane perpendicular to the GCA contained the mechanical axis of the tibia, while the plane perpendicular to the cTEA contained the mechanical axis of the femur. The authors pointed out that this feature had important relevance in the balancing of soft-tissues during TKA. It is a contemporary practice that in TKA the tibial plateau is sectioned using the "classical cut" technique, which is a perpendicular cut to the mechanical axis of the tibia. This study revealed that a "classical cut" is not parallel and bears no relationship with the cTEA. Therefore, if the tibia is cut with the "classical cut" technique and then the femoral implant is aligned to the cTEA (which is still common-practice in TKA), there will be consequences for the soft-tissue balancing and the resulting replaced-knee kinematics. To bring this in perspective, let us use the analogy of two wheels (the femoral condyles) connected by an axle (the FFA) which are rolling on a flat surface (the tibial plateau). If the axle is placed at the location of the cTEA, then with the knowledge that the cTEA is not parallel to the tibial "classical cut" will result in a flat surface that does not touch both wheels at the same instant. Thus, as the axle rotates, there will be out-of-plane movement of the axle in the PD and AP directions as it rolls on the flat surface. Contrariwise, if the axle is placed at the location of the GCA, with the knowledge that the GCA is parallel to the "classical cut" of the tibia, this will result in a scenario where both wheels will make contact with the flat surface. As the wheels and axle roll on the flat-surface, they will display constant contact throughout the ROM. Thus, looking at this issue from a surgical perspective, if the cTEA is used in conjunction with a tibial "classical cut", ligament length and tension will continuously be changing while the articular surfaces will be continuously compressing and distracting to accommodate the out-of-plane motion of the cTEA. If the GCA is used in conjunction with a tibial "classical cut", then ligament length, as well as articular contact, will remain unaffected by motion about this surrogate FEA of the knee. Therefore, the axis selected by the surgeon will directly impact the knee kinematics of the replaced knee while also affecting balance, or imbalance, of the soft-tissue sleeve.

The results and conclusions published by Eckhoff *et al.*'s manuscripts (2001, 2003, 2005 and 2007), support the dual-FEA model theory while also provides evidence that

the singular-FEA model theory is not applicable for the knee. Regarding the agreement with the dual-FEA model theory, the researchers in the above study specifically correlate the identified FFA to the GCA for the range of flexion from 20º to 120º of flexion, which encapsulates the entire applicable range of flexion of the FCA. Taking into consideration the rigorous research methodology employed by Eckhoff *et al.*'s series of studies (2001, 2003, 2005 and 2007), the GCA can be confidently confirmed as the surrogate to the FCA for its entire ROM. Having an anatomically-defined axis which can be easily identified, is ideal for its successful implementation. On the other hand, considering that the FFA that was identified using an open kinematic chain under realistic loads was only applicable for the ROM from 20º to 120º, goes to show that a singular-FEA model is not realistic. The remaining gap lies in the identification of an anatomically-defined surrogate to the ECA, which has so far not been achieved.

Most *et al.* performed an in-vitro study comparing the sensitivity of kinematic data collected using different FEAs (Most *et al.*, 2004). They measured the tibial longitudinal rotation and femoral AP translation (w.r.t each condyle) for the passive motion from full extension to 150˚ flexion using the cTEA and the GCA as the FEAs. They noted a statistically significant difference in all outcome measures (i.e. AP translation and tibial internal-external rotation). They correlated the significant difference in the kinematics to the angular discrepancy that exists between both axes in 3D space, which they reported to be 4.0˚±0.8˚. This statement agrees with Eckhoff's data (average 3D angle of 4.6˚ - Eckhoff *et al.*, 2007a) and supports his statement that the cTEA and the GCA differ significantly.

The study analysed the AP translations by tracking the intersection points of each axis on the medial and lateral condyles independently, which allowed for a more intricate analysis. On the medial side, a large discrepancy in the distance between the two axes was noted (15.5 ± 2.2 mm). Contralaterally, the distance between the two axes was smaller (6.9 ± 0.9 mm). The reader is referred to Figure 35A for a visualisation of the distance between the surrogate FFAs. The significant difference between the medial and lateral condyle translations between both axes (refer to * data points in Figure 35B and Figure 35C) was correlated to the difference that exists between both axes in 3D. Error bars represent one standard deviation from the mean. Lateral AP translations were larger than medial AP translations for both axes throughout the entire ROM, which reflects the medial pivoting of the knee. The lateral end of the cTEA maintained a

greater posterior (positive) translation as compared to the same lateral end of the GCA.

The medial end of the cTEA did not show signs of movement until 30º of flexion and
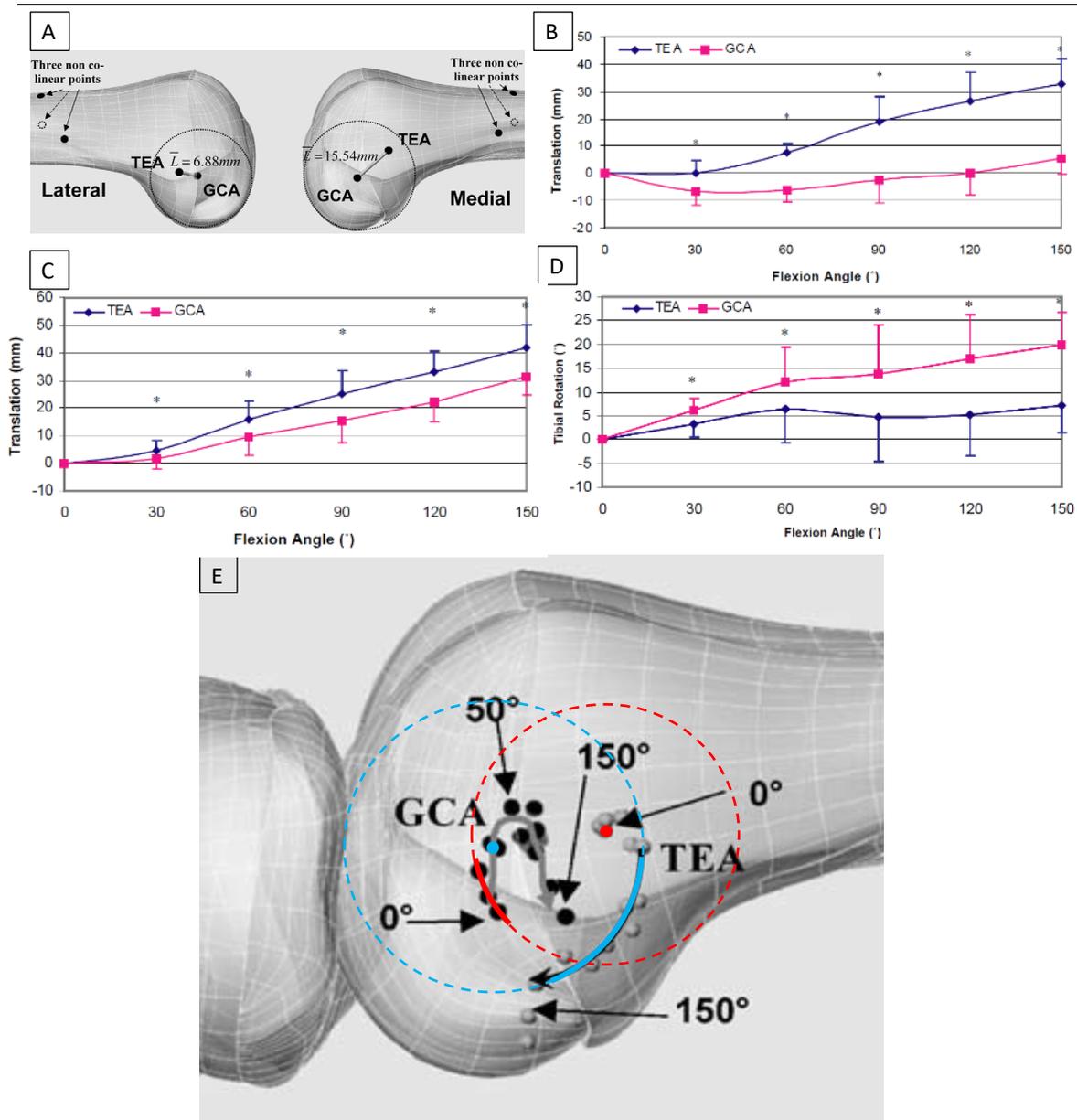
Figure 35: Femoral translation of the cTEA and the GCA on the medial side of the knee. (Most *et al.*, 2004)

A: The 3D model of the knee used in this study, showing the difference in the distances between the cTEA and the GCA on the medial and lateral ends. The three non-co-linear points shown were used in the study to locate the rigid-body pose in 3D.

B: Graphic representation of the anterior (negative) and posterior (positive) translation of the condyle on the medial end. Statistically significant differences between the two profiles are shown with a * ($p<0.05$).

C: Same as C but for the lateral end.

D: Graphic representation of the resulting tibial rotations for both surrogate axes. The GCA showed a greater degree of internal tibial rotation throughout the passive knee flexion motion. Refer to text for explanation.

E: The medial end of the cTEA showed monotonic posterior and distal translation while the GCA first translated anteriorly until 30˚ of flexion and then remained stationary before proceeding to translate posteriorly. Refer to text for explanation of circle overlays.

subsequently maintained constant posterior translation throughout the remaining ROM. The medial end of the GCA maintained a more constant displacement, first moving anteriorly in the first 30º of flexion followed by minimal but constant posterior movement up until 150º (totalling circa 10 mm).

Theoretically, the medial condyle is known to remain fixed until 30º of flexion followed by 2 mm posterior translation until 120º of flexion and a further 8mm until 160º, totalling 10mm of posterior translation (refer to Table 3 in section 2.4.1). Comparing the results presented by Most *et al.* (2004) for the AP translation of the medial condyle with theory, it can be noted that the medial AP translation of the cTEA agrees with theoretical AP translation from hyper-extension through to 30º of flexion for the medial compartment, whereby no movement occurred in the AP direction, but subsequently shows abnormal excessive posterior AP translation. On the other hand, comparing the AP translations reported for the medial end of the GCA with theory, it can be noted that paradoxical anterior translation occurs from hyper-extension through to 30º of flexion, and subsequently follows the theoretical AP translation from 30º of flexion onwards (ultimately agreeing with the theoretical 10 mm posterior translation reported by Freeman *et al.* - Table 3).

On the lateral end, the theory states that the compartment translates 4 mm posteriorly in the first 30º of flexion followed by 15 mm posterior translation until 120º of flexion, and finally a further 5 mm for the remaining flexion until 160º. Comparing the results presented by Most *et al.* (2004) for the AP translation of the lateral condyle, it can be noted that for the cTEA the lateral AP translation from hyper-extension through to 30º of flexion agrees with the theory, where it moves posteriorly by around 4 to 5 mm. Following the 30º flexion mark, the cTEA shows about 30 mm of posterior translation until 120º of flexion and then an additional 10 mm in the last 30º of flexion through to 150º, which does not agree with values reported by Freeman *et al.* (2000). On the other hand, comparing the AP translations reported for the lateral end of the GCA with theory, it can be noted that barely any movement occurs in the first 30º of flexion which disagrees with the theory. This is followed by roughly 20 mm of translation until 120º of flexion and a further 10 mm until it reaches 150º, which is closer to theoretical values than the posterior translation reported for the cTEA.

Taking the assumption that any AP translation being reported which does not follow theoretical values is occurring since the femur is rotating around another axis other than

the axis being investigated (kinematic crosstalk), then the following conclusions can be drawn. Based on the fact that the cTEA AP translations (for both medial and lateral ends) show agreement with the theory before 30º of flexion and the GCA AP translations show agreement with the theory past the same 30º flexion mark, then one can imply that the knee is switching its FFA at 30º of flexion (for the case of the data being reported by Most *et al.* - 2004). Therefore, these results support the dual-FEA model theory and indicate that the cTEA (or an axis in its proximity, that is, the sTEA) may be a viable surrogate to the ECA.

In addition to the above logic, Figure 35E depicts the location of the medial end of the cTEA and GCA, where the black markers identify the GCA locations and the grey markers identify the cTEA. Regarding the cTEA markers for the first 30º of flexion, it can be noted how these markers are all within roughly the same location, which reflects the marginal posterior translations reported in Figure 35B for the medial end up until 30º of flexion. For this ROM it can be noted, how the movement of the corresponding markers for the GCA (that is, the black markers from hyper-extension through to 30º of flexion) follow an arc whose centre is roughly located at the location of the cTEA (refer to red circle overlays in Figure 35E). This shows how the anterior movement being displayed by the GCA is not arbitrary but can be explained by considering rotation around the location of the cTEA (or in the proximity of it) for this ROM. Subsequently, for the ROM from 30º to 120º of flexion, the same can be implied for the arbitrary posterodistal translation occurring at the cTEA. Regarding the blue circle overlays in Figure 35E, it can be seen how the posterodistal translation displayed by the cTEA also follows an arc of a circle, whose centre lies towards the location of the GCA for this ROM. Finally, the markers for flexion beyond the 120º flexion mark for both the GCA and cTEA display posterior translation in the same direction, which supports the statements of Freeman *et al.* (2000) whereby they stated that beyond the 120º flexion mark the knee principally experiences posterior translation as it moves onto the posterior meniscal horn to avoid tissue impingement.

Therefore, based on the results reported by Most *et al.* (2004) in Figure 35B and C, and the correlation which was identified between the pathways of both FEAs, this study also supports the dual-FEA model theory. While the data published by the study was aimed at identifying the sensitivity of using different FEAs to investigate knee kinematics, it also indirectly provided information on the identification of a surrogate

to the ECA. It should be noted that the correlation shown between the pathways of both FEAs (Figure 35E) is solely based on a qualitative analysis of the marker locations reported by Most *et al.* (2004), although it is still supported by the medial and lateral translation plots shown in Figure 35B and C.

Moving on to the tibial rotation (presented in Figure 35D), it was reported that the GCA achieved a larger tibial rotation when compared to the cTEA. Most *et al.* (2004) reported that the GCA displayed larger tibial rotation due to the difference in condylar displacement on the medial end. While lateral displacement for both axes followed a similar profile (although cTEA displayed larger values throughout – refer to Figure 35C), when referring to the GCA the overall displacement of the medial condyle was minimal and when referring to the cTEA, the displacement was larger (Figure 35B). Thus, as a result of the different medial profiles, the cTEA showed an apparent decrease in internal rotation. This statement correlated with a study by Piazza *et al.* who demonstrated that the screw-home mechanism of the knee is noticeably affected by the choice of axes as a result of kinematic crosstalk (Piazza and Cavanagh, 2000). Most *et al.* (2004) concluded that knee kinematics are sensitive to the selection of the FEA, as expected. They suggested that both surrogates can be used to describe knee kinematics if a clear definition of the FEA is given when reporting the kinematics. This statement will be discussed further in a subsequent conclusive statement of this chapter.

In conclusion, the results of Most *et al.* (2004) above, infer that <u>the cTEA is a viable surrogate to the Extension Condylar Axis and the GCA is once again confirmed as the surrogate to the Flexion Condylar Axis</u>.

The validity of the cTEA as the FFA of the knee has been further analysed by Mochizuki *et al.*, this time by quantifying the vertical shift (PD translation) that the cTEA shows during flexion (Mochizuki *et al.*, 2014). They hypothesised that if the cTEA approximates the FFA, it should show minimal to no movement w.r.t the vertical displacement (PD translation) at each of the epicondyles. Any PD movement can, therefore, be attributed to kinematic crosstalk, while keeping in mind the PD profile of the tibial plateau.

They captured a weight-bearing squatting functional movement of twenty healthy volunteers using single-plane fluoroscopy. The epicondyles of the femur were identified, and the cTEA was assembled for all the static frames recorded.
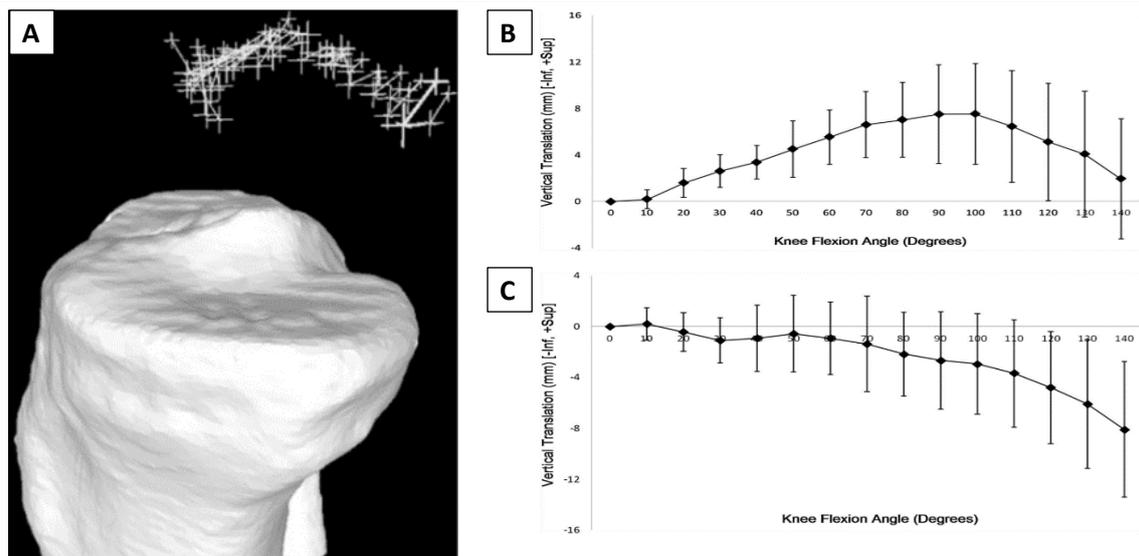
Figure 36: cTEA vertical displacement (Mochizuki *et al.*, 2014)

A: The movement of the cTEA of healthy knees in 3D space during knee flexion.

B: The vertical displacement of the medial end of the cTEA.

C: The vertical displacement of the lateral end of the cTEA.

Subsequently, the vertical displacement of the cTEA was determined by calculating the Z-displacement of the medial and lateral ends from the tibial axial plane (tibial plateaus). From 0° to 140° of knee flexion, the vertical displacements recorded for the medial and lateral ends of the cTEA were as follows. The medial end (Figure 36B) demonstrated superior displacement in the first 100° of flexion (mean 7.5 ± 4.4 mm, range -0.8 to 16.0 mm superior), followed by inferior displacement beyond the 100° mark (mean 5.0 ± 2.1 mm, range 1.6 to 9.7 mm inferior). The lateral end (Figure 36C) demonstrated consistent inferior displacement throughout the entire ROM (mean 8.2 ± 5.4 mm, range -0.6 to 20.1 mm inferior). Mochizuki *et al.* (2014) concluded that the cTEA, based on the relatively large movement that it demonstrated (Figure 36), is not an acceptable surrogate for the FFA.

This study agrees with previously reviewed studies which stated that the cTEA is not an acceptable surrogate to the FFA over the entire ROM of the knee (Most *et al.*, 2004; Eckhoff *et al.*, 2007a; Lustig *et al.*, 2008). Reviewing the data presented by Mochizuki in his study, similarities to the study of Most *et al.* can be noted. The data reported by Mochizuki *et al.* (2014) show that the cTEA displays no vertical displacement in the first 10° of flexion, followed by progressive proximal displacement thereon. This supports the statement mentioned earlier (within the review of the study by Most *et al.* - 2004) where no AP translation was recorded for the cTEA in the first 30° of flexion

(Figure 35C). The discrepancy that exists, that is, that no PD displacement occurred until 10º of flexion and no AP displacement occurred until 30º of flexion can be explained by the Transition phase of flexion, which is known to be subjective and can last from 10º through to 30º of flexion.

Therefore, regarding the data presented by Most *et al.* (2004) and Mochizuki *et al.* (2014), the evidence is showing that:

- the cTEA (or the sTEA due to its proximity) may be viable surrogates to the ECA since they do not display movement in the AP and PD directions during the effective ROM of the ECA, and

- All reviewed studies which suggested that and/or implemented, the cTEA or sTEA as the FEA throughout the entire ROM of the knee are taking an incorrect assumption which is indirectly affecting their results beyond the Transition phase of flexion. Consequently, the conclusions derived in their studies have to be revised, taking into consideration the impact of kinematic crosstalk.

Considering that the location of the ECA was never defined for the femoral ROIs, then having the cTEA, or sTEA, acting as a surrogate would be ideal. The TEA axes can be identified using the location of the epicondyles, therefore allowing for a simplistic implementation in-situ and subsequently allowing for accurately calculating the kinematics of the Extension phase (and to a certain extent the Transition phase), thus avoiding kinematic crosstalk. This would further eliminate the long-standing assumption that the chosen surrogate FEA applies to the full ROM of the knee, which is a prevalent assumption which is taken in the majority of the research reviewed in this thesis. No research, apart from the work of Freeman *et al.*, has so far been reviewed that identifies both the ECA and the FCA of the distal femur individually. It is always assumed (usually without even stating it) that the surrogate FEA being utilised applies to the entire ROM when in reality it has been shown that the knee rotates around the two femoral ML axes (refer to chapter 2.4 and Figure 17), depending on the phase of flexion.

Regarding the above-reviewed studies and interpretations, this theory can be further reinforced since the ECA, which lies proximal to the roof of the intercondylar notch, due to the larger radius of the EFs, lies in the proximity of the TEA. Having the ECA defined by anatomical ROIs makes it easier to implement, since identifying the ECA

in-situ would be more straight-forward. Also, it is known that the TEA lies at the origin of the collateral ligaments, which are taut during the Extension phase (refer to Figure 21). Therefore, having the surrogate to the ECA occurring at the TEA in the initial phases of the flexion cycle (up until the Transition Phase - while it is rotating around the ECA) makes logical sense, since in this ROM the knee is using the collateral ligaments for system stability and rigidity, and thus using them as a fulcrum around which the femur rotates. In fact, using this train of thought, when the knee exceeds 10° of flexion, the collateral ligaments start to become relatively loose, and the cruciate ligaments take over as the major ligaments that provide system stability and rigidity for the knee. Since the collaterals loosen with further flexion, then the TEA no longer acts as the fulcrum for femoral rotation. The FFA then transfers from the origins of the collateral ligaments, posterodistally to the origin of the cruciate ligaments. Eckhoff *et al.* reported that the GCA passes through the origins of the cruciate ligaments in the intercondylar notch (Figure 2A and Figure 4A). Furthermore, in the previously reviewed studies it has been shown through numerous studies that the GCA coincides with the location of the FCA, thus further supporting this theory that the GCA can act as the surrogate to the FEA from 30º through to 120° of flexion. Flexion following the 120° flexion mark (also known as deep- or passive-flexion) does not have an FEA since the principal movement that is occurring is translation, while rotation is minimal. Therefore, in conclusion to this theory, there is the possibility that the cTEA (or the sTEA) is a surrogate to the ECA. Could it be, that the TEAs have been misinterpreted through time as the surrogates of the FFA for all the ROM of the knee when in reality they are only valid for the range of flexion where rotation is occurring around the ECA? So far, no studies investigating this hypothesis have been identified.

Identifying the ideal ECA surrogate (the cTEA versus the sTEA)

So far, in this review, it has been established that the singular-FEA model of the knee is an over-simplified theory to facilitate our perception of knee motion. Using a singular-FEA to describe the entire ROM of the knee will result in the incorrect extraction of kinematics data due to the effects of kinematic crosstalk. In light of the dual-FEA model theory, up to this point, it has been determined that the FCA, or GCA, is the axis of rotation for the Flexion phase (that is, 30º to 120º of flexion). The cTEA has been shown to be a possible surrogate to the ECA from hyper-extension to 10º of

flexion. No studies have been found that directly evaluate the cTEA's applicability to the ECA during its effective ROM.

The cTEA's applicability is over-shadowed by its inadequate reliability and accuracy when defining it in-situ, due to the variability that exists in identifying the anatomical ROIs which define this axis. This is a limitation that impedes on its implementation as a surrogate axis to the ECA. On the other hand, the sTEA (which lies close of the cTEA) has only been briefly discussed to follow the chronological order of events. Considering that the sTEA has been recommended numerous times as the better alternative to the cTEA (Berger *et al.*, 1993; Matsuda *et al.*, 2003; Asano, Akagi and Nakamura, 2005), a concise review of literature of studies investigating the relationship between the sTEA and the FFA will follow. It should be noted that similar to the cTEA, no studies to date investigated the correlation between the sTEA and the ECA specifically. The studies that will be reviewed below investigate the possibility of using the sTEA as the singular FFA of the knee. Data and conclusions from these studies will be reviewed to identify correlations between the sTEA and the applicable ROM of the ECA.

Key research studies on the relationship between the sTEA and the FFA from a kinematic perspective are not as prominent as those found for the cTEA, probably due to its more recent emergence. Berger *et al.* defined the sTEA for intra-operative rotational alignment purposes as an axis which initiates medially from the sulcus of the epicondyle and terminates laterally at the epicondyle. Their findings reported that the sTEA, in comparison to the cTEA, may improve the alignment of the femoral component during surgery since the medial sulcus of the medial epicondyle is noted as a discernible and reproducible landmark in contrast to the stochastic medial epicondyle (Berger *et al.*, 1993).

Matsuda *et al.* compared the sTEA, cTEA and APA (Anteroposterior Axis) in a dynamic study investigating the relationship of these surgical axes to the tibial mechanical axis over the knee's ROM. They concluded that the sTEA, in contrast to the cTEA or the APA maintains a more predictable orientation relative to the tibial mechanical axis while going from flexion to extension (Matsuda *et al.*, 2003).

The first prominent in-vivo weight-bearing study investigating the relationship that exists between the sTEA, cTEA and an algorithm-based FFA was published by Asano *et al.* (Asano, Akagi and Nakamura, 2005). Bi-planar fluoroscopy was used to capture static weight-bearing images of the knee at 15° intervals from 0° to 90° of flexion. The FFA was identified by fitting a circle to the consecutive locations of the centre of the

ankle joint for all the recorded frames (Figure 37A). By minimising the least sum of squares error between the optimal circle and the recorded ankle centre points, the FFA was identified with an average error of 0.61% ± 0.23%. The fitted FFA reflected its validity since it displayed marginal PD translation (less than ±1 mm) and abduction-adduction rotation (less than ±1˚) when viewed in the coronal plane (Figure 37B). They noted that when the FFA was viewed end-on, each femoral condyle was found to conform to the perimeter of a circle, with both circles having collinear centres. While this apparently identifies the GCA, or FCA, upon further investigation, the authors noted that the posterior aspects of the femoral condyles, specifically "the areas which contact the tibia beyond 90˚ of flexion" did not fit on the circles defined earlier (Figure 37C). Considering that the FFA was identified using data for the range of flexion from 0º to 90º, then in light of the dual-FEA model theory, it is expected that the identified singular-FFA encapsulates the majority of the effective range of the ECA and a partial range of the FCA. Therefore, it is safe to assume that the identified FFA in this study would lie between the location of the ECA and FCA, but closer to the FCA, since two-thirds of the captured ROM falls within the effective ROM of the FCA. While the authors failed to explain the reason behind their data, the aforementioned should explain why the fitted circles did not entirely match the posterior condyles of the femur.
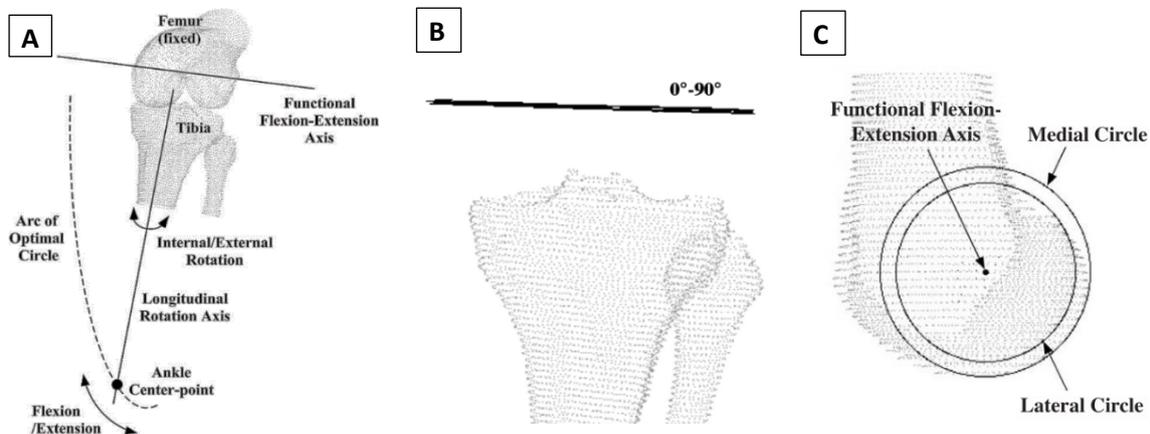
Figure 37: The relationship between the sTEA and the functional FEA. (Asano, Akagi and Nakamura, 2005)

A: Determination of the functional FEA by least squares method. This method od deriving the functional FEA was based on the assumption that during knee flexion consecutive locations of the centre of the ankle joint (distal end of the IEA) lie on the perimeter of a circle.
B: The validity of the derived functional FEA approach is reflected in this coronal view of the knee, showing minimal PD translation and abduction-adduction rotation from 0˚-90˚ of flexion.
C: Viewing the functional FEA end on, each femoral condyle was found to conform to the perimeter of a circle with a common centre on the axis.

The intersections of the identified FFA with the medial and lateral femoral condyles were located and reported. Medially, the FFA intersected at a point 6.3 ± 1.5 mm from

the epicondyle (P<0.001) and 1.0 ± 1.7mm from the sulcus of the medial epicondyle (P=0.10). Laterally, the intersection was 0.6 ± 2.7mm from the epicondyle (P=0.54). The 3D angles were reported w.r.t the PCA (Posterior Condylar Axis) as follows: 6.7° ± 1.5° w.r.t the cTEA, 3.1° ± 1.7° w.r.t the sTEA and 2.7° ± 2.1° w.r.t the FFA. The angles were statistically analysed w.r.t the FFA, with the cTEA and PCA showing a statistically significant difference (P<0.001 and P=0.002, respectively), while the sTEA was not (P=0.60).

The researchers in this study concluded that based on their statistical analysis, the sTEA approximated the identified FFA and proposed the implementation of the sTEA as a singular-FEA of the knee. Keeping in mind that the researchers in this study have unwillingly assumed that the identified FFA applies to the entire ROM of the knee, then the results presented in this study lose their significance when attempting to compare the sTEA to the identified FFA. This is the case since they are attempting to identify correlations between an FFA which was calculated on data ranging from 0° to 90° of flexion, and the sTEA which evidently does not have the same effective ROM. Therefore, while the research methodology used in this study was robust, their data is inconclusive for our purposes due to the assumption of a singular FFA model of the knee.

Asano's work was followed-up by Victor in a review of the literature surrounding the current FFA surrogate axes (Figure 31C) from a surgical perspective (Victor, 2009). Victor agreed with Eckhoff *et al.* that the GCA (referred to as the Femoral Transverse Axis in his study) is perpendicular to the tibial mechanical axis. He also noted that if the GCA is projected into the axial plane of the tibia, it coincides with the tibial transverse axis. Victor further calculated the angle between the GCA and the sTEA and found that they are parallel to each other in the axial plane. Victor concluded that given the pitfalls, outliers and difficulties with identifying the epicondyles of the distal femur, a pre-operative CT scan is still recommended for improved accuracy. This was in agreement with a statement by Aglietti *et al.* (Aglietti *et al.*, 2008). Victor demonstrated that identifying the sTEA on a CT scan produces acceptable inter- and intra-observer variability. A study by Matziolis *et al.* also reported results which were in agreement with Victor's statement above (Matziolis *et al.*, 2011).

Lustig *et al.* published a paper which they referred to as a "critical analysis of the concept of the sTEA as the fixed axis of rotation of the femoral condyles during flexion

of the knee" (Lustig *et al.*, 2008). They performed this anatomical study of the distal part of the femur to address the misconception that the sTEA is applicable as the singular-FEA of the knee. It should be noted, that their aim was not to support the dual-FEA model theory, but simply to affirm that the sTEA is not applicable for the entire ROM of the knee in contrast to conclusions which some prominent studies stated.
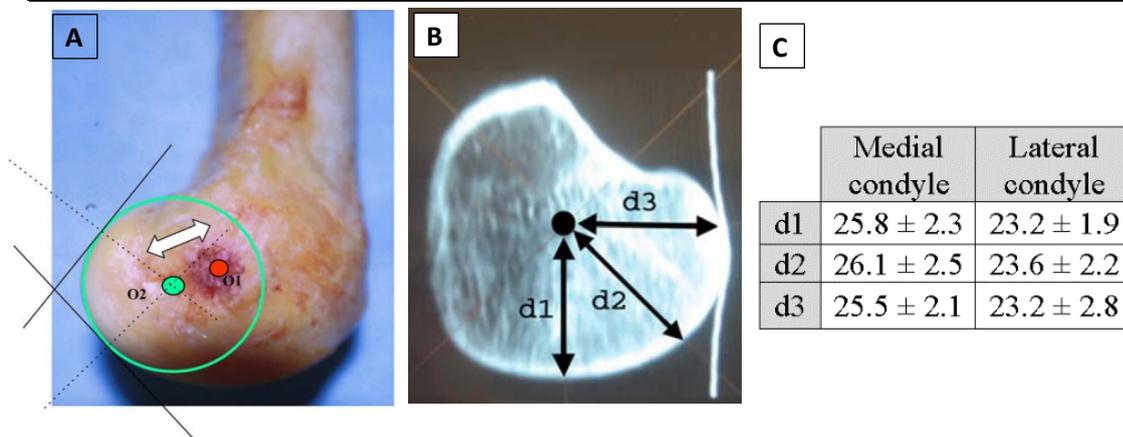
Figure 38: The relationship between the sTEA and the articular surface of the distal femur (Lustig et al., 2008)

A: Distance between the centre of the posterior femoral condyles (O2) and the surgical epicondylar axis (O1).
B: Visual representation of the distances between the sTEA and the distal/anterior (d1), intermediate (d2) and posterior (d3) articular surfaces.
C: Averaged results obtained for the distances shown in B.

They took a geometrical approach by assessing if the distance between the sTEA and the anterior femoral condyle (that is, the femoral EF) is the same as the distance between the sTEA and the posterior femoral condyle (that is, the femoral FF), and also to test if the sTEA shows signs of correlation with the entire contour of the femoral condyles.

They stated that most of the studies performed on the TEA reported inaccuracies w.r.t the location of the TEA itself, thus questioning the reliability of their results. To assure that their study circumvents such inaccuracies, they first identified the medial sulcus and lateral epicondyle in-vitro and inserted metallic bodies at the level of the collateral ligament insertions on 16 dried femurs. They reported that they accurately located the sTEA with an accuracy of 1mm. This also allowed them to precisely locate the sTEA on the AP radiographs and the CT-scans of the dried femurs. The CT scans were taken with the femurs positioned in such a way that the metallic needles were aligned, in order to get the CT slices to be perpendicular to the sTEA. They attempted to fit circles centred at the sTEA to the whole femoral condyles, but no circles could fit either the entire medial or lateral condyles thus providing evidence that the sTEA does not show

signs of correlation with the entire contour of the femoral condyles. Conversely, when trying to fit circles (using either of two methods; circle templates and the tangent method) to the posterior condylar contours they found a good fit, with the centres of these circles theoretically locating the GCA, or FCA, which agreed with previous literature (Kurosawa *et al.*, 1985; Elias, Freeman and Gokcay, 1990; Eckhoff *et al.*, 2003; Freeman and Pinskerova, 2005). Using the location of the GCA, they measured the distance between the centres of the sTEA and the GCA, which was 8.4 ± 2.1mm medially and 6.5 ± 2.8mm laterally (Figure 38). This confirmed that the sTEA does not coincide with the GCA, contrary to the statements of Elias *et al.* (1990), Hollister *et al.* (1993) and Churchill *et al.* (1998). This is further supported by the conclusions of Asano, Akagi and Nakamura (2005) above since they failed to prove that their algorithm based FFA was coincident with both the sTEA and the posterior femoral contours.

The distances between the sTEA and the anterior, intermediate and posterior articular surfaces (that is, the extent of the entire contour where contact occurs throughout the ROM - Figure 38B) of both condyles are shown in Figure 38C. They reported that laterally no statistical difference was found between the three measurements (p = 0.223), which supports the theory of a single radius of curvature for the lateral condyle. Medially a statistical difference was noted (p = 0.023), which again supports the theory that the medial condyle exhibits two (or more) radii of curvature. The average size of the condyles was 25.7 and 23.3mm for the medial and lateral condyles respectively (ratio 1.102), which is comparable to the medial-to-lateral ratios reported by Churchill *et al.* (1998) (1.143), and Asano *et al.* (2005) (1.139). They concluded that the apparent homogeneity of the values d1, d2 and d3 may have been misinterpreted as the sTEA being the centre of curvature of the femoral condyles. They stated that their results were consistent with the concept of the lateral condyle having a single curvature for the anterior and posterior aspects and the medial condyle having different radii for the posterior and anterior aspects, which agrees with the work presented by Freeman *et al.* and the dual-FEA model theory being discussed.

Lustig *et al.* (2008) emphasised that considering the precautions they took in the identification process of the ROIs of the sTEA, their results were accurate, and they were confident that this disagreement with such prominent studies could not be explained by measurement errors. They further highlighted how these prominent

studies showed methodological deficiencies which they correlated to lessened confidence in their results. Lustig *et al.* (2008) stated that the conclusions of these prominent studies, which stated that the sTEA is coincident with the centre of the posterior condyles "was proposed as a theoretical model in an effort to simplify our perception of the knee motion, even if the level of evidence was insufficient". This statement sheds light and agrees with the theory proposed by the international team of Freeman *et al.* (2000) while highlighting the fact that assuming rotation around just one FEA, that is, the singular-FEA model theory is an oversimplification. They finally refer to Asano's study (reviewed above), who accordingly failed to prove the coincidence of the sTEA to the centres of the posterior condyles. They concluded that based on their data, the sTEA is not equidistant from the anterior and posterior femoral condyles and is not located at the centre of the contour of the femoral condyles. Thus, based on these findings, they suggested that the sTEA is not adequate for defining the entire articulation of the femur.

Yin *et al.* performed a kinematic study aimed at identifying the FFA based on kinematic data collected during weight-bearing knee flexion and then comparing it with the two major anatomical axes of the distal femur, the GCA and sTEA (Yin *et al.*, 2015). They hypothesised that the GCA would be located closer to the FFA than the sTEA. They used the angular deviation and distance between the endpoints of each FEA as outcome measures to assess their hypothesis. Twenty healthy volunteers performed a CT scan of their knee and took bi-planar x-rays while performing a single-leg lunge manoeuvre at 0°, 15°, 30°, 60°, 90° and 120°. The CT generated models were registered onto the bi-planar scans via 2D to 3D registration techniques to extract the 3D in-vivo tibiofemoral movements. Subsequently, an anatomical coordinate system was embedded in the tibia as defined by Grood and Suntay (Grood and Suntay, 1983 – reviewed in section 2.6.3.3). The tibial plateau centres were identified using the methods described by Cobb and Victor which were demonstrated to have high precision and reliability (Cobb *et al.*, 2008; Victor, Van Doninck, Labey, Van Glabbeek, *et al.*, 2009).

Yin *et al.* (2015) noted that the conventional methods of calculating the FFA (Hollister *et al.*, 1993; Churchill *et al.*, 1998; Roland, Hull and Howell, 2010) had an inherent drawback since these methods required that the IEA must be calculated independently through repeated movements of internal-external rotations of the knee before locating the FFA. While this method of approach is achievable using in-vitro cadaveric studies,

as noted in previous studies, they are not practical in in-vivo kinematic studies. Therefore, they proposed a new method which is based on a similar approach to the one presented earlier by Asano *et al.* (2005). The algorithm was based on the assumption that the FFA remains at a relatively constant vertical distance from the tibial plateau, regardless of the pattern of motion of the femoral condyles (sliding, rolling or both). This can be again explained by the analogy of an axle with a wheel attached at each end, rolling on a flat surface (as already explained earlier in this text for the explanation of the out-of-plane movement that the cTEA created if it is used as the FFA - Eckhoff *et al.*, 2003). Using this analogy, the FFA was identified by first discretising the femur model into a point cloud, and subsequently tracking the vertical shift that occurs for each point in the distal femur between each frame (Figure 39A). This was termed the Vertical Shift Value, or VSV, and was calculated for each subsequent frame interval. The next step was to compensate for the tibial slope, by identifying the vertical shift that occurred between corresponding tibiofemoral contact points and deducting this value from the VSV of the corresponding frame interval (Figure 39B). The resulting VSVs from all frame intervals are then summated to get the cumulative VSV (cVSV). The FFA was identified by identifying the points with the least cVSV from all the point cloud. By identifying the FFA using solely the cVSVs, the algorithm is independent of any rolling, spinning or sliding of the femur on the tibia, and any transverse movements (such as internal-external rotations) occurring as flexion progresses.

While the sTEA was identified visually, it was mentioned that if they did not confidently locate the sulcus, the epicondyle was chosen instead. This assumption included the possibility of errors in the results since the author did not mention how many sulcus points were not confidently identified. On the other hand, the GCA was identified by passing a line through the centres of spheres which were fitted, in the least-squares sense, to the medial and lateral posterior condyles and connecting their centres. It is good to note that they pointed out that fitting spheres to the posterior condyles, rather than cylinders (as performed by Eckhoff *et al.* - 2003) resulted in identical results but was easier and more robust during the fitting of the model.

The lowest cVSVs converged towards the central portion of the medial and lateral posterior condyles (Figure 39C). The absolute coronal angle (measured in the coronal and transverse plane w.r.t the tibial ML axis) of the FFA was significantly different from the sTEA ($p < 0.001$), but not from the GCA ($p = 0.065$). The absolute transverse
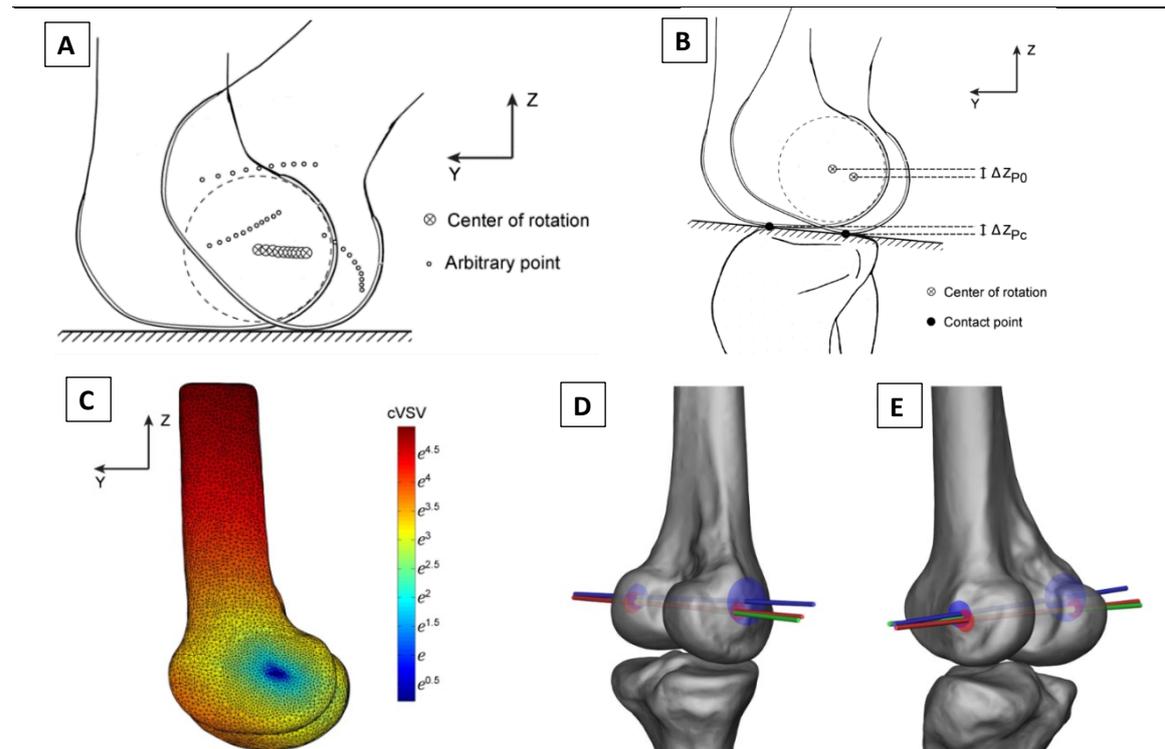
Figure 39: The FFA of the knee as proposed by Yin et al. (Yin et al., 2015)

A: The axis of a rolling object on a flat surface keeps a constant vertical distance w.r.t surface it contacts. Arbitrary points which do not lie on the axis display vertical shifts of different magnitudes which vary depending on their distance relative to the axis.
B: When the rolling object is contacting an oblique surface, the axis naturally follows the path of the surface. For the case of the knee, this is equivalent to the tibial slope, which can be compensated for by taking into consideration the vertical shift displayed by the contact points.
C: The mapping of the cumulative vertical shift value (cVSV). The distribution of the cVSV from 0° to 120° of knee flexion in the left femur as seen from the lateral side. The points with the lowest cVSV converge towards the centre of the posterior condyles.
D: The relationship between the FFA and the sTEA and GCA from a posteromedial view. The FFA is coloured green, the sTEA ids coloured blue and the GCA is coloured red. The circles with the respective colours represent the 95% confidence interval of the positions of the GCA and sTEA. The sTEA and GCA shown represent the average locations of all the subjects.
E: Same as **D** but from a posterolateral view.

different from both the sTEA and GCA (p<0.001 and p=0.007, respectively). The mean 3D between the sTEA and the FFA was $3.45 \pm 1.58°$ (range, $0.27 – 6.36°$) and between the angle of the FFA was significantly angle GCA and the FFA was $1.98 \pm 1.55°$ (range, $0.42 – 6.25°$). For all subjects, the absolute angles and the 3D angles of the GCA was closer to the FFA than those of the sTEA. The distance between the intersection points of the FFA and the sTEA averaged, 6.7 ± 2.2mm (range, $3.4 – 9.4$mm) medially and 3.2 ± 1.5mm (range, $1.7 - 6.7$mm) laterally. For the averaged distances between the FFA and the GCA they reported, 1.9 ± 1.5mm (range, $0.1 – 5.4$mm) medially and 2.0 ± 1.6mm (range, $0.2 – 6.6$mm) laterally. The medial distances were statistically different (p < 0.001), while the lateral distances were not (p = 0.16). The sTEA was

always found superior and anterior to the FFA in all analysed subjects. The GCA did not show any preferential relationship to the FFA but was always much closer to it. They stated that while neither the sTEA nor the GCA perfectly coincided with the FFA, the GCA exhibited better approximation to the FFA than the sTEA did. They concluded that considering the incidence of the GCA to the FFA, an anatomical frame based on the GCA should be used for the distal femur.

The study by Yin *et al.* (2015), suffered the same fate as the study of Asano *et al.* (2005) since they unwillingly assumed that the identified FFA applies to the entire ROM of the knee. Nonetheless, the results presented in this study show signs of correlation to the dual-FEA model theory. The fact that the calculated FFA was found to be significantly different from both the GCA and sTEA shows that neither of them can act as the singular-FEA for the knee, therefore supporting the argument that the singular-FEA model is an over-simplification of knee motion. The fact that the calculated FFA is closer to the GCA than the sTEA makes sense in light of the dual-FEA model theory. If one takes the assumption that the knee rotates around these two axes, then given the captured ROM in this study, it makes sense that the FFA is closer to the GCA, since ¾ (90º of the entire 120º) of the captured ROM occurred around the GCA. This would converge the FFA to lie closer to the GCA. If the singular-axis model was in fact applicable, then the presented results stating that the FFA is statistically different to either the GCA or the sTEA would be contradicting the majority of the reviewed literature which points towards either the GCA or one of the TEA variants as the singular-FEA. Also, concluding that the GCA is to be used as the anatomical frame of reference due to the incidence it showed with the FFA is misleading and will lead to kinematic crosstalk in the results if it were to be implemented over the entire ROM of the knee.

The last study being reviewed was performed by Feng *et al*. The objective of the study was to investigate the femoral condylar motion during a dynamic flexion exercise using a 2D to 3D fluoroscopic technique (Feng *et al.*, 2016). The femoral condylar motion was described using the cTEA, sTEA and GCA axes. The outcome measures analysed were the AP and PD femoral condyle translations. Twenty healthy subjects (1:1 male to female ratio) were asked to perform a CT-scan of the femur and tibia to extract the 3D models of the knee. The cTEA, sTEA and GCA were defined using the standard definitions of the axes. The dynamic motion of the knee was captured using a

fluoroscopic imaging system at a frame rate of 30Hz. The participants were asked to perform a single-leg lunge from full-extension to the maximum comfortable flexion.

The 3D angles between the 3 surrogate axes were 8.2° ± 1.7˚ between the cTEA and GCA, 4.8° ± 1.1˚ between the cTEA and sTEA, and 4.0° ± 1.3˚ between sTEA and GCA. These results agreed with studies by Asano *et al.*(2005), Most *et al.* (2004), Yoshino *et al.* (2014) and Eckhoff *et al.* (2003). Also, they projected the axes in the coronal and transverse planes, and noted that the angular differences between the projected axes were all significantly smaller than those in 3D space, agreeing with the statement by Eckhoff *et al.* (2005). The results for the AP and PD translations of the medial and lateral femoral condyles are presented in Figure 40.

The results presented in this study agreed with the conclusions of Most *et al.* (2004), which stated that the knee kinematics are sensitive to the FEA used. The AP translations of the three FEAs reported different profiles for the medial condyle but similar profiles for the lateral condyle. On the other hand, the PD translations were also different for the medial side, while on the lateral side, the two TEAs were similar (as expected since they share the same ROI). The GCA also had a similar profile to the TEA counter-parts but with a slight distal shift (due to the GCA being located slightly distal to the TEAs) which decreased with increasing flexion (due to the TEAs experiencing kinematic crosstalk w.r.t the GCA). On the lateral side, it was noted that the cTEA and sTEA showed minimal movement from full extension to roughly 60˚ of flexion, with the sTEA displaying less variation. The GCA showed minimal movement in the PD direction from 30˚ to 90˚, while beyond 90˚ slight distal movement occurred, which reflects the sloping posterior surface of the lateral saddle-shaped tibial plateau.

The results presented by Feng *et al.* (2015) support the dual-FEA model theory since the TEAs are showing marginal PD translations during the effective ROM of the ECA, while the GCA is showing marginal PD translations during the effective ROM of the FCA. The validity of the data collected in this study is in line with the results obtained by Most *et al.* (2004 - AP translations) and Mochizuki *et al.* (2014 - PD translations). The data presented in this study is analogous with their data, with the only difference being that Feng *et al.* (2015) did not present the absolute values of the translations. Furthermore, their data was in agreement with other studies which are not presented in this review (Walker *et al.*, 2011; Li *et al.*, 2013; Tanifuji *et al.*, 2013).
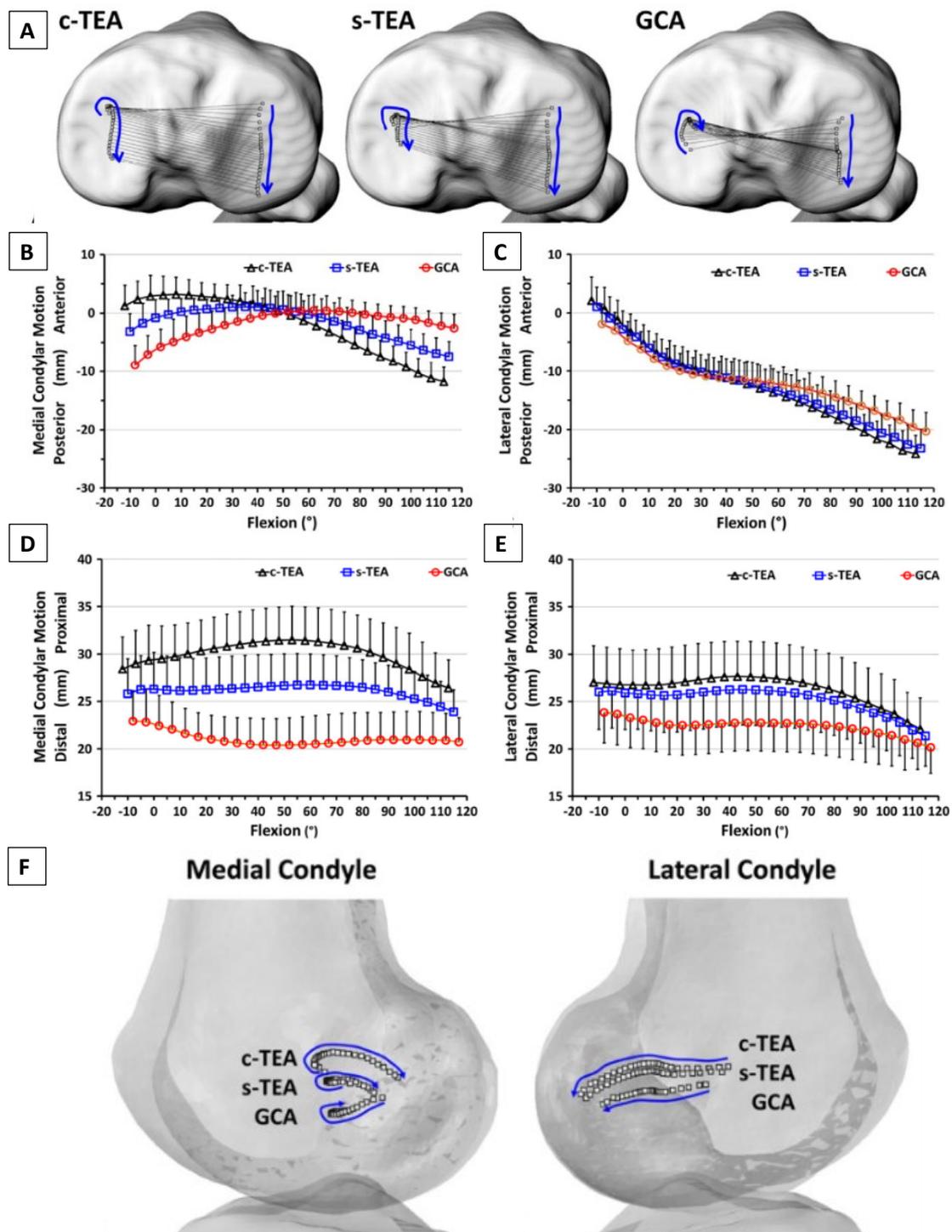
Figure 40: Movement patterns of the three surrogate axed during knee flexion (Feng et al., 2016)

A: A visual representation of the AP translations of each axis.

B: A graphical illustration of the medial AP condylar translations.

C: A graphical illustration of the lateral AP condylar translations.

D: A graphical illustration of the medial PD condylar translations.

E: A graphical illustration of the lateral PD condylar translations.

F: A visual representation of the medial and lateral movement patterns of the three axes.

The researchers pointed out that it is still arguable if any of the two TEA variants are applicable for the use of femoral component alignment in TKA. This statement holds if the singular-FEA model is being considered. For the case of the dual-FEA model and considering the data reviewed so far, this data supports the sTEA as the better surrogate to the ECA and the GCA as the surrogate to the FCA. Regarding Figure 40D and E, it can be noted that the sTEA in comparison to its variant, the cTEA, clearly maintains a more quasi-static vertical displacement from hyper-flexion until around the 60º flexion mark, most prominently in the medial compartment. Conversely, the cTEA shows constant proximal translation medially which reflects kinematic crosstalk. This evidently justifies the sTEA as the better surrogate to the ECA. On the other hand, the GCA maintains a quasi-static PD displacement post the 30º flexion mark while translating distally following the 90º flexion mark (prominently in the lateral compartment) due to the sloping anatomy of the posterior aspect of the lateral tibial plateau (refer to the difference in the sloping anatomy of the posterior tibial anatomy between the medial, in Figure 17B, and the lateral, in Figure 17C - section 2.4). It is good to note that Freeman *et al.* reported that the ECA is applicable until 10º of flexion (with the possibility of being effective until the end of the Transition phase, that is, until 30º of flexion) and the FCA is effective from 30º of flexion onwards. In contrast, in this study, the GCA agreed with the effective ROM of the FCA while the sTEA was reported to maintain marginal PD movement until circa 60º of flexion.

Feng *et al.* (2015) concluded by stating that to standardise results of kinematic studies of the knee, authors need to clearly explain the way the flexion axis was defined, to allow replication of the experiment if need be. The results of this study have confirmed that knee kinematic measurements are sensitive to the selection of the flexion axes.

The review of the study by Feng *et al.* (2015) concludes the literature being reviewed in the quest for the identification of the FEA of the knee. The following recapitulation of reviewed literature is aimed at summarising the key points discussed in this review.

Summary of the reviewed literature

- The Weber brothers (Weber and Weber, 1837) were the first researchers to propose that the femoral condyles had circular profiles. However, their work was contradicted by numerous researchers who claimed that the condyles were helical in shape. Their statements were later dismissed as it was noted that these researchers

were taking true-sagittal plane sections, which showed them a skewed cross-section of the knee, resulting in elongated profiles of the condyles.

- Hollister *et al.* (1993) performed an in-vitro experiment on 6 cadaveric knees to identify the FFA via passive un-loaded flexion-extension cycles of the knee. They were amongst the first researchers who proposed that a singular-fixed FFA exists and passes through the origins of the collateral ligaments and superior to the intersection of the cruciate ligaments. They concluded that the FFA is offset by 7˚ to the anatomical sagittal plane. Their work was supported by numerous clinicians since at the time the cTEA was proven to be the most accurate axis for rotational alignment. Nonetheless, issues of accuracy remained when using the cTEA. Berger *et al.* (1993) suggested the sTEA as a better alternative to the cTEA with better accuracy while also better approximating the anatomical locations identified by Hollister. The methodology used by Hollister *et al.* (1993) was limited to 3 DOF.

- Churchill *et al.* (1998) aimed at building upon the research of Hollister *et al.* (1993) by performing a 6 DOF in-vitro experiment on 15 cadaveric knees to identify the FFA via passive loaded flexion-extension cycles of the knee over the range of 5˚ to 90˚. They concluded that the FFA passes through the posterior femoral condyles but not precisely through their centres. Also, in contrast to the GCA, they reported no statistical difference between the FFA and the cTEA. Nonetheless, they concluded that both axes can be used for kinematic analyses. Their results were based on 2D projections of the axes which were later dismissed (on the basis that 2D projections "flatten" the discrepancy that exists in 3D) by Eckhoff *at al.* (2005) when comparing them to their 3D counterparts.

- The cTEA was reported to suffer from poor reproducibility with reports of up to 22mm of variability in locating its medial ROI. Several researchers suggest that the cTEA is unreliable and should not be used as a surrogate to the FFA. Nonetheless, research at the time still used the cTEA as a surrogate to the FFA.

- A series of studies by Freeman *et al.* (2001, 2003, 2005 and 2007) reinforced the concept of the compound axes model of the knee. The model states that the knee rotates primarily about two fixed axes, an ML axis (FEA) located in the femur and an IEA located in the tibia. For the FEA, they reported that the knee rotates around the extension condylar axis (ECA) from full-extension through to 30˚ after which the knee shifts its rotational axis to the flexion condylar axis (FCA) which is effective

from 30° through to 120° of flexion. A transition phase occurs between 10° and 30° of flexion, which is subjective and activity-dependant. Up to the author's knowledge, Freeman's work has been accepted throughout the research community, and no-one has yet challenged their results, and thus they are considered as gold-standard for the kinematics of the knee. Freeman's work pioneered the dual-FEA model theory.

- Eckhoff *et al.* performed a series of studies (2001, 2003, 2005 and 2007) which identified the GCA as the ideal surrogate to the FFA from 20° to 120°. They confirmed the cylindrical nature of the posterior femoral condyles using three different approaches, each identifying the GCA to pass through the collinear centres of the two fitted-cylinders with different radii. They identified the FFA through a 6 DOF in-vitro dynamic simulator which located the FFA to be coincident with the GCA for the range of 20° to 120°. Given that they assessed the applicability of the cTEA and GCA over the effective ROM of the FCA, they provided evidence that allowed for the dismissal of the cTEA as a surrogate to the FCA. Also, they identified the GCA to be passing through the origin of the cruciate ligaments in the intercondylar notch. This relationship to the knee anatomy along with the perpendicular relationship with the tibial mechanical axis further strengthened the position of the GCA as the ideal surrogate to the FCA.

- The work of Eckhoff was later supported by Lustig *et al.* (2008) when they tried to fit spheres to the entire articular surfaces of the condyles in a plane perpendicular to the cTEA, with no success. This meant that the cTEA could not be used as an FFA that is effective over the entire ROM of the femur. Furthermore, Eckhoff confirmed that the GCA does not apply to the entire ROM as well, such that no FEA has been yet identified that applies to the entire ROM of the femur. These results further support the dual-FEA model theory.

- Most *et al.* (2004) provided evidence that the cTEA undergoes marginal AP movement in the first 30° of flexion, and the GCA undergoes marginal AP movement thereafter. Furthermore, using the published results, it was noted that the profile of the interception points of the axes with the medial condyle indicate that the GCA rotates around the cTEA (or an axis in its proximity) in the first 30° of flexion, followed by the cTEA rotating around the GCA thereafter until 120° of flexion. They concluded that the results were all significantly different, confirming their hypothesis that kinematics are sensitive to the selection of FEA. Based on their

results, and the underlying assumption of the singular-FEA model theory, they stated that researchers could use either of the FEAs as long as they specify which axis was used to define the femoral CS. The author of this thesis advises caution with suggesting such statements, since allowing researchers the freedom of using any axis other than the ideal one will allow for misinterpretation of the actual movement of the knee because of kinematic crosstalk affecting the results. These effects should be well-understood to be able to understand the outputted results and correctly understand the limitations imposed by the surrogate axis used in the implemented kinematic model.

- Mochizuki *et al.* (2014) performed an in-vivo weight-bearing study for a squatting exercise through the range of 0 to 140˚ of flexion, to test the validity of the cTEA as a surrogate to the singular-FEA model. Medially the cTEA demonstrated superior displacement in the first 100º of flexion followed by inferior displacement until 140º. Lateral displacement was always inferior throughout the entire ROM. No PD displacement was recorded in the first 10º of flexion. They concluded that the cTEA is not an acceptable surrogate to the FFA since it demonstrated relatively large movement in the PD direction. In light of the dual-FEA model, this study provided further evidence (in addition to the results presented by Most *et al.*) that the cTEA has the potential of being the surrogate to the ECA.

- Further to research data presented so far, the author of this thesis provided an additional argument in support of one of the TEA variants being the surrogate to the ECA. It was suggested that the TEA might be a suitable surrogate to the ECA due to the location of its anatomically defined ROIs and their coincidence to the collateral ligaments which are known to be taut during the extension phase, thus acting as the fulcrum point of rotation during the extension phase.

- So far in this review of literature, the GCA was defined as the surrogate to the FCA, and the cTEA displayed the most promising results for the possibility of acting as the surrogate to the ECA. However, the sTEA was not yet reviewed due to its more recent emergence relative to the cTEA.

- One of the first studies reviewed for the sTEA was by Matsuda *et al.* (2003). They identified the sTEA as maintaining a more predictable orientation with respect to the tibial mechanical axis relative to the cTEA and APA.

- Asano *et al.* (2005) performed an in-vivo weight-bearing study investigating the relationship of the sTEA to their algorithm-based FFA. The FFA that they identified in their study did not report statistical difference when compared to the sTEA. Based on this, the researchers suggested that the sTEA is applicable as a surrogate to the FFA. The author of this thesis identified shortcomings in their reasoning, mostly due to the underlying assumption of the singular-FEA model, which will produce considerable kinematic crosstalk if implemented. Also, given that they extracted the FFA over the ROM from 0 to 90˚, then such a statement would only be applicable for that given range.

- Victor *et al.* (2009) confirmed that GCA is perpendicular to the tibial mechanical axis, thus supporting the statement of Matsuda *et al.* (2003). Also, they stated that the GCA is parallel to the tibial transverse axis when projected on the tibial plane, and also parallel to the sTEA but not the cTEA. Finally, Victor *et al.* point out that CT imaging should be utilised for the identification of the femoral epicondyles since this method has been shown to provide acceptable accuracy.

- Lustig *et al.* (2008) did a "critical analysis of the concept of the sTEA as the fixed axis of rotation of the femoral condyles during flexion of the knee". This study was purely anatomic and did not involve analysing the dynamic movement of the knee. They attempted to fit a sphere (in a plane perpendicular to the sTEA) to the condyles of the femur, which was not successful. They confirmed that the sTEA and GCA do not coincide. Also, they measured the distance from the sTEA intersection with each condyle to the distal, intermediate and posterior articular surfaces. They noted that laterally the distances were similar, confirming that the lateral condyle has a single curvature. Medially the distances were statistically different, therefore confirming that the medial condyle had two or more curvatures. Based on their results, they concluded that since the distances showed apparent homogeneity, the sTEA might have been misinterpreted as the centre of curvature. They concluded that the sTEA is not adequate for defining the articulation of the entire femur. Apart from the series of studies by Freeman *et al.* this was the only reviewed paper which recognised the fact that an FEA does not apply to the entire ROM of the knee. The researchers did not comment on the applicability of the sTEA to the ECA.

- Yin *et al.* (2015) performed a study investigating the relationship between the FFA and the GCA and sTEA. They obtained kinematics data for 20 healthy subjects under

weight-bearing conditions. They showed that the GCA is closer to the FFA than the sTEA, concluding that the GCA is a better anatomical surrogate for the FFA. Similar to the study of Asano *et al.* this study suffered from the underlying assumption that the knee rotated around a single FEA. Nonetheless, in light of the dual-FEA theory, their results can be appreciated as discussed in the review.

- Feng *et al.* (2016) performed a dynamic in-vivo loaded analysis of femoral condylar motion using the cTEA, sTEA and GCA axes on 20 healthy subjects. They analysed the AP and PD translations of each FEA from full-extension until the maximum comfortable flexion. The two TEA variants showed marginal PD translations during the effective ROM of the ECA, while the GCA showed marginal PD translations during the effective ROM of the FCA. The sTEA, in comparison to the cTEA, clearly maintained a more static vertical displacement from hyper-extension through to 60º, most prominently in the medial compartment (laterally, slight deviations from a static vertical displacement is assumed to have occurred due to the saddle-shaped contour of the lateral tibial plateau). The results reported by Feng *et al.* (2016) support the dual-FEA model theory since the sTEA is displaying marginal kinematic crosstalk during the initial stages of flexion, therefore providing evidence that the distal femur is rotating around this FEA during the Extension and Transition phases of the flexion cycle (-10º to 30º of flexion – although they reported minimal kinematic crosstalk until 60º of flexion). Subsequently, the distal femur transitions its FEA to the GCA until the end of the Flexion phase (30º to 120º of flexion), which reflects the quasi-static PD translations noted for the GCA in the results presented by Feng *et al.* (2016).

Literature Review concluding remarks and observations

The study designs of the reviewed literature had limitations and challenges which undermine the validity of their results when applied to much larger populations. The number of subjects was usually small (under 25) and sampled from a single population across studies (Churchill *et al.*, 1998; Eckhoff *et al.*, 2007b; Victor, Van Doninck, Labey, Innocenti, *et al.*, 2009; Feng *et al.*, 2016). Knee kinematics were collected using different methods, such as cadaver tests using knee simulators (Churchill *et al.*, 1998; Eckhoff *et al.*, 2005) and in-vivo radiographic tracking based on single-planar or biplanar image matching techniques (Asano, Akagi and Nakamura, 2005; Mochizuki *et al.*, 2014; Feng *et al.*, 2016). Meanwhile, the kinematics was under different loading

conditions, such as passive flexion (Most *et al.*, 2004; Eckhoff *et al.*, 2005), quasi-static knee bending (Yin *et al.*, 2015) and active flexion (Asano, Akagi and Nakamura, 2005; Mochizuki *et al.*, 2014; Feng *et al.*, 2016). All these factors affect the results, making it harder to extract a conclusive statement from the reviewed research.

The aim of the above review of literature had been primarily intended to understand which FEA would be ideal for implementing in the practical aspect of this thesis. Following a preliminary reading of the literature, the author of this thesis noted that several contradicting statements were being mentioned in some prominent papers. It is for this reason that it was decided to perform an in-depth and chronological review, to provide clarification on how and why there were such conflicting statements with no consensus being reached amongst researchers in the aspect of identifying the surrogate FEA for the distal femur. Following the in-depth critical review, which has been transcribed in the above text, an emerging trend was noted whereby most researchers unknowingly overlooked the assumption of modelling the knee using the singular-FEA model theory. Implementing the singular-FEA model theory for the analysis of knee kinematics is not wrong in no way whatsoever. The issue emanates if researchers are not aware of the assumptions being taken when implementing such a 'simplified' model, such that incorrect interpretation of the resulting data occurs. This was noted in a majority of the papers using the singular-FEA model since they state in their concluding remarks that given their results, a particular singular-FEA model can be used to evaluate and describe the knee kinematics without taking into consideration the imposed effects of kinematic crosstalk on the results if one were to follow their guidance. Some go a step further stating that their axis of choice can also be used for guiding component alignment in TKA and for the design and development of new implant designs (Churchill *et al.*, 1998; Matsuda *et al.*, 2003; Most *et al.*, 2004; Asano, Akagi and Nakamura, 2005; Yin *et al.*, 2015). Taking into consideration the sensitivity of implant alignments, such as the fact that minor malrotation of 1-4° will result in lateral patellar tracking and other unbalanced tissue loads (Victor, 2009), and that knee implant designs will leave detrimental effects on the patients' kinematics if the slightest geometric discrepancy is taken for granted, then the aforementioned statements in prominent research are to be taken cautiously. Taking into consideration the complex and intricate articulation that is known to occur in knee kinematics, then research should be driven towards understanding the underlying mechanisms of the dual-FEA model

theory rather than trying to identify the ideal singular-FEA to simplify our understanding. Such underlying mechanisms would be the identification of the ideal surrogate to the ECA and the mechanisms which define the Transition phase from the ECA to the FCA. Once these mechanisms are understood and successfully modelled, research will become more centralised allowing for the development of more robust implant designs which replicate the natural knee kinematics, thus reducing implant failures.

Given the current state of research, the singular-FEA model theory remains the most feasible model to use since implementing the dual-FEA model would require the researcher(s) to have answers to the aforementioned underlying mechanisms. Hence, considering that the singular-FEA model is the best current option, the limitations and pitfalls of the singular-FEA model must be understood to allow for valid conclusions to be drawn. Considering the reviewed literature regarding the identification of the ideal singular-FEA, it is not surprising that a conclusive agreement has not yet been agreed. It has been indicated that researchers are not aware of these limitations and pitfalls, leading them to attempt to identify a singular-FEA which applies for the entire ROM of the knee, which is not a tangible outcome given the knowledge of the dual-FEA model theory. By definition, an ideal FEA would be one that would show no relative movement in the following planes. PD translation should be minimal since the knee is assumed to be in contact throughout the ROM. Marginal PD translations are to be accepted if they follow the tilt of the corresponding tibial plateau profile. AP translations should also be minimal while keeping in mind the translations that are expected to occur as a result of the native articulation of the knee, primarily screw-home, medial-pivoting and femoral roll-back.

Additionally, abduction-adduction rotations should show marginal movement during flexion of the knee. It is also important to take note of the effects of kinematic crosstalk which would be dependant on the axis being chosen. The author of this thesis proposes that the sTEA and/or the GCA should be implemented, given the conclusions derived from the above-reviewed literature. With the knowledge that the sTEA is a possible surrogate to the ECA, and the GCA being an excellent surrogate to the FCA, then two approaches are being suggested:

Approach 1: Use either the sTEA <u>or</u> GCA. If this approach is chosen, the user should be aware that once the flexion angle goes outside the applicable ROM of the chosen axes (that is, exceeds 30º of flexion for the sTEA, or below the 30º of flexion and above 120º of flexion for the GCA) then the resulting kinematics will be affected by kinematic crosstalk. The results should then be intricately analysed to understand the effects of crosstalk for this specific case. It should also be noted that the transition phase is subjective and might vary from the theoretical 30º flexion mark proposed above.

Approach 2: Use both the sTEA and GCA. This is the preferred approach since this will avoid having to reason out the effects of kinematic crosstalk. With both axes implemented, the user is only required to identify the point, or range, at which the knee transitioned from the sTEA to the GCA, or vice-versa. The transition point, or range, can be identified by primarily assessing the PD translations and secondarily the AP translations of both the axes to identify when considerable signs of out-of-plane movement occur. Once the point of transition is identified, then the user can consider the range from hyper-extension until the identified transition point for the sTEA and similarly, from the transition point through to 120º of flexion for the GCA.

Given the knowledge gained through this review of literature, the author is confident that using the second approach will result in virtually eliminating kinematic crosstalk, therefore, achieving the most realistic results, until more research is performed on the dual-FEA model theory. Dual-FEA model theory research should primarily focus on the identification of an ideal surrogate for the ECA and FCA and secondarily understand the underlying mechanism of the transition occurring between both axes. Until this information is learnt, all knee-kinematic studies will be tainted by the effects of kinematic crosstalk.

Having a standardised system will have drawbacks to implement since it requires a change in the mentality of several researchers and clinicians who are used to using their preferred system. However, the author believes that this will streamline communication amongst researchers and comparison of reported data. If this is not achieved, it would merely lead to further disagreements and conflicting statements which ultimately impinge on our objective of being able to replicate the natural kinematics of the knee in future implant designs, thus improving patient satisfaction.

2.6.2.2   INTERNAL-EXTERNAL ROTATION AXIS

The IEA of the knee is known to lie in the tibial bone, initiating distally from the centre of the ankle, and proximally, the location of the IEA intersection with the tibial plateau varies depending on the loading conditions, or the activity, imposed on the knee. (Hollister *et al.*, 1993; Churchill *et al.*, 1998). While there have been numerous studies in literature related to the identification of the FEA of the knee, less attention has been directed towards identifying the knee's natural IEA for tibial rotation.

This is probably since it is not the primary axis of the knee, and thus the internal-external rotation of the knee only started gathering attention by biomechanists when knee kinematic analysis in 3-dimensions came into play. The realisation of the importance of the IEA has come to light as an important design feature of modern TKA implants following the early attempts with hinge-type implants utilising a single fixed axis for FEA, with no allowance for internal-external rotational DOF. These designs imposed many restrictions w.r.t the freedom of movement for the replaced knees in which they were implanted, leading to a universally poor result, with failures attributed to loosening at the implant-bone interfaces due to excessive rotational torques being generated at this interface. This brought about a keen interest on learning more about its location in the knee and its relation to the FEA in the compound knee model, to be able to allow implant designers to incorporate rotational freedom into their subsequent designs.

Studies attempting to map the IEA location for varying degrees of flexion have produced a wide variety of interpretations. The IEA was reported to have both fixed and dynamic locations. In vitro, un-loaded studies reported the IEA to pass through the intercondylar eminence (Shaw and Murray, 1974; Hollister *et al.*, 1993), the medial femoral condyle (Brantigan and Voshell, 1941) or being dynamic, with an instantaneous moving centre in the intercondylar eminence (Matsumoto *et al.*, 2000; Boguszewski *et al.*, 2016). Not much has been done w.r.t in-vivo studies, as the reviewed studies only performed tracking of the displacement of the menisci using MRI (Thompson *et al.*, 1991; Vedi *et al.*, 1999) and measured bony landmarks to deduce the location of the IEA (Kaneda *et al.*, 1997).

Hollister *et al.* (1993) used the aforementioned "axis-finder" to locate the IEA through a series of manual internal and external rotation of the tibia on a fixed femur and noted

that it was fixed at the insertion point of the ACL on the tibial plateau (Hollister *et al.*, 1993). It is important to recall that the study of Hollister was criticised since their "axis finder" only allowed rotations to occur (no translational DOF), thus limiting the freedom of movement of the tibia, which might be correlated to the fixed IEA results obtained in their study. Churchill *et al.* also measured the intersection of the IEA with the tibial plateau in 1998 for a loaded knee undergoing a passive squatting movement (Churchill *et al.*, 1998). They reported the functional IEA to intersect the tibial plateau medial and proximal to the centre of the tibial plateau (Figure 41A). Their results represented the sitting of the medial femoral condyle onto the concave medial tibial plateau due to the loading conditions which translated the intersection points to lie more toward the centre of the medial tibial plateau rather than being in the proximity of the medial tibial spine.

A few years later Matsumoto in 2000, used bi-planar photography to identify the location of the IEA upon forced internal and external rotational torques on the tibia and noted that the IEA moved depending on the flexion angle. He reported that on average, it is located between the insertion point of the ACL and PCL. As seen in Figure 41B, Matsumoto reported that the IEA at 0˚ of flexion was slightly posterior to the ACL insertion point, and gradually moved posteriorly until it was slightly posterior to the PCL insertion point at 60˚. Subsequently, it translated again anteriorly to lie equidistant from the insertion point of both cruciate ligaments by 90˚ (Matsumoto *et al.*, 2000).

When relating these results with the functional anatomy of the knee, it correlates to a certain extent with the complex interaction of varying tension between the ACL and PCL during flexion. In an extended knee, the ACL is taut (along with the collateral ligaments) while the PCL is relatively lax, which would result in the ACL acting as a fulcrum for the IEA. As the knee progresses through flexion, the ACL tension is transferred onto the PCL, which correlates with the transition of the IEA location with increasing flexion. This phenomenon was noted by Elias *et al.* for the FEA, with the collateral ligaments acting as fulcrum points for the knee to rotate around during extension (Elias, Freeman and Gokcay, 1990). Thus, using the same reasoning, the IEA might be using the ACL and PCL as fulcrum points, depending on the tension of the cruciate ligaments. This theory is further amplified by an RSA study which recorded a drastic change in the IEA rotation following ACL injury, with the assumption that this

change might imply the beginning of osteoarthritis in an injured knee (Brandsson *et al.*, 2001).
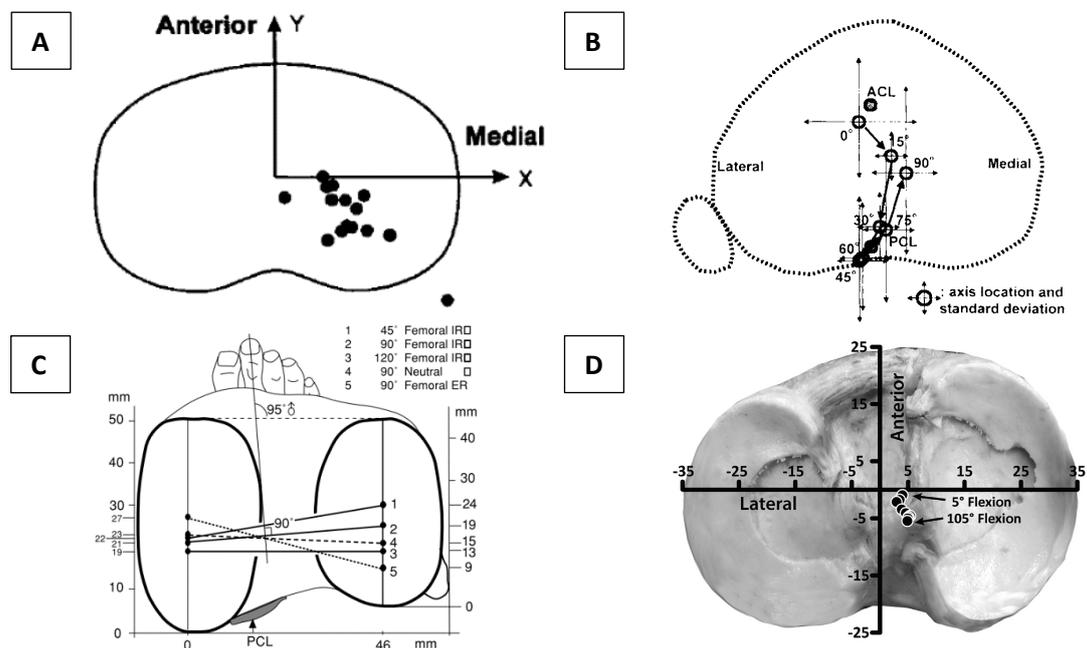
Figure 41: The longitudinal rotation axis of the knee (IEA)

A: A schematic of the tibial plateau overlaid with the recorded intersections of the IEA for the 15 loaded specimens during a passively simulated squatting exercise between full extension and 100˚ of flexion. (Churchill *et al.*, 1998)

B: Location of the axis of tibial rotation. The location of the axis at 15˚ increments is visualised against the locations of the ACL and PCL in this illustration from a superior axial view of the tibial plateau. Refer to text for an explanation (Matsumoto *et al.*, 2000).

C: The proximal penetration point of the IEA was deduced from a series of forced axial rotations at different knee flexion angles. The FFC axes for each recorded position are projected onto the tibial plane for visualisation. (Iwaki, Pinskerova and Freeman, 2000). Note that this image is inverted, in the ML direction, to the ones shown in **A**, **B** and **D**.

D: The IEA "Instantaneous Centre of Location" on the tibial plateau as derived using the Reuleaux method. The IEA locations were always medial to the plateau centre (p < 0.001) (Boguszewski *et al.*, 2016).

This correlation between the IEA location and the cruciate ligaments was further analysed by Boguszewski *et al.* in a recent study. They utilised a custom-built and validated setup which fixed the femur and allowed unconstrained tibial rotation while permitting AP, ML and PD movement as the tibia was manually flexed in small increments under no loading conditions. They identified the "Instantaneous Centre of Rotation" (ICR) using the well-documented and validated method of Reuleaux (Reuleaux, 1875). Their primary finding was that the IEA was dynamic and throughout the range of flexion it was initially located medial and posterior to the centre of the tibial plateau and moved posteriorly with knee flexion (Figure 41D). Concerning the ACL, their results would translate to initiating posterior to the ACL and moving

posteriorly with flexion towards the PCL insertion site. This agrees with the previous unloaded knee studies discussed above and further supports the theory relating the IEA to the tension in the cruciate ligaments.

Regarding the functional anatomy of the knee described in section 2.4, Iwaki *et al.* performed a series of forced axial rotations on the same cadaveric knees which were used to analyse the morphology of the knee to deduce the location of the IEA (Figure 41C). Iwaki suggested that when projecting the FEA of forced axial rotations at specific flexion angles onto the tibial plateau, the intersection point of the projected FEAs can be used to locate in the distal intersection point of the IEA (Iwaki, Pinskerova and Freeman, 2000). This can be seen in Figure 41C for the 90° position, where the neutral, internally- and externally- rotated projected axes penetrate the tibial plateau proximal to the medial tibial spine. They concluded that the IEA is not fixed but varies in the anteroposterior direction on the lateral side of the medial plateau. They further backed their statement by referencing it to the asymmetry of the tibial plateau, which contributes to the longitudinal rotation occurring in the knee, where the saddle-shaped lateral tibial plateau and the concave medial plateau direct the axis of the longitudinal rotation of the knee medially (Fu, Harner and Vince, 1994; Iwaki, Pinskerova and Freeman, 2000). Also, the medial and lateral menisci factor into the medial location of the axis of longitudinal rotation since the medial meniscus is more firmly anchored than the lateral meniscus, thus allowing the lateral meniscus to move posteriorly as much as two times further than the medial meniscus (Thompson *et al.*, 1991; Vedi *et al.*, 1999).

In conclusion, the identified literature about the identification of the functional IEA clarified that the proximal intersection point of the IEA is not fixed in one location but is also continually moving to adapt to the multitude of active forces and passive restraints which are subjective and activity-dependant. An apparent discrepancy can be noted between loaded and unloaded knees, where for loaded knees the IEA is reported to intersect the medial tibial plateau toward its centre, because of the loading conditions which sit the medial femoral condyle in the concave medial tibial plateau. On the other hand, unloaded knees seem to have less dependency on the morphological features of the knee contact areas but are more affected by the effect of ligamentous restraints, namely the cruciate ligaments. The functional IEA for an unloaded knee seems to lie between the insertion points of the cruciate ligaments, toward the medial aspect of the tibial spine.　　Nonetheless, more studies are required to understand better the

relationship between the location of the functional IEA and the ligamentous restraints, load-bearing forces and muscular activities. Additional 3-dimensional research is required to determine the effect of these factors on the axis of motion and resultant in-vivo knee kinematics.

With the inconsistencies that exist in the literature, it is thought-provoking to the author's realisation, that there exist reports in the literature, such as the study by Garling *et al.* (2007) that reported that there are implants (the one in question being a posterior stabilised mobile bearing implant) which are still being sold in the market whose design for the IEA is based on the locations reported by Hollister *et al*. (1993). While the study of Hollister is a notable one and of great scientific value, its sample size is that of only six cadaveric knees without mentioning the fact that the knees being tested were constrained to only 3 DOF. Furthermore, the description of tibial rotation axis placement for other implants is lacking in the literature, leaving the author to question the robustness in the design stage of such implants.

In theory, placing the tibial implant's fixed IEA at the location of the knee's natural IEA should reproduce the normal knee kinematics and maintains the normal balance of forces within the knee, since kinematic crosstalk is being avoided. Here a major limitation of fixed-bearing implants is put into light since the knee has been shown to have a dynamic IEA. Therefore, when the fixed IEA location embedded in the design of the fixed-bearing implants does not match the natural IEA location, the patients are put in the risk of having forced tibial rotations. These unwanted tibial rotations lead to imbalanced forces in the ligamentous restraints, which lead to potential polyethylene wear and possible loosening at the bone-implant interface. Contrarywise in mobile-bearing implants, mal-positioning of the IEA can be accommodated by the movement of the femoral component on the superior surface of the tibial polyethylene insert.

Nonetheless, this could still produce an imbalance of forces on the collateral and cruciate ligaments. This has been studied and reported in numerous in-vivo fluoroscopic patient studies that noted that the centre of the tibiofemoral rotation in mobile-bearing implants did not always coincide with the implant fixed IEA (Garling *et al.*, 2007; Chouteau *et al.*, 2009; Harman *et al.*, 2012). Finally, the evidence of the importance of the IEA of the knee is illustrated in the novel developments of knee prostheses. Recently, new knee prosthesis has been designed with a medial compartment acting as a ball-and-socket joint and the lateral compartment as an

outrigger, allowing the lateral AP translations to occur around the medial-pivot created by the deep medial congruent socket. Although these implant designs have not yet been thoroughly tested to be accepted as a golden-standard, they are showing promising results in their early stages of testing (Banks *et al.*, 2016).

2.6.3 KINEMATIC MATHEMATICAL MODELS OF THE KNEE

When the motion associated with an anatomical joint needs to be measured, a kinematic mathematical model for the anatomical joint must first be established. By definition, a mathematical model is the description of a system using mathematical concepts and language, whose aim is to explain the systems' function and to study the effects of its different components. Therefore, it can be inferred that a kinematic mathematical model describes the motion of objects (without the consideration of forces). In order to define the object's motion a set of rigid bodies need to be defined in space, and the motion of these bodies needs to be constrained by the number of degrees-of-freedom of the joint(s) connecting the said rigid-bodies.

Different kinematic mathematical models use different approaches to interpret the motion that is being investigated. It should be noted that while there are several mathematical models which use different mathematical concepts to define motion in space for anatomical joints, their interpretation, that is the description of the motion being studied, differs. In this section, three different kinematic mathematical models, which are used to describe the motion of anatomical joints, specifically the knee, over time, will be discussed, while highlighting the benefits and limitations of using these models.

A statement that puts into perspective the complexities that go into building these mathematical models was penned by Kinzel and Gutkowski in a review of kinematic mathematical models in 1983. They stated that due to the difficulty to describe general spatial motion quantitatively, only a few investigators attempt it, since:

> *"The unambiguous description of spatial motion is perhaps more difficult than the measurement itself."*
>
> - *Kinzel and Gutkowski, 1983)*

2.6.3.1   THE INSTANTANEOUS CENTRE OF ROTATION MODEL

The first documentation of the morphology of the femur was undertaken by the Weber brothers (Weber and Weber, 1837), who proposed the circular geometry of the posterior condyles. Braune in 1891 and Fick in 1911, challenged these statements, proposing that the condyles were more helical in shape (Braune and Fischer, 1891; Fick, 1911). In 1904, (Zuppinger, 1904) not only performed the first radiological study of the knee kinematics but were also the first to document femoral roll-back and referred to the four-bar linkage model of the knee. While they did not correlate the four-bar linkage mechanism to the roll-and-glide movement of the tibiofemoral joint, they highlighted how the combined action of the cruciate ligaments guided the femur and tibia during flexion and extension of the knee (Zuppinger, 1904). The four-bar linkage mechanism described the motion of the knee in the 'pure' sagittal plane, where the ACL and PCL represented the two rigid bars (or links) connecting the femur and tibia (Figure 42C).

A few decades later in 1971, Frankel *et al.* suggested that at intermittent knee flexion angles the intersection of the ACL and PCL along with the changing radius of curvature of the condyles resulted in an "instantaneous centre of rotation" (ICR) which shifted along a predictable "J" curved pathway as the knee flexed (Frankel, Burstein and Brooks, 1971). The ICR was determined using the method of Reuleaux, which involves a simple yet astute process (Reuleaux, 1875). Two points are chosen on the femur at a particular instant in time, say A_1 and B_1, and then the femur is moved around a static tibia and the exact same points are recorded again, thus having A_1' and B_1' (refer to Figure 42A). The lines joining the same points at different time instants, such as $A_1 A_1'$ and $B_1 B_1'$, represent the displacement of these points. Perpendicular bisecting lines (dotted lines in Figure 42A) are then projected from each of these lines, and their intersection point is termed the centrode or ICR. Due to the shapes of the bones and the restraints on motion imposed by the soft tissues, the ICR of successive flexion angles moves, following a semi-circular pathway (shown in red in Figure 42B), referred to as the "J-curve".

The "instantaneous centre of rotation" and "four-bar linkage" theories were primarily accepted throughout the 20st century, as shown by the large following of engineers until at least the 1980s (Bugnion, 1892; Zuppinger, 1904; Strasser, 1917; Kapandji, 1970; Smidt, 1973; Nordin and Frankel, 1982). This system provided a mechanical explanation of the roll-and-glide motion of the femur on the tibia with increasing

flexion. The ICR model was influential to the extent that it had even influenced contemporary knee implant designs (Floerkemeier *et al.*, 2011). While this theory helped explain the posterior translation of the femur relative to the tibia along with the resistance to posterior drawer motion that occurs during the articulation of the knee, it had a pitfall. This theory assumed a 2-dimensional description of motion, whereas nowadays we are aware that the knee articulates through all 3-dimensions. Studies which correlated knee motion to the "four-bar linkage" mechanism intrinsically failed to analyse the FEA offset from the anatomical sagittal plane, or to take into consideration the coupled internal and external rotation that occurs around the IEA (Soudan, Van Audekercke and Martens, 1979; Hollister *et al.*, 1993).
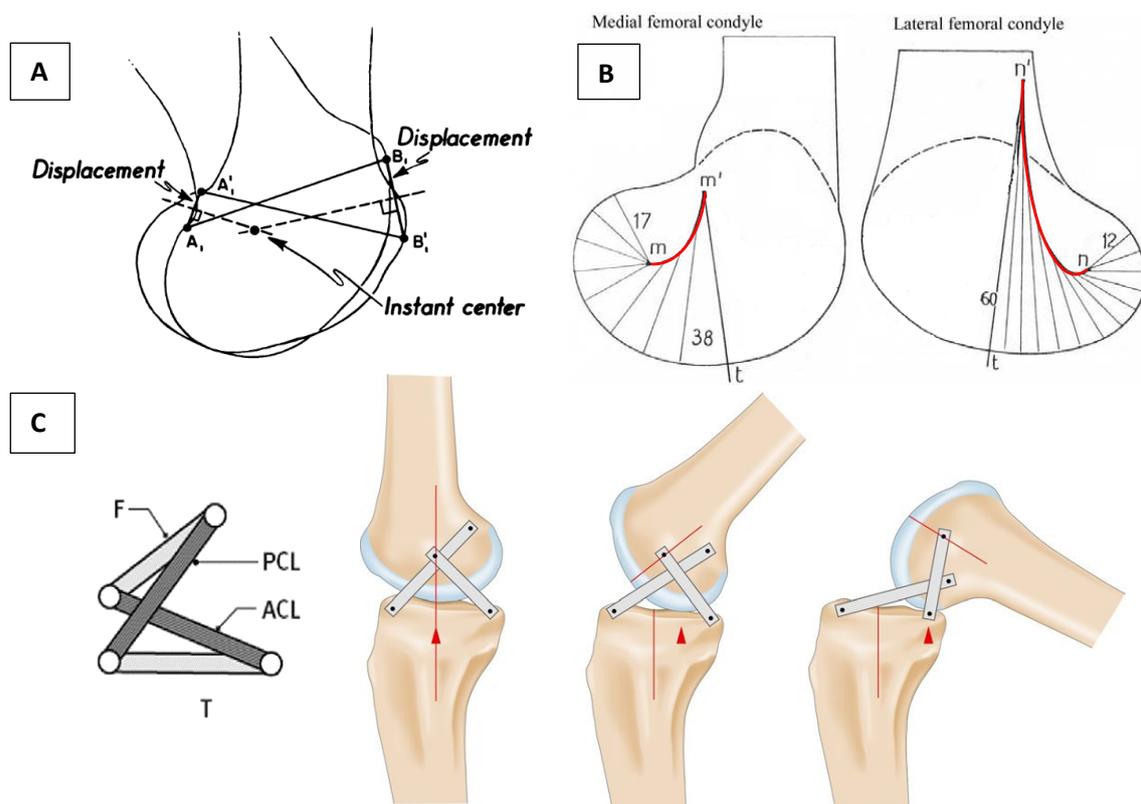
Figure 42: Depiction of the early knee ICR model concept which influenced contemporary knee kinematics.

A: Determination of the instant centre of motion by the method of Reuleaux. Refer to text for explanation. (Frankel, Burstein and Brooks, 1971)

B: A sagittal view of the ICR pathways for the medial and lateral condyles (representing the medial and lateral ends of the axis of knee flexion and extension, according to Kapandji). The distances from the articular surface to the ICR is the radius of curvature, which varies throughout flexion. "t" shows the anterior limit of tibiofemoral contact during hyper-extension. (Kapandji, 1970)

C: The four-bar link mechanism proposed by Zuppinger formed by the fixed distance between the cruciate ligaments (ACL and PCL), the femur attachment sites (F) and the tibia attachment sites (T). The four-bar linkage mechanism action is shown on the right. (Shenoy, Pastides and Nathwani, 2013).

With the advent of medical imaging, researchers could conveniently perform 3-dimensional studies of the knee. This brought about a considerable change in the knee kinematics knowledge of the time. Furthermore, the "four-bar linkage" theory was side-lined when studies investigating the mechanical and anatomical properties of the cruciate ligaments revealed that femoral roll-back did not primarily occur as a result of the cruciate ligaments in the knee (Blankevoort, Huiskes and de Lange, 1988; Smith, Livesay and Woo, 1993). With reference to section 2.4, the manuscripts by Freeman *et al.* (2000) later emphasised how the morphology of the knee's compartments are mainly responsible for the roll-back mechanism of the knee, with the four major ligaments acting as a secondary mechanism providing stability.

Similarly, the 2-dimensional "instantaneous centre of rotation" theory, was discredited by Hollister who suggested that this theory needs to be re-evaluated in 3-dimensions because researchers had repeatedly assumed a flexion axis perpendicular to the sagittal plane of the knee (Hollister *et al.*, 1993). While locating an axis perpendicular to the sagittal plane may have sounded quite intuitive, it is not the case for the knee, as there is yet no anatomical or kinematic data that support the idea that the flexion-extension axis of the knee is perpendicular to the sagittal plane. It was reported by Churchill *et al.* that out-of-plane rotation leads to errors of up to 20mm, which are way too large to accurately describe knee kinematics (Churchill *et al.*, 1998). Also, another argument against the 2-dimensional "instantaneous centre of rotation" theory was that, for most human articulations, the anatomy has evolved to produce the most efficient movement, such as the movement occurring within joints such as the shoulder, elbow and hip. A continually moving axis, as proposed by Braune's theory, is highly inefficient because the inertia will continuously be changing its location, leading to a considerable waste of energy.

Contemporarily studies investigated the application of the ICR theory in 3-dimensions by considering the sagittal offset of the native knee. The 3-dimensional application of the ICR theory was verified to replicate native knee-kinematics theoretically (Fiedler *et al.*, 2011). From a practical perspective (Floerkemeier *et al.*, 2011) the ICR theory was implemented into the design of a novel physiological knee prosthesis (Aequos G1 knee arthroplasty) which replicated the convex (lateral) and concave (medial) morphology of the tibial compartments along with a sagittally-offset FEA. This knee replacement was reported to reconstruct the four-bar linkage mechanism of the native

knee, having displayed induced roll-back mechanism, however physiological knee kinematics were only achieved up until 45º of flexion (Floerkemeier *et al.*, 2011).

In conclusion, while the ICR theory was beneficial for simplifying the understanding of the complex articulation of the knee in the early knee kinematic studies, it is not sufficient for the accurate analysis of the 6 DOF kinematics of the knee. It presented a simplified 2-dimensional explanation for femoral roll-back due to the combined action of the cruciate ligaments which were assumed to guide the femur and tibia during flexion and extension of the knee. Following 3-dimensional studies of the knee, the ICR model was understood to be only adequate for the planar description of knee joint motion. Contemporarily, it has been shown that while the cruciate ligaments have a role in defining the articulation of the knee, they are not the primary mechanisms which define its movement. It has been shown that the morphology of the knee is the principal mechanism which defines the complex articulation of the knee, with the cruciate ligaments acting as secondary stabilising mechanisms.

2.6.3.2   THE HELICAL AXIS MODEL
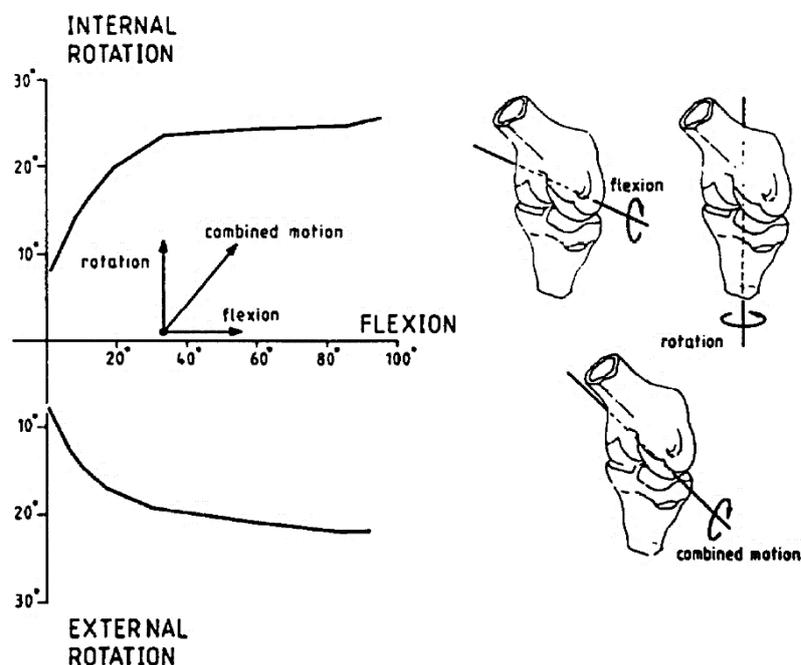
Figure 43: An illustration of the obliquity of the helical axis as a result of the combined axial rotation and flexion

The illustration shows the passive knee joint motion between full extension and 95˚of flexion with internal and external tibial torques of 3Nm. The joint in this case could freely move within its envelope in flexion and axial rotation. The graph on the left shows the reported flexion and tibial rotation (with respect to their corresponding anatomical axes), while the knee depictions on the right show how the helical axis results in an oblique angle due to the combined movement of the FEA and IEA (Blankevoort, Huiskes and de Lange, 1990)

The Helical Axis model offers a complete three-dimensional description of motion, and to a certain extent, can be considered as an extension of the planar (2-dimensional) ICR model explained in the previous section. The helical axis theory is based on Chasles' theorem which states that any Euclidean displacement of a rigid body in three-dimensional space has a screw (or helical) axis that can be decomposed into a rotation about, and translations along, the screw axis (Bottema, Roth and Veldkamp, 1980). As a result of the known coupled-rotational articulation of the tibiofemoral joint, the functional axis of rotation is not parallel to the frontal or coronal planes. The functional axis of a rigid body is defined as one single axis that incorporates the combined movement of the rigid bodies being analysed. Therefore, for the case of the knee, due to the coupled motion of the femur around the FEA and the tibia around the IEA, the functional axis will lie at an oblique angle relative to all anatomical planes (Figure 43).

Many possible paths of motion may be followed by a rigid body when moving from one position to another. Contrary to Euler (or Cardan) angle description of motion (which will be discussed in section 2.6.3.3), helical axes are independent of the order in which the translations and rotations occur. The simplest path of motion for a rigid-body is found by identifying the helical axis (Bull and Amis, 1998). The reader is referred to Figure 44 for a visualisation of the helical axis of a moving tibia around a fixed femur. The mathematical derivation of a helical axis is beyond the scope of this thesis and will only be briefly outlined in the following discussion.

The helical axis model quantifies the relative motion between two rigid-bodies by identifying the *pose of the helical axis* and *the magnitude of rotation and translation* that the moving rigid-body is performing around the fixed rigid-body. First, cartesian coordinate systems are embedded into each body and the corresponding position and rotational matrices for both time steps are extracted in the same way as explained in section 2.6.1. The position and rotational matrices for the two-time steps are manipulated to form what is referred to as a displacement matrix, which holds the information of the mapping of the displacement that the moving body performs around the fixed body. The displacement matrix is then equated with a helical matrix in order to extract eight unknown parameters (contained within the helical matrix) which entirely define the pose of the helical axis and the motion performed around it.

Six parameters define the pose of the helical axis. The first three parameters are contained within the position vector $L = [L_x \quad L_y \quad L_z]$, which is a line connecting the

origin of the fixed body (femur) to the closest point on the helical axis (occurring at the perpendicular intersection - Figure 44). The other three parameters specify the orientation of the helical axis, which is defined by the direction cosine vector $C = [C_x \quad C_y \quad C_z]$ of the axis (refer to Figure 44). With the pose of the helical axis defined, the remaining two parameters define the displacement that the moving body performs around the helical axis. These two parameters are the magnitude of the rotation angle, ω, and the translation, s, that the moving body (tibia) is making around the helical axis. These eight parameters are subsequently extracted from the helical matrix by solving the necessary scalar equations after equating it with the displacement matrix.
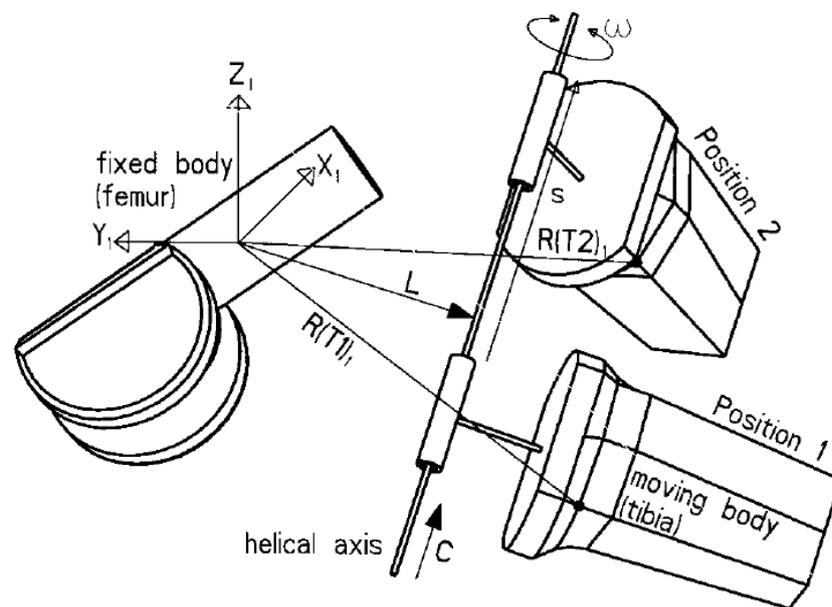
Figure 44: A visualisation of the eight variables defining the pose of the helical axis for a moving tibia and the motion occurring around it.

A fixed body and a moving body at two positions in space are shown. R(T1)₁ and R(T2)₁ represent the position matrices of the moving tibia with respect to the fixed femur. The pose of the helical axis is defined by the position vector L, and the direction cosine vector C. The helical rotation and translation of the moving tibia around the fixed femur are represented by ω and s respectively (Bull and Amis, 1998).

For helical motion, the smaller the increments in time between the movement steps (i.e. as T2-T1 tend to zero), the more the helical axis will approximate the position of the functional axis. While reducing the time-step size will seem beneficial at first, it should be noted that as T2-T1 tends to zero, errors in the position data used to calculate the path of motion of the moving rigid-body will increase, rendering the calculations more inaccurate. Furthermore, the helical axis model suffers from poor reproducibility and consistency unless the utmost care is taken to ensure that the motion pathways between studies are consistent. This is because any variations in the spatial motions between

individual specimens within a study (or even between different studies) will result in a different helical axis (Blankevoort, Huiskes and de Lange, 1990).
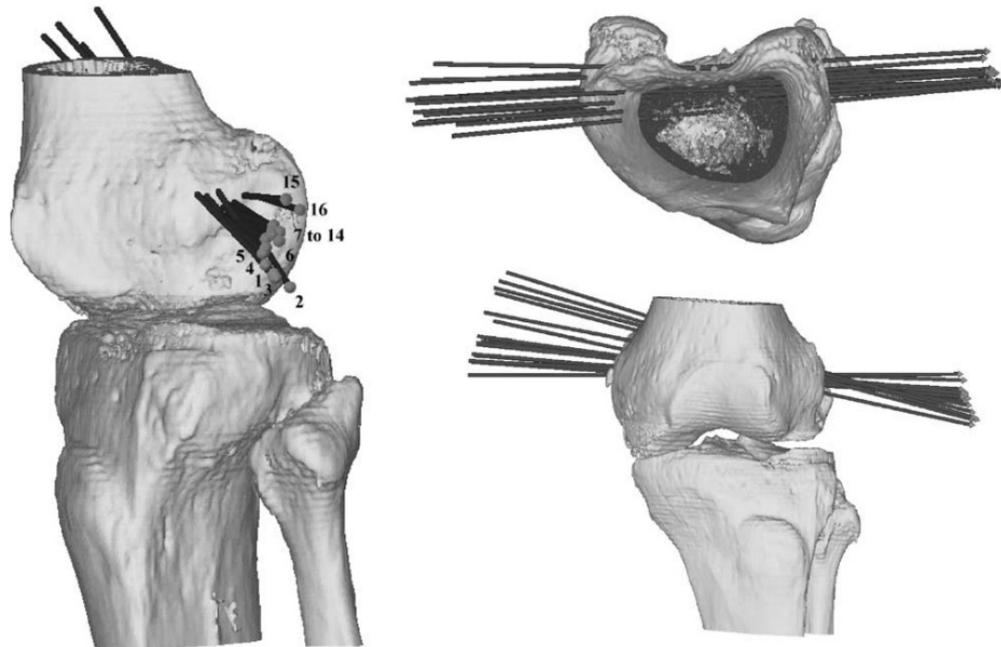
Figure 45: The helical axis of the Left knee.

Left: Lateral View;   **Right Top:** Proximal view;   **Right bottom:** Frontal view.

The helical axis during 16 steps of knee flexion, from full extension to about 80˚ of flexion is shown. ω about each axis was reported to be approximately 5˚, while total translation was 6.15mm. The obliquity of the helical axis can be clearly noted in this illustration. The posterior motion of the helical axis as the knee flexes can also be noted, which correlates with the data reported by Freeman et al, where the knee moves from the EFC to the FFC as flexion progresses. The screw-home mechanism is also clear from the frontal view, where the obliquity gradually decreases during flexion, reaching a horizontal state (end of screw-home mechanism). (Van Sint Jan *et al.*, 2002)

Mathematically, helical motion represents the most complete description of the 6 DOF spatial motion possible. This has led to its extensive use in knee models and as a design tool for prostheses. However, most clinicians find it hard to understand and correlate the results from helical model studies to their work, which is typically based around anatomical planes. With reference to Figure 45, it can be noted that while the helical axis provides a complete description of knee motion, it is not as straight forward as reporting results in the anatomical planes of the knee. The helical description of motion is not comparable to the clinical description of motion, and this led to the pitfall of the helical axis in biomechanics since most clinicians tend to avoid using such models as they are not able to interpret the results into their line of work. The helical axis model is excellent for engineers to model prosthesis designs and other anatomical joint-related

approaches, for example, relating a novel prosthesis model motion pathway with that of a native knee to quantify its effectiveness.

Studies investigating knee kinematics using the helical axis model are lacking since research focused on the JCS model, which is the preferred model to the present day. The JCS model offers a more straightforward approach to presenting knee kinematics, as will be presented in the subsequent section.

2.6.3.3   THE JOINT COORDINATE SYSTEM MODEL

The JCS model is a specific-case of Euler angles, which allows for the calculation of rotations occurring around its principal axes without having sequence dependency. Furthermore, in contrast with the standard Euler angles, this model also caters for joint translation calculations. The JCS axis arrangement, which will be outlined in this section, creates a unique set of angles which are independent of the order in which they are described. This is the case since the sequence is defined by the selection of specific axes embedded within the proximal and distal reference frames. For the application of the JCS to the knee, the sequence of rotations are defined as follows:

1. The proximal embedded axis specifies the first rotation. This axis is embedded within the femur and represents the FEA.

2. The floating axis specifies the second rotation. This axis is not embedded within any of the rigid-bodies being analysed but is continuously perpendicular to the other two axes. This axis represents the Abduction-Adduction axis of the knee.

3. The distal embedded axis specifies the third rotation. This axis is embedded within the tibia and represent the IEA.

In order to assemble a generalised JCS, the first step is to embed two Cartesian Coordinate System (CCS) with origins located at O_A and O_B within the corresponding rigid-bodies A and B, whose relative-motion is being described (Figure 46). In order to calculate the relative angular position and the corresponding rotations between the two arbitrary rigid bodies, three rotational axes need to be defined, which will ultimately characterise the JCS. These axes are symbolised by the vector notations $\widehat{e_1}$, $\widehat{e_2}$ and $\widehat{e_3}$ which are non-orthogonal unit vectors. $\widehat{e_1}$ is the first body fixed axis which is embedded in rigid body A. $\widehat{e_3}$ is the second body fixed axis, which is embedded in rigid body B.
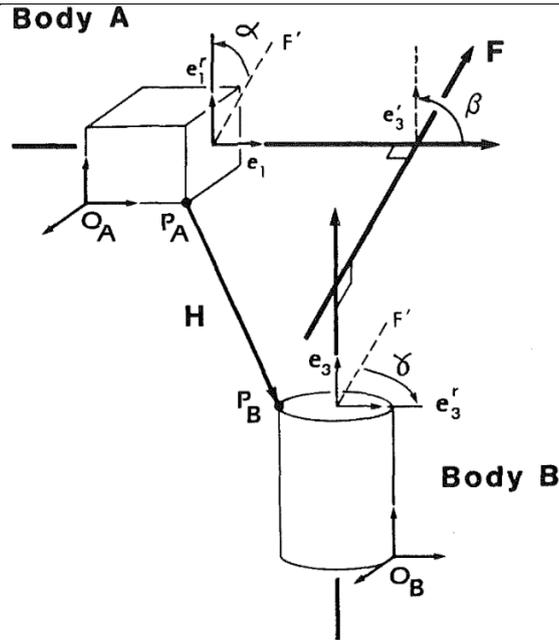
Figure 46: The generalised JCS composed of three axes (Grood and Suntay, 1983)

A CS is embedded in each of the rigid-bodies whose relative motion in 3D space is being described. A specific axis from each of the rigid-body embedded CS is selected as the body-fixed axes. These axes are the unit base vectors, $\widehat{e_1}$ and $\widehat{e_3}$ in the diagram. These two body-fixed axes are subsequently joined with a third axis, $\widehat{F}$, which is the common perpendicular to both body-fixed axes. Since $\widehat{F}$ is not fixed to either body and moves in relation to the body-fixed axes, it is called the floating axis, whose unit base vector is $\widehat{e_2}$.

These two axes can be coincidental with any of the axes in the CCS of their corresponding rigid bodies. These fixed axes will move with the rigid-bodies, so the spatial relationship between them changes with motion. The third axis, $\widehat{e_2}$ ($\widehat{F}$ in Figure 46), is the common perpendicular to the body-fixed axes $\widehat{e_1}$, and $\widehat{e_2}$. Therefore, its orientation is defined by the cross product of the body-fixed axes, as follows:

$$\widehat{e_2} = \frac{\widehat{e_3} \times \widehat{e_1}}{|\widehat{e_3} \times \widehat{e_1}|}$$

$$(21)$$

$\widehat{e_2}$ is referred to as the floating axis because it is not fixed in either body and moves in relation to both. Apart from the three primary body-fixed axes, the JCS requires another axis in each of the body embedded CCS to calculate the relative rotations between the two bodies. These secondary axes are intuitively called the reference axes, since they are used as a reference axis for the calculations of the angles α and γ formed between the floating axis and each of the body-fixed reference axes (shown as $\widehat{e_1^r}$ and $\widehat{e_3^r}$ in Figure 46). The third, and final, relative rotation occurs about the floating axis and is measured by the angle, β, between the two body-fixed axes, as follows:

$$\cos \beta = \widehat{e_1} \cdot \widehat{e_3}$$

$$(22)$$

The three angles α, β and γ, provide a general geometric description of Euler angles.

The relative position of the two reference points, P_A and P_B, located in each body, is used to describe the joint translations, as shown in Figure 46. The vector, $\hat{H}$, characterises the relative position of the reference points and is directed from body A to body B. The projections of $\hat{H}$ onto each of the three principal axes of the JCS, define the components of the translational vector.

The reader should keep in mind the clear distinction between the body-embedded CCS, located in each rigid-body, and the JCS which is composed of the two body fixed axes, $\widehat{e_1}$ and $\widehat{e_3}$ and their mutual perpendicular $\widehat{e_2}$.

In order to apply the generalised JCS, explained above, to the knee, it is necessary to specify:

1. The body-embedded CCS fixed in the femur and tibia,

2. The body-fixed axes and the reference axes of the JCS used to describe the relative rotations between the two bones, and

3. The location of the translation reference point in each bone.
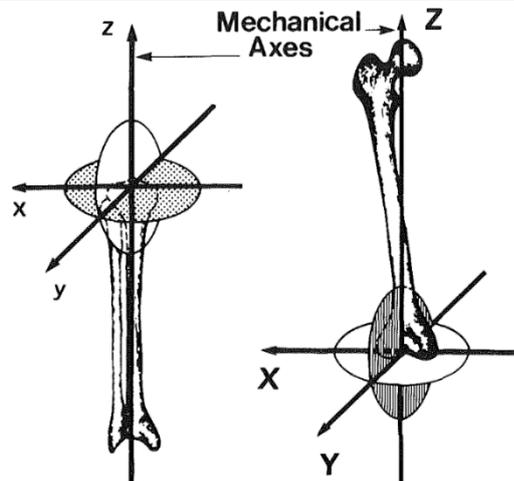
Figure 47: Application of the JCS to the knee (Grood and Suntay, 1983)

The CCSs are defined in each bone. The femoral CCS is denoted by X, Y and Z, while the tibial CCS is denoted by x, y and z. The corresponding unit base vectors of the CCS are $\hat{I}, \hat{J}$ and $\hat{K}$ for the femur and $\hat{i}, \hat{j}$ and $\hat{k}$ for the tibia. For both bones, the z-axis is positive in the proximal direction, and the y-axis is positive in the anterior direction, while the x-axis is positive to the right.

For convenience, the CCS axes fixed in each bone are chosen to be coincident with the body fixed and reference axes of the JCS, while the origin of the body-embedded CCS coincides with the translation reference points. For clarity, the femoral CCS axes will be represented by the capitalised letters X, Y and Z with $\hat{I}$, $\hat{J}$ and $\hat{K}$ as their respective unit base vectors. On the other hand, lower case letters will denote the tibial CCS axes as, x, y and z with $\hat{i}$, $\hat{j}$ and $\hat{k}$ as their respective unit base vectors (Figure 47).

In the upcoming paragraphs, the body-fixed CCSs will be defined. These definitions will be reflected in the implementation of the CCSs in the kinematic analysis software designed for this thesis. While the mathematical model which will be implemented in this thesis is primarily based on the JCS, defined by Grood and Suntay in 1983, some deviations from the model defined by the JCS, will be implemented. This was done in order to minimise the errors due to kinematic crosstalk, which were described in section 2.6.2. The level of detail and emphasis, which was attributed to the review of literature for the identification of the location of the principal functional axes of the knee, will now be put in scope. The knowledge gained allowed for identifying the ideal axes for each body-fixed CCS in order to primarily minimise kinematic crosstalk in the results and secondarily understand the variability which is expected given the choice of axes which will be defined in the following paragraphs.

In contrast with the JCS proposed by Grood and Suntay (1983), the principal difference lies in the definition of the femoral fixed CCS. Grood and Suntay (1983) proposed to locate the femoral body-fixed axis, or the FEA, by first identifying the origin of the CS, as the most distal point on the posterior surface of the femur, midway between the medial and lateral condyles. Then, a line connecting the most posterior points on the femoral condyles is defined. Finally, the FEA is defined by identifying a line parallel to the condylar-defined line, which passes through the predefined origin. This results in an FEA which is not directly related to the femoral morphology, or representative of any other known FEA.

Furthermore, identifying the three subjective anatomical ROI proposed by Grood and Suntay (1983) is not straight-forward since they are not clearly defined by any anatomical surface, making repeatability a point of concern when trying to identify them. The two ROIs located at the most posterior points on the femoral condyles vary depending on the position of the femur when defining the CCS. The position of the femur at which these ROIs are to be defined is not stated in their paper. Therefore, this

raises issues when used in different studies, since it can be interpreted differently, leading to inconsistencies when comparing data across studies.

Given the above concerns, in this thesis, a modified version of the JCS will be implemented. The subsequent paragraphs will outline the fixed body CCS implemented in this thesis.

Joint Coordinate System definition

Throughout this section defining the Joint Coordinate System, reference is made to Figure 49 which visualises the defined CS.

In the femur, the X-axis having the unit vector $\hat{I}$, is chosen to be coincident with the JCS body-fixed axis having the unit vector $\widehat{e_1}$. Rotations around the X-axis will correspond to the clinical motion of flexion-extension of the knee. Following the conclusions reached in section 2.6.2.1, the following axes will be implemented as the FEA of the knee:

- Surgical Trans Epicondylar Axis (sTEA): The first axis of the dual-FEA model. This axis is defined by a line intersecting the medial sulcus and the lateral epicondyle of the distal femur. The sTEA is effective from hyper-extension of the knee until 30º of flexion. Beyond this flexion angle, the sTEA is known to display kinematic crosstalk.

- Geometric Centre Axis (GCA): The second axis of the dual-FEA model. This axis is defined by a line passing through the centres of two spheres, fitted to each posterior femoral condyle. The GCA is effective from 30º of flexion through to 120º of flexion. The GCA displays signs of kinematic crosstalk from hyper-extension through to 30º of flexion when the knee is rotating around the sTEA which lies anterior and proximal to the GCA.

- Functional FEA (FFA): This axis represents a singular-FEA whose location is functionally derived by fitting a line to the points displaying the least Cumulative Vertical Shift Value (cVSV) as proposed by Yin *et al.* (refer to paper reviewed in section 2.6.2.1).

- Joint Coordinate System FEA (JCS): The FEA as defined by Grood and Suntay (1983) in their paper. This axis will be implemented in order to give perspective on the amount of variance which this axis displays due to the subjective way it is defined.

For each of the four axes, a separate JCS model will be implemented. Each model will be practically identical apart of the FEA, which will be defined as explained above. The X-axis is defined to be positive to the right, irrespective of laterality of the knee.

Subsequently, the Z-axis of the femur having the unit vector $\widehat{K}$ is coincident with the femoral mechanical axis. The femoral mechanical axis passes proximally through the centre of the femoral head and distally through the mid-point of the X-axis. The mid-point of the X-axis also defines the origin of the femoral fixed CCS. This method of defining the origin as the mid-point of the FEA was first proposed by Pennock and Clark in a study where they proposed modifications, which were aimed at generalising the JCS (Pennock and Clark, 1990). The Z-axis is defined to be positive in the proximal direction. Finally, the Y-axis of the femur having the unit vector $\widehat{J}$ is obtained by the cross-product of the Z-axis and the X-axis. The unit vector $\widehat{J}$ is coincident with the reference axis $\widehat{e_1^r}$, and the corresponding Y-axis is defined to be directed anteriorly. Figure 47 visualises the above definitions of the femoral CCS.

In the tibia, the primary axis of interest is the IEA, that is the tibial mechanical axis, which is the z-axis in the tibial CCS having the unit vector $\widehat{k}$. For the JCS, the z-axis is coincident with the tibial body-fixed axis, $\widehat{e_3^r}$. As discussed in section 2.6.2.2, the proximal end of the functional IEA varies depending on the loading condition of the knee. For the case of a loaded knee, the IEA is known to be dynamic and varies as a function of the flexion angle and the load being applied through the knee. For an unloaded knee, the IEA is known to lie between the insertion points of the cruciate ligaments, toward the medial aspect of the tibial spine. However, although the functional IEA is known to be dynamic for loaded knees, most studies take the assumption that the proximal end of the IEA is fixed at the centre of the tibial plateau when implementing their mathematical model (Most *et al.*, 2004; Yin *et al.*, 2015; Kang *et al.*, 2018). This assumption holds for studies of flexion of an unloaded knee, since the centre of the tibial plateau lies within a relatively insignificant distance from the medial tibial spine, thus minimising the error due to kinematic crosstalk. Conversely, for loaded knees, this assumption would not hold since the proximal end of the functional tibial mechanical axis would move close to the centre of the medial tibial plateau, which would result in significant kinematic crosstalk.

Therefore, taking into consideration that in the practical aspect of this thesis unloaded knees will be investigated, the definition of the tibial CCS is achieved as follows. First, the z-axis of the tibia having the unit vector $\widehat{k}$, which is coincident with the JCS body-fixed axis having the unit vector $\widehat{e_3}$, is defined. As mentioned above, the z-axis passes distally through the centre of the ankle joint and proximally through the centre of the tibial plateau. Distally, the centre of the ankle is located by identifying the mid-point between the epicondyle of the tibia medially and the epicondyle of the fibula laterally at the level of the ankle (Subburaj, Ravi and Agarwal, 2010). Proximally, the centre of each tibial plateau is located by using the method proposed by Cobb *et al.*, which has been demonstrated to have high precision and reliability (Cobb *et al.*, 2008; Victor, Van Doninck, Labey, Van Glabbeek, *et al.*, 2009). Initially, a two-dimensional circle is fitted to the outline of each tibial cortex in order to locate the centre of each tibial plateau (Figure 48A). The proximal end of the tibial z-axis is then identified as the mid-point between the two plateaus centres, defined by the fitted circles. The z-axis is defined to be positive in the proximal direction.

Subsequently, the x-axis of the tibia having the unit vector $\hat{\imath}$ is defined by projecting the previously located tibial plateau centres distally along the z-axis until they contact the surface of the tibial plateaus. The x-axis is then defined by the line joining the projected points. The x-axis is defined to be positive to the right, irrespective of the laterality of the leg. Finally, the y-axis having the unit vector $\hat{\jmath}$, which corresponds with the reference axis $\widehat{e_3^r}$, is obtained by performing the cross-product of the other two tibial axes. The y-axis is defined as being oriented anteriorly. The above definition of the tibial CCS is visualised in Figure 47.

Table 4: Relationship between rigid-bodies CCS axes and the JCS axes.

	ML axes	*AP axes*	*PD axes*
Femoral CCS	$\widehat{e_1} = \hat{\imath}$	$\widehat{e_1^r} = \hat{\jmath}$	$\widehat{K}$
Tibial CCS	$\hat{\imath}$	$\widehat{e_3^r} = \hat{\jmath}$	$\widehat{e_3} = \hat{k}$

Having the bone embedded CCS defined, the last step is to define the floating axis, $\widehat{e_2}$. The floating axis, $\widehat{e_2}$, is obtained by performing the cross-product of $\widehat{e_3}$ and $\widehat{e_1}$ as shown in equation 21. Using equation 21 always results in a right-handed JCS, if $\widehat{e_3}$ and $\widehat{e_1}$ are defined as explained in the previous paragraphs.
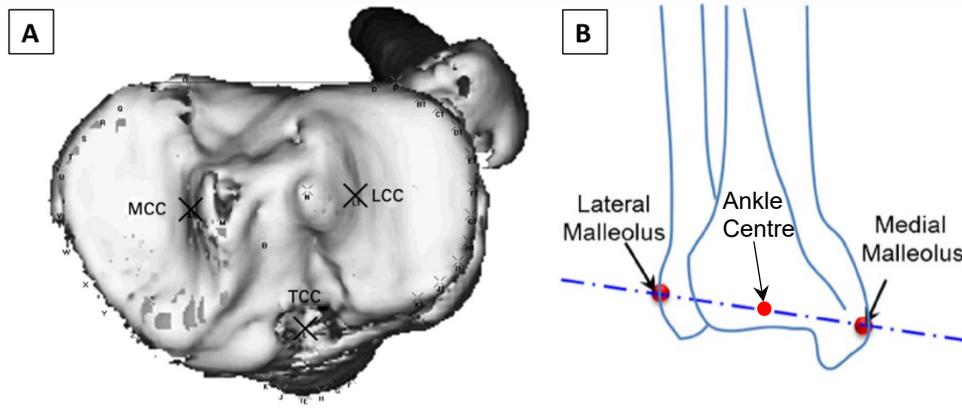
Figure 48: Identification of tibial regions of interest for the assembly of the tibial CCS.

A: The z-axis of the tibial CCS passes proximally through the centre of the tibial surface, which is defined by locating the mid-point between the centres of each tibial plateau. The centres of the tibial plateaus (shown as MCC and LCC in the figure) are located by fitting 2D circles to the tibial cortex of each corresponding plateau (Cobb *et al.*, 2008).

B: The z-axis of the tibial CCS passes distally through the ankle centre, which is defined as the mid-point between the medial and lateral malleolus (Subburaj, Ravi and Agarwal, 2010).

Rotational degrees-of-freedom definition

With the JCS defined, the three relative joint rotations between the femur and tibia can be described. The relative clinical rotation for flexion/extension (designated the term alpha, α) is the angle between $\widehat{\mathbf{e_1^r}}$, the femoral reference axis, and $\widehat{e_2}$, the floating axis (shown in Figure 49 – green circle). In Euclidean geometry, the flexion/extension angle is calculated as follows:

$$\cos \alpha = \left(\widehat{e_2} \cdot \widehat{\mathbf{e_1^r}} \right) \qquad (23)$$

$$\alpha = \cos^{-1}\left(\widehat{e_2} \cdot \widehat{\mathbf{e_1^r}} \right) \qquad (24)$$

Using equation 24 allows for determining the magnitude of the rotation, but it does not determine the direction of the rotation (i.e. flexion or extension). This is due to the symmetry exhibited in the cosine function, which can be interpreted mathematically as:

$$\cos(\alpha) = \cos(-\alpha) \qquad (25)$$

Therefore, in order to surpass this limitation and determine the sign, or direction, of the flexion/extension angle, the sine function is used to replace the cosine function, since :

$$\sin(\alpha) \neq \sin(-\alpha) \qquad (26)$$
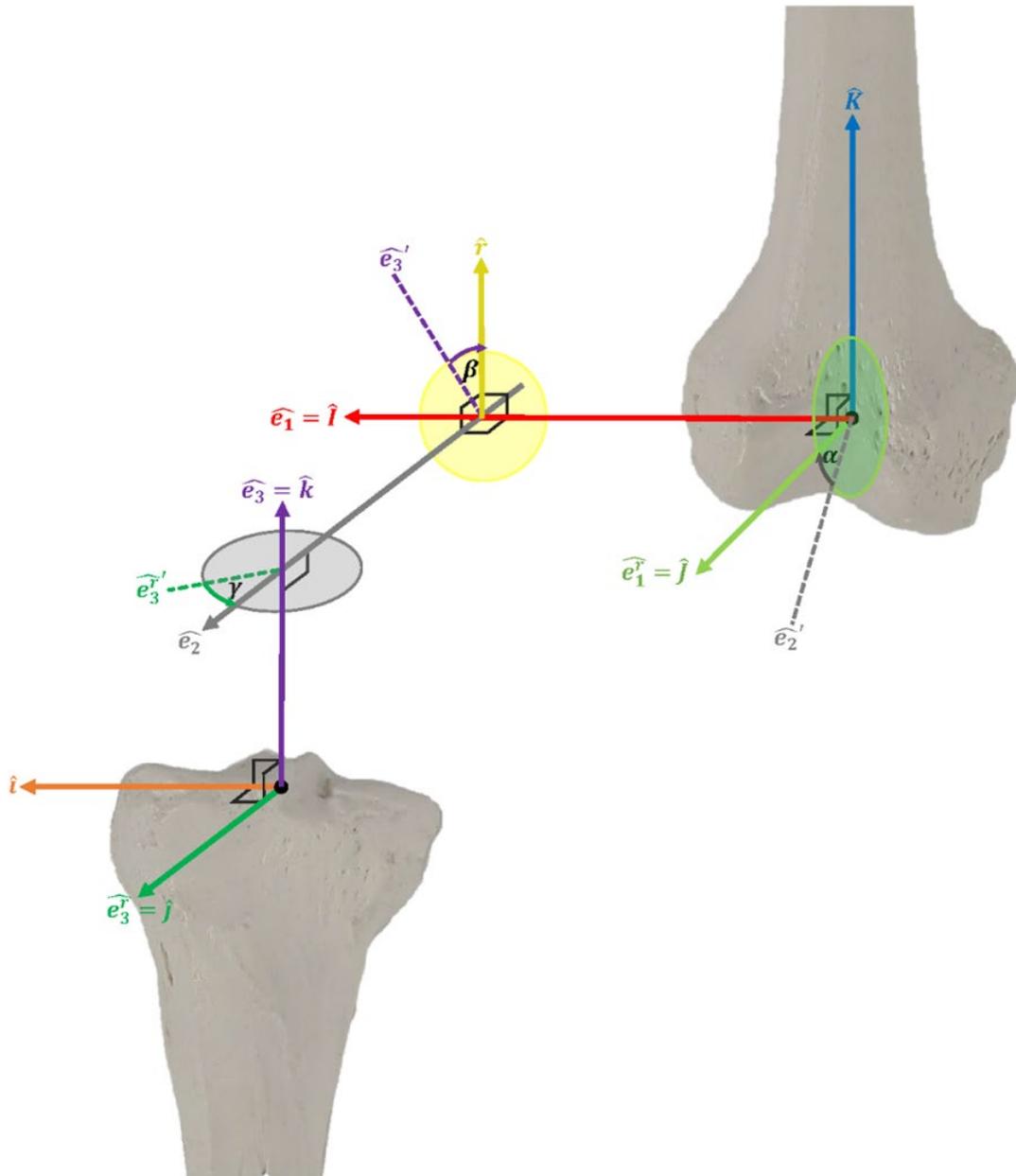
Figure 49: The three rotational DOF of the JCS of the knee (Author's rendition)

The JCS for the application of the knee deconstructs into flexion-extension (green circle) about the femoral body-fixed axis (red axis), external-internal tibial rotation (grey circle) about the fixed tibial axis (purple axis) and abduction-adduction (yellow circle) about the floating axis (grey axis), F.

Note: This diagram is not to scale, its only purpose is to help visualise how the JCS and body-fixed axes interact to quantify the three rotational DOF mentioned in the text.

From the theory of sine and cosine functions, we know that the two functions are 90˚ out of phase w.r.t each other, which can be explained with reference to the following co-function identity:

$$\cos(\alpha + 90) = -\sin \alpha \qquad\qquad (27)$$

If the angle α in equation 23 is the angle between $\widehat{e_2}$ and $\widehat{e_1^r}$, then geometrically the angle $(\alpha + 90)$ in equation 27 is equal to the angle between $\widehat{e_2}$ and $\widehat{K}$. Therefore, using this relationship and applying it to equation 23, we get:

$$\cos(\alpha + 90) = \widehat{e_2} \cdot \widehat{K} \qquad (28)$$

Applying the trigonometric identity presented in equation 27:

$$\sin \alpha = -\left(\widehat{e_2} \cdot \widehat{K}\right) \qquad (29)$$

Equation 29 follows the convention for positive moments where counter-clockwise rotations result in positive angular values. Therefore, using equation 29, the angle of flexion can be determined as follows:

$$\alpha = -\sin^{-1}\left(\widehat{e_2} \cdot \widehat{K}\right) \qquad (30)$$

Using this approach, positive values represent flexion, and negative values represent extension of the knee.

Since the approach proposed by Grood and Suntay (1983) is specific for the case of the knee, if the same equations were to be used with another anatomical joint, then the equations have to be adjusted for the joint being analysed. Cole *et al.* proposed a more generic approach which is essentially an adaptation of the JCS proposed by Grood and Suntay (Cole *et al.*, 1993). In their paper, they proposed a method of standardising the JCS across all anatomical joints. Apart from standardising the JCS, they also proposed revisions to the algorithms which Grood and Suntay defined, mostly for the sake of making them easier to program into software while also presenting them in a more general sense. In order to surpass the limitations due to the symmetric nature of the cosine function, Cole *et al.* (1993) multiply the dot product combinations by a 'sign determinant' in order to define the direction of the rotation. The 'sign determinant', which will be implemented for all three rotational DOF, is consistent with the generally accepted direction for positive moments, which uses the convention where counter-clockwise rotations around the principal axis being analysed are positive. The 'sign determinant' indicates whether the angle between the two chosen vectors is acute ($\widehat{u} \cdot \widehat{v} > 0$) or obtuse ($\widehat{u} \cdot \widehat{v} < 0$), therefore allowing for the determination of the direction. For the case of the flexion/extension angle of the knee, the following equation is proposed:

$$\alpha = \cos^{-1}\big(\widehat{e_2} \cdot \widehat{\mathbf{e_1^r}}\big) \times sign\big(\widehat{e_2} \cdot \widehat{K}\big) \qquad\qquad (31)$$

Considering that the X-axis is defined to be positive to the right, irrespective of laterality of the knee, and that flexion is a clockwise rotation around the FEA, then a negative sign is added in front of equation 31, in order to obtain flexion angles as positive values, as follows:

$$\alpha = -\cos^{-1}\big(\widehat{e_2} \cdot \widehat{\mathbf{e_1^r}}\big) \times sign\big(\widehat{e_2} \cdot \widehat{K}\big) \qquad\qquad (32)$$

Equation 32, therefore, outputs the angle between $\widehat{\mathbf{e_1^r}}$ and the $\big[\hat{\imath} - \widehat{e_3^r}\big]$ plane as measured in the $\big[\widehat{K} - \widehat{\mathbf{e_1^r}}\big]$ plane. After applying the sign correction in equation 32, the resulting angular values are positive for flexion and negative for extension. Any of the two approaches defined above (i.e. equation 30 for the Grood and Suntay (1983) approach and equation 32 for the Cole approach (1993) will result in obtaining the same values.

Using a similar approach, the relative clinical rotation for adduction and/or abduction in the knee (designated the term beta, β) is defined as the angle of rotation around the floating axis $\widehat{e_2}$. Grood and Suntay (1983) quantified this angle by identifying the angle between $\widehat{e_1}$, the femoral body-fixed axis, and $\widehat{e_3}$, the tibial body-fixed axis (shown in Figure 49 – yellow circle).

$$\beta = \cos^{-1}(\widehat{e_1} \cdot \widehat{e_3}) \qquad\qquad (33)$$

Since for the case of the knee, the angle β varies with the laterality of the knee, further manipulation of the resulting angle is required based on the laterality of the knee being investigated, as follows:

$$\text{Left Knee:} \qquad Adduction = 90° - \beta \qquad\qquad (34)$$

$$\text{Right Knee:} \qquad Adduction = \beta - 90° \qquad\qquad (35)$$

The resulting angular values using equations 34 and 35 are positive for adduction and negative for abduction.

Cole *et al.*'s (1993) approach to identifying the abduction/adduction angle does not require the secondary calculation. Mathematically Cole's (1993) alternative approach calculates the magnitude and direction of the angle in one single calculation. Cole *et al.* (1993) first created a new unit vector, $\hat{r}$, which is perpendicular to $\widehat{e_1}$, the femoral body-

fixed axis, and $\widehat{e_2}$, the floating axis (shown as a yellow axis in Figure 49). Mathematically this is calculated as follows:

$$\hat{r} = \frac{\widehat{e_1} \times \widehat{e_2}}{|\widehat{e_1} \times \widehat{e_2}|} \qquad (36)$$

Using this new unit vector, $\hat{r}$, the magnitude of the abduction/adduction angle can then be obtained as follows:

$$\beta = \cos^{-1}(\hat{r} \cdot \widehat{e_3}) \qquad (37)$$

Similar to the calculations performed for the flexion/extension angles, the above equation only solves the magnitude of the abduction/adduction angle. Therefore, in order to identify the direction of the angle, we will similarly implement the 'sign determinant' as follows:

$$\beta = \cos^{-1}(\hat{r} \cdot \widehat{e_3}) \times sign(\widehat{e_1} \cdot \widehat{e_3}) \qquad (38)$$

With reference to Figure 49, equation 38 outputs the angle between $\hat{r}$ and $\widehat{e_3}$ as measured in the $[\widehat{e_1} - \widehat{e_3}]$ plane. After applying the sign determinant in equation 38 the resulting angular values are positive for counter-clockwise rotation around the floating axis, $\widehat{e_2}$. Taking into consideration that abduction/adduction angles switch direction depending on laterality of the knee, then equation 38 is modified as follows, to obtain adduction as the positive angle, irrespective of knee laterality:

Left Knee: $\qquad \beta = -\cos^{-1}(\hat{r} \cdot \widehat{e_3}) \times sign(\widehat{e_1} \cdot \widehat{e_3}) \qquad (39)$

Right Knee: $\qquad \beta = \cos^{-1}(\hat{r} \cdot \widehat{e_3}) \times sign(\widehat{e_1} \cdot \widehat{e_3}) \qquad (40)$

Similar to the equations defined by Grood and Suntay, using equations 39 and 40 always results in positive values representing adduction and negative values representing abduction, irrespective of the laterality of the knee. Again, any of the two approaches defined above (i.e. equations 34 and 35 for the Grood and Suntay approach and equations 39 and 40 for the Cole approach) will result in identical results.

Lastly, the relative clinical rotation between the femur and tibia for internal/external rotation in the knee (designated the term gamma, γ) is defined as the angle of rotation around the tibial body-fixed axis, $\widehat{e_3}$. Grood and Suntay quantified this angle by calculating the angle between $\widehat{e_3^r}$, the tibial reference axis, and $\widehat{e_2}$, the floating axis (refer to Figure 49 – grey circle). The relationship is mathematically defined as follows:

$$\cos \gamma = \widehat{e_3^r} \cdot \widehat{e_2} \qquad\qquad (41)$$

$$\gamma = \cos^{-1}\left(\widehat{e_3^r} \cdot \widehat{e_2}\right) \qquad\qquad (42)$$

Given that the direction of the rotation (i.e. internal or external) is dependent upon the laterality of the knee, an additional calculation is required to identify the correct direction. In order to eliminate the symmetric cosine function, Grood and Suntay (1983) manipulated Equation 41 by referencing a different selection of axes which still calculating the same angle. Instead of quantifying the angle between $\widehat{e_3^r}$ and $\widehat{e_2}$, they used $\hat{\imath}$, the tibial body-fixed x-axis as the reference, which is orthogonal to $\widehat{e_3^r}$. This allowed them to rewrite equation 41 as follows:

Left Knee: $$\cos\left(\pi/2 - \gamma\right) = \widehat{e_2} \cdot \hat{\imath} \qquad\qquad (43)$$

Right Knee: $$\cos\left(\pi/2 + \gamma\right) = \widehat{e_2} \cdot \hat{\imath} \qquad\qquad (44)$$

Then, given Equations 43 and 44, co-function identities were implemented to eliminate the symmetry exhibited by the cosine function. This was achieved by replacing it with the asymmetric sine function, using the identity $\sin \gamma = \cos(\pi/2 - \gamma)$. This results in the following definitions for the internal/external rotation of the tibia:

Left Knee: $$\gamma = \sin^{-1}(\widehat{e_2} \cdot \hat{\imath}) \qquad\qquad (45)$$

Right Knee: $$\gamma = -\sin^{-1}(\widehat{e_2} \cdot \hat{\imath}) \qquad\qquad (46)$$

Using equations 45 and 46 results in positive values representing external tibial rotation and negative values representing internal tibial rotation.

Cole *et al.*'s (1983) approach to quantifying the internal and external tibial rotation of the knee follows a similar train of thought as used for the quantification of the abduction and adduction angles above. Cole *et al.* (1993) quantified this angle in the same way as Grood and Suntay (1983), leading to equation 42. Instead of using the co-function identities to eliminate the symmetric cosine function, the 'sign determinant' is used with equation 42 to define the direction of the rotation being quantified, as follows:

$$\gamma = \cos^{-1}\left(\widehat{e_2} \cdot \widehat{e_3^r}\right) \times sign(\widehat{e_2} \cdot \hat{\imath}) \qquad\qquad (47)$$

With reference to Figure 49, equation 47 outputs the angle between $\widehat{e_3^r}$ and $\widehat{e_2}$ measured in the $\left[\hat{\imath} - \widehat{e_3^r}\right]$ plane. After applying the 'sign determinant' in equation 47 the resulting

angular values are positive for counter-clockwise rotation around the tibial body-fixed axis, $\widehat{e_3}$. Taking into consideration that internal/external angles switch direction depending on laterality of the knee, then in order to always obtain external tibial rotation as the positive angle, irrespective of knee laterality, equation 47 is modified as follows:

$$\text{Left Knee:} \qquad \gamma = \cos^{-1}\left(\widehat{e_2} \cdot \widehat{e_3^r}\right) \times sign(\widehat{e_2} \cdot \hat{\imath}) \qquad (48)$$

$$\text{Right Knee:} \qquad \gamma = -\cos^{-1}\left(\widehat{e_2} \cdot \widehat{e_3^r}\right) \times sign(\widehat{e_2} \cdot \hat{\imath}) \qquad (49)$$

Again, any of the two approaches defined above (i.e. equations 45 and 46 for the Grood and Suntay (1983) approach and equations 48 and 49 for the Cole *et al.*'s (1993) approach) will result in identical results. Positive values represent external tibial rotation, while negative values represent internal tibial rotation.

The above-derived equations conclude the description of the calculations which are required for the extraction of the rotational degrees-of-freedom occurring around the three principal axes of the knee.

Translational degrees-of-freedom definition

Joint translations are defined by the relative position of the two reference points, P_F and P_T. For convenience, these are chosen to be the origins of the body-embedded CCS fixed in the femur and tibia, designated the vector notations O_F and O_T, respectively. The relative position of the origins is characterised by the position vector, $\widehat{H}$, which connects them and is directed from the femoral origin to the tibial origin. The components of $\widehat{H}$ can be defined with respect to the femoral CS, as follows:

$$\widehat{H} = H_x \hat{I} + H_y \hat{J} + H_z \widehat{K} \qquad (50)$$

In equation 50 the position vector is defined w.r.t the femoral CS, where H_x, H_y and H_z are the corresponding $\hat{I}$, $\hat{J}$ and $\widehat{K}$ components of the distance from the tibial origin, O_T, to the femoral origin, O_F, measured along the X, Y and Z axes.

Grood and Suntay (1983) mathematically defined the clinical translations of the knee as follows (refer to Figure 50 for visualisation of these translations):

- Mediolateral (ML) tibial shift, designated q_1, is the motion along the $\widehat{e_1}$ axis. Geometrically, q_1, is taken as the medial-lateral displacement of the tibial origin with respect to the femoral origin.

- Anteroposterior (AP) tibial drawer, designated q_2, is the motion along the floating axis, $\widehat{e_2}$. Geometrically, q_2, is the displacement of the tibial origin along the floating axis, $\widehat{e_2}$.

- Distraction-Compression (also referred to as proximodistal shift), designated q_3, is the motion along the $\widehat{e_3}$ axis. Geometrically, q_3, is the height of the femoral origin above the tibial transverse plane.
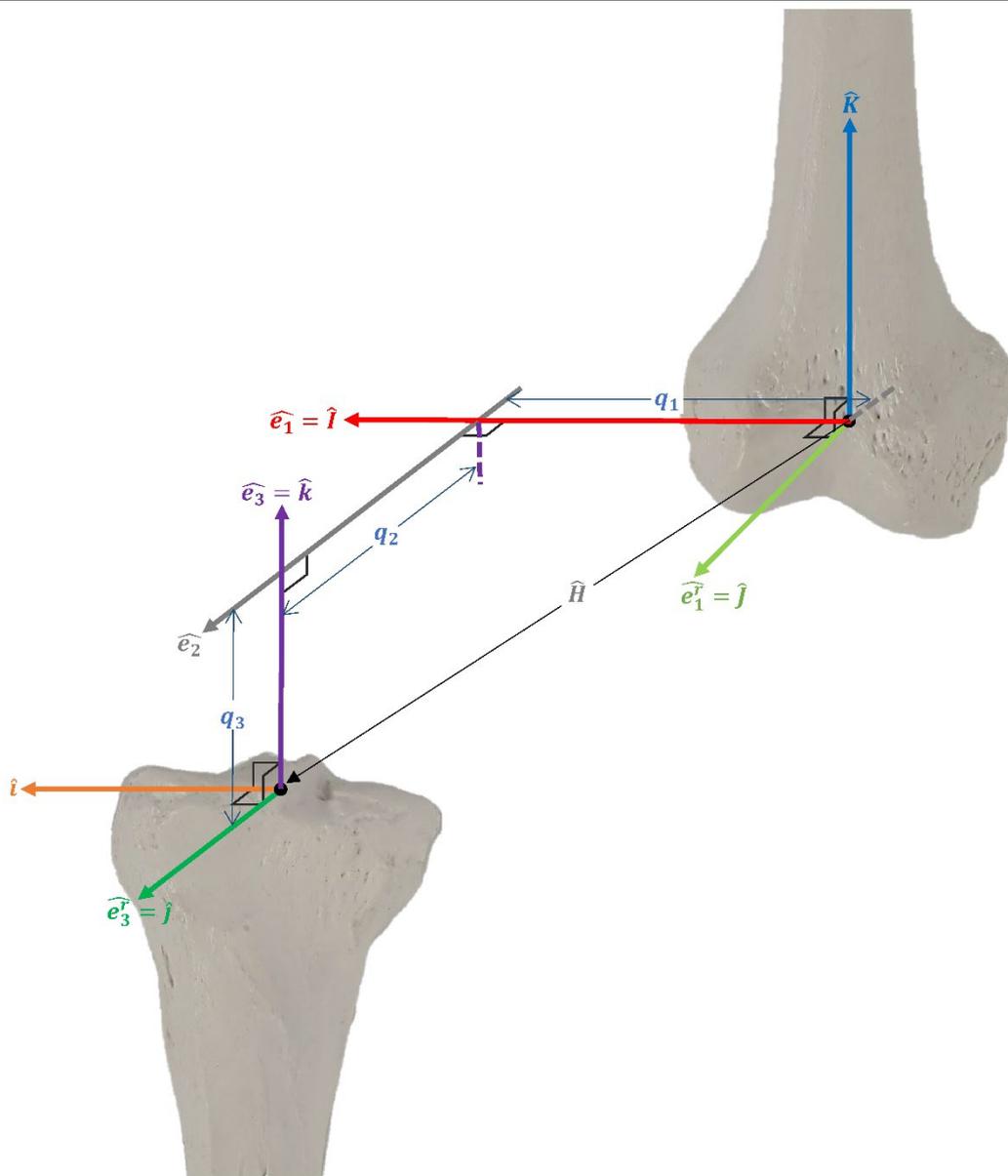
Figure 50: The three translational DOF of the JCS of the knee. (Author's rendition)

This figure visualises the quantification of the clinical translations of the knee, that is, how the position vector, $\widehat{H}$, is decomposed into the three clinical translations, q_i. Refer to text for context.

Note: This diagram is not to scale; its only purpose is to help visualise the multiple references to different CSs, axes and distances mentioned in the text.

In order to measure the clinical translations of the tibial origin, O_T, with respect to the femoral origin, O_F, the orientation of the knee must be considered. With reference to section 2.6.1, the orientation of two rigid bodies can be measured by implementing direction cosines matrices. Furthermore, with reference to equation 50, the knee translations have already been defined in terms of the projections of the position vector onto the femoral CS. Therefore, in order to obtain the clinical translations, the femoral components of the distance from the tibial origin, O_T, to the femoral origin, O_F, measured along the X, Y and Z axes are described in terms of the JCS axes, the $\widehat{e_1}$, $\widehat{e_2}$ and $\widehat{e_3}$ axes, by implementing the following DCM manipulation:

$$\begin{bmatrix} q_1 \\ q_2 \\ q_3 \end{bmatrix} = \begin{bmatrix} \hat{I} \cdot \widehat{e_1} & \hat{J} \cdot \widehat{e_1} & \hat{K} \cdot \widehat{e_1} \\ \hat{I} \cdot \widehat{e_2} & \hat{J} \cdot \widehat{e_2} & \hat{K} \cdot \widehat{e_2} \\ \hat{I} \cdot \widehat{e_3} & \hat{J} \cdot \widehat{e_3} & \hat{K} \cdot \widehat{e_3} \end{bmatrix} \begin{bmatrix} H_x \\ H_y \\ H_z \end{bmatrix} \qquad (51)$$

By implementing equation 51, knee joint distraction will be reported as a negative value, which does not align with known clinical terms. Furthermore, $\widehat{e_1}$ and $\widehat{e_3}$ can be substituted by $\hat{I}$ and $\hat{k}$, respectively. Therefore, in conclusion, equation 51 is adjusted as follows:

$$\begin{bmatrix} q_1 \\ q_2 \\ q_3 \end{bmatrix} = \begin{bmatrix} \hat{I} \cdot \hat{I} & \hat{J} \cdot \hat{I} & \hat{K} \cdot \hat{I} \\ \hat{I} \cdot \widehat{e_2} & \hat{J} \cdot \widehat{e_2} & \hat{K} \cdot \widehat{e_2} \\ -\hat{I} \cdot \hat{k} & -\hat{J} \cdot \hat{k} & -\widehat{K} \cdot \hat{k} \end{bmatrix} \begin{bmatrix} H_x \\ H_y \\ H_z \end{bmatrix} \qquad (52)$$

Equation 52 concludes the concise description of the calculations which are required for the extraction of the clinical translational degrees-of-freedom occurring along the three principal axes of the knee.

Standardisation of the Joint Coordinate System approach

The Standardisation and Terminology Committee (STC) of the International Society of Biomechanics (ISB) in November of 1993, recognised the lack of a standard for reporting joint motion in the field of biomechanics of human movement. This lack of standardisation reflected earlier comments in this thesis, which stated that comparisons among various studies were difficult, if not impossible since every researcher was using their preferred system with no clear alignment amongst all involved stakeholders. Following the publication of the pivotal JCS approach for the clinical description of three-dimensional motion by Grood and Suntay (1983), which was reviewed and presented above, the STC of the ISB selected this approach as the standard approach

for reporting kinematic data due to the advantages it provides in terms of reporting joint motions in clinically relevant terms (Wu and Cavanagh, 1995). This method assisted researchers with achieving more straightforward comparisons of data sets across different studies. Furthermore, this method made the application and interpretation of biomechanical findings easier and more welcoming to clinicians who are usually not accustomed to the terminology used by engineers and researchers.

The committee further formed a number of sub-committees to standardise the description of the movement of individual joints by experts specialising on these joints. Following a concerted effort by these committees, the JCS was adapted, developed and published for the whole body (Wu and Cavanagh, 1995), ankle, hip and spine (Wu *et al.*, 2002) and the shoulder, elbow, wrist and hand (Wu *et al.*, 2005).

2.6.4 SYNOPSIS

In this section, the following outcomes have been established:

- The singular-FEA model theory has been shown to be the primary choice of the research community due to its 'simplified' approach. It has been shown that unless the underlying assumptions of the model are considered, this theory results in the incorrect interpretation of the resulting data. This incorrect interpretation occurs if the effective ROM of the chosen FEA is not taken into consideration, leading to kinematic crosstalk impinging on the data points which fall outside the effective ROM of the implemented FEA.

- The dual-FEA model theory, which was prominently investigated by the research team of Freeman *et al. (2000)*, takes into consideration the complex and intricate articulation that is known to occur within the tibiofemoral complex. While this model theory is well understood, its implementation in research is not yet clearly defined. This is due to the undetermined underlying mechanisms of the Transition Phase, which are responsible for the shifting of the FEA from the ECA to the FCA with progressing flexion. Furthermore, while the GCA has been shown to be an excellent surrogate to the FCA, more research is required to identify the ideal surrogate axis to the ECA. Nonetheless, the sTEA showed marginal signs of kinematic crosstalk during the effective ROM of the ECA, which provides the possibility that it might be a good surrogate to the ECA. More research is required on the underlying mechanisms of the

Transition Phase of flexion and the correlation between the sTEA and the ECA in order to substantiate these claims.

- The JCS which was proposed by Grood *et al.* in 1983 has been established as the standard mathematical model for the quantification of the six DOF kinematics of the knee by the ISB in 1995.

Although the ISB has standardised the mathematical model in order to have a common method of reporting joint motion in the field of biomechanics, this standardisation is being overshadowed by the fact that the research community are yet to agree on the ideal axis, or axes, of choice. The JCS is based on the notion that the body-fixed CS are reproducible and repeatable so that results obtained using this model can be compared across studies. However, as it stands, if researchers do not identify a set of standard axes which will be implemented across all studies, it is futile having a standardised mathematical model, since the resulting data will still not be comparable.

2.7   CONCLUSION

The theory and literature presented in this chapter justify the need for the development of a new supplementary tool which provides clinicians with fundamental 4D kinematic data. This data, which is comprised of the six DOF of the knee, contact profiles and the axial centre of rotation of the knee, provides clinicians with knowledge which is required to make informed decisions and ultimately provide a better patient diagnosis. In contrast to current clinical practices, which rely on 2D ML and AP X-rays for patient diagnosis, the availability of such a tool would transform the way orthopaedic surgeons could evaluate the patients' kinematics pre- and post-operatively on a routine basis.

Apart from justifying the need for the development of this software, in this chapter, research gaps which exist in the literature were highlighted. Primarily, it was shown that there is a need for establishing and standardising the FEA of the femur. This research gap is having detrimental effects on the work of numerous researchers since their results are inconsistent with those of other researchers. It is believed that similar to what the ISB did with the standardisation of the JCS, there is the need for the standardisation of the FEAs of the knee in order to eliminate this confounding variable which is mostly being overlooked by researchers.

Secondarily, it was shown that more studies investigating the mobility of Ultra-Congruent Mobile-Bearing and Fixed-Bearing knees are required. Presently, there is no

consensus on the statements that declare that MB knees present improved mobility over their FB counterparts. More studies are required to build on the current knowledge base mostly in relation to Ultra-Congruent bearing designs which are currently lacking in the reviewed literature.

3   RESEARCH AIMS AND OBJECTIVES

3.1   PRIMARY AIM

Development of the Kinematic Analysis Suite

The primary aim of this thesis is to develop an in-house semi-automated bespoke modular kinematic analysis software, which has the capability of processing 4D CT data, a truly novel paradigm. The software is aimed to be able to extract three principal outcome measures which can be used to assist clinicians in diagnosing the knee(s) being investigated, specifically the:

1. Six DOF Kinematics

2. Contact point profiles

3. Axial centre-of-rotation

The following research objectives were determined in order to facilitate the achievement of this aim:

Objective 1:   Review literature pertaining to the kinematic analysis of healthy and replaced knees.

Objective 2:   Identify kinematic outcome measures used in literature which can be implemented in the software to maximise the clinical benefit of the outputted data, thus providing a comprehensive kinematic description of the knee(s) being investigated.

Objective 3:   Code and compile the software package from the ground up in MATLAB (MATLAB® Release 2016b, The MathWorks, Inc., Massachusetts, United States).

Objective 4:   Implement the kinematic analysis software on healthy and replaced knees in order to verify that this proof-of-concept software prototype is feasible.

3.2   SECONDARY AIM

Do mobile-bearing knee implants provide additional mobility in comparison to their fixed-bearing counterparts?

The secondary aim was directed at addressing the widely debated question in the world of knee orthopaedics, specifically concerning mobile and fixed bearing implants. A pilot study will be performed to add to the already available pool of knowledge on the topic of MB versus FB implants. The following research objectives were determined in order to facilitate the achievement of this aim:

Objective 1: Perform a review of the literature concerning the kinematics of fixed and mobile-bearing knees.

Objective 2: Obtain ethical approval to recruit control and patient participants for this pilot study

Objective 3: Develop a scanning protocol for the radiologists and participants to follow during the execution phase of this study.

Objective 4: Collect the raw data and post-process it using the kinematic analysis software.

Objective 5: Using the processed data, analyse and discuss the extracted kinematic results, focusing on the degree of mobility that the two implant types display in comparison to a healthy control knee.

3.3   TERTIARY AIM

The ideal Flexion-Extension Axes of the Knee

When implementing rigid-body kinematics, it is imperative to be as precise as possible when locating the principal axes of the system of bodies. Otherwise, the collected data will be influenced by kinematic crosstalk. Given the uncertainty that surrounds the current state of research focusing on the identification of FEA surrogates, this tertiary aim is intended to investigate the kinematic crosstalk that different FEAs demonstrate over specific ROMs. At present, the two primary surrogate knee FEAs referenced in the literature are the Trans Epicondylar Axis (TEA) which has two variants (the sTEA and the cTEA), and the Geometric Centre Axis (GCA). Apart from these two surrogate axes, the software will be used to extract a functional FEA of the knee by "reverse-engineering" the relative motion of the tibiofemoral complex. The following research objectives were determined in order to facilitate the achievement of this aim:

Objective 1: Perform an in-depth review of the literature concerning the identification of the ideal surrogate axes to the anatomical FEA(s).

Objective 2: Obtain ethical approval to recruit control and patient participants for this pilot study.

Objective 3: Develop a scanning protocol for the radiologists and participants to follow during the execution phase of this study.

Objective 4: Collect the raw data and post-process it using the kinematic analysis software. Identify the functional FEA of the analysed knees, and embed it into the femoral CS along with the other surrogate FEAs which will be analysed.

Objective 5: Extract the kinematic outcome measures for all the knees whose dynamic movement was captured.

Objective 6: Analyse and discuss the extracted kinematic results for each implemented FEA.

4   METHODOLOGY

In this chapter, an outline of the developed workflow, which was undertaken with the aim of quantifying the dynamic knee joint motion of healthy and replaced knees, will be presented. This workflow was divided into two phases. The first phase was the data collection, which consisted of the design and approval of the experimental method, NHS ethical approval, patient recruitment and implementation of the 4D CT scanning protocol. The second phase was the data processing which consisted of processing the collected data from phase one using the bespoke kinematic analysis software. In the upcoming sections, each step of the workflow will be presented and discussed.

4.1   DATA COLLECTION

4.1.1 STUDY DESIGN

Before delving into the experimental method, which was implemented in this study, it should be noted that the data collection phase for this study was undertaken twice, in two different hospitals within Scotland. This was not planned but occurred as a result of external and unforeseen circumstances.

Initially, the study was planned to take place at the Royal Infirmary of Edinburgh. A Randomised Control Trial (RCT) was designed to investigate the benefits if any, that bespoke TKA instrumentation (patient-specific and single-use variants) present over standard re-usable instrumentation in terms of pain and function to the patient, and the economic impact to the NHS. This RCT was funded by Medacta International SA, a medical device company based in Switzerland. They opened a collaboration with the University of Edinburgh and the University of Strathclyde to investigate the effect of their novel single-use and patient-specific TKA instrumentation on patient outcomes.

The study aimed to analyse three different patient groups which varied by the type of intra-operative instrumentation used to insert the Medacta GMK Sphere™ knee prosthesis, vis-à-vis three outcome measures:

1. The patients' pain pre- and postoperatively was analysed using PROMs (Patient Recorded Outcome Measures).

2. The Economic impact of using one type of instrumentation over the other variants was analysed in a Health Economic Study which was concluded in parallel to this study (as outlined in the preface section of this thesis and presented in Annex G:).

3. The patients' function was to be analysed using two different instrumentation modalities:

   a. Primarily all 172 patients were to be analysed using a Vicon optical infra-red based system, which was adapted to a dual-belt instrumented treadmill. This motion capture system was intended to assess the patients' balance, ROM and limb movement during activities of daily living at the pre-operative stage and one and two-year postoperative intervals.

   b. Secondarily, the function of 10 randomly selected patients was to be assessed in more detail, using the Toshiba Aquilion ONE™ 4D CT scanner at the Clinical Research Imaging Centre (CRIC) within the RIE.

Ethical approval was obtained in April of 2015 (approval letter attached in Annex A:), and subsequently, the study commenced recruitment of patients. For the 4D CT aspect of this RCT study, it was decided to initially scan control participants to fine-tune the scanning protocol, while also having 4D CT data to support the development of the kinematic analysis software. The first two control participants, labelled as participants C003 and C004 in this study, were successfully scanned on the 10th December of 2015 using the intermittent scanning modality for C004 and the continuous scanning modality for C003. Unexpectedly, following the scanning of these two control participants, we were informed that the 4D CT scanner at the CRIC was going to be decommissioned from the institution since the scanner was going to be taken elsewhere. This news brought the 4D CT aspect of the RCT study to a sudden halt. In order to surpass this obstacle, the research team attempted to locate another 4D CT scanner in the vicinity of the RIE, but the closest one that was identified was based in the Queen Elizabeth University Hospital (QEUH) in Glasgow. Since the recruited patients for this RCT were coming from the Lothian part of Scotland, it would not be ethical to ask the patients to travel to Glasgow and back, for the 4D CT scans. Therefore, the functional assessment component using the 4D CT scans was removed from the RCT study.

Taking into consideration that the development of the kinematic analysis software was already underway, and the fact that the 4D CT aspect was a considerable part of the PhD programme, it was decided to shift the study to Glasgow. Dr Philip Riches, the primary supervisor of this PhD programme, kindly offered to use a sub-set of the TKA patients which were taking part in another RCT study in Glasgow (hereon referred to

as study B). Study B compared knee prostheses from the Columbus™ knee system range (Aesculap AG, Tuttlingen, Germany) using another Vicon optical infra-red based system. The study investigated the functional assessment of high congruent knee bearings in fixed and mobile configurations.

Although study B was already underway, recruitment was still ongoing. Therefore, an agreement was reached to use a small sample of the future recruits of study B for this 4D CT study. Taking into consideration, that at this stage, the NHS ethical approval obtained for the RCT study in the RIE was not valid anymore, the process for obtaining ethical approval had to be restarted.

4.1.2 ETHICS

Once the radiology department at the QEUH sanctioned the use of their 4D CT scanner, the process for obtaining ethical approval was initiated. Ethical approval for this study was obtained from the NHS Research Ethics Committee (REC) 3 in December of 2016 (approval letter attached in Annex B:). The study was carried out in accordance with the standards of Good Clinical Practice (GCP) and the Declaration of Helsinki. All research members had their GCP training updated prior to initiating this study.

4.1.3 PATIENT RECRUITMENT

A small subset of ten participants was recruited for this case-controlled pilot study. Four healthy individuals as control participants (two of which were scanned in Edinburgh), while six patient participants were recruited from study B. The patient participants were equally sub-divided in two groups, a FB group and MB group.

The participant sample size was not based on any formal sample size calculation since this was a low-powered pilot study. The sample size was kept as low as possible for a number of reasons:

- To avoid unnecessary radiation to a large number of participants.

- Time was not in our favour due to the unforeseen decommissioning of the 4D CT scanner in Edinburgh, which delayed data collection by more than 14 months.

- Financial constraints were imposed on this study since this study went from being externally funded (by Medacta in Edinburgh) to being internally funded (by the University of Strathclyde).

Furthermore, at the time it was reasoned that should this study reveal significant variation in the kinematics between and within groups, a follow-up study will be envisaged with a larger sample size.

Control participants for this study were recruited from the staff and student population at the University of Strathclyde and also via university links with external community groups. Patient participants were recruited from the patient population of study B, which took place at the University of Strathclyde, in collaboration with the Golden Jubilee National Hospital. Patient recruitment was managed by Dr Alistair Ewan, who was the research member who was already managing patient recruitment for study B. He was directed to approach and ask randomly selected patients from each group to join the study until three volunteers in each group were recruited.

A preliminary letter (attached in Annex C:) was sent to each randomly chosen participant, to invite them to volunteer for this 4D CT study. When the participants accepted to take part in the study, they were given a participant information sheet (attached in Annex D:) which explained the study in detail along with a consent form (attached in Annex E:) which they were required to sign upon clarifying any concerns they might have had. These three documents were all handled by Dr Ewan. Signed consent forms were sent back to the research team for filing purposes. The participants were informed that they had the freedom to withdraw from the study at any time without giving any reason or justification. They were further informed that if they decided not to participate or else withdraw from the study, the healthcare they receive and legal rights were not affected. On the other hand, should they decide to participate in this study, their treatment would be very much the same as it would be if they did not participate in this study, except for a visit to the QEUH for the 4D CT scan postoperatively.

For participants to be eligible for the study, the following criteria had to be met:

- Inclusion criteria for control participants:
  - No pre-existing condition or injury which would have likely influenced the scan results due to being unable to perform the required tasks during the scan.
  - Over 35 years of age.
  - Willing to voluntarily take part in this study.

- Exclusion criteria for control participants:
    - Previous lower limb joint replacement procedure.
    - Unable to give written consent

- Inclusion criteria for patient participants:
    - Patients with osteoarthritis ('wear and tear') of the knee, which was sufficiently symptomatic to require total knee arthroplasty as assessed by their consultant surgeon.
    - Over 35 years of age.
    - Willing to voluntarily take part in this study.

- Exclusion criteria for patient participants:
    - Patients with ligament problems.
    - Patients with significant knee deformities that would have drastically altered the movement of their knee
    - Patients with inflammatory arthritis (e.g. rheumatoid arthritis).
    - Patients who were not suitable to have any of the three study implants.
    - Patients who were unable to give written consent.
    - Patients who were unable to attend the 4D CT scanning sessions.

At the end of this recruitment process, the following patients were recruited:

- 4 control patients
- 3 patients with an Ultra Congruent Fixed bearing
- 3 patients with an Ultra Congruent Mobile bearing

A summary of the participants who were recruited for this study is given in Table 5:

Table 5: Participant details

ID	Sex	Age[3]	Type	Hospital	Scan Date	Implant
C001	Male	58	Control	QEUH	21/02/2017	N/A
C002	Male	50	Control	QEUH	12/05/2017	N/A
C003	Male	42	Control	RIE	10/12/2015	N/A
C004	Male	58	Control	RIE	10/12/2015	N/A
P001	Female	70	Patient	QEUH	21/06/2017	Fixed UC
P002	Female	72	Patient	QEUH	21/08/2017	Mobile UC
P003	Male	56	Patient	QEUH	08/08/2017	Fixed UC
P004	Male	65	Patient	QEUH	08/08/2017	Fixed UC
P005	Male	68	Patient	QEUH	21/08/2017	Mobile UC
P006	Female	73	Patient	QEUH	16/08/2017	Mobile UC

---

[3] The age variation within the two study groups does not influence the results, since they were presented individually in a case-by-case basis. Cross group comparisons were not undertaken due to the low power of the study.

4.1.4 KNEE IMPLANT GROUPS

Patient participants received one of two PCL-sacrificing variants of the Columbus™ knee range. The Columbus™ range is advertised as having superior design features which achieve natural kinematics (Aesculap, 2012). This statement will be evaluated in

Figure 51: PCL-sacrificing UC and UCR Columbus™ implants (Aesculap, 2012)

A, B: The ultra-congruent fixed bearing implant. Figure **A** shows the tibial insert with the elevated anterior edge, while **B** shows the complete three-piece implant.
C, D & E: The ultra-congruent mobile bearing implant. Figure **C** shows the tibial component which contains a central stem upon which the tibial insert rotates, and an elongated rounded rotation stop which limits axial rotation. Figure **D** depicts a proximal view of the tibial insert at one of the extreme points of allowable rotation to depict how the rotation stop mechanism works. Figure **E** shows the assembled tibial component and tibial insert, highlighting the elevated anterior edge.

the results section of this thesis. With reference to Figure 51, the knee implant models utilised in this thesis were:

- The PCL-sacrificing fixed gliding surface Columbus™ UC: This variant is generalised as an ultra-congruent (UC) fixed tibial bearing. The anterior elevated edge is advertised to offer high stability in the AP direction following PCL resection.

- The PCL-sacrificing rotating gliding surface Columbus™ UCR: This variant is generalised as an ultra-congruent rotating (UCR), or mobile, tibial bearing. The mobile tibial plate is advertised to allow for axial rotational freedom of ±20º. Similar to the UC variant, the tibial insert has an elevated anterior edge.

All Columbus™ range knee implants have a posterior slope of 3° and an elevated anterior wall built into the tibial insert which is advertised to facilitate deep flexion and prevent the increase of anterior micro-movements (paradoxical anterior motion). Finally, both implant variants for all patients were affixed to the corresponding bone using cemented fixation.

4.1.5 EXPERIMENTAL METHOD

4.1.5.1 IMAGING EQUIPMENT

As mentioned earlier, in this study, the Toshiba Aquilion ONE™ 4D CT scanner will be used for capturing the dynamic movement of the knee. With reference to section 2.3.1.3, this scanner is a 320-multidetector CT (320-MDCT) scanner. Owing to its wide detector it is capable of producing continuous 3D images in real-time (4D), covering a distance of 16cm along the z-axis (without table movement). This state-of-the-art scanner allows fast and non-invasive dynamic kinematic evaluation of the knee joint in vivo.

Anatomy can be visualised using one of two modalities:

- Intermittent Volumetric scan: This scanning modality captures a volumetric image of the anatomy at certain predetermined time intervals, with a minimum of one second per interval and an additional minimum 0.1-second pause in between each scan.

- Dynamic Volumetric scan: This scanning modality continuously captures a volumetric image of the anatomy with every rotation of the detector, at a maximum frequency of 3.64Hz (0.275 seconds).

In this study, following the pilot scans performed in Edinburgh, it was decided that all the remaining participants were to be scanned using the dynamic modality, for apparent reasons. These being, lower radiation dose, shorter scan time, more natural movement and freedom of the speed of the movement. Therefore, the only participant who was scanned using the intermittent modality was C004 which had a scan taken every 1.5s. Refer to section 5.4 for more detail on the influence that this scanning modality had on the participants' motion.

One of the main drawbacks of CT scanning is the radiation dose which the patient receives during the scan. The Aquilion ONE™ has a 3D Adaptive Integrated Dose Reduction control system (AIDR 3D) which is a sophisticated algorithm capable of reducing the exposure dose by continuously adapting the tube current during the scan to obtain the optimum dose at every instant according to the region being targeted and the patients' anatomy (Toshiba Medical Systems, 2012). The Total Effective Dose for the CT Knee procedure was estimated to be 0.8 mSv. This target dose was estimated to be the total dose that each participant would be exposed to for the whole study. For an adult in normal health, this would result in an increased risk of cancer induction due to exposure to radiation. The estimated lifetime risk of fatal cancer associated with the total study dose of 0.8 mSv is 1 in 25000 (Robb, 1994). The dose is equivalent to 19 weeks of background radiation dose in the UK. This risk was classified as very low by the head of Health Physics in the Radiology Department at the QEUH. The risk was classified in comparison to the lifetime natural risk of a cancer diagnosis, which is 1 in 2 for people born in the UK after 1960. Figure 52A puts these exposure values in context, whereby the estimated radiation dose of this study can be compared against typical radiation doses for routine scans.

Finally, with reference to section 2.3.1.3, this scanner is also integrated with Single Energy Metal Artefact Reduction (SEMAR), which is an iterative reconstruction technique which effectively reduces metallic streak artefacts which occur when scanning metallic objects. This algorithm is intended to improve implant visualisations without compromising the bone and soft tissue. Reference is made to Figure 52B for a sample advertised visualisation of this metal artefact reduction technique.

Diagnostic Procedure	Typical Effective Dose (mSv)[1]	Number of Chest X rays (PA film) for Equivalent Effective Dose[2]	Time Period for Equivalent Effective Dose from Natural Background Radiation[3]
Chest x ray (PA film)	0.02	1	2.4 days
Skull x ray	0.1	5	12 days
Lumbar spine	1.5	75	182 days
I.V. urogram	3	150	1.0 year
Upper G.I. exam	6	300	2.0 years
Barium enema	8	400	2.7 years
CT head	2	100	243 days
CT abdomen	8	400	2.7 years
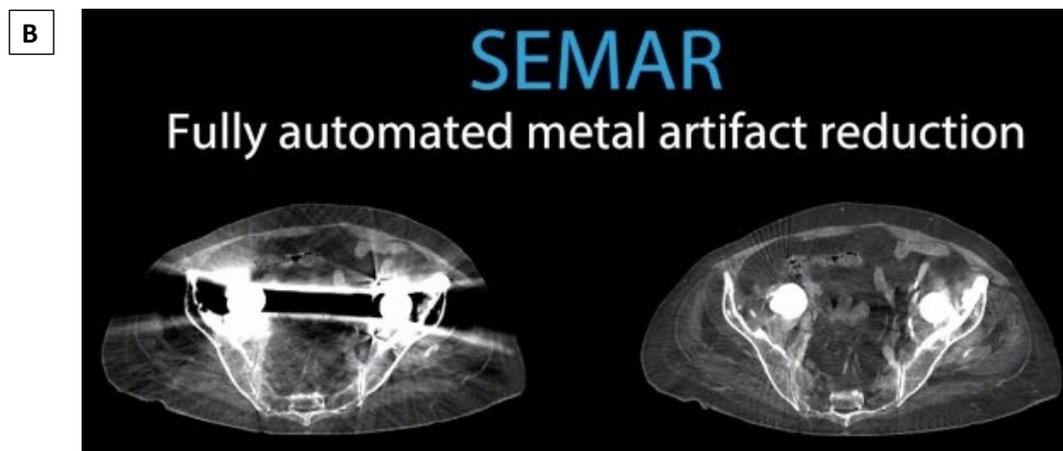
Figure 52: Radiation Exposure table and SEMAR illustration.

A: Radiation exposure for a variety of procedures and how they compare to background radiation (Diaz, 2018).
B: A visualisation of the metal artefact reduction results as advertised by Toshiba Medical Systems.

4.1.5.2   IMAGING PROTOCOL

A scanning protocol was developed for this study to be followed as a standard operating procedure during the scanning sessions of the recruited participants. The scanning protocol was focused on imaging the participants' knees through a double-legged, open-chain, flexion exercise.

The protocol was initially developed for the RIE study in collaboration with CRIC radiologists. This first version of the protocol required the participants to lie face down in a prone position, with a cushion under their lower legs. Initially, the participants were asked to flex their knees until the maximum allowable range of motion was achieved

(refer to Figure 53A). At this point, they were told to start extending their knees until they touch the cushion on the CT bed (refer to Figure 53B). Then, the participant restarted the cyclic motion and continued in this fashion until the radiologist stopped the scanner. Following the learning experience of these two pilot scans and the participant feedback, the participants' prone position proposed in this first protocol was revised. It was noted that in this position, there was the risk that the patella was being pressed down against the CT bed during the functional exercise, which might indirectly affect the knee kinematics.
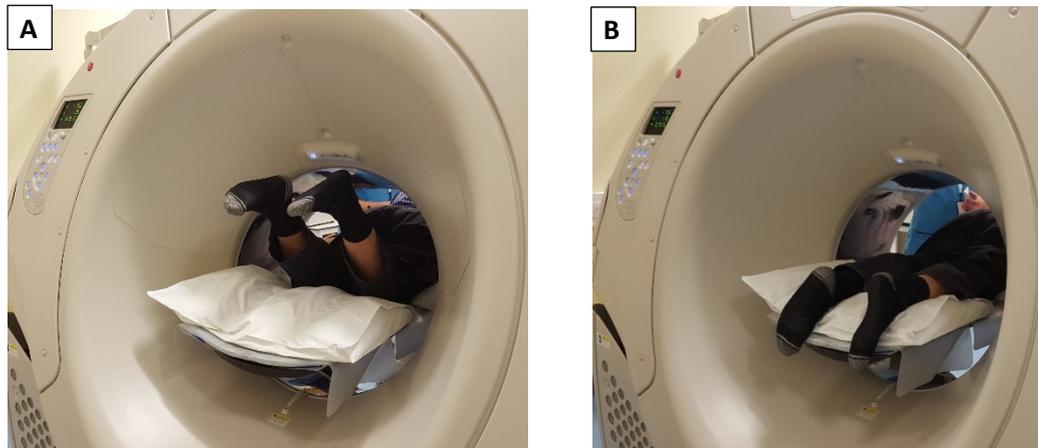
Figure 53: Photographs showing the participant C004's position during the functional exercise, as defined in the first iteration of the study protocol.

A: Participant C004 with his knee in the flexed position just before touching the edge of the gantry.
B: Participant C004 with his knee in a fully extended position.

When the second NHS ethical approval was being sought for the QEUH study, the opportunity was taken to consult further with radiologists from the QEUH on the participants' position during the scan. The outcome of these consultation sessions resulted in the second and final revision of the scanning protocol, which was approved by the NHS REC and subsequently implemented for the remaining 8 participants. The scanning protocol was as follows:

Step 1: When the participants entered into the scanning room, they were guided to lay down, feet first, in a supine position (facing up) on the CT bed (Figure 54A).

Step 2: A 90º cushion padding was placed under their knee to elevate it (refer to Figure 54B).

Step 3: The CT bed was then moved until their knee was positioned to lie in the centre of the gantry. The positioning of the knee was assisted by projected lasers which identified the centre of the gantry (refer to Figure 54B).

Step 4: The participant was then asked to practice a double-legged, open-chain, flexion exercise. During this practice session the participants were directed to fully extend their knee (in order to capture the screw-home mechanism - refer to Figure 54B) and flex their knees as further as possible (practically, until their calf muscles touched with the padding - refer to Figure 54C). Also, if the participants were noted to make contact at their heels, they were informed to maintain an open kinematic chain, that is, no contact between both legs. If the participants were not making contact, they were not informed to perform this adjustment so as not to subconsciously alter their movement to follow our guidelines (also known as motion targeting).

Step 5: Once the participant was performing the functional movement properly, a metronome (using a smartphone device) was placed next to them, set at 60 beats per minute. They were informed to time their movement to go from flexion to extension (or vice-versa) over the period of four beats, that is equivalent to 4 seconds. The aim here was to be able to capture one full cycle over the allowable 4.5 second scan time window.

Step 6: Once the participant was comfortably achieving the functional movement at the right speed, the participant was asked to rest for a few minutes, until the radiologist set up the scanner parameters and made some final adjustments. While the participant was resting, they were asked if they had any questions or required any clarification.

Step 7: In the meantime, the radiologist set the scanner in accordance with another parallel protocol[4] which ensured that the scanning parameters required for this dynamic scan were in order.

Step 8: Once the radiologist confirmed that everything was set, the participant was guided to initiate the functional movement, this time performing it indefinitely until directed to stop by the radiologist through an intercom system.

---

[4] Note: This protocol was designed in collaboration with Toshiba representatives and radiologists during a preliminary meeting which was set to define the scanning position and corresponding scanner parameters. This protocol is attached in Annex F.

Step 9:   While the participant was performing the functional exercise, the radiologist was directed to target the start of the scan to occur just before the participant starts flexing their knee (at maximum extension). The scan was then allowed to record the participant flexing their knees until they achieve the maximum allowable flexion. The radiologist was then expected to stop the scan right after they start extending their knees again.

Step 10: Once the scan was terminated, the participant was informed to stop performing the functional exercise and rest.
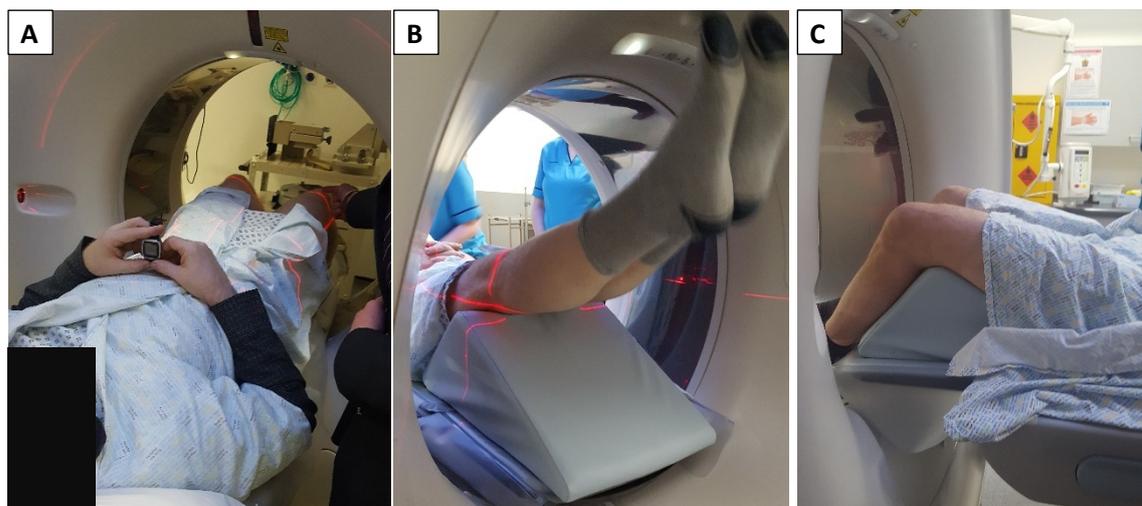
Figure 54: Photographs showing the participant C001's position during the functional exercise, as defined in the second iteration of the study protocol.

A: Participant C001 laying in the supine position while being instructed on how to perform the functional movement outlined in the second iteration of the scanning protocol.
B: Participant C001 with his knee in the fully extended position. In this photograph, the projected laser lines which are used to position the patient in the scanner can be noted. Also, the 90º padded cushion which was used to elevate the knee and thus allow for an extended ROM is visible.
C: Participant C001 with his knee in the maximum flexed position, at which point the calf muscles (gastrocnemius group) makes contact with the padding and prevents any further flexion.

The captured data was subsequently saved on the NHS computers at the radiology department. This data was then anonymised before a copy was produced on DVD and handed over to the research team at the University of Strathclyde. The research team encrypted the data as an additional security measure and stored the data on University computers which were also password protected. The data was then inputted into the bespoke kinematic analysis software, which was used to process the raw 4D CT data until the kinematic outcome measures were extracted. The bespoke software will be presented in the forthcoming section.

4.2 DATA ANALYSIS - KINEMATIC ANALYSIS SUITE

4.2.1 SOFTWARE DESIGN

Initially, before starting to develop the software application, a few baseline requirements were determined in order to clarify what the application will achieve, and how. The requirements were as follows:

- Kinematic analysis: The main requirement was for the software to be able to address the aims of this thesis, by processing the raw 4D CT data and extracting the essential kinematic outcome measures which allow for analysing the dynamic articulation of the investigated knee.

- User-friendly interface: This software is intended for biomedical engineers and clinicians. Therefore, from the end-user perspective, the application was designed to be easy to operate and understand. This was achieved by implementing a straightforward Graphical User Interface (GUI) at each step of the process, which only requires a few interactions by the user to achieve the desired outcome.

- Modular structure: The application was designed to be composed of a series of successive modules (or scripts and functions). These modules will build upon each other while directing the end-user through the workflow, from the inputting of the data until the kinematic outcome measures are obtained. While this modular approach goes hand-in-hand with the previous requirement, it also allows future versions of the software to allow for shuffling of the modules as necessary without the need of re-coding the entire script. This also allows for future in-house biomedical engineers to extend the application of this software to be able to analyse other anatomical joints or even to go beyond kinematic analysis, and allow for kinetics to be incorporated into the software.

- Semi-automated: The software was developed with the aim of automating as much of the process as possible. This way, user interaction will be kept to a minimum, such that the user will only be required to verify the output. If the output is not deemed to be acceptable by the end-user, then the user will be presented with alternative manual approaches to override the automated output.

- Intuitive codebase: The code was written to be easily read and understood, in part and in whole, by future biomedical engineers. The code is commented extensively throughout, to assist future engineers in understanding the purpose of each function, and if need be, amend it as required.

While the presented version of this software achieved the aim of demonstrating the feasibility of using 4D CT data to analyse the kinematics of healthy and replaced knees, this is still a work-in-progress. The continuous development of such an application is necessary to be able to adjust it to the current needs of the end-user while also adapting it to accept the evolving 4D CT data, which is inputted. It should be understood that the workflow being presented in the upcoming sub-sections will always be predisposed to further improvements and developments. As it currently stands, the presented code is a result of intensive time, and effort to achieve a seamlessly working application[5].

The software application, which was written entirely in MATLAB (The Mathworks Inc., 2018), is composed of 101 individual bespoke modules comprising more than 10,000 lines of code (excluding comments, blank lines and function lines). While the entire codebase will be attached as a soft-copy to this thesis[6], the parent module is presented in Annex I: of this thesis.

---

[5] It should be noted that before starting my PhD, I did not have any background knowledge or training on developing code, although I had elementary training in MATLAB via an undergraduate class. Therefore, there was a steep learning curve which I undertook prior to developing this code. Throughout the process of developing this software, I found a passion for computer programming, which complemented my over-arching interest in identifying solutions to existing problems. Programming is fundamentally about creating innovative solutions to problems, which aligns with the skills and qualities that an engineer, like myself, is trained to develop. Developing a software application is analogous to developing a complex mechanical machine which is made up of complex puzzle-like components of interlocking moving parts. Watching these components, or modules in the case of software applications, work in tandem to play out the consequences of the principles on which they were designed gives the developer a sense of achievement and appreciation to the efforts put into the work. This is further corroborated by the opportunity of continuously learning new algorithms and techniques when developing such an application, which stems from the nonrepeating nature of the task.

[6] For the sake of brevity, and the fact that this is a biomedical engineering thesis and not a software engineering one, the focus will be given to the methods which were implemented within the code and not how they were programmed into MATLAB code.

4.2.2 MODULES OUTLINE

The modular structure of the application is presented in the parent script, `SKM.m`, which is presented in Annex I:. Upon execution of the parent script all the other modules are consequently called in a predefined order as visualised in the flowchart in Figure 55.

In the upcoming sections, the purpose of each of these modules will be defined and presented from a biomedical engineering perspective, where applicable, to explain how the data inputted into the specific module was processed and ultimately outputted in preparation for the subsequent module.
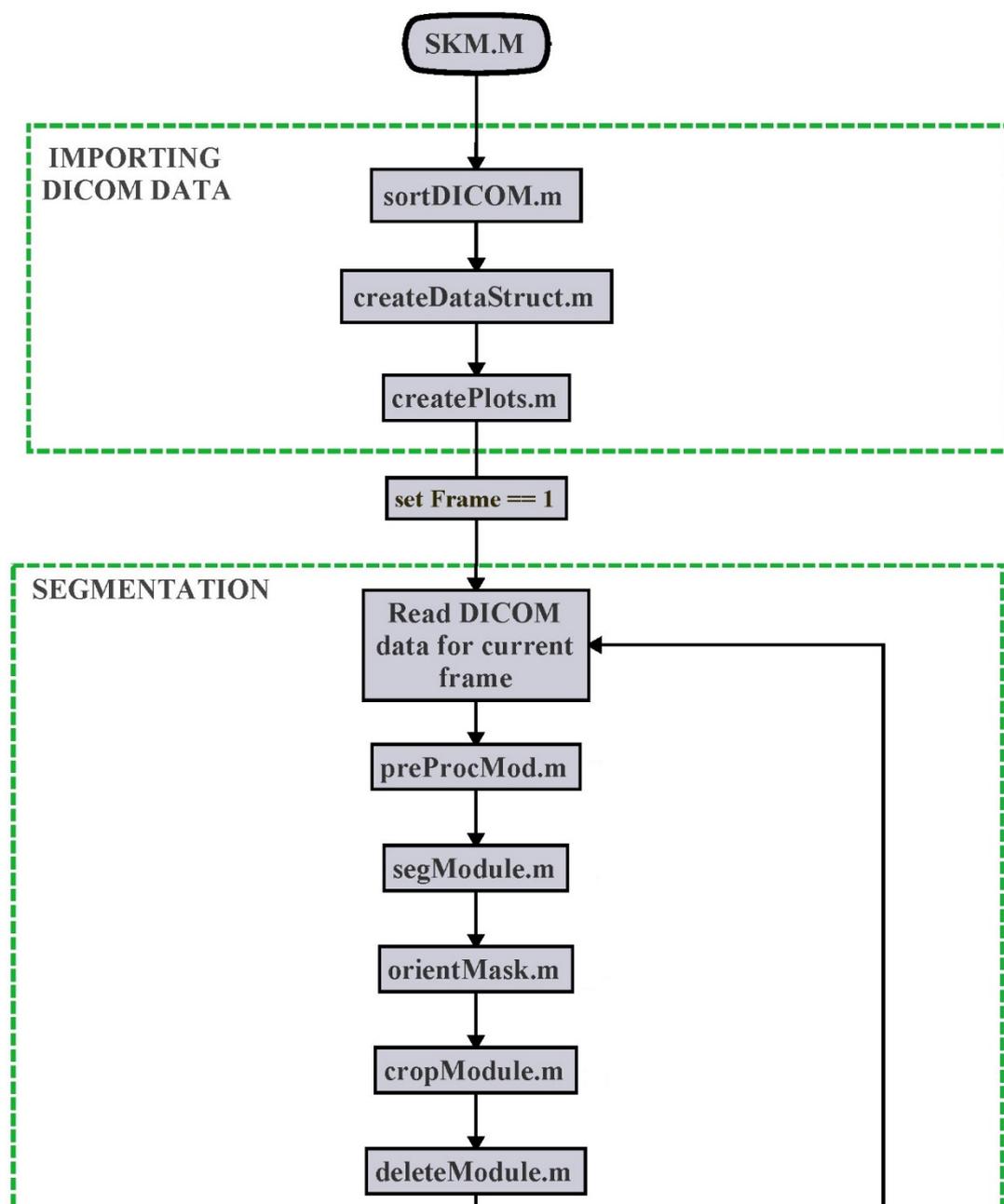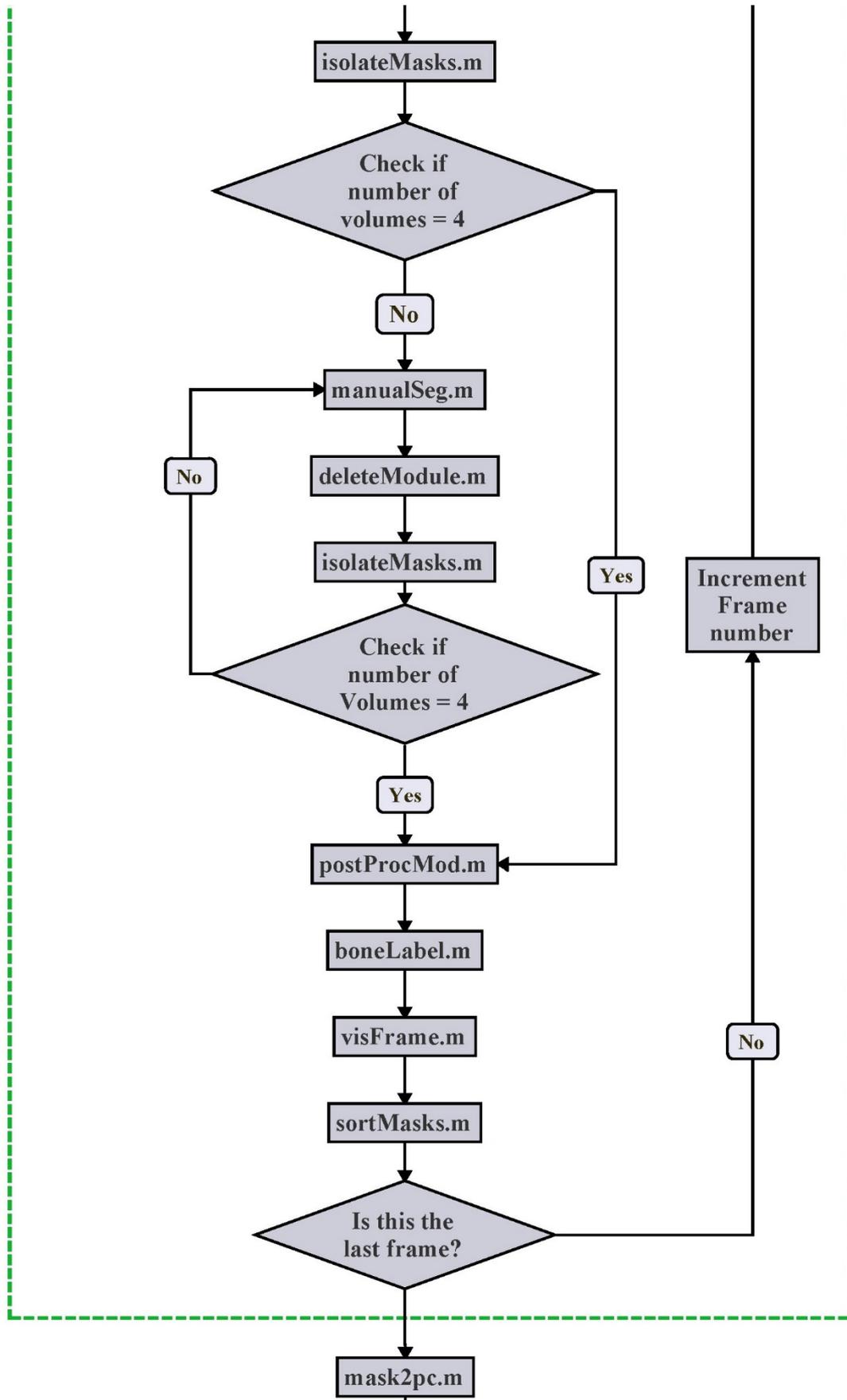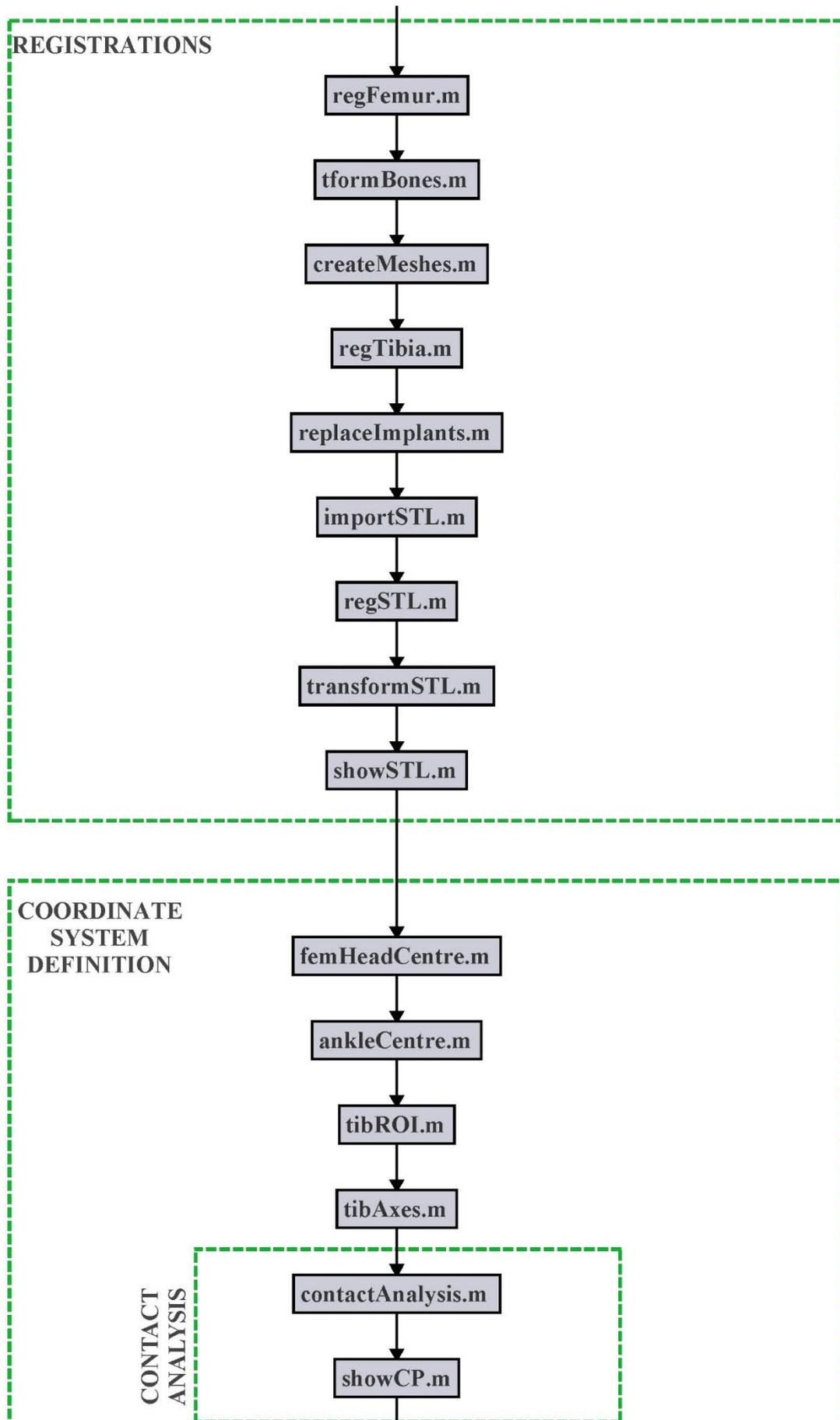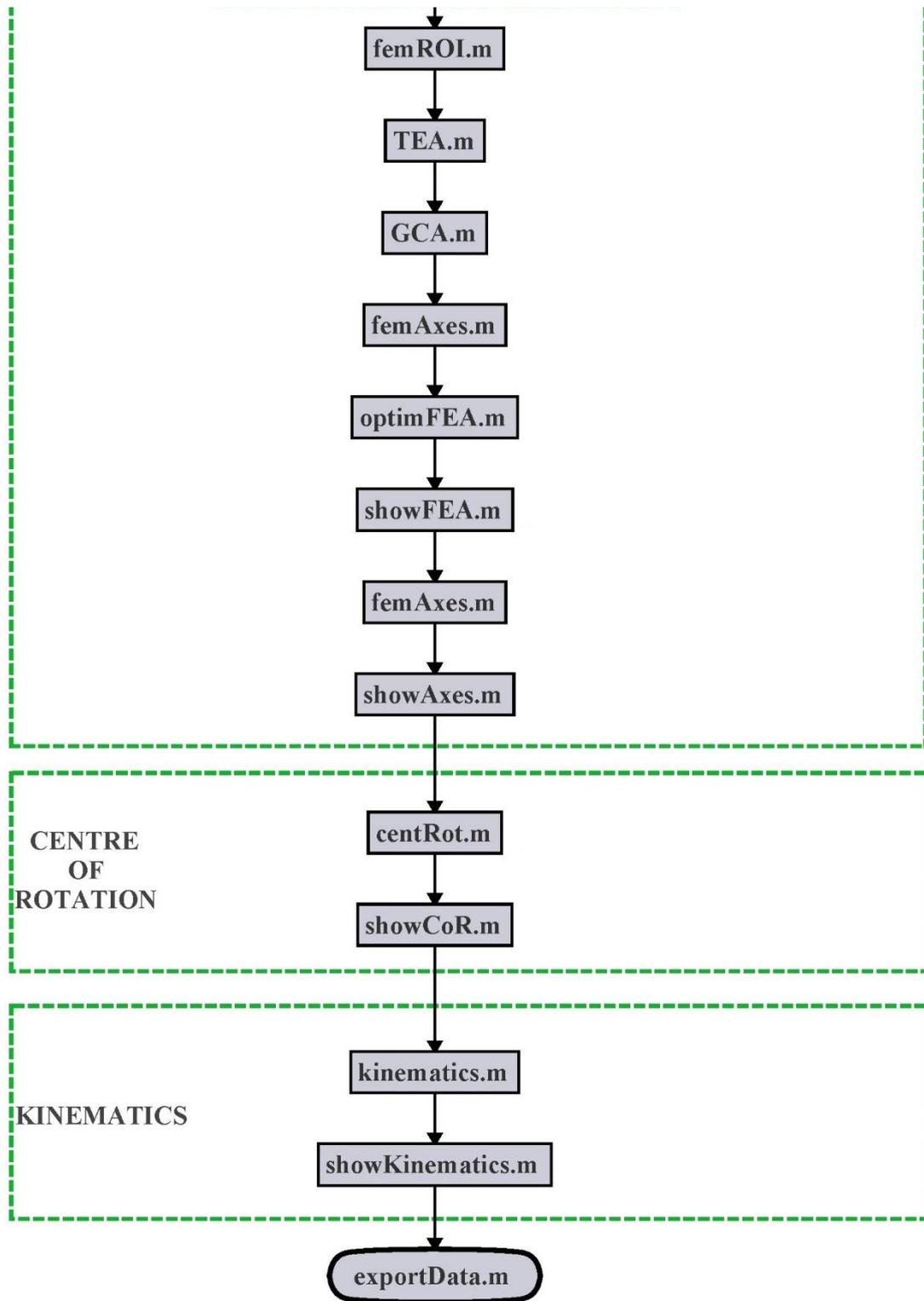
Figure 55: A flowchart of the workflow of the parent module, `SKM.m`

The flowchart presents the logical flow of the kinematic analysis software, which was developed for this thesis. Furthermore, the modules are grouped to clarify their purpose using the green dashed borders.

4.2.3 IMPORTING DICOM DATA

Once the parent module is executed, the MATLAB workspace is refreshed, that is, all existing variables and figures are removed, and the command window is cleared. Then, a structure array, named `data`, is created. This array will house all the data which will be generated throughout the execution of this application into separate containers, called `fields`.

The first module to be called is the `sortDICOM.m` module whose purpose is to load the 4D CT raw DICOM data and sort it in sequential order. A DICOM file[7] contains the volumetric images which were recorded by the 4D CT scanner, along with an extensive list of metadata which includes all the information related to the imaging device settings used during the scan, patient data and radiologist data amongst many more.

In the `sortDICOM.m` module, the 4D CT data is located, loaded and indexed into the `data` structure according to its acquisition time-stamp. Subsequently, the metadata for the scan is also saved as this will be cross-referenced throughout the application, as required, in order to extract certain parameters which would be specific to the particular scan being analysed. Once the entire raw DICOM data is processed, the `data` structure is outputted and passed back to the parent module for further processing.

The next module is a straightforward, yet essential one, whose purpose is simply to define all the fields which make up the `data` structure array in advance. Refer to the "Data Structure Array fields description" PDF document (can be accessed from the folder which contains the entire code base which was developed for this software) for a list of all the fields which are created in the `data` array throughout the execution of the software application, along with a short description of the data that will be stored within each field.

---

[7] DICOM, which stands for Digital Imaging and Communication in Medicine, is the standard for the communication and management of medical imaging and related data. This standard was created out of necessity, back in the 1970s, when it was recognised that there was no standard method for transferring images and associated information between the numerous medical devices which were emerging at the time. Therefore, the DICOM standard was created to facilitate the incorporation of medical imaging data into the Picture Archiving and Communication Systems (PACS), which are found in all hospitals worldwide.

The next module to be called is the `createPlots.m` module, whose sole purpose is to create the basis for the GUI. The GUI for this application was designed to house two main areas, the 'Module UI' and the 'Viewer'. The 'Module UI' provides the end-user with three areas:

- Top area: a description of the purpose behind the current module,

- Middle area: a selection of controls with which the user can interact with the current module (in terms of setting the parameters of the current module and deciding when to progress to the subsequent module, amongst others)

- Bottom: Provide the user with a log of the progress of the functions being executed in the background. This feature is not yet incorporated into the GUI, as it is was halted due to time constraints. As it stands, the progress log can be seen in the MATLAB command window during execution, or by accessing the `log` field after the software terminates.

The 'Viewer' provides the end-user with a platform where the volume(s) being processed are visualised, along with any supplementary overlays, axes and/or objects. The user is allowed to interact with the visualisation (rotating, selecting Regions-of-Interest (ROIs), et cetera) during specific modules as required. Refer to Figure 56 for a model visualisation of the GUI which was implemented in this software application.

4.2.4 SEGMENTATION

Following initialisation of the software application, the upcoming group of modules were developed to process and segment each raw DICOM volumetric frame. The software was developed to be capable of segmenting bilateral femurs and tibias for both healthy and replaced knees, along with their corresponding implant components. Patellas and fibulas were not considered in this study since the focus was on quantifying the kinematics of the tibiofemoral complex.

For replaced knees, the inputted data would preferably be pre-processed using a metal artefact reduction algorithm in order to avoid the detrimental streak artefacts which decompose the image considerably. For this study, as explained in section 4.1.5.1, the 4D CT scanner, which was used to capture the movement of the knee, had the SEMAR algorithm embedded within its data post-processing workflow. While this was effective

in allowing for the delineation of the knee implants, it had some adverse repercussions on the neighbouring osseous tissue, as shown in Figure 57 of section 4.2.4.1.

In the upcoming sub-sections, the developed segmentation workflow is presented. All the segmentation modules are executed for each recorded volumetric frame, or time frame, via the use of a `for` loop which iterates through each frame (refer to Figure 55).

4.2.4.1   STEP 1: VOLUME PRE-PROCESSING

The first step of the segmentation workflow is composed of two pre-processing stages. First, the raw DICOM data is scaled to real-world dimensions, so as to visualise the geometry of the scanned volume correctly. A 3D affine transformation matrix manipulation is used to scale the voxels. In this step, the raw 3D matrix is scaled using the 'pixel spacing' and 'slice thickness' metadata to get each voxel to match real-world dimensions. Following this process, each voxel within each volume has a known dimension of 1mm x 1mm x 1mm.

The next stage, coded in `preProcMod.m`, visualises the participant's bilateral knees[8] in the Viewer UI and allows the user to identify each knee as either a healthy or replaced knee as shown in Figure 56. Once the boundary of each knee is defined, the raw 3D matrix is cropped according to the user-defined boundaries and saved accordingly in the `data` structure array as separate volumes. For the case when both knees are of the same type, the user is not required to define the boundaries of the knees, but simply select the type which applies to both knees, and proceed.

Subsequently, depending on the combination of healthy and replaced knees selected by the user, one of 3 possible combinations is automatically selected by the software:

- Mode 1: Two Healthy Knees (Control Subject)

- Mode 2: One Healthy and one Replaced Knee (Unilateral TKA Patient)

- Mode 3: Two Replaced Knees (Bilateral TKA patient).

---

[8] Throughout the segmentation workflow, all visualisations are voxel-based. The raw voxels are visualised using the `patch` function in MATLAB. This approach, while being memory intensive, allows for the raw data to be accurately visualised throughout this delineation process. With reference to Figures 56 to 62, it can be noted, how all the volumes are composed of a series of cube-like voxels.
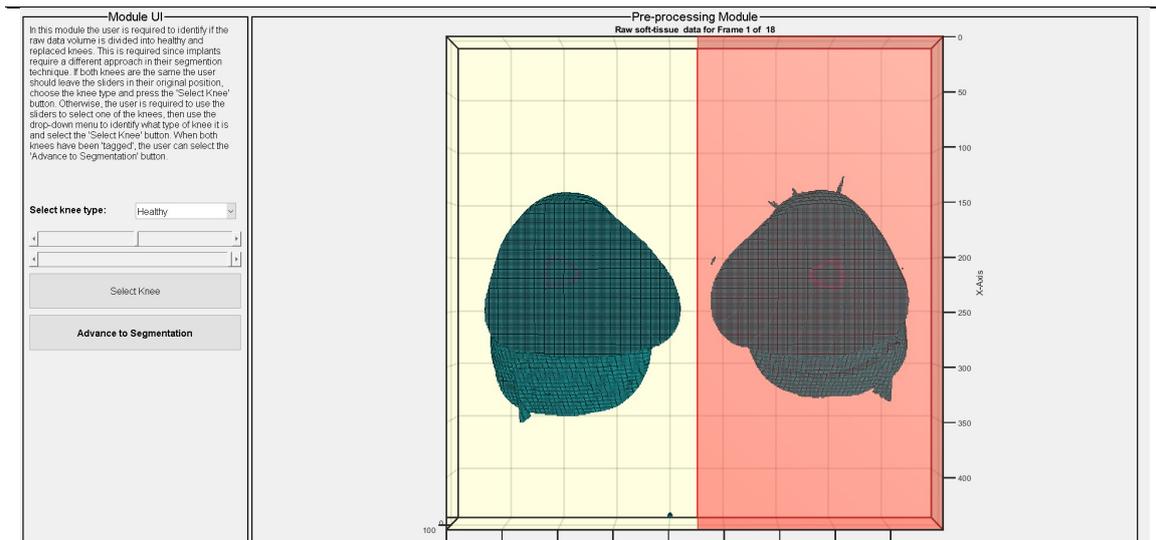
Figure 56: Pre-processing module UI

In the pre-processing module, the knee is visualised, and the user is then allowed to define the boundaries of each knee using the sliders shown in the Module UI section. When the boundary is set (as seen by the red bounding box in the example above), the user then selects the type of knee using the drop-down menu and confirms his selection using the 'Select knee' button.

Depending on the selection of the user, the software automatically identifies the number of segmentation iterations which will be required. The processes involved during each segmentation iteration will be outlined in the upcoming sub-sections.

With reference to the "Volume pre-processing" subsection in Annex I:, the code snippet following `preProcMod.m` determines the number of iterations required for each volume depending on the identified "mode". This approach will be verbalised here for clarification purposes. The raw 4D CT data for healthy knees will only require one iteration of the segmentation process. However, replaced knees will require two iterations. The reason behind the second iteration for replaced knees is that the first iteration will be dedicated to exclusively segment the knee implant while the second iteration will be dedicated to segmenting the bone tissue. This iterative process was implemented to increase the time efficiency of the entire segmentation process when taking into consideration the number of volumes which require to be segmented.

The idea behind this approach is that for a replaced knee, following the segmentation of the first frame, the user would have delineated both the two implant components and their corresponding bones. When it comes to the segmentation of the second frame onwards, the delineation of the bone tissue is not required since it is assumed that the geometrical relationship between the implant components and their corresponding bones, and the morphology of the bones will not change between volumetric frames.

Therefore based on this assumption, the user will only be required to segment the implants from the second frame onwards, which is much simpler and less time consuming than if the user was also required to segment the bones. This approach shaves off a considerable amount of time which would have been wasted segmenting the complex morphology of the bone for all frames, which are usually affected by streak-artefacts from the underlying metallic implants. With reference to Figure 57, it can be noted that although the replaced knees were processed with the SEMAR algorithm, the bones for replaced knees were still heavily-impacted by the streak-artefacts due to flaring. This detrimental effect on the bone tissues was noted in all replaced knees, which were segmented for this study. Furthermore, it was noted that this resulted in the elimination of certain essential ROIs in replaced knees, which imposed certain limitations during the execution of subsequent modules.

Replaced knee
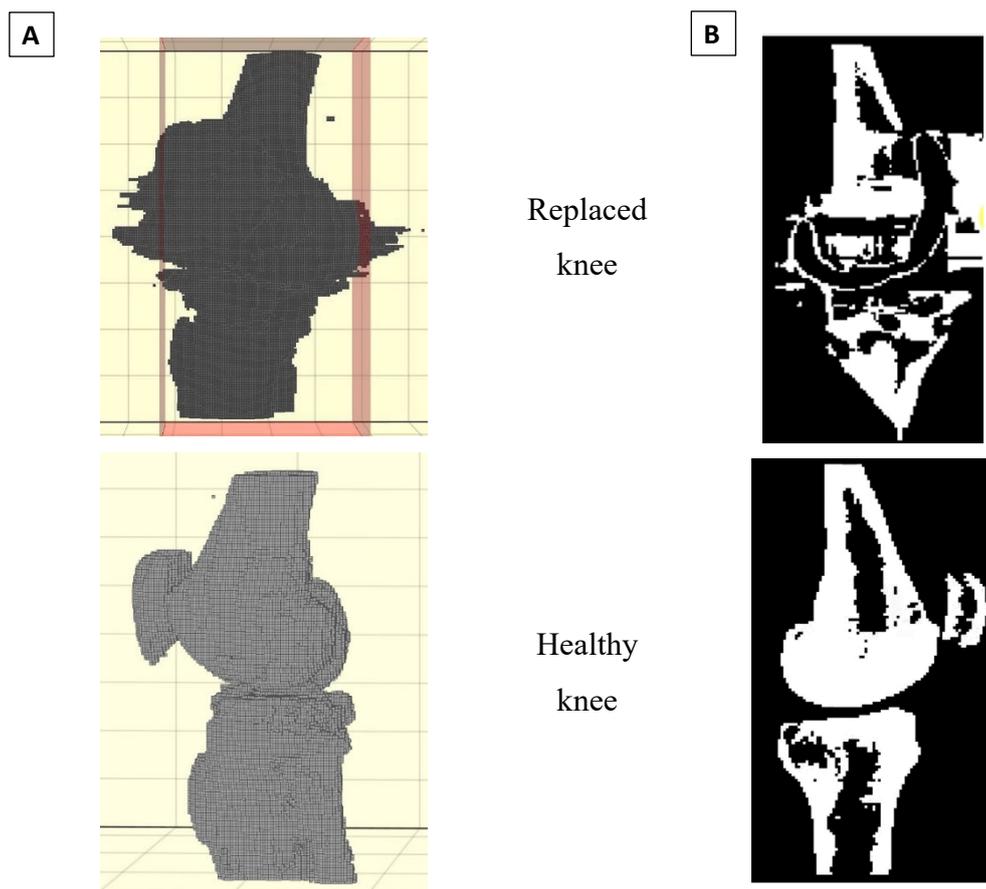
Healthy knee

Figure 57: Streak-artefacts post-SEMAR

A: A 3D sagittal comparison of a replaced knee (top) and a healthy knee (bottom). The streak artefacts can be clearly visualised on the left (anterior end) and right (posterior end) border of 3D volume.
B: A 2D sagittal cross-section, or slice, comparison of the replaced knee (top) and the healthy knee (bottom), highlighting the considerable amount of manual segmentation which was required to segment the SEMAR-processed replaced knees.

Due to this approach for replaced knees, the segmented bone from the first frame will then be registered onto the remaining frames through a series of registration algorithms which will be explained in section 4.2.5.

4.2.4.2   STEP 2: FAST FUZZY C-MEANS (FCM) CLUSTERING ALGORITHM

Following volume pre-processing, the first segmentation algorithm is implemented. This algorithm uses the Fast Fuzzy C-Means (FCM) clustering algorithm, which was explained in section 2.3.2.2. This segmentation algorithm was acquired from the MATLAB File Exchange, which is an online repository where users share their algorithms for open-access use. Credit is given to Anton Semechko for making this algorithm available. This algorithm uses the histogram of image intensities during the clustering process to classify the different tissues. In comparison to the conventional method of classifying an image using the raw HU values, this histogram-based approach results in high computational efficiency.

For this algorithm to be processed, two parameters (defined in section 2.3.2.2) need to be inputted, the 'number of clusters' and the 'fuzzy weighting exponent'. During the testing phase of this algorithm, different values for these two parameters were tested to assess the outputted segmentation results for different knee types. Depending on whether the knee is healthy or replaced, specific values were identified to obtain the best segmentation results. In order to guide the user in choosing the right values, the software automatically inputs the predetermined parameter values which match the type of knee being segmented based on which of the three "modes" was selected in the pre-processing step, and the iteration step of the process. The user can further adjust these values if the resulting volumes do not delineate the bone tissue or implants accurately.

Therefore, in `segModule.m`, the following approach was developed to segment the different knee types (refer to Figure 58 and Figure 59):

- For the case when both knees are defined to be healthy (Mode 1), the cluster size is set to default to a value of 4, and the fuzzy weighting exponent is set to default to a value of 1.6. The entire raw 3D matrix is segmented using these values, which results in the delineation of the bone tissue as one of the four clusters (Figure 58).

- For the case when one knee is healthy, and the other knee is replaced (Mode 2), the following approach is taken. Recall that, for this case, both knee volumes were cropped and stored in the `data` structure array as separate volumes. First, the

healthy knee is segmented using the parameter values defined for option 1. Then, for the replaced knee, the selected values will vary depending on the iteration number, since the densities of the volumes being segmented will vary between the first and second iteration. For the first iteration (implant segmentation), the cluster size is set to default to a value of 3, and the fuzzy weighting exponent is set to default to a value of 1.1 (refer to Figure 59). For the second iteration (bone tissue segmentation), the cluster size is set to default to a value of 3, and the fuzzy weighting exponent is set to default to a value of 4.4.
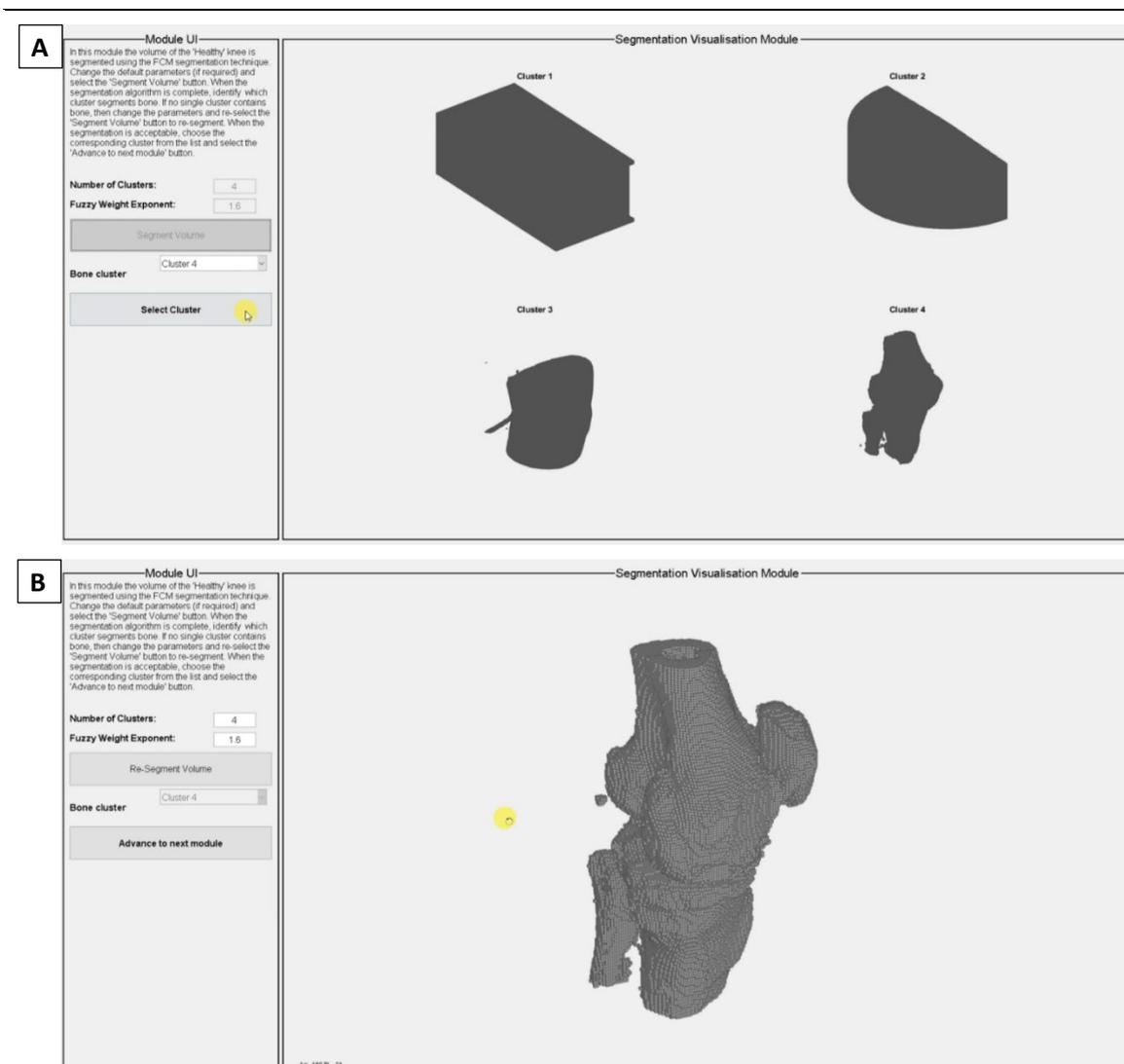
Figure 58: Segmentation module UI – Healthy Knee

A: The user is allowed to vary the Fast FCM segmentation default parameters before initiating segmentation. Following segmentation, the different clusters are visualised so the user can select the cluster of choice.
B: When the user selects the preferred cluster, the UI visualises an enlarged version of the selected cluster for the user to analyse the quality of the segmentation better.

- For the case when both knees are replaced (option 3), the entire raw 3D matrix is segmented over two iterations using the same procedure outlined for the replaced knee in "Mode 2". This results in the segmentation of the implants in the first iteration, and the bones (without the implants) in the second iteration.

Once the user is satisfied with the segmentation results, the user selects the cluster of choice from a drop-down menu (refer to Module UI in Figure 58A for healthy knees and Figure 59A for replaced knees). The user is then shown an enlarged version of the selected cluster to evaluate the quality of the segmentation. If the segmentation is satisfactory, the user can proceed to the next module, or else change the parameters and
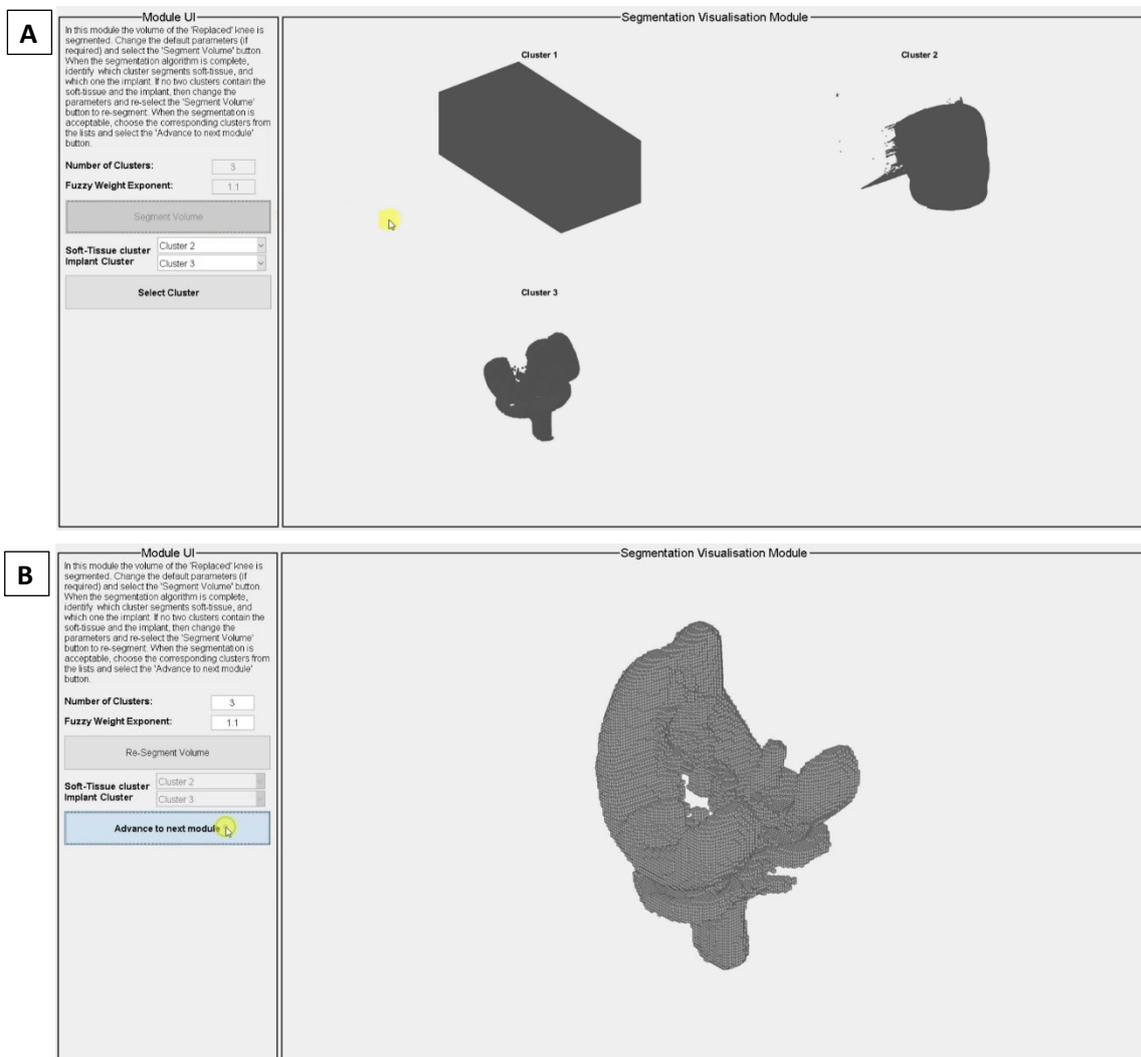
Figure 59: Segmentation module UI – Replaced knee (Iteration 1)

A: For the first iteration of FCM segmentation for replaced knee segmentation, the user is presented with three clusters. The user is guided to select which cluster represents the soft tissues (and bone) and which one represents the implant cluster. The soft-tissue cluster is saved for the second segmentation iteration.
B: The visualisation of the resulting segmentation of a patient participant implant is shown enlarged following the user selection of the implant cluster.

re-run the segmentation. Before proceeding, the selected cluster is saved in the `data` structure array as a binary mask[9]. For replaced knees, following the first iteration of the first volume, the generated soft tissue (and bone) mask is temporarily saved. The implant mask is processed through a series of modules (defined in the steps below) which further clean the binary implant mask. Once the implant segmentation is finalised, the soft tissue (and bone) mask is passed back to `segModule.m` for the second iteration of segmentation processing to extract the bone tissue.

4.2.4.3   STEP 3: SEGMENTED MASK POST-PROCESSING

Following fast FCM segmentation, the outputted binary mask is post-processed through a series of modules in preparation for the second and last segmentation method, manual segmentation, which is only executed if required.

The first module, `orientMask.m`, visualises the segmented mask and asks the user to verify the orientation of the mask with respect to specific labels which identify the required laterality of the mask (refer to Figure 60A). If the user notices that the mask's orientation does not agree with the predetermined labels, then the user can rotate the array until the laterality of the mask(s) agree with the labels. The correct orientation of the mask is imperative for subsequent modules which require the knee mask orientation to be known. This module ensures that all knees are oriented in the same manner irrespective of the participants' position on the CT bed (supine or prone) or the proprietary settings of the scanner that was used.

The second module, `cropModule.m`, is a straightforward module which visualises the segmented mask overlaid with a translucent red box (refer to Figure 60B). The user is allowed to adjust the boundaries of the overlaid box in order to crop out any artefacts, or unwanted bone, from the mask. Any voxels lying outside the box will be subsequently deleted. This module is useful on replaced knee masks due to the streak artefacts which occur as a result of the flaring in the neighbouring areas of the implant.

The third module, `deleteModule.m`, performs a series of binary operations on the binary mask to clean it of any isolated voxels which exist within the mask. The user

---

[9] A binary mask is a 3D array composed entirely of 0s and 1s. The segmented volume is represented by voxels which are assigned the value of 1 while the remaining voxels are assigned the value 0.

can specify a threshold value for the size of the connected voxel volumes which will be deleted. Based on the chosen value, the user is presented with a visualisation of the isolated voxel volumes which are smaller than the set threshold (refer to Figure 60C). The user is also shown the remaining number of volumes in the mask once the selected voxels are deleted, to assist with selecting the correct threshold value. Once the user is satisfied with the threshold value, the voxels are deleted.

The fourth and last module before manual segmentation is the `isolateMasks.m` module. This module takes the output of the `deleteModule.m` and isolates all separate voxel volumes into individual masks. This is performed so that individual bone masks are obtained prior to performing manual segmentation. This will aid with processing the masks more efficiently during manual segmentation.

4.2.4.4   STEP 4: MANUAL SEGMENTATION

For the case when the binary knee mask still requires further segmentation following the aforementioned modules, then the manual segmentation module, `manualSeg.m`, is executed. Manual segmentation involves the process of manually delineating the ROI in a slice by slice manner. While this method is time-consuming, it is recognised as the golden standard for segmentation since the user uses apriori knowledge of the ROI's anatomy to segment it appropriately.

The module for manual segmentation, which was also developed from the ground up, allows the user to visualise each slice of the volume being analysed from all three perspectives, that is, the sagittal, coronal and transverse planes. This allows the user to identify any pixels which are connecting one bone to another adjacent bone, and delete them accordingly (refer to patellofemoral interface in Figure 61A and Figure 61B).

Following manual segmentation, the user is again presented with the `deleteModule.m` and `isolateMasks.m` modules to clean the binary mask. The first run of these modules (before manual segmentation) was intended solely for cleaning the mask from any isolated voxels which remained following FCM segmentation. However, this second run also has the purpose of identifying the patella and fibula, which at his point should appear as disconnected voxel volumes following manual segmentation (refer to Figure 61C). Therefore, these two modules are called again to identify and delete the voxels which correspond with the patella and fibula, and subsequently, isolate the femur and tibia bone masks and store them individually.
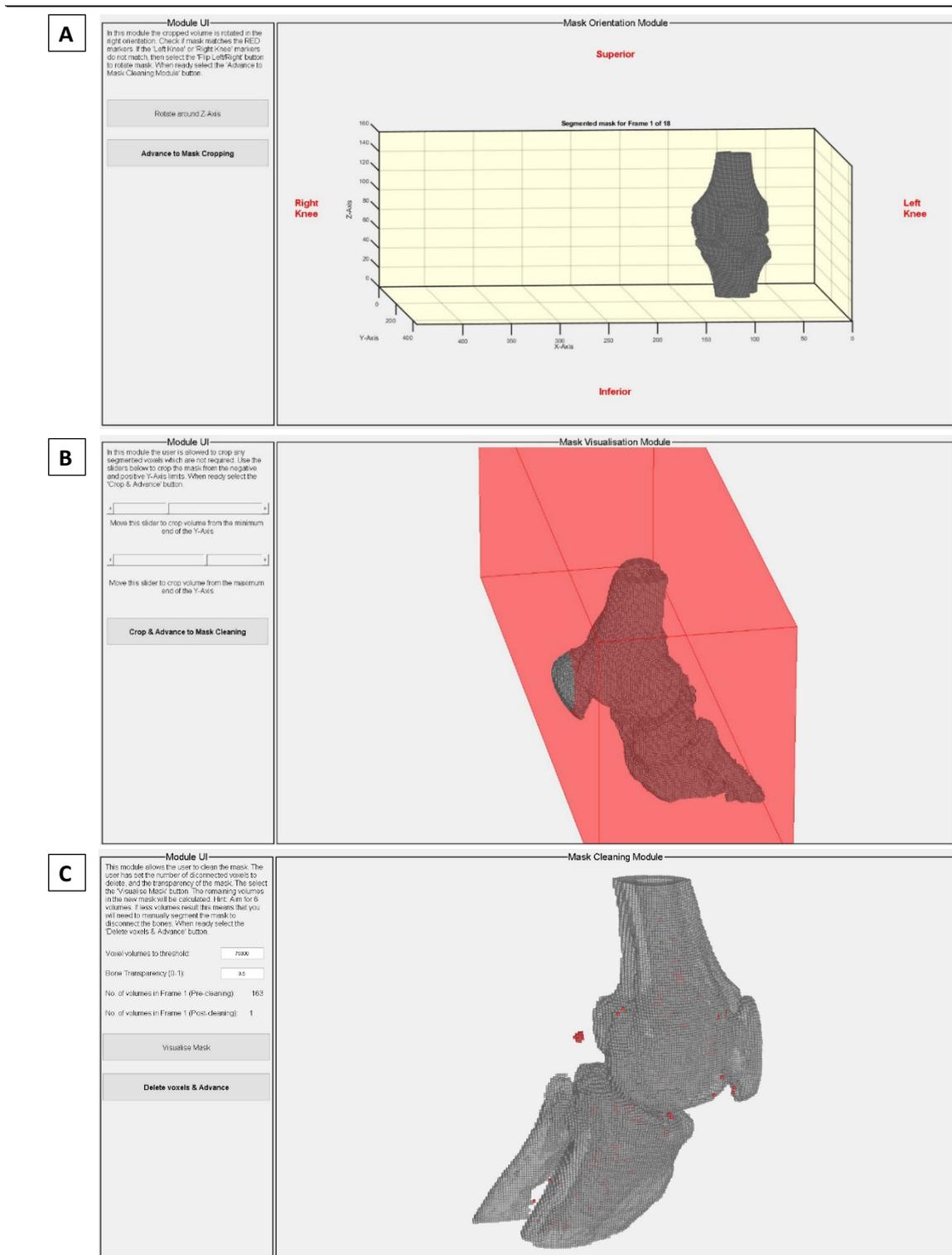
Figure 60: Segmented mask cleaning UI

A: In the mask orientation module, the mask is visualised in relation to a predetermined set of markers. The user is guided to rotate the masks, if required, in order to ensure the correct mask orientation.
B: In the crop module, the user is allowed to crop the knee mask as a coarse method of mask cleaning. This module's effectiveness is mostly appreciated in replaced knee masks since they usually display flaring artefacts which impact the neighbouring regions of the implant.
C: In the delete module, the user chooses a threshold value for the size of the voxel volumes to be deleted. Subsequently, the user is presented with a visualisation as shown in this figure, which highlights the voxel which will be deleted in red, while making the remaining voxels translucent.
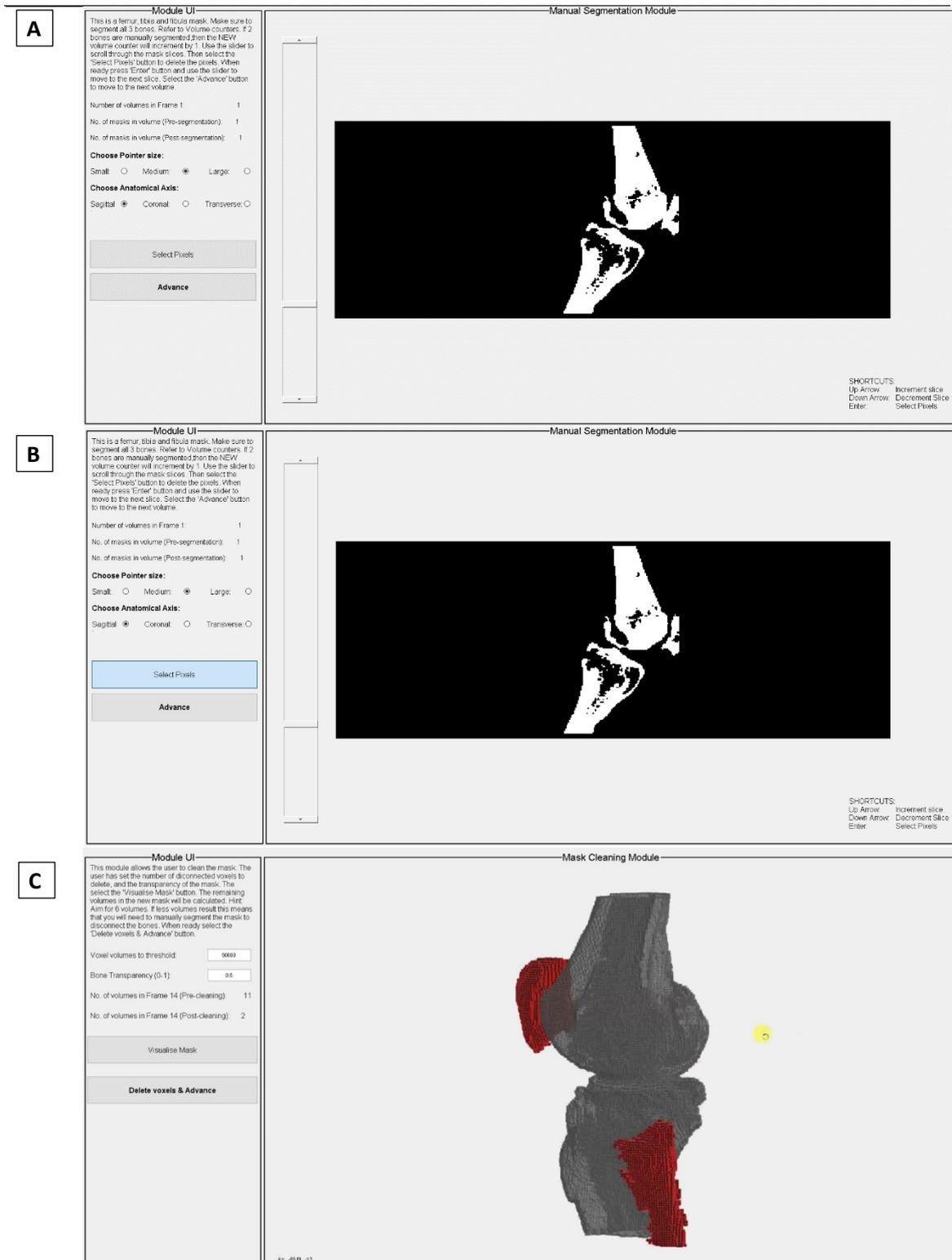
Figure 61: Manual segmentation module UI
A: The manual segmentation module UI allows the user to manually segment the binary mask by viewing individual slices in any of the three anatomical planes. The user is allowed to choose from three different pointer sizes to assist with accurately segmenting specific ROIs.
B: This figure visualises the manual segmentation performed on the slice shown in **A**, where the patella and the femur were separated by deleting the pixels which were connecting both bones.
C: After manual segmentation, the mask cleaning module identifies the bones which are now disconnected from the femur and tibia, thus allowing for the software to delete them accordingly.

4.2.4.5 STEP 5: BONE MASKS POST-PROCESSING

With the individual bone masks stored in the `data` structure array, the next module, `postProcMod.m`, performs a series of checks to identify the present stage of the segmentation workflow and prepares the data for the upcoming iterations or modules. The module processes the data based on the knee being segmented, as follows:

- Mode 1: For these volumes, this module simply is not required to perform any computations and terminates.

- Mode 2: For this case, if the healthy knee has just been segmented, then the module saves the segmented volumes for later access and prepares the `data` structure array for the segmentation of the replaced knee. The segmented data is required to be saved, otherwise, the data will be overwritten in the subsequent segmentation run. If the module identifies that the replaced knee has just been segmented, then it determines the iteration number. For Iteration 1, that is, the knee implant components have been successfully segmented, if the first frame is being segmented, the module saves the segmented volumes for later access and prepares the `data` structure array for the segmentation of the bones of the replaced knee. Alternatively, for the remaining frames in Iteration 1 and the first frame of Iteration 2, that is, the bones of the replaced knee, the module combines the segmented bone and implant masks back together.

- Mode 3: For this case, the module follows the same process implemented for the replaced knee aspect of Mode 2, with the difference that the step of combining the bone masks, in the end, is omitted as it is not required.

While this module preforms background tasks which the user is not aware of, it has a pivotal role in maintaining the segmentation workflow in working order.

With the above-outlined modules, segmentation of both healthy and replaced knee types was possible in a relatively time-efficient manner.

4.2.4.6 STEP 5: BONE LABELLING AND INDEXING

Following the segmentation of all femurs and tibias and corresponding implant components, the software progresses to two modules which are dedicated to labelling and indexing the segmented masks in preparation for the registration phase of the software.

The first module, `boneLabel.m`, asks the user to label each segmented mask so that these masks can be subsequently indexed accordingly. The module UI visualises the segmented masks and identifies them sequentially using a red translucent box to encapsulate the mask (refer to Figure 62). The software automatically suggests the laterality of the mask (based on the mediolateral labelling which occurred in the orientation module) and the bone type (based on the proximodistal labelling). Once the user verifies the labels for all four segmented masks, the module terminates.
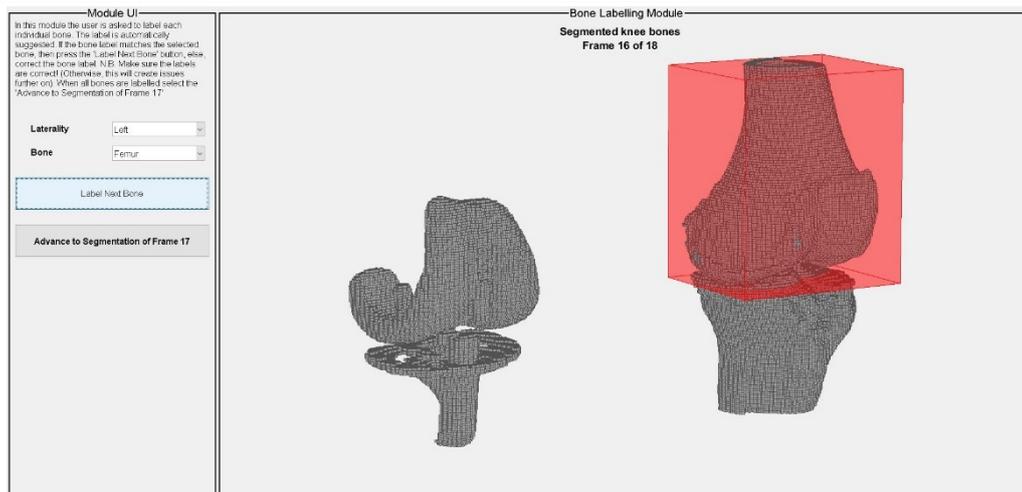
Figure 62: Bone labelling module UI

Following the labelling of each segmented mask, the software calls `sortMasks.m` to index the masks into four categories which will simplify cross-referencing throughout the remaining code. These four indexing categories were chosen to be able to identify which masks form part of the left knee, `LBonesIdx`, and the right knee, `RBonesIdx`, and which masks refer to the femur (bone or implant), `femurIdx`, and which refer to the tibia (bone or implant), `tibiaIdx`.

Once the indexing is complete, the last module in the segmentation workflow, `visFrame.m`, visualises the segmented frame and saves specific views of the segmented masks. Once all volumes are segmented, these frames are combined and the user if shown a 360º visualisation of the segmentation results for all recorded frames.

Once `visFrame.m` terminates, the segmentation for the next frame commences, by incrementing the marker identifying the frame number and going back to the start of the `for` loop, that is, the `preProcMod.m` module.

4.2.5 REGISTRATION MODULES

Following the segmentation of all frames, the binary masks are processed using custom and fully-automated registration algorithms. The aim of the registrations is three-fold:

1. To get the femur to be fixed in 3D space while the tibial bones and implants to rotate around the fixed femur, effectively eliminating the movement occurring for the tibiofemoral complex as a whole in relation to the global CS. This approach is considered necessary since it simplifies the extraction and subsequent interpretation of the kinematic outcome measures. Also, it will allow for reducing human error in subsequent modules which identify ROIs. The idea here is that rather than identifying the same ROI for all the frames, thus allowing room for human error, the ROI is identified once and it will be applicable to all frames since the femur is fixed.

2. To identify the transformation matrices (TMs) which define the rigid transformations occurring between the tibial bone or implant in the first frame and all subsequent frames. This approach will also assist in reducing human error during ROI identification, since the ROIs will only be required to be found on the model of the first frame, and they will be subsequently transformed onto the other frames using the TMs obtained in this step.

3. Also, since the proximal extremity of the femur and the distal extremity of the tibia were not in the field of view of the scanner, a pair of generic STL models of the femur and tibia are registered onto the segmented masks in order to identify the ROIs at the extremity of these bones. These ROIs are necessary for defining the femoral and tibial coordinate systems.

In the upcoming sub-sections, the developed registration workflow is presented. The workflow is broken down into three significant steps, as follows:

1. The registration of femoral bones (or implants for replaced knees),

2. The registration of tibial bones (or implants for replaced knees), and

3. The registration of the generic STL models onto the segmented masks.

Prior to initialising the registration modules, the binary masks are inputted into the `mask2pc.m` module, which converts the binary masks into point clouds. The 3D coordinates of each segmented voxel within each binary mask are extracted by indexing

the location of the voxel in terms of its row, column and slice number. Given that the voxel aspect ratio is 1:1:1 (following the scaling performed in the volume pre-processing stage defined in section 4.2.4.1), then it can be implied that the voxel's location within the 3D binary mask array represents its distance away from the origin. Once the 3D coordinates of each segmented voxel are calculated, the data is saved, and the module terminates.

4.2.5.1   STEP 1: FEMORAL REGISTRATIONS

The first step in the registration workflow of this software was to register the femur bone or implant masks of the second until the last frame, onto the first frame. In order to fully automate the 3D registrations of the point cloud data, a meticulous approach was developed, which revolves around the modified implementation of the Iterative Closest Point (ICP) registration algorithm.

The ICP algorithm used in this software was obtained from the MATLAB File Exchange[10]. Credit is given to Dirk-Jan Kroon from the University of Twente for making this algorithm available (Kroon, 2016). The ICP algorithm receives two point cloud data sets, the static and moving point clouds, and a set of registration options which define the parameters of the algorithm. The algorithm first sorts the static points into a grid of overlapping blocks. The block nearest to a moving point will contain its closest static point, thus allowing for faster registrations. The algorithm ultimately outputs the point cloud data sets of the transformed moving point cloud, the TM which maps the moving point cloud onto the static point cloud and the error of the registration in terms of the RMSE and NRMSE (normalised RMSE). This algorithm required four parameters to be defined before it is executed, as follows:

1. Registration type: This parameter defines the type of transformations which are allowed for approximating the moving point cloud to the static point cloud. For this case, rigid transformations were only allowed, since scaling and shearing would distort the segmented bones or implants.

2. Optimiser type: Given that this is an iterative algorithm, an optimisation method needs to be defined. An optimisation method is a function which searches for the

---

[10]   https://www.mathworks.com/matlabcentral/fileexchange/24301-finite-iterative-closest-point

minimum value of a problem, that is, until the solver converges to the solution of the problem. For this case, the user is allowed to choose between three different types of optimisation methods, `fminsearch`, `fminlbfgs` and `lsqnonlin`. By default, the user is guided to use the `fminsearch` method, since following extensive testing, this method produced the best results without compromising on time-efficiency.

3. Convergence tolerance: This parameter defines the threshold position tolerance, which is allowed. If the absolute difference in the position of the moving point cloud between two consecutive iterations is smaller than this value, then the operation is terminated, since convergence is considered to have been achieved. By default, the user is guided to use a convergence tolerance of 0.001mm.

4. Error tolerance: This parameter defined the threshold error tolerance, which is allowed. If the absolute difference in the error between the static and the moving point clouds between two consecutive iterations is smaller than this value, then this operation is terminated, since convergence is considered to have been achieved. By default, the user is guided to use an error tolerance of 0.001mm.

The approach developed for the registration of the femur bones or implants is presented in `regFemur.m`, and is processed as follows:

Step 1: The point cloud data of the femur bone, or implant, of the first frame, is imported and labelled as the static point cloud. The point cloud data of the femur bone, or implant, of the frame which is being registered onto the static point cloud, is imported and labelled as the moving point cloud.

Step 2: In this step, if there was a previous run of the registration for the current frame, or else if the previous frame has already been registered, then the TM which was obtained from this previous registration is applied to the moving point cloud. This acts as a preliminary coarse approximation of the moving point cloud onto the static point cloud.

Step 3: Before performing a fine registration using all the data points (usually around 80,000 points), which is time-consuming, a coarse registration is performed to better approximate the location of the moving point cloud to the static counterpart. In order to perform a coarse registration, the usual practice is to down-sample the original point cloud considerably and perform the

registration on the down-sampled point cloud to reduce the computational load on the processor. However, in this software, an alternative approach was tested and resulted in faster and better registrations. Instead of down-sampling the original point cloud, a convex hull, or an alpha-shape, was calculated for both point clouds using the `boundaryFacets` MATLAB function. This function basically 'wraps' around the original point cloud and provides a boundary point cloud, or border, of the shape, thus eliminating all the data points inside the bone while maintaining its morphological features. This results in the original point cloud being reduced to roughly 15,000 data points while maintaining the morphology of the bone or implant being registered.

Step 4: Following the extraction of the boundary shapes, two stages of coarse registration are performed. First, the static and moving boundary point clouds are registered using the ICP algorithm mentioned above. The resulting TM is saved and also applied to the boundary point cloud of the moving femur bone or implant. Subsequently, based on the fact that the length of the femur model might change between frames[11], an extra check is performed to improve the accuracy of the coarse registration further. The length of the two boundary point clouds is compared, and if the moving point cloud is determined to be longer, or shorter, than the static point cloud, then the moving point cloud is translated so that it aligns with the distal end of the femur. Subsequently, the proximal end of the longer boundary point cloud is cropped so that the length of the two boundary point clouds match. The TM defining the translation of the moving point cloud is saved. Now, the second coarse ICP registration is performed, and the resulting TM is saved.

Step 5: Before performing the fine registration on the full point cloud data sets, the TMs which were generated in the previous steps are collated together in order to capture all the transformations performed so far into a single TM. The resulting TM is then applied to the full moving point cloud data set in order to transform it to the location which was achieved following the coarse

---

[11] The length of the femur might change between consecutive frames due to the fact that the scanner might capture different sections of the femur as the knee bends. Refer to Figure 13A for a case in point.

registrations. At this point, the fine registration is performed. The resulting TM is applied to the moving point cloud data, and the resulting errors are saved.
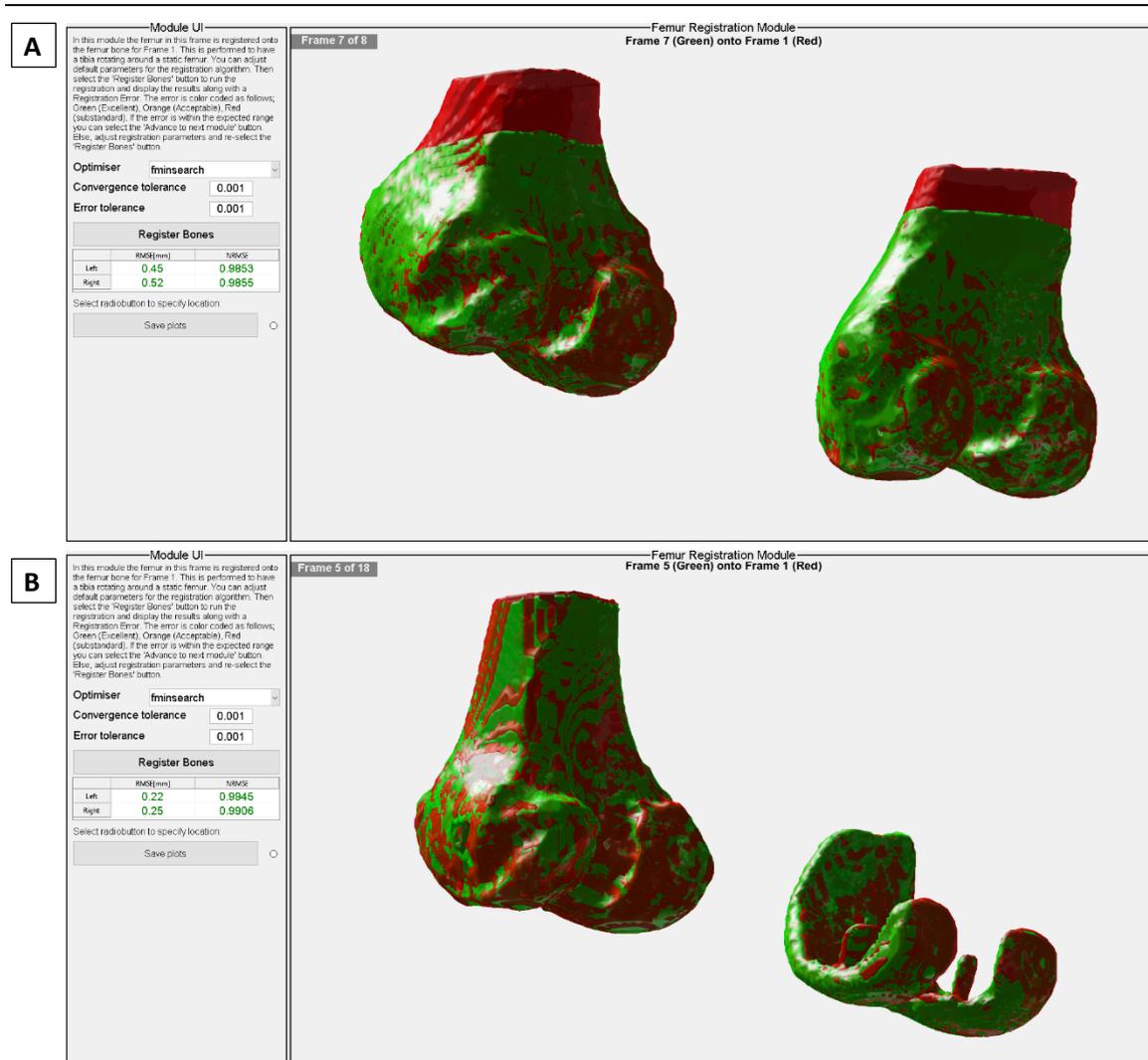
Figure 63: Femur registrations module UI

A: A visualisation of the registration results for one of the control participants. This visualisation highlights the effectivity of the adjustment for the different femur lengths during the coarse registration. Here, the green femur model from frame 7 was registered onto the red femur model from frame 1.
B: A visualisation of the registration results for one of the patient-participants, highlighting the high accuracy of the registration results of both bone and implant models. Here, the green femur model from frame 5 was registered onto the red femur model for frame 1.

Step 6: The user is now shown the registration results along with the corresponding RMSE and NRMSE errors. The user then analyses the quantitative and qualitative results of the registration, and if they are satisfactory, the user can proceed to the next registration. Otherwise, the parameters of the registration algorithm can be modified, and the registration is performed again. The user is guided, through colour-coding of the displayed errors (refer to Figure 63), to accept registration results with errors of less than 0.75 mm (shown in green),

and proceed with caution for errors between 0.75 and 1 mm (shown in orange). Errors over 1 mm are to be avoided (shown in red). Once the user accepts the registrations, the generated TMs and corresponding registration errors are saved.

Following the registration of all femur bone or implant point clouds of all frames, (except the first frame), onto the first frame, the module `tformBones.m`, is called. This module gets the TMs for all the registrations performed in the previous module and applies them to the corresponding femur and tibia 3D coordinate data. While no transformations are applied for the first frame, from the second frame onwards the following is performed. The TM for the second frame, for the left femur, is applied to the left femur and tibia, while the TM for the same frame, for the right femur, is applied to the right femur and tibia. The same transformations are performed on the remaining frames. As explained earlier, this results in the femur being fixed with respect to the GCS throughout all frames, and the tibias rotating around it with each consecutive frame. The updated 3D coordinate data and corresponding point cloud data is stored in the `data` structure array.

Finally, the module `createMeshes.m` is called to create triangular surface plots of the boundary surfaces of the updated point cloud data sets for all frames[12]. The boundary surfaces were opted for plotting the bones and implants in order to conserve memory since using all the data points would drastically increase the number of triangles and vertices for no additional graphical benefit. At this point, the triangular surface plots are only created and not visualised.

4.2.5.2 STEP 2: TIBIAL REGISTRATIONS

The next step in the registration workflow is to perform rigid ICP registration of the previously transformed tibial bone or implant masks, of the second until the last frame, onto the first frame. This registration step will ultimately identify the TMs, which represents the movement occurring in the tibial bone or implants between consecutive frames. In contrast to the TM obtained for the femoral registrations, these will not be

---

[12] The visualisations being shown post-segmentation workflow, are all triangular surface plots which were generated using the `trisurf` function in MATLAB. This approach was implemented as it drastically reduces the memory intensity while maintaining accuracy and improving the aesthetic nature of the visualised bone or implant models.

used to actively transform the 3D coordinates of the tibial bones or implants, but they will be used in subsequent modules to simplify the procedure of ROI identification. Using the TMs obtained in this step, the user will only be required to identify the tibial ROIs for the first frame. The ROIs will then be transformed onto the remaining frames using the TMs obtained in this step, therefore decreasing user input, while increasing accuracy and reducing human error in the identification of the same ROI over consecutive frames.

The approach developed for the registration of the tibial bones or implants is similar to the approach developed for the registration of the femoral bones or implants. The difference in the approach will be highlighted below. The procedure is presented in `regTibia.m`, is processed as follows:

Step 1: The original point cloud data of the tibial bone, or implant, of the first frame, is imported and labelled the static point cloud. The transformed point cloud data of the tibia bone, or implant, of the frame which is being registered onto the static point cloud, is imported and labelled as the moving point cloud.

Step 2: Similar to the femur registration approach, the first coarse approximation occurs if there were any previous runs of the registration of the current frame, or else if the previous frame has already been registered onto the first frame. In this case, the TM, which was obtained from any of these previous registrations, is applied to the moving point cloud.

Step 3: The boundary point clouds for both the static and moving point clouds are calculated.

Step 4: The two-step coarse registration, similar to the femoral registration algorithm, is implemented. First, the static and moving boundary point clouds undergo a preliminary coarse registration using the ICP algorithm. Subsequently, the same check performed on the femoral bones is performed on the tibial bones, that is, the comparison of the length of the tibias, and subsequent cropping and translating if there is a mismatch in the lengths. For this tibial coarse registration step, the algorithm enforces a minimum of three iterations of registration, cropping and translating, and a maximum of six iterations. This was performed, since in contrast to the femoral bone, the tibial bone is affected by a diagonal cut along the tibial shaft due to the orientation of the tibia in

relation to the scanner's field-of-view during data capture (refer to Figure 64A for a case in point). This diagonal cut resulted in a more significant discrepancy in the consecutive bone models, such that more iterations were required by the ICP algorithm to converge on the static bone model properly. The TMs generated during this iterative processed are joined together and saved.

Step 5: Before performing the fine registration on the full point cloud data sets, the TMs which were generated during the coarse registration are combined and applied to the original moving point cloud data set (defined in step 1) in order to transform the tibial bone, or implant, to the same location which was achieved during the coarse registration. At this point, the fine registration is performed, and the resulting TM is applied to the moving point cloud data while the resulting registration errors are saved.

Step 6: The user is now shown the registration results along with the corresponding RMSE and NRMSE errors. The user analyses the quantitative and qualitative results of the registration, and if they are satisfactory, the user proceeds to the registration of the consecutive frame. Otherwise, the parameters of the registration algorithm can be modified, and the registration is performed again. The user is guided to accept or reject the registrations based on the same colour-coding system used for the femur registrations. Once the user accepts the registrations, the generated TMs and corresponding registration errors are saved.

Following the registration of all tibial bone or implant point clouds of all frames, (except the first frame), onto the first frame, the module `replaceImplants.m`, is executed. The purpose of this module is to transform the segmented replaced knee bone masks onto the rest of the frames using the registration TMs obtained in the previous modules. The procedure implemented in this module is as follows:

Step 1: The 3D coordinates for the replaced knee femur and tibia bone masks which were extracted in the `mask2pc.m` module are imported.

Step 2: For the case of the femur replaced knee, the 3D coordinates extracted in step 1 are concatenated to the femur implant 3D coordinates of the first frame. This is the only manipulation that is required for the case of the femur since the remaining frames have all been registered onto the first frame, such that the

concatenated 3D coordinates for the first frame are applicable to all the consecutive frames.
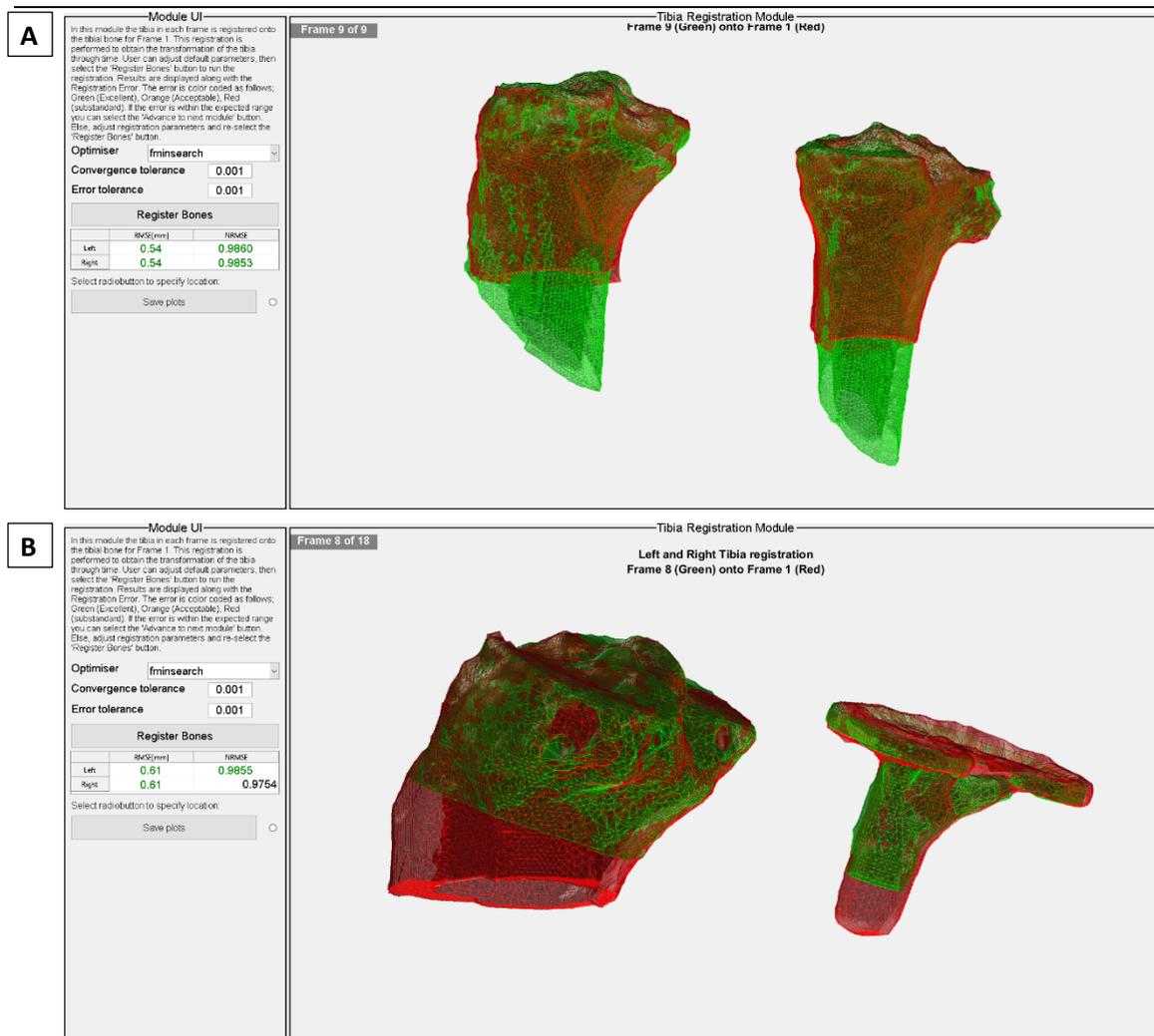
Figure 64: Tibia registrations module UI

A: A visualisation of the registration results for one of the control participants. This visualisation highlights the effectivity of the adjustment for the different tibia lengths during the coarse registration. Here, the green femur model from frame 9 was registered onto the red femur model from frame 1.
B: A visualisation of the registration results for one of the patient-participants, highlighting the high accuracy of the registration results of both bone and implant models. Here, the green tibia model from frame 8 was registered onto the red tibia model for frame 1.

Step 3: For the case of the tibia replaced knee, the 3D coordinates imported in step 1 are concatenated to the tibial implant 3D coordinates of the first frame. However, for the remaining consecutive frames, the corresponding 3D coordinates which were imported in step 1 are inversely transformed using the corresponding TM extracted in the previous module, `regTibia.m`. Following the inverse transformation, the 3D coordinates are concatenated to the corresponding 3D coordinates of the tibial implants. This approach results in the replaced knee bone coordinate data being merged to the corresponding

implant coordinate data such that all frames with replaced knees are now represented with both the bone and implant coordinate data.

Step 4: Finally, the boundary surfaces of the merged coordinate data for the replaced knee are calculated and saved. The corresponding triangular surface plots of the boundary surfaces are created for all frames and saved for subsequent visualisation steps.

This module concludes the second step of the registration workflow. At present, the registration algorithms which were implemented achieved the following:

- Eliminated the collective motion of the knee in 3D space via the implementation of the TMs of consecutive frames for the femur bone or implant. The resulting bone and implant models represent a fixed femur in 3D space with the tibia maintaining its original relative motion.

- Identified the TMs which represent the tibial motion that is occurring in consecutive frames.

- Merged the replaced knee bone masks to the corresponding implant masks, For the femur, this involved concatenating the 3D coordinate data for the implant and bone, while for the tibia, this involved the inverse transformation of the replaced knee bone coordinate data onto all the frames and the subsequent concatenation of the 3D coordinate data.

4.2.5.3   STEP 3: GENERIC STL MODEL REGISTRATIONS

The third and final step in the registration workflow is the registration of generic femur and tibia STL bone models onto the transformed bone models. This step, as mentioned earlier, is required in order to identify the extremity ROIs which are required for the definition of the mechanical axes of the femur and tibia.

The generic STL bone models which are used in this software were obtained from an open-source repository which was managed by the Biomedical Research and Technology community called Biomed Town. While the website[13] of this community has since been taken off the internet, at the time when the models were downloaded,

---

[13] https://www.biomedtown.org/biomed_town/LHDL/Reception/datarepository/repositories/
VAKHUM_home

this webpage was intended as an open space for biomedical researchers to discuss and share their ongoing research. The downloaded STL models were obtained from a full-body CT scan of a healthy 45 year old male with his knees in the fully-extended position. These STL models will be attached as a soft-copy to this thesis along with the entire codebase of this software. These STL models will be referred to as the *generic STL bone models*.

The approach developed for the importation, registration and transformation of the generic STL bone models is as follows:

Step 1: The `importSTL.m` module is called to ask the user to select the directory where the STL models are saved. Subsequently, the STL faces and vertices are extracted from each individual STL model, to extract the coordinate data and allow for visualisations to be generated later on. Finally, each imported STL model is labelled according to the laterality of the bone (left or right) and the bone type. For the implementation of these STL models, the following bone models were imported: left and right femurs, left and right tibias and left and right combined tibias and fibulas. Once the labelling process was finished, the module terminated.

Step 2: Following `importSTL.m`, the `regSTL.m` module is called. In this module, the generic STL models of the femur and tibia for both the left and right knees will be registered onto the femur and tibia models in frame 1. The first step is to import the vertex data of the femur and tibia STL model. The vertex data represents the 3D coordinates of the vertices of each triangular element within the STL model. Using this data, the 3D coordinates of the STL models can be registered onto the 3D coordinate data of the femur and tibia models obtained from the scanner.

Step 3: For the preliminary coarse ICP registration of the STL models onto the scanned models, the boundary point cloud data sets for the scanned femur and tibia of frame 1 are used. The STL models are rotated to align them with the scanned bone models. Subsequently, the STL coordinates are cropped by half the length of the entire bone. For the femur, the proximal half of the bone is cropped out, while for the tibia, the distal half is cropped out. In order to scale the STL models to match the dimensions of the scanned models, the mediolateral

extremities of both femurs are compared, and the STL model is scaled to match the mediolateral width of the scanned model. For the tibia, both the mediolateral and the anteroposterior dimensions are compared, due to its different morphology which required this additional step to achieve better scaling. The TMs generated from the scaling are saved. Then, the STL models are translated to be roughly located close to the scanned models. For the femur, the centre of the mediolateral and anteroposterior extremities at the most distal end of the scanned femur is compared to the same location for the STL femur. The STL model is then translated along a vector connecting these two points. For the tibia, the same procedure is applied with the difference that the most proximal end is considered in this case. Following the translation transformations, the TMs are saved. At this point, the STL model is coarsely approximated to the scanned models, and therefore ICP registration can be performed. The same procedure implemented for the coarse registration of the tibial bones in `regTibia.m` is implemented here. Once the registration converges, the TMs are saved. All the TMs generated throughout this coarse registration process are combined together and saved.

Step 4: The TMs are applied to the original 3D coordinate (vertex) data of the STL bone models to replicate the location which was calculated in the coarse registration. Subsequently, the fine ICP registration is performed on the coarsely transformed STL point cloud data and the full femur or tibia point cloud data. The user then analyses the quantitative and qualitative results of the registration (refer to Figure 65) and proceeds as necessary. Taking into consideration that this time the registration algorithm is attempting to register two bone morphologies from different individuals, the error ranges were more lenient than those suggested for the previous registrations. For this case, the user was guided to accept RMSE errors which are smaller than 1.75 mm (shown in green), proceed with caution for RMSE errors between 1.75 mm and 2 mm (shown in orange) and reject RMSE errors greater than 2 mm. Finally, the TMs are combined and saved along with the registration errors.
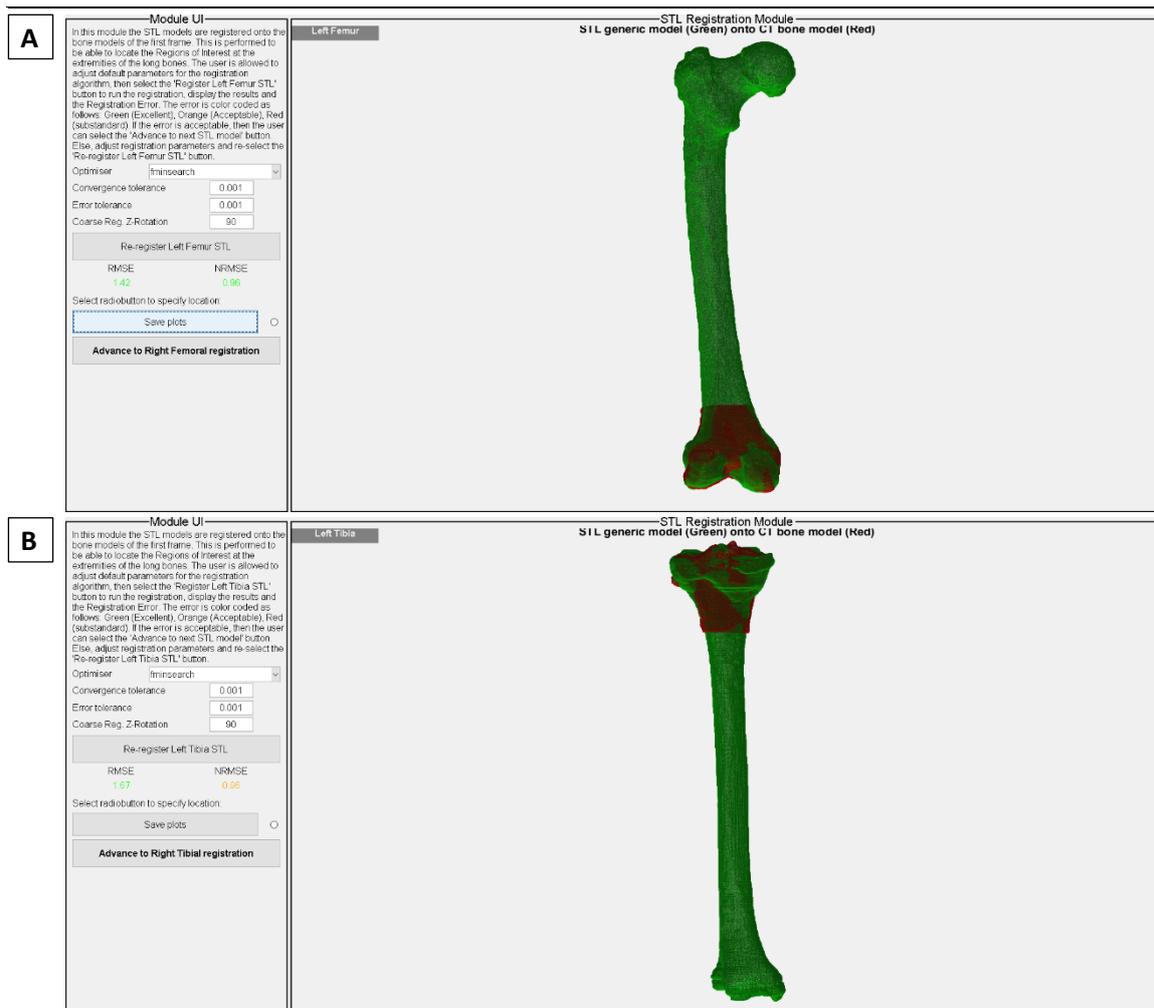
Figure 65: STL registration module UI

A: A visualisation of the registration results for one of the participants, highlighting the effective registration of the generic STL femur model and the corresponding scanned femur bone model. Here, the green generic STL femur model was registered onto the red scanned femur model for frame 1.
B: Another visualisation of the registration results for the green generic tibia STL model onto the red scanned tibia model for frame 1.

Step 5: Following the registration algorithm for the STL models onto the scanned models in frame 1, the next step was to use the TMs calculated in `regSTL.m`, and the TMs obtained in `regTibia.m` to transform the STL models onto all the bone models in all frames. For the case of the femur, no transformations are required since all the femur models in all frames are in the same identical location (fixed femur). Therefore, the registered femur STL model is simply copied for the remaining frames. For the case of the tibia, the STL model needs to be inversely transformed onto the remaining frames. In this case, it should be noted that before applying these transformations, the vertices for the STL model, which contains the combined tibia and fibula are imported. This STL model will be used instead of the tibia STL model since the fibula is required for the identification of the centre of the ankle. Therefore, first, the combined

tibia and fibula STL model is transformed using the TM, which was calculated in `regSTL.m`, so that it will match the location of the registered tibia STL model. Subsequently, the TMs calculated in `regTibia.m` are used to inversely transform the combined tibia and fibula STL model, which is currently located on the scanned tibia model of frame 1, onto the remaining frames.
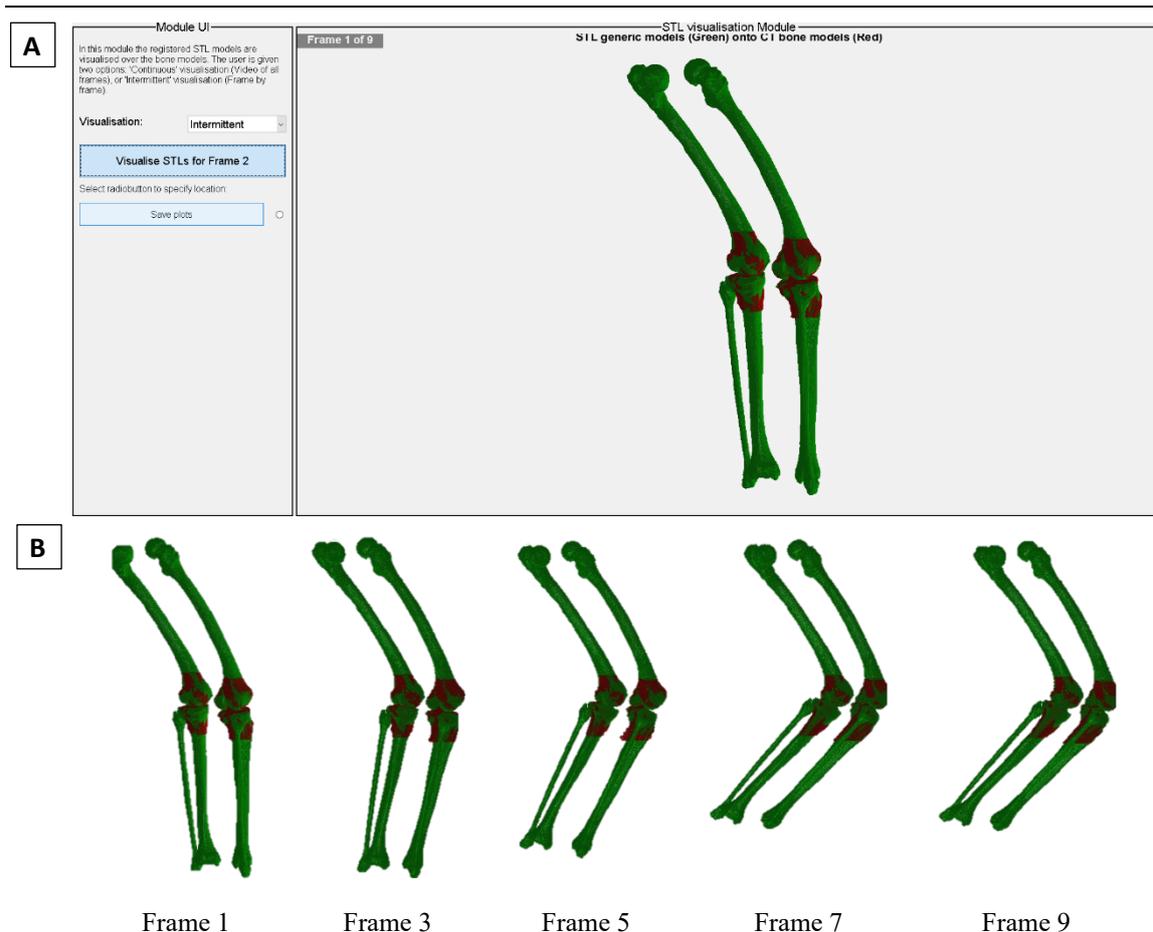
Figure 66: STL visualisation module UI

A: The user is presented with a visualisation module which allows the user to visualise the results of the entire registration workflow in an intermittent or continuous manner. The visualised motion is representative to the motion which was dynamically captured with the 4D CT scanner.
B: A model visualisation of the flexion exercise performed by participant C003. The registered STL bone models are overlaid onto the scanned models. The motion is simplified as the tibia rotates around the fixed femur.

Step 6: Finally, the `showSTL.m` module is called to visualise the results of the entire registration workflow to the user. With reference to Figure 66A, the user is presented with a visualisation of the generic STL bone models in green, overlaid over the scanned bone models in red. The user can visualise the consecutive frames intermittently or continuously, as preferred. The dynamic

motion that is visualised reflects the dynamic motion which was captured during the data capture with the 4D CT scanner, apart for the femur bone being fixed in 3D space. A case visualisation is shown in Figure 66B for alternate frames which were captured for participant C003.

Up to this point, through the extensive use of volumetric image analysis and processing the developed software has achieved segmentation of healthy and replaced knees, and visual representation of the dynamic motion which was captured during the data capture stage. The raw 4D CT data was manipulated explicitly in order to prepare it for the upcoming modules, which are aimed at accurately identifying specific ROIs in the bone models. This will subsequently allow for defining the required CSs, which will be implemented within the bone models to allow for the extraction of the kinematic outcome measures.

4.2.6 COORDINATE SYSTEMS DEFINITION MODULES

The upcoming subsections will present the way that the tibial and femoral CSs were assembled. In the developed workflow of the software, first, the tibial CS is defined then, before presenting the assembly of the four femoral CS, the identification of the tibiofemoral contact points is presented. The contact point analysis precedes the femoral CS definitions since the location of the contact points is required for specific modules used in the subsequent femoral CS definition modules. In this text, the modules responsible for the identification and visualisation of the tibiofemoral contact points will be presented in section 4.2.7, along with the modules which are responsible for the extraction of the kinematic outcome measures. For this reason, it should be noted that in the following subsections when referring to the identified contact points, it should be assumed that these are already identified in the workflow, although not yet presented in this text. The reader is referred to Figure 55, which presents the software's workflow.

4.2.6.1 TIBIAL COORDINATE SYSTEM

Reference is made to the text defining the assembly of the tibial CS, in section 2.6.3.3. In this software, in line with the description given in the text referred above, prior to assembling the tibial CS, three essential ROIs need to be identified, namely the ankle centre, and the centre of each tibial plateau. Using these three ROIs, the tibial CS can then be assembled. In the following text, the developed approach to identify these three ROIs and the subsequent assembly of the tibial CS will be presented.

Ankle centre identification

The `ankleCentre.m` module locates the medial and lateral malleoli of the ankle using the registered STL models. The STL 3D coordinates, or vertices, of the tibia being analysed, are imported and cropped so as only to visualise the distal fifth of the entire bone. The user is then presented with a UI which visualises the distal fifth of the tibia and fibula. The software then attempts to identify the medial and lateral malleoli of the ankle by locating the points which lie at both extremes on the x-axis of the global coordinate system (GCS). These points are visualised with red markers. A third marker, shown in blue, represents the mid-point between the two aforementioned markers, which locates the ankle centre (refer to Figure 67A). Since the mediolateral axis of the tibia STL model is not yet defined and also not aligned with the x-axis of the GCS, the automatically identified markers at the current stage usually need to be revised by the user.
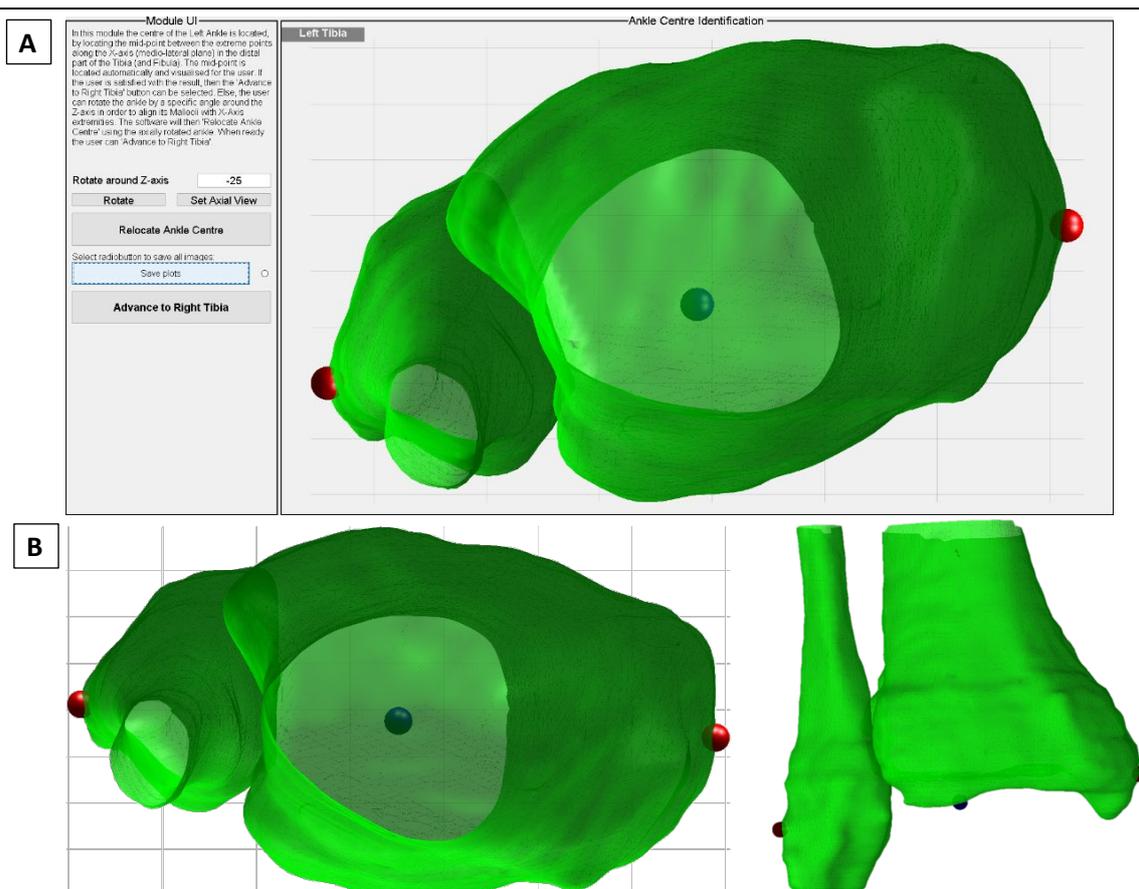
Figure 67: Ankle Centre identification module UI

A: The user is initially presented with an automated identification of the ankle centre. Due to the tibia STL not being aligned with the x-axis of the GCS (shown with the grey horizontal lines behind the ankle) the tibia needs to be rotated using the UI to align it with the x-axis.

B: Following rotation of the tibia STL, the tibia is aligned with the x-axis of the GCS and then the software locates the medial malleoli. Left: Axial view and Right: Coronal view of the identified malleoli.

The user is guided to use the module UI to visualise the tibia from the axial perspective and subsequently rotate the tibia until the markers on the malleoli are located in their correct location. The user can specify the degree of rotation around the z-axis, and iteratively align the tibia until the malleoli are labelled correctly.

Once the user is satisfied with the identified ankle centre, the TM which was generated to rotate the tibial STL model is used to inversely transform the identified ankle centre back to the original location of the tibia STL model. Furthermore, the location of the ankle centre is transformed onto the remaining frames by using the TMs generated in the `regTibia.m` module to perform an inverse transformation of its coordinates onto the other frames. The locations of the ankle centres for all frames are saved, and the user then advances to the contralateral tibia to repeat the process.

Tibial plateau centres identification

For the identification of the centre of the tibial plateaus, the method proposed by Cobb *et al.* (2008) is implemented (refer to section 2.6.3.3). This method, which is presented in `tibROI.m`, has been demonstrated to have high precision and reliability. The user is guided through the following steps to identify the proximal end of the IEA or the mechanical axis of the tibia:

Step 1: Outline both the medial and lateral cortices of the tibial plateaus. The software uses these selected points to fit a plane[14] to the surface of the tibial plateaus. The user is shown a visualisation of this plane and is guided to verify its orientation in relation to the tibial plateau surface (refer to Figure 68A for its application on a healthy knee and Figure 69A for a replaced knee).

Step 2: The user is subsequently guided to outline any of the two tibial plateau cortices. The software uses the points selected by the user to fit a 2D circle to the selected points. Once the circle is defined, it is visualised for the user to confirm the fitting process (refer to Figure 68B and C for its application on a healthy

---

[14] The algoithm used to fit a plane to a set of 3D points in this software was obtained from MATLAB File Exchange. Credit goes to David Legland for making the algorithm available. The algorithm performs a moment of inertia analysis on the 3D points. To estimate the moment of inertia of the 3D points, it is assumed that the best-fit plane passes through the centroid of the identified points. A covariance matrix is constructed from the vectors linking the centroid to the 3D points. Principal Component Analysis is then used to extract the moment of inertia axes. These axes are used to define the fitted plane.

knee and Figure 69B and C for a replaced knee). The user is also presented with the RMSE and NRMSE error of the fitting process. Colour coding is used to assist the user with accepting or rejecting (and repeating) the fitting process. Once the user accepts the fitted circle, the software projects the centre of the fitted circle onto the plane defined in step 1. This point is defined as the centre of the tibial plateau that is being analysed. The user then repeats the same process on the contralateral tibial plateau. Once both plateau centres are defined, the 3D coordinates for each tibial plateau centre, the plane defined in step 1 and the fitting errors are saved.

Step 3: The user is guided to perform the same process on the contralateral tibia.

Step 4: The TMs generated in `regTibia.m` are used to perform an inverse transformation of the tibial plateau centres identified in the previous steps onto the other frames. The transformed locations of the tibial plateaus centres for all frames are saved, and the module terminates.
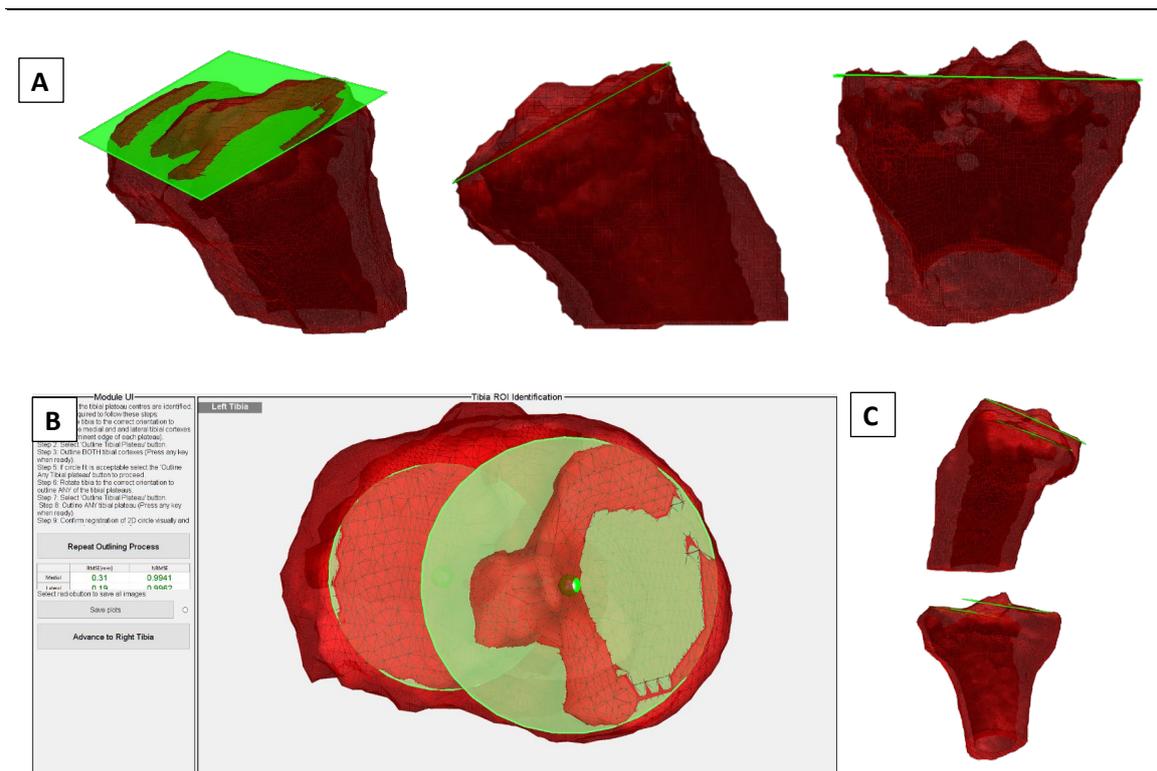
Figure 68: Tibial plateau Centre Module UI – Healthy knees

A: After the first round of tibial cortex identification, the user is presented with a plane which is fitted to the selected points. Left: Orthographic view, Centre: Sagittal view, Right: Coronal View of the fitted plane.
B: During the second round of tibial cortex identification, the user is presented with 2D circles which are fitted to selected points outlining the tibial plateau. The centre of the corresponding tibial plateau is defined by the centre of the fitted circle. The image shows the axial view of the two fitted circles.
C: Same as **B**, from different perspectives. Left: Coronal view, Right: Sagittal view.
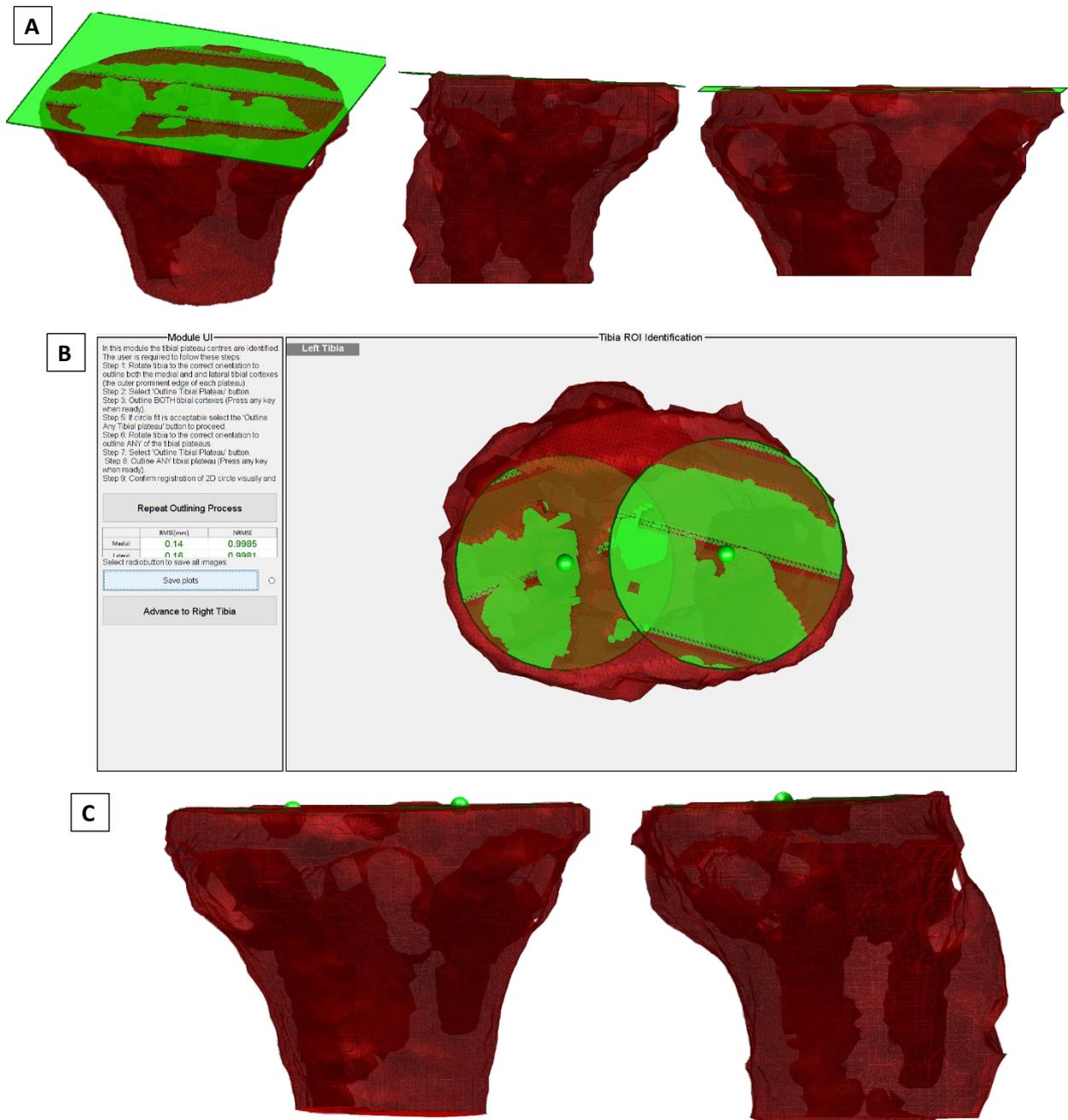
Figure 69: Tibial plateau Centre Module UI – Replaced knees

A: The plane that was fit to the user selected points outlining the entire tibial plateau. Left: Orthographic view, Centre: Sagittal view, Right: Coronal View of the fitted plane.
B: The 2D circles which are fitted to the user selected points outlining each tibial plateau. The image shows the axial view of the two fitted circles for the replaced knee of P003.
C: Same as **B**, from different perspectives. Left: Coronal view, Right: Sagittal view.

Defining the Tibial Coordinate System

Following the identification to the three ROIs of the tibia, `tibAxes.m` is called to assemble the anatomical, or local, tibial CS as defined in section 2.6.3.3. The approach taken to achieve this is as follows:

Step 1: The ROI coordinates for the current frame, which were located in the previous modules, are imported.

Step 2: The origin is identified as the mid-point between the medial and lateral tibial plateau centres.

Step 3: The tibial z-axis, which is coincident with the JCS body-fixed axis having the unit vector $\widehat{e_3}$, representing the IEA of the JCS, is defined as the vector which distally passes through the ankle centre and proximally through the origin defined in Step 2. The vector is defined by subtracting the location of the ankle centre from the location of the origin. The vector is then converted into a unit vector.

Step 4: The tibial x-axis is defined as the vector which passes through the two plateau centres. This is defined by subtracting the location of the medial plateau centre from the location of the lateral plateau centre for the right knee and vice versa for the left knee. This ensures that the x-axis is always oriented so as to be positive towards the right. The vector is then converted to a unit vector.

Step 5: The tibial y-axis, which is coincident with the JCS tibial reference axis having the unit vector $\widehat{e_3^r}$, is defined by completing the right-handed coordinate system. The vector is defined by the cross product of the z-axis and the x-axis. The vector is then converted to a unit vector.

Step 6: All the three vectors, their corresponding unit vectors and the origin of the tibia are saved.

Step 7: Steps 1 to 6 are repeated for all frames using the inversely transformed ROIs generated in the two previous modules.

Step 8: Finally, the user is shown a visualisation of the generated tibial CS for all frames (refer to Figure 70).

This concludes the developed approach for the definition of the tibial anatomical CS.
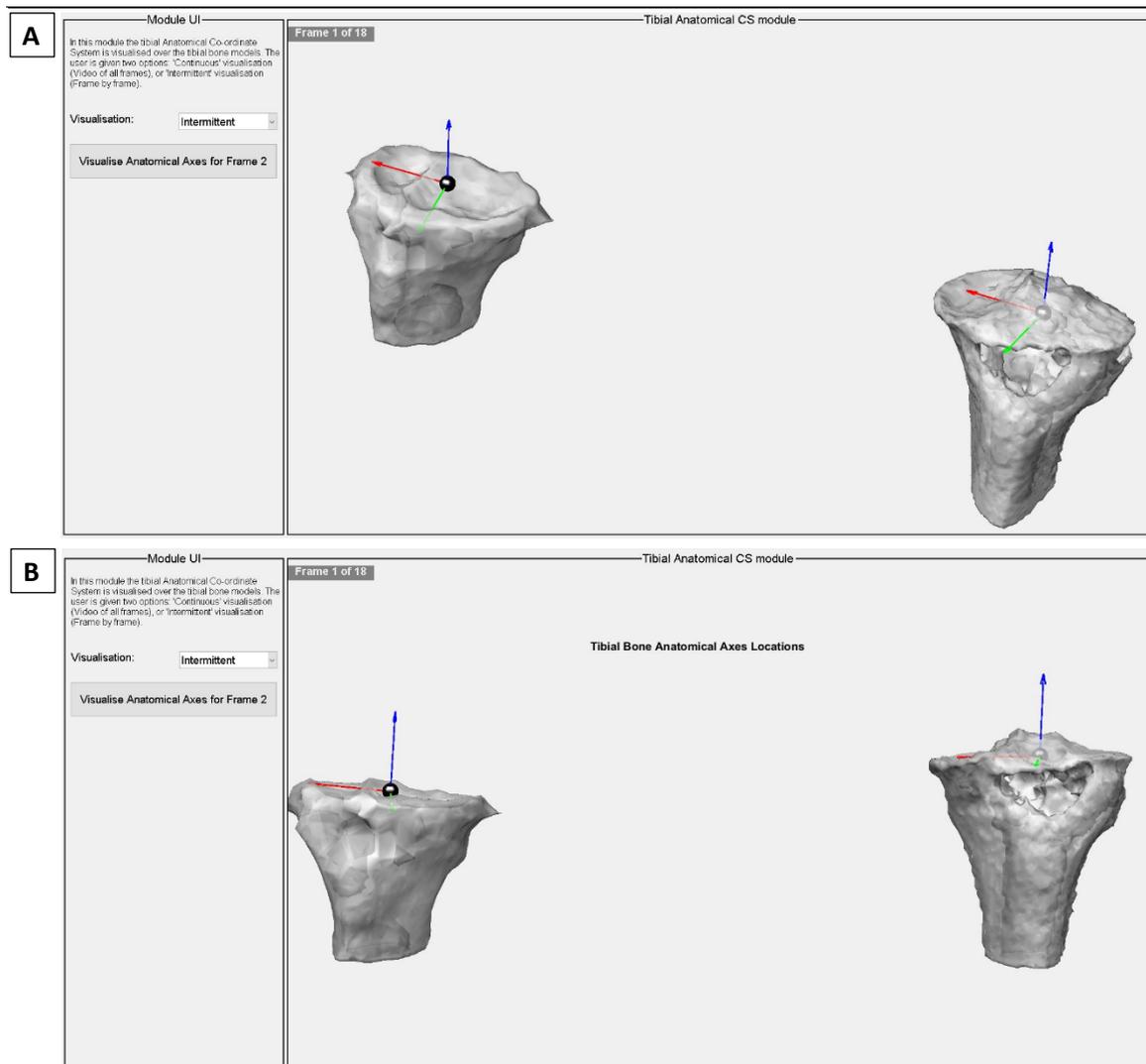
Figure 70: Tibial Anatomical CS module UI

A: An orthographic view of the generated tibial CS for patient participant P001.
B: A coronal view of the generated tibial CS for patient participant P001.

4.2.6.2   FEMORAL COORDINATE SYSTEM

Reference is made to the definition of the femoral LCSs, in section 2.6.3.3. In this software, in line with the description given in the text referred above, prior to assembling the femoral CSs, the centre of the femoral head needs to be identified, and four femoral FEAs will need to be defined. Subsequently, the LCSs are assembled and implemented in the scanned knees to understand how the reported kinematics will vary between the four cases over the captured ROM. The four FEAs are namely the:

1. FEA as defined by Grood and Suntay (1983) in the paper defining the JCS. While this FEA axis is known to be inadequately defined, it is being implemented to highlight the kinematic crosstalk that would result when improper axis placement occurs. This axis will be referred to as the "JCS" FEA.

2. GCA, or Geometric Centre Axis, is defined as a line passing through the centre of the posterior femoral condyles. Although this axis is well established within the research community, in this study, its applicability over the captured ROM of the knee will be assessed.

3. sTEA, or Surgical Trans Epicondylar Axis, is defined by a line intersecting the medial sulcus and the lateral epicondyle of the distal femur. Similar to the GCA, although this axis is well established in the research community (along with its neighbouring clinical Trans Epicondylar Axis), in this study, its applicability over the captured ROM of the knee will be assessed.

4. FFA, or functional FEA, is a functionally derived axis whose location is identified by fitting a line to the points displaying the least cVSV (cumulative Vertical Shift Value – as proposed by Yin *et al.* in 2015) or the least cED (cumulative Euclidean Distance – an alternative approach being tested in this study) over the entire recorded ROM.

For each of the four FEAs, a separate local femur CS will be assembled. The upcoming text will describe the approach taken to identify the centre of the femoral head, the four FEAs and their corresponding CS.

Femoral head centre identification

The centre of the femoral head is the only common point to all four CSs. The approach taken to identify this ROI is defined in `femHeadCentre.m`, and is processed as follows:

Step 1: The 3D STL coordinates of the femur are imported and then cropped so as only to visualise the proximal fifth of the entire femur.

Step 2: The proximal fifth of the femur is visualised along with a translucent red box (refer to Figure 71A). The user is guided to rotate the femur model around the y-axis of the GCS until the femoral head is aligned with the box.

Step 3: Once the box is aligned to the femoral head, the box's dimensions can be adjusted to ensure it encapsulated the femoral head. Then a sphere is fitted and visualised along with the corresponding RMSE and NRMSE errors. The user is guided, through colour-coding of the displayed errors (refer to Figure 71B), to accept registration results with errors of less than 0.5 mm (shown in green),

and proceed with caution for errors between 0.5 and 1 mm (shown in orange). Errors over 1 mm are to be avoided (shown in red).

Step 4: The user analyses the quantitative and qualitative results of the sphere fitting, and if it is deemed satisfactory, the user can proceed to the contralateral femur. Otherwise, the sphere fitting process can be repeated.

Step 5: The centre of the sphere is saved as the centre of the corresponding femoral head. The location is copied onto the remaining frames, and the module terminates.
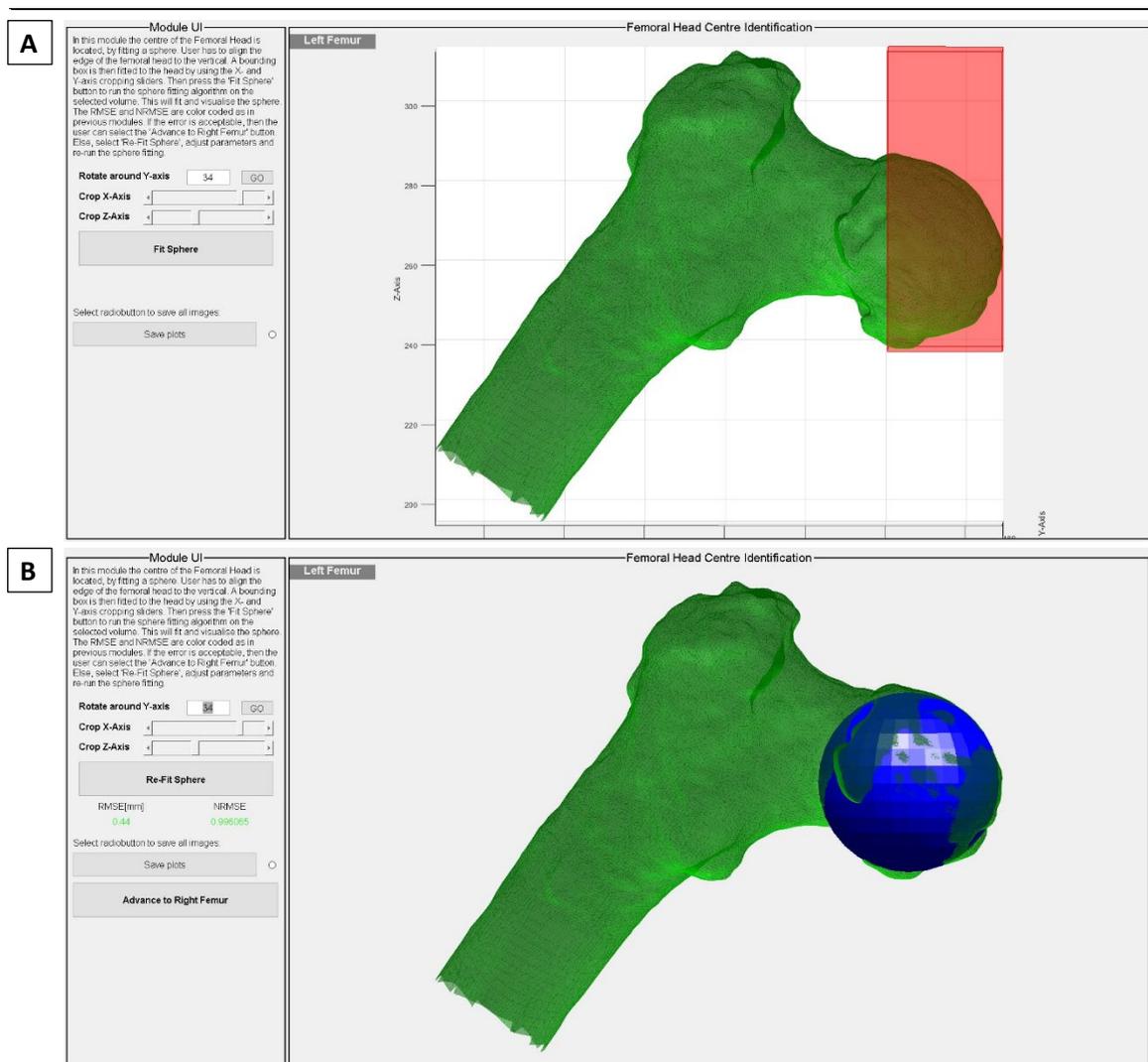
Figure 71: Femoral head centre identification module UI

A: The proximal fifth of the femur is visualised for the user to be able to select the femoral head. The first step is for the user to use the UI to rotate the femur to align it with the red translucent box.
B: The centre of the femoral head is defined by fitting a sphere to the highlighted part of the femur which was selected by user using the red translucent bounding box.

JCS defined FEA

With reference to the description of the JCS given in section 2.6.3.3, in their paper, Grood and Suntay (1983) defined the FEA using three femoral ROIs, specifically:

1. The most distal point on the posterior surface of the femur (midway between the medial and lateral condyles).

2. The most posterior point on the medial femoral condyle.

3. The most posterior point on the lateral femoral condyle.

These three ROIs are identified within the `femROI.m` module. The user is guided through the following steps to identify them:

Step 1: Manually identify the most distal point on the posterior surface of the femur. The user is guided to rotate the femur model in order to identify this correctly. Once the user selects the ROI, a marker visualises its location for the user to verify the location (refer to Figure 72A). If the user is satisfied with its location, the software advances to the identification of the next two ROIs; otherwise, the user can repeat the identification process.

Step 2: For the identification of the most posterior point of each femoral condyle, the definition[15] given by Matsuda is implemented (Matsuda *et al.*, 2004). The user is asked to select two points at the most superior aspect of the femoral articular surface of the posterior condyle. A plane is created connecting the two points selected by the user and the contact point (identified earlier in the workflow). The midpoint of the two points selected by the user is identified and labelled point X. Subsequently, the midpoint between point X and the contact point is located and labelled point D. The normal of the plane created earlier is found, and a line is projected, passing through point D and oriented along the normal to the plane. Finally, the most posterior point of the femoral condyle is identified as the point of intersection of this line with the femoral condyle.

---

[15] With reference to the inset image in Figure 21B, the most posterior point on the femoral condyle is identified by connecting point A, the contact point with the tibia, to point B, the most superior point of the femoral articular surface of the condyle. The mid-point of the line connecting these two points is identified, and subsequently a line perpendicular to line AB is project at the mid-point. Point C, the most posterior point on the femoral condyle is the location where the projected line intersects the condyle.

Step 3: The user is shown a visualisation of the calculated point (refer to Figure 72B). If the user confirms its location the software proceeds to the contralateral condyle, otherwise, the user can repeat the selection of the two points.

When all three ROIs have been defined the software replicates all three locations onto the remaining frames (no transformation required), saves all the locations and the module subsequently terminates.
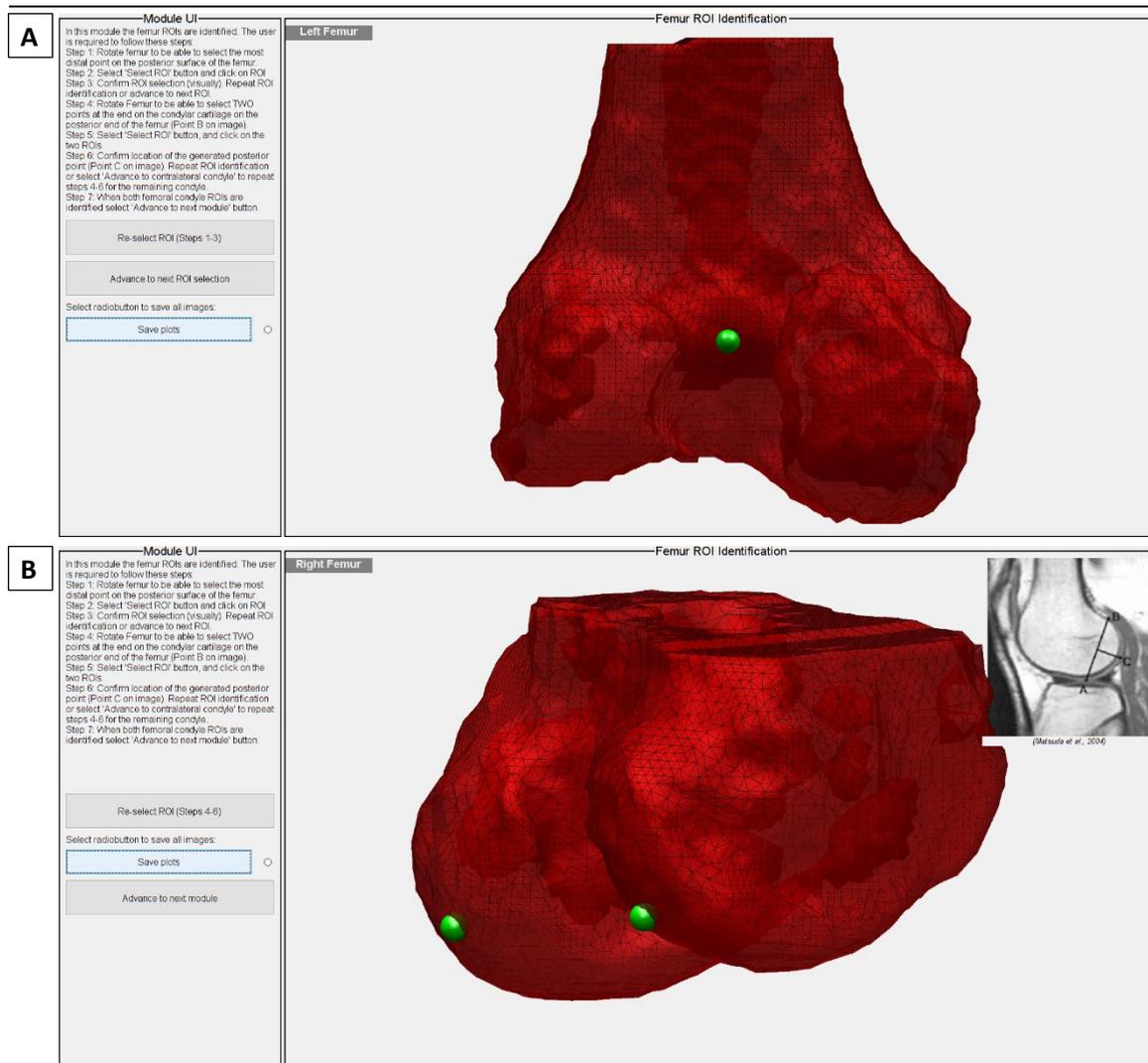
Figure 72: Femur ROI (JCS FEA) Module UI

A: A visualisation of the most distal point on the posterior surface of the femur.
B: A visualisation of the most posterior points of the femoral condyle which are automatically identified following the selection of two points at the location of point B in the inset image.

GCA as the FEA

With reference to section 2.6.2.1, the GCA is defined by the centres of the posterior femoral condyles. While Eckhoff *et al.* (2003) fitted cylinders to each femoral condyle, Yin *et al.* (2015) stated that fitting a sphere to the condyles results in more robust and

reproducible results, while achieving identical results to the cylinder fitting method. This statement was tested in this software, and it was indeed noted that sphere fitting is more robust than the cylinder fitting method. For this reason, the sphere fitting method is implemented in the developed approach.

The identification of the centre of the posterior femoral condyles, and the subsequent definition of the GCA is outlined in GCA.m, and is processed as follows:

Step 1: The femur being analysed is visualised, and the user is guided to rotate it in order to orient it in a way to allow for outlining the cartilaginous areas of the posterior femoral condyles.

Step 2: Once the user orients the knee, any of the posterior femoral condyles can be outlined. The outlining is performed by selecting different locations on the cartilage of the condyle until the posterior aspect of the femoral condyle is outlined.

Step 3: The software then fits a sphere to the outlined points on the condyle and visualises it. The user is shown the corresponding RMSE and NRMSE errors of the fitting process and is guided through colour-coding of the displayed errors (using the ranges implemented for the fitting process of the femoral head).

Step 4: The user then analyses the quantitative and qualitative results of the sphere fitting, and if it is satisfactory, the user can proceed to the contralateral femur. Otherwise, the sphere fitting process can be repeated.

Step 5: When the user outlines and accepts the sphere fitting of the contralateral femoral condyles, the software uses the locations of the centre of the two spheres to calculate the GCA. The GCA is visualised (refer to Figure 73), and then the user is asked to confirm its location[16]. The user can then either repeat the entire sphere fitting process or proceed to the contralateral femur.

---

[16] Apart from visually assessing the fitted spheres and the location of the GCA relative to the condyles, the user can refer to the relative size of the two spheres for guidance, whereby the medial sphere is expected to be larger than its lateral counterpart at a ratio of ranging between 1.1 and 1.15. Furthermore, the GCA is expected to pass distal to the intercondylar notch, through the origin of the ACL (Refer to section 2.6.2.1).

The software then saves the location of the centres of the spheres, their radii, the corresponding errors and the equation of the line defining the GCA. The saved data is copied for the remaining frames, and the module terminates.
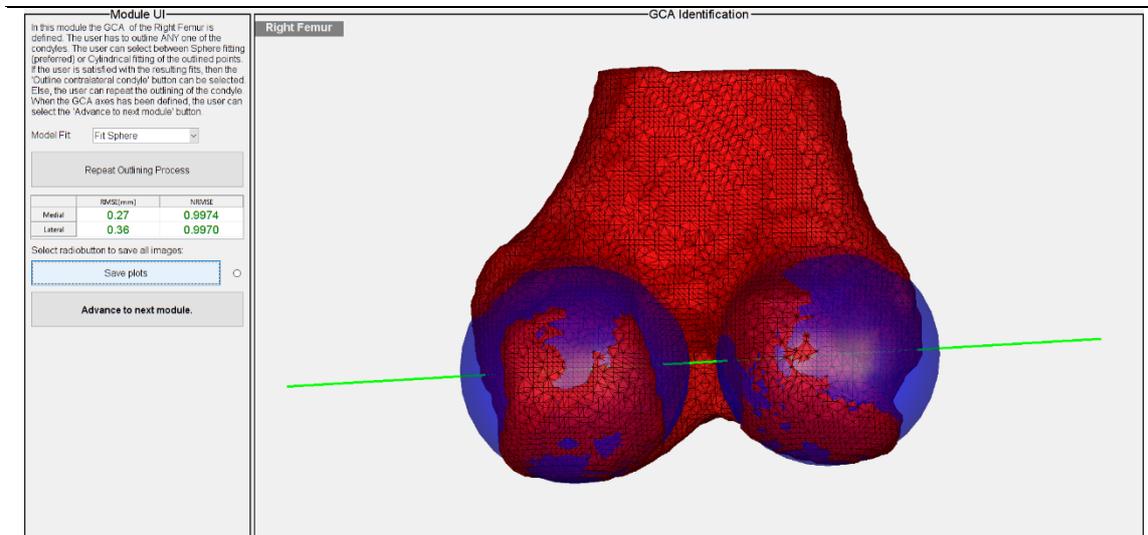
Figure 73: GCA identification module UI

This module initially fits a sphere to each of the femoral lateral condyles. Then, a line passed through the sphere centres is calculated, defining the GCA.

TEA as the FEA

With reference to section 2.6.2.1, the computer-assisted epicondyle identification method proposed by Eckhoff *et al.* in his paper (Eckhoff *et al.*, 2005) is implemented. In the `TEA.m` module, the GCA axis, which was defined in the previous module, is used to guide the identification of the TEA. A cylinder defined by the GCA axis is created and extended along its axis mediolaterally until only one point remains outside of the cylinder on both ends (refer to Figure 34C). These identified points are used to guide the user in manually identifying the epicondyles. Given that the TEA has two variants, the clinical and surgical TEAs, the user is guided to identify the surgical variant of the TEA preferably. If the medial sulcus (sTEA) cannot be confidently identified, the user is guided to identify the medial epicondyle (cTEA) instead.

The identification of the epicondyles and the subsequent definition of the TEA is processed as follows:

Step 1: The point cloud data points for the femur being analysed are imported and transformed into the CS which was defined for the GCA axis in the previous module. This results in all the femur data points being defined with respect to the GCA CS.
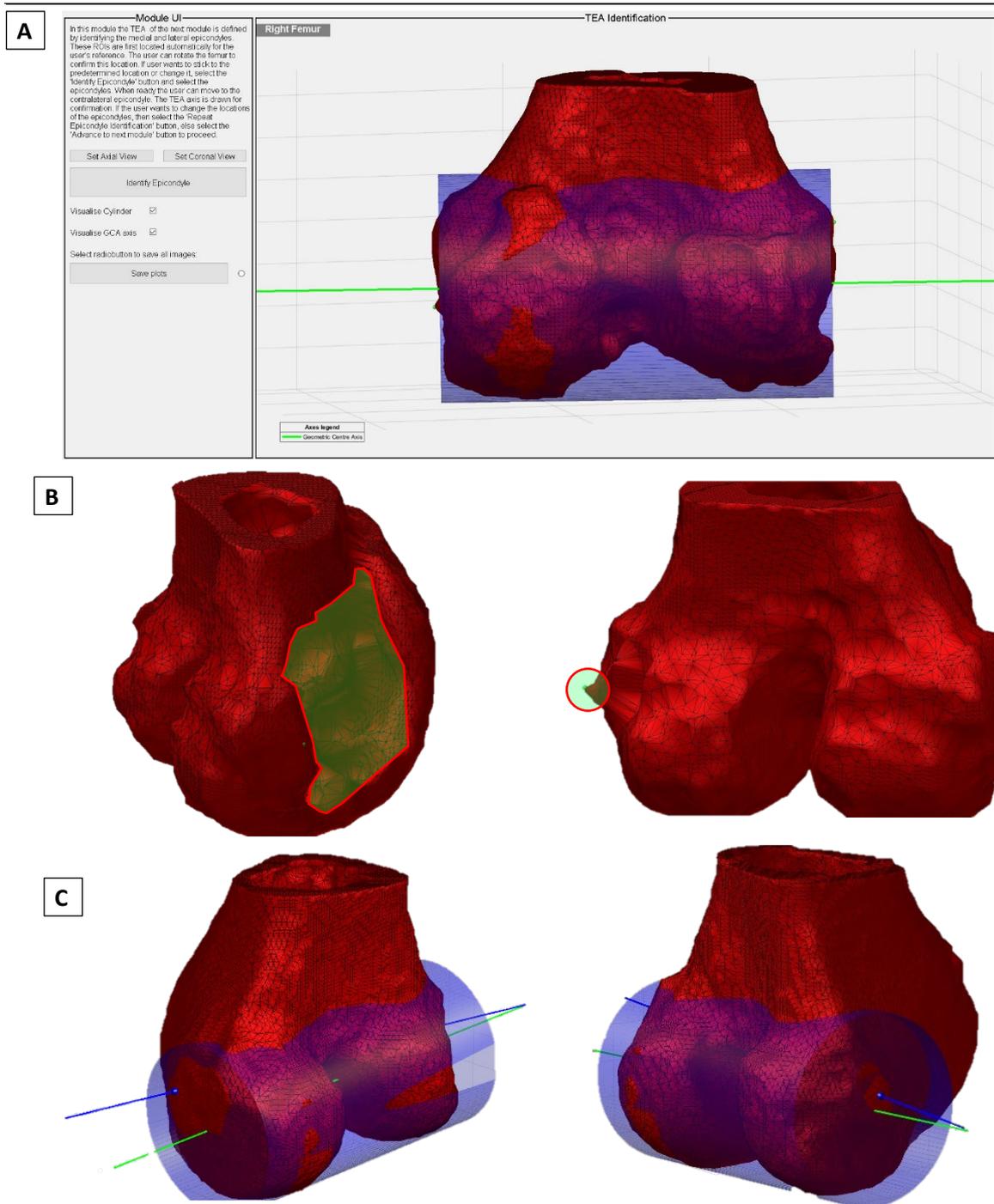
Figure 74: TEA identification module UI

A: A visualisation of the initial estimation of the medial and lateral epicondyles along with the GCA axis (green) and its translucent cylinder.

B: SEMAR impacted femur models in replaced knees. Left: Missing condylar osseous tissue, highlighted in green, which was removed following the SEMAR post-processing algorithm in an attempt to reduce flaring from the metallic implants. This resulted in ROIs being eliminated, thus not allowing for their identification. Right: Another SEMAR artefact, highlighted in green, is the erratic condyle contours which resulted for replaced knees. This negatively impacted the identification of the TEA ROIs in replaced knees.

C: Orthographic views of the user identified TEA ROIs and the corresponding TEA axis for participant C002. Left: Medial condyle, Right: Lateral condyle.

Step 2: The most medial and lateral points on the transformed femur point cloud are identified and labelled as the medial and lateral epicondyles, respectively (refer to small green spheres in Figure 74A and B). These points will be used to guide the user in better identifying the epicondyles.

Step 3: The femur point cloud data and the automatically identified ROIs are transformed back to the GCS and visualised, along with the GCA axis. A translucent cylinder defined by the GCA is overlaid over the other visualisations to assist the user in identifying the most medial and lateral aspects of the femur condyles (refer to Figure 74C).

Step 4: Using the preliminary estimated epicondyle locations, the user is guided to either confirm the automatically identified ROIs or else to manually re-define the location of the ROIs. It should be noted that while automatically generated ROIs define the epicondyles, the user should preferably identify the sulcus medially, as this will identify the sTEA which is preferred over the cTEA.

Step 5: Once the ROIs are selected by the user, the TEA axis is defined by a line passing through both ROIs. The TEA is then visualised alongside the GCA axis for the user to confirm its location (refer to Figure 74C). The user can then choose to either repeat the manual identification process or proceed to the contralateral femur.

The software then saves the location of the identified ROIs and the equation of the line defining the TEA axis. The saved data is copied for the remaining frames, and the module terminates.

With reference to Figure 74B, during the execution of this module on the collected participant data, it was noted that the SEMAR processed replaced knees negatively impacted the initial estimation process in identifying the medial and lateral epicondyles due to the irregular surfaces which resulted following segmentation of replaced knee bone tissue. The impact of the over-processed replaced knees resulted in cases of replaced knees which did not have any remaining bone tissue on the surface of the condylar areas, as shown in Figure 74B. For these cases, the TEA could not be defined and will, unfortunately, not be included in the analysis of the individual results. The participant knees which were affected to this extent by the SEMAR processing will be highlighted in the results section.

Functional Axis as the FEA

In this software, the functional FEA (FFA) method proposed by Yin *et al.* (2015)*,* which was reviewed in section 2.6.2.1, will be implemented along with a variation of the same method. Apart from the cVSV approach, which measures the cumulative vertical shift value of each voxel over the captured ROM, in this software, an alternative cumulative euclidean distance (cED) approach will be investigated.

This alternative method measures the cED of each voxel and then subsequently fits an axis to the voxels with the lowest cED values, in an attempt to identify the FFA. This alternative method of identifying the FFA was considered since the cVSV method was not converging as expected during preliminary testing[17] (refer to Figure 75C and D). This was primarily attributed to the relatively smaller captured ROM in comparison to Yin *et al.*'s (2015) implementation, which covered 120º of flexion. Secondarily this was attributed to the fact that the cVSV method utilises only the z-value of the coordinate data.

Therefore, in an attempt to surpass these limitations the cED approach was considered to evaluate if including the x- (mediolateral) and y- (anteroposterior) values in addition to the z-values would assist the algorithm to converge on the FFA. However, it should be appreciated that since the x- and y-values are being inputted into the algorithm, the ML and AP translations, of the femur relative to the tibia, will weigh into the algorithm and will subsequently skew the resulting FFA when using the cED approach. Therefore, when analysing the results of the FFA, the ML and AP translations and their effect on the position of the FFA should be considered.

The implementation of the cVSV and cED approach to extract the FFA is presented in `optimFEA.m` and `showFEA.m`, and is processed as follows:

Step 1: The tibial and femoral coordinate data points are converted from the GCS to the tibial CS of the frame being processed. This is performed in order to allow for measuring the movement of the femur relative to a fixed tibia.

---

[17] In this context, the algorithm is assumed to converge when it outputs an axis which lies in the vicinity of the TEA or the GCA. Refer to Figure 75C and D for cases which do not converge.

Step 2: The VSV is measured by identifying the difference in the z-value of each point in the femur over two consecutive frames. The Euclidean distance travelled by each point in the femur over two consecutive frames is also measured.

Step 3: The cVSVs are added cumulatively from the first to the last frame to obtain a unique value for each femoral data point. The same is performed for the cED values, such that two unique values exist for each point in the femur.

Step 4: The cVSVs are then sorted in ascending order, and the femur data points which recorded the smallest 1% cVSVs are saved for further processing. The same procedure is applied for the cED values.

Step 5: The weighted mean of the stored values is identified by using the following exponential weighting metric which gives more weight to the data points which reported the smallest values, while exponentially decreases the weighting metric as the values increase:

$$f(x) = e^{1-\frac{1}{x^2}}$$

Step 6: Having the weighted mean identified, the remaining component in order to define the vector defining the FFA is the direction vector. This is achieved by performing singular value decomposition (SVD) of the femur data points stored in step 4 for both the cVSV and the cED selected data points. SVD locates the largest singular vector, or eigenvector, which is assumed to represent the direction vector of the FFA.

Step 7: The weighted mean and the direction vector extracted in steps 5 and 6 are used to define the FFA for the cVSV and the cED.

Step 8: Finally, for the femur visualisations, each data point in the femur is coloured so as to visualise the corresponding cVSV and cED values. The femur data points exhibiting the smallest movement are coloured blue, with the colour changing to red as the values increase (using the MATLAB jet colourmap – Figure 75).

Step 9: The user is presented with a visualisation of the coloured surface points of the femur which are indexed to the corresponding cVSV or cED values. Furthermore, the identified FFA for the cVSV or cED (depending on the user's choice) and the GCA and TEA are also visualised for reference (Figure 75A and B).
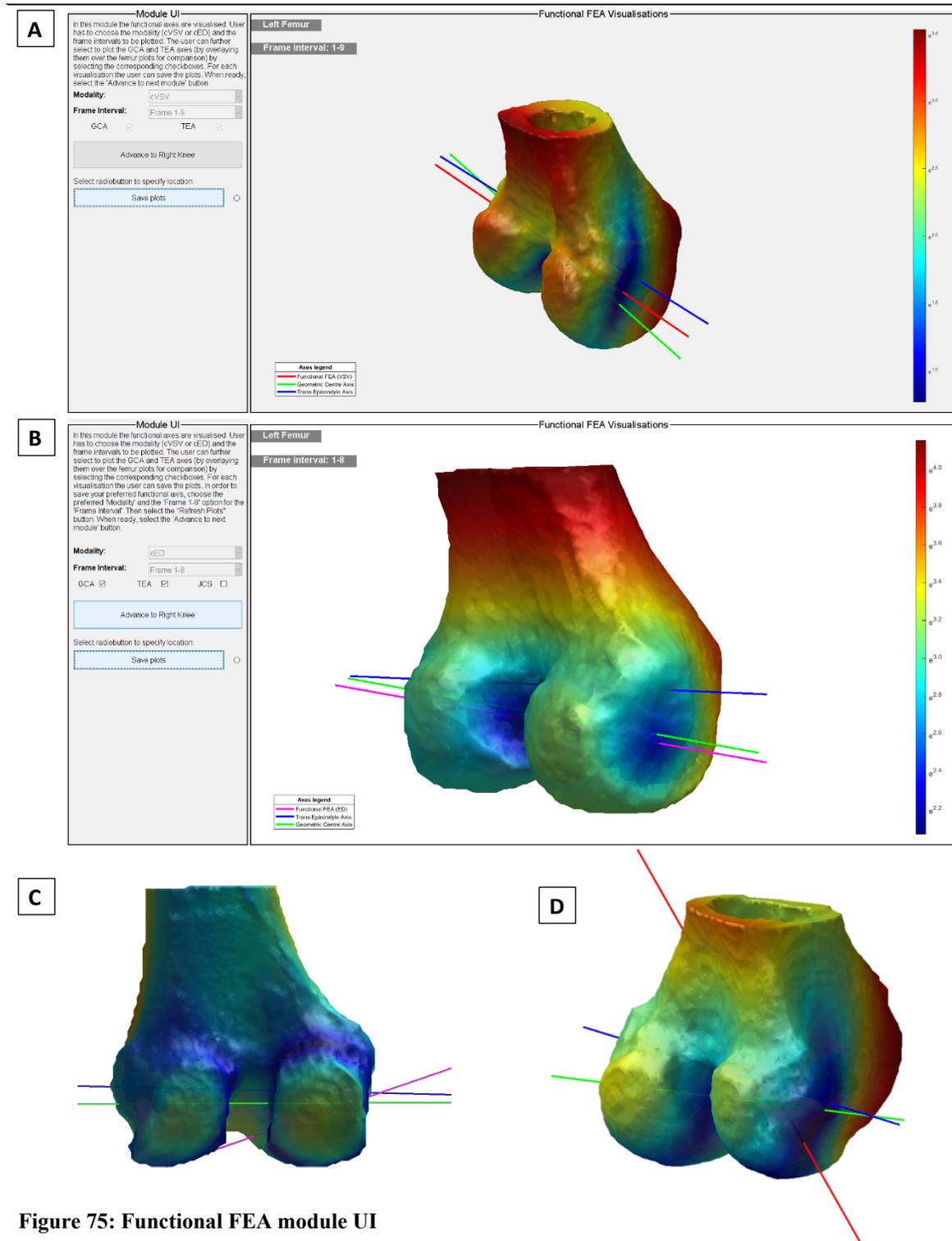
Figure 75: Functional FEA module UI

A: The user is shown a visualisation of the calculated cVSV values for each femoral data point by applying a colourmap which is indexed to the corresponding cVSV values. The fitted FFA is visualised alongside the GCA and TEA for reference.

B: The user is allowed to choose between visualising the cVSV, as shown in **A** or the cED values, as shown in this image.

C: The user is also given the opportunity of visualising the cVSV or cED values for different frame intervals. In this image, the Left Femur cED values and corresponding FFA axis are shown for the frame interval from frame 1 to frame 5. Generally, the smaller the frame interval, the less the FFA convergences.

D: A cVSV (or cED) result which does not converge does not show a relationship to any of the anatomically defined axes, that is, the GCA and TEA.

Step 10: The user can then save the cED and cVSV plots and advance to the contralateral femur. Subsequently, the software saves the equation of the fitted lines and their corresponding intersection points with the femur surfaces.

It should be noted that the functional FEA module described above, apart from allowing the user to visualise the cVSV and cED values over the entire frame interval range, that is, from the first to the last frame, it also allows the user to visualise the cED and cVSV results over three other predefined frame interval ranges, as follows:

> A. Frame Intervals: $1 - 2$, $1 - 3$, …, $1 - n$
>
> B. Frame Intervals: $1 - 3$, $2 - 4$, …, $(n - 2) - n$
>
> C. Frame Intervals: $1 - 4$, $2 - 5$, … , $1 - n$

The intention behind calculating the cVSV and cED values for these various frame intervals was to be able to calculate and visualise the FFA over the extension and flexion ranges of motion so that the ECA and FCA can be related to the FFAs identified over specific ranges. However, the algorithms were not robust enough to be able to converge for frame intervals which do not represent a considerable ROM (refer to Figure 75C). This dependence on the ROM was noticed to be the principal limitation with this method of identifying the FFA, which will be noted in the results which are reported in chapter 5.

Defining the Femur Coordinate System

Following the identification of the femoral head and the definition of the four FEA variants of the femur, `femAxes.m` is called to assemble the four local femoral CSs as defined in section 2.6.3.3. The approach taken to assemble each of the four CSs is identical, and the procedure followed for any of the four CSs is as follows:

Step 1: The ROI coordinate data and the FEA equation, which were identified in the previous modules, are imported.

Step 2: The origin is defined as follows for each case:

> a. JCS CS: The most distal point on the posterior surface of the femur
>
> b. TEA CS: The mid-point between the medial and lateral epicondyles
>
> c. GCA CS: The midpoint between the medial and lateral centres of the posterior femoral condyles.

d. FFA CS: The midpoint between the intersection points of the FFA with the medial and lateral femoral condyles.

Step 3: The femoral Z-axis is defined as the vector which distally passes through the origin, defined in step 2, and proximally through the centre of the femoral head. The vector is defined by subtracting the location of the origin from the location of the femoral head centre, therefore ensuring that the Z-axis is always oriented so as to be positive in the proximal direction. The vector is then converted to a unit vector.

Step 4: The femoral X-axis, which is coincident with the JCS body-fixed axis having the unit vector $\widehat{e_1}$, representing the FEA of the JCS is defined for each FEA variant depending on the laterality of the knee being analysed. For the left knee, the lateral ROI of the FEA being analysed is subtracted from the medial ROI, while for the right knee, the medial ROI is subtracted from the lateral ROI. This approach ensures that the X-axis is always oriented so as to be positive to the right. The vector is then converted to a unit vector.

Step 5: The femoral Y-axis, which is coincident with the JCS femoral reference axis having the unit vector $\widehat{e_1^r}$, is defined by completing the right-handed coordinate system. The vector is defined by the cross product of the Z-axis with the X-axis. The vector is then converted to a unit vector.

Step 6: All the three vectors, their corresponding unit vectors and origin, are saved.

Step 7: Once all vectors and origins for all four FEA variants are defined and saved, the generated vector and coordinate data are copied for the remaining frames. The module subsequently terminates

Following the execution of `femAxes.m`, another module, `showAxes.m` is called to provide the user with the ability to visualise the tibial CS and any of the four femoral CSs. The user is given the freedom of visualising any of the CSs independently in order to understand their relative orientation. Furthermore, the CSs can be visualised for all recorded frames. Refer to Figure 76 for images of the Anatomical CS visualisation module showing two possible combinations that can be visualised. The visualisation module, `showAxes.m`, concludes the workflow for the definition of the tibial CS and all the femoral CSs.
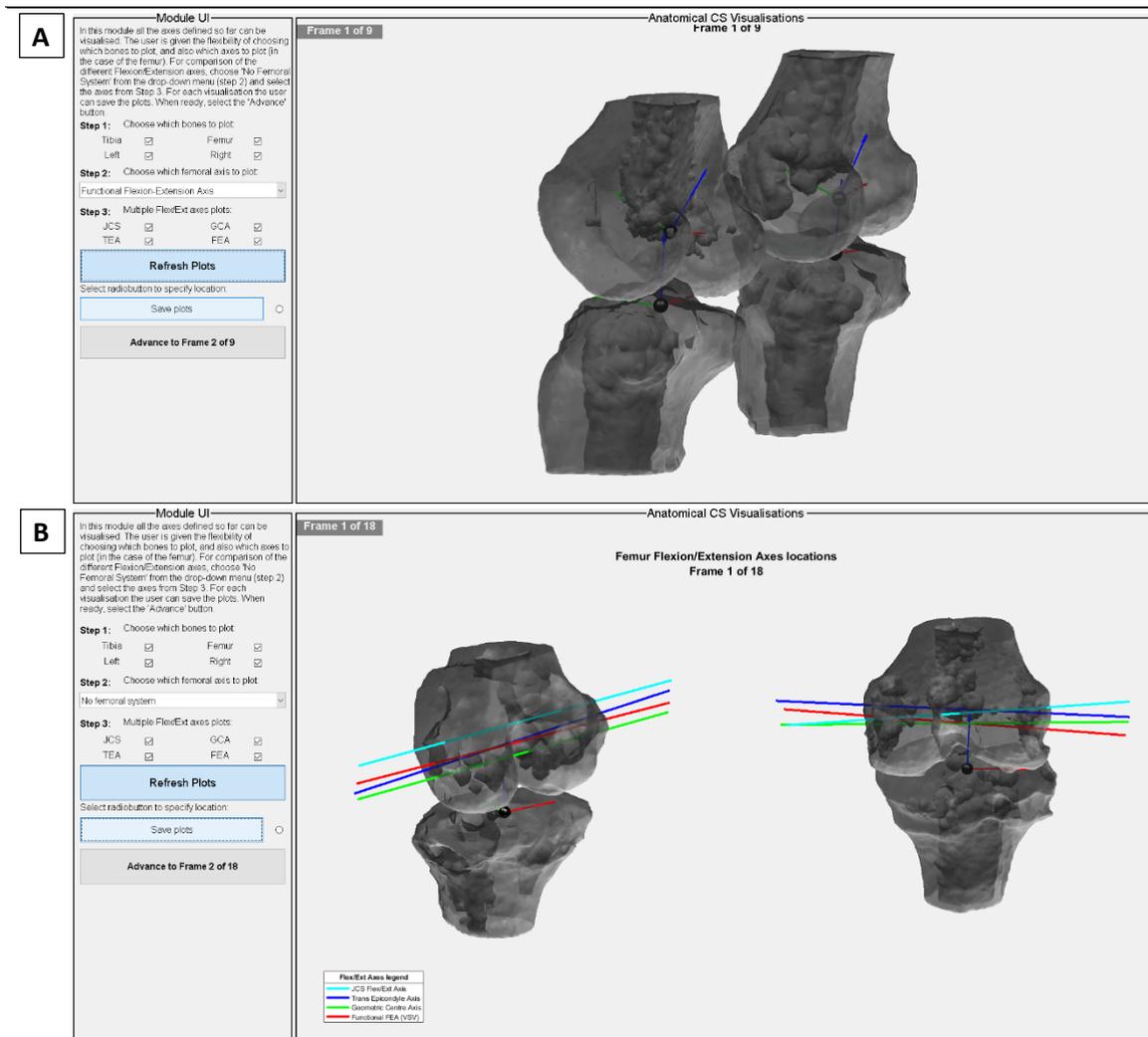
Figure 76: Anatomical CS module UI

The user can visualise any chosen femoral CS (visualising FFA in **A**) or any of the four FEAs (visualising all FEAs in **B**), the tibial CS and any one of the bone models, in any combination for each recorded frame using the options provided in the module UI on the left.

The remaining text will discuss the developed approach for the extraction of the kinematic outcome measures, that is, the tibiofemoral contact points, the axial centre of rotation and the six DOF kinematics.

4.2.7 KINEMATIC OUTCOME MEASURES MODULES

Following the definition of all the local CSs, the software enters into its final phase of the developed workflow, which calculates the kinematic outcome measures. With reference to the introductory statement in section 4.2.6, the tibiofemoral contact point modules are executed between the modules defining the tibial and femoral CS. For the sake of coherence in the text, it is being presented along with the remaining kinematic outcome measures modules.

4.2.7.1   CONTACT POINT ANALYSIS

With reference to section 2.4.4, a tibial contact point is defined as the location where the subchondral bone of the femur and the tibia most closely approach each other. Mathematically this is interpreted as the shortest Euclidean distance that exists between the tibial and femoral bones. However, merely calculating the shortest Euclidean distance between the femur and the tibia will not usually result in the correct tibiofemoral CPs being identified.

The irregular and asymmetric morphology of the tibiofemoral complex along with artefacts from the segmentation process, make the identification process less intuitive and more prone to false-positive results when identifying CPs. With reference to Figure 77, examples of common false-positive CP areas within the knee joint are presented. Such situations arise when the participants' morphology displays a relatively shorter distance between the tibia's intercondylar tubercles and the medial aspect of the femoral condyles (highlighted with a red circle in Figure 77A) than between the cartilaginous contact areas of the femoral condyles and the tibial plateaus (shown with a green circle). This effect is usually amplified in symptomatic knees due to the asymmetric reduction
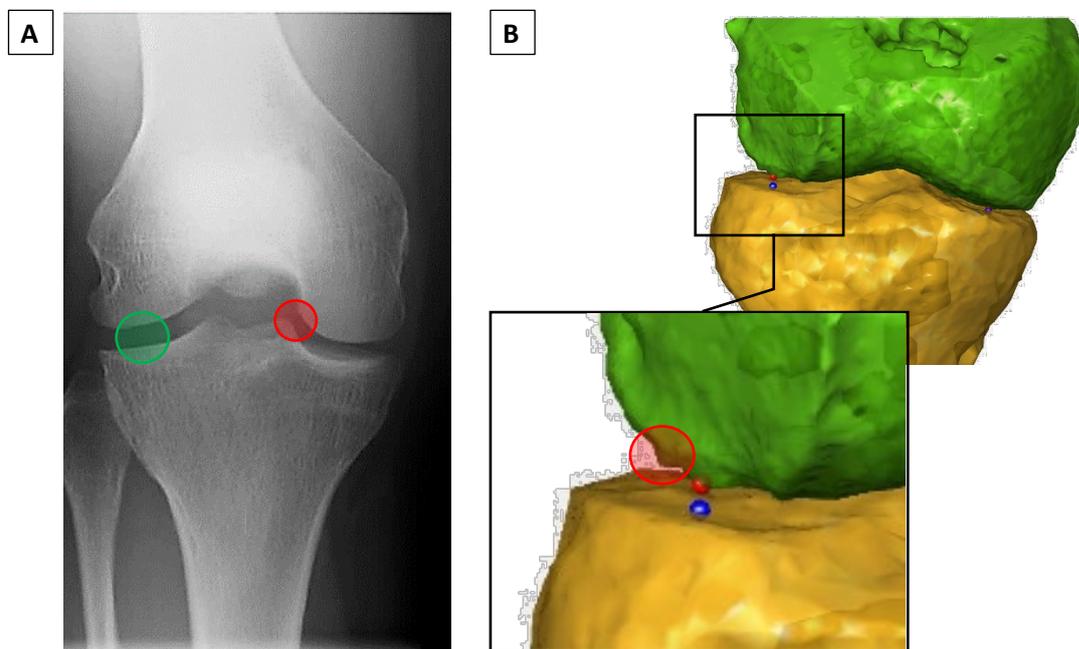
Figure 77: False-positive CP areas within the TF complex

A: An image highlighting an area which is commonly mistaken as the CP due to the proximity it displays between the femur and tibia. Refer to text for more detail. (Tsujii *et al.*, 2018)
B: The image shows the CPs identified for a particular frame for one of the participants during module testing. The femur (shown in green) and tibia (shown in yellow) made contact at the point marked by the red and blue spheres. The inset focuses on the uneven surface of the femoral condyle, which may create false-positive results when attempting to identify the TF CPs.

in the joint space, which distorts the positional relationship of the TF complex. Furthermore, as a result of segmentation artefacts, minor protrusions in the surface morphology of the femur or tibia create areas which can be mistakenly identified as contact points (refer to Figure 77B).

In the developed approach to identify the CPs occurring throughout the recorded ROM, several measures were taken to overcome the identification of false-positive CPs. The procedure taken to identify the tibiofemoral CPs while mitigating the incorrect identification of false-positive results is presented in `contactAnalysis.m`. The process is automated and processes each frame consecutively as follows:

Step 1: The femur and tibia models are divided into the medial and lateral components. This is performed in order to isolate the point cloud data so that the medial and lateral CPs can be identified individually.

Step 2: For each compartment (four in total; medial Left, lateral Left, medial Right and lateral Right), the corresponding tibial plateau plane defined in step 1 of the `tibROI.m` module, is imported. The Euclidean distances between all femur points and the corresponding tibial plateau plane are identified. The Euclidean distance is calculated by solving the dot product of the point being analysed and the normal of the plane.

Step 3: The measured distances are sorted in ascending order and subsequently stored.

Step 4: The points which are indexed to the smallest 100 distances are selected. These points are checked for any outliers by assessing if the X-, Y- and Z-values of each point lie more than 1.5 scaled Median Absolute Deviations[18] (MAD) away from the corresponding median coordinate values of the selected 100 points. Any identified outliers are removed, and subsequently, the remaining points are inputted back to the original list of femur points and corresponding Euclidean distances. This is the first of a series of checks which are performed in order to eliminate any outlier data points which might lead to the identification of a false-positive CP.

---

[18] The MAD is a robust statistic which measures statistical dispersion. It is more resilient to outliers in a data set than the standard deviation. When using standard deviations, large deviations are weighted more heavily, thus outliers can heavily influence its value. In MAD, the deviations of a small number of outliers are irrelevant.

Step 5: As a second step designed to eliminate outliers, the same process performed in step 4 is repeated, this time for the points which are indexed to the 200 smallest distances.

Step 6: The third and final step, which is intended to reduce the possibility of identifying false positives is first to identify the point which displays the shortest Euclidean distance (following the elimination of outliers in the previous two steps). Then the algorithm identifies and selects all the points whose Euclidean distance falls within 0.5mm of the shortest distance. The centroid of these points is calculated and labelled the femoral contact point.

Step 7: In order to identify the corresponding tibial contact point, an algorithm proposed by Möller and Trumbore (Moller and Trumbore, 1998) is implemented. This algorithm creates a line, or ray, which originates from the femoral contact point, defined in the previous step, and oriented along the normal of the tibia plateau plane. It then identifies the coordinates of the intersection point between this line and the tibial bone. This intersection point is defined as the tibial contact point.

Step 8: When all four compartments of the frame being analysed undergo the steps outlined above, the contact point data is saved, and the user is shown a visualisation of the identified contact points (refer to Figure 78A).

Step 9: The module terminates once it iterates through the above steps for all the recorded frames.

Subsequently, the `showCP.m` module is executed to present the user with a visualisation of the progression of the contact points on the tibial and femoral models (refer to Figure 78B and C). This concludes the algorithm for the identification and visualisation of the TF CPs.

4.2.7.2 AXIAL CENTRE OF ROTATION

In this module, the Tibial Axial Plots mentioned throughout section 2.4, will be compiled, along with the identification of the axial, or transverse, centre of rotation (COR). These diagrams, when combined with the CP profiles extracted in the previous module, provide a comprehensive understanding of the relative motion of the TF interface. The axial COR is a singular metric which aims to represent the relative motion occurring between the femoral condyles and the tibial plateau.
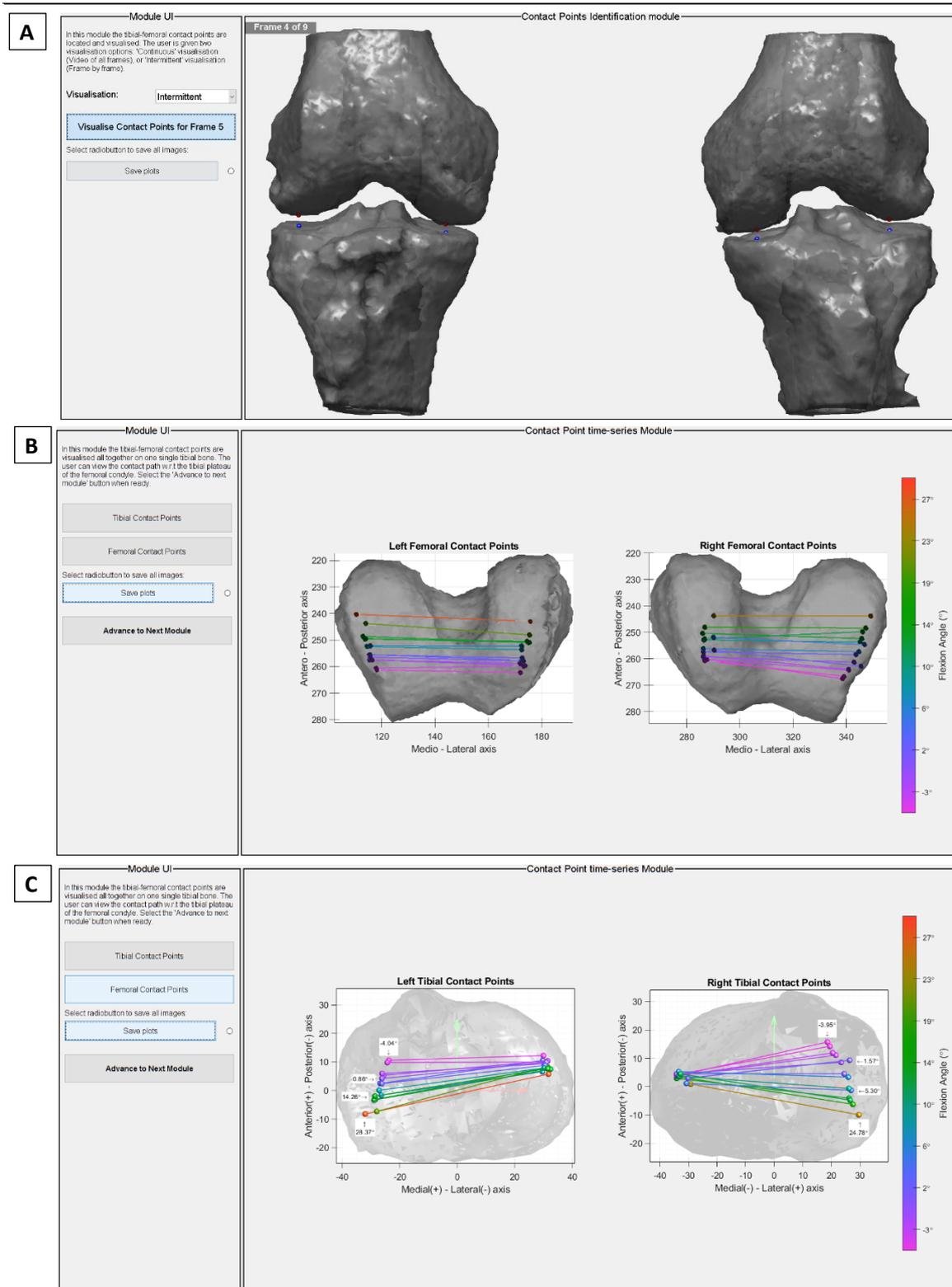
Figure 78: Contact Point Analysis Module UIs

A: Following the identification of the contact points for each frame, the user is presented with a visualisation of the CPs before the next frame is processed.
B & C: Following the identification of all CPs for all captured frames, the user is presented with a visualisation of how the CP locations change with progressing flexion. The femur CPs are presented in **B** and the tibia CPs in **C**.

The procedure for the identification of the COR is presented in `centRot.m`, and the subsequent visualisation of the tibial axial plots, including the CP profiles and the centre of rotation are presented in `showCoR.m`. The approach taken in both modules is as follows:

Step 1: The equations of the lines defining the FEA being analysed for the left and right femurs for all frames are imported. (Note: the `centRot.m` module loops four times, once for each FEA variant).

Step 2: Using the TMs obtained in `regTibia.m`, the line equations of the FEA are inversely transformed from the GCS to the tibial LCS, such that all line equations are now defined with respect to the corresponding tibial LCS.

Step 3: Each transformed FEA line equation is projected onto the tibial XY plane. At this point, all the FEA line equations for all frames are defined with respect to the tibial CS, such that, if they were to be plotted on the tibial LCS, they show the movement of the ML axes with progressing flexion.

Step 4: The location of the axial COR is calculated by solving the least-squares system of the line equations obtained in step 3, as proposed by Banks and Hodge in their paper in 2004 (Banks and Hodge, 2004). The resulting coordinate data, which defines the axial COR, is saved.

Step 5: The module loops through all four FEA variants, identifying the axial COR for each case, and subsequently saving the data for later access in the visualisation module.

Subsequently, the `showCoR.m` module is called to visualise the progressive movement of each femoral FEA variant. With reference to Figure 79, this module visualises the tibia from the axial perspective, with the FEA axes for all frames being projected onto the tibial plateau plane. The CP profiles are underlaid with dashed lines connecting the CPs of corresponding frames. Finally, if the COR falls within the tibial plateau area, it is visualised using a black cross, along with its ML and AP coordinates which are defined with respect to the tibial origin. These Tibial Axial Plots allow for an additional perspective into the complex articulation of the TF complex, which could provide further insight into the underlying mechanisms of healthy and replaced knees.
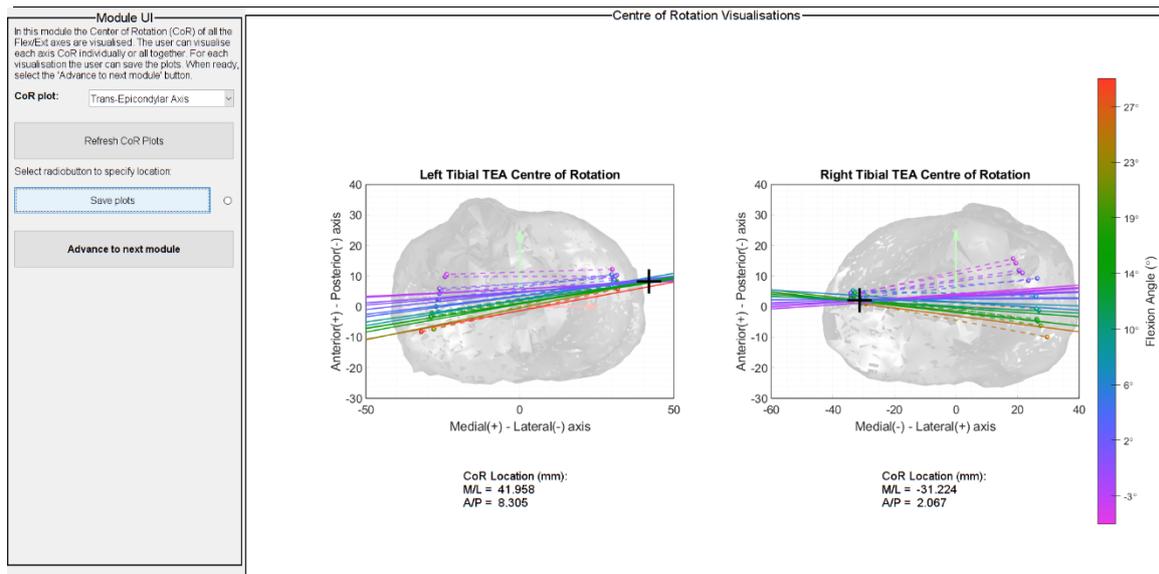
Figure 79: Centre of rotation module UI

Following the identification of the COR, the user is presented with a visualisation of the projected FEA axis (in this case the TEA) and its corresponding COR location (shown with the blaxk cross). The contact points identified for this participant are underlaid. This allows the user to visualise the relationship between the CP profile and the movement of the FEA, which allows for another perspective into the TF kinematics of the knee being investigated.

4.2.7.3 SIX DOF KINEMATIC DATA

The final step in the entire workflow of the Kinematic Analysis Suite developed and implemented in this thesis is the assembly and implementation of the JCS and the subsequent extraction of the six DOF of the knee over the captured ROM.

Up to this point, the only remaining axes to be defined before assembling the JCS is the floating axis. With reference to section 2.6.3.3, the floating axis is defined by performing the cross product of the two body-fixed axes, that is, the X-axis of the femur CS and the z-axis of the tibial CS. Subsequently, the equations outlined in section 2.6.3.3 can be implemented to extract the three rotational DOF and the three translational DOF. These remaining calculations are presented in `kinematics.m` and are processed as follows for each consecutive frame:

Step 1: The tibial and femoral CS data is imported. This includes the three tibial unit vectors and the tibial origin, and the four FEA variant unit vectors, the corresponding Y- and Z- unit vectors and the four corresponding origins.

Step 2: The floating axis is then defined for all four FEA variants. This is achieved by performing the cross product between each variant of the femur body-fixed axis, $\widehat{e_1}$, and the tibial body-fixed axis, $\widehat{e_3}$, using equation 21.

Step 3: The translational vector $\hat{\boldsymbol{H}}$, is calculated for each FEA variant by identifying the vector connecting the corresponding femoral origin to the tibial origin.

Step 4: The rotational angles are then calculated by implementing:

      a. Equation 32 for identifying the flexion-extension angles,

      b. Equations 36, 39 (for left knees) and 40 (for right knees) for identifying the abduction-adduction angles, and,

      c. Equation 48 (for left knees) and 49 (for right knees) for identifying the internal-external rotation angles.

Step 5: The translations are then calculated by using the corresponding vector $\hat{\boldsymbol{H}}$, defined in step 3, and solving the matrix defined in equation 52.

Step 6: Lastly, all the resulting rotations and translations are saved.

Step 7: The module then loops through steps 1 to 6 for all recorded frames until all the rotations and translations for all frames are calculated.

Following the calculation of the six DOF kinematics, the `showKinematics.m` module is called. Through the execution of this module, the user is presented with a series of options to visualise the kinematic plots in various ways. With reference to the module UI section in Figure 80, the user is allowed to choose from the following options:

- Plotting the calculated kinematics either against the frame number or against the flexion angle.

- Plotting the raw kinematic data or smoothing it through a binomial-weighted average filter.

- Choose to either plot results for one single FEA variant or all FEA variants together on one plot.

- Display either any one of the six DOF results or else display all six plots next to each other (for comparison). If the user selects the option to display a single plot, then the user is required to select the DOF of choice to be visualised.

Figure 80: Kinematic plots module UI

A: All the six DOF are plotted for all four FEA variants against the flexion angle.
B: All the six DOF are plotted for one of the FEA variants, specifically the GCA, against the frame number.
C: One DOF, specifically the Ab/Adduction angles, is plotted for all four FEA variants against the flexion angle. Specific data points are labelled to support further analysis of the data.

When the user finishes visualising the data, the module can be terminated through the UI. Before the Kinematic Analysis Suite is terminated, the principal data, collected throughout the execution of the software, is extracted to an MS Excel database so that it can be analysed further, should it be required. This process of extracting the data to MS Excel is presented in `exportData.m`.

Once the data is exported, the module terminates, and the software closes. At this point, the user is guided to save the data structure array, which contains the entire data that was generated throughout the processing of the participant data. This can be done by inputting the following code into the MATLAB command window: `save('name','-v7.3')`. A description of the data which is saved within the fields of the structure array can be found within the PDF document which is supplied with the entire code base that was developed for this software, under the name "Data Structure Array fields description".

This concludes the description of the bespoke Kinematic Analysis Suite, which was developed for the analysis of 4D CT data of healthy and replaced knees.

In this chapter, the reader has been presented with a detailed outline of the workflow, which was designed and developed to quantify the dynamic knee joint motion of healthy and replaced knees. Following the completion of the software, and the scanning of all the ten participants, their DICOM data was processed, individually, until the results were extracted. The processed data will be presented and discussed in chapter 5 via a case-by-case approach.

For documentation purposes, the developed code was built on MATLAB R2016 to R2018, and the data presented in this thesis was extracted using MATLAB R2019. The code as supplementarily presented with this thesis, is stable and runs without errors from start to finish. The latest version of MATLAB which was tested on this software was R2020.

5   RESULTS

Having all the 4D CT data collected and subsequently post-processed using the developed software as described in Chapter 4 of this thesis, the extracted results will be presented in this chapter. The 4D-CT data collected for each of the 10 participants (four control and six patient participants) will be presented via a case-by-case approach. For each participant, the following kinematic outcome measures will be presented:

- Functional FEA

- Six DOF kinematics (three rotations and three translations)

- Tibiofemoral contact points

- Transverse centre-of-rotation (COR)

A biomechanical interpretation of the collected results in light of the objectives of this thesis will be discussed in this chapter. This discussion will shed light on how the collected data for each case compares to the reviewed theory and literature presented in Chapter 2 of this thesis. A holistic discussion will follow this in chapter 6, which will review all the collected data and discuss it from a broader perspective while addressing the aims and objectives outlined in Chapter 3 of this thesis. The raw kinematic data collected during the post-processing for each case, which was used to compile the figures presented in this chapter, will be made available in Annex H:.

The results for the control and patient participants will be tackled differently in order to address their respective objectives. Control participant data, which is comprised entirely of healthy knees, will be used to address two of the three aims defined in Chapter 3 of this thesis, as follows:

- Assess if the kinematic outcome measures extracted via the kinematic analysis software agree with the reviewed theory and literature in Chapter 2. This extracted kinematic data will indicate the capability of the developed software in processing knee kinematics using the collected 4D CT data.

- Investigate if the TEA is a good surrogate to the Extension Condylar Axis during the Extension Phase of the flexion cycle. Secondary to this, the healthy knee data will also be used to assess how the kinematics for the four FE axes vary as a function of the flexion angle of each control participant.

The patient participant data, which is comprised of two types of replaced knees (UC FB and UC MB knees) and arthritic knees, will be used to address the third objective of this thesis, as follows:

- The kinematic outcome measures collected will be used to identify any differences which exist between fixed and mobile-bearing knees with respect to their mobility (that is, the capability of allowing axial rotation with increasing flexion)

The kinematic analysis software designed for this study had the capability of calculating the four FEA variants, namely:

1. The JCS defined FE axis,

2. The TEA,

3. The GCA, and

4. The functional FE axis (FFA)

While all four FEA variants were located and extracted in the developed software, these will only be compared for control participants. The focus will be given to the TEA and GCA results, for the reasons explained within section 2.6.2.1. The FFA will only be considered if any of the two algorithms (cED or cVSV – refer to 4.2.6.2) for each individual case converges such that the FFA axis lies in the region of the TEA or GCA axis. The JCS axis, as defined in the paper by Grood and Suntay (1983), is being regarded as mal-defined due to the subjective ROI locations which raise concerns of repeatability, leading to considerable crosstalk as explained in section 2.6.3.3. For patient participants, the focus will only be given to the GCA axis while disregarding the TEA, since the patient knee models were all affected by metal streak artefacts which resulted in the segmented bone models having missing bone in the epicondylar area, thus not allowing for confidently locating the epicondyles. The FFA results for patient participants will still be evaluated if any of the two algorithms converge.

The six DOF kinematics and the axial COR will be compared for all participants (focusing on the FE axes which apply to either control or patient participants). For control participants, the six DOF kinematics and axial COR will be analysed to highlight any differences which occurred as a result of assuming rotation around the different FE axis. From all the six DOF, emphasis will be given to the three principal DOF, namely Flexion-Extension and Internal-External rotations and the AP

translations, since as described earlier, these three DOF display the most significant variations with progressive flexion. The other three DOF will be discussed where their relevance is deemed necessary to support an argument.

It should be noted that while extensive effort has been invested in defining each of the FE axes correctly, limitations still existed. As described in section 4.2 and above, these limitations occurred mostly as a result of distorted volumes due to the metal artefacts which occur when scanning replaced knees, which ultimately limited the identification of specific bony landmarks required to define certain axis. Another limitation which can be noted in the results section was the limited ROM which was captured for some of the participants. This was due to the fact that, while the participant being scanned was continuously performing the cyclic flexion exercise described in section 4.1.5.2, the radiologists, who were recording the scans, had to time the starting point, when the scanner starts to capture the data, to match with either end of the cyclic movement. Furthermore, this study was the first time that the radiologists ever used the 4D CT function of the scanner, which led to a learning-curve effect in identifying the right point-in-time when they should initiate the scans. Due to the ROM which was captured for specific participants, the FFA algorithm defined in section 4.2.6.2 did not always converge as expected, which resulted in a skewed and mal-positioned FFA due to insufficient data points. These specific cases will be identified and discussed in the following sections.

In conclusion, control participant data will be evaluated by primarily analysing the results for the FFA in order to determine if the identified axis should be considered in the subsequent results which were calculated based on this specific axis. Subsequently, the six DOF kinematics will be presented and discussed. The kinematics are followed by the Contact Point analysis results and finally, the axial COR results are presented. On the other hand, patient participant data will be analysed by primarily examining the FFA results, and subsequently analysing the six DOF kinematics, contact point analysis and axial COR data, primarily for the GCA (and FFA if converged).

5.1   CONTROL PARTICIPANT #1

Control Participant #1 performed the cyclic flexion-extension exercise while in the supine position. His movement was recorded from circa 30º of flexion going to full-extension and subsequently flexing until circa 20º of flexion (refer to Figure 81). The captured movement for C001 is illustrative of the issues faced by the radiologists in properly timing the scan with the patients' movement. The following participant data was collected for Control Participant #1:

- Reference: C001

- Age: 58 years

- Gender: Male

- Left and Right Knee: Both healthy, with no knee-related symptoms reported throughout the participants life.
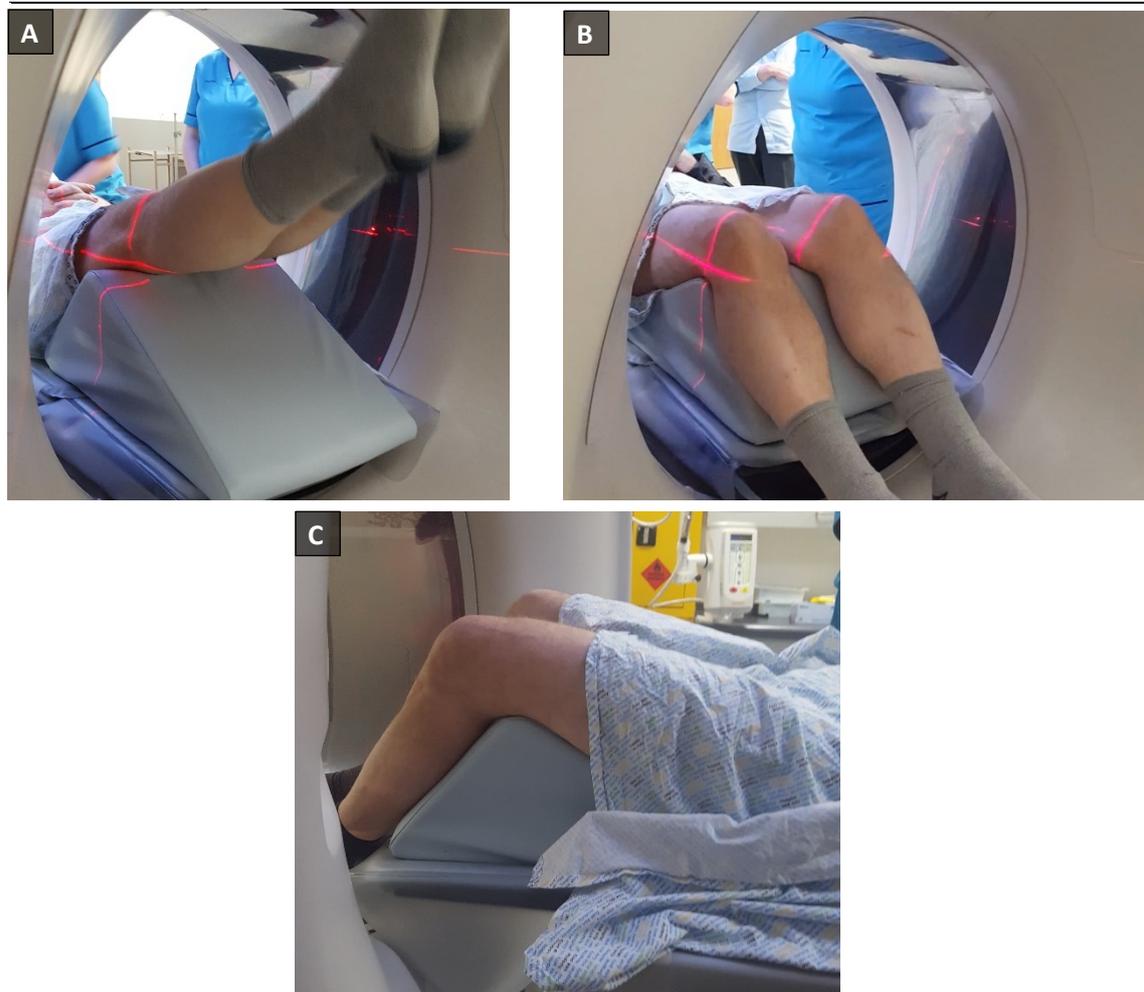
Figure 81: Photographs of participant C001 during pre-scanning setup

A: C001 at full-extension.
B: C001 at the maximum flexion which could be achieved given the limitations of the equipment.
C: C001 at maximum flexion (Sagittal view).
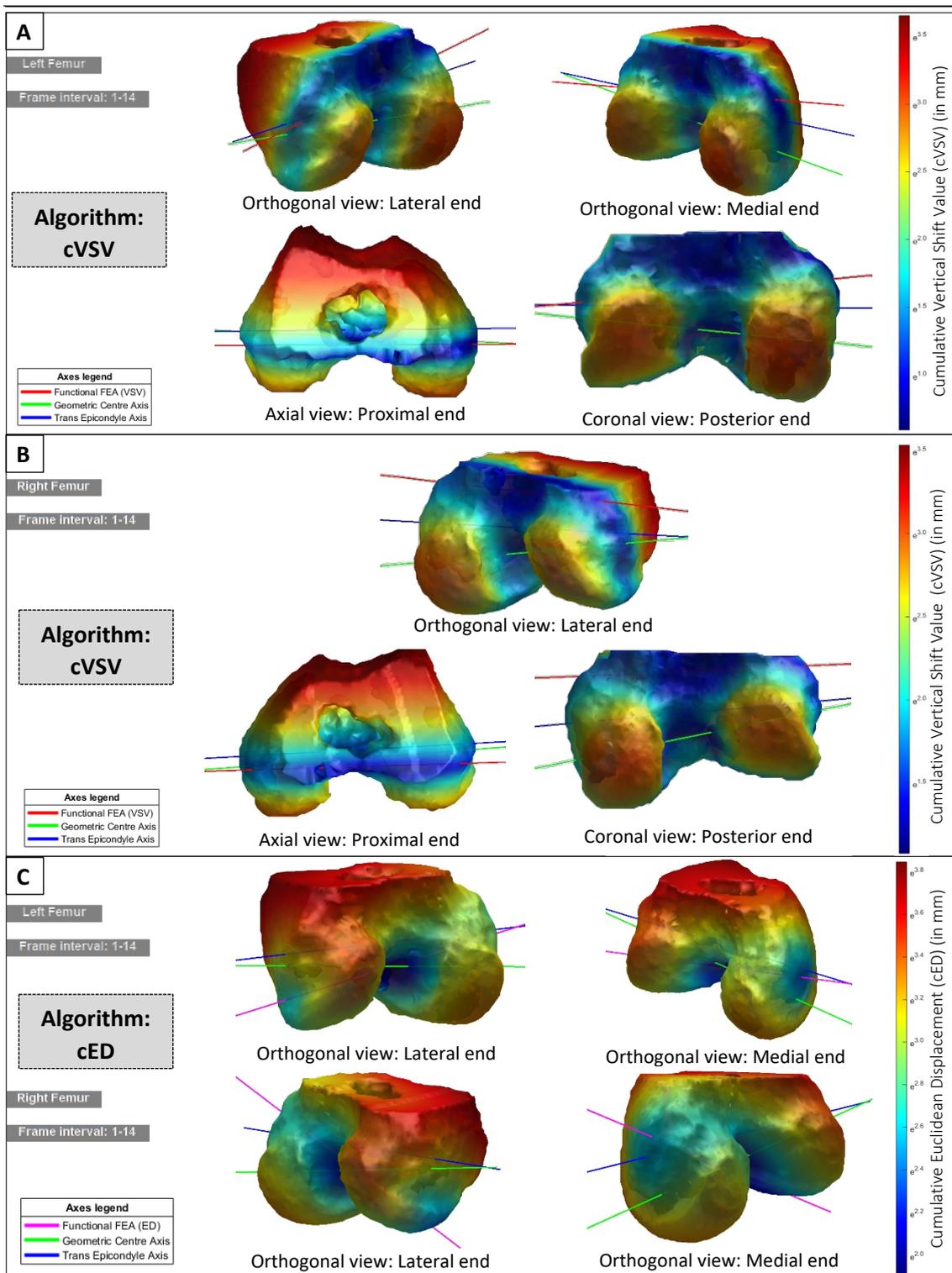
Figure 82: The Functional FE axis (FFA)– Participant C001

A: FFA results based on the cVSV algorithm. The inlays show the relationship between the FFA (cVSV axis in red), the TEA (blue) and GCA (green) for the left knee.

B: FFA results based on the cVSV algorithm. The inlays show the relationship between the FFA (cVSV axis in red), the TEA (blue) and GCA (green) for the right knee.

C: FFA results based on the cED algorithm. The relationship between the FFA (cED axis in magenta), the TEA (blue) and GCA (green) for the left (top) and right (bottom) knee.
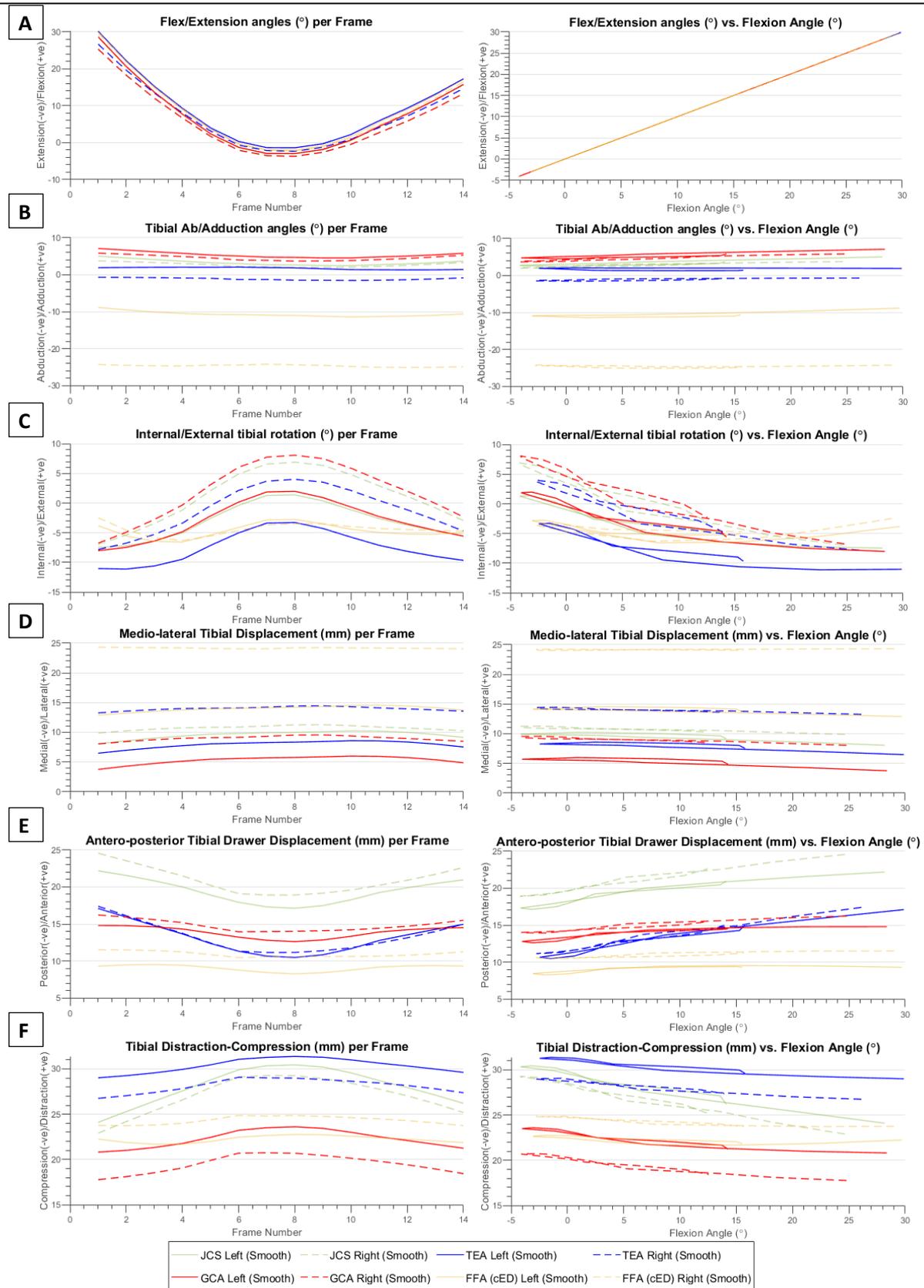
Figure 83: Kinematics for all FE axes for all 6 DOF of the knee – Participant C001

The kinematics based on the four FE axes variants, for the movement performed by control participant C001. The rotational DOF (A-C) are presented per Frame (Left) and against the Flexion Angle (Right). The translational DOF (D-F) are presented per Frame (Left) and against Flexion Angle (Right).
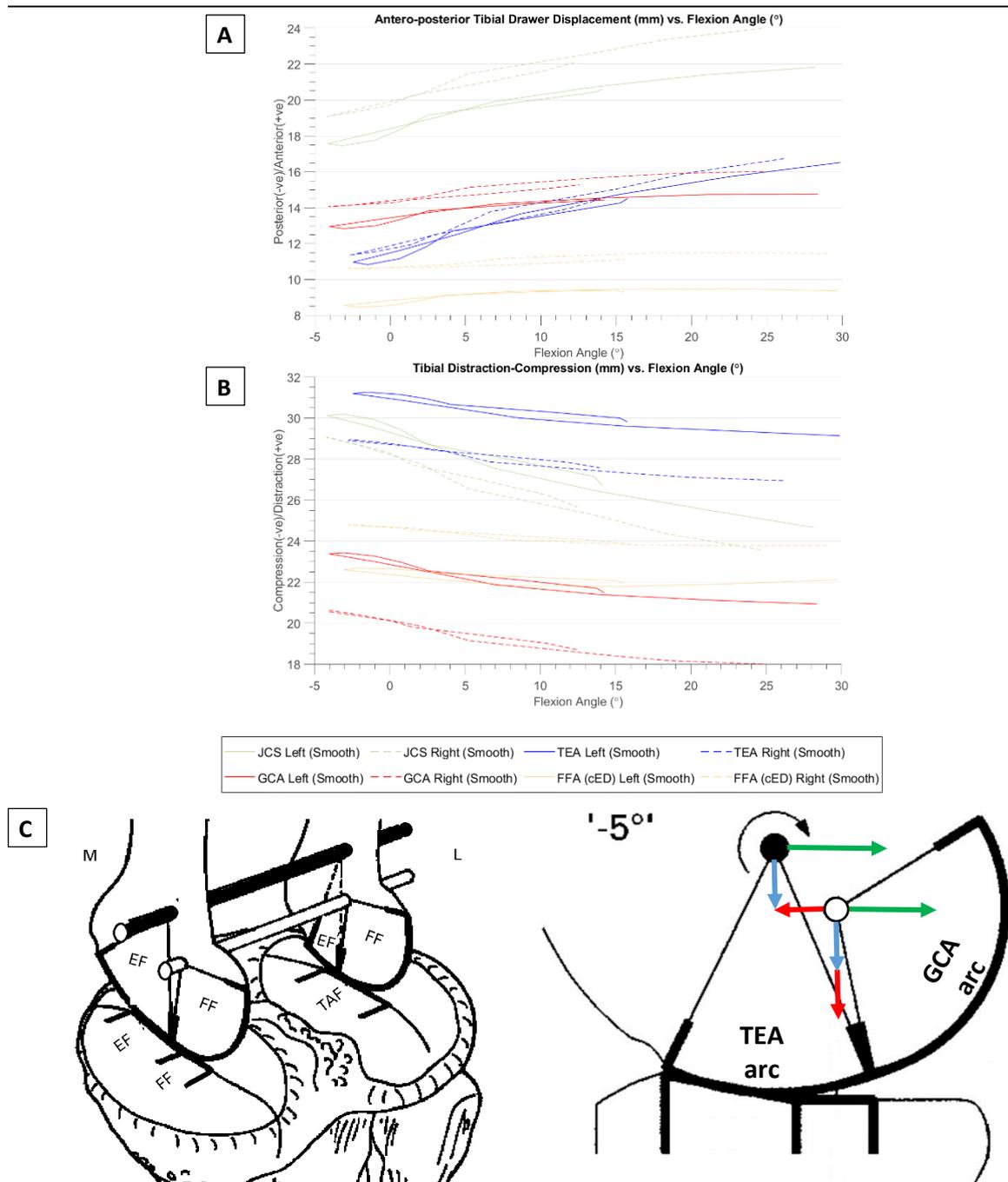
Figure 84: AP and PD translations for C001.

A: AP translations for all four FEA variants
B: PD translations for all four FEA variants
C: An illustration to explain the kinematic crosstalk occurring at the GCA and TEA. The left image is showing the theoretical location of the Extension Condylar Axis (Black axis) and the Flexion Condylar axis (White Axis) (Iwaki, Pinskerova and Freeman, 2000). The Right image (author's rendition) is a sagittal 2D view of the image on the left, identifying the GCA and TEA axis and the translations which these axis should be experiencing as the knee starts flexing from hyper-extension. The green arrows show the AP translation recorded by the TEA based kinematics, which represents actual motion of the rigid body (femur) in space, thus acting as well on the GCA. Similarly the blue arrows show the PD translation recorded by the TEA based kinematics, thus also acting on the GCA. The red arrows identify the translations which the GCA is experiencing as a result of kinematic crosstalk.
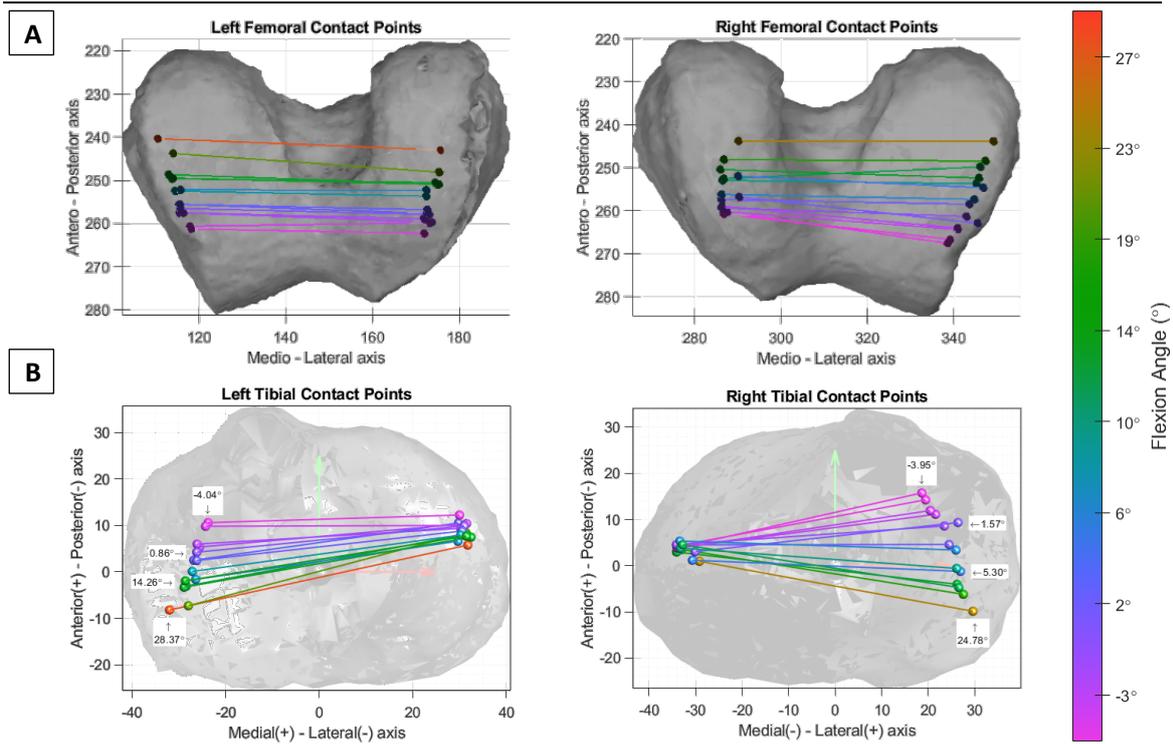
Figure 85: Tibiofemoral contact points - Participant C001

A: Femoral contact points calculated for the movement performed by control participant C001.
B: Tibial contact points calculated for the movement performed by control participant C001.
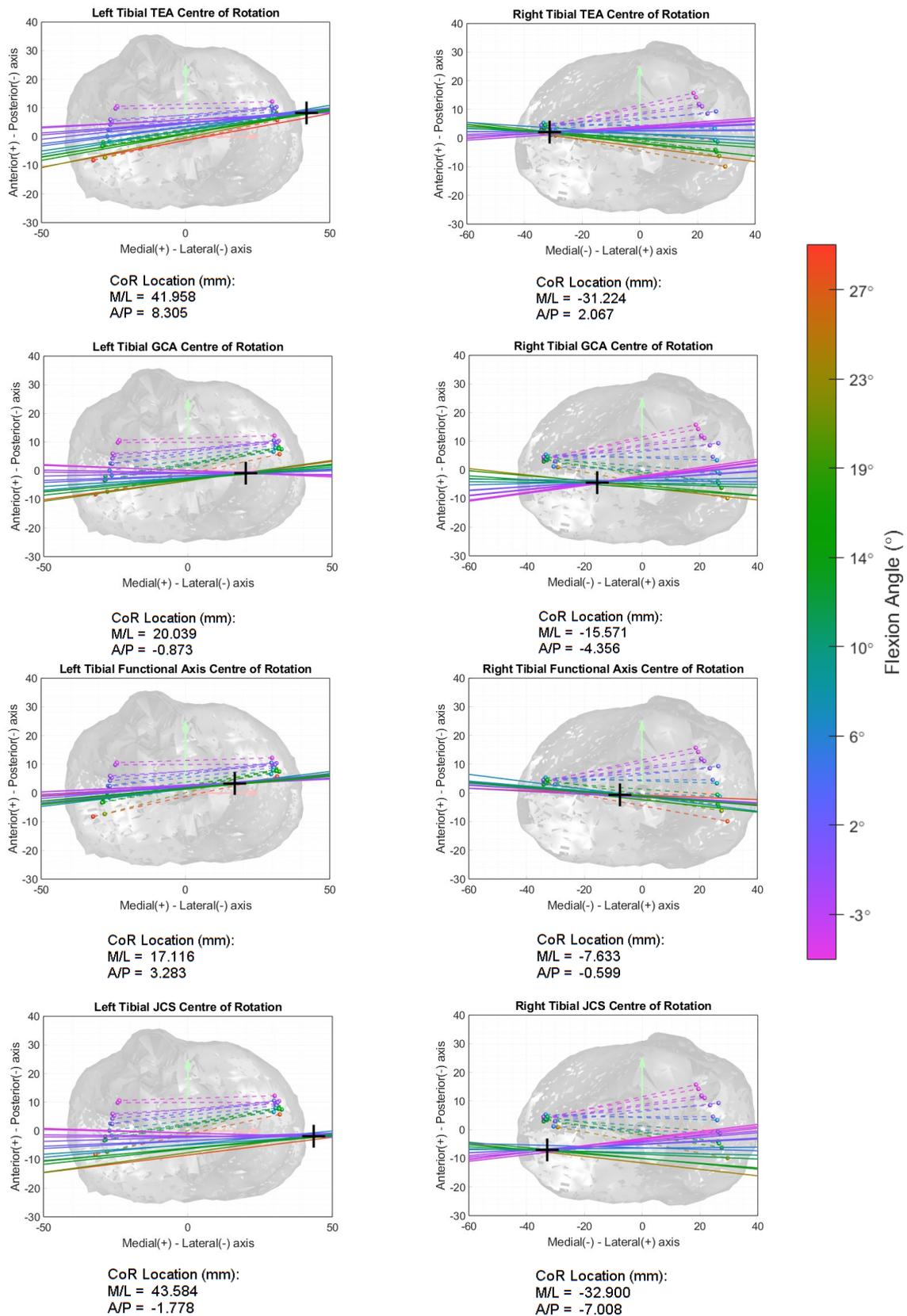
Figure 86: Axial Centre-of-Rotation of the four FE axis variants – Participant C001

The COR plots for the TEA, GCA, FFA and the JCS are plotted for the movement performed by control participant C001. The location of each COR location is plotted and also reported in terms of mediolateral and anteroposterior distance from the tibial origin below each plot.

Functional FEA (FFA)

With reference to Figure 82, it can be noted that both algorithms for the FFA (Figure 82A and B - cVSV algorithm; C - cED algorithm) did not converge for C001, for both the left (Figure 82A and C) and right knee (Figure 82B and C). Regarding the cVSV-based FFA, the left knee better converged towards the GCA and TEA in comparison to the contralateral knee. This is assumed to be related to the slightly larger ROM, which was captured for the left knee (Figure 83A - a total of 3.5º more). This brings to light the dependency of this algorithm on the inputted ROM, where the larger the ROM captured, the better it will approximate the FFA.

With reference to the cVSV results of the left knee, it can be noted that the lateral end of the FFA converged closer to the other surrogate axes than the medial end. This is occurring, since the lateral condyle of the knee has a quasi-single radius (refer to section 2.4.3) which in this case would assist the algorithm with converging towards the real anatomical FE axis. With reference to the orthogonal views, the concept of a single lateral radius can be appreciated since all surrogate axes converge to the same area laterally, while medially the axes are more dispersed. Irrespective of the location of the FFA on the lateral end, the location of the FFA on the medial left knee and both ends on the right knee are incorrect as they represent no correlation with any anatomical structures which drive, or guide, the motion at the knee. Therefore, given the results obtained for the cVSV-based FFA, these axes will be disregarded for C001.

Similarly, the results for the cED-based FFA (Figure 82C) for both left and right knee did not converge. The results obtained for the cED-based FFA highlight a notable difference between the cED and cVSV algorithms. From theory, we are aware that during the captured ROM of C001, which lies within the range of -5º and 25º of flexion, the femur is predominantly rotating around the medial condyle during the screw-home mechanism. This results in the medial femoral condyle gliding on the tibia (theoretically achieving pure rotation around the EFC) while the lateral condyle rolls on the surface of the tibia (simultaneous rotation and translation). This medial gliding is captured in the cED results by the smaller cED values, which can be noted on the medial end in comparison to the lateral end (predominantly in the left femur). Furthermore, the rolling of the lateral condyle can be appreciated in the cED results for both bilateral femurs, since the points showing the least cED values are at the contact areas of the lateral TF interface. This is captured in the cED values since the ML, and AP movement of the femur are a function of the cED values (in contrast to the cVSV). Nevertheless, the results for the cED-based FFA axes can be considered to be incorrect as well. As a result of the above, all FFA results presented hereon for C001 will only be for reference and can be overlooked since the FFA axes did not converge.

Six DOF Kinematics

The six DOF kinematics for C001 are presented in Figure 83. The kinematics of all four FEA variants were extracted using the post-processing outlined in section 4.2.7.3. In Figure 83 focus is given to the plots of the TEA (blue) and the GCA (red), while the plots for the JCS (green), and the FFA (orange) are presented in a faded manner since these are not deemed applicable to this participant. The left columns of the graphs in Figure 83 show the six DOF kinematics plotted against the frame of capture, while the right columns show the same six DOF kinematics plotted against the flexion angle. All the data for all participants has been smoothed by passing it through a binomial weighted average filter (Marchand and Marmet, 1983) with a window size of seven. The benefit of using a binomial weighted average filter is that it allows the final average number to reflect the relative importance of each number that is being averaged, taking into account the relative importance of each number in the sample. This maintains the data's integrity while making the data more understandable when viewing it all at once.

For participant C001, the first frame was captured as he was extending his knees at 29.88º of flexion for the left knee and 26.11º of flexion for the right knee (the reported angles for C001 are based on the TEA kinematics). C001 continued to extend his knee to full extension reaching 2.46º hyper-extension for the left knee and 2.76º hyper-extension for the right knee. The participant subsequently flexed his knee until the last frame was captured at 15.77º of flexion for the left knee and 13.93º of flexion for the right knee (refer to Figure 83A). While the ROM that was captured was not ideal, this data will be a great opportunity to identify any trends in how the healthy knee articulates while the screw-home and subsequently, the screw-away mechanism are in action.

With reference to Figure 83B, the TEA-based kinematics reported that the tibia for both left and right knees showed minor changes in the adduction with progressive flexion. Both knees maintained constant adduction angles as they extended, which had a range of 0.1º for the left knee and 0.7º for the right knee. As the participant changed into flexion, the adduction angles again varied slightly with a range of 0.5º for both knees. With reference to Figure 83B, the GCA-based kinematics reported that both tibias experienced relatively larger changes in their adduction angles (range of 2º) over the TEA values. Based on the captured ROM for C001, theoretically, during this phase of flexion, the knee should be rotating around the Extension Condylar Axis, which we are assuming to be approximated by the TEA. Therefore this increase in adduction is being

correlated to kinematic crosstalk. This is justified due to the fact that the GCA is skewed with respect to the TEA (by 6.7˚±4.3˚, Eckhoff *et al.*, 2003). Apart from this, it is also located posterodistal to it. These discrepancies are assumed to be responsible for the increase in adduction with progressive flexion for the GCA values. Contrariwise, the quasi-constant adduction angles reported by the TEA support the argument that this axis lies close to the Extension Condylar Axis, therefore for the captured ROM this axis is expected to show minimal kinematic crosstalk, which is the case so far.

Moving on to the internal/external tibial rotation results (Figure 83C), the screw-home (and subsequently, the screw-away) mechanism can be observed for both knees. As the knee was extending into hyper-extension and subsequently flexing away from hyper-extension the tibia externally and internally rotated, respectively, as expected. While it is hard to determine the point at which this mechanism is initiated, from the plots against the flexion angles, it can be assumed that this occurs around the 7º flexion mark, at which point the gradient slightly reduces for both knees with progressive flexion. This agrees with theoretical values reported earlier in this text, that state that the screw-home mechanism initiates anywhere between 0º and 10º of flexion.

The translational degrees-of-freedom for the TEA are presented in Figure 83 (D-F). The ML translation calculated for C001 shows minimal translation with a range of 1.5 mm (6.7 mm to 8.2 mm) for the left knee and a range of 1 mm (14.3 mm to 13.3 mm) for the right knee. From the results for the ML displacement, it can be noted that the left tibia is better aligned to the left femur than the right tibia, which is roughly 7.5 mm laterally displaced in relation to the right femur. This might be as a result of the morphology within the participants' right knee, or else it might be due to slight errors in the definition of either the tibial CS or femoral CS.

The AP translation agrees with theory, whereas the tibia moves anteriorly with progressing flexion. Theoretically, it is known that during the Extension and Transition phases of flexion (i.e. from 0º to 30º of flexion), the knee rotates around the Extension Condylar Axis, which is assumed to be approximated by the TEA and then in subsequent phases of flexion the knee transfers its axis of rotation onto the Flexion Condylar Axis, which coincides with the GCA (refer to section 2.6.2.1). With this in mind, considering C001 is not exceeding 30º of flexion, then we should expect the AP and PD translations for the GCA based kinematics (Figure 83 – red lines) to be displaying out-of-plane movement (kinematic crosstalk) since the knee should be

rotating around the TEA during the captured ROM. The calculated ranges for the AP and PD translations of the GCA and TEA (refer to Figure 83E and Figure 83F or Figure 84A and Figure 84B - enlarged) are listed in Table 6 as follows:

Table 6: AP and PD translations for the TEA and GCA kinematics for C001

	TEA		GCA	
	Left	Right	Left	Right
AP range (mm)	5.55	5.38	1.8	1.95
PD range (mm)	2.05	1.95	2.45	2.55

It can be noted that the recorded TEA AP translations are relatively larger than the GCA AP translations, while the TEA PD translations are slightly smaller than the GCA. At first glance, since the TEA is experiencing larger AP translations than the GCA one might assume that this increase in movement is occurring due to kinematic crosstalk, but this is not the case. If this specific case is broken down, visualised and understood, one can appreciate that although the GCA is showing smaller translations, it is still the axis which is being affected by kinematic crosstalk. With reference to Figure 84C, at hyper-extension, the femur is rotating around the Extension Condylar Axis (black axis - approximated by the TEA) shown on the left image. If we take a sagittal-view of the knee at this instant (right image in Figure 84C), one can visualise how both the TEA and GCA axis are translating at this point in time.

During the Extension and Transition phases of flexion, we know from theory that the entire femur does not only rotate around the Extension Condylar Axis (assumed to be approximated by the TEA), but it also translates posteriorly (green arrows in Figure 84C) and slightly compresses (distal femoral translation – blue arrows in Figure 84C) due to the downward tibial slope. Since the rotation is not occurring around the GCA, then the GCA should experience further translations due to its location relative to the TEA. We know that the GCA is located posterodistal to the TEA, such that if flexion (clock-wise rotation) is occurring around the TEA, as should be the case for C001, then the GCA will experience anterior and distal translations (red arrows in Figure 84C) which are attributed solely to kinematic crosstalk. If all these aforementioned translations occurring at both axes are summated, one can appreciate that if rotation is occurring around the TEA, then the GCA should experience larger distal (compressive) translation and smaller proximal translation (here it is assumed that the anterior translation due to kinematic crosstalk is smaller than the posterior translation occurring in the entire femur), which is the case as one can note in the results reported in Table 6,

Figure 84A and Figure 84B. These results along with the results for the adduction angles reported earlier for this participant, support the argument presented in section 2.6.2.1 whereby it is being questioned whether the TEA can act as a surrogate to the Extension Condylar Axis for its effective range, after which the rotation of the femur moves onto the Flexion Condylar Axis (represented by the GCA).

Tibiofemoral Contact Points

The contact points obtained for C001 (Figure 85) followed the expected path for healthy knees. Comparing the contact profile obtained for C001 to the contact profiles found in the literature for healthy knees (refer to Figure 22A), both profiles approximate the theoretical profiles closely, emphasising the medial pivoting of the knee along with the posterior translation of the lateral condyle with increasing flexion. With reference to the flexion angles attributed to each plotted contact point in Figure 85B, it can be noted, that for both knees the majority of the rotation is occurring during the screw-home mechanism (up until circa 7º of flexion) while for the remaining 20º of flexion, the knee, relatively, rotates much less. With reference to Figure 85A, the femoral contact points are also visualised for a more comprehensive understanding of the contact points profile.

While the Tibiofemoral contact points offer a distinct perspective on the articulation occurring within the knee, when these results are combined with the axial COR results, the movement of the knee can be better appreciated, as will be discussed in the following section.

Axial COR

Theoretically, the axial COR of a healthy knee is expected to be located on the medial plateau, towards the medial tibial spine. With reference to the calculated axial COR results for all four variants of the FEA in Figure 86, it can be noted that while all the eight COR results are located on the medial side, some of them are located just outside the tibial plateau. This is being assumed to be the case since the least-squares algorithm used to calculate this metric did not have sufficient data points (due to the limited ROM for C001) therefore not converging onto the tibial plateau. With reference to the theory mentioned in section **Error! Reference source not found.**, when the results of the axial COR are combined with those of the tibiofemoral contact points, the clinician is given a different perspective for understanding the articulation occurring within the knee. With reference to the TEA results presented in Figure 86, it can be noted that the

projections of the TEA onto the tibial plateau closely match the profile of the contact points. When compared with the theoretical results of Pinskerova *et al.* (2004), the results obtained for C001 clearly reflect those of a healthy non-weight-bearing knee. The TEA results display a distinct similarity between the axial COR profiles and their corresponding contact points, while the GCA displays no similarity, as expected.

When comparing the location of the axial COR results and the contact points results for the TEA, it can be noted that both results converge towards the same location in the AP and ML dimensions. This further supports the argument that the femur is rotating around the TEA during this range of flexion. If we take the analogy of the axel (axis) with two attached wheels (femoral condyles), then it is logical that if the femur is rotating around the TEA, then the contact points will be located directly beneath it, as long as the wheel (condyle) is contacting a horizontal surface. This is the case until the knee starts moving into the late stages of extension, at which point the tibial plateau starts tilting upwards displaying an increase in gradient beneath the Anterior Meniscal Horn (refer to Figure 4). This was noted in the results for the TEA, as the contact points in the final stages of extension lie anterior to the projected TEA lines. With reference to the results of the GCA, it can be noted that there is only a slight correlation between the contact points and the projected GCA axes. Nonetheless, the results still have relevance with theory, since the projected GCA axes are posterior to the contact points, as expected due to its geometric relationship with the TEA. Also, this brings to light the misconceptions that can lead to incorrect interpretation of results, since, if the GCA axial COR results were to be plotted on their own (no contact point visualisations), then one would easily misinterpret the GCA results as the better case when compared to the TEA results since the GCA axial COR is located more medial than that of the TEA.

In conclusion, the results obtained for C001 have shown that the biomechanics of this participant followed the theoretical values and profiles which were expected for healthy knees for the captured ROM. Also, using the data for C001, it has been shown that during the Extension (-5º to 5º of flexion) and Transition Phase (5º to 30º of flexion) the knee rotates around the TEA, which we are assuming to approximate the Extension Condylar Axis. This statement is based on the fact that the AP and ML translational results and the adduction results for the GCA showed clear signs of kinematic crosstalk in comparison to the TEA, and similarly, the axial COR and contact point results also pointed towards the fact that the knee is rotating around an axis which can be approximated by the TEA.

5.2   CONTROL PARTICIPANT #2

Control Participant #2 performed the flexion-extension exercise in the same position as C001. The following information was collected for Control Participant #2:

- Reference: C002

- Age: 50 years

- Gender: Male

- Left and Right Knee: Both healthy, with no knee-related symptoms reported throughout the participants' life.

The movement that was captured for participant C002 initiated during the screw-away mechanism, from 0º of flexion for the left knee and 4º for the right knee (based on TEA kinematics). C001 proceeded to flex both his knees until he achieved maximum flexion at 63º for both the left and right knee. The participant then started extending his knees until 58º of flexion for both knees, at which point the scanner reached its maximum allowed number of frames and stopped recording data. Given the ROM recorded for this participant, the extracted kinematic data is expected to shed light on the way the knee transitions its FE axis of rotation from the Extension Condylar Axis (represented by the TEA) to the Flexion Condylar Axis (represented by the GCA). Given the range of motion achieved, the functional FE axis is expected to lie in between the TEA and GCA.

It is important to note that while all participants were instructed to perform the cyclic flexion-extension exercise with feet apart (open kinematic chain), while analysing the data collected for C001, it was noted that this participant's feet made contact. With reference to Figure 90A, it can be observed how, as C002 flexes his knees, his left tibia gradually adducts, reducing the gap between the ankles from s_a to s_b (refer to Figure 90C), until it makes contact with the right lower leg. Although this had no implications on the scanning procedure itself, this led to both legs experiencing the undesirable closed kinematic chain mechanism, which reduces the mobility on the 'links' (in our case the bones) that make up the 'chain' (refer to the definition of a kinematic chain given in section 2.4.3). From a visual analysis of the path followed by the ankle, it is assumed that the feet made contact in the vicinity of the 8th Frame, which translated to circa 20º of flexion (Figure 90C). The exact point of contact is being assumed as it cannot be precisely determined since the movement during the scan was not video-recorded. The consequences of this manoeuvre were noticeable in the kinematic results obtained for this participant, as will be highlighted below.
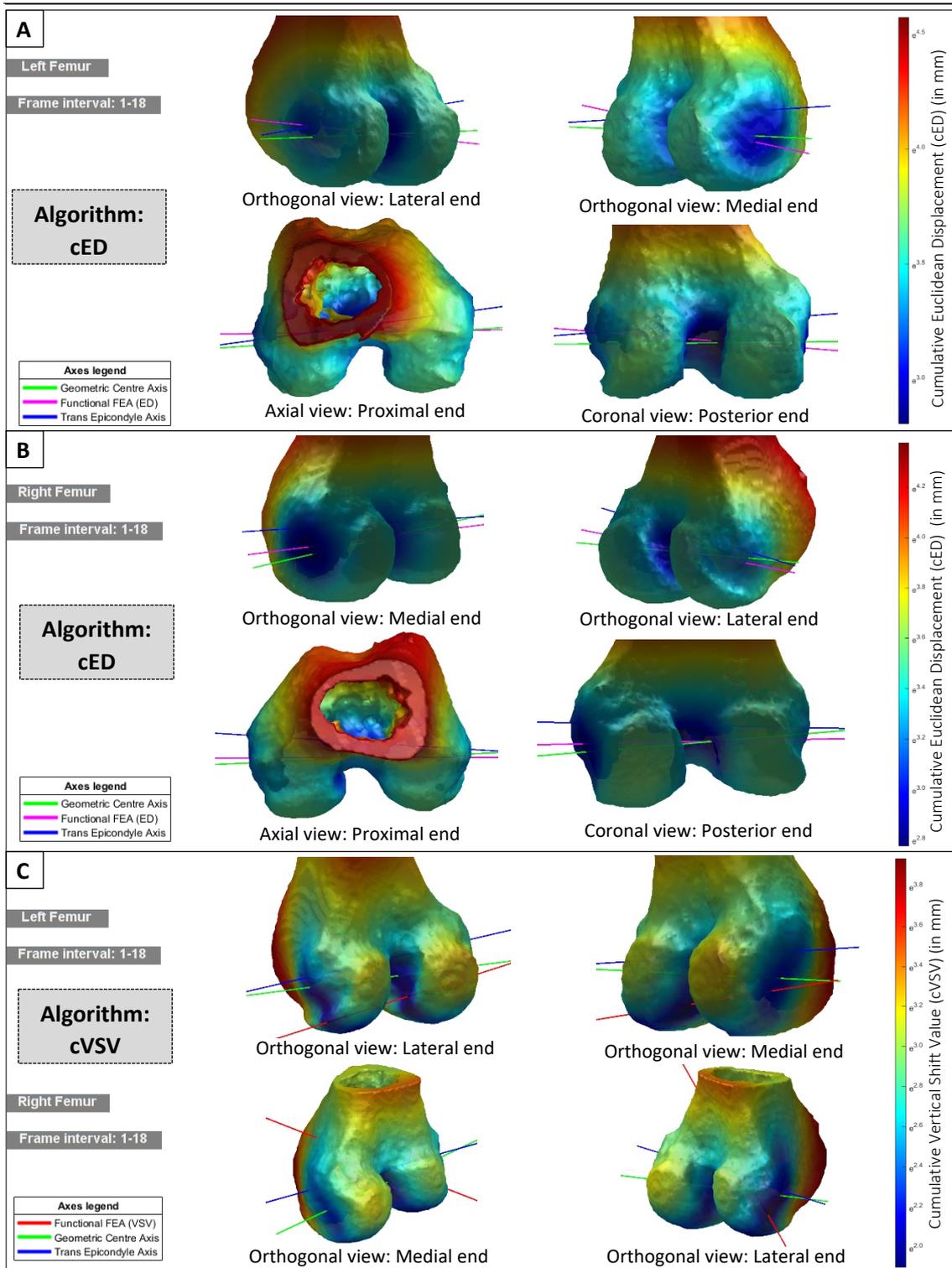
Figure 87: The Functional FE axis (FFA)– Participant C002

A: FFA results based on the cED algorithm. The inlays show the relationship between the FFA (cED axis in magenta), the TEA (blue) and GCA (green) for the left knee.
B: FFA results based on the cED algorithm. The inlays show the relationship between the FFA (cED axis in magenta), the TEA (blue) and GCA (green) for the right knee.
C: FFA results based on the cVSV algorithm. The relationship between the FFA (cVSV axis in red), the TEA (blue) and GCA (green) for the left (top) and right (bottom) knee.
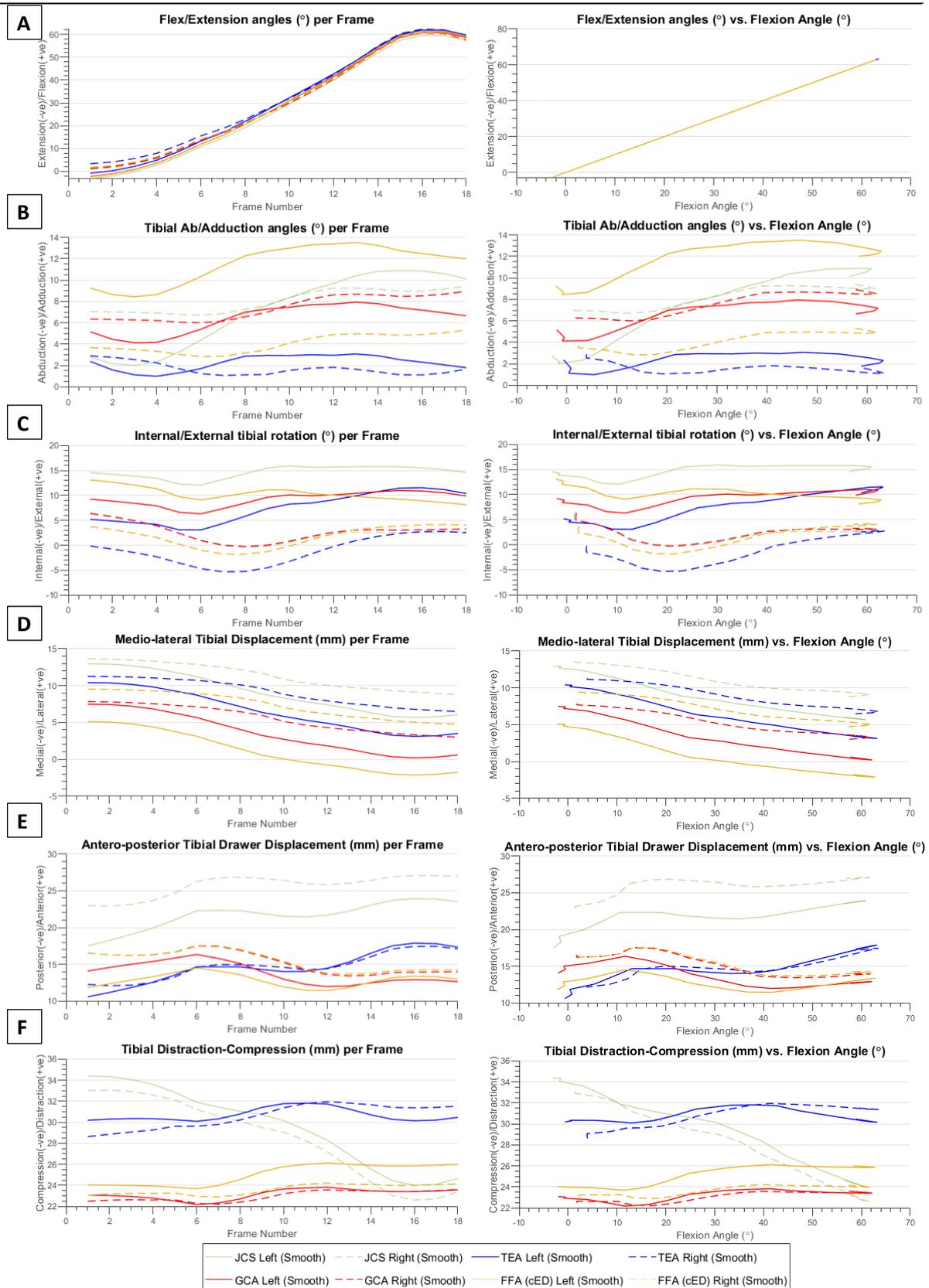
Figure 88: Kinematics for all FE axes for all 6 DOF of the knee – Participant C002

The kinematics based on the four FE axes variants, for the movement performed by control participant C002. The rotational DOF (A-C) are presented per Frame (Left) and against the Flexion Angle (Right). The translational DOF (D-F) are presented per Frame (Left) and against Flexion Angle (Right).
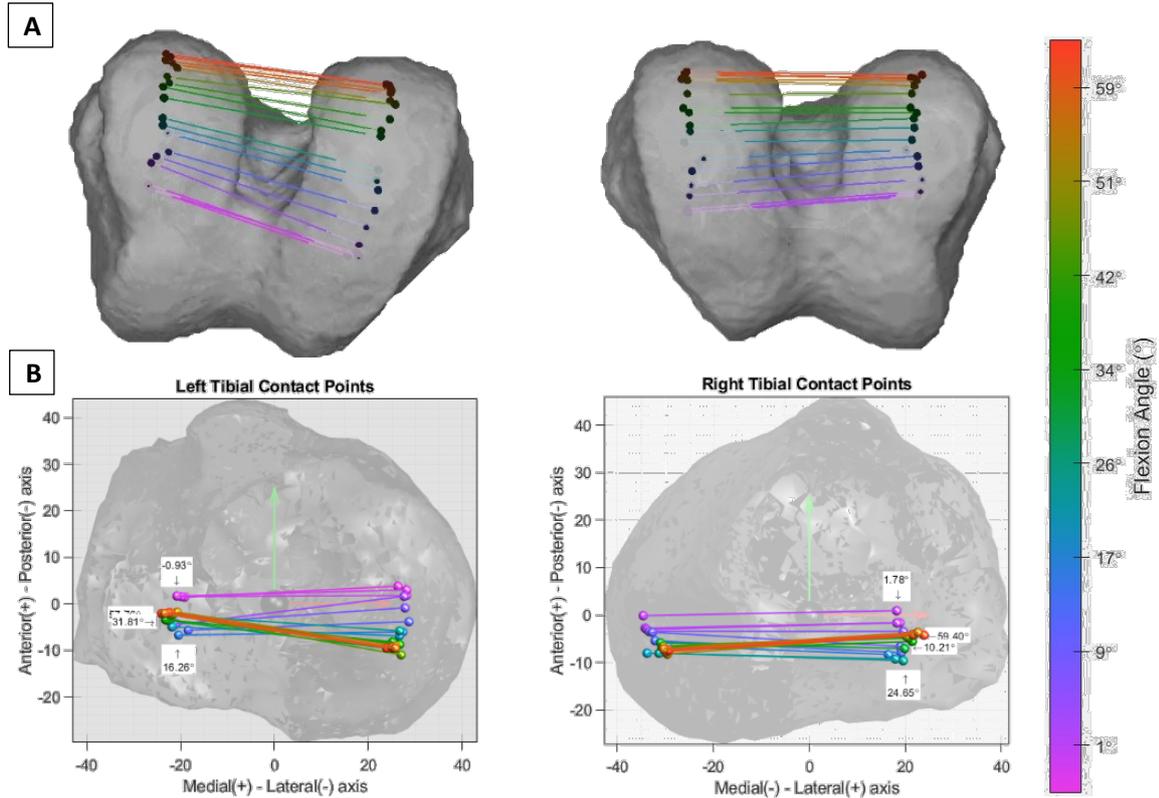
Figure 89: Tibiofemoral contact points - Participant C002

A: Femoral contact points calculated for the movement performed by control participant C002.
B: Tibial contact points calculated for the movement performed by control participant C002.
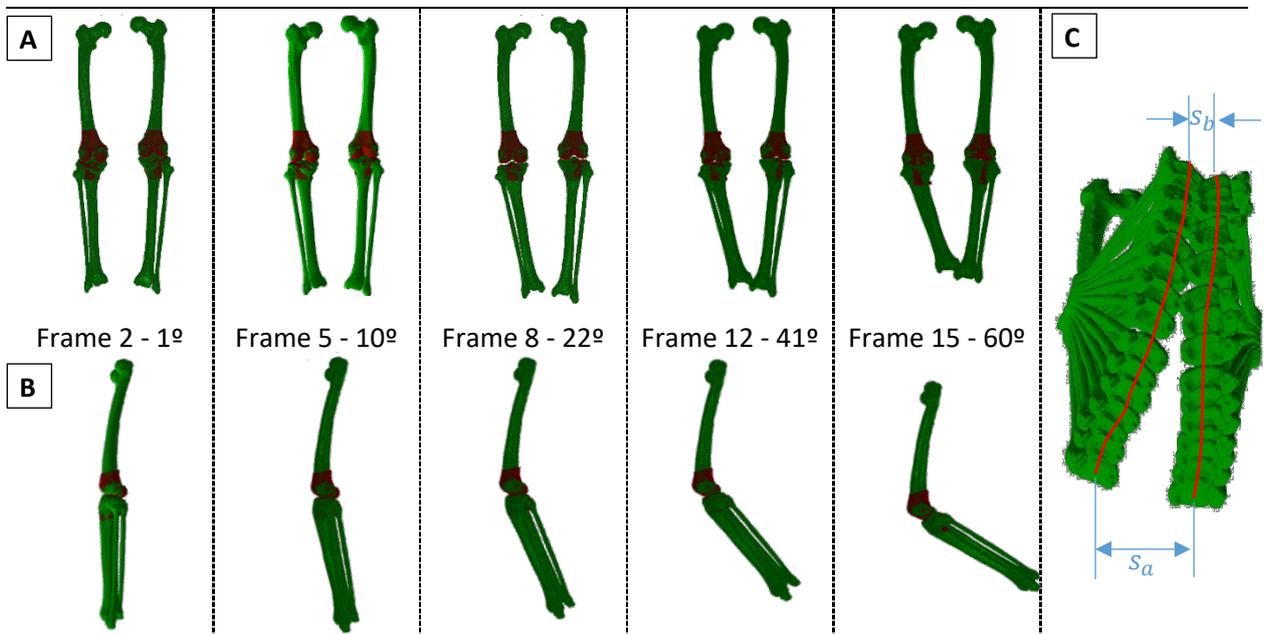
Figure 90: Visualisation of the CT scan models (red) and registered STL models (green) for a sample of the frames recorded, showing the ROM of C002.

A: Coronal View (Posterior)
B: Sagittal View
C: Distal view of all frames overlaid on each other to help visualise the manoeuvre performed by C001 (refer to text). s_a and s_b represent the initial and final widths between both ankles.
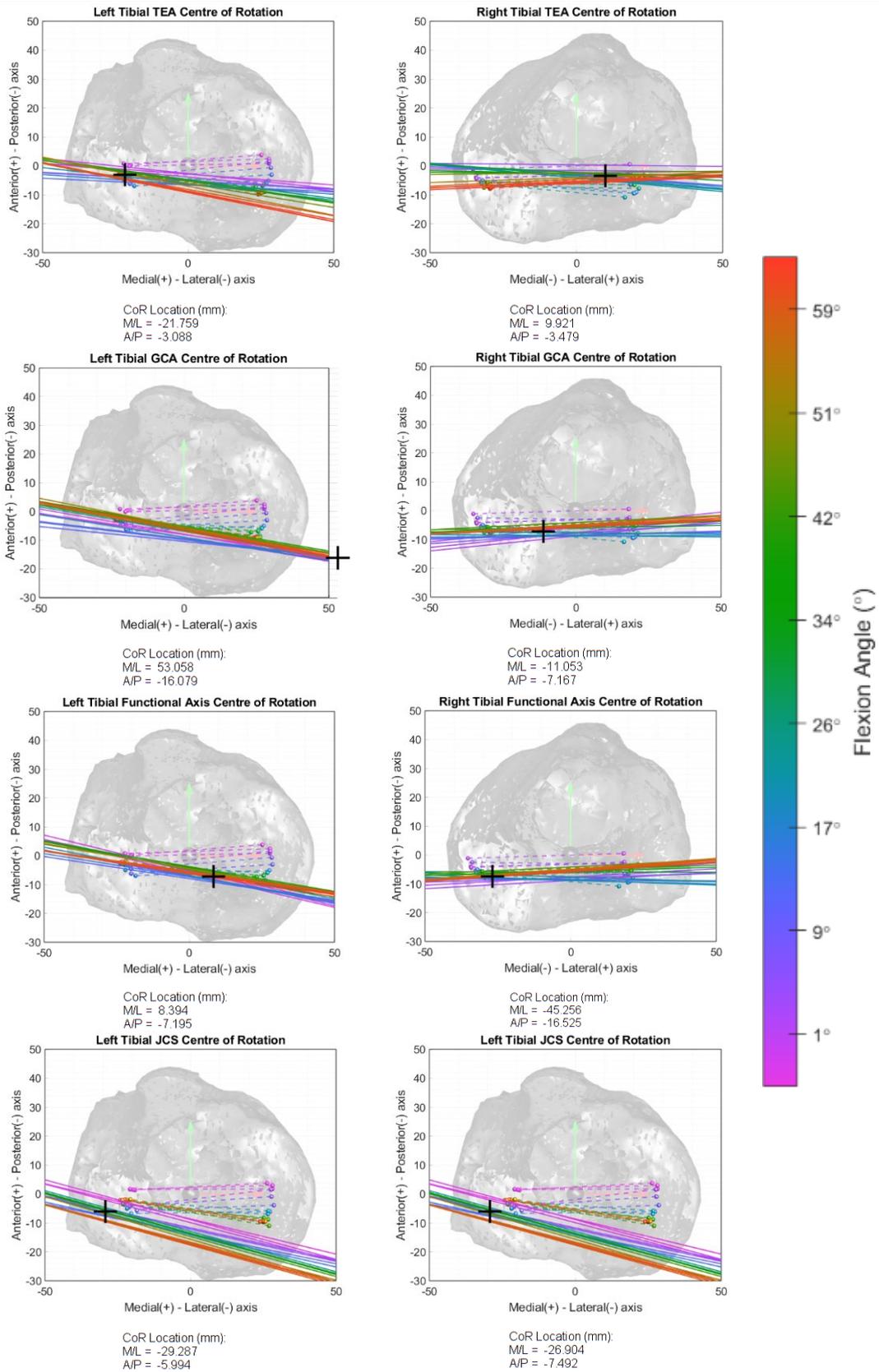
Figure 91: Axial Centre-of-Rotation of the four FE axis variants – Participant C002

The COR plots for the TEA, GCA, FFA and the JCS are plotted for the movement performed by control participant C002. The location of each COR location is reported in terms of mediolateral and anteroposterior distance from the tibial origin.

Functional FEA (FFA)

The results obtained for the functional FEA (FFA) as calculated using the cED based algorithm are presented in Figure 87A and Figure 87B, while the results obtained for the FFA as calculated using the cVSV based algorithm are presented in Figure 87C. At first glance, it can be noted that the results for the cED based algorithm converged, to a certain extent. The cED algorithm for the left knee (Figure 87A) produced an FFA that medially intersected the femoral surface close to the GCA's medial intersection point, while laterally the cED FFA intercepted the femoral bone close to the lateral epicondyle which is also the TEA's lateral point of intersection. For the right knee (Figure 87B), the cED based FFA similarly intersected the femoral condyle close to the GCA's medial intersection point, while laterally in contrast to the left knee the cED FFA intercepted the femoral condyle closer to the GCA's intersection point than the TEA's, although both lie in close proximity (as is the case for the left knee).

On the other hand, the cVSV based algorithm did not converge for both knees. Similar to the results of C001, this might be the case due to the ROM recorded. For the case of C002, although the ROM is nearly double that recorded for C001, it still seems to be limiting the algorithm in converging on the anatomical location of the FEA. Given the location obtained for the cVSV based algorithm, these results will be omitted and will not be considered for this participant.

With reference to the FFA obtained using the cED based algorithm (Figure 87A and B), these results are being considered as applicable since they lie in the proximity of the two principal FE axis. The results obtained hereon using this FFA need to be dealt with caution due to the fact that their location, as explained above, is still not optimal, and there is a considerable chance of kinematic crosstalk. In the images presented in Figure 87A and B, one can note how all three axes converge laterally onto the same location, which agrees with theory, which states that while the lateral condyle is composed of two arcs, the intersection points on the lateral condyle are close enough such that they can be considered as one in some cases. Contralaterally on the medial end, given the ROM, captured for C002, the medial location of both FFAs is realistic since from theory we expect the FFA to start at the location of the medial sulcus (or epicondyle) at full extension and subsequently transitioning towards the intersection of the GCA, which agrees with the results obtained using the cED based algorithm.

Six DOF Kinematics

The six DOF kinematics for C002 are presented in Figure 88, where the kinematics for all four FE axes are outlined. In Figure 88, the focus is given to all the FE axes apart of the JCS derived axes (shown in faded green). The reported FFA results (orange) are for the FFA, which was derived using the cED based algorithm.

As mentioned earlier, the 4D CT scanner started recording the movement of participant C002 as he started flexing his knees following hyper-extension. Subsequently, C002 reached his maximum allowable flexion angle, given the limitations on the equipment, and subsequently started extending in the last two captured frames. The flexion angles reported for the three chosen FE axes (TEA, GCA and FFA), are reported below:

Table 7: Flexion angles reported for each FE axes for the ROM captured for C002.

	TEA		GCA		FFA	
	Left	**Right**	**Left**	**Right**	**Left**	**Right**
Start (Max Extension)	-0.67	3.97	-2.04	1.87	-2.23	2.36
Max Flexion	63.24	63.49	62.19	61.89	62.83	62.03
Finish	58.84	58.80	57.76	57.14	58.34	57.31

With reference to Figure 88B, the left knee appears to adduct until it reaches the 20° mark after which all three axes seem to stabilise. This is attributed to the manoeuvre performed by C002, whereby the left knee noticeably adducts more in relation to the contralateral knee until it touches the right leg in the 8th frame which corresponds to circa 20° of flexion. In the right knee, the GCA recorded no change in adduction until the 16° mark, after which it starts adducting and stabilises after the 40° mark. Considering that all three axes followed the same path of motion, albeit slight variations in magnitude between one another, then it is safe to assume that this is due to the participant's movement.

The effect of this movement is also noted in the axial rotation displayed by C002. Both tibias initially were internally rotating as expected during this phase of flexion, but at circa 15°, for the left knee, and 20° for the right knee, the effect of the contact occurring distally was noticeable. This distal contact indirectly influenced the knee joint to adjust for this reduction in freedom of movement (as a result of the closed kinematic chain) by changing its direction of axial rotation as can be noted in Figure 90C. Following this change in direction, the kinematics, based on the TEA, showed continuous external rotation until maximum flexion, while the GCA and the FFA plateaued at around the

40º mark. This difference towards the terminal stages of flexion (for this given ROM) is attributed to the fact that after the 40º flexion mark, the femur is known to be rotating around the GCA, while the TEA will be undergoing out-of-plane movement. The repercussions of the reduction in freedom of movement in the lower leg were also noted in the results calculated for the contact points and axial COR (discussed below).

The translational DOF are presented in Figure 88 (D-E). The ML tibial translation calculated for C002 showed constant medial translation for both contralateral knees, with the left tibia translating 3mm more than the right knee. This difference in translation is correlated to the larger adduction angles reported by the left knee, which consequently translated the knee medially.

The AP and PD translations will be reviewed together, similar to discussion performed for C001, but this time focusing on later stages of flexion in light of the specific movement performed by C002. With reference to Figure 92A, the profiles for both translations were divided into 3 phases based on trends which were noted in the translation profiles for these 2 DOF. During the first phase, marked ❶ in Figure 92A, both tibias followed theoretical motion by translating anteriorly while maintaining their PD location, albeit some kinematic crosstalk being displayed by the GCA (and the FFA – but with smaller magnitudes) which agrees with the justifications given earlier for the AP and PD translations of C001 (refer to Figure 84). During phase ❶ the results for C002 agree with the assumption that rotation is occurring around the TEA, while the GCA displays out-of-plane movement in the form of lesser femoral posterior translation and greater femoral distal translation (compression), as noted in the plots presented in phase ❶ in Figure 92A.

Moving on to phase ❷, it can be noted that the anterior tibial motion ceases at around the 20º flexion mark. Theoretically, during this phase, the TEA kinematics are expected to report anterior tibial motion. However, no tibial movement was reported in the AP dimension, which is assumed to have been counter-acted by the manoeuvre which C002 performed. The GCA kinematics (along with the FFA) reported that posterior tibial translation occurred, having its gradient decreasing from 15º of flexion until the end of this phase when the GCA and FFA AP translations plateau. With reference to Figure 92B, this paradoxical posterior tibial motion can be explained by assuming rotation at 15º of flexion to be occurring around the TEA, such that the GCA experienced the paradoxical posterior tibial motion due to kinematic crosstalk (refer to red arrow). The

transition from the TEA to the GCA is assumed to occur at the 40º flexion mark. Theoretically, the Transition phase of flexion lasts until around the 30º flexion mark, but this is subjective. In fact, towards the final quarter of phase ❷ this transition of the FE axis can be noted to start as the gradient of the GCA AP profile decreases while the gradient of the TEA increases. With reference to the PD translation during phase ❷, all three axes reported that both knees distracted by 1.5 mm over this flexion range. Due to the similar magnitudes, this movement is not attributed to kinematic crosstalk and can be assumed to be occurring as a result of the entire knee distracting, maybe as a result of the closed kinematic chain manoeuvre.

In phase ❸, both the AP and PD translations for the GCA (and FFA) stabilise while the TEA based kinematics display clear signs of kinematic crosstalk. Theoretically, from 40° of flexion onwards, the femur rotates around the Flexion Condylar Axis (GCA). Taking this assumption, and with reference to Figure 92C, it can be understood that at
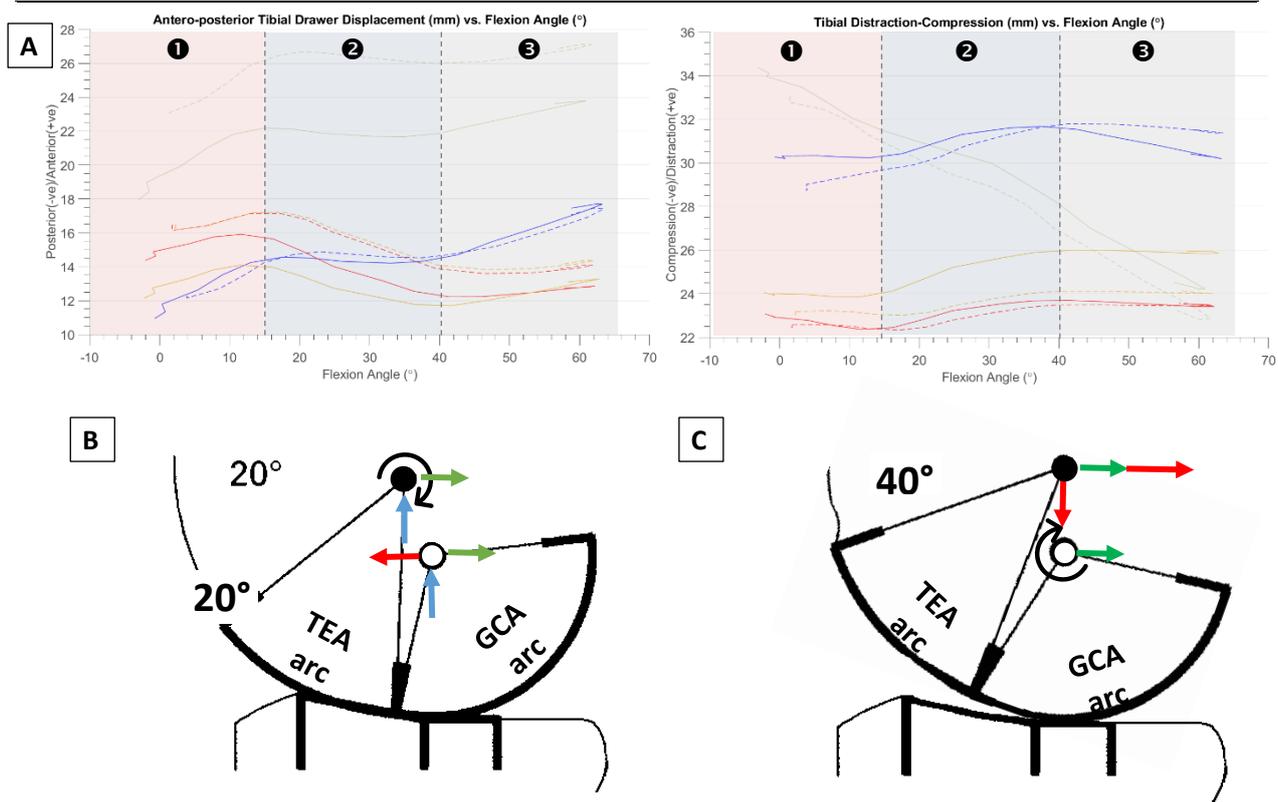
Figure 92: AP and PD translations for C002

A: AP (left) and PD (right) translations calculated for the left and right tibia based on the four different FE axes.

B and C: An illustration to explain the kinematic crosstalk occurring at the GCA and TEA at the instances when the knee is during the Transition phase (left image) and the Flexion phase (right image). The blue arrows show the PD translation, recorded by the TEA based kinematics, which represents the actual motion of the rigid body in space, thus acting as well on the GCA. The green arrows show the AP translation, recorded by the GCA based kinematics, which represents the actual motion of the rigid body in space, thus acting as well on the TEA. The red arrows identify the translations which the GCA (left image) and the TEA (right image) are experiencing as a result of kinematic crosstalk.

this point in the flexion cycle the TEA should be experiencing posterior and distal (compressive) translation due to kinematic crosstalk. It should be noted that while the GCA is not showing any movement in the PD dimension, the AP dimension is showing slight posterior movement for the femur, which agrees with theory. Therefore, based on the above, and with reference to Figure 92A, the tibial anterior and proximal translation reported by the TEA-based kinematics during phase ❸ can be attributed to kinematic crosstalk.

So far, based on the substantiated evidence shown for C001, it was determined that during the Extension and the Transition phases of flexion, the FE axis of rotation could be approximated by the TEA. Using the data collected for C002, the FE axes model being proposed in section 2.6.2.1 can be also corroborated. Given the ROM captured for C002 and the corresponding extracted kinematics discussed above, it has been shown that during the late Transition phase of flexion the FE axis transitions onto the GCA. Furthermore, as the knee progresses into the Flexion Phase, the femur utilises the GCA as its FE axis. The validation of this model will be revisited during the discussion of the kinematics of C003 and C004, in order to confirm its applicability in healthy knees.

Tibiofemoral Contact Points

The contact points calculated for C002 (Figure 89) followed the same trend noted in the kinematics presented so far for this participant. Initially, up until circa 20º of flexion, the contact points showed posterior translation, with marginal signs of medial pivoting with increasing flexion. From the 20º flexion mark onwards, the contact profile patterns do not follow the expected path, which is exhibited by healthy knees. This, again, is attributed to the fact that the participant made contact at his feet, therefore restricting the freedom of movement of the tibia, whereby the tibia had to adjust its position in response to the closed kinematic chain that was created upon contact. For the left knee, it can be noted how, beyond the 20º flexion mark (represented by the lines with the blue shades in Figure 89B), the contact points in the lateral compartment which are expected to move posteriorly at this point in the flexion cycle in a healthy knee, instead have translated anteriorly. On the other hand, the contact points in the medial compartment, which were expected to remain roughly in the same location for a healthy knee, showed posterior translation. The movement that occurred for the contact points in both compartment is the opposite of what typically occurs in a healthy knee, resulting in external rotation of the tibia. These results are correlated with the results obtained for the axial rotation where it was noted that the tibia initially undergoes internal rotation followed by a sudden shift, switching to external rotation. A similar trend is noticed in the right knee, although not as prominent as the effect imparted on the left knee. The

right knee still manages to show marginal signs of medial pivoting, notwithstanding the manoeuvre performed by C002.

Axial COR

Similar to the results obtained above, the axial COR results (presented in Figure 91) were affected by the closed kinematic chain created by the contact at the participants' feet. The axial COR results for the TEA reported that the COR lies in the lateral compartment for both knees. This follows the same reasoning explain above for the Contact Point results obtained for C002. Here it is good to note that, similar to the axial COR results presented for C001, the initial TEA contact points and axial COR for C002 were located above each other (refer to magenta to blue lines), showing that rotation is occurring around the TEA axes in these initial stages of flexion. Even so, the results beyond roughly the 20º flexion mark are erroneous and can be ignored.

For the GCA, although the COR for both knees was located on the medial side, the profile of projected GCA axes is affected by C002's manoeuvre. The GCA COR results lie directly above the contact points occurring beyond the 40º flexion mark (green to red shaded lines), which shows an agreement with the theory that rotation beyond the Transition Phase of flexion occurs around the GCA. This also applies to the COR results for the cED based FFA. Given the above, these results will not be considered due to the effect of the closed kinematic chain on them.

While the kinematic results presented above for C002 were vastly affected by the undesired movement of the participant, these results shed light on the importance of knowing the implications that either an open or closed kinematic chain will have on the results being investigated. Whereas these results only provided limited correlation to known trends in the kinematics of a healthy knee, these results reflect the statement by Churchill *et al.* (1998), mentioned in section 2.6.2.1:

> *"When one of the rotational axes is not allowed to move, the resulting kinematics will change such that the axis that is allowed to rotate does not remain fixed but will move in order to accommodate for the reduction in the DOF of the anatomical joint."*
>
> *- Churchill et al., 1998*

With reference to the results presented for C002, it was noted that the tibia was forced into an externally rotated state due to the closed kinematic chain that was imposed on the knees. In light of the statement by Churchill *et al.* (1998), this had direct implications in all the other DOF, as seen in the calculated and presented results for C002.

5.3   CONTROL PARTICIPANT #3

Control participant #3 performed the flexion-extension exercise while lying down on the CT bed in a prone position. His movement was recorded as he was flexing his knee from circa 20º through to 75º at which point his heel made contact with the CT gantry, thus restricting any further flexion (refer to Figure 93A and B). The CT gantry was tilted at the maximum allowable tilt angle of 15º (Figure 93C) in order to be able to capture the largest flexion angles possible. The following participant data was collected:

- Reference: C003
- Age: 43 years
- Gender: Male
- Left and Right Knee: Both healthy. C003 had a bone pin surgically inserted medial to the tibial tubercle of his right tibia (Figure 93D). C003 noted that this did not have any impact on his movement.

Figure 93: Photographs of Control Participant #3

A & B:C003 in the prone position during pre-scanning setup
C: 4D CT scanner tilt angle. Used to increase the participants' ROM in the prone position.
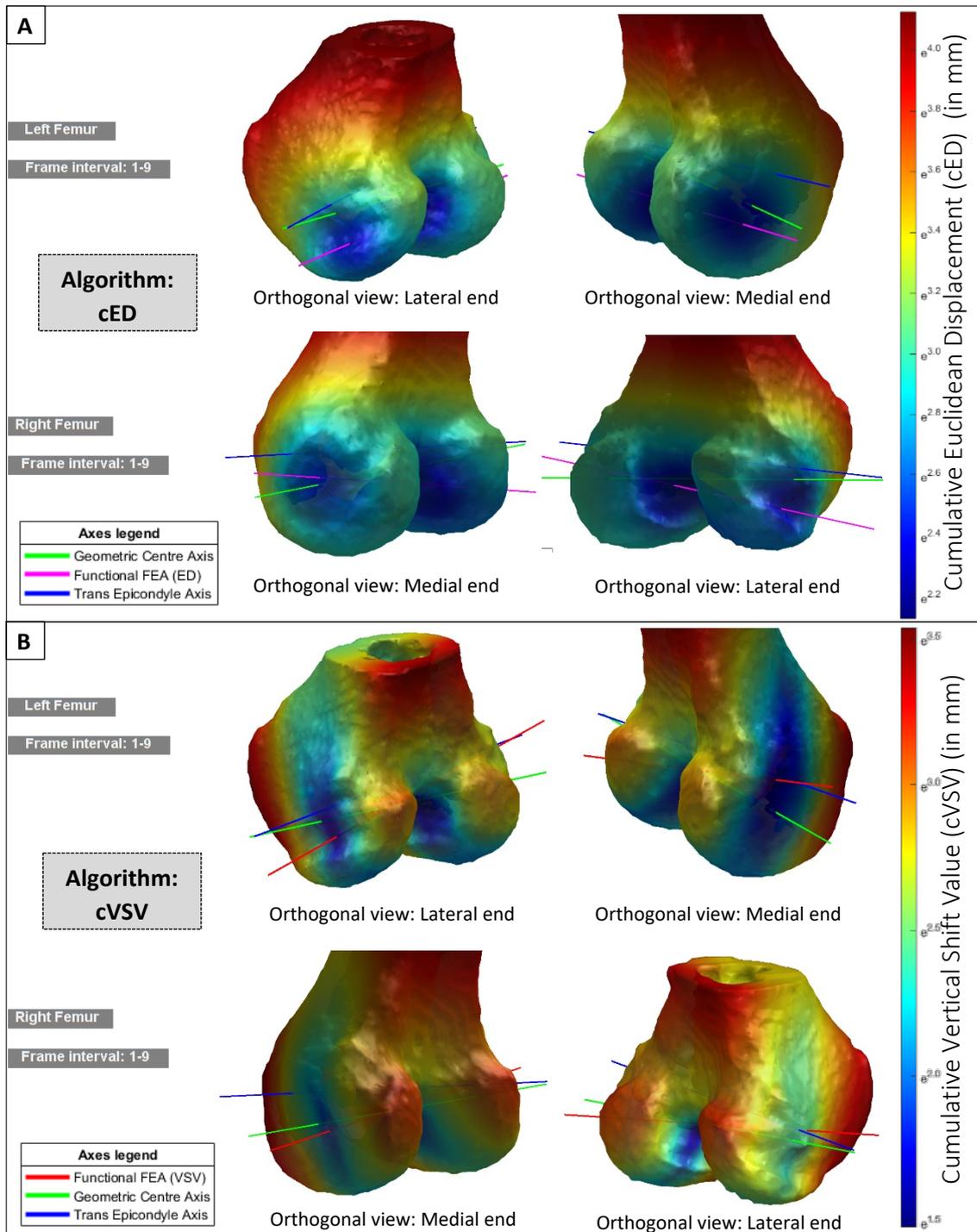
Figure 94: The Functional FE axis (FFA)– Participant C003

A: FFA results based on the cED algorithm. The inlays show the relationship between the FFA (cED axis in magenta), the TEA (blue) and GCA (green) for the left (top row) and right (bottom row) knees.

B: FFA results based on the cVSV algorithm. The inlays show the relationship between the FFA (cVSV axis in red), the TEA (blue) and GCA (green) for the left (top row) and right (bottom row) knees.

D: Two orthogonal views of the tibial bone-pin hole in C003's right tibia.
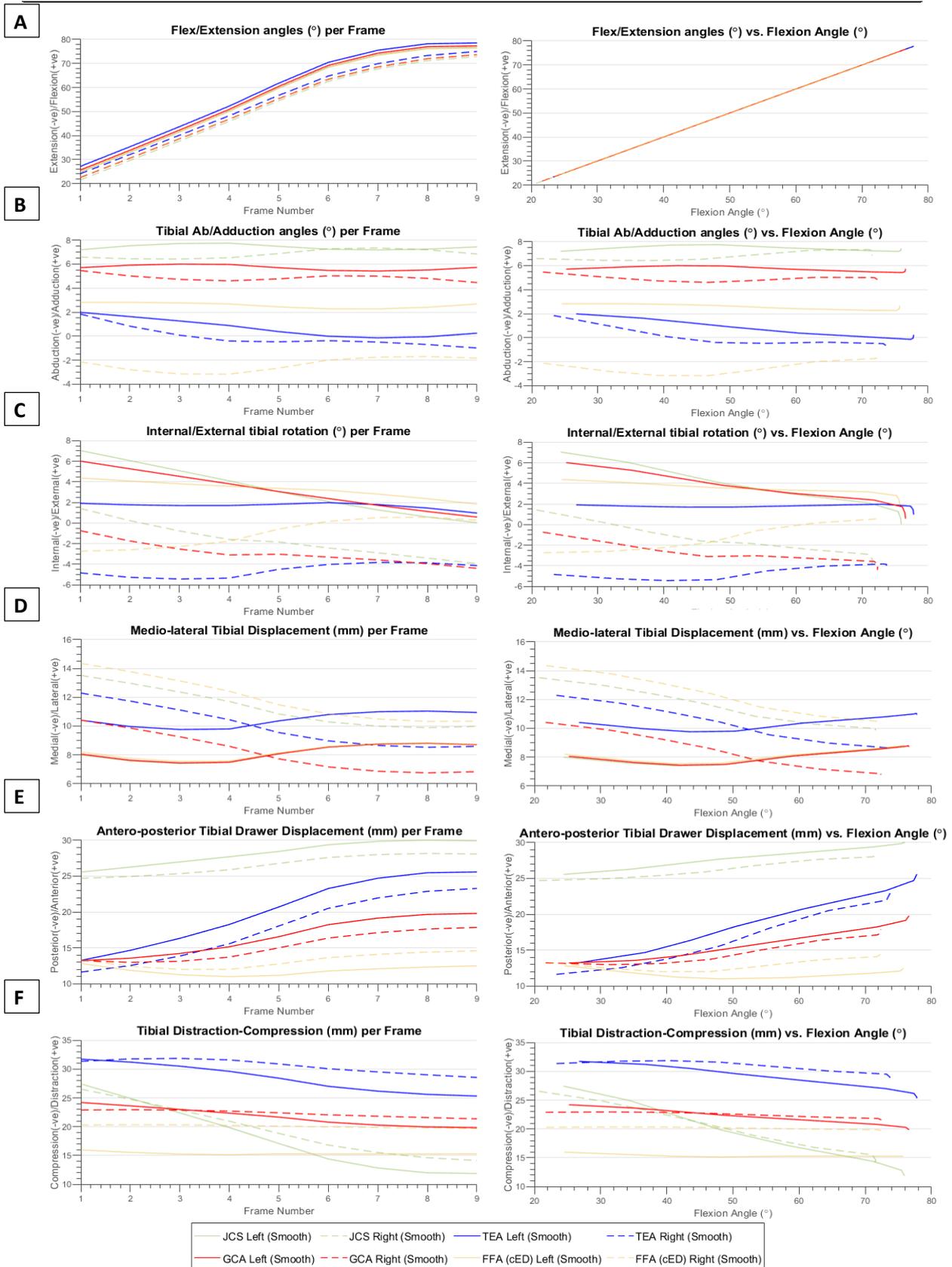
Figure 95: Kinematics for all FE axes for all 6 DOF of the knee – Participant C003

The kinematics based on the four FE axes variants, for the movement performed by control participant C003. The rotational DOF (A-C) are presented per Frame (Left) and against the Flexion Angle (Right). The translational DOF (D-F) are presented per Frame (Left) and against Flexion Angle (Right).
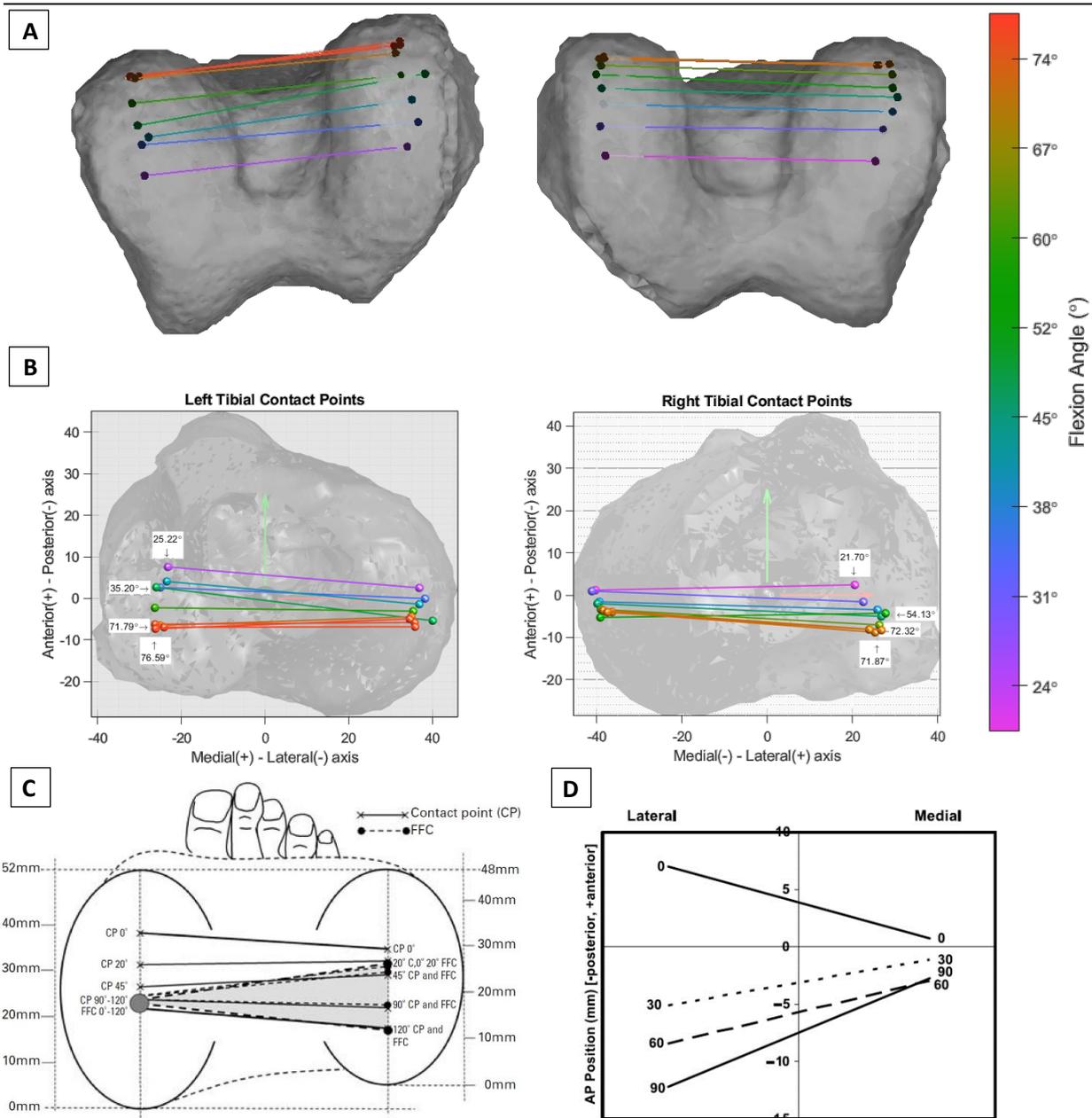
Figure 96: Tibiofemoral contact points - Participant C003

A: Femoral contact points calculated for the movement performed by control participant C003.

B: Tibial contact points calculated for the movement performed by control participant C003.

C: Diagram of the contact profile and COR patterns for non-weight-bearing in-vivo tibial knees (n=5) during a deep knee bend (0-120º flexion). (Pinskerova *et al.*, 2004).

D: The average medial and lateral condyle contact positions for a healthy knee (n=10) during a deep knee bend (0-90º flexion) (Dennis *et al.*, 2003)
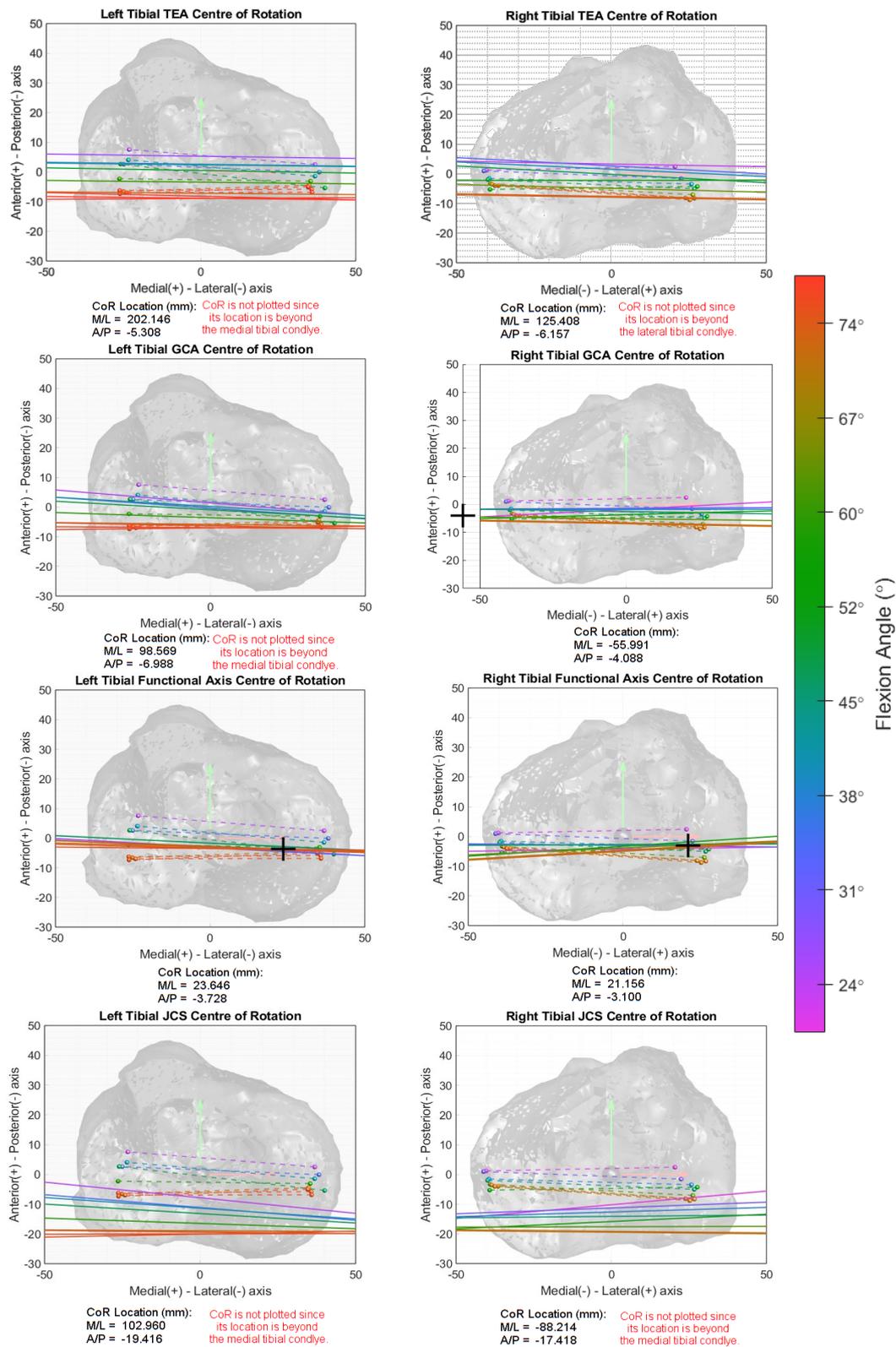
Figure 97: Axial Centre-of-Rotation of the four FE axis variants – Participant C003

The COR plots for the TEA, GCA, FFA and the JCS are plotted for the movement performed by C003. The location of each COR location is reported in terms of mediolateral and anteroposterior distance from the tibial origin. The COR location is plotted on each graph (unless it is outside the tibial plateau, in which case its location is defined by the AP and ML locations below each plot).

Functional FEA

The movement that was captured for C003 initiated towards the end of the Transition Phase of flexion, subsequent to the screw-away mechanism. Considering that the majority of the captured ROM occurred during the Flexion phase, it is expected that the FFA algorithms converge towards the GCA.

The results obtained for the functional FEA (FFA) are presented in Figure 94 (A - cED algorithm; B – cVSV algorithm). With reference to the cED based algorithm, both left and right FFAs converged to similar locations. Medially, both FFAs converged towards the GCA, with the right knee better approximating the GCA intersection point medially. Laterally, similar to C001, both axes converged towards the femoral condyle edges. This is attributed to the effect of considering the X (mediolateral) and Y (anteroposterior) values in the cED algorithm, which are effectively skewing the results. A trend is emerging, where laterally the cED axis is being located towards the surfaces of the condyles, where contact with the tibia occurs, rather than towards the centre of the posterior condyles. This is resulting due to the lateral condyle experiencing more AP and ML motion in relation to its contralateral condyle, such that the FFA does not converge towards the expected locations.

With reference to the cVSV algorithm (Figure 94B), both left and right FFAs did not converge. The cVSV based FFA for the left knee converged to an apparent correct location medially, since it lied between the TEA and GCA, but it was still located too proximal to both. Laterally, the FFA was located relatively far from the expected location, towards the edges of the condyles, similar to the cED based FFA result. The cVSV based FFA for the right knee, converged to a satisfactory location medially, lying close to the GCA. Also, laterally the FFA axes pass in close proximity of the TEA and GCA intersection points laterally. Nonetheless, the resulting FFA axis for the right knee is still considerably skewed in relation to the TEA and GCA.

Given the above results for the cED and cVSV algorithm, none of the FFAs will be considered to have sufficiently converged. Nonetheless, the results for the cVSV based FFA will be reported in the upcoming results for reference only.

Six DOF Kinematics

The six DOF kinematics for C003 are presented in Figure 95, giving focus to the GCA and TEA, while the FFA and JCS are faded since their axes are not being considered to be located correctly, for the reasons given above. With reference to the GCA results (blue) in Figure 95A, the captured movement for C003 started from 25.29º of flexion for the left knee and 21.77º of flexion for the right knee. Subsequently, C003 flexed his knee until the last frame was captured, when he reached 76.64º of flexion for the left knee and 72.39º of flexion for the right knee.

With reference to Figure 95B, the adduction angles calculated for the movement performed by C003 were as expected. For the GCA, marginal variation in the adduction angles was reported, having a range of 1.5º (4.9º to 6.4º) for the left knee, and 1.8º (4.1º to 5.9º) for the right knee. Conversely, the TEA reported steadily increasing abduction angles which were attributed to kinematic crosstalk. The ranges reported for the TEA were 2.5º (-0.7º to 1.8º) for the left knee and 3º (-1.1º to 1.9º) for the right knee.

Moving on to the axial rotation of the knee, it is known from theory that for the given range of flexion covered by C003, slight internal rotation of the tibia is expected (refer to Figure 20A). The majority of the internal rotation of the tibia (or external rotation of the femur) occurs during the Extension and Transition phase of flexion (as seen in the results obtained for C001). With reference to the internal/external tibial rotation results presented in Figure 95C, it can be noted that for the left knee the TEA showed minimal signs of internal rotation while the GCA internally rotated by an additional 5º. Contralaterally, the same movement is reflected apart for the TEA, which displayed external tibial rotation following the 45º flexion mark. With reference to the results presented for the contact points (Figure 96B), it can be noted that the left knee displays constant internal rotation while the right knee also internally rotates, although not as much as the contralateral knee. Also, the right knee does not display any signs of external tibia rotation, as reported in the axial rotation values of the right TEA. Based on the above, it can be concluded that the TEA values are effected by kinematic crosstalk, while the GCA values agree with theory for this given range of flexion.

The ML translation values presented in Figure 95D show identical profiles when comparing the TEA to the GCA. This identical motion is attributed to actual ML movement occurring between the femur and tibia, and not kinematic crosstalk. As noticed with previous participant data, the ML translation is the least of all translational DOF to be impacted by kinematic crosstalk since the FE axes around which the majority of the movement occurs is also the axis along which the ML translation is measured. This is reflected in the results obtained for ML translations, where the difference

between the ranges of the TEA and GCA axes are only 0.05 mm and 0.1 mm for the left and right knee, respectively, which can be considered negligible.

The AP and PD translations for C003 are in agreement with the results obtained for C002 during the Flexion phase for the same two DOF (refer to Figure 92A and C). As a result of kinematic crosstalk, the TEA axis reported larger tibial anterior displacement and also larger tibial proximal (compressive) translations.

Tibiofemoral Contact Points

The TF contact points calculated for C003 (Figure 96) agree with theoretical profiles over the same flexion range (Figure 96C and D). Medially the contact points are only spread out over a range of 7.5 mm (left) and 6.5 mm (right) in the AP direction. Laterally the contact points are spread out over a range of 14.9 mm (left knee) and 11.2 mm (right knee) in the AP direction. These values reflect the ranges reported in the qualitative results found in the literature (Figure 96C and D).

Axial COR

The axial COR results for C003 are presented in Figure 97. With reference to Figure 96C, it can be noted that for the range of flexion recorded for C003, the axial COR profiles are expected to show slight medial pivoting, while also relating with the contact point locations from circa 45º onwards. Previous to this, the contact points are expected to lie anterior to the corresponding axial COR profiles.

The TEA axial COR profiles reflect the kinematics discussed, for this FE axis, above, where due to the kinematic crosstalk, the resulting axial rotation for both knees was quasi-constant. This resulted in quasi-parallel TEA profiles in the tibial axial plots, which further supports the argument that the TEA is not the FFA for this given ROM, since no signs of medial pivoting is occurring, while also showing disagreement between the axial COR results and the corresponding Contact Point results.

The GCA axial COR results showed the expected slight medial pivoting of the knee with progressing flexion. The GCA profiles agreed with the theoretical profiles presented in Figure 96C, and are also in agreement with the contact points overlay, with the exception of the profiles corresponding to flexion up until 30º. The profiles before 30º of flexion (transition phase of flexion) do not match with the contact points since during this range of flexion the knee is assumed to be rotating around the ECA, or TEA (refer to TEA axial COR profiles before 30º of flexion).

The axial COR profiles for the FFA and the JCS do not show agreement with theory or with the contact point profiles, as expected.

5.4   CONTROL PARTICIPANT #4

Control participant #4 performed the flexion-extension exercise while lying down on the CT bed in a prone position, similar to C003. In contrast to C003 and the rest of the participants in this study, the movement of this participant was recorded using the intermittent scanning feature described in section 4.1.5.1. The scanner was set to scan the participant once every 1.5 seconds, for a total of 12 seconds, producing 8 volumetric images of the participants' movement. This resulted in the participant having to bend his knees at a third of the speed that the other participants were performing the same flexion-extension movement. It should be noted that the participant remarked that when trying to sluggishly flex the lower leg during the early degrees of flexion he felt a sense of instability which receded with increasing flexion. While this sense of instability is mostly due to the slow speeds which the participant was required to maintain, the instability was further enhanced in the early stages of flexion, when in prone position, due to the following reasons (refer to Figure 100C):

- The centre of mass of the shank and foot initially lies far from the knee joint. Subsequently, the centre of mass approaches the knee with increasing flexion (refer to the difference between s_1 and s_8 in Figure 100C), thus reducing the moments generated at the knee,

- The moment arm of the Hamstring muscle group, F_H, and to a certain extent the Gastrocnemius muscles, F_G is initially very small. This increases with flexion, thus increasing the effectivity while reducing the effort of force transmission, and

- The Transition phase of flexion (which occurs during the initial stages of capture for C004) is a phase during which the knee experiences increased knee instability due to the "rocking" of the condyles when transitioning to the Flexion Condylar axis.

The CT gantry was again tilted at the maximum allowable tilt angle of 15º in order to be able to capture the largest flexion angles possible. Using this intermittent approach this control participant was able to flex his knee from circa 10º to 70º. The following participant data was collected for participant #4:

- Reference: C004
- Age: 58 years
- Gender: Male
- Left and Right Knee: Both healthy, with no knee-related symptoms reported throughout the participants life.
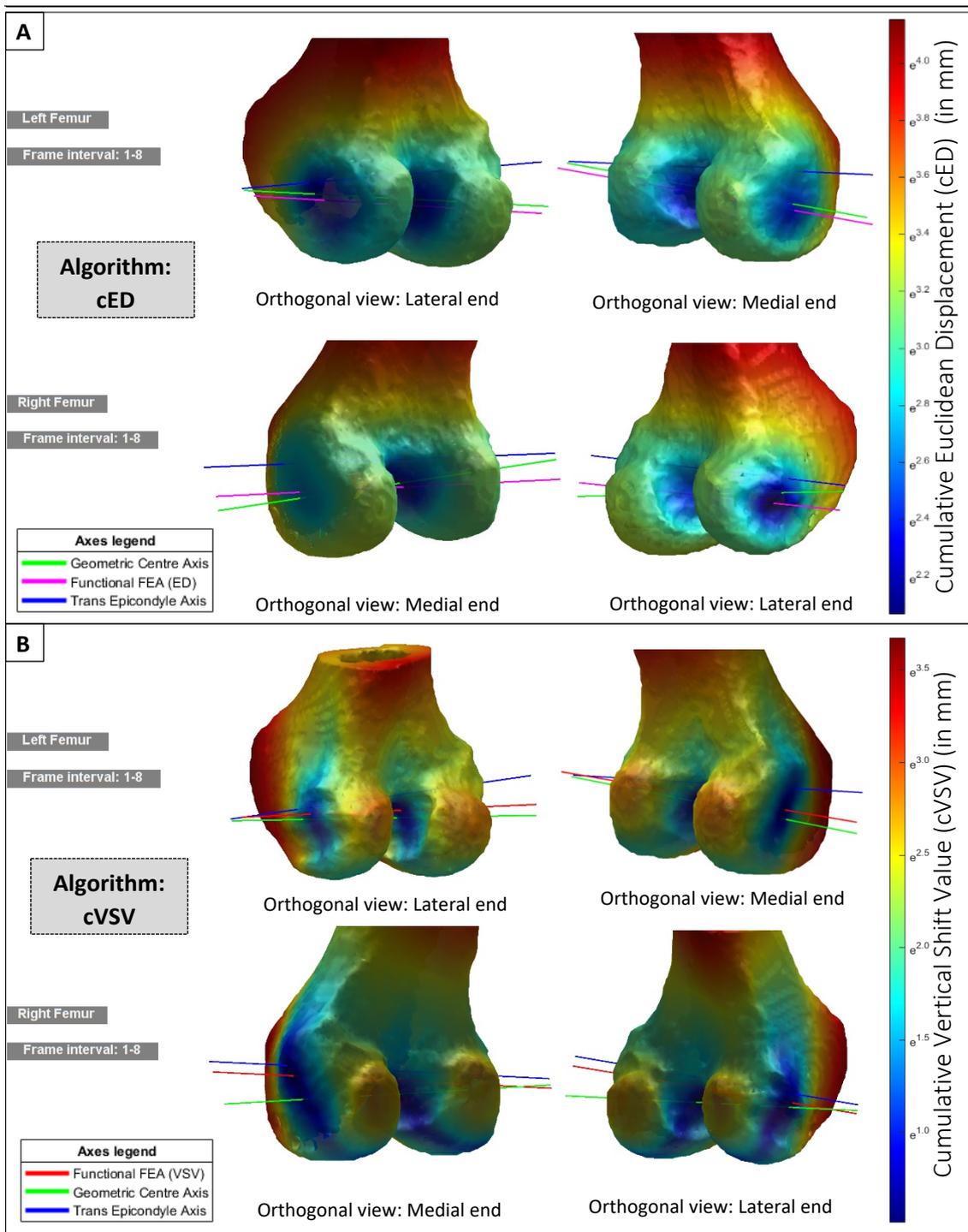
Figure 98: The Functional FE axis (FFA)– Participant C004

A: FFA results based on the cED algorithm. The inlays show the relationship between the FFA (cED axis in magenta), the TEA (blue) and GCA (green) for the left (top row) and right (bottom row) knees.

B: FFA results based on the cVSV algorithm. The inlays show the relationship between the FFA (cVSV axis in red), the TEA (blue) and GCA (green) for the left (top row) and right (bottom row) knees.
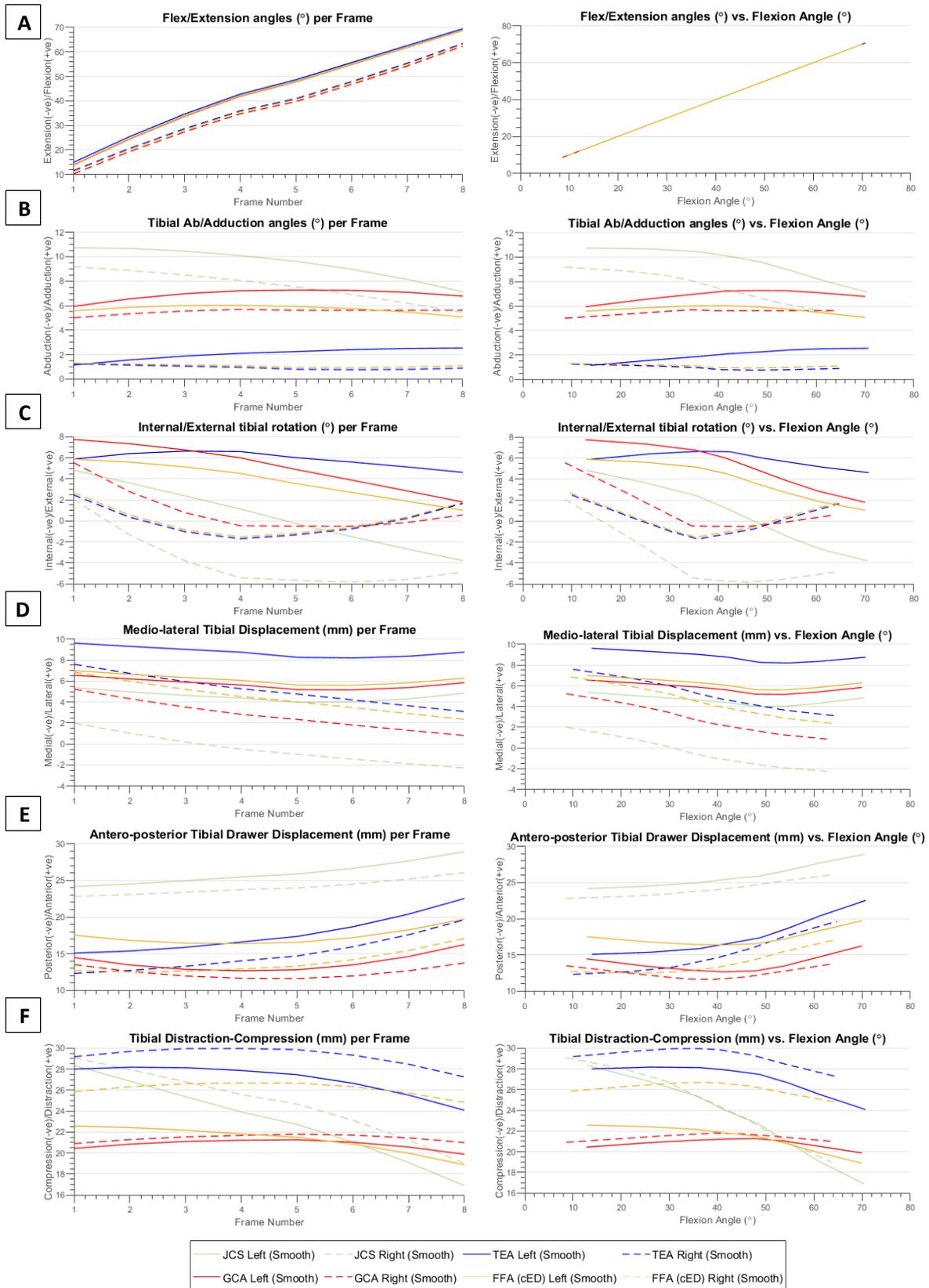
Figure 99: Kinematics for all FE axes for all 6 DOF of the knee – Participant C004

The kinematics based on the four FE axes variants, for the intermittent movement performed by control participant C004. The rotational DOF (A-C) are presented per Frame (Left) and against the Flexion Angle (Right). The translational DOF (D-F) are presented per Frame (Left) and against Flexion Angle (Right).
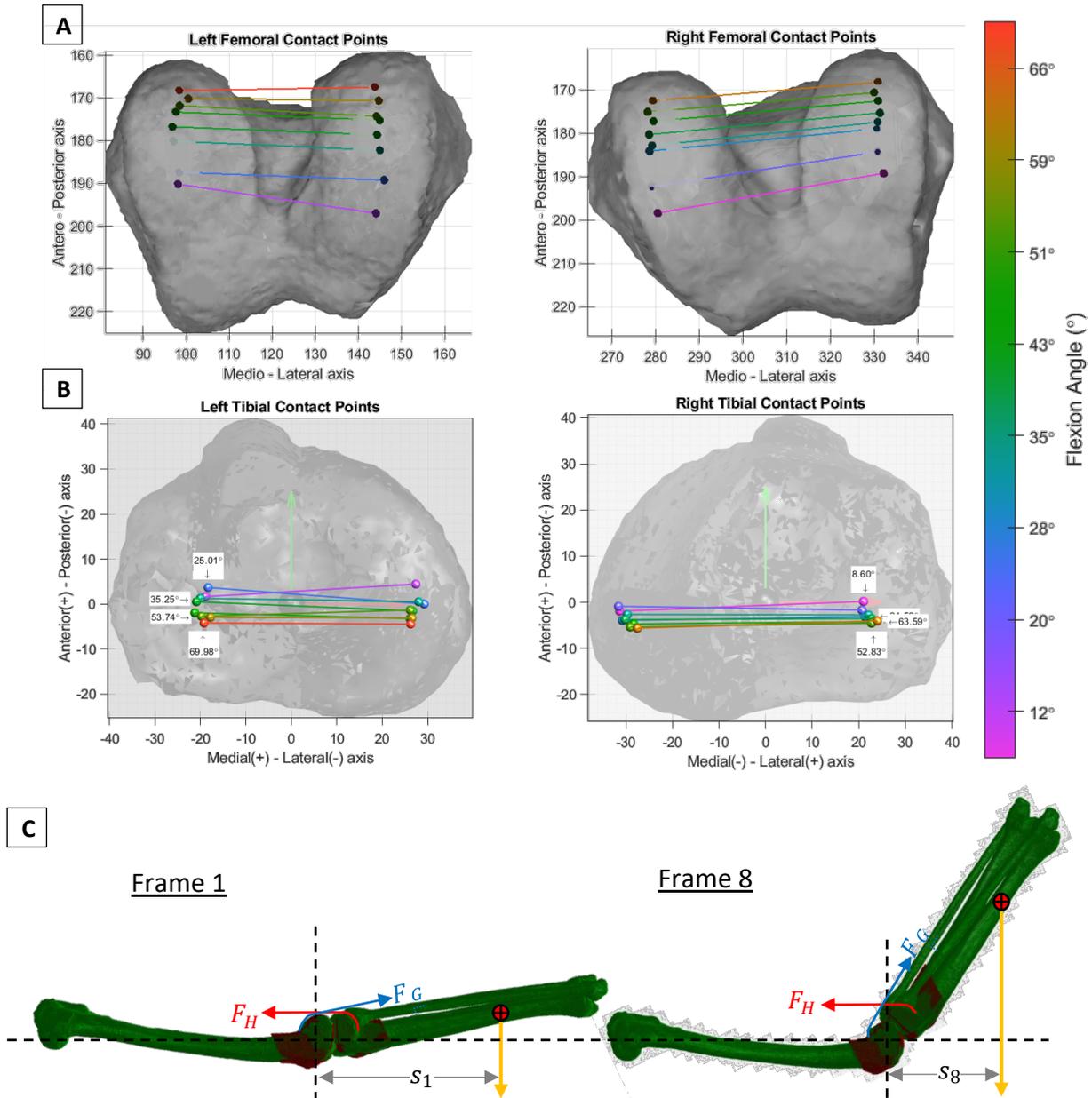
Figure 100: Tibiofemoral contact points - Participant C004

A: Femoral contact points calculated for the movement performed by control participant C004.
B: Tibial contact points calculated for the movement performed by control participant C004.
C: Visualisation of the forces acting on the knee and the lower leg during the ROM of C004.
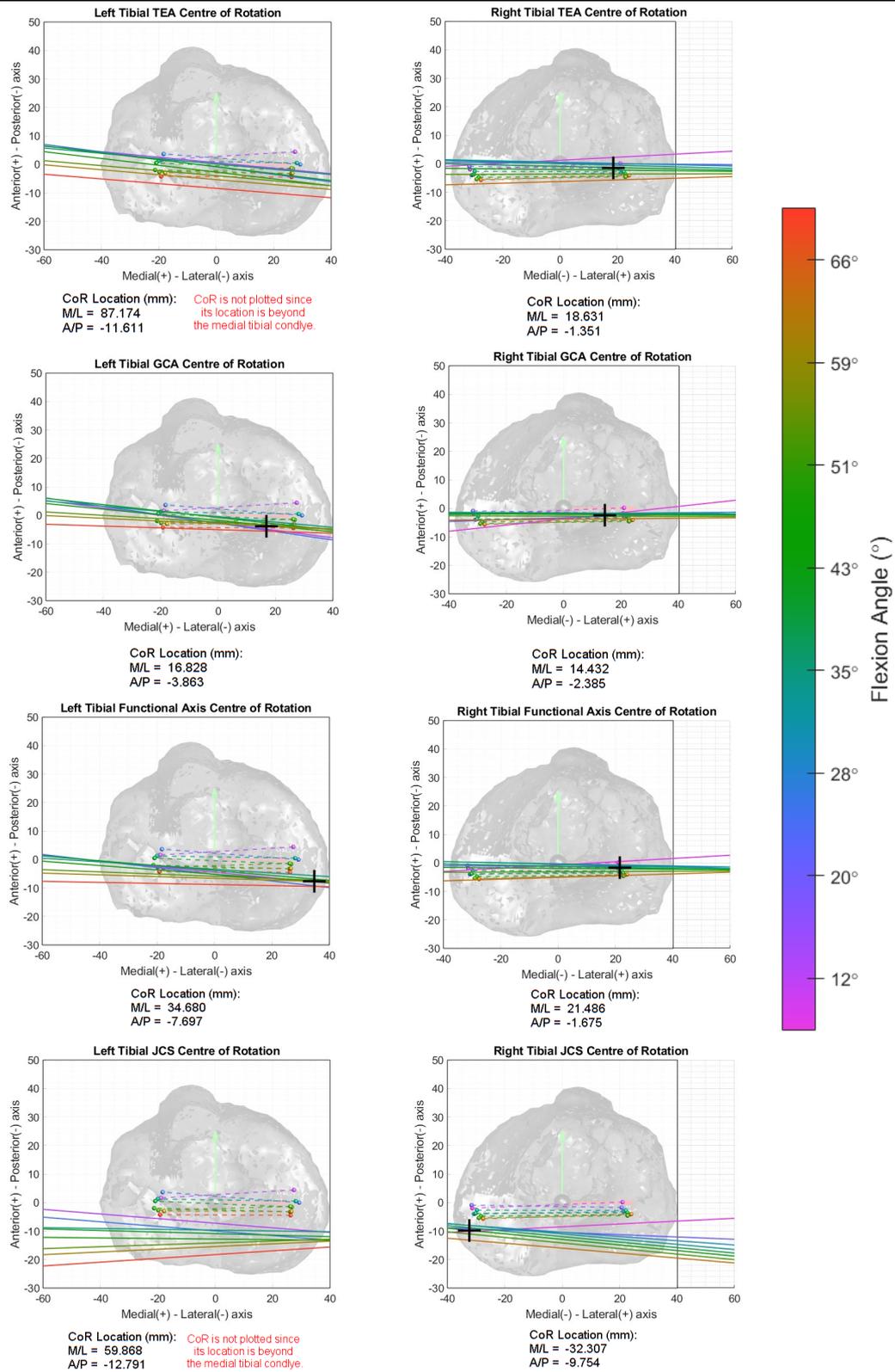
Figure 101: Axial Centre-of-Rotation of the four FE axis variants – Participant C004

The COR plots for the TEA, GCA, FFA and the JCS are plotted for the movement performed by control participant C004. The location of each COR location is reported in terms of mediolateral and anteroposterior distance from the tibial origin. The COR location is plotted on each graph (unless it is outside the tibial plateau, in which case its location is defined by the red text below each plot).

Functional FEA

The functional FEA (FFA) results for C004 are presented in Figure 98 (A – cED algorithm; B – cVSV algorithm). Given the captured ROM for C004, it is expected that at the beginning of the flexion cycle, when the knees would be at the beginning of the Transition phase of flexion, the functional FE axis would be located in close proximity of the TEA. Subsequently, until roughly 30º of flexion, the functional FE axis is expected to have transitioned from the location of the TEA to that of the GCA, after which it will stabilise there until the end of capture (similar to C002).

At first glance, the results obtained for C004 show better convergence of the algorithm than any of the previously presented results so far. With reference to the results obtained for the cED based algorithm, the left converged towards the GCA as expected. Medially, the FFA intersects the femoral condyle in close proximity to the intersection point of the GCA, although slightly distal to it. Laterally, the FFA also intersects in close proximity to the GCA, although, this time, slightly posterior to the GCA intersection point. With reference to the cED based FFA for the right knee, it can be noted how the FFA approached the GCA medially, as expected. Laterally, the same behaviour noted with the results for C003 occurred, although not so prominently. Laterally, the intersection of the FFA with the femoral condyle was relatively more posterior than that of the GCA, such that the FFA was skewed in relation to the GCA, but roughly parallel to the TEA.

With reference to the results obtained for the cVSV based algorithm, the FFA for the left knee converged towards the GCA, as expected, for both the medial and lateral ends. In contrast with the cED based FFA, the intersections medially and laterally were proximal in relation to the GCA intersection points. Nonetheless, the cVSV based algorithm for the left knee is considered to have converged for this case. Contralaterally, the cVSV based FFA, also converged to the expected area between the TEA and GCA intersection points, but this time lying closer to the TEA. Medially the FFA intersected the femoral condyle close to the TEA, while laterally the FFA intersected closer to the GCA. It can be noted how, similar to the result obtained for the cED FFA of the right knee (above), the cVSV based FFA in the right knee is roughly parallel to the TEA. With reference to Figure 99A, this increased correlation to the TEA is being attributed

to the fact that the right knee lasted longer in the Transition Phase of flexion (10˚ to 30˚ flexion), such that the algorithm for the right knee was inputted more data pointing towards the FFA being located close to TEA, than the left knee.

Considering the above, while the cED FFA results are satisfactory, the cVSV results were chosen on the premise that FFA results for the right knee converged better for the cVSV than for the cED. Therefore, the results for the cVSV FFA will be presented and discussed in the upcoming results.

Six DOF Kinematics

The six DOF kinematics for C004 are presented in Figure 99, giving focus to the GCA, TEA and cVSV based FFA, while the JCS is shown in faded green. With reference to the GCA results (blue) in Figure 99A, the captured movement for C003 started from 12.8º of flexion for the left knee and 8.6º of flexion for the right knee. Subsequently C004 intermittently flexed his knee until he achieved 70.0º of flexion for the left knee and 63.6º for the right knee.

The tibial adduction angles (Figure 99B) calculated for C004 showed no deviations or irregularities. With reference to the GCA results, the left knee slightly adducted over a range of 1.7º (9.2º to 10.9º) while the right knee abducted over a range of 2º (7.7º to 9.7º). Similarly with reference to the TEA, the left knee slightly adducted over a range of 1.5º (1.3º to 2.8º) while the right knee slightly abducted over a range of 0.7º (0.6º to 1.2º).

Due to the fact that the Extension phase of flexion was not captured for C004, therefore intrinsically not capturing the screw-home mechanism in action, the axial rotation is not expected to vary much, with most of the axial rotation expected to occur during the first few degrees of flexion. With reference to the GCA kinematics, the axial rotation of the knee displayed internal rotation for both knees as expected. Discrepancies were noted between the results of the left and right knee. The left knee reported slight internal rotation until 40º of flexion for the GCA, followed by larger changes in the internal rotation angles until the end of the flexion cycle. Contralaterally, the right knee displayed relatively larger increases in the internal rotation of the tibia until 40º of flexion, followed by a much lesser degree of internal rotation from there on. The results for the left knee are contradictory in the sense that for the given ROM the tibia is expected to achieve most of its internal rotation until the end of the Transition phase,

after which the knee only internally rotates as a result of the posterior translation in the lateral compartment, which results in smaller internal rotation angles. With that being said, it should be noted that both knees managed to achieve similar overall internal rotation values, with the left knee internally rotating by 6.62º and the right knee internally rotating by 6.65º. Therefore, given the above, it is being assumed that this irregular axial rotation happened due to the instability the participant commented about following the scan. Due to the slow flexion speeds required by the participant for the intermittent scanning, the femoral condyles were allowed enough time to slightly re-position themselves with respect to the tibia in order to try to stabilise the knee in these quasi-static positions, which as a result adjusted the internal rotation angles.

 The AP and PD translations are analysed in Figure 102. Recall that the TEA is being assumed to be the anatomical FEA until circa 10º, followed by a transition period until the 30º flexion mark during which the anatomical FEA transitions to the location of the GCA. With reference to phase ❶ in Figure 102, it can be noted how the TEA is reporting anterior tibial motion, as expected, while the GCA and FFA are reporting posterior motion which is occurring due to kinematic crosstalk (refer to Figure 92B). The GCA (and FFA) is displaying out-of-plane motion until the 40º flexion mark, at which point the TEA starts displays signs of kinematic crosstalk. During phase ❷, the GCA follows expected motion, displaying anterior and slight compressive motion, while the TEA displays excessive anterior and compressive motions, which are correlated with kinematic crosstalk (similar to C002).
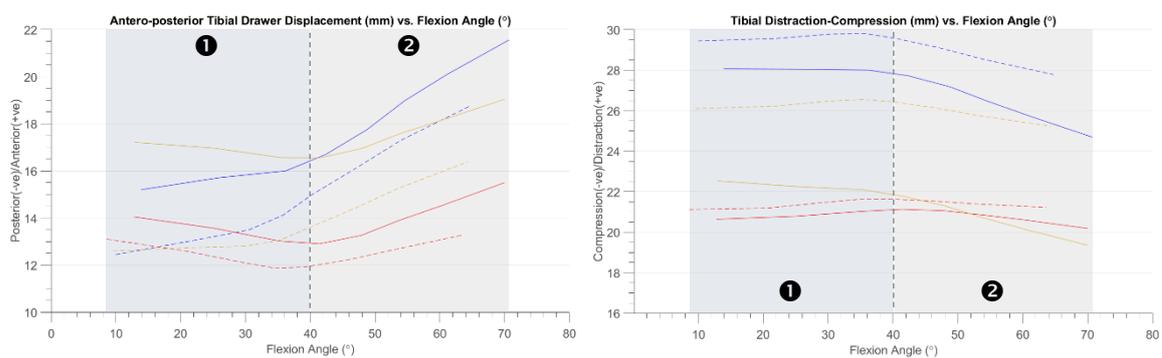
Figure 102: Analysis of the AP and PD translations for C004.

Tibiofemoral Contact Points

The TF contact points calculated for C004 (Figure 100) fail to show the internal rotation of the tibia during the Transition phase of flexion. It is expected that the contact points up until the 30º flexion mark are anterior and internally rotated with respect to the subsequent contact points which usually follow a quasi-parallel path while moving slightly posterior with progressive flexion. The first contact point for the left knee (occurring at 12.8º flexion) is atypically externally rotated while the subsequent contact points follow the expected slight internal rotation (medial pivoting) along with the minor posterior displacement. The first CP reflects the TEA axial rotation results, which reported minor external rotation. The contact points for the right knee follow the same trend displayed by the left knee but the external rotation is not so prominent, and occurs in the CPs of the second frame.

This mildly erratic behaviour in the first two frames is being assumed to be happening as a result of the instability reported by the participant during the intermittent scanning procedure. Due to the slow speeds which the participant was required to maintain, the TF interface was allowed to adjust its relative position in response to the external and internal forces and resulting moments which existed at these specific positions. Following the 30º flexion mark, the CPs for both knees relate the theoretical profiles, as the CPs translate posteriorly while displaying slight medial pivoting.

Axial COR

The axial COR results for C004 are presented in Figure 101. With reference to the TEA COR results, the projected TEA axes for the left knee do not show agreement with their corresponding Contact Points. For the captured ROM, it is expected that the TEA axes would match the location of their corresponding CPs for the flexion angles up until 40º (considering that the Transition phase for C004 lasted until 40º as shown in Figure 102). Subsequently the TEA axes are expected to move posteriorly in a parallel manner, as shown in the TEA axial COR results for C003. The results for the projected TEA axes of the right knee show better agreement with theory, since the projected axes and the corresponding CPs lie in close proximity until the 30º flexion mark. This is with the exception of the first frame which is located anterior to its corresponding CP. The disagreement displayed for the TEA COR plots is again associated to the slow flexion speeds of C004.

The GCA axial COR profiles for the left knee followed theoretical profiles while also corresponding with the CPs for flexion angles larger than 40º. The profiles before the 40º flexion mark did not agree with theoretical locations of the profiles and with the CPs of the corresponding flexion angle. The right knee COR results were affected by the profile of the first frame which pushed the COR laterally. Apart from this, towards the end of the flexion cycle the COR profiles lie anterior to their CP counter-parts. The FFA axial COR results for the left knee were posteriorly located with respect to their corresponding CPs, which reflects the location of the converged axes w.r.t the GCA. On the other hand, the FFA axial COR result for the right knee agrees with the corresponding CPs throughout the entire ROM, including the first frame. Furthermore, while the COR profiles agree with the CPs' locations, the COR location is irregularly located on the lateral plateau which contradicts theory for a deep flexion exercise. The JCS axial COR profiles show no sign of agreement with the corresponding CPs or theoretical profile patterns.

In conclusion, the results for C004 followed theoretical values and profiles expected for a flexion exercise from 10º to 70º. The TEA was shown to be acting as the anatomical FEA until 40º of flexion, and subsequently, the GCA approximated the anatomical FEA until the end of flexion. It was noted that the first few degrees of flexion, particularly the first two frames, were affected by the sluggish flexion motion which the participant was required to maintain in order to align with timings of the intermittent scanning procedure. This had a direct result on the captured kinematics, mostly in the first 30º of flexion, after which the knee seemed to be more stable, such that the kinematics better reflected those expected during a simple knee flexion exercise. This instability is prominent in the results of C004, due to the slow speed of the flexion exercise, which is assumed to have allowed the TF interface to adjust its position in response to the muscle and ligament forces acting on the knee at that instant, the corresponding moments (torques) and also the moment of inertia imposed on it by the centre of mass of the shank and foot.

5.5   PATIENT PARTICIPANT #1

Patient Participant #1 had a left arthritic knee and a right replaced knee. The replaced knee was an Ultra-Congruent Fixed Bearing knee. Patient participant #1 performed the cyclic flexion-extension exercise while in the supine position with an elevated cushion under her knees to increase the ROM. The movement was captured from circa 20º of flexion as the participant was extending her knees. Subsequently, she extended to her maximum allowable extension and then proceeded to flex her knees until the last frame was captured at circa 55º of flexion. The following participant data was collected for Patient Participant #1:

- Reference: P001
- Age: 70 years
- Gender: Female
- Left Knee: Arthritic with clear signs of osteophyte growth on the peripheries of the femoral condyles (refer to left knee models in Figure 103).
- Right Knee: Replaced with an Ultra-Congruent Fixed-Bearing BBraun implant.

It should be noted that the TEA location identified for the right replaced knee was only selected based on the remaining bone tissue following segmentation (refer to right knee models in Figure 103). As a result of the majority of the medial and lateral condylar bone being segmented due to the metal artefacts from the implants, the exact location of the epicondyles could not be confidently identified. Therefore, the identified TEA for the right knee should not be considered as applicable. In fact, when comparing the TEA location for the right replaced knee with the TEA locations identified for the control participants, the TEA for this replaced knee appears to be incorrect as it does not approach the GCA laterally while also displaying a quasi-parallel orientation to the GCA. Based on this, any results for the TEA of the right knee are to be disregarded for P001.

The analysis of the left knee is only going to be presented for reference since it is beyond the scope of this thesis to analyse the kinematics of arthritic knees.
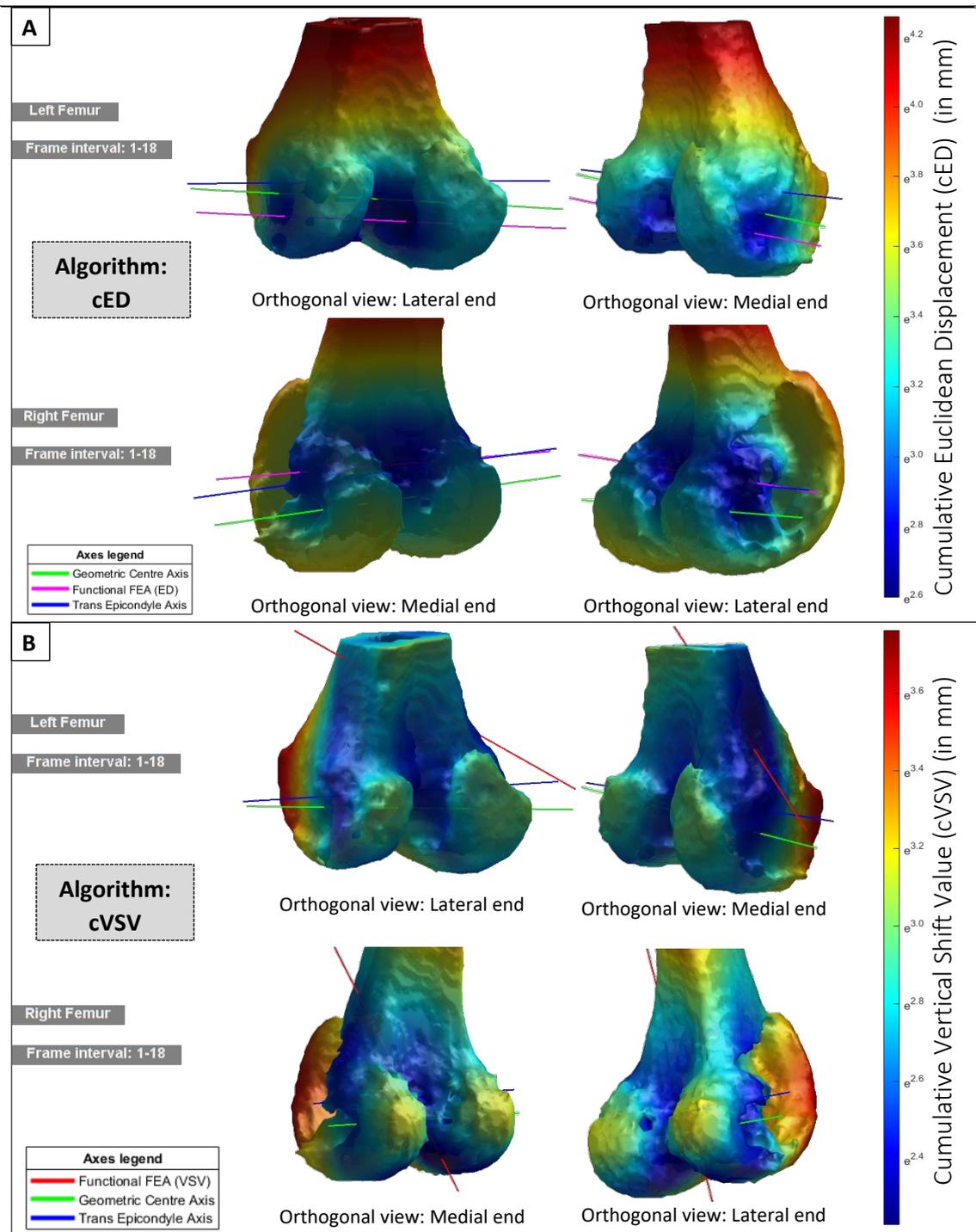
Figure 103: The Functional FE axis (FFA)– Participant P001

A: FFA results based on the cED algorithm. The inlays show the relationship between the FFA (cED axis in magenta), the TEA (blue) and GCA (green) for the left (top row) and right (bottom row) knees.
B: FFA results based on the cVSV algorithm. The inlays show the relationship between the FFA (cVSV axis in red), the TEA (blue) and GCA (green) for the left (top row) and right (bottom row) knees.
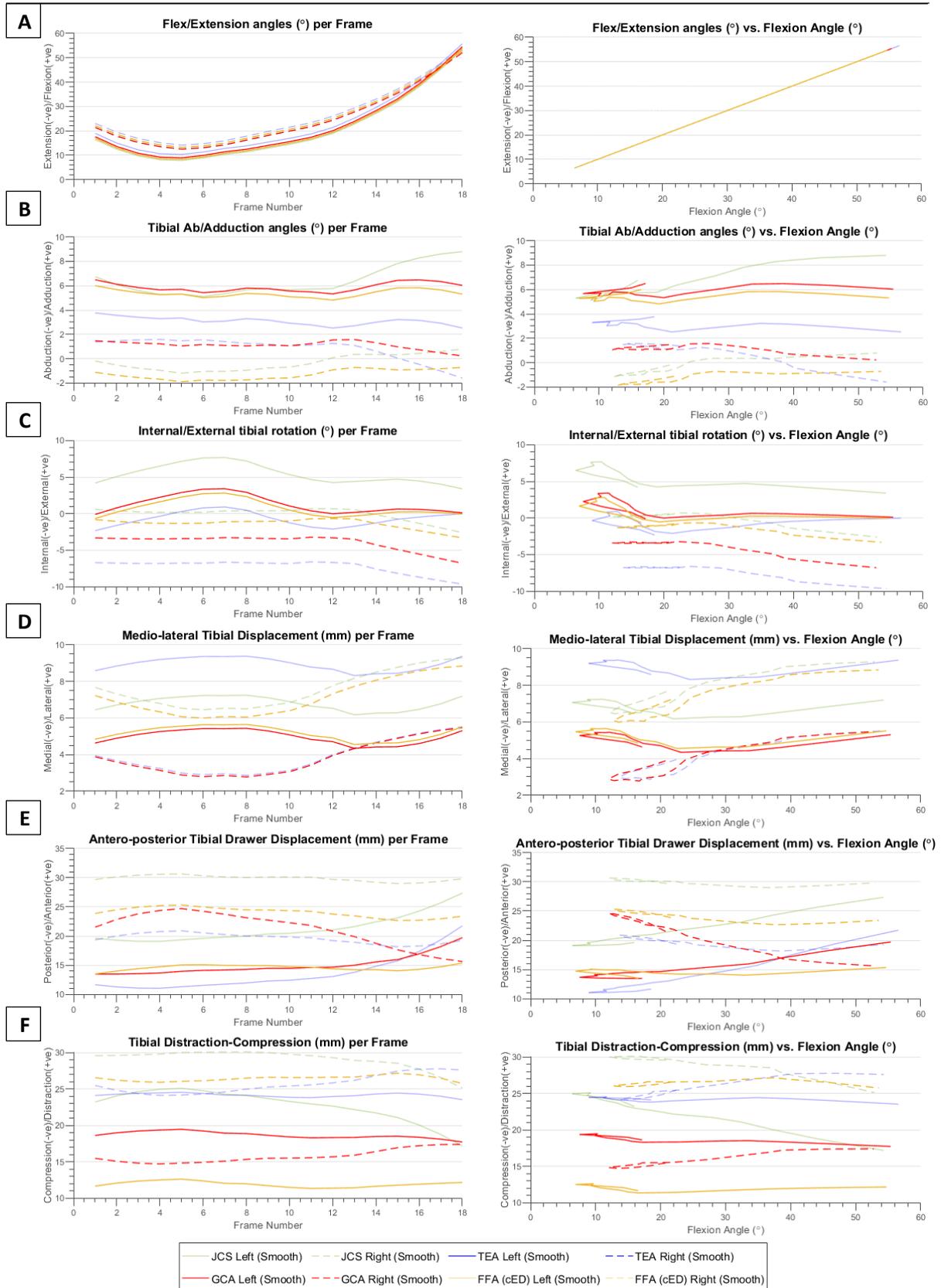
Figure 104: Kinematics for all FE axes for all 6 DOF of the knee – Participant P001

The kinematics based on the four FE axes variants, for the movement performed by patient participant P001. The rotational DOF (A-C) are presented per Frame (Left) and against the Flexion Angle (Right). The translational DOF (D-F) are presented per Frame (Left) and against Flexion Angle (Right).
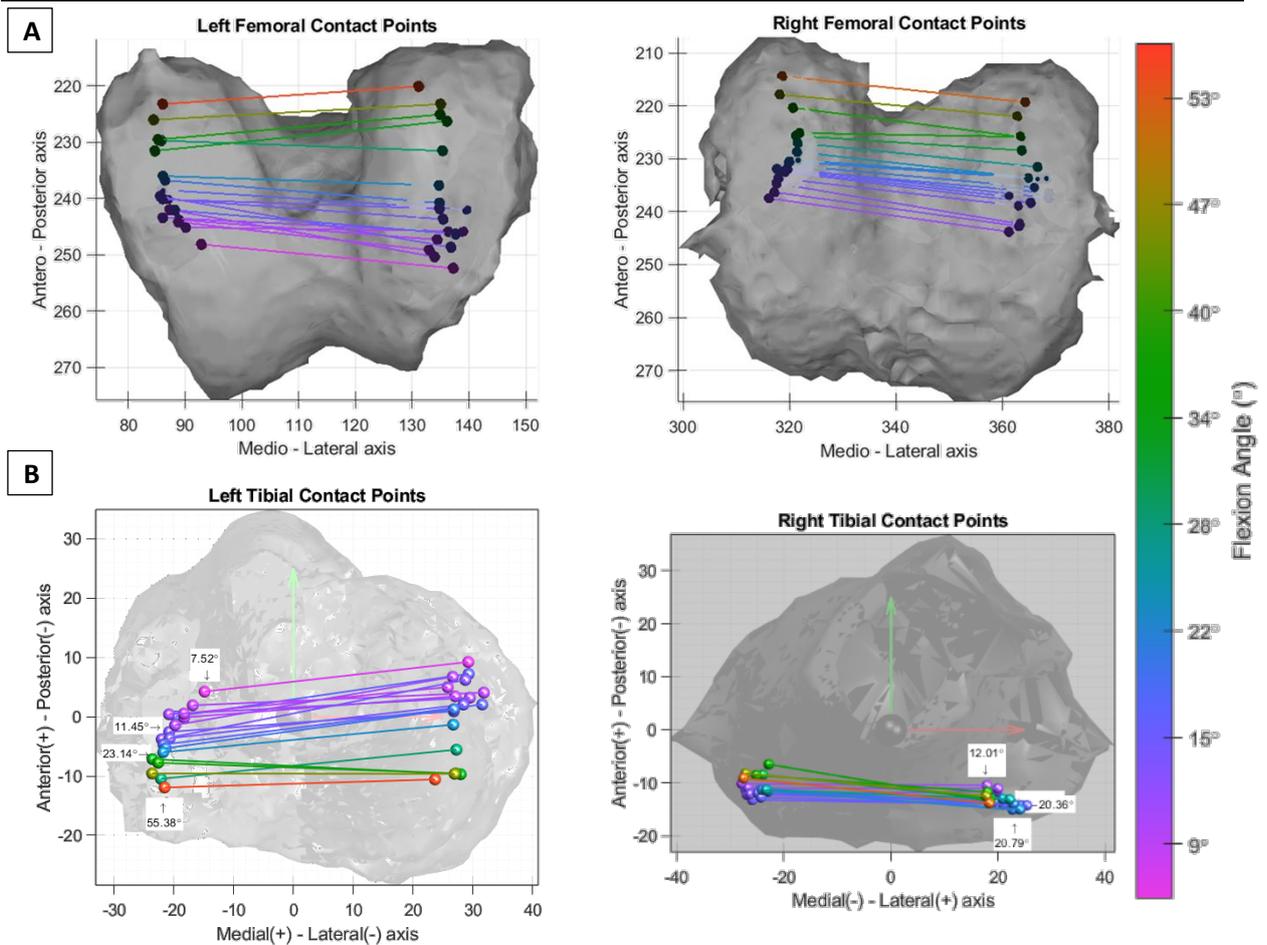
Figure 105: Tibiofemoral contact points - Participant P001

A: Femoral contact points calculated for the movement performed by patient participant P001.
B: Tibial contact points calculated for the movement performed by patient participant P001.
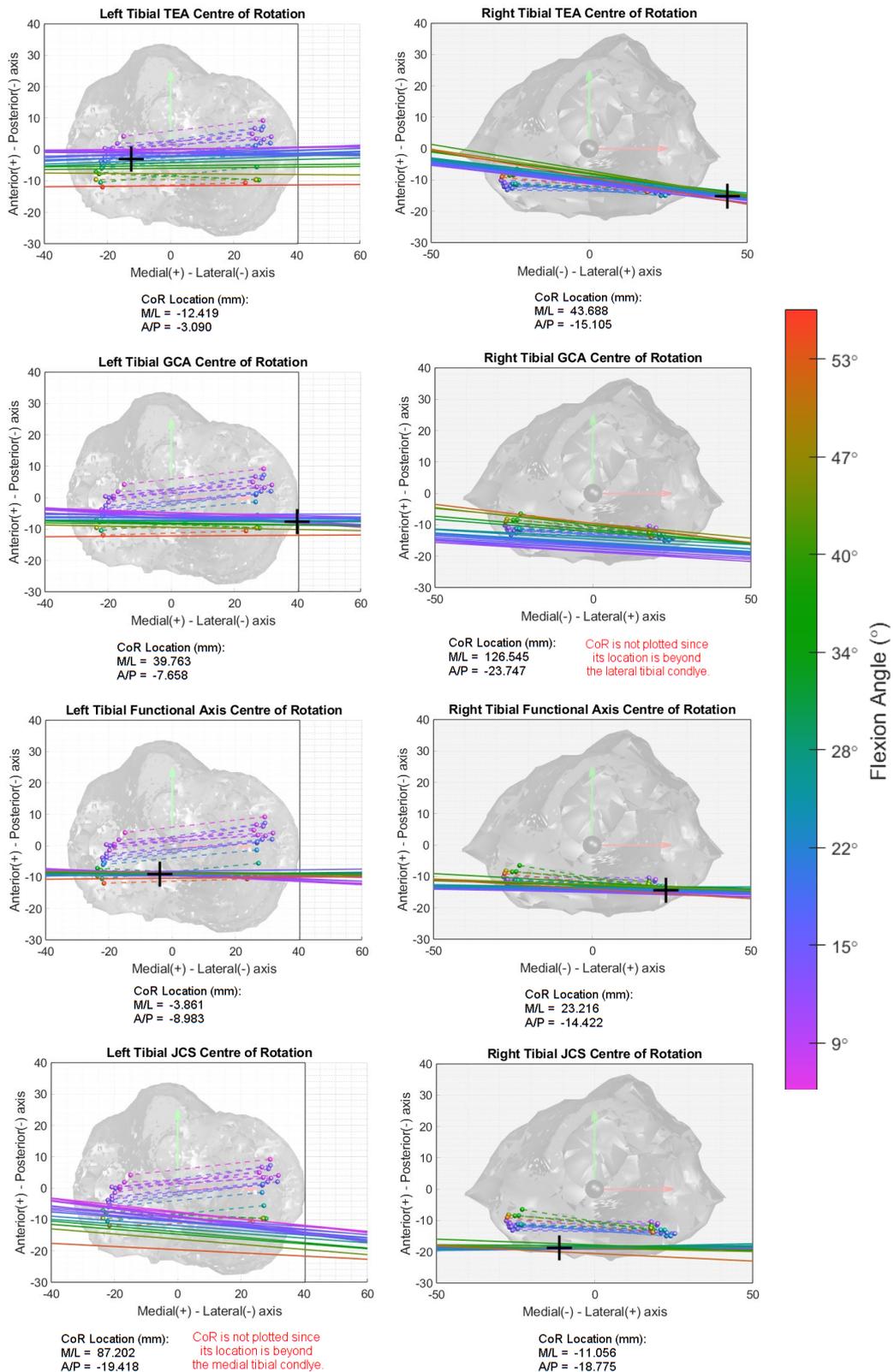
Figure 106: Axial Centre-of-Rotation of the four FE axis variants – Participant P001

The COR plots for the TEA, GCA, FFA and the JCS are plotted for the movement performed by patient participant P001. The location of each COR location is reported in terms of mediolateral and anteroposterior distance from the tibial origin. The COR location is plotted on each graph (unless it is outside the tibial plateau, in which case its location is defined by the red text below each plot).

Functional FEA

With reference to Figure 103, it can be noted that both algorithms for the FFA (Figure 103A – cED algorithm; B – cVSV algorithm) did not converge for P001, for both left and right knees. It was expected that the algorithm for the right replaced knee would converge to a location lying between the TEA and the GCA, given the captured ROM for P001. However, it should be noted that the design curvatures of the implants used in this study, which dictate the FEA that the implant is designed to rotate around, is not known. Therefore, the FFA results for the right knee cannot be really anticipated. However, as mentioned in section 4.1.4, the implants are advertised to achieve the natural kinematics of a healthy knee, so technically the same theory that applies to the healthy knees should apply to the replaced knees.

Regarding the cED based FFA, the left knee converged to a location distal and quasi-parallel to the GCA. Given that P001's ROM cycled between the transition and flexion phase, the resulting location of the FFA for the left knee is considered as non-converged. The cED based FFA for the right knee shows no correlation to the GCA (recall that the TEA is not confidently identified for this knee). Therefore, the cED based FFA is not considered to have converged and will be disregarded.

The results calculated for the cVSV based FFAs of both the left and right knee show very irregular locations for both converged results. Both cVSV based axes are to be disregarded. Therefore, in conclusion, the TEA and GCA are the only applicable axes to be considered for the left knee, while the GCA is the only applicable axes for the right knee. The mobility of the UC FB implant will hence be assessed based on the GCA results only while taking into consideration the recorded ROM.

Six DOF Kinematics

The six DOF kinematics for P001 are presented in Figure 104. While the results for all four FE axes are presented, the focus is given to the GCA results. The TEA, FFA and JCS are faded out since they are not applicable to this participants' replaced knee, as explained above.

With reference to the GCA based kinematic results, the first frame for P001 was captured as she was extending her knees at 17.15º for the left arthritic knee and 20.79º for the right UC FB knee. P001 continued to extend her knees until she reached 7.52º in her left knee and 12º in her right knee. The participant subsequently flexed her knee

until the last frame was captured at 55.38º for the left knee and 52.77º for the right knee (refer to Figure 104A). Considering that all participants were informed to extend their knees to the furthest extent possible, the results reported highlight the limitations that arthritic and replaced knees impose on the user. For arthritic knees, this is expected since the knee is swollen and the effectivity of the associated muscular and ligamentous structures in an arthritic knee is usually reduced leading to several limitations which restrict the normal motion of the degrading knee. The flexion angles reported for P001, show that the arthritic knee, which is already being limited due to its symptomatic nature still managed to achieve larger extension and flexion angles over the UC FB model. For the replaced knee, considering that this is an UC FB model, achieving hyper-flexion (beyond the 0º flexion mark) and angles of deep-flexion (usually beyond the 120º flexion mark) is difficult due to the constraints imposed by the UC design of the implant. This ultimately also has implication on the identification of the different phases of flexion, since the theoretical phases of flexion outlined in section 2.4 are not applicable to the replaced knee unless they were considered during the design stages of the implant. For this reason, the results presented for the replaced knees of all patient participants will only be compared to these theoretical phases of flexion to identify any relationships which might exist. With reference to addressing the secondary aim of this thesis, defined in section 3.2, the focus will be on the mobility of the replaced knee in terms of the capability of the two different implant modalities in achieving axial rotation and the corresponding AP motion with respect to the flexion angles.

The adduction angles reported for the movement performed by P001 (Figure 104B), show a quasi-parallel path when flexing and extending her knees. It can be noted that when the participant was changing from extension to flexion, there seems to have been a phase of instability in the arthritic knee. This effect was minimal in the replaced knee.

With reference to the axial rotation angles obtained for P001 (refer to Figure 104C), it can be noted how, although the left arthritic knee only extended to 17.15º (which technically falls within the Transition Phase of flexion) she still managed to achieve 3.6º of internal rotation during the screw-away mechanism. The late occurrence of the screw-away mechanism is being associated to the fact that the left knee is arthritic in nature, therefore as explained earlier, its ROM would have been considerably reduced such that the knee is not capable of extending as far as a healthy knee, therefore pushing the screw-away mechanism initiation point along with it. Subsequently, the knee shows

a clear change in gradient when it reaches the 0º axial rotation mark, identifying the terminal stages of the screw-away mechanism. The left knee then proceeded to maintain the axial rotation position until the last frame of capture, which contradicts theory since a healthy knee usually maintains a slight internal tibial rotation for the captured ROM.

Moving on to the right UC FB knee, the axial rotation angles calculated for this knee followed expected theoretical profiles for FB implants. The UC FB knee showed no signs of screw-away during its early stages of extension, which was expected considering the fixed bearing nature of the design. Subsequently, as the knee progressed with flexion, the right knee displayed 4.1º of further internal rotation according to the GCA. While this internal rotation agrees with the theory for healthy knees, this gradual internal rotation could be occurring as a result of kinematic crosstalk of the GCA. This might occur in the case that the GCA is not aligned with the FEA that the implant was designed to rotate around, therefore, experiencing out of plane motion.

The AP translation results for P001, presented in Figure 104E, show that the left arthritic knee still managed minor anterior tibial displacement with increasing flexion, which is in agreement with AP translations for a healthy knee. The right UC FB knee displayed the controversial paradoxical anterior femoral movement, which is known to occur in replaced knees. This happens due to the removal of the PCL, which controls anterior femoral translation with progressive flexion. Considering that this is a UC FB knee, 8.8mm of anterior translation is considerable and might be as a result of kinematic crosstalk of the GCA. Recall that it is not known what axis is utilised for the femoral component of the BBraun implants used in this study. With reference to the FFA based kinematics for the right knee (which is located in the region of the epicondyles for this knee), it can be noted that the AP translation undergoes much smaller magnitudes of posterior translation (range of 3.1 mm), which is more realistic when considering the design features of this implant.

The PD translation results for the left knee followed theoretical profiles, such that the femur moved distally during the screw-away mechanism due to the downward tibial slope. Subsequently, gradual distal movement of the femur occurs, which is expected. Contrariwise, the right replaced knee displayed proximal femoral translation (distraction) with progressing flexion over a range of 3 mm throughout the captured ROM, stabilising towards the last 10º of flexion. This movement is also contradictory in nature, since considering that this is an ultra-congruent implant, the design of the

femoral component should consistently correspond with the design of the tibial insert. This distraction might be as a result of an incorrectly chosen axis of rotation for the femoral component. If this is the case, the femoral component will create out-of-plane movement with increasing flexion, therefore pushing the femur (or tibia) to lift-off in order to accommodate the out-of-plane motion. Here it should be noted that the FFA based results also reported increasing distraction with increasing flexion, but again with a slightly smaller range (2 mm).

With reference to the AP and PD translations reported by the GCA and FFA, the one showing the least kinematic crosstalk can be derived using the same reasoning used with control participant data (Figure 84 and Figure 92). Considering the locations of the GCA and FFA, if the femur was translating anteriorly while rotating around the FFA, it is expected that the GCA based kinematics would report larger tibial posterior translations and increased knee distraction (tibial distal translation). Conversely, if the femur was translating anteriorly while rotating around the GCA, then it is expected that the FFA based kinematics would report smaller tibial posterior translations and increased compression (tibial proximal translation) in relation to the GCA values. By referring to the AP and PD translations reported by both the GCA and FFA, it can be noted that the GCA displays both larger tibial posterior translations and tibial distal translations, while the FFA does display smaller tibial posterior translations but compression was only marginal. Therefore it can be inferred that for P001, the FFA (whose relative position is not defined) is considered to approximate the axis of rotation of the femoral component better than the GCA. This supports the same conclusion, which was derived using the data for AP translations above; that is, the implant is showing preference towards an axis that passes through the epicondylar region.

Tibiofemoral Contact Points

The TF contact point results for P001 are presented in Figure 105 (A – Femoral CPs; B – Tibial CPs). For the left arthritic knee the CPs on the lateral side show posterior translation with progressing flexion, but medially the CPs also posteriorly translate with increasing flexion which does not agree with healthy knee theory. As a result, the CPs did not display the expected medial pivoting, which is correlated to the fact that the knee is arthritic.

The reported CPs for the right replaced knee were as expected. Due to the UC FB design, the femur is constrained in the axial and AP direction, such that all the CPs lie in the same region, for both the medial and lateral condyles. These results highlight the extent of the constraints that exists in the kinematics which this kind of implant imposes on the replaced knee.

Axial COR

The axial COR results calculated for P001 are presented in Figure 106. The TEA based axial COR results for the left arthritic knee show lateral pivoting and posterior medial translation, which do not agree with theory and are correlated to the arthritic nature of the knee.

For the right replaced knee, the TEA based axial COR results for the right knee are externally rotated with respect to the underlying CPs, which further supports the statement above that the TEA is not confidently identified and should be disregarded for P001.

The axial COR results for the GCA of the left knee again show gradual agreement with the underlying CPs with progressing flexion. The results for the right knee show that the GCA is not in agreement with the underlying CPs until roughly the 30º flexion mark, which further support the above-mentioned statement that the knee is not rotating around this axis. However, the tibial axial plot for the FFA shows a closer relationship between the CPs and the projected axes. This further supports the statement above, that the FFA (which lies close to the assumed location of the TEA) is showing signs of approximation to the axis of rotation of the femoral implant.

In summary, the results calculated for P001, show that the left arthritic knee displayed similar trends to the control participants, such as rotation around the TEA in the early stages of flexion, followed by transitioning of the axis of rotation to the GCA. Nonetheless, the kinematics showed considerable variations from those of healthy knee. On the other hand, the right replaced knee displayed expected trends for a UC FB knee. The paradoxical posterior tibial translation and the marginal signs of axial rotation are characteristic of such designs, due to their highly constrained nature. Also, the FFA results showed signs of approximation to the axis of rotation due to more stable kinematic results and agreement between the CPs and axial profiles. This will be discussed further in the holistic discussion in chapter 6.

5.6   PATIENT PARTICIPANT #2

Patient participant #2 had a left arthritic knee and a right replaced knee. The replaced knee was an Ultra-Congruent Mobile bearing knee. Patient participant #2 performed the cyclic flexion-extension exercise while in the supine position with the elevated cushion under her knees to maximise the ROM. The movement that was captured was similar to that of P001, where the first frame was captured from circa 25º of flexion as the participant was extending her knees. Subsequently, she extended her knees to her maximum allowable extension and then proceeded to flex her knees until the last frame was captured at circa 55º of flexion. The following participant data was collected for Patient Participant #2:

- Reference: P002
- Age: 72 years
- Gender: Female
- Left Knee: Arthritic with signs of osteophyte growth on the peripheries of the femoral condyles (refer to left knee models in Figure 107).
- Right Knee: Replaced with an Ultra-Congruent Mobile Bearing BBraun implant.

Similar to P001, the TEA location identified for the right knee is being considered to be incorrect, since the epicondyles could not be confidently identified. The bone in the medial and lateral epicondylar area was primarily affected by metal artefacts such that the bone in this area was segmented due to the SEMAR processing.

Also, the analysis of the left knee is only going to be presented and briefly discussed for reference only, since the knee is considered to be arthritic. This thesis is focusing solely on the kinematics of healthy and replaced knees, therefore considering that the kinematics of the degrading knee are known to be different from the kinematics of healthy or replaced knees, the analysis of such arthritic knees is beyond the scope of this thesis.
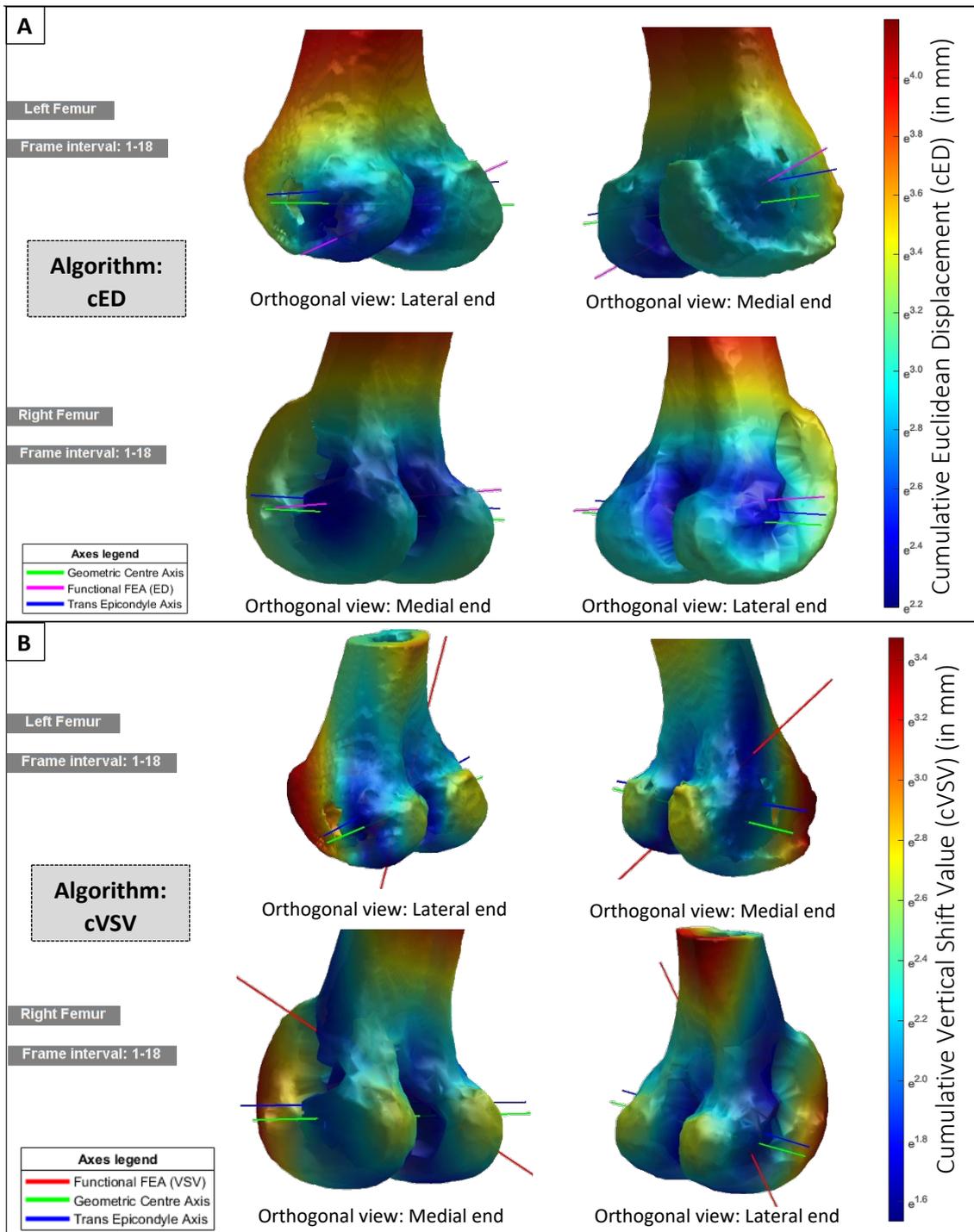
Figure 107: The Functional FE axis (FFA)– Participant P002

A: FFA results based on the cED algorithm. The inlays show the relationship between the FFA (cED axis in magenta), the TEA (blue) and GCA (green) for the left (top row) and right (bottom row) knees.
B: FFA results based on the cVSV algorithm. The inlays show the relationship between the FFA (cVSV axis in red), the TEA (blue) and GCA (green) for the left (top row) and right (bottom row) knees.
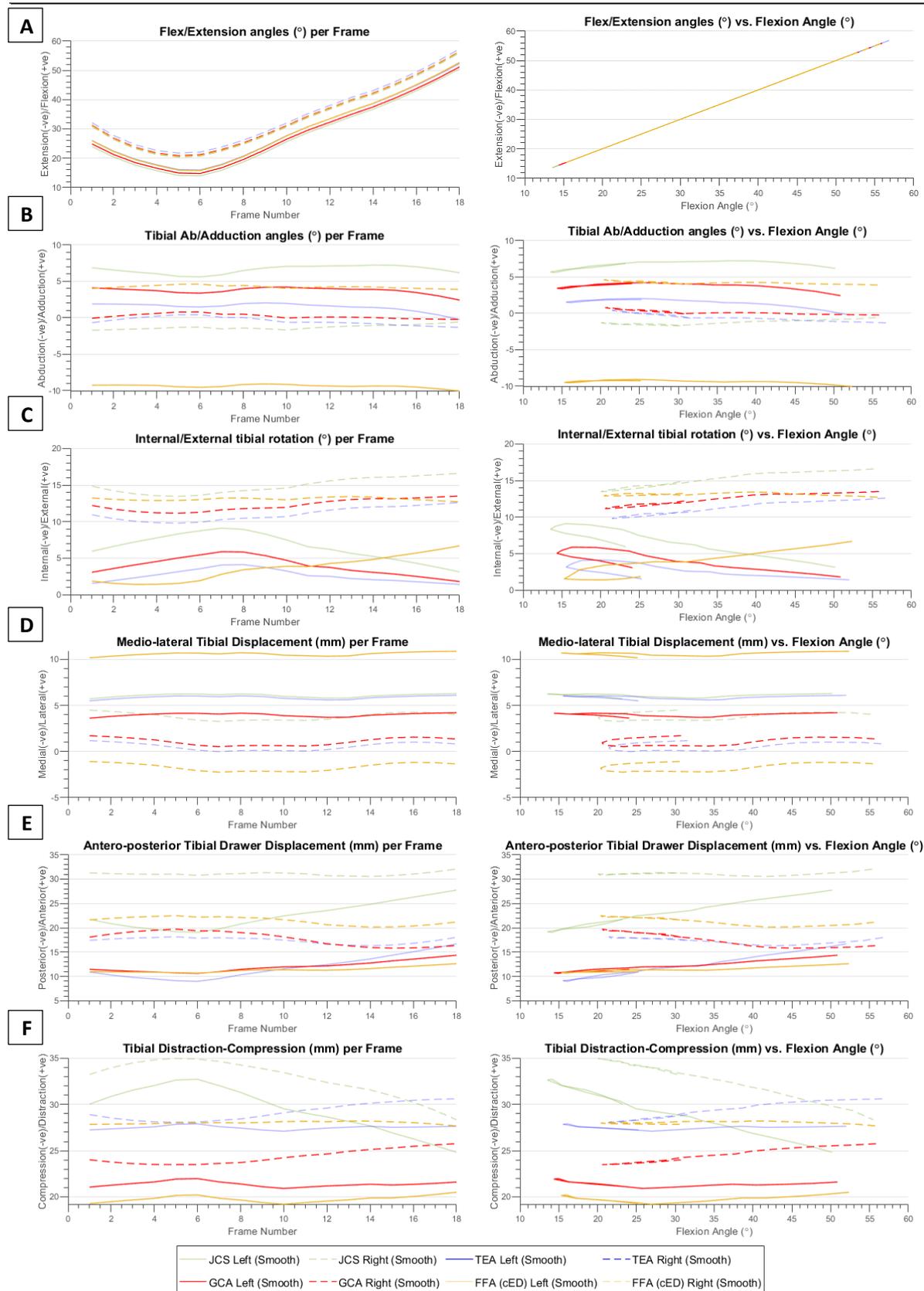
Figure 108: Kinematics for all FE axes for all 6 DOF of the knee – Participant P002

The kinematics based on the four FE axes variants, for the movement performed by patient participant P002. The rotational DOF (A-C) are presented per Frame (Left) and against the Flexion Angle (Right). The translational DOF (D-F) are presented per Frame (Left) and against Flexion Angle (Right).
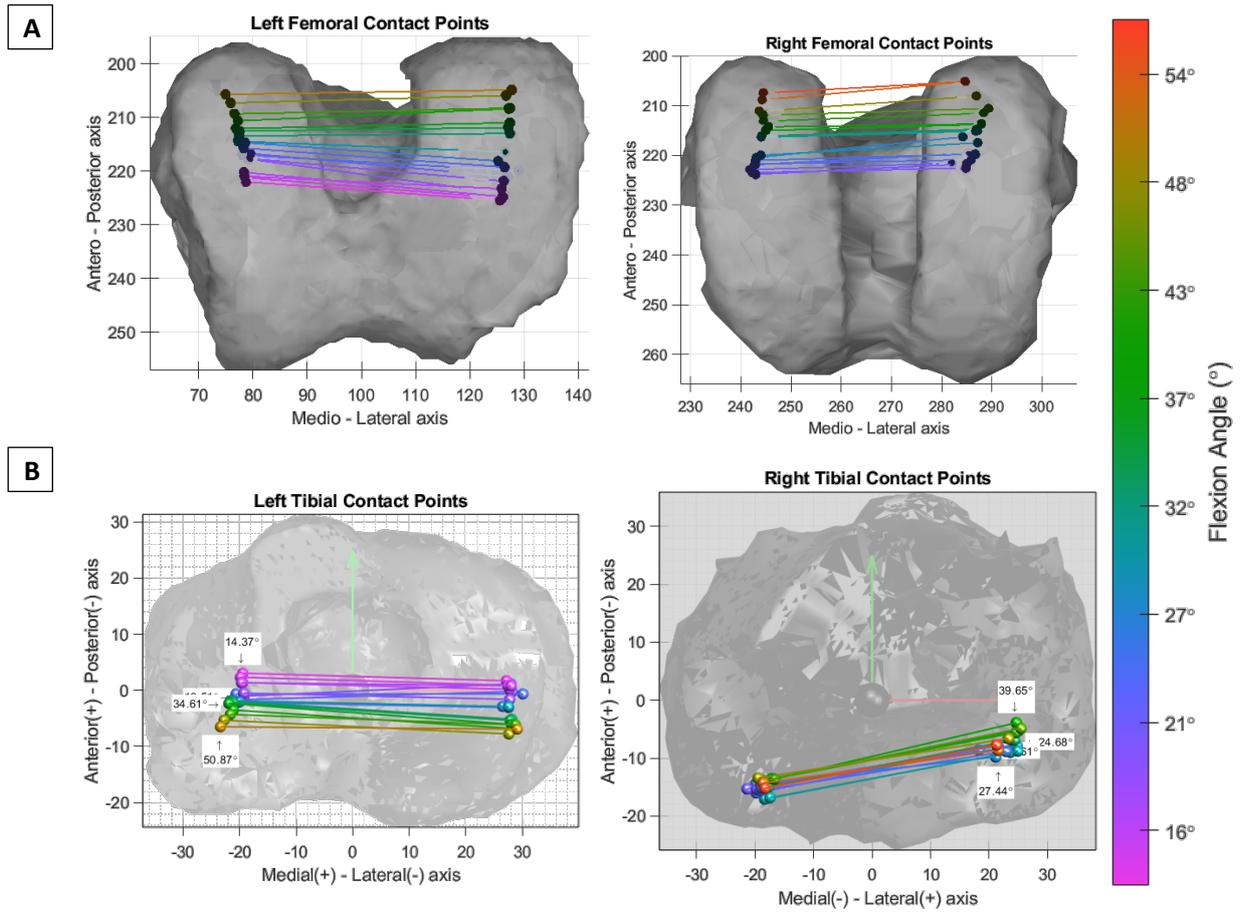
Figure 109: Tibiofemoral contact points - Participant P002

A: Femoral contact points calculated for the movement performed by control participant P002.
B: Tibial contact points calculated for the movement performed by control participant P002.
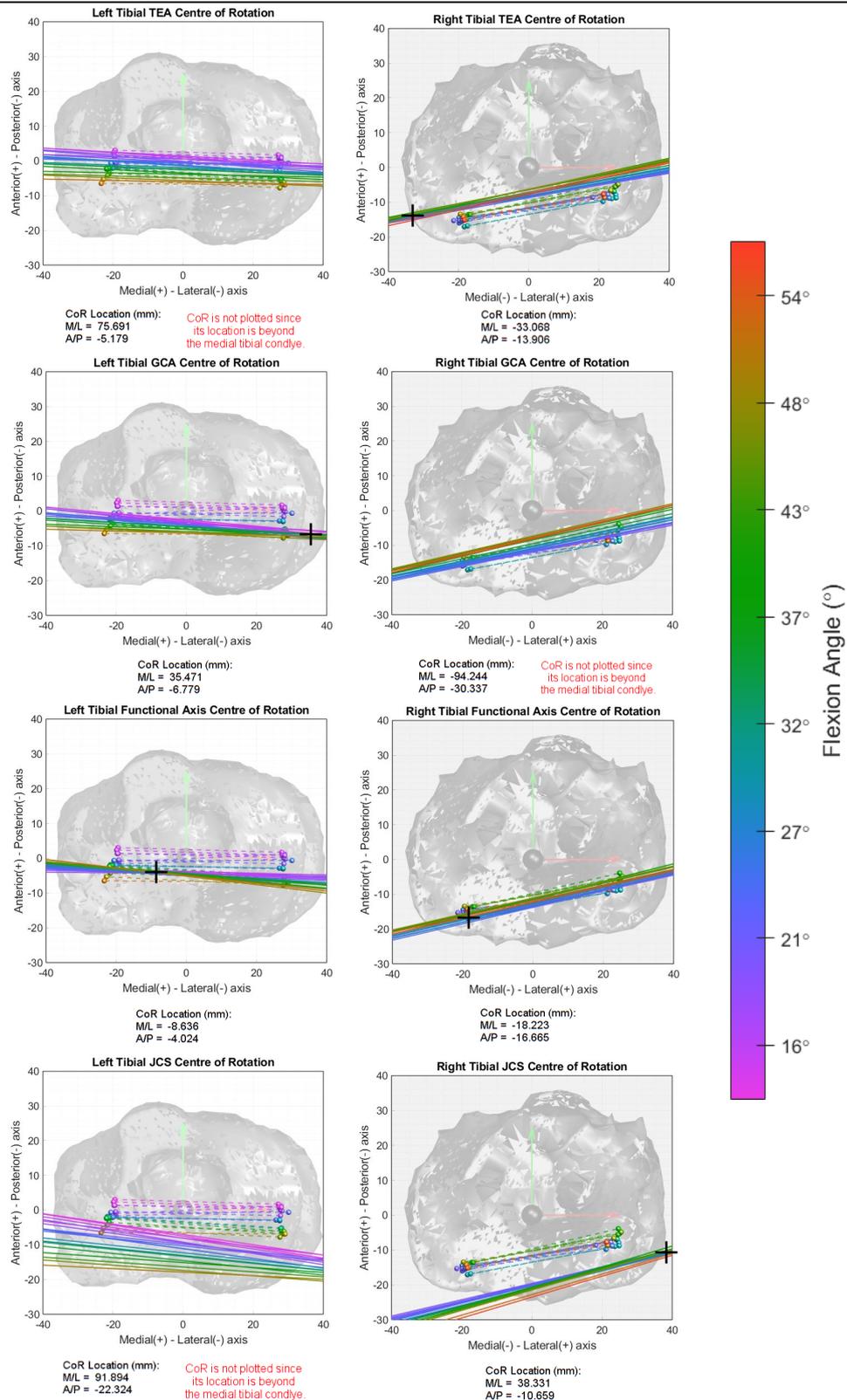
Figure 110: Axial Centre-of-Rotation of the four FE axis variants – Participant P002

The COR plots for the TEA, GCA, FFA and the JCS are plotted for the movement performed by patient participant P002. The location of each COR location is reported in terms of mediolateral and anteroposterior distance from the tibial origin. The COR location is plotted on each graph (unless it is outside the tibial plateau, in which case its location is defined by the red text below each plot).

Functional FEA

The results for the FFA are presented in Figure 107 (A – cED algorithm; B – cVSV algorithm). The cED based FFA for the left knee did not converge and will be disregarded in the kinematic analysis of P002. Conversely, the cED based FFA for the right knee converged to a location slightly proximal to the GCA. Medially it intercepts the medial condyle proximal and slightly posterior to the GCA, while laterally the FFA intercepts the lateral condyle proximal and anterior to the GCA, approximating the location of the FFA for the replaced knee of P001. While this shows disagreement with the expected FFA for a healthy knee, this is a replaced knee, and it is expected that the FFA will converge to a location close to the axis of rotation of the femoral component (which is not known). Therefore, based on the above, the cED based FFA result for the right knee is going to be considered and the kinematic results obtained for this axis will be used to determine if this axis shows signs of kinematic crosstalk in comparison to the GCA.

The results for the cVSV based FFAs of both the left and right knee show very irregular locations for both knees, similar to the cVSV results obtained for P001. Therefore, in conclusion, since no FFA converged for the left knee, only the TEA and GCA are being considered as applicable FFAs for this knee. Contralaterally, only the cED based FFA converged for the right knee, such that the GCA and the cED based FFA are being considered as applicable for the right replaced knee.

Six DOF Kinematics

The six DOF kinematics for P002 are presented in Figure 108. While the results for all four FE axes are presented, the focus is given to the GCA and FFA based results. The TEA and JCS are faded since they are not applicable to this participants' replaced knee, as explained above.

With reference to the GCA based kinematic results, the first frame for P002 was captured as she was extending her knees at 24.1º for the left arthritic knee and 30.7º for the right replaced knee. P002 continued to extend her knees until she reached 14.4º for the left knee and 20.6º for the right knee. P002 subsequently flexed her knee until the last frame was captured at 50.9º for the left knee and 56º for the right knee (refer to Figure 108A). Similar to the results obtained for P001, the replaced knee didn't manage to extend as much as the contralateral non-replaced knee. This is a limitation in the

design of UC implants, which restricts the ROM of the knee due to the anterior ridge, which limits the knee from going into extension, not to mention hyperextension.

The adduction angles recorded for both knees show that the movement performed by P002 was as instructed, whereas the knees were kept parallel to each other in order to avoid having a closed kinematic chain which would impact the results obtained.

With reference to the axial rotation results calculated for P002 (refer to Figure 108C), the left arthritic knee shows constant internal tibial rotation, but no sign of the screw-away mechanism. This could be either due to the arthritic nature of the knee, or else due to the patient not extending her left knee enough to activate the screw-home mechanism. With reference to the ROM of P002, it can be noted that similar to the ROM of P001 the arthritic knee did not extend into the Extension phase of flexion. While the axial rotation results for P001 showed clear signs of the screw-away mechanism, the axial rotation results for P002 did not. Contralaterally, the axial rotation of the UC MB knee showed slight external rotation over a range of 3º, which is similar to P001. On the other hand, the FFA results displayed an external rotation of 1.7º. Considering that the axial rotation of the FB implant of P001 had a range of 4.1º and the axial rotation for the MB implant had a range of 3º for the same FEA, then it can be inferred that the implied mobility of the mobile bearing implant is not evident for P002, but rather diminished.

The AP and PD translation results for P002 are presented in Figure 108E and F. The left tibia translated anteriorly and slightly compressed with increasing flexion, as expected. Here it can be noted how both the AP and PD translation for the TEA and GCA of the left arthritic knee follow the same trends identified earlier (Figure 84 and Figure 92) but displaying smaller magnitudes. This indicates that the TEA is approximating the anatomical FEA during the early stages of flexion after which the GCA approximated the anatomical FEA.

The right UC MB knee translated posteriorly, which reflects the results obtained for the P001. Here it should be pointed out that the GCA results reported 4.2 mm of posterior tibial translation, while the FFA results reported a 2.1 mm translation. Similar to the reasoning used for P001, the AP and PD translation data will be used to identify which axes amongst the GCA and FFA best approximates the anatomical FEA. With reference to the PD translation recorded for the right replaced knee, the GCA kinematics reported

that throughout the ROM of P002 the femur distracted by a range of 2.6 mm, while the FFA kinematics reported that the femur distracted by a marginal 1mm. Therefore, using the same reasoning which was used for other participants for these DOF, the FFA is considered to approximate the axis of rotation of the femoral component better than the GCA.

Tibiofemoral Contact Points

The TF contact point results for P002 are presented in Figure 109. For the left arthritic knee, the CPs show a quasi-parallel orientation, which is similar to the CPs identified for the arthritic knee of P001, except that the CPs for P002 cover a smaller range in the AP direction. The CPs support the assumption that the left arthritic knee did not go through the Extension phase of flexion (thus not capturing the screw-away mechanism). The left arthritic knee again failed to show the medial pivoting, which is expected for the given ROM. This is attributed to the arthritic nature of the knee.

The CPs for the right UC MB knee, showed no signs of axial rotation, which the mobile bearing implant should be achieving, given its design. The CPs also show a malalignment in the relationship between the CPs and the Tibial CS (shown faded in the centre). This either represents a mal-aligned component which resulted in permanently rotating the femur internally, or the tibial mobile insert is locked in place forcing the femur into an internally rotated orientation. These results further support the statement given earlier, where it was stated that the mobility of the mobile bearing implant is evidently inexistent.

Axial COR

The axial COR results calculated for P002 are presented in Figure 110. The TEA based axial COR results for the left arthritic knee shows alignment with the underlying CPs for the captured ROM. Conversely, the GCA results better relate to the expected results for a healthy knee, since the GCA COR identifies medial pivoting and the CPs for angles smaller than 30º (the extension phase) lie anterior to the GCA profiles, while the CPs above 30º align with the GCA profiles. In view of these left knee tibial axial plot results for the TEA and GCA, these results support the statement that the TEA is initially approximating the anatomical FEA followed by the GCA.

The TEA axial COR results for the right knee can be disregarded as the TEA is not applicable for the replaced knee. The axial COR results for the GCA show considerable

agreement with the underlying CPs, although the axial profiles are slightly translated anteriorly. The axial COR results for the FFA on the right knee show better agreement with the underlying CPs since they overlay the CP locations throughout the entire captured ROM. Furthermore, the location of the axial COR is located directly above the medial CPs. Therefore, the results for the GCA and FFA of this replaced knee, also support the aforementioned statement that the FFA (which again lied proximal to the GCA in the region of the TEA) better approximates the axis of rotation of the femoral component than the GCA.

In conclusion, the results for P002, have shown that the left arthritic knee displayed similarities with the kinematics of healthy knees for the captured ROM, which shows that the arthritic nature of the knee is not yet advanced enough to modify its kinematics considerably. Nonetheless, the arthritic knee did not display any sign of medial pivoting due to the posteriorly translating medial CPs, which is being assumed to be occurring due to the arthritic nature of the knee. In contrast, the right replaced knee failed to display any sign of axial rotation, which should be occurring given the mobility design factor of such an implant. Furthermore, the femur is internally rotated with respect to the tibia, which might be due to the tibial insert being stuck in an internally rotated position, or else due to a poorly aligned tibial plate during surgery. Similar to the results for P001, the cED based FFA (which approximates the TEA) displayed a closer relation the axis of rotation of the femoral component in comparison to the GCA, which supports the assumption that this implant design is using the TEA as its singular-FEA.

5.7   PATIENT PARTICIPANT #3

Patient participant #3 had a Left replaced knee and a Right arthritic knee. The replaced knee was an Ultra-Congruent Fixed-Bearing knee. Patient participant #3 performed the cyclic flexion-extension exercise while in the supine position with an elevated cushion under his knees. The movement was captured from circa 20º of flexion as the participant was extending his knees. Subsequently, he extended to his maximum allowable extension and then proceeded to flex his knees until the last captured frame at circa 60º of flexion. The following participant data was collected for Patient Participant #3:

- Reference: P003
- Age: 56 years
- Gender: Male
- Left Knee: Replaced with an Ultra-Congruent Fixed-Bearing BBraun implant.
- Right Knee: Arthritic with clear signs of osteophyte growth on the peripheries of the femoral condyles and reduced bone thickness at the condylar level (refer to right knee models in Figure 111).

The TEA identified for the left replaced knee is to be disregarded for this participant as well, since, similar to the previous participants, the medial and lateral epicondyles could not be confidently identified. Also, the analysis of the right knee is going to be presented for informational purposes only since the kinematic analysis of arthritic knees is beyond the scope of this thesis.
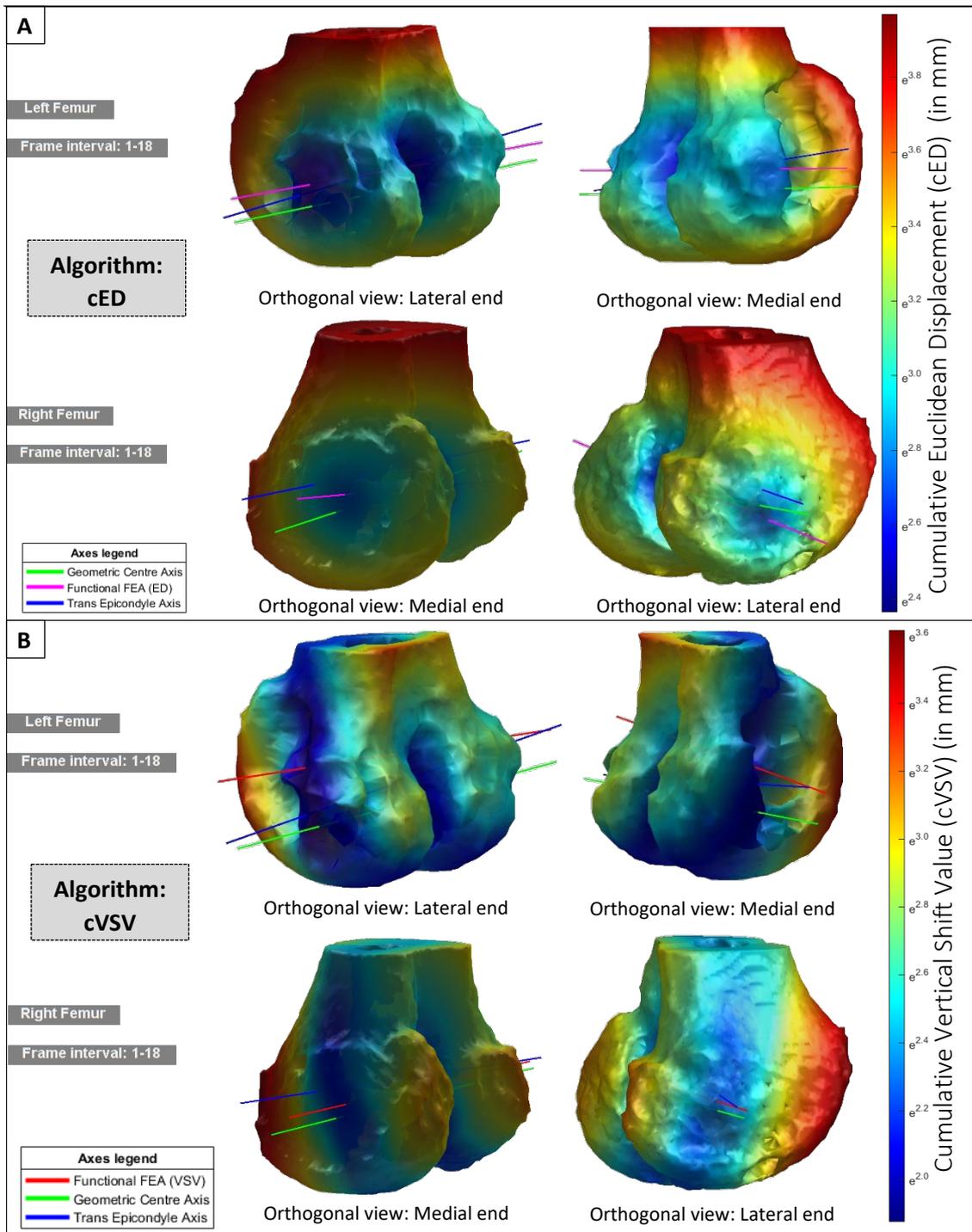
Figure 111: The Functional FE axis (FFA)– Participant P003

A: FFA results based on the cED algorithm. The inlays show the relationship between the FFA (cED axis in magenta), the TEA (blue) and GCA (green) for the left (top row) and right (bottom row) knees.
B: FFA results based on the cVSV algorithm. The inlays show the relationship between the FFA (cVSV axis in red), the TEA (blue) and GCA (green) for the left (top row) and right (bottom row) knees.
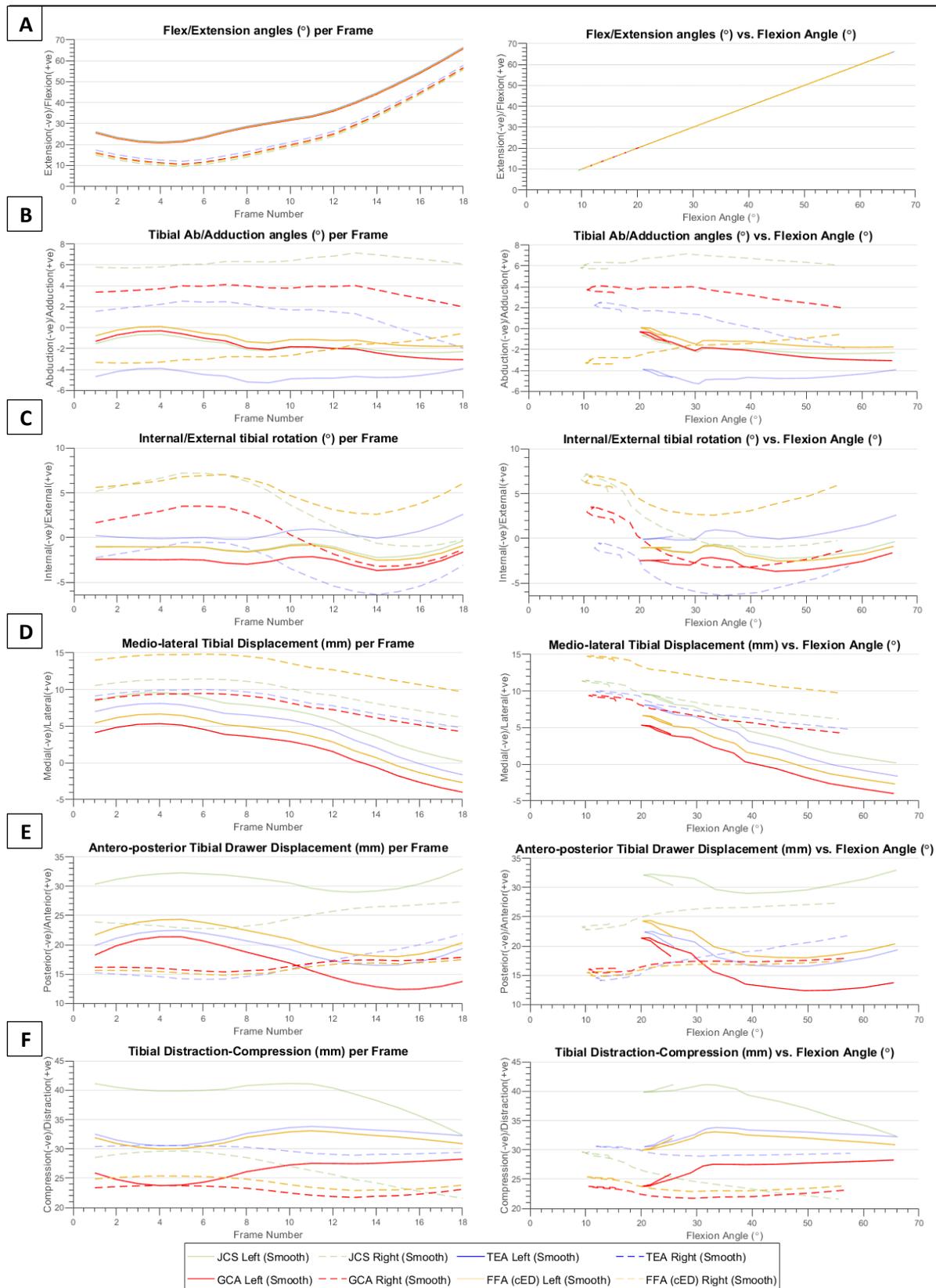
Figure 112: Kinematics for all FE axes for all 6 DOF of the knee – Participant P003

The kinematics based on the four FE axes variants, for the movement performed by patient participant P003. The rotational DOF (A-C) are presented per Frame (Left) and against the Flexion Angle (Right). The translational DOF (D-F) are presented per Frame (Left) and against Flexion Angle (Right).
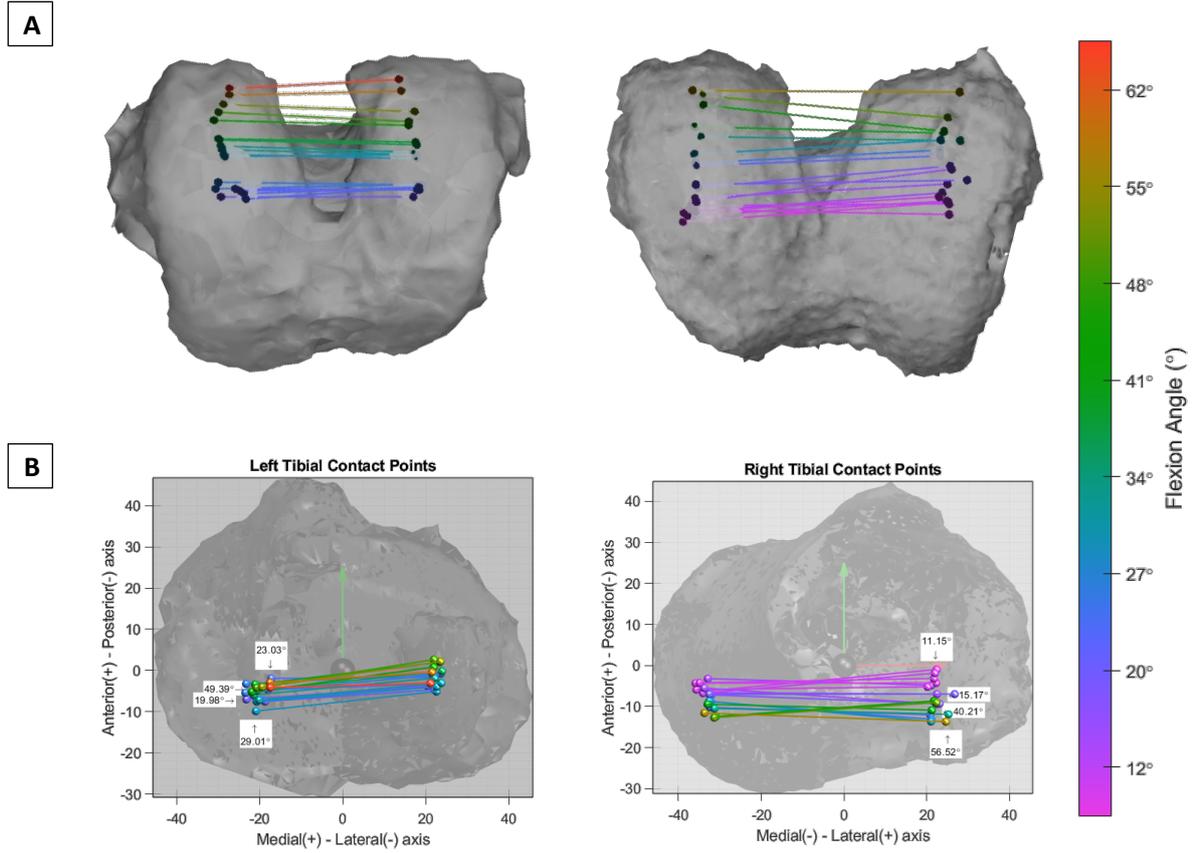
Figure 113: Tibiofemoral contact points - Participant P003

A: Femoral contact points calculated for the movement performed by control participant P003.
B: Tibial contact points calculated for the movement performed by control participant P003.
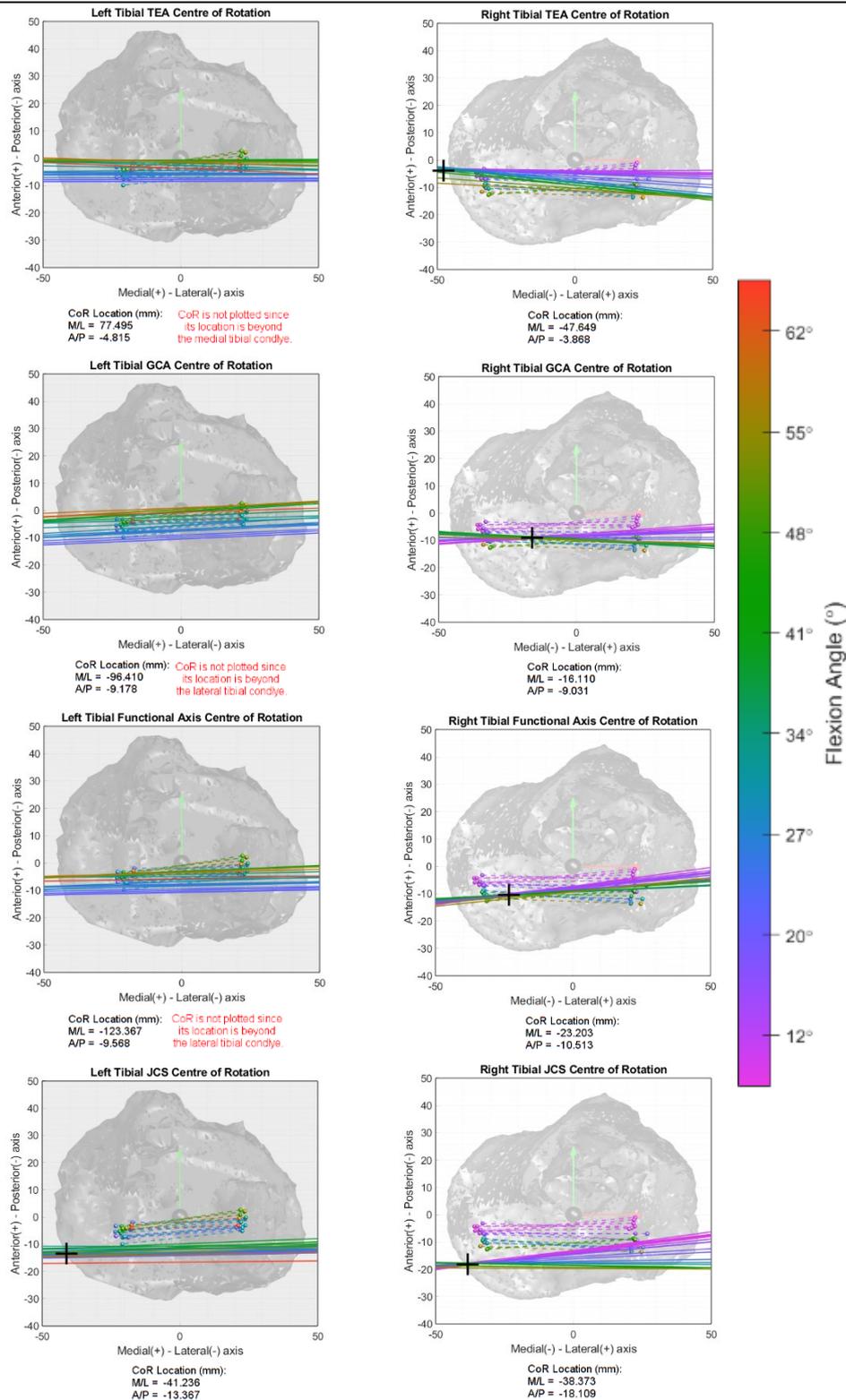
Figure 114: Axial Centre-of-Rotation of the four FE axis variants – Participant P003

The COR plots for the TEA, GCA, FFA and the JCS are plotted for the movement performed by patient participant P003. The location of each COR location is reported in terms of mediolateral and anteroposterior distance from the tibial origin. The COR location is plotted on each graph (unless it is outside the tibial plateau, in which case its location is defined by the red text below each plot).

Functional FEA

The results for the FFA are presented in Figure 111 (A – cED algorithm; B – cVSV algorithm). The cED based FFA for the left replaced knee converged to a location proximal to the GCA. Medially, the FFA intercepts the medial condyle proximal and slightly posterior to the GCA, while laterally the FFA intercepted the lateral condyle proximally and also slightly posterior to the GCA. This resulted in the FFA showing a quasi-parallel orientation to the GCA. The resulting FFA for the left replaced knee was noted to lie in a similar location to the converged cED based FFA for the replaced knee of P001 and P002. The cED based FFA for the arthritic right knee was located proximal to the GCA medially and distal to it laterally. This resulted in a skewed axis in relation to both the GCA and TEA, such that it can be presumed that the algorithm did not have enough data points to converge for this knee.

The results for the cVSV based FFA of the left knee did not converge, as it was calculated to lie very proximal to the GCA. Contralaterally, the cVSV based FFA for the arthritic right knee converged close to the GCA, showing a quasi-parallel orientation to it. Medially, it intersected the condyle slightly proximal and anterior to the GCA, while laterally it intersected the condyle right in between the TEA and GCA intersection points which agrees with the expected location for the captured ROM of P003.

Therefore in conclusion, ideally the cED based FFA would be considered for the left knee, while the cVSV based FFA would be considered for the right knee. Regrettably, the kinematic analysis software was only coded to choose either the cED or the cVSV axes and not a selection of each. Therefore, due to this limitation, and considering that the results for P003 are concerned with the kinematics for the replaced knee, the cED based FFA will be chosen since this algorithm best fitted the FFA of the left replaced knee. As a result, the FFA for the right knee will not be considered as applicable for the aforementioned converged cED based results for this knee.

In summary, the cED based FFA and the GCA are being considered as applicable for the left replaced knee, while the GCA and TEA are being considered as applicable for the arthritic right knee.

Six DOF Kinematics

The six DOF kinematics for P003 are presented in Figure 112. Focus is given to the GCA and FFA results, as these are the axes which are being considered as applicable for the left replaced knee.

With reference to the GCA based kinematic results in Figure 112A, the first frame captured for P003's movement occurred as he was extending his knee at 25.4º of flexion for the left knee and 15.5º of flexion for the right knee. P003 then extended his knees to the maximum allowable extension angles of 20º for the left knee and 10.5º for the right knee. Subsequently, he kept flexing his knees until the last frame was captured at 65.5º for the left knee and 56.5º for the right knee. This resulted in the participant covering a maximum flexion range of 45.5º for the left knee and 46º for the right knee. Again, the replaced knee was not allowed to extend as far as the arthritic knee. This is becoming a clear trend in the result obtained so far, whereas the replaced UC design imposes limitations on the ROM which the patient manages to achieve, mostly in their "Extension phase".

The adduction angles reported for both knees show that the movement performed by P003 followed the given instructions, apart for some slight abduction with progressive flexion. Also, for the left replaced knee a sudden but minor change in the adduction angles was noted at the 30º flexion mark, which is being considered to have occurred as a result of P003 correcting his motion pathway. It can be noted that before the 30º mark P003 was considerably abducting his left knee, and after 30º the abduction was muted. With reference to the flexion angles vs frame plot, this correction is also noted, as the flexion gradient is reduced following frame 9 (equivalent to 30º of flexion), resembling the slight reduction in flexion speed, to allow for the correction in the adduction angles.

With reference to the axial rotation results calculated for P003 (refer to Figure 112C), the left replaced knee did not display any sign of axial rotation in its early stages of extension, neither during the screw-home mechanism nor during the screw-away mechanism. Subsequently, at circa 30º of flexion, the replaced knee displays a sudden 1.5º external rotation which is recovered by the 40º flexion mark. This paradoxical axial rotation is being linked to the participants' correction of his motion pathway, whereby the knee reacted to the reduction of flexion speed and abduction by adjusting its axial rotation. Apart from the above abnormal pattern, the left knee displays minimal axial rotation, which was expected for a UC FB knee. It should be noted that following the 50º flexion mark, the left knee shows a slight increase in external rotation until it

reached the same angle of rotation which was initially recorded in the first few frames. Contralaterally, the axial rotation for the arthritic right knee followed the expected internal tibial rotation with progressing flexion, although the screw-home and screw-away mechanisms were not prominently visible. This is correlated to the arthritic nature of the knee, which is known to vary its kinematics depending on the OA severity of the knee.

The AP and PD translation results for P003 are presented in Figure 112E and F. The left UC FB knee displayed continuous paradoxical posterior tibial translation with progressing flexion until circa 50º, at which point the translation stopped, and the knee stabilised showing minor anterior tibial translation until the end of capture. The GCA results reported 9.3 mm posterior tibial translation, while the FFA results reported a 6.4 mm translation. For the PD translations, the left knee displayed gradual distraction of the knee until the 30º flexion mark followed by minimal movement in the PD direction until the end of capture. The GCA results reported 5.2 mm of distraction (tibial distal translation), while the FFA results reported 3.8 mm of distraction. Similar to the reasoning presented for P001 and P002, the results obtained for the AP and PD translations of P003, point towards the FFA as the axes that is better approximating the anatomical axis of rotation. The GCA displays more significant anterior translations and tibial distal translations which are correlated with kinematic crosstalk.

For the arthritic right knee, the AP translations displayed minor anterior tibial translations, which agree with the translation reported for previous arthritic knees over a similar ROM. The PD translations for the right knee were also similar to those reported earlier for arthritic knees. The knee showed minor compression in the first 10º of flexion, which occurred in response to the tibial slope.

Tibiofemoral Contact Points

The TF contact point results for P003 are presented in Figure 113 (A – Femoral CPs; B – Tibial CPs). The CPs for the left replaced UC FB knee were as expected, showing slight AP movement with progressing flexion, but practically being constrained to same region throughout, both medially and laterally.

The CPs for the arthritic right knee also show similar results to other arthritic knees presented so far, such that the CPs translated posteriorly while maintaining a roughly parallel orientation. This led to the CPs not displaying the medial pivoting, which is generally noticed in healthy knees.

Axial COR

The axial COR results calculated for P003 are presented in Figure 114. The TEA based axial COR results for the arthritic right knee initially shows an agreement with the underlying CPs, and subsequently, the axial COR profiles fall anterior to the CP locations. This reflects results obtained for healthy knees, which represented the TEA being the axis which approximated the location of the anatomical FEA during the Extension phase of flexion. The TEA based result for the left replaced knee is to be disregarded since the TEA is not applicable for the replaced knee.

The GCA based axial COR results for the left UC FB knee shows a correlation between the GCA profiles and the underlying CPs, apart for the first few degrees which are found to lie posterior to the location of the corresponding CPs. The constrained mobility of the fixed bearing knee is reflected in the quasi-parallel profiles of the GCA in these results, showing the marginal axial rotation that is occurring throughout flexion. The GCA based axial COR results of the right knee show partial agreement in the later stages of flexion while falling posterior to the CPs which correspond to the Extension phase. This again shows that the arthritic knee still shows similarities to the healthy knee, whereby the TEA is initially approximating the anatomical FEA followed by the GCA, although not as effective as shown in the results of the healthy knee.

Finally, the FFA based axial COR results show similar results to those reported by the GCA, but with the difference that the FFA based results show the slight external rotation following the 50º of flexion, which was reported in the kinematics section of P003. Also, the projected FFA profiles are less dispersed than the GCA profiles, which indicates a better correlation with the corresponding CPs. The remaining axial COR plots are to be disregarded as they are not being considered to be applicable.

In conclusion, the results obtained for P003 have displayed the constrained mobility (in terms of axial rotation) of the fixed bearing knee via the axial rotation results, contact point pathways and axial COR results. The replaced knee results showed that thee cED based FFA axis displayed less kinematic crosstalk than its GCA counterpart. Contrariwise, the arthritic right knee displayed similarities to the kinematics of a healthy knee although discrepancies were evident, such as the absence of medial pivoting and the screw-away mechanism.

5.8   PATIENT PARTICIPANT #4

Patient participant #4 had a left mildly arthritic knee and a right replaced knee. The replaced knee was an Ultra-congruent Fixed-bearing knee. Patient participant #4 performed the cyclic flexion-extension exercise while in the supine position with an elevated cushion under his knees. The movement for this patient participant was captured from the maximum allowable extension of each knee as the participant was about to start flexing his knee. Subsequently, he flexed until the maximum allowable flexion at circa 65º and then proceeded to start extending his knees again until the last frame was captured at circa 60º. The following participant data was collected:

- Reference: P004

- Age: 65 years

- Gender: Male

- Left Knee: Mild signs of osteoarthritis due to regions of thin condylar bone which can be noted in the generated bone models for this knee (refer to left knee models in Figure 115).

- Right Knee: Replaced with an Ultra-Congruent Fixed-Bearing BBraun implant.

The TEA identified for the right replaced knee is to be disregarded for this participant since the medial and lateral epicondyles could not be confidently identified. Also, the analysis of the left arthritic knee will only be presented for informational purposes. Although this knee did not show clear signs of OA, it cannot be assumed to be healthy and will, therefore, be only briefly discussed to relate its kinematics to those of healthy knees.
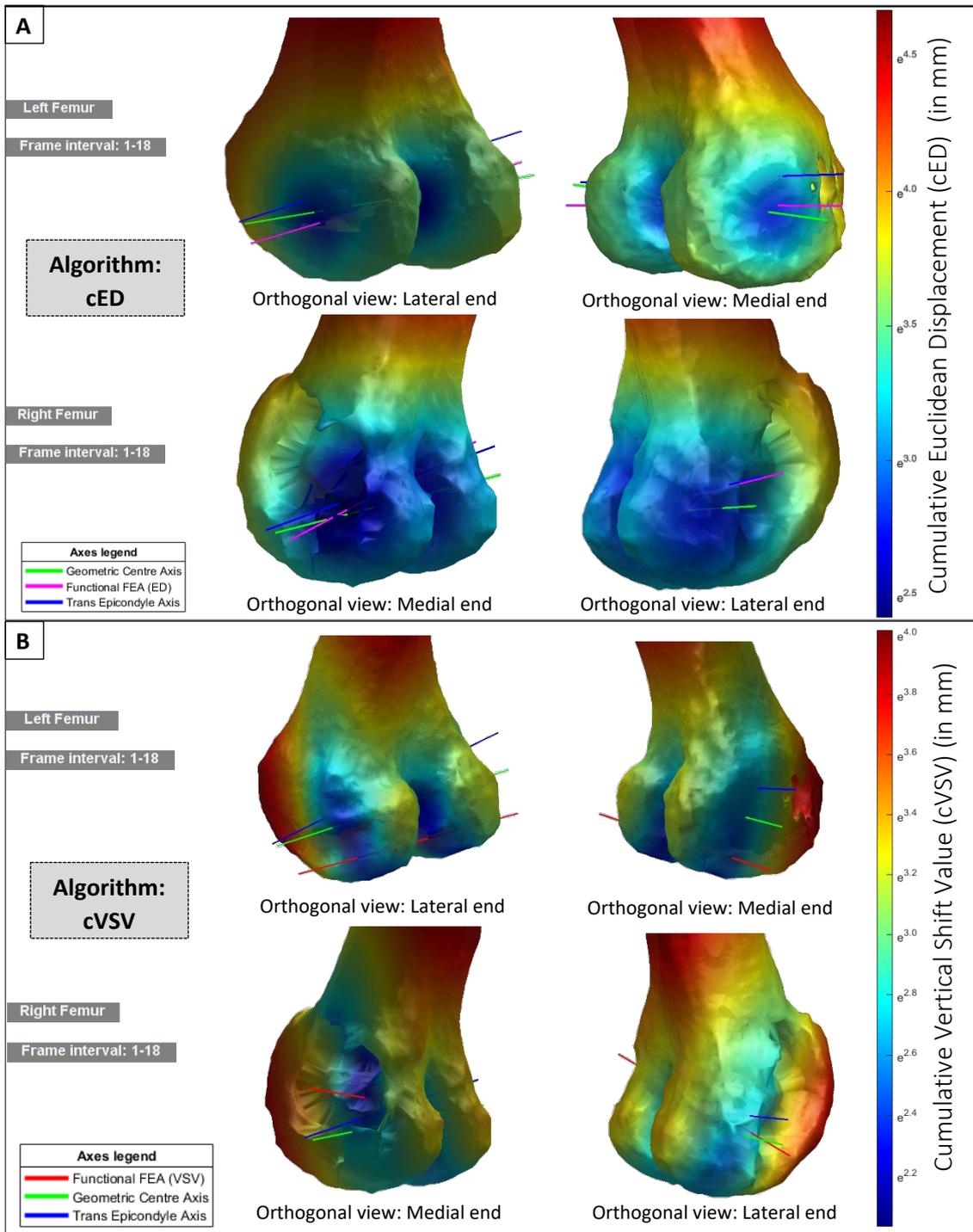
Figure 115: The Functional FE axis (FFA)– Participant P004

A: FFA results based on the cED algorithm. The inlays show the relationship between the FFA (cED axis in magenta), the TEA (blue) and GCA (green) for the left (top row) and right (bottom row) knees.
B: FFA results based on the cVSV algorithm. The inlays show the relationship between the FFA (cVSV axis in red), the TEA (blue) and GCA (green) for the left (top row) and right (bottom row) knees.
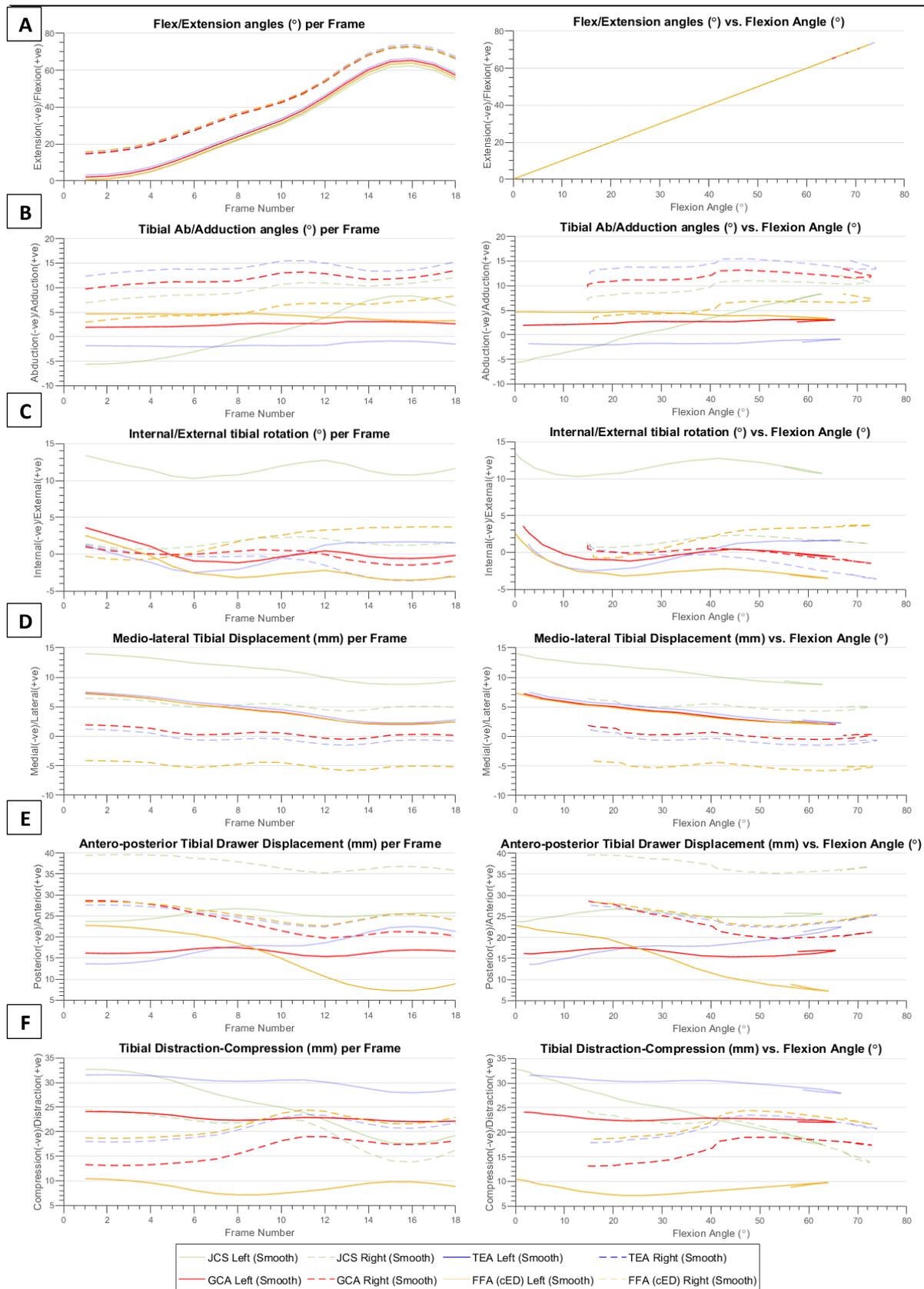
Figure 116: Kinematics for all FE axes for all 6 DOF of the knee – Participant P004

The kinematics based on the four FE axes variants, for the movement performed by patient participant P004. The rotational DOF (A-C) are presented per Frame (Left) and against the Flexion Angle (Right). The translational DOF (D-F) are presented per Frame (Left) and against Flexion Angle (Right).
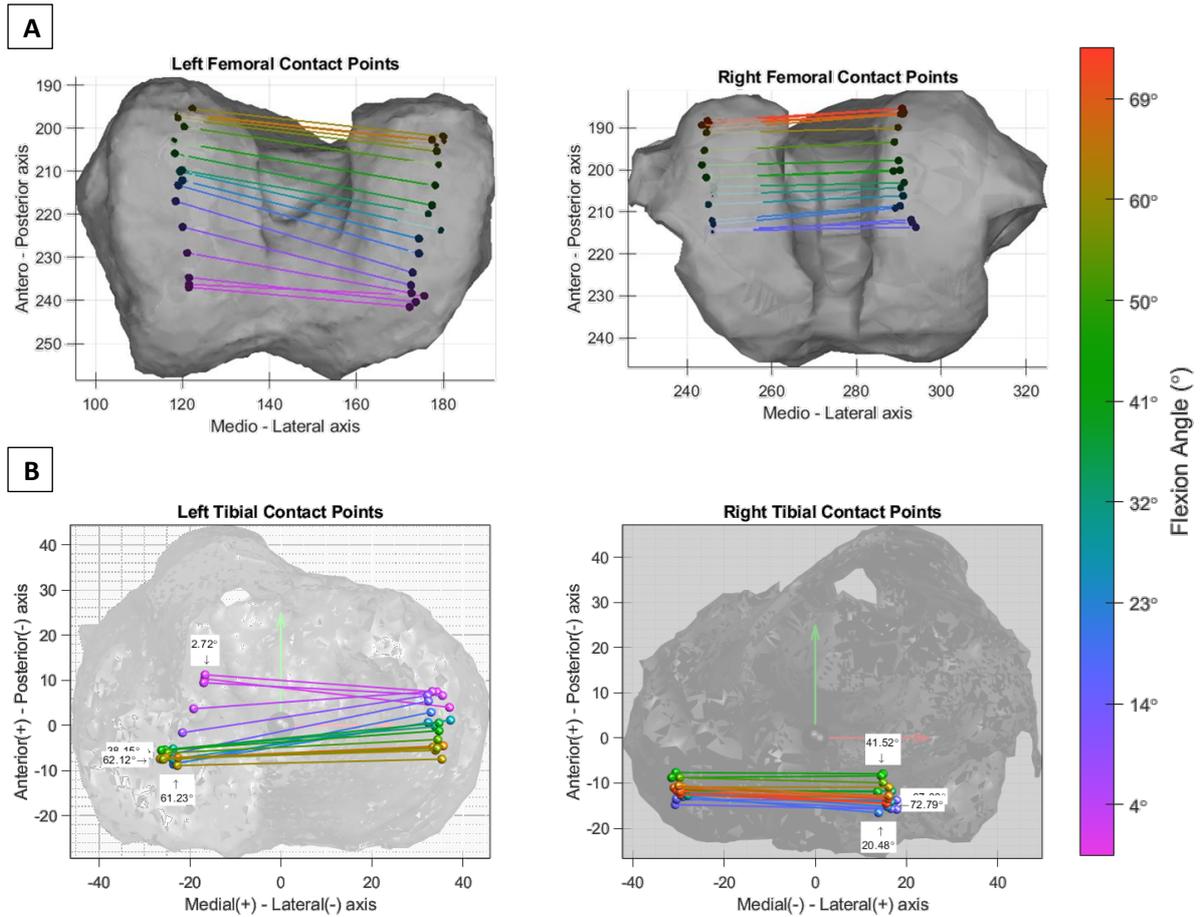
Figure 117: Tibiofemoral contact points - Participant P004

A: Femoral contact points calculated for the movement performed by control participant P004.
B: Tibial contact points calculated for the movement performed by control participant P004.
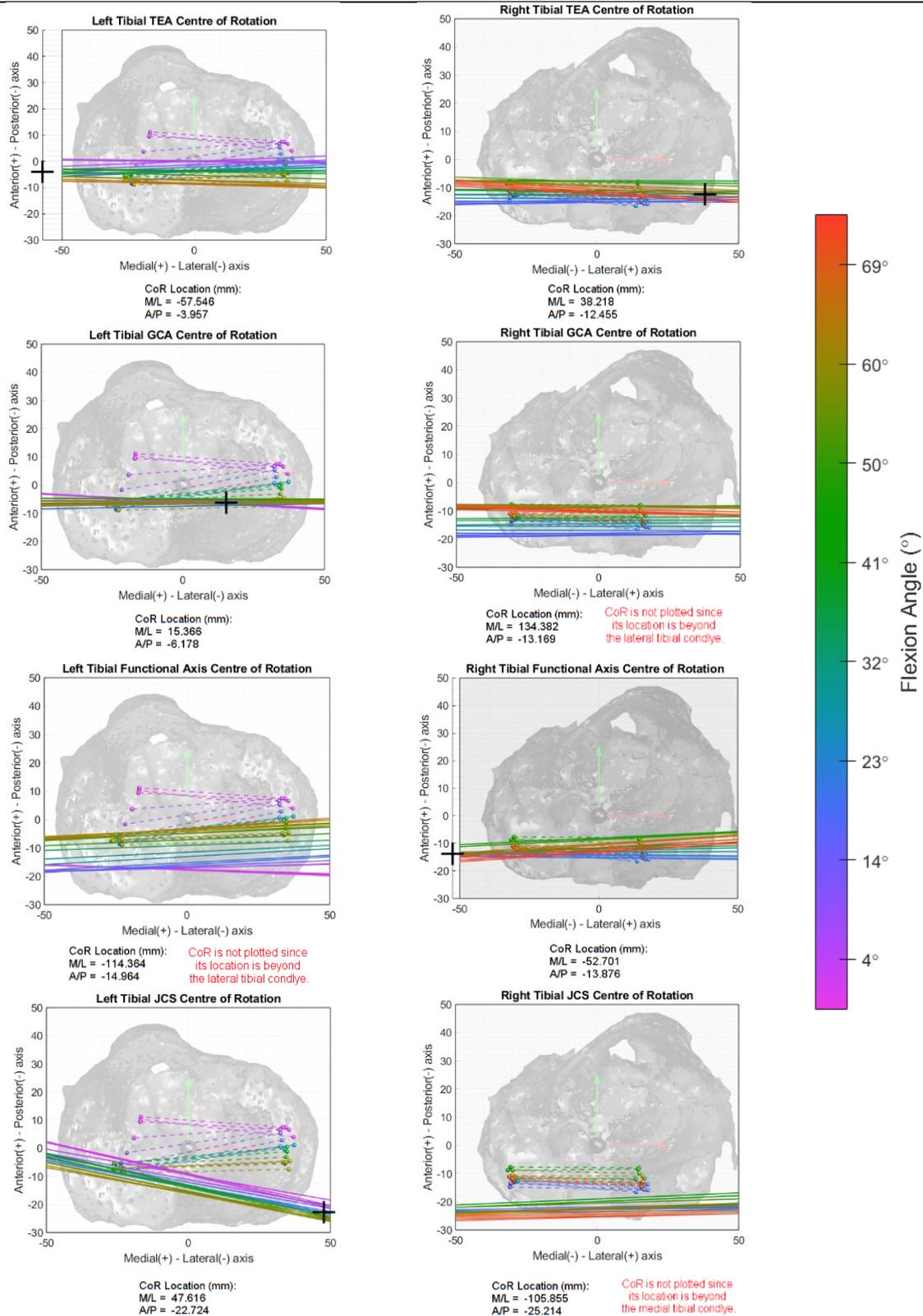
Figure 118: Axial Centre-of-Rotation of the four FE axis variants – Participant P004

The COR plots for the TEA, GCA, FFA and the JCS are plotted for the movement performed by patient participant P004. The location of each COR location is reported in terms of mediolateral and anteroposterior distance from the tibial origin. The COR location is plotted on each graph (unless it is outside the tibial plateau, in which case its location is defined by the red text below each plot).

Functional FEA

The results for the FFA are presented in Figure 115 (A – cED algorithm; B – cVSV algorithm). The cED based FFA for the left arthritic knee converged to a location close to the GCA. Medially it intercepted the condyle slightly anterior and proximal to the GCA intersection point, and laterally it intersected the condyle slightly posterior and distal to the GCA intersection point. This resulted in the FFA being skewed in relation to the GCA. The cED based FFA for the right replaced knee did not converge. The FFA intersected the medial condyle at exactly the GCA intersection point, while laterally the FFA intersected the lateral condyle anterior and proximal to the GCA intersection point. In contrast to the previously analysed replaced knees, this cED based FFA displays no relation to the expected location of the TEA.

The results for the cVSV based FFA of the left arthritic knee clearly did not converge and will be disregarded. Contralaterally, it is interesting to note how the resulting FFA compares to the cED based FFA. The cVSV based FFA intersects the medial condyle proximal to the GCA intersection point, towards what would be the medial epicondyle location, although this cannot be confirmed. Laterally, the FFA intersects the lateral condyle close to the GCA intersection point. This resulted in an FFA which is skewed in the opposite orientation to the cED based FFA. With reference to theory, it is known that laterally the axes are expected to converge to the same point since the knee has a quasi-single radius of curvature laterally. Medially there exists a discrepancy between the radii of the extension and flexion condylar axes, which is reflected in the distance between the intersection points of the extension and flexion condylar axes. The cVSV based FFA resulted in an axis which better agrees with theory since the GCA and FFA both converged to the same location laterally while they are further away from each other medially (approximating the expected location of the medial epicondyle). Therefore based on the above, the cVSV based FFA will be chosen as the better approximate for the functional FEA. The cED based FFA results will thus be disregarded for P004.

In summary, the GCA and TEA are being considered as applicable for the left arthritic knees, while the cVSV based FFA and the GCA are being considered as applicable for the right replaced knee.

Six DOF Kinematics

The six DOF kinematics for P004 are presented in Figure 116. Focus is again given to the GCA and cVSV based FFA results, as these were chosen as the applicable axes for the right replaced knee.

With reference to the GCA based kinematic results in Figure 116A, the first frame was captured for P004's movement as he was about to start flexing his knees at 1.7º of flexion for the left knee and 14.9º of flexion for the right knee. P004 then flexed his knee until he reached the maximum allowable flexion angle (that is, when his calves compressed against the elevated cushion) of 65.5º of flexion for the left arthritic knee and 72.9º for the right replaced knee. Subsequently, he started extending his knee for the last two frames until the last frame was captured at 57.7º of flexion for the left knee and 67º for the right knee. Similar to the trend noted in the previous patient participants, the replaced knee showed a restricted ROM, mostly toward the extension phase, which is being attributed to the UC feature in the implants being investigated in this study. It can be noted that this participant achieved the largest recorded ROM, which is expected to shed light on how the UC FB implant responds during the later stages of flexion. The range of flexion for the left knee was 63.8º, while 58º was achieved for the right knee.

The adduction angles reported for both knees show that the participant maintained the same adduction angles throughout the flexion cycle for both knees. With reference to the right knee, it should be noted that this participant performed an adjusting manoeuvre similar to P003 to correct his motion pathway. It can be noted that right before the 40º flexion mark (which corresponds to Frame 8) the participant slowed down his flexion speed in order to perform this manoeuvre.

With reference to the axial rotation results calculated for P004 (Figure 116C), the results for the left knee displayed the expected screw-away mechanism during the initial stages of flexion. This was followed by a quasi-constant phase of no axial rotation until circa the 40º flexion mark when the tibia starts showing further internal rotation. This agrees with the expected axial rotation for a healthy knee, which demonstrates that the left knee is in fact still in good shape and the mild arthritic nature has not yet impacted the kinematics of the knee as drastically as with the previously discussed arthritic knees. The right replaced knee showed gradual external rotation for the cVSV based FFA, which was muted following the 40º flexion mark. The GCA maintained a more constant

rotation until the 40º flexion mark, and subsequently, marginal internal rotation occurred. The FFA reported 4.7º of external rotation, while the GCA reported 2.5º or internal rotation.

The AP and PD translation results for P004 are presented in Figure 116E, and F. The left mildly arthritic knee displayed healthy knee profiles for both the GCA and TEA based AP and PD translations. This further supports the results presented above, which demonstrate the healthy nature of the left knee. The right UC FB replaced knee displayed continuous paradoxical posterior tibial translation until the 60º flexion mark. Subsequently, the tibia maintained its position in the AP dimension, while showing marginal anterior translation following the 70º flexion mark. The GCA reported an AP range of 9.2 mm while the FFA reported an AP range of 6 mm. For the PD translations, the right replaced knee displayed continuous distraction until the 40º flexion mark, followed by minimal movement in the PD direction until 50º of flexion. Subsequently, the knee started showing minor signs of compression until the end of capture. The GCA and FFA based PD translations reported a range of 6.3 mm.

In retrospect, now that the kinematic results from all three UC FB models have been reviewed, it can be noted how this implant design has shown a trend. In the region of the 40º flexion mark, the tibial implant seems to display a sudden but minor change in position in relation to its corresponding femoral component. While, so far, this was being attributed to the participants adjusting their motion pathway in order to maintain a parallel path during the flexion cycle, it might be that this movement is occurring intrinsically as a result of the geometry of the implant. While we do not have enough data to substantiate this claim, it is not to be overlooked, since this change in position is slightly noted in P001, and prominently noted in P003 and P004, although in P003, it occurred at the 30º flexion mark. Due to the fact that CT scanners are not capable of capturing the geometry of low-density materials, such as the tibial insert, it is not possible to assess if this movement is occurring due to inconsistencies in the congruency of both implant components.

Tibiofemoral Contact Points

The TF contact points results for P004 are presented in Figure 117 (A – Femoral CPs; B – Tibial CPs). The CPs for the left mildly arthritic knee followed healthy knee profiles, showing medial pivoting of the knee, although the medial CPs are slightly more dispersed than those noted for healthy knees. The CPs for the right UC FB knee were as expected, showing slight movement in the AP direction with progressing flexion while showing no signs on rotation occurring throughout the captured ROM. Here it can be noted how, at the 40º flexion mark, the CPs show marginally more anterior locations than the rest of the CPs. This slight deviation from the location of the remaining CPs is being attributed to the irregular kinematics noted earlier. With reference to section 2.5.3, these anterior CPs may be as a result of the concept of mid-flexion instability, which occurs in most traditional TKA designs due to the elimination of the cruciate ligaments which are responsible for stability during this period of the flexion cycle.

Axial COR

The axial COR results for P004 are presented in Figure 118. The TEA based axial COR results for the left mildly arthritic knee show agreement with the underlying CPs throughout the entire ROM except for the initial few degrees. Considering that the TEA has been so far shown to approximate the functional FEA during the Extension phase of flexion, it was expected that the TEA axial profiles would be more anteriorly located. This discrepancy is being attributed to the arthritic nature of the knee. The TEA axial profiles for the right replaced knee are to be disregarded since the TEA is not applicable for the replaced knee.

The GCA based axial COR results for the left mildly arthritic knee follow expected results for the GCA, as they correspond to the underlying CPs for flexion angles following the 30º flexion mark (after the Transition phase of flexion). It can be noted that despite the agreement shown with the underlying CPs, the GCA axial profiles displays negligible signs of posterior translation, which normally occurs in healthy knees. Again, this is attributed to the arthritic nature of the knee, which would directly impact the kinematics of the knee. The GCA based axial COR profiles of the right replaced knee display signs of agreement with the CPs following the 30º of flexion. Before the 30º flexion mark, the profiles fall posterior to the CPs, which demonstrates

that the GCA is not approximating the functional FEA of the replaced knee during these early stages of flexion. It can also be noted, that the axial profiles show no sign of axial rotations, which corresponds to the design of the replaced knee.

Finally, the FFA based axial COR results for the right replaced knee show agreement with the underlying CPs until the 40º flexion mark. Subsequently, following an abrupt but minor change in axial rotation, the axial profiles maintain their axial rotation while moving posteriorly. In contrast with the GCA, the axial profiles fall within the AP range of the underlying CPs. This identifies the cVSV based FFA as a better approximation of the functional axis of the femoral component than the GCA. This is also supported by the AP ranges reported earlier for the GCA and FFA kinematic results, which demonstrated less displacement for the FFA profiles in comparison to the GCA profiles.

In conclusion, the results obtained for P004, have again shown that the UC FB implants constrain the knees mobility both in the AP direction and the axial rotation. This is supported by the six DOF kinematic results, TF CP patterns and the axial profile pathways (of the applicable axes). Furthermore, it was also noted how all the FB models analysed in this study displayed an abrupt but minor change in the kinematics of the replaced knee towards the 40º flexion mark, which is being attributed to the well known mid-flexion instability of replaced knees. The results obtained for the left mildly arthritic knee displayed similarities to healthy knees, although discrepancies were noted.

5.9   PATIENT PARTICIPANT #5

Patient participant #5 was the only patient participant who had both knees replaced. The left knee was the BBraun Columbus Ultra-Congruent Mobile-Bearing knee, while the right knee was unknown since the patient did not know what kind or brand the implant in his right knee was. Also, Dr Alistair Ewen, who was the research member responsible for managing the participant data, was not able to identify what kind of implant this participant had in his right knee. During the segmentation of the knee model, it was noted that the right knee showed similarities to the fixed bearing models used in this study, although geometrical differences were noted as well. Therefore, this knee can be assumed to be of a FB design, but the geometry of the component contours unquestionably varied in comparison to the BBraun models being used in this study. Given the uncertainty surrounding this implant, the data extracted will only be presented but not discussed since comparison to an unidentified implant design is futile.

Patient participant #5 performed the cyclic flexion-extension exercise while in the supine position with the elevated cushion under his knees to maximise the ROM. The movement that was captured is similar to that of C001 since it initiated at circa 35º of flexion as the participant was extending his knees. Subsequently, he reached his maximum allowable extension and started flexing again until the last frame was captured at around 35º of flexion. This data is expected to highlight the mobility of the UC MB knee since it is during this phase of flexion that the majority of the axial rotation occurs. The following participant data was collected for Patient Participant #5:

- Reference: P005
- Age: 68 years
- Gender: Male
- Left Knee: Replaced with an Ultra-Congruent Mobile Bearing implant from the B.Braun Columbus series.
- Right Knee: Replaced with likely a Fixed-Bearing implant. Implant brand is unknown.

Similar to previous patient participants, the TEAs identified for the replaced knees of P005 were not confidently identified due to the missing bone on the epicondylar regions following segmentation. Although the identified locations for both knees do seem to approximate the locations of the TEA in healthy knees, the confidence in their location cannot be ensured and will, therefore, be disregarded.
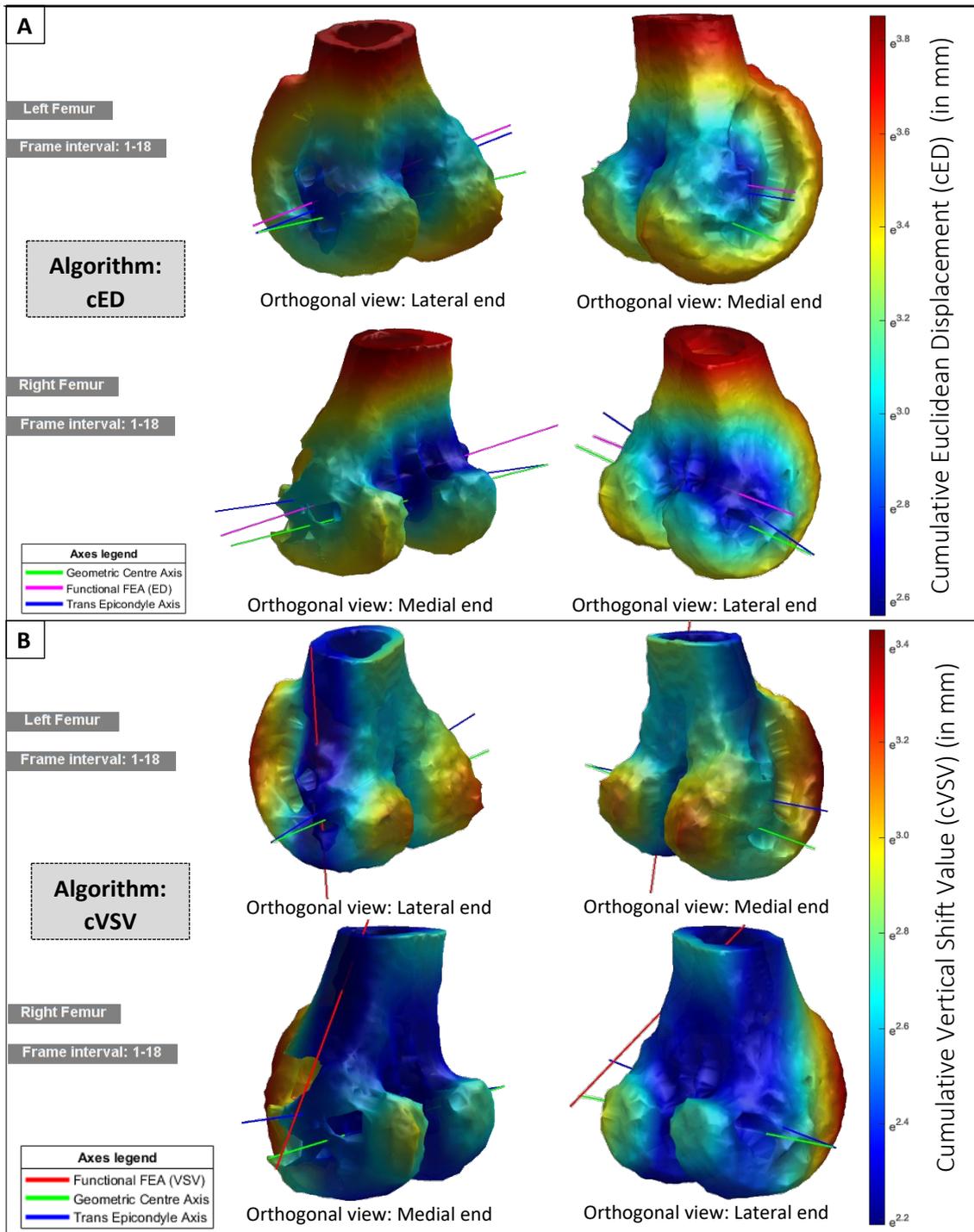
Figure 119: The Functional FE axis (FFA)– Participant P005

A: FFA results based on the cED algorithm. The inlays show the relationship between the FFA (cED axis in magenta), the TEA (blue) and GCA (green) for the left (top row) and right (bottom row) knees.
B: FFA results based on the cVSV algorithm. The inlays show the relationship between the FFA (cVSV axis in red), the TEA (blue) and GCA (green) for the left (top row) and right (bottom row) knees.
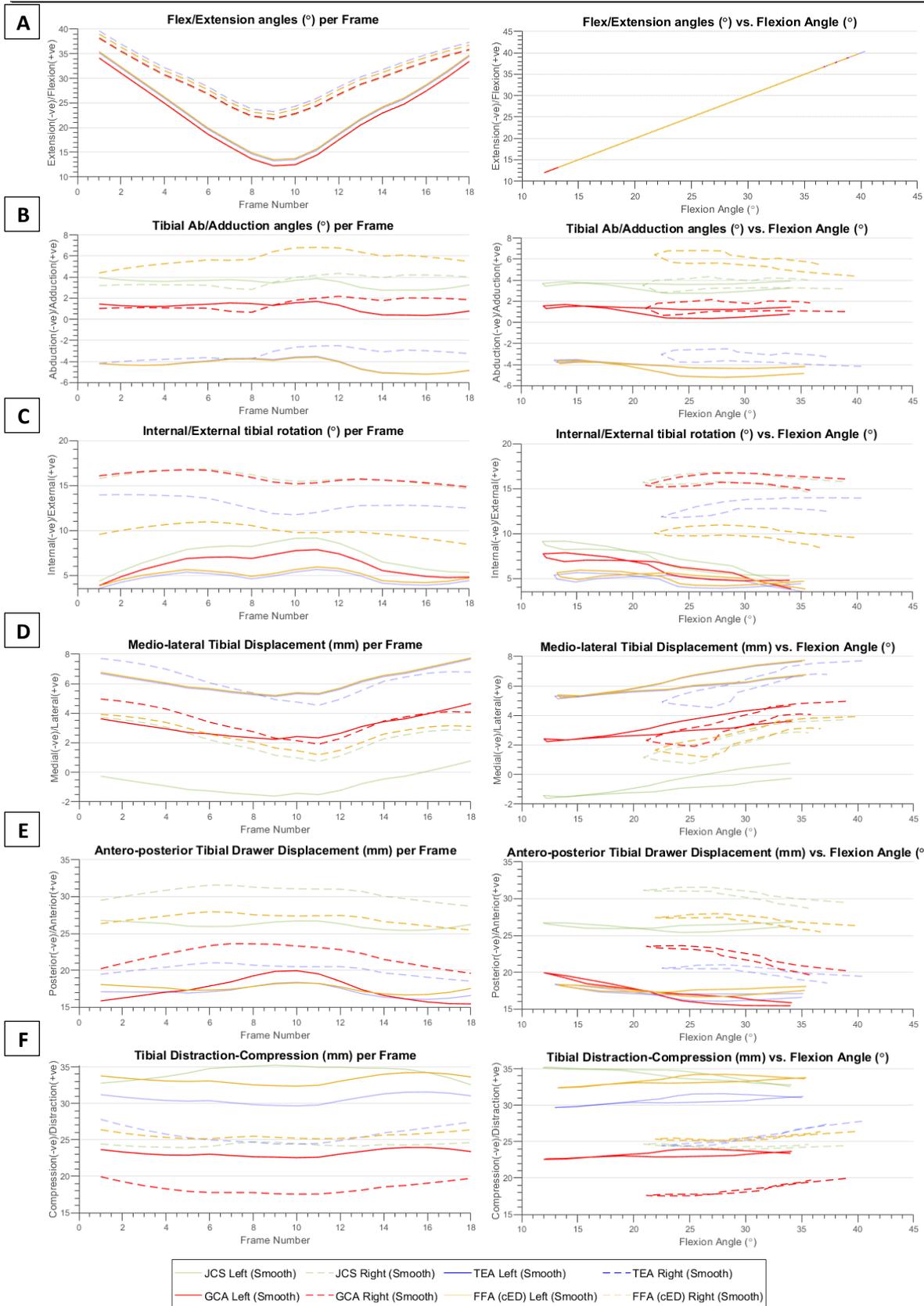
Figure 120: Kinematics for all FE axes for all 6 DOF of the knee – Participant P005

The kinematics based on the four FE axes variants, for the movement performed by patient participant P005. The rotational DOF (A-C) are presented per Frame (Left) and against the Flexion Angle (Right). The translational DOF (D-F) are presented per Frame (Left) and against Flexion Angle (Right).
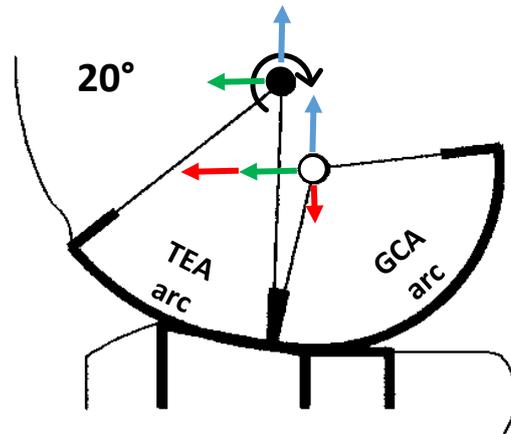
Figure 121: AP and PD translations for P005.

An illustration to explain the kinematic crosstalk occurring at the GCA and FFA (approximating the TEA). The green arrows show the AP translation recorded by the TEA based kinematics, which represents the actual motion of the rigid body (femur) in space, thus acting as well on the GCA. Similarly, the blue arrows show the PD translation recorded by the TEA based kinematics, thus also acting on the GCA. The red arrows identify the translations which the GCA is experiencing as a result of kinematic crosstalk.
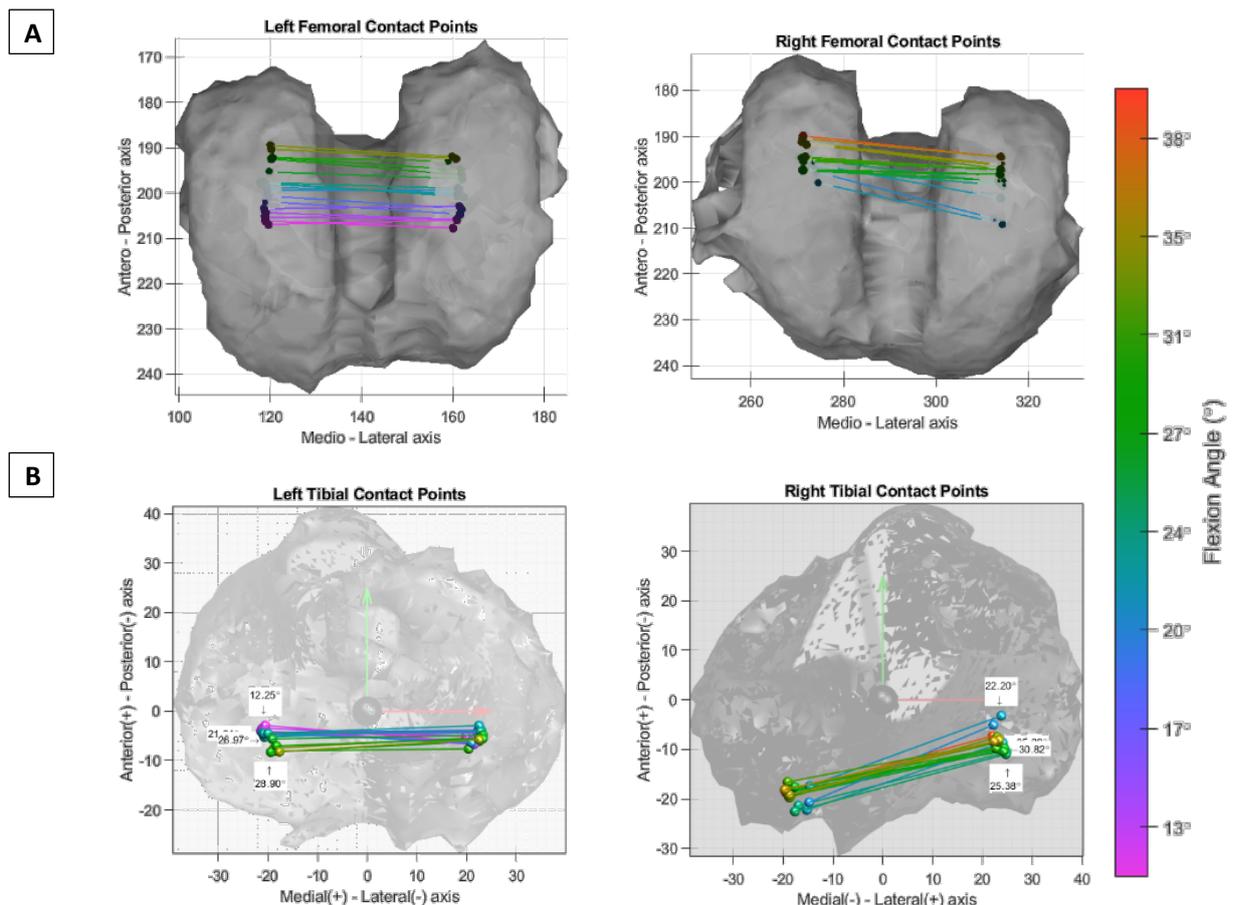
Figure 122: Tibiofemoral contact points - Participant P005

A: Femoral contact points calculated for the movement performed by control participant P005.
B: Tibial contact points calculated for the movement performed by control participant P005.
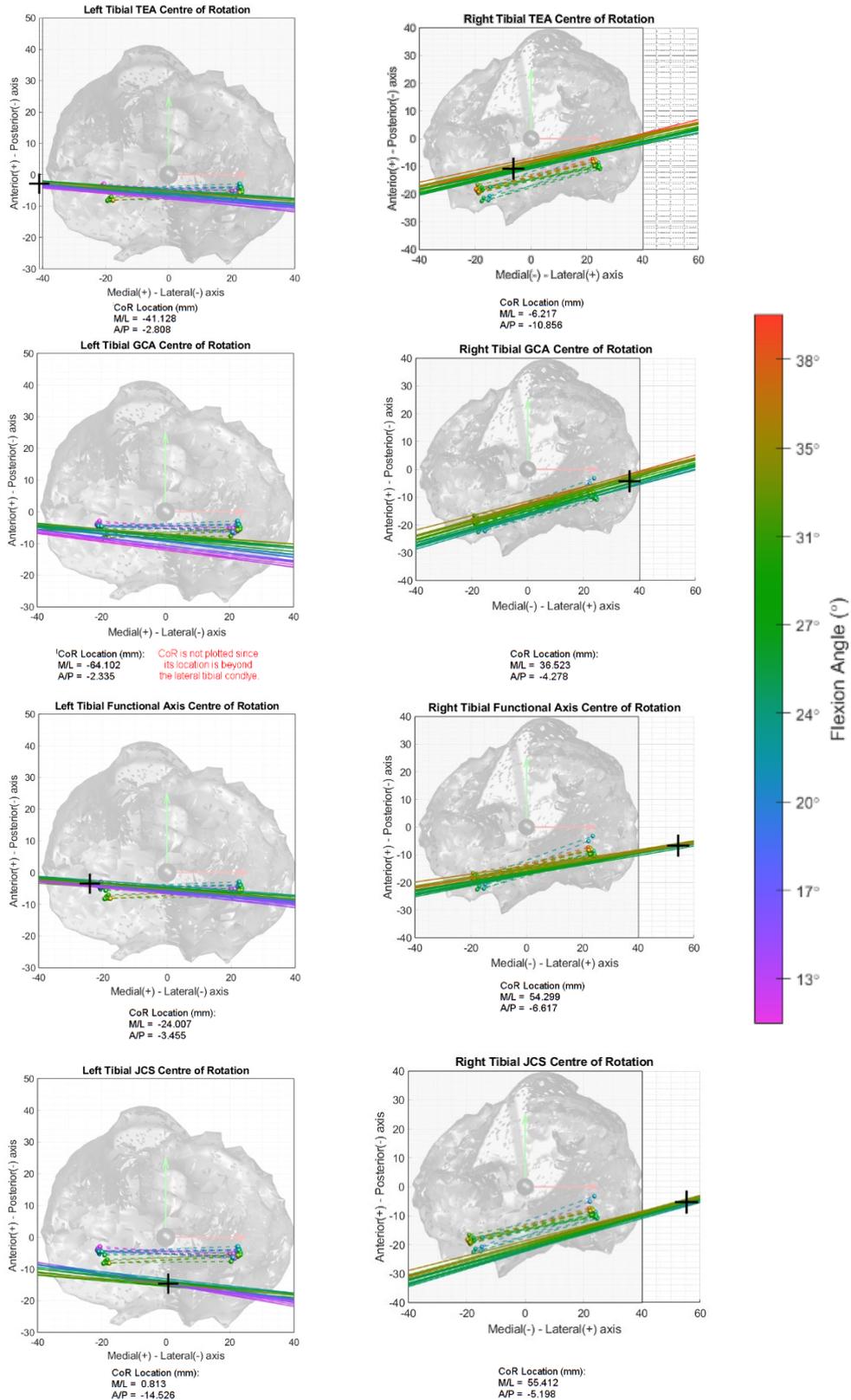
Figure 123: Axial Centre-of-Rotation of the four FE axis variants – Participant P005

The COR plots for the TEA, GCA, FFA and the JCS are plotted for the movement performed by patient participant P005. The location of each COR location is reported in terms of mediolateral and anteroposterior distance from the tibial origin. The COR location is plotted on each graph (unless it is outside the tibial plateau, in which case its location is defined by the red text below each plot).

Functional FEA

The results for the FFA are presented in Figure 119 (A – cED algorithm; B – cVSV algorithm). Similar to previously analysed replaced knees, the cED based FFA for the left UC MB converged towards the TEA location (keeping in mind that the TEA could not be confidently identified). While the morphology of the interface between the femoral component and the tibial insert define the path of motion, the supporting soft tissues still influence the path of motion. The collateral ligaments, which are taut during the Extension phase of flexion, act as a fulcrum point at the epicondylar regions of the femur (which coincide with the origins of the LCL and MCL) which in turn guide the femur to rotate around the epicondyles which define the TEA. Therefore, having the cED based FFA lying close to the TEA during the Extension phase further supports its applicability. The cED based FFA for the right knee is to be disregarded since the kinematics of this knee are not being assessed.

The cVSV based FFAs of both knees clearly did not converge. The location of the FFAs is as a result of the relatively small captured ROM for P005, which summed up to a range of 22.2º of flexion for the left knee and 17.9º of flexion for the right knee. Due to these small ranges, the algorithm had insufficient data to work with in order to approximate the location of the functional FEA.

In conclusion, the GCA and FFA are being considered as applicable for the left UC MB knee (the TEA is to be considered with caution, keeping in mind the fidelity of its identified location). Contralaterally, the GCA is the only applicable axis.

Six DOF Kinematics

The six DOF kinematics for P005 are presented in Figure 120. The plotted graphs give focus to the GCA and FFA based profiles since these were the applicable axis for the left UC MB knee. Conversely, the TEA and JCS are faded out.

With reference to the GCA based kinematics for rotation around the FEA (Figure 120A), the first frame for P005 was captured as the participant was extending his knees at 34.1º for the left UC MB knee and 38.9º for the right FB knee. P005 continued to extend his knees until his maximum allowable extension angle, which occurred at 12º for the left knee and 21.1º for the right knee. P005 subsequently flexed his knees until the last frame was captured at 34º for the left UC MB knee and 35.8º for the right FB knee. The reported flexion angles for the left UC MB knee, again show limited extension angles in comparison to healthy knees, which is being assumed to occur due to the anterior ridge of the UC tibial insert. The right FB knee only achieved 21.1º of

Extension, which is very irregular even for a replaced knee. This might have happened as a result of the geometry of the implant, or else due to the participant limiting his extension angle sub-consciously. Nonetheless, the kinematics of the right knee are not of relevance for this study.

The adduction angles reported for both knees (Figure 120B) show that the participant maintained his tibias in a parallel path throughout the extension cycle, and then during the initial stages of the flexion cycle (circa frame 11, which corresponds to 14º of flexion) he slightly adjusted his adduction angles and then proceeded to maintain this angle until the end of capture.

The axial rotation results calculated for the captured movement of P005 (Figure 120C) shows marginal signs of internal rotation with progressing flexion in the left knee, with the GCA reporting a range of 4.3º and the FFA reporting 2.6º of internal rotation. In comparison to C001, who achieved 9º of internal rotation over a smaller ROM during the Extension Phase, the internal rotation angles were still considerably smaller. Furthermore, considering that this is a MB implant, it is expected that the implant would allow more internal rotation to be achieved during these early phases of flexion. Recall that this MB implant is advertised to have axial rotational freedom of ±20º. Therefore, the MB implant axial rotation recorded only achieves a fraction of its designed allowances. Similar to the results obtained for P002 (UC MB implant), so far the UC MB implant is not showing any significant indications of additional freedom of axial rotation (mobility) in comparison to the results obtained for the UC FB implants. With reference to the GCA and FFA profiles, it can be noted how the FFA profile demonstrated less axial rotation than the GCA alternative. The excess axial rotation displayed by the GCA is being attributed to kinematic crosstalk, based on the fact that so far the data collected, analysed and discussed has pointed towards an axis is the vicinity of the TEA to be its FFA, similar to P005.

Also, with reference to the axial rotation vs frame plot, when comparing the rate of external rotation experienced during extension with the rate of internal tibial rotation experienced during flexion, it can also be noted that at the instant when the participant slightly adjusted his adduction angles, the rate of internal rotation increased proportionally (this can also be appreciated in the plot against flexion angles). This same response, as a consequence of a change in adduction angles, was also noted in P001 (at frame 12) and P003 (at frame 9) but not in healthy or arthritic knees. Therefore it can be assumed that this might be occurring as a result of the constrained design of the replaced knee. Logically, considering that the UC design ensures congruity between

the tibial and femoral components throughout the entire ROM, then if the user suddenly changes the adduction angle one of the femoral condyles will act as a fulcrum and the contralateral condyle will distract opening room in the AP direction where the distracted condyle can translate. Due to the constrained design of the knee, the "released" femoral condyle will move anteroposteriorly in response to the active and passive constraints on the knee at the instant of distraction, thus performing axial rotation until it again contacts the tibial insert.

The axial rotations for the right Fixed Bearing knee demonstrate similar magnitudes of internal rotation which again supports the argument that MB knees do not provide more mobility than their FB counterparts. However, there is no concrete evidence which determines if the right knee is fixed or mobile.

Moving on to the AP and PD translations for P005 (Figure 120E and F), it can be noted how both knees displayed the paradoxical posterior tibial translation along with marginal signs of distraction with progressing flexion. Again both these motions are contradictory to the health knee, which usually shows anterior tibial translation along with slight compression with increasing flexion. With reference to translations displayed by the GCA and FFA, it can be noted that the GCA kinematics reported that the tibia translated posteriorly by 5 mm and distracted by 1.6 mm, while the FFA kinematics reported that the tibia translated posteriorly by 2.1 mm and distracted by 2.1 mm. With reference to the features of the UC MB implant, it is known that the tibial insert only allows axial rotation while it restricts anterior translation, while the UC feature ensures that the TF contact is maximised throughout the flexion cycle. Therefore, theoretically, the kinematics should be reporting no anterior translations and distraction translations. Based on the above, it is logical that the FFA is better approximating the theoretical kinematics since its AP translation is more than halved over the GCA values, while the distraction is marginally increased. With reference to Figure 121 and taking the assumption that the femur is rotating around the FFA (which is approximating the TEA for this case), it can be understood that the GCA should be showing increased posterior translation and less distraction, which is the case. This further supports the argument that the identified FFA is approximating the axis of rotation of the femoral implant.

Tibiofemoral Contact Points

The TF contact point results for P005 are presented in Figure 122. The CPs for the left UC MB knee again showed minimal signs of rotation throughout the captured ROM. The first few CPs (plotted in purple) show a slightly internally rotated orientation,

which reflects the femurs attempt at responding to the screw-away mechanism, but ultimately being hindered by the constrained design of the UC MB implant. These CP results further support the argument that the MB design does not achieve its designed target of allowing axial rotation within the knee, consequently replicating the movement of a FB design.

Axial COR

The axial COR results calculated for the left UC MB knee of P005 are presented in Figure 123. The GCA based axial profiles fail to show agreement with the underlying CPs apart for a slight overlap on the lateral plateau. This supports the statement that the GCA is not approximating the axis of rotation of the femoral component. Apart from the marginal correlation between the axial COR profiles and the underlying CPs, the GCA based axial COR also demonstrates a COR which lies far out of the tibial plateau laterally.

On the other hand, the axial COR profiles for the FFA (and the TEA) show agreement with the underlying CPs apart for the final few frames which lie slightly posterior of the axial profiles. The FFA axial profiles are noted to be slightly internally rotated with respect to the orientation of the CPs and the Local Tibial CS (shown faded in the centre). This might be as a result of a slight mal-alignment when installing the implant components, or else it might be the case that the tibial insert ceased in an internally rotated position, therefore acting as a UC FB implant. This mal-rotation was also noted in P002 which also had an UC MB implant. Also, the axial profiles are not entirely parallel, showing marginal internal rotation, which is reflected in the location of the COR for the FFA.

In conclusion, the results for the UC MB implant of P005 have shown that the axis of rotation of the femoral component is approximated by the location of the cED based FFA which shows a correlation with the TEA. This has also been noted in other patient participants, notable in P001 and P004. Also, the six DOF results and the axial COR results have shown that the FFA is displaying less kinematic crosstalk than the GCA. Furthermore, this UC MB also showed the paradoxical anterior femoral translation, which agrees with literature. The results obtained for the UC MB models have so far shown no improvement in the axial rotation achieved over UC FB models (including the FB model installed in the right knee of this participant).

5.10   PATIENT PARTICIPANT #6

Patient participant #6 had a left arthritic knee and a right replaced knee. The replaced knee was a BBraun Columbus Ultra-Congruent Mobile-Bearing knee. Patient participant #6 performed the cyclic flexion-extension exercise while in the supine position with the elevated cushion under her knees to maximise the ROM. The movement that was captured initiated during the terminal stages of extension, subsequently the patient flexed her knees until the last frame was captured at circa 50º of flexion for the left knee and circa 40º of flexion for the right knee. The following participant data was collected for Patient Participant #6:

- Reference: P006
- Age: 73 years
- Gender: Female
- Left Knee: Arthritic with clear signs of osteophyte growth on the peripheries of the femoral condyles (refer to left knee models in Figure 124).
- Right Knee: Replaced with an Ultra-Congruent Mobile Bearing BBraun implant.

Similar to previous patient-participants, the TEA identified for the replaced knee was not confidently identified due to the missing bone on the epicondylar regions as a result of segmentation artefacts. As a result of this, the TEA based kinematic outcome measures for the replaced knee should be disregarded. Also, the results of the left arthritic knee are only going to be presented and briefly discussed since the analysis of arthritic knees goes beyond the scope of this thesis.
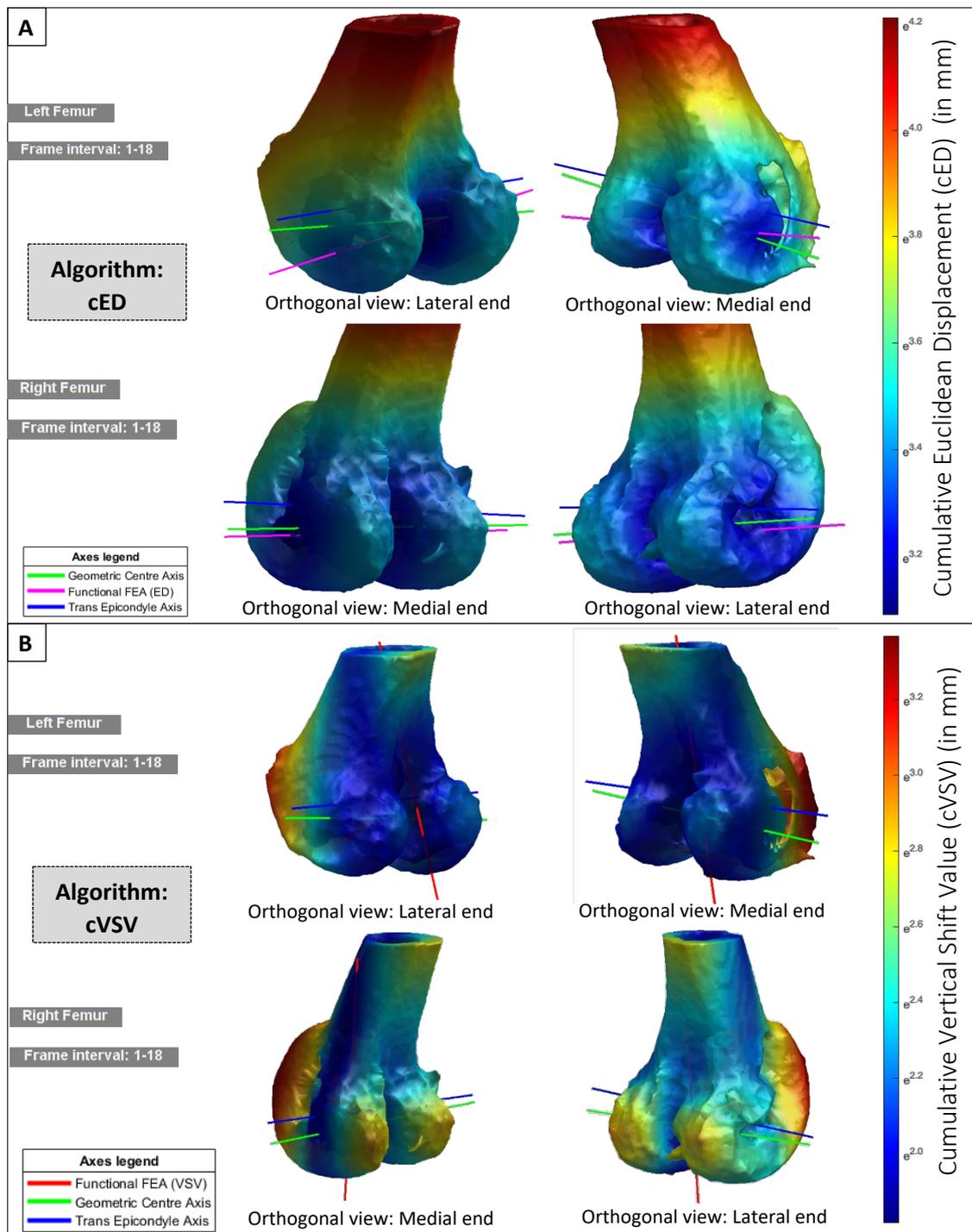
Figure 124: The Functional FE axis (FFA)– Participant P006

A: FFA results based on the cED algorithm. The inlays show the relationship between the FFA (cED axis in magenta), the TEA (blue) and GCA (green) for the left (top row) and right (bottom row) knees.
B: FFA results based on the cVSV algorithm. The inlays show the relationship between the FFA (cVSV axis in red), the TEA (blue) and GCA (green) for the left (top row) and right (bottom row) knees.
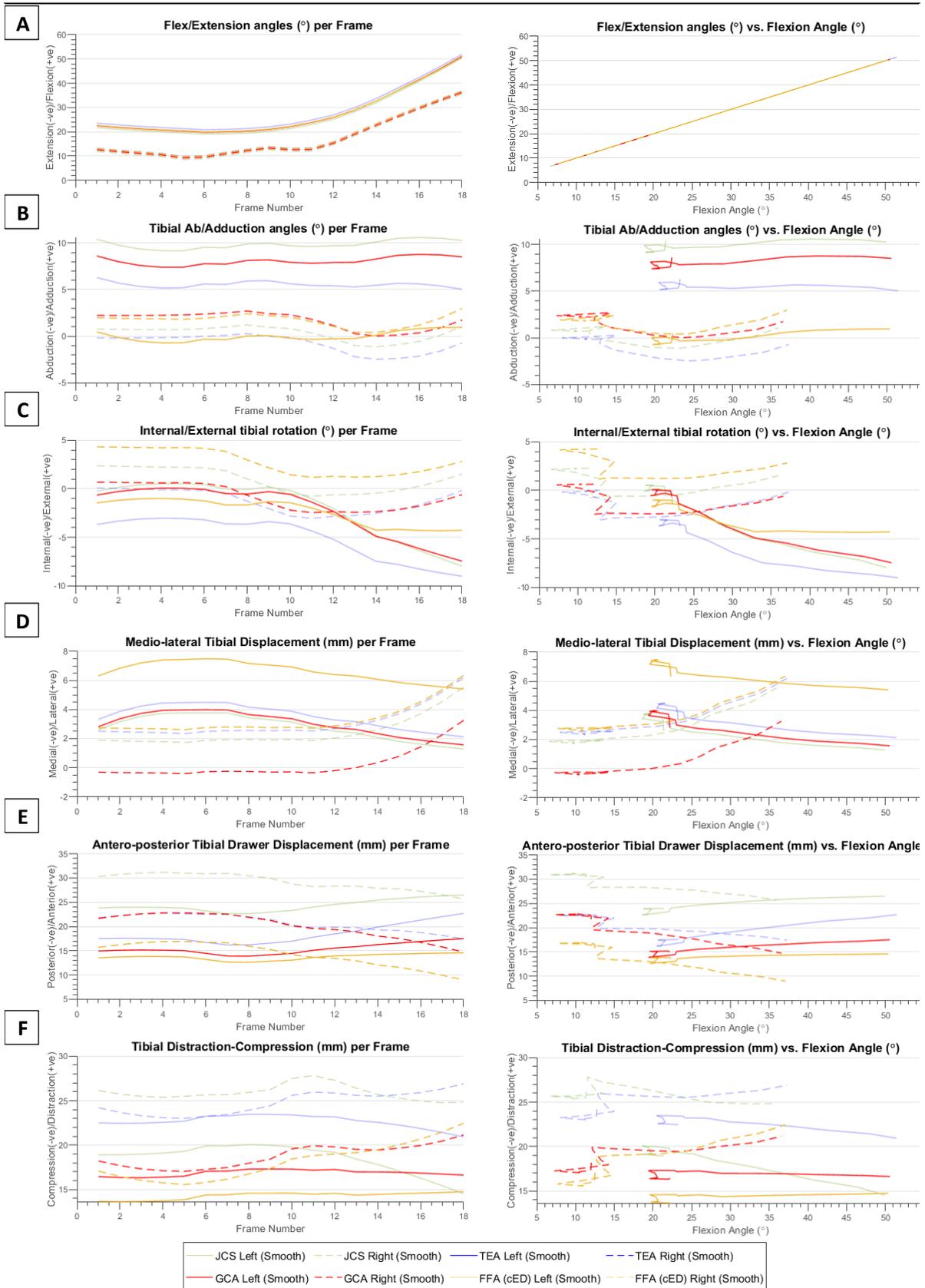
Figure 125: Kinematics for all FE axes for all 6 DOF of the knee – Participant P006

The kinematics based on the four FE axes variants, for the movement performed by patient participant P006. The rotational DOF (A-C) are presented per Frame (Left) and against the Flexion Angle (Right). The translational DOF (D-F) are presented per Frame (Left) and against Flexion Angle (Right).
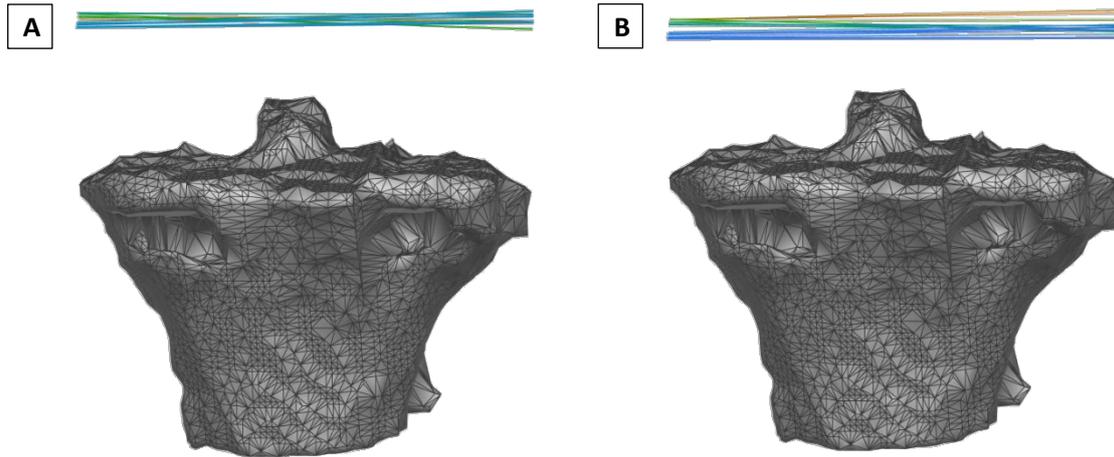
Figure 126: Coronal view of the applicable axes for the right knee – Participant P006

The validity of the derived cED based FFA is reflected in this coronal view of the knee. This view visualises the difference between the GCA-based (A – Left) and the FFA-based (B – Right) PD translations and abduction-adduction rotations for the captured ROM.
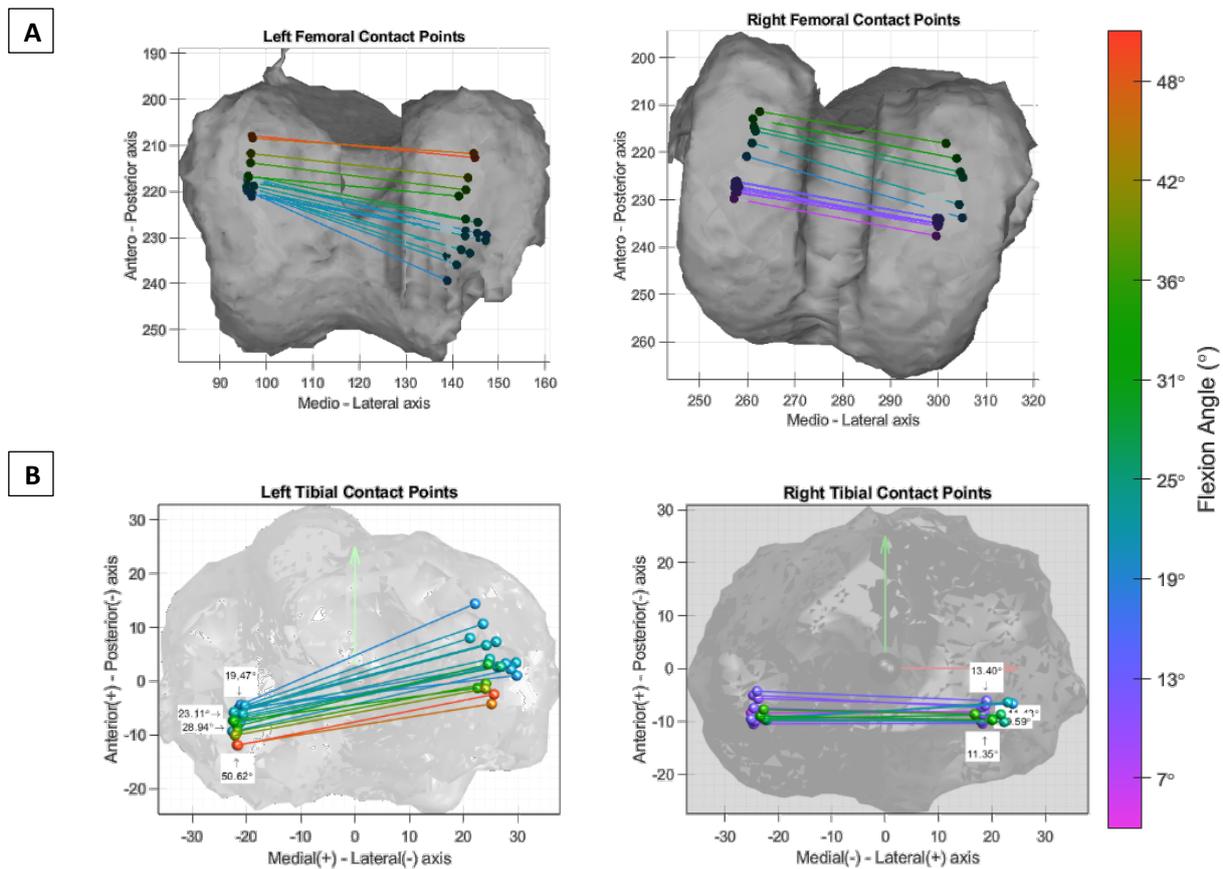
Figure 127: Tibiofemoral contact points - Participant P006

A: Femoral contact points calculated for the movement performed by control participant P006.
B: Tibial contact points calculated for the movement performed by control participant P006.
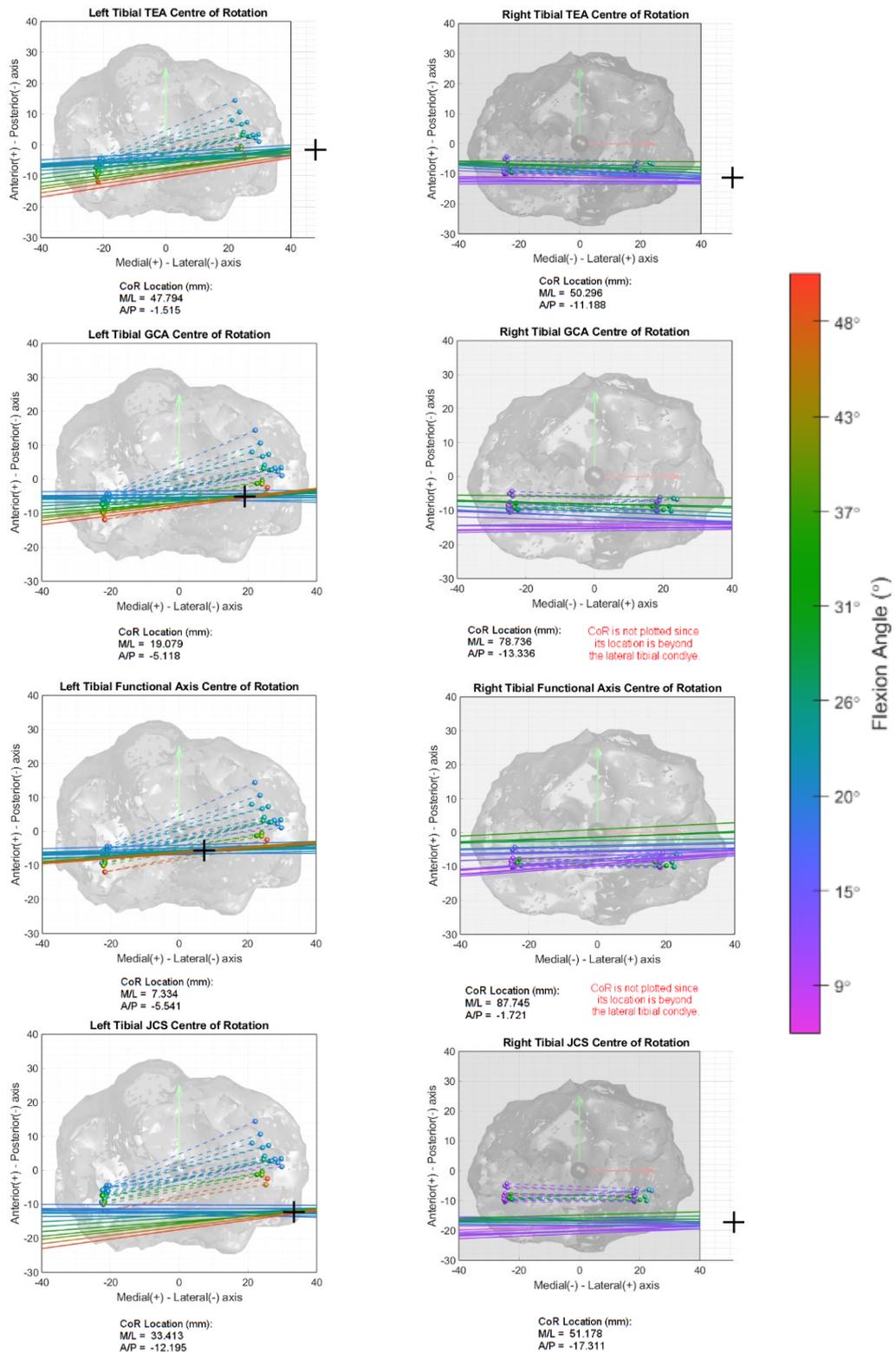
Figure 128: Axial Centre-of-Rotation of the four FE axis variants – Participant P006

The COR plots for the TEA, GCA, FFA and the JCS are plotted for the movement performed by patient participant P006. The location of each COR location is reported in terms of mediolateral and anteroposterior distance from the tibial origin. The COR location is plotted on each graph (unless it is outside the tibial plateau, in which case its location is defined by the red text below each plot).

Functional FEA

The results for the FFA are presented in Figure 124 (A – cED algorithm; B – cVSV algorithm). The cED based FFA for the left arthritic knee did not converge. This location shows no kind of relation to the functional anatomy of the knee, it can be noted that medially it intersects close to the GCA intersection point, while laterally it intersects distal to the GCA and TEA intersection points. This resulted in a skewed axis to both the GCA and TEA showing no relation to neither one. Therefore, this cED based FFA for the left knee is to be disregarded. Contralaterally, the cED based FFA for the right replaced knee showed indications of approximating the GCA, although there are discrepancies between the locations of both axes. Medially the FFA is approximating the intersection point of the GCA, while laterally it is not, but rather lies in the anterodistal direction from the GCA intersection point. This resulted in an FFA that is skewed in relation to the GCA. Although the identified TEA is considered to be irregularly located, if the identified FFA was to be compared to the expected theoretical location of the TEA, the FFA still does not show similarities to the theoretical location of the TEA. With reference to Figure 126, it can be noted that the coronal-view of the FFA based profiles show larger PD displacement when compared to the alternative GCA axis. This shows that the identified FFA experiences considerable kinematic crosstalk since ideally the FFA would be one that experiences the least PD translations and adduction/abduction rotations. Therefore, based on the above, the cED based FFA for the right replaced knee is to be disregarded.

The results for the cVSV based FFAs of both the left and right knee show very irregular locations for both knees, which is similar to the cVSV results obtained for P001, P002 and P005. Therefore, in conclusion, since no FFA converged for the left knee, only the TEA and GCA are being considered as applicable FFAs for this knee. Contralaterally, neither of the two FFA algorithms converged for the right knee, such that only the GCA is being considered as applicable for the right replaced knee. Nonetheless, given that the software required the choice of one of the FFAs to be selected for the presentation of the results, then the cED based FFAs were selected as they showed signs of convergence. It should be kept in mind that both FFA results are not applicable.

Six DOF Kinematics

The six DOF kinematics for P006 are presented in Figure 125. While the results for all the FE axes are presented, the focus is given to the GCA as it is the only applicable axes identified for the right replaced knee, which is the emphasis of the results being presented for P006. Conversely, the TEA, FFA and JCS are presented in a faded manner.

With reference to the GCA based kinematic results for rotation about the FEA (Figure 125A), the first frame for P006 was captured as the participant was reaching the end of her extension cycle at 22.2º for the left arthritic knee and 12º for the right UC MB knee. Subsequently, P006 reached her maximum allowable extension for the left knee at 19.4º of flexion in frame 8, while for the right replaced knee the maximum allowable extension was achieved in frame 6, at 7.3º of flexion. Afterwards, the participant proceeded to flex her knees until the last frame was captured at 50.6º of flexion for the left knee and 36.6º of flexion for the right knee. The results for P006, are the only results to display larger extension angles for the replaced knee in comparison to the contralateral arthritic knee. Furthermore, with reference to the plot of the flexion angles per frame (Figure 125A left), it can be noted that when the participant reached the maximum allowable extension in the right replaced knee, the contralateral knee had not yet reached the maximum allowable extension, which occurred two frames later. As a result of this, the participant initiated flexion in the right knee, while the contralateral knee was still extending. Then at frame 9, just after the left knee reached the maximum extension, the participant halted the flexion of the right knee for three frames and then proceeded with flexion until the end of capture. This manoeuvre is being assumed to have been performed by P006 in order to synchronise the movement of both knees.

With reference to the adduction angles calculated for P006 (Figure 125B), it can be noted that prior to the manoeuvre of the right knee, the participant maintained a constant adduction angle in the right knee. Following frame 8, the right knee was abducted at a constant rate until frame 14, after which the knee is adducted again, possibly to correct the abduction that was just performed. In light of the discussion presented in the analysis of the results of P005, it was noted that any changes in the adduction angles reverberated in the results of the axial rotation. Therefore, this back and forth adduction movement is expected to affect the axial rotations of the replaced knee. Contralaterally,

the adduction angles of the left knee reported a quasi-constant adduction angle throughout the entire captured ROM.

The axial rotation results calculated for the captured movement of P006 (Figure 125C) demonstrated that the left arthritic knee displayed the expected internal tibial rotation with progressing flexion. On the other hand, the right replaced knee displayed internal rotation during the duration of the manoeuvre and subsequently stabilised in a fixed internally rotated position until the end of capture. Given that so far a trend has been noted, where the axial rotation is directly affected when the replaced knee varies its adduction angles, this internal rotation of the UC MB knee is being attributed to this manoeuvre and not as a result of the mobile bearing actually rotating. This will be further supported by the results that will be presented for the contact points below. In the last few frames, the replaced knee displayed external tibial rotation similar to P002. P006, similar to the other two participants who had the UC MB implant, did not experience any significant additional mobility as a result of having the Mobile-Bearing model over the Fixed-Bearing model.

The AP and PD translations for P006 (Figure 125E and F) again follow similar trends noted in previous participants for both the arthritic and replaced knees. For the left arthritic knee, the GCA based kinematics reported slight anterior tibial translation and marginal signs of compression with progressing flexion which reflects the kinematics of a healthy knee, although on a smaller scale of magnitudes. The right UC MB knee demonstrated the paradoxical posterior tibial translation with progressing flexion, which was noted in all replaced knees analysed in this study. Also, the replaced knee distracted in response to the adduction manoeuvre, which was also noted in other replaced knees when they were abducted/adducted. It can be noted that a sudden increase in distraction occurs during the phase when the replaced knee ceased flexion momentarily (frames 9-11). This supports the argument presented in the discussion of the axial rotation of P005. When the replaced knee abducted, one of the femoral condyles (possibly the lateral one) acted as a fulcrum point and lifted off the tibial insert. As a result, the contralateral femoral condyle was "released" from its UC constraints and thus had room to move in the AP direction, thus simultaneously creating axial rotation. Based on the above, it can be inferred that the distractions occurring within the replaced knee are not occurring as a function of flexion but in response to changes in the adduction angles.

Tibiofemoral Contact Points

The TF contact points calculated for P006 are presented in Figure 127 (A – femoral CPs; B – tibial CPs). The CPs for the left arthritic knee displayed lateral pivoting, which is the opposite of what occurs in a healthy knee. With reference to the femoral CPs of the left knee, it can be noted, how the lateral femoral condyle has all the CPs until circa 30º of flexion located in the same area. When comparing these CP patterns with other arthritic knees (which so far showed quasi-parallel TF CPs), it can be understood that the lateral femoral condyle did not rotate as expected until the 30º mark, but instead experienced sliding. This might have happened due to some physiological defect as a consequence of the OA. Furthermore, in light of the kinematic axial rotation results and the axial profiles discussed below, it can be noted that although the CPs show lateral pivoting, the axial rotation still shows medial pivoting (internal tibial rotation). This will be discussed further below.

The CPs for the right UC MB knee again showed marginal signs of axial rotation throughout the captured ROM. These results again support the conclusion that MB knees have no increased mobility over their FB counterparts.

Axial COR

The axial COR results calculated for P006's movement are presented in Figure 128. The axial profiles for the left arthritic knee, namely the GCA based profiles, demonstrate the aforementioned medial pivoting, which is characteristic of a healthy knee. However, these profiles do not show agreement with all the medial CPs which lie anterior to the GCA axial profiles. Contrariwise, the lateral CPs show agreement with the GCA profiles throughout the entire ROM. Due to the arthritic nature of the left knee these results might be occurring as a consequence of many factors such as a damaged medial meniscus, or damage to any of the primary ligaments which constrain the knee medially. Nonetheless, the analysis of these results is beyond the scope of this thesis and will not be discussed further.

The GCA axial profiles of the right UC MB knee demonstrate agreement with the CPs following 30º of flexion. Before that, the GCA projected profiles do not agree with the corresponding CPs and in fact lie posterior to their corresponding CPs. Conversely, the TEA plots show better agreement with the underlying CPs. While the location of the TEA cannot be confirmed, it is lying in the region of its expected theoretical location.

Based on this assumption and the results obtained in the tibial axial plots, the TEA is better approximating the axis of rotation of the implant due to its correlation with the underlying CPs. The FFA results, albeit the axis being malpositioned, shows agreement in the extension phases, but not through the later flexion angles. Based on the results obtained for the axial COR, in contrast to previously discussed replaced knees, there is not one axis which shows agreement throughout the captured ROM. The TEA is the axis that is showing the best agreement, which agrees with the results obtained in previous participants with replaced knees.

In conclusion, the results for the UC MB implant for P006 have once again shown that the MB model did not show significant improvement over the FB model in terms of axial rotation. This is supported by the results of the other two UC MB implants analysed in this study. Apart from the futile purpose of the mobile tibial insert, which is aimed at providing the knee increased freedom of movement, these results have also provided evidence that the UC feature of these implants in conjunction with the fixed nature of the tibial inserts (FB or MB), is resulting in an overly constrained knee. This is subsequently causing the knee to react abruptly when the knee is "released" from these constraints. Even if this freedom occurs momentarily, the knee adjusts its position to its naturally perceived orientation, creating instability in the patients' knee, due to the sudden change in kinematics. Also, it can be confidently stated that the kinematics calculated for both UC models are anything but close to those calculated for the healthy knees. This would consequently result in abnormal stresses in the replaced knee, which ultimately leads to patient dissatisfaction and implant failures.

6   DISCUSSION & CONCLUSIONS

The primary aim of this thesis was to develop a proof of concept kinematics analysis tool which has the capability of processing 4D CT imaging data for assessing patient-specific knee kinematics.   The secondary and tertiary aims were intended as pilot studies to assess the functionality of the kinematic analysis tool. The secondary aim was to perform a low-powered pilot study to analyse whether mobile bearing knee implants provide additional mobility in comparison to their fixed bearing counterparts. The third aim was directed towards investigating the kinematic crosstalk that different flexion-extension axes demonstrate over specific ROMs. In this section, each aim and their corresponding research questions will be answered and discussed in light of the results obtained and the reviewed literature. The lessons that were learnt throughout the development and implementation of this study will also be mentioned. Before delving into addressing the aims and objectives which were set out in chapter 3, the studies' limitations will be presented.

6.1   STUDY LIMITATIONS

This study had a number of limitations that presented a direct and repercussive effect on the results that were obtained. The allowable ROM of the 4D CT scanner was one of the principal limiting factors in the study, which when combined with the inconsistent ROMs which were captured during the scanning procedures, this resulted in limiting the amount of information that could be extracted from the processed data. Due to the radiologists not being trained in using the 4D CT features of the scanner, the timing of the acquisition was drastically affected as can be seen in the contrasting captured ROMs for the majority of the participants. Furthermore, due to time limitations on the time-window of the 4D CT scanner availabilities during the data collection phase of this study, the participants might not have been given enough time to practice the movement, which resulted in noticeable artefacts in the results. Also, while the SEMAR algorithm, which processed the captured raw data from the scanner to remove the metal artefacts, allowed for the delineation of the metallic implants, it negatively affected the surrounding bone tissue to the extent that all replaced knees had their medial and lateral femoral condylar surfaces segmented as a result of the processing performed on the raw data. The number of participants that were recruited was also a limiting factor which led to the study being a low-powered one. The number of participants is justified by the time constraints which were indirectly imposed on the

study when the 4D CT scanner in the CRIC in Edinburgh was unexpectedly decommissioned. This also burdened the study from a financial perspective, as explained in section 4.1.1, thus further limiting the number of scans which could be commissioned for the study. Notwithstanding, the time and financial constraints, the number of participants for such a study needs to be conservative due to radiation effects of CT scanners. Exposing people to unnecessary radiation is not ethical and has to be adequately justified in order to be allowed to proceed. Therefore, even if there were no financial and time constraints, the number of participants chosen for the study would have to be kept as low as possible without compromising the study's statistical power.

6.2 PRIMARY AIM: DEVELOPMENT OF THE KINEMATIC ANALYSIS SUITE

Table 8: Objectives defined in chapter 3 for the primary aim

Objective	Description	Achieved
1	Review literature pertaining to the kinematic analysis of healthy and replaced knees.	Yes
2	Identify kinematic outcome measures used in literature which can be implemented in the software to maximise the clinical benefit of the outputted data, thus providing a comprehensive kinematic description of the knee(s) being investigated.	Yes
3	Code and compile the software package from the ground up in MATLAB (MATLAB® Release 2016b, The MathWorks, Inc., Massachusetts, United States).	Yes
4	Implement the kinematic analysis software on healthy and replaced knees in order to verify that this proof-of-concept software prototype is feasible.	Yes

The majority of the effort put into the work presented in this thesis was dedicated to the exhaustive task of developing the proof of concept kinematics analysis tool which assesses both healthy and replaced patient-specific knee kinematics. Following the in-depth review of the literature presented in section 2, the features that the kinematic analysis tool was required to have, in order to assess patient-specific knee kinematics confidently, were determined (such as segmentation methods, registration methods, CS implementation methods, et cetera). The review of the literature also highlighted which kinematic outcome measures were required in order to assess patient-specific knee kinematics. These kinematic outcome measures, namely the six DOF kinematics, the contact point profiles and the tibial axial plots (containing the axial COR) were

identified as essential metrics which provide a comprehensive understanding of patient-specific knee kinematics.

The software, which was described in detail in section 4.2, successfully calculated the three kinematic outcome measures of both healthy and replaced knees, as shown by the results which were presented earlier in section 5. The software, which remains a work in progress (refer to chapter 6.6 for future work which is planned to continue building on the achievements presented in this thesis), sufficiently demonstrated the feasibility of using 4D CT scanning technology for the assessment of patient-specific knee kinematics, through its successful implementation on the collected data.

While its success was rewarding, given the time and effort invested in its development, the software unfortunately still carries intrinsic weaknesses. The primary concern with the developed software was that the reliability, repeatability and reproducibility were not quantified and assessed. Each process which was integrated into the workflow of the software was developed in a way so as to ensure that reliability, repeatability and reproducibility are not compromised. This was achieved via the use of validated methods which were found in the literature (such as the tibial plateau identification method proposed by Cobb *et al.* (2008), and the TEA identification method proposed by Eckhoff *et al.* (2007), amongst others), and reducing user input to avoid human error (such as the identification of the transformation matrices which defined the movement of the femoral and tibial bones over time). Typical quality assurance procedures recommend to primarily assess the feasibility of a novel tool, secondarily to validate it and lastly to implement it. At the outset, the plan was to follow these recommendations by performing these validation studies once the software tool is shown to be feasible. This would then allow for assessing the reliability, repeatability and reproducibility of each module individually and also the software in its entirety. However, due to the unforeseen time constraints imposed on this study and the fact that these type of reliability, repeatability and reproducibility studies are time-consuming, it was decided that these validation studies will be proposed for future work (refer to chapter 6.6). Another intrinsic drawback of the software is that it requires the user to be knowledgeable of the anatomy of the knee. The user is required to perform manual segmentation of the knee and accurately select specific ROIs on the segmented models, which, as noted in the results, is not always ideally segmented. Therefore, prior anatomical knowledge is essential for confidence to be ensured. Finally, the registration

of the generic STL bone models onto the scanned model is considered to be a limitation which can be avoided in future studies. If a low resolution (thus low dose) preliminary scan of the ankle, knee and hip areas of the patients is performed, then the relative location of the ankle and the hip with respect to the knee can be accurately obtained. This would eliminate errors which result from the registration of the generic models.

6.3 SECONDARY AIM: DO MOBILE-BEARING KNEE IMPLANTS PROVIDE ADDITIONAL MOBILITY IN COMPARISON TO THEIR FIXED-BEARING COUNTERPARTS?

Table 9: Objectives defined in chapter 3 for the secondary aim

Objective	Description	Achieved
1	Perform a review of the literature concerning the kinematics of fixed and mobile-bearing knees.	Yes
2	Obtain ethical approval to recruit control and patient participants for this pilot study	Yes
3	Develop a scanning protocol for the radiologists and participants to follow during the execution phase of this study.	Yes
4	Collect the raw data and post-process it using the kinematic analysis software.	Yes
5	Using the processed data, analyse and discuss the extracted kinematic results, focusing on the degree of mobility that the two implant types display in comparison to a healthy control knee.	Yes

The patient participant results, which were presented and discussed in this chapter, did not report any significant increase in the mobility of mobile bearing (MB) implants in comparison to their fixed-bearing (FB) counterparts. However, it should be noted that due to the low-powered nature of this pilot study, this statement must be considered with caution since no statistical comparison of the two groups were performed. Performing a statistical comparison on such a low powered study reduces the chance of detecting a true effect, and also risks the consequence of overestimating the true effect.

With that being said, the results obtained for the patient participants revealed that the axial rotation and AP translations reported for the MB implants did not show any significant variations and were similar to those obtained for the FB implants. This was also reflected in the contact point profiles obtained for both groups. Due to the different captured ROMs for the different participants, performing an intra-patient comparison of the data was not practical. The comparison was further impeded by the slight deviations that were recorded in the participants' movements which added to the factors

which made the comparison less feasible. Nonetheless, the individual analyses and discussions presented for each participant are believed to have sufficiently answered this research question given the limitations imposed on the study and the fact that this was a pilot study aimed at assessing the feasibility of the developed kinematic analysis software on replaced knees.

Furthermore, all the implants analysed in this study reported the paradoxical anterior motion, which is a common repercussion of cruciate-deficient implants. With reference to section 2.5.3, the BBraun implants used in this study have a higher anterior wall incorporated into their design which is intended to counteract this paradoxical anterior motion. However, following the analysis of the individual results, it seems that this functional design feature is not achieving its purpose. Another statement which was in disagreement with the results obtained in this study was the statement that the BBraun implants used in this study achieved natural kinematics due to its "superior design". All six DOF results obtained for the replaced knees showed considerable variation in comparison to healthy (natural) knees. The replaced knees were noted to limit the patient in achieving full extension, with the maximum extension angle never going beyond 7.3° (positive). The axial rotation failed to report any signs of the screw-away or screw-home mechanism for the MB knees, while the CP profiles were mostly stacked on top of each other, showing minimal to no signs of axial rotation in MB knees. Furthermore, it was noted that the UC feature in the implant components was resulting in the knee being over-constrained. In instances when the participants adjusted their path of motion, and intrinsically ab/adducted their knee, one of the condyles lifted off the tibia. In response to this reduction in constraint, the femur was noted to opportunistically adjust the remaining DOF to accommodate this reduction in the freedom of movement and attempt to return to its natural position.

In conclusion, while the data collected for the patient participants indicated that MB implants do not provide increased mobility over their FB counterparts, it is being acknowledged that the statement cannot be confidently stated since it is not back by a statistical analysis of plausible power.

6.4 TERTIARY AIM: THE IDEAL FLEXION-EXTENSION AXES OF THE KNEE.

Table 10: Objectives defined in chapter 3 for the tertiary aim

Objective	Description	Achieved
1	Perform an in-depth review of the literature concerning the identification of the ideal surrogate axes to the anatomical FEA(s).	Yes
2	Obtain ethical approval to recruit control and patient participants for this pilot study.	Yes
3	Develop a scanning protocol for the radiologists and participants to follow during the execution phase of this study.	Yes
4	Collect the raw data and post-process it using the kinematic analysis software. Identify the functional FEA of the analysed knees, and embed it into the femoral CS along with the other surrogate FEAs which will be analysed.	Yes
5	Extract the kinematic outcome measures for all the knees whose dynamic movement was captured.	Yes
6	Analyse and discuss the extracted kinematic results for each implemented FEA.	Yes

The control participant results which were presented and comprehensively discussed in this chapter were fitted with four different femoral CS and analysed individually to understand the kinematic crosstalk that each CS displays in light of the reviewed theory and literature in chapter 2. Recall, that in the conclusions derived from the reviewed literature, two theories were identified, the singular-FEA model theory and the dual-FEA model theory. The singular-FEA model theory is being considered as an over-simplified theory in an attempt to facilitate our perception of knee motion, while the dual-FEA theory uses the theory published by the team of Freeman (Hill *et al.*, 2000; Iwaki, Pinskerova and Freeman, 2000; Karrholm, Brandsson and Freeman, 2000; Nakagawa *et al.*, 2000), which has not been challenged to date to the author's knowledge. The dual-FEA theory is based on the fact that the knee rotates around two principal axes, the ECA and the FCA, during the Extension and the Flexion phases respectively. Through reviewed literature, it has been shown that the ECA seems to be approximated by the TEA while the FCA was shown to be excellently approximated by the GCA. The approximation is measured in terms of kinematic crosstalk.

The TEA and GCA were confidently identified for all control participants in this study. In an attempt to identify the functional FEA (FFA) over specific ROMs, therefore allowing for the identification of an FFA for the ECA and FCA separately, the method

proposed by Yin *et al.* (2015) was implemented in the developed software. Upon testing the implemented method over these specific ROMs, that is the Extension and Flexion phases, the algorithm did not converge for any case. As explained in section 4.2.6.2, it was therefore decided to apply the developed FFA methods over the entire captured ROM and comparing the resulting FFA with the other established FEA. Finally, the JCS FEA was implemented in order to emphasis the effects of using a malpositioned FEA.

The TEA showed promising results during both the Extension and the Transition phases of flexion for all control participants. Notwithstanding the undesirable effects which resulted due to participants deviating from the path of motion, the TEA showed minimal signs of kinematic crosstalk for participants whose motion was captured during the Extension and Transition phases (C001, C002 and C004). Apart from the analysis of the six DOF kinematics for the detection of kinematic crosstalk, the Tibial Axial Plots also reflected the TEAs applicability over this ROM due to the CPs and projected FEAs aligning and agreeing with the theory for the applicable phases. On the other hand, the TEA displayed clear signs of kinematic crosstalk during the flexion phase. These were clearly explained and visualised in the corresponding results section.

The GCA, on the other hand, displayed signs of kinematic crosstalk during the Extension and Transition phases, as expected and in agreement with theory. Conversely, during the Flexion phase, the GCA reported minimal signs of kinematic crosstalk in the 6 DOF kinematics and the Tibial Axial Plots. This also agreed with the theory and literature reviewed earlier in this text.

The identified FFAs that is the cVSV, and the cED based variants showed sporadic convergence throughout the entire study population, with no clear trend being identified for any of the two methods. With reference to section 4.2.6.2, the cED based FFA was implemented in an attempt to improve upon the cVSV method (since it was not converging), but there was no apparent improvement vis-à-vis the cVSV's rate of convergence. However, it is good to note that the cED did show signs of improved convergence when implemented on the replaced knees. This might be due to the fact that the replaced knees did not allow the femur to move in the AP and PD directions, therefore allowing for better convergence of the FFA. Conversely, the cVSV showed a reduced incidence of convergence when implemented on the replaced knees. Given the above, the confidence in the converged cases was not strong, such that the FFA results

were considered with caution. The author suggests that this method of identifying the FFA should only be confidently implemented in cases whose ROM exceeds at least 90º.

Finally, the JCS defined FEA, proved its purpose, that is, it clearly showed that a malpositioned FEA, although being defined as per the guidelines given in the JCS paper, results in excessive out of plane rotations and translations, and no correlation in the Tibial Axial Plots. In view of the results obtained for this axis, the reader can appreciate the reason behind the emphasis given to kinematic crosstalk throughout this thesis. It is only when these axes are intricately compared and analysed that the kinematic discrepancies between them become evident.

6.5   CONCLUSION

In this thesis, a 4D CT based analysis of knee kinematics was successfully achieved. A 4D CT scanning protocol was defined, which allowed for capturing the articulation of both healthy and replaced knees. Initially, a comprehensive theoretical and literature review of the current state of research was performed to understand the several aspects that were required to be taken into consideration during the development of the kinematic analysis software. A proof of concept software was developed to process the raw data from the 4D CT scanner and subsequently, segment and extract the relevant knee kinematics for analysis. In order to assess the feasibility of the developed software, two separate low-powered pilot studies were undertaken. Ten participants were recruited on a voluntary basis, had both their knees dynamically scanned, and their collected data was successfully processed through the developed software. The participants' data was used to build on the current research, specifically focusing on two research questions. The mobility of MB and FB knees was assessed for patient participants, while the control participant data was used to identify the applicable ROM for different FEAs.

While the results obtained in this thesis are not statistically significant, given the low-powered nature of the study, they supported the claims and statements posed by the author in the reviewed literature. The MB knees analysed in this study showed no evident difference in their mobility in relation to their fixed bearing counterparts. It was noted that the kinematics that both the FB and MB knees reported are a far cry from the kinematics of a healthy knee, and these discrepancies justify the relatively low patient

satisfaction rates when it comes to TKA. It is envisaged that with the technological leaps that the TKA industry is currently experiencing (such as CAOS, patient-specific implants and surgical tools, robotic surgeries, et cetera) and advanced knee implant designs (such as medially pivoted knees and bicompartmental designs which maintain the vital cruciate ligaments intact) will be more successful in restoring the native kinematics and therefore restoring the knee's original function, leading to a higher incidence of patient satisfaction.

For the applicable ROM of different FEAs, it was evident that neither the TEA nor the GCA is applicable over the <u>entire</u> ROM of the knee. These results highlighted the importance of understanding the joint CSs which are implemented into the anatomical joints when assessing the kinematics. In the reviewed literature, it was evident that numerous researchers overlooked the choice of the axes and seemed to blindly follow the status-quo when it comes to assembling their CSs in their studies. Based on the pilot-study results presented in this thesis for the TEA and the GCA, the research community should further investigate the applicability of these two FEAs over the knees' ROM in order to better understand this theory and disseminate it amongst the research community for further debate and perspectives.

The developed software, although still in its native stages, showed strong potential in extracting knee kinematic data from 4D CT raw data. Considering the rise in the uptake of 4D CT scanners in hospitals worldwide, the short scan times and relatively low doses, this developed technology has the potential of being implemented in routine care to enhance the quality of the treatment given to the patients, thus enhancing their quality of life. The developed software also has the potential of assessing post-operative implant function, assisting with patient rehabilitation, being used as a pre-operative assessment tool for TKAs and revision surgeries and can also be implemented into the design and development processes of future implant designs.

6.6 FUTURE WORK

The work performed in this project provides a basis for future research. The author suggests the following improvements for the developed software:

- Investigating more advanced segmentation algorithms to enhance the quality of the segmented models, such as statistical shape modelling, edge detection methods, deformable modelling and marching cube algorithms. This would allow for enhancing the automated nature of the segmentation workflow while reducing the time-consuming manual segmentation.

- Test out, and, if feasible, implement, the registration of non-segmented (raw) scanned data, to extract the TM that represent the movement occurring between frames. This will avail the user by only having to segment the first frame, while the remaining frames will not be required, since the segmented model of the first frame can be inversely transformed to the original using the TM extracted from the registration of the raw models.

- Replacing the registration of generic STL bone models to identify the ankle and hip centres. This can be achieved by implementing a Statistical Shape Model which would deform to match the scanned models, therefore increasing the accuracy of the registration. Otherwise, a preferred approach would be to eliminate the registration of bone models and instead of performing a preliminary low dose scan of the ankle, knee and hip region of the patient to be able to measure the location of the extremities while avoiding the errors that are introduced with the registration algorithms.

- Remove the JCS FEA module.

- Replace the FFA algorithm. The method proposed by Asano, Akagi and Nakamura (2005), is considered to be a potential candidate for replacing the method of Yin *et al.* (2015) The method of Asano utilises the ankle centre location for the identification of the FFA. Using the ankle centre will magnify the arc of the path of motion in comparison to using the voxel data of the femur, which lies much closer to the FFA than the ankle centre.

- Provide the user with more quantitative results to support in taking the decisions on specific outcomes. For example, the GCA sphere-fitting process can be supported by the medial to lateral ratio following the sphere fitting on both condyles. If the ratio falls within the acceptable range defined earlier in literature,

then the user can proceed. Another instance would be to provide the user with the 3D angle between the GCA and TEA axes and determining if the reported angle falls within the acceptable range identified in the literature. These features will assist the user in making better-informed decisions.

- Allow for plotting a specific selection of FE axes on the plot. As it currently stands, the software only allows for either plotting all FE axes or else plotting them individually (as shown in the results section). The code is to be revised in order to allow the user to plot a selection of axes for comparison.

The following studies are suggested for future work:

- Investigate how to improve the scanning protocol in terms of:

    o Maintaining a more consistent movement during the exercise,

    o Incorporating a live feed of the participants' legs to assist the radiologist in timing the start of the scan.

    o Design a rig to maximise the ROM that can be achieved, and if possible load the knee during the flexion-extension exercise.

- Perform a validity study of the software's modules and the entire software package. This should involve a reliability, repeatability and reproducibility study. A reliability study relates the magnitude of the measurement error in a number of observed measurements. A repeatability study identifies the variation that exists when repeated measurements are made on the same subject under the same conditions (e.g. same observer). A reproducibility study (also known as a method comparison study) is similar to a repeatability study but for varying conditions (e.g. different observers, or methods of measurement). These studies will establish the accuracy and variation of the results being reported by the software, and identify areas of improvement to minimise these errors.

- Perform the two studies which were presented in this thesis with a larger sample size in order to maximise the statistical power of the studies and have clinically significant data which can highlight statistically significant differences between the groups. The focus should be towards the identification of the ideal FEA surrogates to the ECA and FCA, as more research and data collection is required in order to establish the dual-FEA theory in practice.

BIBLIOGRAPHY

Aesculap (2012) *Columbus Knee Design Rationale Brochure*. Palo Alto. Available at: https://www.aesculapimplantsystems.com/content/dam/aesculap-us/us/website/aesculap-implant_systems/hp-section/ortho-product-pages/ortho-resources-pdfs/DOC616-RevA-Columbus-Knee-Design-Rationale-Brochure.pdf.

Aglietti, P. *et al.* (2008) 'Rotational position of femoral and tibial components in TKA using the femoral transepicondylar axis', in *Clinical Orthopaedics and Related Research*. doi: 10.1007/s11999-008-0452-8.

Aly, A. A., Bin Deris, S. and Zaki, N. (2011) 'Research Review for Digital Image Segmentation Techniques', *International Journal of Computer Science and Information Technology*, 3(5). doi: 10.5121/ijcsit.2011.3509.

American Academy of Orthopaedic Surgeons (2014) *Arthritis of the Knee*. Available at: https://orthoinfo.aaos.org/en/diseases--conditions/arthritis-of-the-knee/ (Accessed: 5 October 2019).

AO foundation (2008) *Lateral parapatellar approach to the distal femur*. Available at: https://www2.aofoundation.org/wps/portal/!ut/p/a0/04_Sj9CPykssy0xPLMnMz0vMA fGjzOKN_A0M3D2DDbz9_UMMDRyDXQ3dw9wMDAzMjfULsh0VAbWjLW0!/? approach=Lateral parapatellar approach&bone=Femur&segment=Distal&showPage=approach&contentUrl=/srg/33/ 04-Approaches/A21-lat (Accessed: 12 July 2018).

Argenson, J. N. A. *et al.* (2012) 'The outcome of rotating-platform total knee arthroplasty with cement at a minimum of ten years of follow-up', *Journal of Bone and Joint Surgery - Series A*. doi: 10.2106/JBJS.K.00263.

Asano, T., Akagi, M. and Nakamura, T. (2005) 'The Functional Flexion-Extension Axis of the Knee Corresponds to the Surgical Epicondylar Axis', *The Journal of Arthroplasty*, 20(8), pp. 1060–1067. doi: 10.1016/j.arth.2004.08.005.

Bach, J. M. and Hull, M. L. (1995) 'A New Load Application System for In Vitro Study of Ligamentous Injuries to the Human Knee Joint', *Journal of Biomechanical Engineering*. doi: 10.1115/1.2794195.

Bamberg, F. *et al.* (2011) 'Metal artifact reduction by dual energy computed

tomography using monoenergetic extrapolation', *European Radiology*. doi: 10.1007/s00330-011-2062-1.

Banks, S. *et al.* (2016) 'In Vivo kinematics of a medially conforming and rotationally unconstrained TKA design', *Orthopaedic Proceedings*, 98-B(SUPP_1), p. 35. doi: 10.1302/1358-992X.98BSUPP_1.ISTA2014-035.

Banks, S. A. and Hodge, W. A. (2004) '2003 Hap Paul Award paper of the International Society for Technology in Arthroplasty', *The Journal of Arthroplasty*, 19(7), pp. 809–816. doi: 10.1016/j.arth.2004.04.011.

Barrett, W. P. *et al.* (2011) 'Comparison of Radiographic Alignment of Imageless Computer-Assisted Surgery vs Conventional Instrumentation in Primary Total Knee Arthroplasty', *The Journal of Arthroplasty*, 26(8), pp. 1273-1284.e1. doi: 10.1016/j.arth.2011.04.037.

Bellemans, J. *et al.* (2012) 'The Chitranjan Ranawat Award: Is Neutral Mechanical Alignment Normal for All Patients?: The Concept of Constitutional Varus', *Clinical Orthopaedics and Related Research®*. doi: 10.1007/s11999-011-1936-5.

Bellemans, J., Ries, M. D. and Victor, J. M. K. (2005) *TKA - A Guide To Better Performance*.

Berger, R. A. *et al.* (1993) 'Determining the Rotational Alignment of the Femoral Component in Total Knee Arthroplasty Using the Epicondylar Axis', *Clinical Orthopaedics and Related Research*, (286), pp. 40–47. doi: 10.1097/00003086-199301000-00008.

Berme, N., Engin, A. E. and Correia da Silva, K. M. (eds) (1985) *Biomechanics of Normal and Pathological Human Articulating Joints*, *Biomechanics of Normal and Pathological Human Articulating Joints*. Dordrecht: Springer Netherlands. doi: 10.1007/978-94-009-5117-4.

Bistolfi, A. *et al.* (2013) 'Comparison of fixed and mobile-bearing total knee arthroplasty at a mean follow-up of 116 months', *Journal of Bone and Joint Surgery - Series A*. doi: 10.2106/JBJS.L.00327.

Blankevoort, L. and Huiskes, R. (1996) 'Validation of a three-dimensional model of the knee', *Journal of Biomechanics*. doi: 10.1016/0021-9290(95)00149-2.

Blankevoort, L., Huiskes, R. and de Lange, A. (1988) 'The envelope of passive knee

joint motion', *Journal of Biomechanics*, 21(9), pp. 705–720. doi: 10.1016/0021-9290(88)90280-1.

Blankevoort, L., Huiskes, R. and de Lange, A. (1990) 'Helical axes of passive knee joint motions', *Journal of Biomechanics*. doi: 10.1016/0021-9290(90)90379-H.

Blunn, G. W. *et al.* (1997) 'Wear in retrieved condylar knee arthroplasties: A comparison of wear in different designs of 280 retrieved condylar knee prostheses', *Journal of Arthroplasty*. doi: 10.1016/S0883-5403(97)90024-3.

Boguszewski, D. V. *et al.* (2016) 'Location of the natural knee axis for internal–external tibial rotation', *The Knee*, 23(6), pp. 1083–1088. doi: 10.1016/j.knee.2015.11.003.

Bottema, D., Roth, B. and Veldkamp, G. R. (1980) 'Theoretical Kinematics', *Journal of Applied Mechanics*. doi: 10.1115/1.3153630.

Van der Bracht, H. *et al.* (2010) 'Is there any superiority in the clinical outcome of mobile-bearing knee prosthesis designs compared to fixed-bearing total knee prosthesis designs in the treatment of osteoarthritis of the knee joint?', *Knee Surgery, Sports Traumatology, Arthroscopy*. doi: 10.1007/s00167-009-0973-z.

Brandsson, S. *et al.* (2001) 'Kinematics after tear in the anterior cruciate ligament: Dynamic bilateral radiostereometric studies in 11 patients', *Acta Orthopaedica Scandinavica*. doi: 10.1080/000164701753542032.

Brantigan, O. C. and Voshell, A. F. (1941) 'THE MECHANICS OF THE LIGAMENTS AND MENISCI OF THE KNEE JOINT', *J Bone Joint Surg Am*.

Braune, C. W. and Fischer, O. (1891) *Die bewegungen des kniegelenks nach einer neuen methode am lebenden menschen gemessen*. Edited by S. Hirzel. Leipzig.

Brook, O. R. *et al.* (2012) 'Spectral CT with metal artifacts reduction software for improvement of tumor visibility in the vicinity of gold fiducial markers', *Radiology*. doi: 10.1148/radiol.12111170.

Buechel, F. F. *et al.* (2001) 'Twenty-year evaluation of meniscal bearing and rotating platform knee replacements', in *Clinical Orthopaedics and Related Research*. doi: 10.1097/00003086-200107000-00008.

Buechel, F. F. and Pappas, M. J. (1986) 'The New Jersey low-contact-stress knee

replacement system: Biomechanical rationale and review of the first 123 cemented cases', *Archives of Orthopaedic and Traumatic Surgery*. doi: 10.1007/BF00435480.

Buechel, F. F. and Pappas, M. J. (1989) 'New Jersey low contact stress knee replacement system. Ten-year evaluation of meniscal bearings', *Orthopedic Clinics of North America*.

Bugnion, E. (1892) *Le mechanism du genou. Extrait du recueil inaugural de l'Universitie Lausanne.* Lausanne.

Bull, A. M. J. and Amis, A. A. (1998) 'Knee joint motion: Description and measurement', *Proceedings of the Institution of Mechanical Engineers, Part H: Journal of Engineering in Medicine*. doi: 10.1243/0954411981534132.

Callaghan, J. *et al.* (2000) 'Mobile-Bearing Knee Replacement : Concepts and Results*+.', *J Bone Joint Surg Am*, 82(7), p. 1020. Available at: http://ovidsp.ovid.com/ovidweb.cgi?T=JS&PAGE=reference&D=yrovftd&NEWS=N &AN=00004623-200007000-00013.

Callaghan, J. J. *et al.* (2010) 'Cemented Rotating-Platform Total Knee Replacement', *The Journal of Bone and Joint Surgery-American Volume*. doi: 10.2106/jbjs.i.01012.

Cappozzo, A. (1991) 'Three-dimensional analysis of human walking: Experimental methods and associated artifacts', *Human Movement Science*. doi: 10.1016/0167-9457(91)90047-2.

Carothers, J. T. *et al.* (2011) 'Mobile-Bearing Total Knee Arthroplasty. A Meta-Analysis', *Journal of Arthroplasty*. doi: 10.1016/j.arth.2010.05.015.

Cherian, J. J. *et al.* (2014) 'Mechanical, Anatomical, and Kinematic Axis in TKA: Concepts and Practical Applications', *Current Reviews in Musculoskeletal Medicine*, 7(2), pp. 89–95. doi: 10.1007/s12178-014-9218-y.

Chouteau, J. *et al.* (2009) 'Mobile-bearing insert translational and rotational kinematics in a PCL-retaining total knee arthroplasty', *Orthopaedics and Traumatology: Surgery and Research*. doi: 10.1016/j.otsr.2009.03.012.

Churchill, D. L. *et al.* (1996) 'A compound pinned hinge model of knee joint kinematics.', *Trans Orthop Res. Soc.*, 21(717).

Churchill, D. L. *et al.* (1998) 'The Transepicondylar Axis Approximates the Optimal

Flexion Axis of the Knee', *Clinical Orthopaedics and Related Research*, 356, pp. 111–118. doi: 10.1097/00003086-199811000-00016.

Cobb, J. P. *et al.* (2008) 'The anatomical tibial axis', *The Journal of Bone and Joint Surgery. British volume*, 90-B(8), pp. 1032–1038. doi: 10.1302/0301-620X.90B8.19905.

Cole, G. K. *et al.* (1993) 'Application of the Joint Coordinate System to Three-Dimensional Joint Attitude and Movement Representation: A Standardization Proposal', *Journal of Biomechanical Engineering*, 115(4A), p. 344. doi: 10.1115/1.2895496.

Colizza, W. A., Insall, J. N. and Scuderi, G. R. (1995) 'The posterior stabilized total knee prosthesis: Assessment of polyethylene damage and osteolysis after a ten-year-minimum follow-up', *Journal of Bone and Joint Surgery - Series A*. doi: 10.2106/00004623-199511000-00011.

D'Entremont, A. G. *et al.* (2013) 'Do dynamic-based MR knee kinematics methods produce the same results as static methods?', *Magnetic Resonance in Medicine*. doi: 10.1002/mrm.24425.

D'Entremont, A. G. *et al.* (2014) 'Effect of opening-wedge high tibial osteotomy on the three-Dimensional kinematics of the knee', *Bone and Joint Journal*. doi: 10.1302/0301-620X.96B9.32522$2.00.

D'Lima, D. D. *et al.* (2001) 'Polyethylene wear and variations in knee kinematics', in *Clinical Orthopaedics and Related Research*. doi: 10.1097/00003086-200111000-00015.

D'Lima, D. D., Chen, P. C. and Colwell, C. W. (2001) 'Polyethylene Contact Stresses, Articular Congruity, and Knee Alignment', *Clinical Orthopaedics and Related Research*, 392, pp. 232–238. doi: 10.1097/00003086-200111000-00029.

Daniilidis, K. *et al.* (2012) 'Highly conforming polyethylene inlays reduce the in vivo variability of knee joint kinematics after total knee arthroplasty', *Knee*. doi: 10.1016/j.knee.2011.04.001.

Dennis, D. A. *et al.* (1996) 'In vivo knee kinematics derived using an inverse perspective technique', in *Clinical Orthopaedics and Related Research*. doi: 10.1097/00003086-199610000-00015.

Dennis, D. A. *et al.* (2003) 'Multicenter Determination of in Vivo Kinematics after Total Knee Arthroplasty', in *Clinical Orthopaedics and Related Research*.

Dennis, D. A. *et al.* (2005) 'Mobile-bearing total knee arthroplasty: Do the polyethylene bearings rotate?', in *Clinical Orthopaedics and Related Research*. doi: 10.1097/01.blo.0000185464.23505.6e.

Deserno, Thomas M. (2011) *Biomedical Image Processing*. 1st edn. Edited by Thomas Martin Deserno. Berlin, Heidelberg: Springer Berlin Heidelberg (Biological and Medical Physics, Biomedical Engineering). doi: 10.1007/978-3-642-15816-2.

Diaz, G. (2018) *Radiation from X-rays*, *GrepMed*. Available at: https://www.grepmed.com/images/1828/risks-comparison-table-imaging-patientinfo-radiation-background.

Dieppe, P. (2000) 'Towards a better understanding of osteoarthritis of the knee joint', *The Knee*, 7(3), pp. 135–137. doi: 10.1016/S0968-0160(00)00043-0.

van Dijk, R., Huiskes, R. and Selvik, G. (1979) 'Roentgen stereophotogrammetric methods for the evaluation of the three dimensional kinematic behaviour and cruciate ligament length patterns of the human knee joint', *Journal of Biomechanics*, 12(9), pp. 727–731. doi: 10.1016/0021-9290(79)90021-6.

Doral Medical Imaging (2006) *Magnetic Resonance Imaging*. Available at: http://www.doralmri.com/images/mri picture.jpg (Accessed: 14 August 2019).

Draper, C. E. *et al.* (2008) 'Feasibility of using real-time MRI to measure joint kinematics in 1.5T and open-bore 0.5T systems', *Journal of Magnetic Resonance Imaging*. doi: 10.1002/jmri.21413.

Dzung, L., Chenyang, X. and Prince, J. L. (1998) 'A survey of current methods in medical image segmentation', *Department of ECE, Johns Hopkins Univ., Tech. Rep.*.

Eckhoff, D. *et al.* (2007a) 'An ABJS best paper: Difference between the epicondylar and cylindrical axis of the knee', in *Clinical Orthopaedics and Related Research*. doi: 10.1097/BLO.0b013e318112416b.

Eckhoff, D. *et al.* (2007b) 'Difference Between the Epicondylar and Cylindrical Axis of the Knee', *Clinical Orthopaedics and Related Research*, PAP, pp. 238–44. doi: 10.1097/BLO.0b013e318112416b.

Eckhoff, D. G. *et al.* (2001) 'Three-Dimensional Morphology of the Distal Part of the Femur Viewed in Virtual Reality - Part I', *The Journal of Bone and Joint Surgery-American Volume*, 83, pp. 43–50. doi: 10.2106/00004623-200100021-00010.

Eckhoff, D. G. *et al.* (2003) 'Three-Dimensional Morphology and Kinematics of the Distal Part of the Femur Viewed in Virtual Reality - Part II', *The Journal of Bone and Joint Surgery-American Volume*, 85(SUPPL. 4), pp. 97–104. doi: 10.2106/00004623-200300004-00012.

Eckhoff, D. G. *et al.* (2005) 'Three-dimensional mechanics, kinematics, and morphology of the knee viewed in virtual reality', in *Journal of Bone and Joint Surgery - Series A*. doi: 10.2106/00004623-200511002-00009.

Elias, S. G., Freeman, M. A. R. and Gokcay, E. I. (1990) 'A Correlative Study of the Geometry and Anatomy of the Distal Femur', *Clinical Orthopaedics and Related Research*, (260), pp. 98–103. doi: 10.1097/00003086-199011000-00018.

Endo, M. *et al.* (2003) 'Four-dimensional computed tomography (4D CT) - Concepts and preliminary development', *Radiation Medicine - Medical Imaging and Radiation Oncology*.

Esses, D. *et al.* (2004) 'Ability of CT to alter decision making in elderly patients with acute abdominal pain', *American Journal of Emergency Medicine*. doi: 10.1016/j.ajem.2004.04.004.

Essner, A. *et al.* (2011) 'The influence of material and design on total knee replacement wear.', *The journal of knee surgery*.

Fantozzi, S. *et al.* (2006) 'Femoral rollback of cruciate-retaining and posterior-stabilized total knee replacements: In vivo fluoroscopic analysis during activities of daily living', *Journal of Orthopaedic Research*. doi: 10.1002/jor.20306.

Feng, Y. *et al.* (2016) 'In-vivo analysis of flexion axes of the knee: Femoral condylar motion during dynamic knee flexion', *Clinical Biomechanics*, 32, pp. 102–107. doi: 10.1016/j.clinbiomech.2015.12.006.

Fick, A. (1877) 'Zur Mechanik des Kniegelenks.', *Arch Anat Entw Gesch*, pp. 440–448.

Fick, R. (1911) 'Handbuch der Anatomie und Mechanik der Gelenke.', 2, pp. 109–17.

Fiedler, C. *et al.* (2011) 'Mathematical study on the guidance of the tibiofemoral joint as theoretical background for total knee replacements.', *Acta of bioengineering and biomechanics*, 13(4), pp. 38–49. Available at: http://www.ncbi.nlm.nih.gov/pubmed/22339245.

Floerkemeier, T. *et al.* (2011) 'Physiologically shaped knee arthroplasty induces natural roll-back.', *Technology and health care : official journal of the European Society for Engineering and Medicine*, 19(2), pp. 91–102. doi: 10.3233/THC-2011-0616.

Frankel, V., Burstein, A. and Brooks, D. (1971) 'Biomechanics of Internal Derangement of the Knee', *J Bone Joint Surg [Br]*, 53(5), pp. 945–77. doi: 10.1097/00004623-197153050-00010.

Freeman, M. A. R. and Pinskerova, V. (2005) 'The movement of the normal tibio-femoral joint', *Journal of Biomechanics*. doi: 10.1016/j.jbiomech.2004.02.006.

Fu, F. H., Harner, C. D. and Vince, K. . (1994) 'Anatomy of the Knee', in Fu, F. H., Harner, C. D., and Vince, K. G. (eds) *Knee Surgery1*. Volume 1. Baltimore: Williams & Wilkins, pp. 1–54.

Fuchs, V. R. and Sox, H. C. (2001) 'Physicians' views of the relative importance of thirty medical innovations.', *Health affairs (Project Hope)*, 20(5), pp. 30–42. Available at: http://www.ncbi.nlm.nih.gov/pubmed/11558715.

Fuller, J. *et al.* (1997) 'A comparison of lower-extremity skeletal kinematics measured using skin-and pin-mounted markers', *Human Movement Science*. doi: 10.1016/S0167-9457(96)00053-X.

Garg, A. and Walker, P. S. (1990) 'Prediction of total knee motion using a three-dimensional computer-graphics model', *Journal of Biomechanics*. doi: 10.1016/0021-9290(90)90368-D.

Garling, E. H. *et al.* (2007) 'Limited rotation of the mobile-bearing in a rotating platform total knee prosthesis', *Journal of Biomechanics*, 40, pp. S25–S30. doi: 10.1016/j.jbiomech.2007.02.013.

Gergely, I. *et al.* (2017) 'Will Total Knee Replacement Ever Provide Normal Knee Function ?', *Journal of Interdisciplinary Medicine*, 2(38), pp. 22–26. doi: 10.1515/jim-2017-0040.

Ghonge, N. P. (2013) 'Computed Tomography in the 21st century: Current status & future prospects', *Journal International Medical Sciences Academy*, 26(1), pp. 35–42.

Gilles, B. *et al.* (2005) 'Bone motion analysis from dynamic MRI: Acquisition and tracking', in *Academic Radiology*. doi: 10.1016/j.acra.2005.08.006.

Goebel, D. and Schultz, W. (2012) 'The Columbus Knee System: 4-Year Results of a New Deep Flexion Design Compared to the NexGen Full Flex Implant', *Arthritis*. doi: 10.1155/2012/213817.

Goldman, L. W. (2007) 'Principles of CT and CT technology', *Journal of Nuclear Medicine Technology*. doi: 10.2967/jnmt.107.042978.

Gondim Teixeira, P. A. *et al.* (2014) 'Total hip prosthesis CT with single-energy projection-based metallic artifact reduction: Impact on the visualization of specific periprosthetic soft tissue structures', *Skeletal Radiology*. doi: 10.1007/s00256-014-1923-5.

Gondim Teixeira, P. A. *et al.* (2015) 'Musculoskeletal wide detector CT: Principles, techniques and applications in clinical practice and research', *European Journal of Radiology*, 84(5), pp. 892–900. doi: 10.1016/j.ejrad.2014.12.033.

Gonzalez, R. C., Woods, R. E. and Masters, B. R. (2009) 'Digital Image Processing, Third Edition', *Journal of Biomedical Optics*. doi: 10.1117/1.3115362.

Griffin, F. M. *et al.* (2000) 'Anatomy of the epicondyles of the distal femur: MRI analysis of normal knees', *Journal of Arthroplasty*. doi: 10.1016/S0883-5403(00)90739-3.

Grood, E. S. and Suntay, W. J. (1983) 'A Joint Coordinate System for the Clinical Description of Three-Dimensional Motions: Application to the Knee', *Journal of Biomechanical Engineering*. doi: 10.1115/1.3138397.

Grupp, T. M. *et al.* (2009) 'Fixed bearing knee congruency - Influence on contact mechanics, abrasive wear and kinematics', *International Journal of Artificial Organs*. doi: 10.1177/039139880903200405.

H. Shaikh, M., Panbude, S. and Joshi, A. (2014) 'Image Segmentation Techniques and its applications for Knee Joints: a Survey', *IOSR Journal of Electronics and Communication Engineering*, 9(5), pp. 23–28. doi: 10.9790/2834-09542328.

Hakki, S. *et al.* (2013) 'Columbus navigated TKA system: Clinical and radiological results at a minimum of 5 years with survivorship analysis', *Orthopedics*. doi: 10.3928/01477447-20130222-19.

Hamelynck, K. J. and Stiehl, J. B. (2002) *LCS® Mobile Bearing Knee Arthroplasty*. 1st edn. Berline: Springer-Verlag Berlin Heidelberg. doi: 10.1007/978-3-642-59347-5.

Han, J., Kamber, M. and Pei, J. (2012) *Data Mining: Concepts and Techniques*. 3rd edn. Morgan Kaufmann. doi: 10.1016/C2009-0-61819-5.

Haralick, R. M. and Shapiro, L. G. (1985) 'Image segmentation techniques', *Computer Vision, Graphics, and Image Processing*, 29(1), pp. 100–132. doi: 10.1016/S0734-189X(85)90153-7.

Harman, M. K. *et al.* (2012) 'Prosthesis alignment affects axial rotation motion after total knee replacement: A prospective in vivo study combining computed tomography and fluoroscopic evaluations', *BMC Musculoskeletal Disorders*. doi: 10.1186/1471-2474-13-206.

Harner, C. D. *et al.* (1995) 'The Human Posterior Cruciate Ligament Complex: An Interdisciplinary Study: Ligament Morphology and Biomechanical Evaluation', *The American Journal of Sports Medicine*. doi: 10.1177/036354659502300617.

Harwin, S. F. (2003) 'Complications of unicompartmental knee arthroplasty', *Seminars in Arthroplasty*, 14(4), pp. 232–244. doi: 10.1053/j.sart.2003.09.001.

Hatayama, K. *et al.* (2011) 'Relationship Between Femoral Component Rotation and Total Knee Flexion Gap Balance on Modified Axial Radiographs', *Journal of Arthroplasty*. doi: 10.1016/j.arth.2010.05.029.

Hill, P. F. *et al.* (2000) 'Tibiofemoral movement 2: the loaded and unloaded living knee studied by MRI', *The Journal of Bone and Joint Surgery*, 82(8), pp. 1196–1198. doi: 10.1302/0301-620X.82B8.10716.

Hirschmann, M. T. and Becker, R. (2015) *The Unhappy Total Knee Replacement*. Edited by M. T. Hirschmann and R. Becker. Cham: Springer International Publishing. doi: 10.1007/978-3-319-08099-4.

Hofmann, A. A. *et al.* (2000) 'Posterior stabilization in total knee arthroplasty with use of an ultracongruent polyethylene insert', *Journal of Arthroplasty*. doi:

10.1054/arth.2000.6633.

Hohmann, E. and Bryant, A. (2007) 'Closing or Opening Wedge High Tibial Osteotomy: Watch Out for the Slope', *Operative Techniques in Orthopaedics*. doi: 10.1053/j.oto.2006.09.010.

Hollister, A. M. *et al.* (1993) 'The Axes of Rotation of the Knee', *Clinical Orthopaedics and Related Research*. doi: 10.1097/00003086-199305000-00033.

Hricak, H. *et al.* (2011) 'Managing radiation use in medical imaging: A multifaceted challenge', *Radiology*. doi: 10.1148/radiol.10101157.

Hsu, R. W. W. *et al.* (1990) 'Normal axial alignment of the lower extremity and load-bearing distribution at the knee', *Clinical Orthopaedics and Related Research*.

Huang, C. H. *et al.* (2003) 'Long-Term Results of Low Contact Stress Mobile-Bearing Total Knee Replacements', *Clinical Orthopaedics and Related Research*. doi: 10.1097/01.blo.0000093890.12372.46.

Huang, C. H., Liau, J. J. and Cheng, C. K. (2007) 'Fixed or mobile-bearing total knee arthroplasty', *Journal of Orthopaedic Surgery and Research*. doi: 10.1186/1749-799X-2-1.

Huang, L. (2017) *A Concise Introduction to Mechanics of Rigid Bodies*. 2nd edn. Edited by L. Huang. Cham: Springer International Publishing. doi: 10.1007/978-3-319-45041-4.

Hung, M. C. and Yang, D. L. (2001) 'An efficient fuzzy C-means clustering algorithm', in *Proceedings - IEEE International Conference on Data Mining, ICDM*.

Hunt, M. A. *et al.* (2008) 'Towards a biopsychosocial framework of osteoarthritis of the knee.', *Disability and rehabilitation*, 30(1), pp. 54–61. doi: 10.1080/09638280701189960.

Incavo, S., Beynnon, B. and Coughlin, K. (2005) 'In vitro kinematics of the replaced knee', in *Total Knee Arthroplasty: A Guide to Get Better Performance*. doi: 10.1007/3-540-27658-0_23.

Iwaki, H., Pinskerova, V. and Freeman, M. A. R. (2000) 'Tibiofemoral movement 1: the shapes and relative movements of the femur and tibia in the unloaded cadaver knee', *The Journal of Bone and Joint Surgery*. doi: 10.1302/0301-620X.82B8.10717.

Jacobs, W. C. H. *et al.* (2012) 'Functional performance of mobile versus fixed bearing total knee prostheses: a randomised controlled trial', *Knee Surgery, Sports Traumatology, Arthroscopy*, 20(8), pp. 1450–1455. doi: 10.1007/s00167-011-1684-9.

Jacobs, W. C. H., Clement, D. J. and Wymenga, A. B. (2005) 'Retention versus removal of the posterior cruciate ligament in total knee replacement: A systematic literature review within the Cochrane framework', *Acta Orthopaedica*. doi: 10.1080/17453670510045345.

Jerosch, J. *et al.* (2002) 'Interindividual reproducibility in perioperative rotational alignment of femoral components in knee prosthetic surgery using the transepicondylar axis', *Knee Surgery, Sports Traumatology, Arthroscopy*. doi: 10.1007/s00167-001-0271-x.

Jones, O. (2017) *TheTibia*, *TeachMeAnatomy*. Available at: http://teachmeanatomy.info/lower-limb/bones/the-tibia/#Proximal.

Jones, O. (2018a) *The Femur*, *TeachMeAnatomy*. Available at: http://teachmeanatomy.info/lower-limb/bones/femur/.

Jones, O. (2018b) *The Knee Joint*. Available at: http://teachmeanatomy.info/lower-limb/joints/the-knee-joint/.

Jonsson, H., Kärrholm, J. and Elmqvist, L.-G. (1989) 'Kinematics of active knee extension after tear of the anterior cruciate ligament', *The American Journal of Sports Medicine*, 17(6), pp. 796–802. doi: 10.1177/036354658901700613.

Kadaba, M. P., Ramakrishnan, H. K. and Wootten, M. E. (1990) 'Measurement of lower extremity kinematics during level walking.', *Journal of orthopaedic research : official publication of the Orthopaedic Research Society*. London: Springer London, 8(3), pp. 383–92. doi: 10.1002/jor.1100080310.

Kaiser, J. *et al.* (2016) 'Accuracy of model-based tracking of knee kinematics and cartilage contact measured by dynamic volumetric MRI', *Medical Engineering and Physics*. doi: 10.1016/j.medengphy.2016.06.016.

Kalender, W. A., Hebel, R. and Ebersberger, J. (1987) 'Reduction of CT artifacts caused by metallic implants', *Radiology*. doi: 10.1148/radiology.164.2.3602406.

Kaneda, Y. *et al.* (1997) 'Experimental Study on External Tibial Rotation of the Knee', *The American Journal of Sports Medicine*, 25(6), pp. 796–800. doi:

10.1177/036354659702500611.

Kang, K.-T. *et al.* (2018) 'Comparison of Kinematics in Cruciate Retaining and Posterior Stabilized for Fixed and Rotating Platform Mobile-Bearing Total Knee Arthroplasty with respect to Different Posterior Tibial Slope.', *BioMed research international*, 2018, p. 5139074. doi: 10.1155/2018/5139074.

Kapandji, I. A. (1970) 'The Knee.', in Kapandji, I. A. (ed.) *The physiology of the Joints*. 2nd edn. Edinburgh: Churchill Livingstone, pp. 72–135.

Kapandji, I. A. (1971) 'The physiology of the joints, vol. 2: Lower Limb. By I. A. Kapandji, Paris. Second edition. 11 × 8½ in. Pp. 219. Illustrated. 1970. Edinburgh and London: E. & S. Livingstone Ltd. £2.75', *British Journal of Surgery*. Wiley, 58(5), pp. 403–403. doi: 10.1002/bjs.1800580528.

Karrholm, J., Brandsson, S. and Freeman, M. A. R. (2000) 'Tibiofemoral movement 4 : changes of axial tibial rotation caused by forced rotation at the weight-bearing knee studied by RSA', *Journal of Bone and Joint Surgery - British Volume*, 82(B), pp. 1201–1203. doi: 0301-620X/00/810715.

Karuppal, R. (2016) 'Kinematic alignment in total knee arthroplasty: Does it really matter?', *Journal of Orthopaedics*, 13(4), pp. A1–A3. doi: 10.1016/j.jor.2016.10.001.

Katz, M. A. *et al.* (2001) 'Determining femoral rotational alignment in total knee arthroplasty', *The Journal of Arthroplasty*, 16(3), pp. 301–305. doi: 10.1054/arth.2001.21456.

Kauffmann, C. *et al.* (2003) 'Computer-aided method for quantification of cartilage thickness and volume changes using MRI: Validation study using a synthetic model', *IEEE Transactions on Biomedical Engineering*. doi: 10.1109/TBME.2003.814539.

Kidoh, M. *et al.* (2014) 'Reduction of dental metallic artefacts in CT: Value of a newly developed algorithm for metal artefact reduction (O-MAR)', *Clinical Radiology*. doi: 10.1016/j.crad.2013.08.008.

Kinzel, G. L. and Gutkowski, L. J. (1983) 'Joint models, degrees of freedom, and anatomical motion measurement.', *Journal of biomechanical engineering*. doi: 10.1115/1.3138385.

Kinzel, V., Ledger, M. and Shakespeare, D. (2005) 'Can the epicondylar axis be defined accurately in total knee arthroplasty?', *Knee*. doi:

10.1016/j.knee.2004.09.003.

Koo, S. and Andriacchi, T. P. (2008) 'The knee joint center of rotation is predominantly on the lateral side during normal walking', *Journal of Biomechanics*, 41(6), pp. 1269–1273. doi: 10.1016/j.jbiomech.2008.01.013.

Kozanek, M. *et al.* (2009) 'Tibiofemoral kinematics and condylar motion during the stance phase of gait', *Journal of Biomechanics*. doi: 10.1016/j.jbiomech.2009.05.003.

Kroon, D.-J. (2016) 'Finite Iterative Closest Point'. MATLAB Central File Exchange. Available at: www.mathworks.com/matlabcentral/fileexchange/24301-finite-iterative-closest-point.

Kurosawa, H. *et al.* (1985) 'Geometry and motion of the knee for implant and orthotic design', *Journal of Biomechanics*. doi: 10.1016/0021-9290(85)90663-3.

Kurtz, S. M. *et al.* (2009) 'Future Young Patient Demand for Primary and Revision Joint Replacement: National Projections from 2010 to 2030', *Clinical Orthopaedics and Related Research®*, 467(10), pp. 2606–2612. doi: 10.1007/s11999-009-0834-6.

LaPrade, R. F. (2007) 'The Anatomy of the Medial Part of the Knee', *The Journal of Bone and Joint Surgery (American)*, 89(9), p. 2000. doi: 10.2106/JBJS.F.01176.

Laskin, R. S. *et al.* (2000) 'Deep-dish congruent tibial component use in total knee arthroplasty: A randomized prospective study', in *Clinical Orthopaedics and Related Research*. doi: 10.1097/00003086-200011000-00006.

Last, R. J. (1950) 'THE POPLITEUS MUSCLE AND THE LATERAL MENISCUS', *The Journal of Bone and Joint Surgery. British volume*, 32-B(1), pp. 93–99. doi: 10.1302/0301-620X.32B1.93.

Lee, T. Y. and Chhem, R. K. (2010) 'Impact of new technologies on dose reduction in CT', *European Journal of Radiology*. doi: 10.1016/j.ejrad.2010.06.036.

Lewis, J. L. and Lew, W. D. (1978) 'A Method for Locating an Optimal "Fixed" Axis of Rotation for the Human Knee Joint', *Journal of Biomechanical Engineering*. doi: 10.1115/1.3426209.

Li, G., Wuerz, T. H. and DeFrate, L. E. (2004) 'Feasibility of Using Orthogonal Fluoroscopic Images to Measure In Vivo Joint Kinematics', *Journal of Biomechanical Engineering*, 126(2). doi: 10.1115/1.1691448.

Li, J. S. *et al.* (2013) 'Kinematic characteristics of the tibiofemoral joint during a step-up activity', *Gait and Posture*. doi: 10.1016/j.gaitpost.2013.03.004.

Li, N. *et al.* (2014) 'Posterior cruciate-retaining versus posterior stabilized total knee arthroplasty: A meta-analysis of randomized controlled trials', *Knee Surgery, Sports Traumatology, Arthroscopy*. doi: 10.1007/s00167-012-2275-0.

Lu, T. W. and O'Connor, J. J. (1999) 'Bone position estimation from skin marker co-ordinates using global optimisation with joint constraints', *Journal of Biomechanics*. doi: 10.1016/S0021-9290(98)00158-4.

Lucchetti, L. *et al.* (1998) 'Skin movement artefact assessment and compensation in the estimation of knee-joint kinematics', *Journal of Biomechanics*. doi: 10.1016/S0021-9290(98)00083-9.

Lustig, S. *et al.* (2008) 'Relationship between the surgical epicondylar axis and the articular surface of the distal femur: An anatomic study', *Knee Surgery, Sports Traumatology, Arthroscopy*. doi: 10.1007/s00167-008-0551-9.

Lützner, J. *et al.* (2017) 'No difference in range of motion between ultracongruent and posterior stabilized design in total knee arthroplasty: a randomized controlled trial', *Knee Surgery, Sports Traumatology, Arthroscopy*, 25(11). doi: 10.1007/s00167-016-4331-7.

Mahfouz, M. *et al.* (2012) 'Three-dimensional morphology of the knee reveals ethnic differences', in *Clinical Orthopaedics and Related Research*. doi: 10.1007/s11999-011-2089-2.

Mahoney, O. M. *et al.* (2012) 'No functional advantage of a mobile bearing posterior stabilized TKA.', *Clinical Orthopaedics and Related Research*, 470(1), pp. 33–44. doi: 10.1007/s11999-011-2114-5.

Majeed, A. and Aylin, P. (2005) 'The ageing population of the United Kingdom and cardiovascular disease', *BMJ*, 331(7529), p. 1362. doi: 10.1136/bmj.331.7529.1362.

De Man, B. *et al.* (2000) 'Reduction of metal streak artifacts in x-ray computed tomography using a transmission maximum a posteriori algorithm', *IEEE Transactions on Nuclear Science*.

Maniar, R. (2006) 'Rationale for the posterior-stabilized rotating-platform knee', *Orthopedics*.

Manner, P. W. (2016) *Knee Replacement Implants*, *OrthoInfo*. Available at: https://orthoinfo.aaos.org/en/treatment/knee-replacement-implants/ (Accessed: 9 June 2019).

Maravi, P. *et al.* (2015) 'Role of MRI in Orthopedics', *Orthopaedic Journal of M.P. Chapter*, 21(2), pp. 74–77. Available at: http://ojmpc.com/index.php/OJMPC/article/download/31/25.

Marchand, P. and Marmet, L. (1983) 'Binomial smoothing filter: A way to avoid some pitfalls of least-squares polynomial smoothing', *Review of Scientific Instruments*, 54(8). doi: 10.1063/1.1137498.

Martini, F. H., Nath, J. L. and Bartholomew, E. F. (2018) *Fundamentals of Anatomy and Physiology*. 11th edn, *Learning*. 11th edn. Edited by S. Beauparlant. Pearson Education, Inc. doi: 612.

Maruyama, S. *et al.* (2004) 'Functional comparison of posterior cruciate-retaining versus posterior stabilized total knee arthroplasty', *Journal of Arthroplasty*. doi: 10.1016/j.arth.2003.09.010.

De Marzi, L. *et al.* (2013) 'Calibration of CT Hounsfield units for proton therapy treatment planning: Use of kilovoltage and megavoltage images and comparison of parameterized methods', *Physics in Medicine and Biology*. doi: 10.1088/0031-9155/58/12/4255.

Matsuda, S. *et al.* (2003) 'A comparison of rotational landmarks in the distal femur and the tibial shaft', *Clinical Orthopaedics and Related Research*. doi: 10.1097/01.blo.0000072904.36018.79.

Matsuda, S. *et al.* (2004) 'Anatomical analysis of the femoral condyle in normal and osteoarthritic knees', *Journal of Orthopaedic Research*. doi: 10.1016/S0736-0266(03)00134-7.

Matsumoto, H. *et al.* (2000) 'Axis location of tibial rotation and its change with flexion angle', *Clinical Orthopaedics and Related Research*. doi: 10.1097/00003086-200002000-00022.

Matziolis, G. *et al.* (2011) 'Kinematic analysis of the flexion axis for correct femoral component placement', *Knee Surgery, Sports Traumatology, Arthroscopy*. doi: 10.1007/s00167-011-1554-5.

Mazzoli, V. *et al.* (2017) 'Accelerated 4D self-gated MRI of tibiofemoral kinematics', *NMR in Biomedicine*. doi: 10.1002/nbm.3791.

McCollough, C. H. *et al.* (2012) 'Achieving routine submillisievert CT scanning: Report from the Summit on Management of Radiation Dose in CT', *Radiology*. doi: 10.1148/radiol.12112265.

Mehranian, A. *et al.* (2013) '3D prior image constrained projection completion for x-ray ct metal artifact reduction', *IEEE Transactions on Nuclear Science*. doi: 10.1109/TNS.2013.2275919.

Mensch, J. and Amstutz, H. (1975) 'Knee morphology as a guide to knee replacement.', *Clinical Orthopaedics and Related Research®,* 112, pp. 231–41. Available at: https://www.ncbi.nlm.nih.gov/m/pubmed/1192638/.

Mettler, F. A. *et al.* (2008) 'Medical radiation exposure in the U.S. in 2006: Preliminary results', in *Health Physics*. doi: 10.1097/01.HP.0000326333.42287.a2.

Meyer, E. *et al.* (2012) 'Frequency split metal artifact reduction (FSMAR) in computed tomography', *Medical Physics*. doi: 10.1118/1.3691902.

Miki, K. *et al.* (2016) 'Single-energy metal artefact reduction with CT for carbonion radiation therapy treatment planning', *British Journal of Radiology*. doi: 10.1259/bjr.20150988.

Mink, J. H., Levy, T. and Crues, J. V (2014) 'Tears of the anterior cruciate ligament and menisci of the knee: MR imaging evaluation.', *Radiology*. doi: 10.1148/radiology.167.3.3363138.

Mochizuki, T. *et al.* (2014) 'The clinical epicondylar axis is not the functional flexion axis of the human knee', *Journal of Orthopaedic Science*, 19(3), pp. 451–456. doi: 10.1007/s00776-014-0536-0.

Moller, T. and Trumbore, B. (1998) *Fast, minimum storage ray-triangle intersection, Doktorsavhandlingar vid Chalmers Tekniska Hogskola*.

Moore, D. C. *et al.* (2015) 'Computed Tomography Image-Based Kinematic Analysis: An Overview', in Neu, C. P. and Genin, G. M. (eds) *Handbook of Imaging in Biological Mechanics*. Florida: CRC Press, p. 556.

Moreland, J. R., Bassett, L. W. and Hanker, G. J. (1987) 'Radiographic analysis of the

axial alignment of the lower extremity', *Journal of Bone and Joint Surgery - Series A*. doi: 10.2106/00004623-198769050-00016.

Morsbach, F. *et al.* (2013) 'Reduction of metal artifacts from hip prostheses on CT images of the pelvis: Value of iterative reconstructions', *Radiology*. doi: 10.1148/radiol.13122089.

Moskowitz, R. W. (1984) *Osteoarthritis: Diagnosis and Management*. 2nd, Illustr edn. Saunders.

Most, E. *et al.* (2004) 'Sensitivity of the knee joint kinematics calculation to selection of flexion axes', *Journal of Biomechanics*, 37(11), pp. 1743–1748. doi: 10.1016/j.jbiomech.2004.01.025.

Nakagawa, S. *et al.* (2000) 'Tibiofemoral movement 3: full flexion in the living knee studied by MRI', *The Journal of Bone and Joint Surgery*, 82(8), pp. 1199–1200. doi: 10.1302/0301-620X.82B8.10718.

Narkhede, H. P. (2013) 'Review of Image Segmentation Techniques', *International Journal of Science and Modern Engineering*, (18).

Nguyen, K. T. *et al.* (2016) 'Quantitative analysis of knee movement patterns through comparative visualization', in *Mathematics and Visualization*. doi: 10.1007/978-3-319-24523-2_12.

Noble, P. C. *et al.* (2005) 'Does total knee replacement restore normal knee function?', *Clinical orthopaedics and related research*, (431), pp. 157–65. Available at: http://www.ncbi.nlm.nih.gov/pubmed/15685070.

Noble, P. C. *et al.* (2006) 'The John Insall Award: Patient Expectations Affect Satisfaction with Total Knee Arthroplasty', *Clinical Orthopaedics and Related Research*, 452, pp. 35–43. doi: 10.1097/01.blo.0000238825.63648.1e.

Nordin, M. and Frankel, V. (1982) 'Biomechanics of the Knee', in Helfet, A. (ed.) *Disorders of the Knee*. 2nd edn. Cambridge: JB Lippincott, pp. 19–33.

Nowakowski, A. (2006) 'Das Transversalträger-Tibiaplateau (TTTP)', *Orthopädische Praxis*, 42(7), pp. 419–28.

Oxford Economics (2010) 'The Economic Costs of Arthritis for the UK Economy', (Final Report).

Pal, N. R. and Pal, S. K. (1993) 'A review on image segmentation techniques', *Pattern Recognition*, 26(9). doi: 10.1016/0031-3203(93)90135-J.

Pan, T. (2005) 'Comparison of helical and cine acquisitions for 4D-CT imaging with multislice CT', *Medical Physics*, 32(2). doi: 10.1118/1.1855013.

Patel, A. *et al.* (2015) 'The epidemiology of revision total knee and hip arthroplasty in England and Wales', *The Bone & Joint Journal*, 97-B(8), pp. 1076–1081. doi: 10.1302/0301-620X.97B8.35170.

Patel, V. V. *et al.* (2004) 'A three-dimensional MRI analysis of knee kinematics', *Journal of Orthopaedic Research*. doi: 10.1016/j.orthres.2003.08.015.

Paudel, M. R. *et al.* (2014) 'Clinical evaluation of normalized metal artifact reduction in kVCT using MVCT prior images (MVCT-NMAR) for radiation therapy treatment planning', *International Journal of Radiation Oncology Biology Physics*. doi: 10.1016/j.ijrobp.2014.02.040.

Pennock, G. R. and Clark, K. J. (1990) 'An anatomy-based coordinate system for the description of the kinematic displacements in the human knee', *Journal of Biomechanics*. doi: 10.1016/0021-9290(90)90378-G.

Pham, D. L. and Prince, J. L. (1999) 'An adaptive fuzzy C-means algorithm for image segmentation in the presence of intensity inhomogeneities', *Pattern Recognition Letters*. doi: 10.1016/S0167-8655(98)00121-4.

Piazza, S. J. and Cavanagh, P. R. (2000) 'Measurement of the screw-home motion of the knee is sensitive to errors in axis alignment', *Journal of Biomechanics*, 33(8), pp. 1029–1034. doi: 10.1016/S0021-9290(00)00056-7.

Pierrart, J. *et al.* (2014) 'New dynamic three-dimensional MRI technique for shoulder kinematic analysis', *Journal of Magnetic Resonance Imaging*. doi: 10.1002/jmri.24204.

Pinskerova, V. *et al.* (2004) 'Does the femur roll-back with flexion?', *Journal of Bone and Joint Surgery - Series B*. doi: 10.1302/0301-620X.86B6.14589.

Pinskerova, V. *et al.* (2009) 'The knee in full flexion: AN ANATOMICAL STUDY', *Journal of Bone and Joint Surgery - British Volume*, 91-B(6), pp. 830–834. doi: 10.1302/0301-620X.91B6.22319.

Post, Z. D. *et al.* (2010) 'Mobile-bearing total knee arthroplasty. Better than a fixed-bearing?', *Journal of Arthroplasty*. Elsevier Inc., 25(6), pp. 998–1003. doi: 10.1016/j.arth.2009.07.014.

Power, S. P. *et al.* (2016) 'Computed tomography and patient risk: Facts, perceptions and uncertainties', *World Journal of Radiology*. doi: 10.4329/wjr.v8.i12.902.

Preston, D. C. (2006) *Magnetic Resonance Imaging (MRI): Basics*. Available at: https://case.edu/med/neurology/NR/MRI Basics.htm#:~:text=The most common MRI sequences,longer TE and TR times.

Ranawat, C. S. *et al.* (2004) 'In Vivo Kinematics for Fixed and Mobile-Bearing Posterior Stabilized Knee Prostheses', *Clinical Orthopaedics and Related Research*. doi: 10.1097/00003086-200401000-00030.

Ranawat, C. S., Luessenhop, C. P. and Rodriguez, J. A. (1997) 'The press-fit condylar modular total knee system. Four-to-six-year results with a posterior-cruciate-substituting design', *Journal of Bone and Joint Surgery - Series A*.

Randen, A. *et al.* (2008) 'Acute appendicitis: Meta-analysis of diagnostic performance of CT and graded compression US related to prevalence of disease', *Radiology*. doi: 10.1148/radiol.2483071652.

Reilly, R. and M. (2019) *Medical Imaging for Health Professionals: Technologies and Clinical Applications*. First. Hoboken, NJ: Wiley.

Reuleaux, F. (1875) *Lehrbuch der kinematik, Vol.1*. 1st edn. F. Vieweg. Available at: https://books.google.com.mt/books?id=MsdJAAAAMAAJ&source=gbs_book_other_versions.

Robb, J. (1994) *Estimates of radiation detriment in a UK population*. Chilton. Available at: https://inis.iaea.org/search/search.aspx?orig_q=source:%22ISBN 0 85951 385 0%22.

Robertson, P. L. *et al.* (2014) 'Anterior cruciate ligament tears: evaluation of multiple signs with MR imaging.', *Radiology*. doi: 10.1148/radiology.193.3.7972833.

Robertsson, O. *et al.* (2000) 'Patient satisfaction after knee arthroplasty: A report on 27,372 knees operated on between 1981 and 1995 in Sweden', *Acta Orthopaedica Scandinavica*, 71(3), pp. 262–267. doi: 10.1080/000164700317411852.

Roland, M., Hull, M. L. and Howell, S. M. (2010) 'Virtual Axis Finder: A New Method to Determine the Two Kinematic Axes of Rotation for the Tibio-Femoral Joint', *Journal of Biomechanical Engineering*, 132(1), p. 011009. doi: 10.1115/1.4000163.

Rosen, M. P. *et al.* (2000) 'Impact of abdominal CT on the management of patients presenting to the emergency department with acute abdominal pain', *American Journal of Roentgenology*. doi: 10.2214/ajr.174.5.1741391.

Rosen, M. P. *et al.* (2003) 'Value of abdominal CT in the emergency department for patients with abdominal pain', *European Radiology*.

Sandhya, P. H. and Kumar, S. (2017) 'A Survey on Fuzzy C-means Clustering Techniques', *International Journal of Engineering Development and Research (IJEDR)*, 5(4), pp. 1151–1155. Available at: https://ijedr.org/papers/IJEDR1704186.pdf.

Sando, T. *et al.* (2015) 'Ten-year results comparing posterior cruciate-retaining versus posterior cruciate-substituting total knee arthroplasty', *Journal of Arthroplasty*. doi: 10.1016/j.arth.2014.09.009.

Sankur, B. (2004) 'Survey over image thresholding techniques and quantitative performance evaluation', *Journal of Electronic Imaging*. doi: 10.1117/1.1631315.

Sathasivam, S. and Walker, P. S. (1997) 'A computer model with surface friction for the prediction of total knee kinematics', *Journal of Biomechanics*. doi: 10.1016/S0021-9290(96)00114-5.

Schmidt, R. *et al.* (2003) 'Fluoroscopic analyses of cruciate-retaining and Medial Pivot knee implants', in *Clinical Orthopaedics and Related Research*. doi: 10.1097/01.blo.0000063565.90853.a4.

Scott, W. N. (2018) *Surgery of the Knee, Insall & Scott Surgery of the Knee*. Elsevier. doi: 10.1016/B978-1-4377-1503-3.00078-0.

Sharkey, P. F. *et al.* (2014) 'Why Are Total Knee Arthroplasties Failing Today—Has Anything Changed After 10 Years?', *The Journal of Arthroplasty*, 29(9), pp. 1774–1778. doi: 10.1016/j.arth.2013.07.024.

Shaw, J. A. and Murray, D. G. (1974) 'The Longitudinal Axis of the Knee and the Role of the Cruciate Ligaments in Controlling Transverse Rotation', *The Journal of*

Bone & Joint Surgery, 56(8), pp. 1603–1609. doi: 10.2106/00004623-197456080-00008.

Sheldon, S. (1994) *Orthopaedic Basic Science*. Edited by S. Sheldon. American Academy of Orthopaedics.

Shenoy, R., Pastides, P. S. and Nathwani, D. (2013) '(iii) Biomechanics of the knee and TKR', *Orthopaedics and Trauma*, 27(6), pp. 364–371. doi: 10.1016/j.mporth.2013.10.003.

Shiavi, R. *et al.* (1987a) 'Helical motion analysis of the knee-II. Kinematics of uninjured and injured knees during walking and pivoting', *Journal of Biomechanics*. doi: 10.1016/0021-9290(87)90032-7.

Shiavi, R. *et al.* (1987b) 'Helical motion analysis of the knee—I. Methodology for studying kinematics during locomotion', *Journal of Biomechanics*, 20(5), pp. 459–469. doi: 10.1016/0021-9290(87)90247-8.

Sikorski, J. M. (2008) 'Alignment in total knee replacement', *The Journal of Bone and Joint Surgery. British volume*, 90-B(9), pp. 1121–1127. doi: 10.1302/0301-620X.90B9.20793.

Van Sint Jan, S. *et al.* (2002) 'Registration of 6-DOFs electrogoniometry and CT medical imaging for 3D joint modeling', *Journal of Biomechanics*. doi: 10.1016/S0021-9290(02)00074-X.

Siu, D. *et al.* (1996) 'Femoral articular shape and geometry: A three-dimensional computerized analysis of the knee', *Journal of Arthroplasty*. doi: 10.1016/S0883-5403(05)80012-9.

Smidt, G. L. (1973) 'Biomechanical analysis of knee flexion and extension', *Journal of Biomechanics*, 6(1), pp. 79–92. doi: 10.1016/0021-9290(73)90040-7.

Smith, B. A., Livesay, G. A. and Woo, S. L. (1993) 'Biology and biomechanics of the anterior cruciate ligament.', *Clinics in sports medicine*, 12(4), pp. 637–70. doi: 10.1080/19397030902947041.

Soudan, K., Van Audekercke, R. and Martens, M. (1979) 'Methods, difficulties and inaccuracies in the study of human joint kinematics and pathokinematics by the instant axis concept. Example: The knee joint', *Journal of Biomechanics*, 12(1), pp. 27–33. doi: 10.1016/0021-9290(79)90006-X.

Steindler, A. (1955) *Kinesiology of the Human Body under Normal and Pathological Conditions.*, *Journal of Bone and Joint Surgery - British Volume*. Available at: https://journals.lww.com/jbjsjournal/Citation/1955/37060/Kinesiology_of_the_Human_Body_under_Normal_and.27.aspx.

Stiehl, J. B. *et al.* (1997) 'In Vivo Kinematic Analysis of a Mobile Bearing Total Knee Prosthesis', *Clinical Orthopaedics and Related Research*. doi: 10.1097/00003086-199712000-00010.

Strasser, H. (1917) *Lehrbuch der Muskel und Gelenkmechanik.* 3rd edn. Berlin: Springer Verlag.

Subburaj, K., Ravi, B. and Agarwal, M. (2010) 'Computer-aided methods for assessing lower limb deformities in orthopaedic surgery planning', *Computerized Medical Imaging and Graphics*. doi: 10.1016/j.compmedimag.2009.11.003.

Sun, Y., Teo, E. C. and Zhang, Q. H. (2006) 'Discussions of knee joint segmentation', in *ICBPE 2006 - Proceedings of the 2006 International Conference on Biomedical and Pharmaceutical Engineering*. doi: 10.1109/ICBPE.2006.348611.

Tanifuji, O. *et al.* (2013) 'Three-dimensional in vivo motion analysis of normal knees employing transepicondylar axis as an evaluation parameter', *Knee Surgery, Sports Traumatology, Arthroscopy*. doi: 10.1007/s00167-012-2010-x.

Tay, S. C. *et al.* (2007) 'Four-dimensional computed tomographic imaging in the wrist: Proof of feasibility in a cadaveric model', *Skeletal Radiology*. doi: 10.1007/s00256-007-0374-7.

The Mathworks Inc. (2018) 'MATLAB'. NAtick, Massachusettes. Available at: www.mathworks.com.

Thompson, W. O. *et al.* (1991) 'Tibial meniscal dynamics using three-dimensional reconstruction of magnetic resonance images', *The American Journal of Sports Medicine*, 19(3), pp. 210–216. doi: 10.1177/036354659101900302.

Toshiba Medical Systems (2008) 'Dynamic Volume Imaging - Special Issue', *Toshiba Medical Systems Journal*. Available at: https://ch.medical.canon/wp-content/uploads/sites/33/2017/01/2008-VISIONS-Special-Dynamic-Volume-ImagingFINAL.pdf.

Toshiba Medical Systems (2012) *Product Data No. MPDCT0314EA*.

Tsujii, A. *et al.* (2018) 'Arthroscopic minimum saucerization and inferior-leaf meniscectomy for a horizontal tear of a complete discoid lateral meniscus: Report of two cases', *International Journal of Surgery Case Reports*. doi: 10.1016/j.ijscr.2018.11.027.

Udupa, J. K. and Saha, P. K. (2003) 'Fuzzy connectedness and image segmentation', in *Proceedings of the IEEE*. doi: 10.1109/JPROC.2003.817883.

Uecker, M. *et al.* (2010) 'Real-time MRI at a resolution of 20 ms', *NMR in Biomedicine*. doi: 10.1002/nbm.1585.

UNSCEAR (2000) *Sources and Effects of Ionizing Radiation, United Nations Scientific Committee on the Effects of Atomic Radiation UNSCEAR 2000 Report to the General Assembly, with Scientific Annexes*, *UNSCEAR 2000 Report*.

Vaishya, R., Agarwal, A. K. and Vijay, V. (2016) 'Extensor Mechanism Disruption after Total Knee Arthroplasty: A Case Series and Review of Literature', *Cureus*. doi: 10.7759/cureus.479.

Varadarajan, K. M. *et al.* (2009) 'Can in vitro systems capture the characteristic differences between the flexion-extension kinematics of the healthy and TKA knee?', *Medical Engineering and Physics*. doi: 10.1016/j.medengphy.2009.06.005.

Vedi, V. *et al.* (1999) 'Meniscal movement', *The Journal of Bone and Joint Surgery*, 81(1), pp. 37–41. doi: 10.1302/0301-620X.81B1.8928.

Veselko, M., Jenko, M. and Lipuscek, I. (1998) 'The use of the co-ordinate measuring machine for the study of three-dimensional biomechanics of the knee.', *Computers in biology and medicine*, 28(4), pp. 343–57. Available at: http://www.ncbi.nlm.nih.gov/pubmed/9805195.

Victor, J., Van Doninck, D., Labey, L., Van Glabbeek, F., *et al.* (2009) 'A common reference frame for describing rotation of the distal femur', *The Journal of Bone and Joint Surgery. British volume*, 91-B(5), pp. 683–690. doi: 10.1302/0301-620X.91B5.21827.

Victor, J., Van Doninck, D., Labey, L., Innocenti, B., *et al.* (2009) 'How precise can bony landmarks be determined on a CT scan of the knee?', *Knee*. doi: 10.1016/j.knee.2009.01.001.

Victor, J. (2009) 'Rotational alignment of the distal femur: A literature review',

Orthopaedics & Traumatology: Surgery & Research, 95(5), pp. 365–372. doi: 10.1016/j.otsr.2009.04.011.

Waldman, S. D. and Campbell, R. S. D. (2011) *Imaging of Pain*. doi: 10.1016/C2009-0-39533-1.

Walker, P. S. *et al.* (2011) 'Reference axes for comparing the motion of knee replacements with the anatomic knee', *Knee*. doi: 10.1016/j.knee.2010.07.005.

Walker, P. S. and Erkiuan, M. J. (1975) 'The Role of the Menisci in Force Transmission Across the Knee', *Clinical Orthopaedics and Related Research*, 109, pp. 184–92. doi: 10.1097/00003086-197506000-00027.

Weber, W. and Weber, E. (1837) 'Ueber die Mechanik der menschlichen Gehwerkzeuge, nebst der Beschreibung eines Versuchs über das Herausfallen des Schenkelkopfs aus der Pfanne im luftverdünnten Raume', *Annalen der Physik und Chemie*, 116(1), pp. 1–13. doi: 10.1002/andp.18371160102.

Whittle, Michael (2012) *Whittle's gait analysis.* 5th edn. Edited by J. Richards, D. Levine, and Micheal Whittle. Churchill Livingstone.

Wilson, D. A. (2011) *Clinical Veterinary Advisor: The Horse*. doi: 10.1016/C2009-0-38641-9.

Woolf, A. D. and Pfleger, B. (2003) 'Burden of major musculoskeletal conditions.', *Bulletin of the World Health Organization*, 81(9), pp. 646–56. Available at: http://www.scirp.org/journal/doi.aspx?DOI=10.4236/abb.2012.324063.

Wu, G. *et al.* (2002) 'ISB recommendation on definitions of joint coordinate system of various joints for the reporting of human joint motion—part I: ankle, hip, and spine', *Journal of Biomechanics*. doi: 10.1016/S0021-9290(01)00222-6.

Wu, G. *et al.* (2005) 'ISB recommendation on definitions of joint coordinate systems of various joints for the reporting of human joint motioN, Part II: shoulder, elbow, wrist and hand', *Journal of Biomechanics*. doi: 10.1016/j.jbiomech.2004.05.042.

Wu, G. and Cavanagh, P. R. (1995) 'ISB recommendations for standardization in the reporting of kinematic data', *Journal of Biomechanics*. doi: 10.1016/0021-9290(95)00017-C.

Wylde, V. *et al.* (2008) 'Patient-reported outcomes after fixed- versus mobile-bearing

total knee replacement', *The Journal of Bone and Joint Surgery. British volume*, 90-B(9), pp. 1172–1179. doi: 10.1302/0301-620X.90B9.21031.

Yamazaki, T. *et al.* (2007) '3D kinematics of normal knee using X-ray fluoroscopy and CT images', in *World Congress on Medical Physics and Biomedical Engineering 2006*. doi: 10.1007/978-3-540-36841-0_706.

Yao, J. *et al.* (2014) 'In vivo measurements of patellar tracking and finite helical axis using a static magnetic resonance based methodology', *Medical Engineering and Physics*. doi: 10.1016/j.medengphy.2014.08.014.

Yau, W. P., Chiu, K. Y. and Tang, W. M. (2007) 'How Precise is the Determination of Rotational Alignment of the Femoral Prosthesis in Total Knee Arthroplasty. An In Vivo Study', *Journal of Arthroplasty*. doi: 10.1016/j.arth.2006.12.043.

Yin, L. *et al.* (2015) 'Identifying the Functional Flexion-extension Axis of the Knee: An In-Vivo Kinematics Study', *PLOS ONE*. Edited by L. Ren, 10(6), p. e0128877. doi: 10.1371/journal.pone.0128877.

Yoshioka, Y. *et al.* (1989) 'Tibial Anatomy and Functional Axes', *Journal of Orthopaedic Research*, 7(1), pp. 132–7. doi: 10.1002/jor.1100070118.

Yoshioka, Y., Siu, D. and Cooke, T. D. V. (1987a) 'The anatomy and functional axes of the femur.', *The Journal of Bone & Joint Surgery*, 69(6), pp. 873–880. doi: 10.2106/00004623-198769060-00012.

Yoshioka, Y., Siu, D. and Cooke, T. D. V. (1987b) 'The anatomy and functional axes of the femur', *Journal of Bone and Joint Surgery - Series A*. doi: 10.2106/00004623-198769060-00012.

You, B. M. *et al.* (2001) 'In vivo measurement of 3-D skeletal kinematics from sequences of biplane radiographs: Application to knee kinematics', *IEEE Transactions on Medical Imaging*, 20(6). doi: 10.1109/42.929617.

Zhai, G. *et al.* (2007) 'A longitudinal study of the association between knee alignment and change in cartilage volume and chondral defects in a largely non-osteoarthritic population', *Journal of Rheumatology*.

Zhang, Y. J. (1996) 'A survey on evaluation methods for image segmentation', *Pattern Recognition*, 29(8). doi: 10.1016/0031-3203(95)00169-7.

Zhao, S. *et al.* (2002) 'A wavelet method for metal artifact reduction with multiple metallic objects in the field of view', *Journal of X-Ray Science and Technology*.

Zuppinger, H. (1904) 'Die aktive Flexion im unbelasteten Kniegelenk [Active flexion of the unloaded knee joint].', *Anatomische Hefte. Beiträge und Referate zur Anatomie und Entwicklungsgeschichte*, 77, pp. 701–64.

Aesculap (2012) *Columbus Knee Design Rationale Brochure*. Palo Alto. Available at: https://www.aesculapimplantsystems.com/content/dam/aesculap-us/us/website/aesculap-implant_systems/hp-section/ortho-product-pages/ortho-resources-pdfs/DOC616-RevA-Columbus-Knee-Design-Rationale-Brochure.pdf.

Aglietti, P. *et al.* (2008) 'Rotational position of femoral and tibial components in TKA using the femoral transepicondylar axis', in *Clinical Orthopaedics and Related Research*. doi: 10.1007/s11999-008-0452-8.

Aly, A. A., Bin Deris, S. and Zaki, N. (2011) 'Research Review for Digital Image Segmentation Techniques', *International Journal of Computer Science and Information Technology*, 3(5). doi: 10.5121/ijcsit.2011.3509.

American Academy of Orthopaedic Surgeons (2014) *Arthritis of the Knee*. Available at: https://orthoinfo.aaos.org/en/diseases--conditions/arthritis-of-the-knee/ (Accessed: 5 October 2019).

AO foundation (2008) *Lateral parapatellar approach to the distal femur*. Available at: https://www2.aofoundation.org/wps/portal/!ut/p/a0/04_Sj9CPykssy0xPLMnMz0vMA fGjzOKN_A0M3D2DDbz9_UMMDRyDXQ3dw9wMDAzMjfULsh0VAbWjLW0!/? approach=Lateral parapatellar approach&bone=Femur&segment=Distal&showPage=approach&contentUrl=/srg/33/ 04-Approaches/A21-lat (Accessed: 12 July 2018).

Argenson, J. N. A. *et al.* (2012) 'The outcome of rotating-platform total knee arthroplasty with cement at a minimum of ten years of follow-up', *Journal of Bone and Joint Surgery - Series A*. doi: 10.2106/JBJS.K.00263.

Asano, T., Akagi, M. and Nakamura, T. (2005) 'The Functional Flexion-Extension Axis of the Knee Corresponds to the Surgical Epicondylar Axis', *The Journal of Arthroplasty*, 20(8), pp. 1060–1067. doi: 10.1016/j.arth.2004.08.005.

Bach, J. M. and Hull, M. L. (1995) 'A New Load Application System for In Vitro Study of Ligamentous Injuries to the Human Knee Joint', *Journal of Biomechanical Engineering*. doi: 10.1115/1.2794195.

Bamberg, F. *et al.* (2011) 'Metal artifact reduction by dual energy computed tomography using monoenergetic extrapolation', *European Radiology*. doi:

10.1007/s00330-011-2062-1.

Banks, S. *et al.* (2016) 'In Vivo kinematics of a medially conforming and rotationally unconstrained TKA design', *Orthopaedic Proceedings*, 98-B(SUPP_1), p. 35. doi: 10.1302/1358-992X.98BSUPP_1.ISTA2014-035.

Banks, S. A. and Hodge, W. A. (2004) '2003 Hap Paul Award paper of the International Society for Technology in Arthroplasty', *The Journal of Arthroplasty*, 19(7), pp. 809–816. doi: 10.1016/j.arth.2004.04.011.

Barrett, W. P. *et al.* (2011) 'Comparison of Radiographic Alignment of Imageless Computer-Assisted Surgery vs Conventional Instrumentation in Primary Total Knee Arthroplasty', *The Journal of Arthroplasty*, 26(8), pp. 1273-1284.e1. doi: 10.1016/j.arth.2011.04.037.

Bellemans, J. *et al.* (2012) 'The Chitranjan Ranawat Award: Is Neutral Mechanical Alignment Normal for All Patients?: The Concept of Constitutional Varus', *Clinical Orthopaedics and Related Research®*. doi: 10.1007/s11999-011-1936-5.

Bellemans, J., Ries, M. D. and Victor, J. M. K. (2005) *TKA - A Guide To Better Performance*.

Berger, R. A. *et al.* (1993) 'Determining the Rotational Alignment of the Femoral Component in Total Knee Arthroplasty Using the Epicondylar Axis', *Clinical Orthopaedics and Related Research*, (286), pp. 40–47. doi: 10.1097/00003086-199301000-00008.

Berme, N., Engin, A. E. and Correia da Silva, K. M. (eds) (1985) *Biomechanics of Normal and Pathological Human Articulating Joints*, *Biomechanics of Normal and Pathological Human Articulating Joints*. Dordrecht: Springer Netherlands. doi: 10.1007/978-94-009-5117-4.

Bistolfi, A. *et al.* (2013) 'Comparison of fixed and mobile-bearing total knee arthroplasty at a mean follow-up of 116 months', *Journal of Bone and Joint Surgery - Series A*. doi: 10.2106/JBJS.L.00327.

Blankevoort, L. and Huiskes, R. (1996) 'Validation of a three-dimensional model of the knee', *Journal of Biomechanics*. doi: 10.1016/0021-9290(95)00149-2.

Blankevoort, L., Huiskes, R. and de Lange, A. (1988) 'The envelope of passive knee joint motion', *Journal of Biomechanics*, 21(9), pp. 705–720. doi: 10.1016/0021-9290(88)90280-1.

Blankevoort, L., Huiskes, R. and de Lange, A. (1990) 'Helical axes of passive knee joint motions', *Journal of Biomechanics*. doi: 10.1016/0021-9290(90)90379-H.

Blunn, G. W. *et al.* (1997) 'Wear in retrieved condylar knee arthroplasties: A comparison of wear in different designs of 280 retrieved condylar knee prostheses', *Journal of Arthroplasty*. doi: 10.1016/S0883-5403(97)90024-3.

Boguszewski, D. V. *et al.* (2016) 'Location of the natural knee axis for internal–external tibial rotation', *The Knee*, 23(6), pp. 1083–1088. doi: 10.1016/j.knee.2015.11.003.

Bottema, D., Roth, B. and Veldkamp, G. R. (1980) 'Theoretical Kinematics', *Journal of Applied Mechanics*. doi: 10.1115/1.3153630.

Van der Bracht, H. *et al.* (2010) 'Is there any superiority in the clinical outcome of mobile-bearing knee prosthesis designs compared to fixed-bearing total knee prosthesis designs in the treatment of osteoarthritis of the knee joint?', *Knee Surgery, Sports Traumatology, Arthroscopy*. doi: 10.1007/s00167-009-0973-z.

Brandsson, S. *et al.* (2001) 'Kinematics after tear in the anterior cruciate ligament: Dynamic bilateral radiostereometric studies in 11 patients', *Acta Orthopaedica Scandinavica*. doi: 10.1080/000164701753542032.

Brantigan, O. C. and Voshell, A. F. (1941) 'THE MECHANICS OF THE LIGAMENTS AND MENISCI OF THE KNEE JOINT', *J Bone Joint Surg Am*.

Braune, C. W. and Fischer, O. (1891) *Die bewegungen des kniegelenks nach einer neuen methode am lebenden menschen gemessen*. Edited by S. Hirzel. Leipzig.

Brook, O. R. *et al.* (2012) 'Spectral CT with metal artifacts reduction software for improvement of tumor visibility in the vicinity of gold fiducial markers', *Radiology*. doi: 10.1148/radiol.12111170.

Buechel, F. F. *et al.* (2001) 'Twenty-year evaluation of meniscal bearing and rotating platform knee replacements', in *Clinical Orthopaedics and Related Research*. doi: 10.1097/00003086-200107000-00008.

Buechel, F. F. and Pappas, M. J. (1986) 'The New Jersey low-contact-stress knee replacement system: Biomechanical rationale and review of the first 123 cemented cases', *Archives of Orthopaedic and Traumatic Surgery*. doi: 10.1007/BF00435480.

Buechel, F. F. and Pappas, M. J. (1989) 'New Jersey low contact stress knee replacement system. Ten-year evaluation of meniscal bearings', *Orthopedic Clinics of North America*.

Bugnion, E. (1892) *Le mechanism du genou. Extrait du recueil inaugural de l'Universitie Lausanne*. Lausanne.

Bull, A. M. J. and Amis, A. A. (1998) 'Knee joint motion: Description and measurement', *Proceedings of the Institution of Mechanical Engineers, Part H: Journal of Engineering in Medicine*. doi: 10.1243/0954411981534132.

Callaghan, J. *et al.* (2000) 'Mobile-Bearing Knee Replacement : Concepts and Results*+.', *J Bone Joint Surg Am*, 82(7), p. 1020. Available at: http://ovidsp.ovid.com/ovidweb.cgi?T=JS&PAGE=reference&D=yrovftd&NEWS=N&AN=00004623-200007000-00013.

Callaghan, J. J. *et al.* (2010) 'Cemented Rotating-Platform Total Knee Replacement', *The Journal of Bone and Joint Surgery-American Volume*. doi: 10.2106/jbjs.i.01012.

Cappozzo, A. (1991) 'Three-dimensional analysis of human walking: Experimental methods and associated artifacts', *Human Movement Science*. doi: 10.1016/0167-9457(91)90047-2.

Carothers, J. T. *et al.* (2011) 'Mobile-Bearing Total Knee Arthroplasty. A Meta-Analysis', *Journal of Arthroplasty*. doi: 10.1016/j.arth.2010.05.015.

Cherian, J. J. *et al.* (2014) 'Mechanical, Anatomical, and Kinematic Axis in TKA: Concepts and Practical Applications', *Current Reviews in Musculoskeletal Medicine*, 7(2), pp. 89–95. doi: 10.1007/s12178-014-9218-y.

Chouteau, J. *et al.* (2009) 'Mobile-bearing insert translational and rotational kinematics in a PCL-retaining total knee arthroplasty', *Orthopaedics and Traumatology: Surgery and Research*. doi: 10.1016/j.otsr.2009.03.012.

Churchill, D. L. *et al.* (1996) 'A compound pinned hinge model of knee joint kinematics.', *Trans Orthop Res. Soc.*, 21(717).

Churchill, D. L. *et al.* (1998) 'The Transepicondylar Axis Approximates the Optimal Flexion Axis of the Knee', *Clinical Orthopaedics and Related Research*, 356, pp. 111–118. doi: 10.1097/00003086-199811000-00016.

Cobb, J. P. *et al.* (2008) 'The anatomical tibial axis', *The Journal of Bone and Joint Surgery. British volume*, 90-B(8), pp. 1032–1038. doi: 10.1302/0301-620X.90B8.19905.

Cole, G. K. *et al.* (1993) 'Application of the Joint Coordinate System to Three-Dimensional Joint Attitude and Movement Representation: A Standardization Proposal', *Journal of Biomechanical Engineering*, 115(4A), p. 344. doi: 10.1115/1.2895496.

Colizza, W. A., Insall, J. N. and Scuderi, G. R. (1995) 'The posterior stabilized total knee prosthesis: Assessment of polyethylene damage and osteolysis after a ten-year-minimum follow-up', *Journal of Bone and Joint Surgery - Series A*. doi: 10.2106/00004623-199511000-00011.

D'Entremont, A. G. *et al.* (2013) 'Do dynamic-based MR knee kinematics methods produce the same results as static methods?', *Magnetic Resonance in Medicine*. doi: 10.1002/mrm.24425.

D'Entremont, A. G. *et al.* (2014) 'Effect of opening-wedge high tibial osteotomy on the three-Dimensional kinematics of the knee', *Bone and Joint Journal*. doi: 10.1302/0301-620X.96B9.32522$2.00.

D'Lima, D. D. *et al.* (2001) 'Polyethylene wear and variations in knee kinematics', in *Clinical Orthopaedics and Related Research*. doi: 10.1097/00003086-200111000-

00015.

D'Lima, D. D., Chen, P. C. and Colwell, C. W. (2001) 'Polyethylene Contact Stresses, Articular Congruity, and Knee Alignment', *Clinical Orthopaedics and Related Research*, 392, pp. 232–238. doi: 10.1097/00003086-200111000-00029.

Daniilidis, K. *et al.* (2012) 'Highly conforming polyethylene inlays reduce the in vivo variability of knee joint kinematics after total knee arthroplasty', *Knee*. doi: 10.1016/j.knee.2011.04.001.

Dennis, D. A. *et al.* (1996) 'In vivo knee kinematics derived using an inverse perspective technique', in *Clinical Orthopaedics and Related Research*. doi: 10.1097/00003086-199610000-00015.

Dennis, D. A. *et al.* (2003) 'Multicenter Determination of in Vivo Kinematics after Total Knee Arthroplasty', in *Clinical Orthopaedics and Related Research*.

Dennis, D. A. *et al.* (2005) 'Mobile-bearing total knee arthroplasty: Do the polyethylene bearings rotate?', in *Clinical Orthopaedics and Related Research*. doi: 10.1097/01.blo.0000185464.23505.6e.

Deserno, T. M. (2011) *Biomedical Image Processing*. 1st edn. Edited by Thomas Martin Deserno. Berlin, Heidelberg: Springer Berlin Heidelberg (Biological and Medical Physics, Biomedical Engineering). doi: 10.1007/978-3-642-15816-2.

Diaz, G. (2018) *Radiation from X-rays*, *GrepMed*. Available at: https://www.grepmed.com/images/1828/risks-comparison-table-imaging-patientinfo-radiation-background.

Dieppe, P. (2000) 'Towards a better understanding of osteoarthritis of the knee joint', *The Knee*, 7(3), pp. 135–137. doi: 10.1016/S0968-0160(00)00043-0.

van Dijk, R., Huiskes, R. and Selvik, G. (1979) 'Roentgen stereophotogrammetric methods for the evaluation of the three dimensional kinematic behaviour and cruciate ligament length patterns of the human knee joint', *Journal of Biomechanics*, 12(9), pp. 727–731. doi: 10.1016/0021-9290(79)90021-6.

Doral Medical Imaging (2006) *Magnetic Resonance Imaging*. Available at: http://www.doralmri.com/images/mri picture.jpg (Accessed: 14 August 2019).

Draper, C. E. *et al.* (2008) 'Feasibility of using real-time MRI to measure joint kinematics in 1.5T and open-bore 0.5T systems', *Journal of Magnetic Resonance Imaging*. doi: 10.1002/jmri.21413.

Dzung, L., Chenyang, X. and Prince, J. L. (1998) 'A survey of current methods in medical image segmentation', *Department of ECE, Johns Hopkins Univ., Tech. Rep*.

Eckhoff, D. *et al.* (2007a) 'An ABJS best paper: Difference between the epicondylar and cylindrical axis of the knee', in *Clinical Orthopaedics and Related Research*. doi:

10.1097/BLO.0b013e318112416b.

Eckhoff, D. *et al.* (2007b) 'Difference Between the Epicondylar and Cylindrical Axis of the Knee', *Clinical Orthopaedics and Related Research*, PAP, pp. 238–44. doi: 10.1097/BLO.0b013e318112416b.

Eckhoff, D. G. *et al.* (2001) 'Three-Dimensional Morphology of the Distal Part of the Femur Viewed in Virtual Reality - Part I', *The Journal of Bone and Joint Surgery-American Volume*, 83, pp. 43–50. doi: 10.2106/00004623-200100021-00010.

Eckhoff, D. G. *et al.* (2003) 'Three-Dimensional Morphology and Kinematics of the Distal Part of the Femur Viewed in Virtual Reality - Part II', *The Journal of Bone and Joint Surgery-American Volume*, 85(SUPPL. 4), pp. 97–104. doi: 10.2106/00004623-200300004-00012.

Eckhoff, D. G. *et al.* (2005) 'Three-dimensional mechanics, kinematics, and morphology of the knee viewed in virtual reality', in *Journal of Bone and Joint Surgery - Series A*. doi: 10.2106/00004623-200511002-00009.

Elias, S. G., Freeman, M. A. R. and Gokcay, E. I. (1990) 'A Correlative Study of the Geometry and Anatomy of the Distal Femur', *Clinical Orthopaedics and Related Research*, (260), pp. 98–103. doi: 10.1097/00003086-199011000-00018.

Endo, M. *et al.* (2003) 'Four-dimensional computed tomography (4D CT) - Concepts and preliminary development', *Radiation Medicine - Medical Imaging and Radiation Oncology*.

Esses, D. *et al.* (2004) 'Ability of CT to alter decision making in elderly patients with acute abdominal pain', *American Journal of Emergency Medicine*. doi: 10.1016/j.ajem.2004.04.004.

Essner, A. *et al.* (2011) 'The influence of material and design on total knee replacement wear.', *The journal of knee surgery*.

Fantozzi, S. *et al.* (2006) 'Femoral rollback of cruciate-retaining and posterior-stabilized total knee replacements: In vivo fluoroscopic analysis during activities of daily living', *Journal of Orthopaedic Research*. doi: 10.1002/jor.20306.

Feng, Y. *et al.* (2016) 'In-vivo analysis of flexion axes of the knee: Femoral condylar motion during dynamic knee flexion', *Clinical Biomechanics*, 32, pp. 102–107. doi: 10.1016/j.clinbiomech.2015.12.006.

Fick, A. (1877) 'Zur Mechanik des Kniegelenks.', *Arch Anat Entw Gesch*, pp. 440–448.

Fick, R. (1911) 'Handbuch der Anatomie und Mechanik der Gelenke.', 2, pp. 109–17.

Fiedler, C. *et al.* (2011) 'Mathematical study on the guidance of the tibiofemoral joint as theoretical background for total knee replacements.', *Acta of bioengineering and*

biomechanics, 13(4), pp. 38–49. Available at: http://www.ncbi.nlm.nih.gov/pubmed/22339245.

Floerkemeier, T. *et al.* (2011) 'Physiologically shaped knee arthroplasty induces natural roll-back.', *Technology and health care : official journal of the European Society for Engineering and Medicine*, 19(2), pp. 91–102. doi: 10.3233/THC-2011-0616.

Frankel, V., Burstein, A. and Brooks, D. (1971) 'Biomechanics of Internal Derangement of the Knee', *J Bone Joint Surg [Br]*, 53(5), pp. 945–77. doi: 10.1097/00004623-197153050-00010.

Freeman, M. A. R. and Pinskerova, V. (2005) 'The movement of the normal tibio-femoral joint', *Journal of Biomechanics*. doi: 10.1016/j.jbiomech.2004.02.006.

Fu, F. H., Harner, C. D. and Vince, K. . (1994) 'Anatomy of the Knee', in Fu, F. H., Harner, C. D., and Vince, K. G. (eds) *Knee Surgery1*. Volume 1. Baltimore: Williams & Wilkins, pp. 1–54.

Fuchs, V. R. and Sox, H. C. (2001) 'Physicians' views of the relative importance of thirty medical innovations.', *Health affairs (Project Hope)*, 20(5), pp. 30–42. Available at: http://www.ncbi.nlm.nih.gov/pubmed/11558715.

Fuller, J. *et al.* (1997) 'A comparison of lower-extremity skeletal kinematics measured using skin-and pin-mounted markers', *Human Movement Science*. doi: 10.1016/S0167-9457(96)00053-X.

Garg, A. and Walker, P. S. (1990) 'Prediction of total knee motion using a three-dimensional computer-graphics model', *Journal of Biomechanics*. doi: 10.1016/0021-9290(90)90368-D.

Garling, E. H. *et al.* (2007) 'Limited rotation of the mobile-bearing in a rotating platform total knee prosthesis', *Journal of Biomechanics*, 40, pp. S25–S30. doi: 10.1016/j.jbiomech.2007.02.013.

Gergely, I. *et al.* (2017) 'Will Total Knee Replacement Ever Provide Normal Knee Function ?', *Journal of Interdisciplinary Medicine*, 2(38), pp. 22–26. doi: 10.1515/jim-2017-0040.

Ghonge, N. P. (2013) 'Computed Tomography in the 21st century: Current status & future prospects', *Journal International Medical Sciences Academy*, 26(1), pp. 35–42.

Gilles, B. *et al.* (2005) 'Bone motion analysis from dynamic MRI: Acquisition and tracking', in *Academic Radiology*. doi: 10.1016/j.acra.2005.08.006.

Goebel, D. and Schultz, W. (2012) 'The Columbus Knee System: 4-Year Results of a New Deep Flexion Design Compared to the NexGen Full Flex Implant', *Arthritis*. doi: 10.1155/2012/213817.

Goldman, L. W. (2007) 'Principles of CT and CT technology', *Journal of Nuclear Medicine Technology*. doi: 10.2967/jnmt.107.042978.

Gondim Teixeira, P. A. *et al.* (2014) 'Total hip prosthesis CT with single-energy projection-based metallic artifact reduction: Impact on the visualization of specific periprosthetic soft tissue structures', *Skeletal Radiology*. doi: 10.1007/s00256-014-1923-5.

Gondim Teixeira, P. A. *et al.* (2015) 'Musculoskeletal wide detector CT: Principles, techniques and applications in clinical practice and research', *European Journal of Radiology*, 84(5), pp. 892–900. doi: 10.1016/j.ejrad.2014.12.033.

Gonzalez, R. C., Woods, R. E. and Masters, B. R. (2009) 'Digital Image Processing, Third Edition', *Journal of Biomedical Optics*. doi: 10.1117/1.3115362.

Griffin, F. M. *et al.* (2000) 'Anatomy of the epicondyles of the distal femur: MRI analysis of normal knees', *Journal of Arthroplasty*. doi: 10.1016/S0883-5403(00)90739-3.

Grood, E. S. and Suntay, W. J. (1983) 'A Joint Coordinate System for the Clinical Description of Three-Dimensional Motions: Application to the Knee', *Journal of Biomechanical Engineering*. doi: 10.1115/1.3138397.

Grupp, T. M. *et al.* (2009) 'Fixed bearing knee congruency - Influence on contact mechanics, abrasive wear and kinematics', *International Journal of Artificial Organs*. doi: 10.1177/039139880903200405.

H. Shaikh, M., Panbude, S. and Joshi, A. (2014) 'Image Segmentation Techniques and its applications for Knee Joints: a Survey', *IOSR Journal of Electronics and Communication Engineering*, 9(5), pp. 23–28. doi: 10.9790/2834-09542328.

Hakki, S. *et al.* (2013) 'Columbus navigated TKA system: Clinical and radiological results at a minimum of 5 years with survivorship analysis', *Orthopedics*. doi: 10.3928/01477447-20130222-19.

Hamelynck, K. J. and Stiehl, J. B. (2002) *LCS® Mobile Bearing Knee Arthroplasty*. 1st edn. Berline: Springer-Verlag Berlin Heidelberg. doi: 10.1007/978-3-642-59347-5.

Han, J., Kamber, M. and Pei, J. (2012) *Data Mining: Concepts and Techniques*. 3rd edn. Morgan Kaufmann. doi: 10.1016/C2009-0-61819-5.

Haralick, R. M. and Shapiro, L. G. (1985) 'Image segmentation techniques', *Computer Vision, Graphics, and Image Processing*, 29(1), pp. 100–132. doi: 10.1016/S0734-189X(85)90153-7.

Harman, M. K. *et al.* (2012) 'Prosthesis alignment affects axial rotation motion after total knee replacement: A prospective in vivo study combining computed tomography and fluoroscopic evaluations', *BMC Musculoskeletal Disorders*. doi: 10.1186/1471-

2474-13-206.

Harner, C. D. *et al.* (1995) 'The Human Posterior Cruciate Ligament Complex: An Interdisciplinary Study: Ligament Morphology and Biomechanical Evaluation', *The American Journal of Sports Medicine*. doi: 10.1177/036354659502300617.

Harwin, S. F. (2003) 'Complications of unicompartmental knee arthroplasty', *Seminars in Arthroplasty*, 14(4), pp. 232–244. doi: 10.1053/j.sart.2003.09.001.

Hatayama, K. *et al.* (2011) 'Relationship Between Femoral Component Rotation and Total Knee Flexion Gap Balance on Modified Axial Radiographs', *Journal of Arthroplasty*. doi: 10.1016/j.arth.2010.05.029.

Hill, P. F. *et al.* (2000) 'Tibiofemoral movement 2: the loaded and unloaded living knee studied by MRI', *The Journal of Bone and Joint Surgery*, 82(8), pp. 1196–1198. doi: 10.1302/0301-620X.82B8.10716.

Hirschmann, M. T. and Becker, R. (2015) *The Unhappy Total Knee Replacement*. Edited by M. T. Hirschmann and R. Becker. Cham: Springer International Publishing. doi: 10.1007/978-3-319-08099-4.

Hofmann, A. A. *et al.* (2000) 'Posterior stabilization in total knee arthroplasty with use of an ultracongruent polyethylene insert', *Journal of Arthroplasty*. doi: 10.1054/arth.2000.6633.

Hohmann, E. and Bryant, A. (2007) 'Closing or Opening Wedge High Tibial Osteotomy: Watch Out for the Slope', *Operative Techniques in Orthopaedics*. doi: 10.1053/j.oto.2006.09.010.

Hollister, A. M. *et al.* (1993) 'The Axes of Rotation of the Knee', *Clinical Orthopaedics and Related Research*. doi: 10.1097/00003086-199305000-00033.

Hricak, H. *et al.* (2011) 'Managing radiation use in medical imaging: A multifaceted challenge', *Radiology*. doi: 10.1148/radiol.10101157.

Hsu, R. W. W. *et al.* (1990) 'Normal axial alignment of the lower extremity and load-bearing distribution at the knee', *Clinical Orthopaedics and Related Research*.

Huang, C. H. *et al.* (2003) 'Long-Term Results of Low Contact Stress Mobile-Bearing Total Knee Replacements', *Clinical Orthopaedics and Related Research*. doi: 10.1097/01.blo.0000093890.12372.46.

Huang, C. H., Liau, J. J. and Cheng, C. K. (2007) 'Fixed or mobile-bearing total knee arthroplasty', *Journal of Orthopaedic Surgery and Research*. doi: 10.1186/1749-799X-2-1.

Huang, L. (2017) *A Concise Introduction to Mechanics of Rigid Bodies*. 2nd edn. Edited by L. Huang. Cham: Springer International Publishing. doi: 10.1007/978-3-319-45041-4.

Hung, M. C. and Yang, D. L. (2001) 'An efficient fuzzy C-means clustering algorithm', in *Proceedings - IEEE International Conference on Data Mining, ICDM.*

Hunt, M. A. *et al.* (2008) 'Towards a biopsychosocial framework of osteoarthritis of the knee.', *Disability and rehabilitation*, 30(1), pp. 54–61. doi: 10.1080/09638280701189960.

Incavo, S., Beynnon, B. and Coughlin, K. (2005) 'In vitro kinematics of the replaced knee', in *Total Knee Arthroplasty: A Guide to Get Better Performance.* doi: 10.1007/3-540-27658-0_23.

Iwaki, H., Pinskerova, V. and Freeman, M. A. R. (2000) 'Tibiofemoral movement 1: the shapes and relative movements of the femur and tibia in the unloaded cadaver knee', *The Journal of Bone and Joint Surgery.* doi: 10.1302/0301-620X.82B8.10717.

Jacobs, W. C. H. *et al.* (2012) 'Functional performance of mobile versus fixed bearing total knee prostheses: a randomised controlled trial', *Knee Surgery, Sports Traumatology, Arthroscopy*, 20(8), pp. 1450–1455. doi: 10.1007/s00167-011-1684-9.

Jacobs, W. C. H., Clement, D. J. and Wymenga, A. B. (2005) 'Retention versus removal of the posterior cruciate ligament in total knee replacement: A systematic literature review within the Cochrane framework', *Acta Orthopaedica.* doi: 10.1080/17453670510045345.

Jerosch, J. *et al.* (2002) 'Interindividual reproducibility in perioperative rotational alignment of femoral components in knee prosthetic surgery using the transepicondylar axis', *Knee Surgery, Sports Traumatology, Arthroscopy.* doi: 10.1007/s00167-001-0271-x.

Jones, O. (2017) *TheTibia*, *TeachMeAnatomy*. Available at: http://teachmeanatomy.info/lower-limb/bones/the-tibia/#Proximal.

Jones, O. (2018a) *The Femur*, *TeachMeAnatomy*. Available at: http://teachmeanatomy.info/lower-limb/bones/femur/.

Jones, O. (2018b) *The Knee Joint*. Available at: http://teachmeanatomy.info/lower-limb/joints/the-knee-joint/.

Jonsson, H., Kärrholm, J. and Elmqvist, L.-G. (1989) 'Kinematics of active knee extension after tear of the anterior cruciate ligament', *The American Journal of Sports Medicine*, 17(6), pp. 796–802. doi: 10.1177/036354658901700613.

Kadaba, M. P., Ramakrishnan, H. K. and Wootten, M. E. (1990) 'Measurement of lower extremity kinematics during level walking.', *Journal of orthopaedic research : official publication of the Orthopaedic Research Society*. London: Springer London, 8(3), pp. 383–92. doi: 10.1002/jor.1100080310.

Kaiser, J. *et al.* (2016) 'Accuracy of model-based tracking of knee kinematics and cartilage contact measured by dynamic volumetric MRI', *Medical Engineering and*

Physics. doi: 10.1016/j.medengphy.2016.06.016.

Kalender, W. A., Hebel, R. and Ebersberger, J. (1987) 'Reduction of CT artifacts caused by metallic implants', *Radiology*. doi: 10.1148/radiology.164.2.3602406.

Kaneda, Y. *et al.* (1997) 'Experimental Study on External Tibial Rotation of the Knee', *The American Journal of Sports Medicine*, 25(6), pp. 796–800. doi: 10.1177/036354659702500611.

Kang, K.-T. *et al.* (2018) 'Comparison of Kinematics in Cruciate Retaining and Posterior Stabilized for Fixed and Rotating Platform Mobile-Bearing Total Knee Arthroplasty with respect to Different Posterior Tibial Slope.', *BioMed research international*, 2018, p. 5139074. doi: 10.1155/2018/5139074.

Kapandji, I. A. (1970) 'The Knee.', in Kapandji, I. A. (ed.) *The physiology of the Joints*. 2nd edn. Edinburgh: Churchill Livingstone, pp. 72–135.

Kapandji, I. A. (1971) 'The physiology of the joints, vol. 2: Lower Limb. By I. A. Kapandji, Paris. Second edition. 11 × 8½ in. Pp. 219. Illustrated. 1970. Edinburgh and London: E. & S. Livingstone Ltd. £2.75', *British Journal of Surgery*. Wiley, 58(5), pp. 403–403. doi: 10.1002/bjs.1800580528.

Karrholm, J., Brandsson, S. and Freeman, M. A. R. (2000) 'Tibiofemoral movement 4 : changes of axial tibial rotation caused by forced rotation at the weight-bearing knee studied by RSA', *Journal of Bone and Joint Surgery - British Volume*, 82(B), pp. 1201–1203. doi: 0301-620X/00/810715.

Karuppal, R. (2016) 'Kinematic alignment in total knee arthroplasty: Does it really matter?', *Journal of Orthopaedics*, 13(4), pp. A1–A3. doi: 10.1016/j.jor.2016.10.001.

Katz, M. A. *et al.* (2001) 'Determining femoral rotational alignment in total knee arthroplasty', *The Journal of Arthroplasty*, 16(3), pp. 301–305. doi: 10.1054/arth.2001.21456.

Kauffmann, C. *et al.* (2003) 'Computer-aided method for quantification of cartilage thickness and volume changes using MRI: Validation study using a synthetic model', *IEEE Transactions on Biomedical Engineering*. doi: 10.1109/TBME.2003.814539.

Kidoh, M. *et al.* (2014) 'Reduction of dental metallic artefacts in CT: Value of a newly developed algorithm for metal artefact reduction (O-MAR)', *Clinical Radiology*. doi: 10.1016/j.crad.2013.08.008.

Kinzel, G. L. and Gutkowski, L. J. (1983) 'Joint models, degrees of freedom, and anatomical motion measurement.', *Journal of biomechanical engineering*. doi: 10.1115/1.3138385.

Kinzel, V., Ledger, M. and Shakespeare, D. (2005) 'Can the epicondylar axis be defined accurately in total knee arthroplasty?', *Knee*. doi: 10.1016/j.knee.2004.09.003.

Koo, S. and Andriacchi, T. P. (2008) 'The knee joint center of rotation is predominantly on the lateral side during normal walking', *Journal of Biomechanics*, 41(6), pp. 1269–1273. doi: 10.1016/j.jbiomech.2008.01.013.

Kozanek, M. *et al.* (2009) 'Tibiofemoral kinematics and condylar motion during the stance phase of gait', *Journal of Biomechanics*. doi: 10.1016/j.jbiomech.2009.05.003.

Kroon, D.-J. (2016) 'Finite Iterative Closest Point'. MATLAB Central File Exchange. Available at: www.mathworks.com/matlabcentral/fileexchange/24301-finite-iterative-closest-point.

Kurosawa, H. *et al.* (1985) 'Geometry and motion of the knee for implant and orthotic design', *Journal of Biomechanics*. doi: 10.1016/0021-9290(85)90663-3.

Kurtz, S. M. *et al.* (2009) 'Future Young Patient Demand for Primary and Revision Joint Replacement: National Projections from 2010 to 2030', *Clinical Orthopaedics and Related Research®*, 467(10), pp. 2606–2612. doi: 10.1007/s11999-009-0834-6.

LaPrade, R. F. (2007) 'The Anatomy of the Medial Part of the Knee', *The Journal of Bone and Joint Surgery (American)*, 89(9), p. 2000. doi: 10.2106/JBJS.F.01176.

Laskin, R. S. *et al.* (2000) 'Deep-dish congruent tibial component use in total knee arthroplasty: A randomized prospective study', in *Clinical Orthopaedics and Related Research*. doi: 10.1097/00003086-200011000-00006.

Last, R. J. (1950) 'THE POPLITEUS MUSCLE AND THE LATERAL MENISCUS', *The Journal of Bone and Joint Surgery. British volume*, 32-B(1), pp. 93–99. doi: 10.1302/0301-620X.32B1.93.

Lee, T. Y. and Chhem, R. K. (2010) 'Impact of new technologies on dose reduction in CT', *European Journal of Radiology*. doi: 10.1016/j.ejrad.2010.06.036.

Lewis, J. L. and Lew, W. D. (1978) 'A Method for Locating an Optimal "Fixed" Axis of Rotation for the Human Knee Joint', *Journal of Biomechanical Engineering*. doi: 10.1115/1.3426209.

Li, G., Wuerz, T. H. and DeFrate, L. E. (2004) 'Feasibility of Using Orthogonal Fluoroscopic Images to Measure In Vivo Joint Kinematics', *Journal of Biomechanical Engineering*, 126(2). doi: 10.1115/1.1691448.

Li, J. S. *et al.* (2013) 'Kinematic characteristics of the tibiofemoral joint during a step-up activity', *Gait and Posture*. doi: 10.1016/j.gaitpost.2013.03.004.

Li, N. *et al.* (2014) 'Posterior cruciate-retaining versus posterior stabilized total knee arthroplasty: A meta-analysis of randomized controlled trials', *Knee Surgery, Sports Traumatology, Arthroscopy*. doi: 10.1007/s00167-012-2275-0.

Lu, T. W. and O'Connor, J. J. (1999) 'Bone position estimation from skin marker co-ordinates using global optimisation with joint constraints', *Journal of Biomechanics*.

doi: 10.1016/S0021-9290(98)00158-4.

Lucchetti, L. *et al.* (1998) 'Skin movement artefact assessment and compensation in the estimation of knee-joint kinematics', *Journal of Biomechanics*. doi: 10.1016/S0021-9290(98)00083-9.

Lustig, S. *et al.* (2008) 'Relationship between the surgical epicondylar axis and the articular surface of the distal femur: An anatomic study', *Knee Surgery, Sports Traumatology, Arthroscopy*. doi: 10.1007/s00167-008-0551-9.

Lützner, J. *et al.* (2017) 'No difference in range of motion between ultracongruent and posterior stabilized design in total knee arthroplasty: a randomized controlled trial', *Knee Surgery, Sports Traumatology, Arthroscopy*, 25(11). doi: 10.1007/s00167-016-4331-7.

Mahfouz, M. *et al.* (2012) 'Three-dimensional morphology of the knee reveals ethnic differences', in *Clinical Orthopaedics and Related Research*. doi: 10.1007/s11999-011-2089-2.

Mahoney, O. M. *et al.* (2012) 'No functional advantage of a mobile bearing posterior stabilized TKA.', *Clinical Orthopaedics and Related Research*, 470(1), pp. 33–44. doi: 10.1007/s11999-011-2114-5.

Majeed, A. and Aylin, P. (2005) 'The ageing population of the United Kingdom and cardiovascular disease', *BMJ*, 331(7529), p. 1362. doi: 10.1136/bmj.331.7529.1362.

De Man, B. *et al.* (2000) 'Reduction of metal streak artifacts in x-ray computed tomography using a transmission maximum a posteriori algorithm', *IEEE Transactions on Nuclear Science*.

Maniar, R. (2006) 'Rationale for the posterior-stabilized rotating-platform knee', *Orthopedics*.

Manner, P. W. (2016) *Knee Replacement Implants*, *OrthoInfo*. Available at: https://orthoinfo.aaos.org/en/treatment/knee-replacement-implants/ (Accessed: 9 June 2019).

Maravi, P. *et al.* (2015) 'Role of MRI in Orthopedics', *Orthopaedic Journal of M.P. Chapter*, 21(2), pp. 74–77. Available at: http://ojmpc.com/index.php/OJMPC/article/download/31/25.

Marchand, P. and Marmet, L. (1983) 'Binomial smoothing filter: A way to avoid some pitfalls of least-squares polynomial smoothing', *Review of Scientific Instruments*, 54(8). doi: 10.1063/1.1137498.

Martini, F. H., Nath, J. L. and Bartholomew, E. F. (2018) *Fundamentals of Anatomy and Physiology*. 11th edn, *Learning*. 11th edn. Edited by S. Beauparlant. Pearson Education, Inc. doi: 612.

Maruyama, S. *et al.* (2004) 'Functional comparison of posterior cruciate-retaining versus posterior stabilized total knee arthroplasty', *Journal of Arthroplasty*. doi: 10.1016/j.arth.2003.09.010.

De Marzi, L. *et al.* (2013) 'Calibration of CT Hounsfield units for proton therapy treatment planning: Use of kilovoltage and megavoltage images and comparison of parameterized methods', *Physics in Medicine and Biology*. doi: 10.1088/0031-9155/58/12/4255.

Matsuda, S. *et al.* (2003) 'A comparison of rotational landmarks in the distal femur and the tibial shaft', *Clinical Orthopaedics and Related Research*. doi: 10.1097/01.blo.0000072904.36018.79.

Matsuda, S. *et al.* (2004) 'Anatomical analysis of the femoral condyle in normal and osteoarthritic knees', *Journal of Orthopaedic Research*. doi: 10.1016/S0736-0266(03)00134-7.

Matsumoto, H. *et al.* (2000) 'Axis location of tibial rotation and its change with flexion angle', *Clinical Orthopaedics and Related Research*. doi: 10.1097/00003086-200002000-00022.

Matziolis, G. *et al.* (2011) 'Kinematic analysis of the flexion axis for correct femoral component placement', *Knee Surgery, Sports Traumatology, Arthroscopy*. doi: 10.1007/s00167-011-1554-5.

Mazzoli, V. *et al.* (2017) 'Accelerated 4D self-gated MRI of tibiofemoral kinematics', *NMR in Biomedicine*. doi: 10.1002/nbm.3791.

McCollough, C. H. *et al.* (2012) 'Achieving routine submillisievert CT scanning: Report from the Summit on Management of Radiation Dose in CT', *Radiology*. doi: 10.1148/radiol.12112265.

Mehranian, A. *et al.* (2013) '3D prior image constrained projection completion for x-ray ct metal artifact reduction', *IEEE Transactions on Nuclear Science*. doi: 10.1109/TNS.2013.2275919.

Mensch, J. and Amstutz, H. (1975) 'Knee morphology as a guide to knee replacement.', *Clinical Orthopaedics and Related Research®*, 112, pp. 231–41. Available at: https://www.ncbi.nlm.nih.gov/m/pubmed/1192638/.

Mettler, F. A. *et al.* (2008) 'Medical radiation exposure in the U.S. in 2006: Preliminary results', in *Health Physics*. doi: 10.1097/01.HP.0000326333.42287.a2.

Meyer, E. *et al.* (2012) 'Frequency split metal artifact reduction (FSMAR) in computed tomography', *Medical Physics*. doi: 10.1118/1.3691902.

Miki, K. *et al.* (2016) 'Single-energy metal artefact reduction with CT for carbonion radiation therapy treatment planning', *British Journal of Radiology*. doi: 10.1259/bjr.20150988.

Mink, J. H., Levy, T. and Crues, J. V (2014) 'Tears of the anterior cruciate ligament and menisci of the knee: MR imaging evaluation.', *Radiology*. doi: 10.1148/radiology.167.3.3363138.

Mochizuki, T. *et al.* (2014) 'The clinical epicondylar axis is not the functional flexion axis of the human knee', *Journal of Orthopaedic Science*, 19(3), pp. 451–456. doi: 10.1007/s00776-014-0536-0.

Moller, T. and Trumbore, B. (1998) *Fast, minimum storage ray-triangle intersection*, *Doktorsavhandlingar vid Chalmers Tekniska Hogskola*.

Moore, D. C. *et al.* (2015) 'Computed Tomography Image-Based Kinematic Analysis: An Overview', in Neu, C. P. and Genin, G. M. (eds) *Handbook of Imaging in Biological Mechanics*. Florida: CRC Press, p. 556.

Moreland, J. R., Bassett, L. W. and Hanker, G. J. (1987) 'Radiographic analysis of the axial alignment of the lower extremity', *Journal of Bone and Joint Surgery - Series A*. doi: 10.2106/00004623-198769050-00016.

Morsbach, F. *et al.* (2013) 'Reduction of metal artifacts from hip prostheses on CT images of the pelvis: Value of iterative reconstructions', *Radiology*. doi: 10.1148/radiol.13122089.

Moskowitz, R. W. (1984) *Osteoarthritis: Diagnosis and Management*. 2nd, Illustr edn. Saunders.

Most, E. *et al.* (2004) 'Sensitivity of the knee joint kinematics calculation to selection of flexion axes', *Journal of Biomechanics*, 37(11), pp. 1743–1748. doi: 10.1016/j.jbiomech.2004.01.025.

Nakagawa, S. *et al.* (2000) 'Tibiofemoral movement 3: full flexion in the living knee studied by MRI', *The Journal of Bone and Joint Surgery*, 82(8), pp. 1199–1200. doi: 10.1302/0301-620X.82B8.10718.

Narkhede, H. P. (2013) 'Review of Image Segmentation Techniques', *International Journal of Science and Modern Engineering*, (18).

Nguyen, K. T. *et al.* (2016) 'Quantitative analysis of knee movement patterns through comparative visualization', in *Mathematics and Visualization*. doi: 10.1007/978-3-319-24523-2_12.

Noble, P. C. *et al.* (2005) 'Does total knee replacement restore normal knee function?', *Clinical orthopaedics and related research*, (431), pp. 157–65. Available at: http://www.ncbi.nlm.nih.gov/pubmed/15685070.

Noble, P. C. *et al.* (2006) 'The John Insall Award: Patient Expectations Affect Satisfaction with Total Knee Arthroplasty', *Clinical Orthopaedics and Related Research*, 452, pp. 35–43. doi: 10.1097/01.blo.0000238825.63648.1e.

Nordin, M. and Frankel, V. (1982) 'Biomechanics of the Knee', in Helfet, A. (ed.) *Disorders of the Knee*. 2nd edn. Cambridge: JB Lippincott, pp. 19–33.

Nowakowski, A. (2006) 'Das Transversalträger-Tibiaplateau (TTTP)', *Orthopädische Praxis*, 42(7), pp. 419–28.

Oxford Economics (2010) 'The Economic Costs of Arthritis for the UK Economy', (Final Report).

Pal, N. R. and Pal, S. K. (1993) 'A review on image segmentation techniques', *Pattern Recognition*, 26(9). doi: 10.1016/0031-3203(93)90135-J.

Pan, T. (2005) 'Comparison of helical and cine acquisitions for 4D-CT imaging with multislice CT', *Medical Physics*, 32(2). doi: 10.1118/1.1855013.

Patel, A. *et al.* (2015) 'The epidemiology of revision total knee and hip arthroplasty in England and Wales', *The Bone & Joint Journal*, 97-B(8), pp. 1076–1081. doi: 10.1302/0301-620X.97B8.35170.

Patel, V. V. *et al.* (2004) 'A three-dimensional MRI analysis of knee kinematics', *Journal of Orthopaedic Research*. doi: 10.1016/j.orthres.2003.08.015.

Paudel, M. R. *et al.* (2014) 'Clinical evaluation of normalized metal artifact reduction in kVCT using MVCT prior images (MVCT-NMAR) for radiation therapy treatment planning', *International Journal of Radiation Oncology Biology Physics*. doi: 10.1016/j.ijrobp.2014.02.040.

Pennock, G. R. and Clark, K. J. (1990) 'An anatomy-based coordinate system for the description of the kinematic displacements in the human knee', *Journal of Biomechanics*. doi: 10.1016/0021-9290(90)90378-G.

Pham, D. L. and Prince, J. L. (1999) 'An adaptive fuzzy C-means algorithm for image segmentation in the presence of intensity inhomogeneities', *Pattern Recognition Letters*. doi: 10.1016/S0167-8655(98)00121-4.

Piazza, S. J. and Cavanagh, P. R. (2000) 'Measurement of the screw-home motion of the knee is sensitive to errors in axis alignment', *Journal of Biomechanics*, 33(8), pp. 1029–1034. doi: 10.1016/S0021-9290(00)00056-7.

Pierrart, J. *et al.* (2014) 'New dynamic three-dimensional MRI technique for shoulder kinematic analysis', *Journal of Magnetic Resonance Imaging*. doi: 10.1002/jmri.24204.

Pinskerova, V. *et al.* (2004) 'Does the femur roll-back with flexion?', *Journal of Bone and Joint Surgery - Series B*. doi: 10.1302/0301-620X.86B6.14589.

Pinskerova, V. *et al.* (2009) 'The knee in full flexion: AN ANATOMICAL STUDY', *Journal of Bone and Joint Surgery - British Volume*, 91-B(6), pp. 830–834. doi: 10.1302/0301-620X.91B6.22319.

Post, Z. D. *et al.* (2010) 'Mobile-bearing total knee arthroplasty. Better than a fixed-bearing?', *Journal of Arthroplasty*. Elsevier Inc., 25(6), pp. 998–1003. doi: 10.1016/j.arth.2009.07.014.

Power, S. P. *et al.* (2016) 'Computed tomography and patient risk: Facts, perceptions and uncertainties', *World Journal of Radiology*. doi: 10.4329/wjr.v8.i12.902.

Preston, D. C. (2006) *Magnetic Resonance Imaging (MRI): Basics*. Available at: https://case.edu/med/neurology/NR/MRI Basics.htm#:~:text=The most common MRI sequences,longer TE and TR times.

Ranawat, C. S. *et al.* (2004) 'In Vivo Kinematics for Fixed and Mobile-Bearing Posterior Stabilized Knee Prostheses', *Clinical Orthopaedics and Related Research*. doi: 10.1097/00003086-200401000-00030.

Ranawat, C. S., Luessenhop, C. P. and Rodriguez, J. A. (1997) 'The press-fit condylar modular total knee system. Four-to-six-year results with a posterior-cruciate-substituting design', *Journal of Bone and Joint Surgery - Series A*.

Randen, A. *et al.* (2008) 'Acute appendicitis: Meta-analysis of diagnostic performance of CT and graded compression US related to prevalence of disease', *Radiology*. doi: 10.1148/radiol.2483071652.

Reilly, R. and M. (2019) *Medical Imaging for Health Professionals: Technologies and Clinical Applications*. First. Hoboken, NJ: Wiley.

Reuleaux, F. (1875) *Lehrbuch der kinematik, Vol.1*. 1st edn. F. Vieweg. Available at: https://books.google.com.mt/books?id=MsdJAAAAMAAJ&source=gbs_book_other_versions.

Robb, J. (1994) *Estimates of radiation detriment in a UK population*. Chilton. Available at: https://inis.iaea.org/search/search.aspx?orig_q=source:%22ISBN 0 85951 385 0%22.

Robertson, P. L. *et al.* (2014) 'Anterior cruciate ligament tears: evaluation of multiple signs with MR imaging.', *Radiology*. doi: 10.1148/radiology.193.3.7972833.

Robertsson, O. *et al.* (2000) 'Patient satisfaction after knee arthroplasty: A report on 27,372 knees operated on between 1981 and 1995 in Sweden', *Acta Orthopaedica Scandinavica*, 71(3), pp. 262–267. doi: 10.1080/000164700317411852.

Roland, M., Hull, M. L. and Howell, S. M. (2010) 'Virtual Axis Finder: A New Method to Determine the Two Kinematic Axes of Rotation for the Tibio-Femoral Joint', *Journal of Biomechanical Engineering*, 132(1), p. 011009. doi: 10.1115/1.4000163.

Rosen, M. P. *et al.* (2000) 'Impact of abdominal CT on the management of patients presenting to the emergency department with acute abdominal pain', *American Journal of Roentgenology*. doi: 10.2214/ajr.174.5.1741391.

Rosen, M. P. *et al.* (2003) 'Value of abdominal CT in the emergency department for patients with abdominal pain', *European Radiology*.

Sandhya, P. H. and Kumar, S. (2017) 'A Survey on Fuzzy C-means Clustering Techniques', *International Journal of Engineering Development and Research (IJEDR)*, 5(4), pp. 1151–1155. Available at: https://ijedr.org/papers/IJEDR1704186.pdf.

Sando, T. *et al.* (2015) 'Ten-year results comparing posterior cruciate-retaining versus posterior cruciate-substituting total knee arthroplasty', *Journal of Arthroplasty*. doi: 10.1016/j.arth.2014.09.009.

Sankur, B. (2004) 'Survey over image thresholding techniques and quantitative performance evaluation', *Journal of Electronic Imaging*. doi: 10.1117/1.1631315.

Sathasivam, S. and Walker, P. S. (1997) 'A computer model with surface friction for the prediction of total knee kinematics', *Journal of Biomechanics*. doi: 10.1016/S0021-9290(96)00114-5.

Schmidt, R. *et al.* (2003) 'Fluoroscopic analyses of cruciate-retaining and Medial Pivot knee implants', in *Clinical Orthopaedics and Related Research*. doi: 10.1097/01.blo.0000063565.90853.a4.

Scott, W. N. (2018) *Surgery of the Knee*, *Insall & Scott Surgery of the Knee*. Elsevier. doi: 10.1016/B978-1-4377-1503-3.00078-0.

Sharkey, P. F. *et al.* (2014) 'Why Are Total Knee Arthroplasties Failing Today—Has Anything Changed After 10 Years?', *The Journal of Arthroplasty*, 29(9), pp. 1774–1778. doi: 10.1016/j.arth.2013.07.024.

Shaw, J. A. and Murray, D. G. (1974) 'The Longitudinal Axis of the Knee and the Role of the Cruciate Ligaments in Controlling Transverse Rotation', *The Journal of Bone & Joint Surgery*, 56(8), pp. 1603–1609. doi: 10.2106/00004623-197456080-00008.

Sheldon, S. (1994) *Orthopaedic Basic Science*. Edited by S. Sheldon. American Academy of Orthopaedics.

Shenoy, R., Pastides, P. S. and Nathwani, D. (2013) '(iii) Biomechanics of the knee and TKR', *Orthopaedics and Trauma*, 27(6), pp. 364–371. doi: 10.1016/j.mporth.2013.10.003.

Shiavi, R. *et al.* (1987a) 'Helical motion analysis of the knee-II. Kinematics of uninjured and injured knees during walking and pivoting', *Journal of Biomechanics*. doi: 10.1016/0021-9290(87)90032-7.

Shiavi, R. *et al.* (1987b) 'Helical motion analysis of the knee—I. Methodology for studying kinematics during locomotion', *Journal of Biomechanics*, 20(5), pp. 459–469. doi: 10.1016/0021-9290(87)90247-8.

Sikorski, J. M. (2008) 'Alignment in total knee replacement', *The Journal of Bone and Joint Surgery. British volume*, 90-B(9), pp. 1121–1127. doi: 10.1302/0301-620X.90B9.20793.

Van Sint Jan, S. *et al.* (2002) 'Registration of 6-DOFs electrogoniometry and CT medical imaging for 3D joint modeling', *Journal of Biomechanics*. doi: 10.1016/S0021-9290(02)00074-X.

Siu, D. *et al.* (1996) 'Femoral articular shape and geometry: A three-dimensional computerized analysis of the knee', *Journal of Arthroplasty*. doi: 10.1016/S0883-5403(05)80012-9.

Smidt, G. L. (1973) 'Biomechanical analysis of knee flexion and extension', *Journal of Biomechanics*, 6(1), pp. 79–92. doi: 10.1016/0021-9290(73)90040-7.

Smith, B. A., Livesay, G. A. and Woo, S. L. (1993) 'Biology and biomechanics of the anterior cruciate ligament.', *Clinics in sports medicine*, 12(4), pp. 637–70. doi: 10.1080/19397030902947041.

Soudan, K., Van Audekercke, R. and Martens, M. (1979) 'Methods, difficulties and inaccuracies in the study of human joint kinematics and pathokinematics by the instant axis concept. Example: The knee joint', *Journal of Biomechanics*, 12(1), pp. 27–33. doi: 10.1016/0021-9290(79)90006-X.

Steindler, A. (1955) *Kinesiology of the Human Body under Normal and Pathological Conditions.*, *Journal of Bone and Joint Surgery - British Volume*. Available at: https://journals.lww.com/jbjsjournal/Citation/1955/37060/Kinesiology_of_the_Human_Body_under_Normal_and.27.aspx.

Stiehl, J. B. *et al.* (1997) 'In Vivo Kinematic Analysis of a Mobile Bearing Total Knee Prosthesis', *Clinical Orthopaedics and Related Research*. doi: 10.1097/00003086-199712000-00010.

Strasser, H. (1917) *Lehrbuch der Muskel und Gelenkmechanik.* 3rd edn. Berlin: Springer Verlag.

Subburaj, K., Ravi, B. and Agarwal, M. (2010) 'Computer-aided methods for assessing lower limb deformities in orthopaedic surgery planning', *Computerized Medical Imaging and Graphics*. doi: 10.1016/j.compmedimag.2009.11.003.

Sun, Y., Teo, E. C. and Zhang, Q. H. (2006) 'Discussions of knee joint segmentation', in *ICBPE 2006 - Proceedings of the 2006 International Conference on Biomedical and Pharmaceutical Engineering*. doi: 10.1109/ICBPE.2006.348611.

Tanifuji, O. *et al.* (2013) 'Three-dimensional in vivo motion analysis of normal knees employing transepicondylar axis as an evaluation parameter', *Knee Surgery, Sports Traumatology, Arthroscopy*. doi: 10.1007/s00167-012-2010-x.

Tay, S. C. *et al.* (2007) 'Four-dimensional computed tomographic imaging in the

wrist: Proof of feasibility in a cadaveric model', *Skeletal Radiology*. doi: 10.1007/s00256-007-0374-7.

The Mathworks Inc. (2018) 'MATLAB'. NAtick, Massachusettes. Available at: www.mathworks.com.

Thompson, W. O. *et al.* (1991) 'Tibial meniscal dynamics using three-dimensional reconstruction of magnetic resonance images', *The American Journal of Sports Medicine*, 19(3), pp. 210–216. doi: 10.1177/036354659101900302.

Toshiba Medical Systems (2008) 'Dynamic Volume Imaging - Special Issue', *Toshiba Medical Systems Journal*. Available at: https://ch.medical.canon/wp-content/uploads/sites/33/2017/01/2008-VISIONS-Special-Dynamic-Volume-ImagingFINAL.pdf.

Toshiba Medical Systems (2012) *Product Data No. MPDCT0314EA*.

Tsujii, A. *et al.* (2018) 'Arthroscopic minimum saucerization and inferior-leaf meniscectomy for a horizontal tear of a complete discoid lateral meniscus: Report of two cases', *International Journal of Surgery Case Reports*. doi: 10.1016/j.ijscr.2018.11.027.

Udupa, J. K. and Saha, P. K. (2003) 'Fuzzy connectedness and image segmentation', in *Proceedings of the IEEE*. doi: 10.1109/JPROC.2003.817883.

Uecker, M. *et al.* (2010) 'Real-time MRI at a resolution of 20 ms', *NMR in Biomedicine*. doi: 10.1002/nbm.1585.

UNSCEAR (2000) *Sources and Effects of Ionizing Radiation, United Nations Scientific Committee on the Effects of Atomic Radiation UNSCEAR 2000 Report to the General Assembly, with Scientific Annexes*, *UNSCEAR 2000 Report*.

Vaishya, R., Agarwal, A. K. and Vijay, V. (2016) 'Extensor Mechanism Disruption after Total Knee Arthroplasty: A Case Series and Review of Literature', *Cureus*. doi: 10.7759/cureus.479.

Varadarajan, K. M. *et al.* (2009) 'Can in vitro systems capture the characteristic differences between the flexion-extension kinematics of the healthy and TKA knee?', *Medical Engineering and Physics*. doi: 10.1016/j.medengphy.2009.06.005.

Vedi, V. *et al.* (1999) 'Meniscal movement', *The Journal of Bone and Joint Surgery*, 81(1), pp. 37–41. doi: 10.1302/0301-620X.81B1.8928.

Veselko, M., Jenko, M. and Lipuscek, I. (1998) 'The use of the co-ordinate measuring machine for the study of three-dimensional biomechanics of the knee.', *Computers in biology and medicine*, 28(4), pp. 343–57. Available at: http://www.ncbi.nlm.nih.gov/pubmed/9805195.

Victor, J., Van Doninck, D., Labey, L., Van Glabbeek, F., *et al.* (2009) 'A common

reference frame for describing rotation of the distal femur', *The Journal of Bone and Joint Surgery. British volume*, 91-B(5), pp. 683–690. doi: 10.1302/0301-620X.91B5.21827.

Victor, J., Van Doninck, D., Labey, L., Innocenti, B., *et al.* (2009) 'How precise can bony landmarks be determined on a CT scan of the knee?', *Knee*. doi: 10.1016/j.knee.2009.01.001.

Victor, J. (2009) 'Rotational alignment of the distal femur: A literature review', *Orthopaedics & Traumatology: Surgery & Research*, 95(5), pp. 365–372. doi: 10.1016/j.otsr.2009.04.011.

Waldman, S. D. and Campbell, R. S. D. (2011) *Imaging of Pain*. doi: 10.1016/C2009-0-39533-1.

Walker, P. S. *et al.* (2011) 'Reference axes for comparing the motion of knee replacements with the anatomic knee', *Knee*. doi: 10.1016/j.knee.2010.07.005.

Walker, P. S. and Erkiuan, M. J. (1975) 'The Role of the Menisci in Force Transmission Across the Knee', *Clinical Orthopaedics and Related Research*, 109, pp. 184–92. doi: 10.1097/00003086-197506000-00027.

Weber, W. and Weber, E. (1837) 'Ueber die Mechanik der menschlichen Gehwerkzeuge, nebst der Beschreibung eines Versuchs über das Herausfallen des Schenkelkopfs aus der Pfanne im luftverdünnten Raume', *Annalen der Physik und Chemie*, 116(1), pp. 1–13. doi: 10.1002/andp.18371160102.

Whittle, M. (2012) *Whittle's gait analysis.* 5th edn. Edited by J. Richards, D. Levine, and Micheal Whittle. Churchill Livingstone.

Wilson, D. A. (2011) *Clinical Veterinary Advisor: The Horse*. doi: 10.1016/C2009-0-38641-9.

Woolf, A. D. and Pfleger, B. (2003) 'Burden of major musculoskeletal conditions.', *Bulletin of the World Health Organization*, 81(9), pp. 646–56. Available at: http://www.scirp.org/journal/doi.aspx?DOI=10.4236/abb.2012.324063.

Wu, G. *et al.* (2002) 'ISB recommendation on definitions of joint coordinate system of various joints for the reporting of human joint motion—part I: ankle, hip, and spine', *Journal of Biomechanics*. doi: 10.1016/S0021-9290(01)00222-6.

Wu, G. *et al.* (2005) 'ISB recommendation on definitions of joint coordinate systems of various joints for the reporting of human joint motioN, Part II: shoulder, elbow, wrist and hand', *Journal of Biomechanics*. doi: 10.1016/j.jbiomech.2004.05.042.

Wu, G. and Cavanagh, P. R. (1995) 'ISB recommendations for standardization in the reporting of kinematic data', *Journal of Biomechanics*. doi: 10.1016/0021-9290(95)00017-C.

Wylde, V. *et al.* (2008) 'Patient-reported outcomes after fixed- versus mobile-bearing total knee replacement', *The Journal of Bone and Joint Surgery. British volume*, 90-B(9), pp. 1172–1179. doi: 10.1302/0301-620X.90B9.21031.

Yamazaki, T. *et al.* (2007) '3D kinematics of normal knee using X-ray fluoroscopy and CT images', in *World Congress on Medical Physics and Biomedical Engineering 2006*. doi: 10.1007/978-3-540-36841-0_706.

Yao, J. *et al.* (2014) 'In vivo measurements of patellar tracking and finite helical axis using a static magnetic resonance based methodology', *Medical Engineering and Physics*. doi: 10.1016/j.medengphy.2014.08.014.

Yau, W. P., Chiu, K. Y. and Tang, W. M. (2007) 'How Precise is the Determination of Rotational Alignment of the Femoral Prosthesis in Total Knee Arthroplasty. An In Vivo Study', *Journal of Arthroplasty*. doi: 10.1016/j.arth.2006.12.043.

Yin, L. *et al.* (2015) 'Identifying the Functional Flexion-extension Axis of the Knee: An In-Vivo Kinematics Study', *PLOS ONE*. Edited by L. Ren, 10(6), p. e0128877. doi: 10.1371/journal.pone.0128877.

Yoshioka, Y. *et al.* (1989) 'Tibial Anatomy and Functional Axes', *Journal of Orthopaedic Research*, 7(1), pp. 132–7. doi: 10.1002/jor.1100070118.

Yoshioka, Y., Siu, D. and Cooke, T. D. V. (1987a) 'The anatomy and functional axes of the femur.', *The Journal of Bone & Joint Surgery*, 69(6), pp. 873–880. doi: 10.2106/00004623-198769060-00012.

Yoshioka, Y., Siu, D. and Cooke, T. D. V. (1987b) 'The anatomy and functional axes of the femur', *Journal of Bone and Joint Surgery - Series A*. doi: 10.2106/00004623-198769060-00012.

You, B. M. *et al.* (2001) 'In vivo measurement of 3-D skeletal kinematics from sequences of biplane radiographs: Application to knee kinematics', *IEEE Transactions on Medical Imaging*, 20(6). doi: 10.1109/42.929617.

Zhai, G. *et al.* (2007) 'A longitudinal study of the association between knee alignment and change in cartilage volume and chondral defects in a largely non-osteoarthritic population', *Journal of Rheumatology*.

Zhang, Y. J. (1996) 'A survey on evaluation methods for image segmentation', *Pattern Recognition*, 29(8). doi: 10.1016/0031-3203(95)00169-7.

Zhao, S. *et al.* (2002) 'A wavelet method for metal artifact reduction with multiple metallic objects in the field of view', *Journal of X-Ray Science and Technology*.

Zuppinger, H. (1904) 'Die aktive Flexion im unbelasteten Kniegelenk [Active flexion of the unloaded knee joint].', *Anatomische Hefte. Beiträge und Referate zur Anatomie und Entwicklungsgeschichte*, 77, pp. 701–64.

Aesculap (2012) *Columbus Knee Design Rationale Brochure*. Palo Alto. Available at: https://www.aesculapimplantsystems.com/content/dam/aesculap-us/us/website/aesculap-implant_systems/hp-section/ortho-product-pages/ortho-resources-pdfs/DOC616-RevA-Columbus-Knee-Design-Rationale-Brochure.pdf.

Aglietti, P. *et al.* (2008) 'Rotational position of femoral and tibial components in TKA using the femoral transepicondylar axis', in *Clinical Orthopaedics and Related Research*. doi: 10.1007/s11999-008-0452-8.

Aly, A. A., Bin Deris, S. and Zaki, N. (2011) 'Research Review for Digital Image Segmentation Techniques', *International Journal of Computer Science and Information Technology*, 3(5). doi: 10.5121/ijcsit.2011.3509.

American Academy of Orthopaedic Surgeons (2014) *Arthritis of the Knee*. Available at: https://orthoinfo.aaos.org/en/diseases--conditions/arthritis-of-the-knee/ (Accessed: 5 October 2019).

AO foundation (2008) *Lateral parapatellar approach to the distal femur*. Available at: https://www2.aofoundation.org/wps/portal/!ut/p/a0/04_Sj9CPykssy0xPLMnMz0vMA fGjzOKN_A0M3D2DDbz9_UMMDRyDXQ3dw9wMDAzMjfULsh0VAbWjLW0!/? approach=Lateral parapatellar approach&bone=Femur&segment=Distal&showPage=approach&contentUrl=/srg/33/ 04-Approaches/A21-lat (Accessed: 12 July 2018).

Argenson, J. N. A. *et al.* (2012) 'The outcome of rotating-platform total knee arthroplasty with cement at a minimum of ten years of follow-up', *Journal of Bone and Joint Surgery - Series A*. doi: 10.2106/JBJS.K.00263.

Asano, T., Akagi, M. and Nakamura, T. (2005) 'The Functional Flexion-Extension Axis of the Knee Corresponds to the Surgical Epicondylar Axis', *The Journal of Arthroplasty*, 20(8), pp. 1060–1067. doi: 10.1016/j.arth.2004.08.005.

Bach, J. M. and Hull, M. L. (1995) 'A New Load Application System for In Vitro Study of Ligamentous Injuries to the Human Knee Joint', *Journal of Biomechanical Engineering*. doi: 10.1115/1.2794195.

Bamberg, F. *et al.* (2011) 'Metal artifact reduction by dual energy computed tomography using monoenergetic extrapolation', *European Radiology*. doi: 10.1007/s00330-011-2062-1.

Banks, S. *et al.* (2016) 'In Vivo kinematics of a medially conforming and rotationally unconstrained TKA design', *Orthopaedic Proceedings*, 98-B(SUPP_1), p. 35. doi: 10.1302/1358-992X.98BSUPP_1.ISTA2014-035.

Banks, S. A. and Hodge, W. A. (2004) '2003 Hap Paul Award paper of the International Society for Technology in Arthroplasty', *The Journal of Arthroplasty*,

19(7), pp. 809–816. doi: 10.1016/j.arth.2004.04.011.

Barrett, W. P. *et al.* (2011) 'Comparison of Radiographic Alignment of Imageless Computer-Assisted Surgery vs Conventional Instrumentation in Primary Total Knee Arthroplasty', *The Journal of Arthroplasty*, 26(8), pp. 1273-1284.e1. doi: 10.1016/j.arth.2011.04.037.

Bellemans, J. *et al.* (2012) 'The Chitranjan Ranawat Award: Is Neutral Mechanical Alignment Normal for All Patients?: The Concept of Constitutional Varus', *Clinical Orthopaedics and Related Research®*. doi: 10.1007/s11999-011-1936-5.

Bellemans, J., Ries, M. D. and Victor, J. M. K. (2005) *TKA - A Guide To Better Performance*.

Berger, R. A. *et al.* (1993) 'Determining the Rotational Alignment of the Femoral Component in Total Knee Arthroplasty Using the Epicondylar Axis', *Clinical Orthopaedics and Related Research*, (286), pp. 40–47. doi: 10.1097/00003086-199301000-00008.

Berme, N., Engin, A. E. and Correia da Silva, K. M. (eds) (1985) *Biomechanics of Normal and Pathological Human Articulating Joints*, *Biomechanics of Normal and Pathological Human Articulating Joints*. Dordrecht: Springer Netherlands. doi: 10.1007/978-94-009-5117-4.

Bistolfi, A. *et al.* (2013) 'Comparison of fixed and mobile-bearing total knee arthroplasty at a mean follow-up of 116 months', *Journal of Bone and Joint Surgery - Series A*. doi: 10.2106/JBJS.L.00327.

Blankevoort, L. and Huiskes, R. (1996) 'Validation of a three-dimensional model of the knee', *Journal of Biomechanics*. doi: 10.1016/0021-9290(95)00149-2.

Blankevoort, L., Huiskes, R. and de Lange, A. (1988) 'The envelope of passive knee joint motion', *Journal of Biomechanics*, 21(9), pp. 705–720. doi: 10.1016/0021-9290(88)90280-1.

Blankevoort, L., Huiskes, R. and de Lange, A. (1990) 'Helical axes of passive knee joint motions', *Journal of Biomechanics*. doi: 10.1016/0021-9290(90)90379-H.

Blunn, G. W. *et al.* (1997) 'Wear in retrieved condylar knee arthroplasties: A comparison of wear in different designs of 280 retrieved condylar knee prostheses', *Journal of Arthroplasty*. doi: 10.1016/S0883-5403(97)90024-3.

Boguszewski, D. V. *et al.* (2016) 'Location of the natural knee axis for internal–external tibial rotation', *The Knee*, 23(6), pp. 1083–1088. doi: 10.1016/j.knee.2015.11.003.

Bottema, D., Roth, B. and Veldkamp, G. R. (1980) 'Theoretical Kinematics', *Journal of Applied Mechanics*. doi: 10.1115/1.3153630.

Van der Bracht, H. *et al.* (2010) 'Is there any superiority in the clinical outcome of mobile-bearing knee prosthesis designs compared to fixed-bearing total knee prosthesis designs in the treatment of osteoarthritis of the knee joint?', *Knee Surgery, Sports Traumatology, Arthroscopy*. doi: 10.1007/s00167-009-0973-z.

Brandsson, S. *et al.* (2001) 'Kinematics after tear in the anterior cruciate ligament: Dynamic bilateral radiostereometric studies in 11 patients', *Acta Orthopaedica Scandinavica*. doi: 10.1080/000164701753542032.

Brantigan, O. C. and Voshell, A. F. (1941) 'THE MECHANICS OF THE LIGAMENTS AND MENISCI OF THE KNEE JOINT', *J Bone Joint Surg Am*.

Braune, C. W. and Fischer, O. (1891) *Die bewegungen des kniegelenks nach einer neuen methode am lebenden menschen gemessen*. Edited by S. Hirzel. Leipzig.

Brook, O. R. *et al.* (2012) 'Spectral CT with metal artifacts reduction software for improvement of tumor visibility in the vicinity of gold fiducial markers', *Radiology*. doi: 10.1148/radiol.12111170.

Buechel, F. F. *et al.* (2001) 'Twenty-year evaluation of meniscal bearing and rotating platform knee replacements', in *Clinical Orthopaedics and Related Research*. doi: 10.1097/00003086-200107000-00008.

Buechel, F. F. and Pappas, M. J. (1986) 'The New Jersey low-contact-stress knee replacement system: Biomechanical rationale and review of the first 123 cemented cases', *Archives of Orthopaedic and Traumatic Surgery*. doi: 10.1007/BF00435480.

Buechel, F. F. and Pappas, M. J. (1989) 'New Jersey low contact stress knee replacement system. Ten-year evaluation of meniscal bearings', *Orthopedic Clinics of North America*.

Bugnion, E. (1892) *Le mechanism du genou. Extrait du recueil inaugural de l'Universitie Lausanne*. Lausanne.

Bull, A. M. J. and Amis, A. A. (1998) 'Knee joint motion: Description and measurement', *Proceedings of the Institution of Mechanical Engineers, Part H: Journal of Engineering in Medicine*. doi: 10.1243/0954411981534132.

Callaghan, J. *et al.* (2000) 'Mobile-Bearing Knee Replacement : Concepts and Results*+.', *J Bone Joint Surg Am*, 82(7), p. 1020. Available at: http://ovidsp.ovid.com/ovidweb.cgi?T=JS&PAGE=reference&D=yrovftd&NEWS=N&AN=00004623-200007000-00013.

Callaghan, J. J. *et al.* (2010) 'Cemented Rotating-Platform Total Knee Replacement', *The Journal of Bone and Joint Surgery-American Volume*. doi: 10.2106/jbjs.i.01012.

Cappozzo, A. (1991) 'Three-dimensional analysis of human walking: Experimental methods and associated artifacts', *Human Movement Science*. doi: 10.1016/0167-9457(91)90047-2.

Carothers, J. T. *et al.* (2011) 'Mobile-Bearing Total Knee Arthroplasty. A Meta-Analysis', *Journal of Arthroplasty*. doi: 10.1016/j.arth.2010.05.015.

Cherian, J. J. *et al.* (2014) 'Mechanical, Anatomical, and Kinematic Axis in TKA: Concepts and Practical Applications', *Current Reviews in Musculoskeletal Medicine*, 7(2), pp. 89–95. doi: 10.1007/s12178-014-9218-y.

Chouteau, J. *et al.* (2009) 'Mobile-bearing insert translational and rotational kinematics in a PCL-retaining total knee arthroplasty', *Orthopaedics and Traumatology: Surgery and Research*. doi: 10.1016/j.otsr.2009.03.012.

Churchill, D. L. *et al.* (1996) 'A compound pinned hinge model of knee joint kinematics.', *Trans Orthop Res. Soc.*, 21(717).

Churchill, D. L. *et al.* (1998) 'The Transepicondylar Axis Approximates the Optimal Flexion Axis of the Knee', *Clinical Orthopaedics and Related Research*, 356, pp. 111–118. doi: 10.1097/00003086-199811000-00016.

Cobb, J. P. *et al.* (2008) 'The anatomical tibial axis', *The Journal of Bone and Joint Surgery. British volume*, 90-B(8), pp. 1032–1038. doi: 10.1302/0301-620X.90B8.19905.

Cole, G. K. *et al.* (1993) 'Application of the Joint Coordinate System to Three-Dimensional Joint Attitude and Movement Representation: A Standardization Proposal', *Journal of Biomechanical Engineering*, 115(4A), p. 344. doi: 10.1115/1.2895496.

Colizza, W. A., Insall, J. N. and Scuderi, G. R. (1995) 'The posterior stabilized total knee prosthesis: Assessment of polyethylene damage and osteolysis after a ten-year-minimum follow-up', *Journal of Bone and Joint Surgery - Series A*. doi: 10.2106/00004623-199511000-00011.

D'Entremont, A. G. *et al.* (2013) 'Do dynamic-based MR knee kinematics methods produce the same results as static methods?', *Magnetic Resonance in Medicine*. doi: 10.1002/mrm.24425.

D'Entremont, A. G. *et al.* (2014) 'Effect of opening-wedge high tibial osteotomy on the three-Dimensional kinematics of the knee', *Bone and Joint Journal*. doi: 10.1302/0301-620X.96B9.32522$2.00.

D'Lima, D. D. *et al.* (2001) 'Polyethylene wear and variations in knee kinematics', in *Clinical Orthopaedics and Related Research*. doi: 10.1097/00003086-200111000-00015.

D'Lima, D. D., Chen, P. C. and Colwell, C. W. (2001) 'Polyethylene Contact Stresses, Articular Congruity, and Knee Alignment', *Clinical Orthopaedics and Related Research*, 392, pp. 232–238. doi: 10.1097/00003086-200111000-00029.

Daniilidis, K. *et al.* (2012) 'Highly conforming polyethylene inlays reduce the in vivo

variability of knee joint kinematics after total knee arthroplasty', *Knee*. doi: 10.1016/j.knee.2011.04.001.

Dennis, D. A. *et al.* (1996) 'In vivo knee kinematics derived using an inverse perspective technique', in *Clinical Orthopaedics and Related Research*. doi: 10.1097/00003086-199610000-00015.

Dennis, D. A. *et al.* (2003) 'Multicenter Determination of in Vivo Kinematics after Total Knee Arthroplasty', in *Clinical Orthopaedics and Related Research*.

Dennis, D. A. *et al.* (2005) 'Mobile-bearing total knee arthroplasty: Do the polyethylene bearings rotate?', in *Clinical Orthopaedics and Related Research*. doi: 10.1097/01.blo.0000185464.23505.6e.

Deserno, Thomas M. (2011) *Biomedical Image Processing*. 1st edn. Edited by Thomas Martin Deserno. Berlin, Heidelberg: Springer Berlin Heidelberg (Biological and Medical Physics, Biomedical Engineering). doi: 10.1007/978-3-642-15816-2.

Diaz, G. (2018) *Radiation from X-rays*, *GrepMed*. Available at: https://www.grepmed.com/images/1828/risks-comparison-table-imaging-patientinfo-radiation-background.

Dieppe, P. (2000) 'Towards a better understanding of osteoarthritis of the knee joint', *The Knee*, 7(3), pp. 135–137. doi: 10.1016/S0968-0160(00)00043-0.

van Dijk, R., Huiskes, R. and Selvik, G. (1979) 'Roentgen stereophotogrammetric methods for the evaluation of the three dimensional kinematic behaviour and cruciate ligament length patterns of the human knee joint', *Journal of Biomechanics*, 12(9), pp. 727–731. doi: 10.1016/0021-9290(79)90021-6.

Doral Medical Imaging (2006) *Magnetic Resonance Imaging*. Available at: http://www.doralmri.com/images/mri picture.jpg (Accessed: 14 August 2019).

Draper, C. E. *et al.* (2008) 'Feasibility of using real-time MRI to measure joint kinematics in 1.5T and open-bore 0.5T systems', *Journal of Magnetic Resonance Imaging*. doi: 10.1002/jmri.21413.

Dzung, L., Chenyang, X. and Prince, J. L. (1998) 'A survey of current methods in medical image segmentation', *Department of ECE, Johns Hopkins Univ., Tech. Rep.*

Eckhoff, D. *et al.* (2007a) 'An ABJS best paper: Difference between the epicondylar and cylindrical axis of the knee', in *Clinical Orthopaedics and Related Research*. doi: 10.1097/BLO.0b013e318112416b.

Eckhoff, D. *et al.* (2007b) 'Difference Between the Epicondylar and Cylindrical Axis of the Knee', *Clinical Orthopaedics and Related Research*, PAP, pp. 238–44. doi: 10.1097/BLO.0b013e318112416b.

Eckhoff, D. G. *et al.* (2001) 'Three-Dimensional Morphology of the Distal Part of the

Femur Viewed in Virtual Reality - Part I', *The Journal of Bone and Joint Surgery-American Volume*, 83, pp. 43–50. doi: 10.2106/00004623-200100021-00010.

Eckhoff, D. G. *et al.* (2003) 'Three-Dimensional Morphology and Kinematics of the Distal Part of the Femur Viewed in Virtual Reality - Part II', *The Journal of Bone and Joint Surgery-American Volume*, 85(SUPPL. 4), pp. 97–104. doi: 10.2106/00004623-200300004-00012.

Eckhoff, D. G. *et al.* (2005) 'Three-dimensional mechanics, kinematics, and morphology of the knee viewed in virtual reality', in *Journal of Bone and Joint Surgery - Series A*. doi: 10.2106/00004623-200511002-00009.

Elias, S. G., Freeman, M. A. R. and Gokcay, E. I. (1990) 'A Correlative Study of the Geometry and Anatomy of the Distal Femur', *Clinical Orthopaedics and Related Research*, (260), pp. 98–103. doi: 10.1097/00003086-199011000-00018.

Endo, M. *et al.* (2003) 'Four-dimensional computed tomography (4D CT) - Concepts and preliminary development', *Radiation Medicine - Medical Imaging and Radiation Oncology*.

Esses, D. *et al.* (2004) 'Ability of CT to alter decision making in elderly patients with acute abdominal pain', *American Journal of Emergency Medicine*. doi: 10.1016/j.ajem.2004.04.004.

Essner, A. *et al.* (2011) 'The influence of material and design on total knee replacement wear.', *The journal of knee surgery*.

Fantozzi, S. *et al.* (2006) 'Femoral rollback of cruciate-retaining and posterior-stabilized total knee replacements: In vivo fluoroscopic analysis during activities of daily living', *Journal of Orthopaedic Research*. doi: 10.1002/jor.20306.

Feng, Y. *et al.* (2016) 'In-vivo analysis of flexion axes of the knee: Femoral condylar motion during dynamic knee flexion', *Clinical Biomechanics*, 32, pp. 102–107. doi: 10.1016/j.clinbiomech.2015.12.006.

Fick, A. (1877) 'Zur Mechanik des Kniegelenks.', *Arch Anat Entw Gesch*, pp. 440–448.

Fick, R. (1911) 'Handbuch der Anatomie und Mechanik der Gelenke.', 2, pp. 109–17.

Fiedler, C. *et al.* (2011) 'Mathematical study on the guidance of the tibiofemoral joint as theoretical background for total knee replacements.', *Acta of bioengineering and biomechanics*, 13(4), pp. 38–49. Available at: http://www.ncbi.nlm.nih.gov/pubmed/22339245.

Floerkemeier, T. *et al.* (2011) 'Physiologically shaped knee arthroplasty induces natural roll-back.', *Technology and health care : official journal of the European Society for Engineering and Medicine*, 19(2), pp. 91–102. doi: 10.3233/THC-2011-0616.

Frankel, V., Burstein, A. and Brooks, D. (1971) 'Biomechanics of Internal Derangement of the Knee', *J Bone Joint Surg [Br]*, 53(5), pp. 945–77. doi: 10.1097/00004623-197153050-00010.

Freeman, M. A. R. and Pinskerova, V. (2005) 'The movement of the normal tibio-femoral joint', *Journal of Biomechanics*. doi: 10.1016/j.jbiomech.2004.02.006.

Fu, F. H., Harner, C. D. and Vince, K. . (1994) 'Anatomy of the Knee', in Fu, F. H., Harner, C. D., and Vince, K. G. (eds) *Knee Surgery1*. Volume 1. Baltimore: Williams & Wilkins, pp. 1–54.

Fuchs, V. R. and Sox, H. C. (2001) 'Physicians' views of the relative importance of thirty medical innovations.', *Health affairs (Project Hope)*, 20(5), pp. 30–42. Available at: http://www.ncbi.nlm.nih.gov/pubmed/11558715.

Fuller, J. *et al.* (1997) 'A comparison of lower-extremity skeletal kinematics measured using skin-and pin-mounted markers', *Human Movement Science*. doi: 10.1016/S0167-9457(96)00053-X.

Garg, A. and Walker, P. S. (1990) 'Prediction of total knee motion using a three-dimensional computer-graphics model', *Journal of Biomechanics*. doi: 10.1016/0021-9290(90)90368-D.

Garling, E. H. *et al.* (2007) 'Limited rotation of the mobile-bearing in a rotating platform total knee prosthesis', *Journal of Biomechanics*, 40, pp. S25–S30. doi: 10.1016/j.jbiomech.2007.02.013.

Gergely, I. *et al.* (2017) 'Will Total Knee Replacement Ever Provide Normal Knee Function ?', *Journal of Interdisciplinary Medicine*, 2(38), pp. 22–26. doi: 10.1515/jim-2017-0040.

Ghonge, N. P. (2013) 'Computed Tomography in the 21st century: Current status & future prospects', *Journal International Medical Sciences Academy*, 26(1), pp. 35–42.

Gilles, B. *et al.* (2005) 'Bone motion analysis from dynamic MRI: Acquisition and tracking', in *Academic Radiology*. doi: 10.1016/j.acra.2005.08.006.

Goebel, D. and Schultz, W. (2012) 'The Columbus Knee System: 4-Year Results of a New Deep Flexion Design Compared to the NexGen Full Flex Implant', *Arthritis*. doi: 10.1155/2012/213817.

Goldman, L. W. (2007) 'Principles of CT and CT technology', *Journal of Nuclear Medicine Technology*. doi: 10.2967/jnmt.107.042978.

Gondim Teixeira, P. A. *et al.* (2014) 'Total hip prosthesis CT with single-energy projection-based metallic artifact reduction: Impact on the visualization of specific periprosthetic soft tissue structures', *Skeletal Radiology*. doi: 10.1007/s00256-014-1923-5.

Gondim Teixeira, P. A. *et al.* (2015) 'Musculoskeletal wide detector CT: Principles, techniques and applications in clinical practice and research', *European Journal of Radiology*, 84(5), pp. 892–900. doi: 10.1016/j.ejrad.2014.12.033.

Gonzalez, R. C., Woods, R. E. and Masters, B. R. (2009) 'Digital Image Processing, Third Edition', *Journal of Biomedical Optics*. doi: 10.1117/1.3115362.

Griffin, F. M. *et al.* (2000) 'Anatomy of the epicondyles of the distal femur: MRI analysis of normal knees', *Journal of Arthroplasty*. doi: 10.1016/S0883-5403(00)90739-3.

Grood, E. S. and Suntay, W. J. (1983) 'A Joint Coordinate System for the Clinical Description of Three-Dimensional Motions: Application to the Knee', *Journal of Biomechanical Engineering*. doi: 10.1115/1.3138397.

Grupp, T. M. *et al.* (2009) 'Fixed bearing knee congruency - Influence on contact mechanics, abrasive wear and kinematics', *International Journal of Artificial Organs*. doi: 10.1177/039139880903200405.

H. Shaikh, M., Panbude, S. and Joshi, A. (2014) 'Image Segmentation Techniques and its applications for Knee Joints: a Survey', *IOSR Journal of Electronics and Communication Engineering*, 9(5), pp. 23–28. doi: 10.9790/2834-09542328.

Hakki, S. *et al.* (2013) 'Columbus navigated TKA system: Clinical and radiological results at a minimum of 5 years with survivorship analysis', *Orthopedics*. doi: 10.3928/01477447-20130222-19.

Hamelynck, K. J. and Stiehl, J. B. (2002) *LCS® Mobile Bearing Knee Arthroplasty*. 1st edn. Berline: Springer-Verlag Berlin Heidelberg. doi: 10.1007/978-3-642-59347-5.

Han, J., Kamber, M. and Pei, J. (2012) *Data Mining: Concepts and Techniques*. 3rd edn. Morgan Kaufmann. doi: 10.1016/C2009-0-61819-5.

Haralick, R. M. and Shapiro, L. G. (1985) 'Image segmentation techniques', *Computer Vision, Graphics, and Image Processing*, 29(1), pp. 100–132. doi: 10.1016/S0734-189X(85)90153-7.

Harman, M. K. *et al.* (2012) 'Prosthesis alignment affects axial rotation motion after total knee replacement: A prospective in vivo study combining computed tomography and fluoroscopic evaluations', *BMC Musculoskeletal Disorders*. doi: 10.1186/1471-2474-13-206.

Harner, C. D. *et al.* (1995) 'The Human Posterior Cruciate Ligament Complex: An Interdisciplinary Study: Ligament Morphology and Biomechanical Evaluation', *The American Journal of Sports Medicine*. doi: 10.1177/036354659502300617.

Harwin, S. F. (2003) 'Complications of unicompartmental knee arthroplasty', *Seminars in Arthroplasty*, 14(4), pp. 232–244. doi: 10.1053/j.sart.2003.09.001.

Hatayama, K. *et al.* (2011) 'Relationship Between Femoral Component Rotation and Total Knee Flexion Gap Balance on Modified Axial Radiographs', *Journal of Arthroplasty*. doi: 10.1016/j.arth.2010.05.029.

Hill, P. F. *et al.* (2000) 'Tibiofemoral movement 2: the loaded and unloaded living knee studied by MRI', *The Journal of Bone and Joint Surgery*, 82(8), pp. 1196–1198. doi: 10.1302/0301-620X.82B8.10716.

Hirschmann, M. T. and Becker, R. (2015) *The Unhappy Total Knee Replacement*. Edited by M. T. Hirschmann and R. Becker. Cham: Springer International Publishing. doi: 10.1007/978-3-319-08099-4.

Hofmann, A. A. *et al.* (2000) 'Posterior stabilization in total knee arthroplasty with use of an ultracongruent polyethylene insert', *Journal of Arthroplasty*. doi: 10.1054/arth.2000.6633.

Hohmann, E. and Bryant, A. (2007) 'Closing or Opening Wedge High Tibial Osteotomy: Watch Out for the Slope', *Operative Techniques in Orthopaedics*. doi: 10.1053/j.oto.2006.09.010.

Hollister, A. M. *et al.* (1993) 'The Axes of Rotation of the Knee', *Clinical Orthopaedics and Related Research*. doi: 10.1097/00003086-199305000-00033.

Hricak, H. *et al.* (2011) 'Managing radiation use in medical imaging: A multifaceted challenge', *Radiology*. doi: 10.1148/radiol.10101157.

Hsu, R. W. W. *et al.* (1990) 'Normal axial alignment of the lower extremity and load-bearing distribution at the knee', *Clinical Orthopaedics and Related Research*.

Huang, C. H. *et al.* (2003) 'Long-Term Results of Low Contact Stress Mobile-Bearing Total Knee Replacements', *Clinical Orthopaedics and Related Research*. doi: 10.1097/01.blo.0000093890.12372.46.

Huang, C. H., Liau, J. J. and Cheng, C. K. (2007) 'Fixed or mobile-bearing total knee arthroplasty', *Journal of Orthopaedic Surgery and Research*. doi: 10.1186/1749-799X-2-1.

Huang, L. (2017) *A Concise Introduction to Mechanics of Rigid Bodies*. 2nd edn. Edited by L. Huang. Cham: Springer International Publishing. doi: 10.1007/978-3-319-45041-4.

Hung, M. C. and Yang, D. L. (2001) 'An efficient fuzzy C-means clustering algorithm', in *Proceedings - IEEE International Conference on Data Mining, ICDM*.

Hunt, M. A. *et al.* (2008) 'Towards a biopsychosocial framework of osteoarthritis of the knee.', *Disability and rehabilitation*, 30(1), pp. 54–61. doi: 10.1080/09638280701189960.

Incavo, S., Beynnon, B. and Coughlin, K. (2005) 'In vitro kinematics of the replaced

knee', in *Total Knee Arthroplasty: A Guide to Get Better Performance*. doi: 10.1007/3-540-27658-0_23.

Iwaki, H., Pinskerova, V. and Freeman, M. A. R. (2000) 'Tibiofemoral movement 1: the shapes and relative movements of the femur and tibia in the unloaded cadaver knee', *The Journal of Bone and Joint Surgery*. doi: 10.1302/0301-620X.82B8.10717.

Jacobs, W. C. H. *et al.* (2012) 'Functional performance of mobile versus fixed bearing total knee prostheses: a randomised controlled trial', *Knee Surgery, Sports Traumatology, Arthroscopy*, 20(8), pp. 1450–1455. doi: 10.1007/s00167-011-1684-9.

Jacobs, W. C. H., Clement, D. J. and Wymenga, A. B. (2005) 'Retention versus removal of the posterior cruciate ligament in total knee replacement: A systematic literature review within the Cochrane framework', *Acta Orthopaedica*. doi: 10.1080/17453670510045345.

Jerosch, J. *et al.* (2002) 'Interindividual reproducibility in perioperative rotational alignment of femoral components in knee prosthetic surgery using the transepicondylar axis', *Knee Surgery, Sports Traumatology, Arthroscopy*. doi: 10.1007/s00167-001-0271-x.

Jones, O. (2017) *TheTibia*, *TeachMeAnatomy*. Available at: http://teachmeanatomy.info/lower-limb/bones/the-tibia/#Proximal.

Jones, O. (2018a) *The Femur*, *TeachMeAnatomy*. Available at: http://teachmeanatomy.info/lower-limb/bones/femur/.

Jones, O. (2018b) *The Knee Joint*. Available at: http://teachmeanatomy.info/lower-limb/joints/the-knee-joint/.

Jonsson, H., Kärrholm, J. and Elmqvist, L.-G. (1989) 'Kinematics of active knee extension after tear of the anterior cruciate ligament', *The American Journal of Sports Medicine*, 17(6), pp. 796–802. doi: 10.1177/036354658901700613.

Kadaba, M. P., Ramakrishnan, H. K. and Wootten, M. E. (1990) 'Measurement of lower extremity kinematics during level walking.', *Journal of orthopaedic research : official publication of the Orthopaedic Research Society*. London: Springer London, 8(3), pp. 383–92. doi: 10.1002/jor.1100080310.

Kaiser, J. *et al.* (2016) 'Accuracy of model-based tracking of knee kinematics and cartilage contact measured by dynamic volumetric MRI', *Medical Engineering and Physics*. doi: 10.1016/j.medengphy.2016.06.016.

Kalender, W. A., Hebel, R. and Ebersberger, J. (1987) 'Reduction of CT artifacts caused by metallic implants', *Radiology*. doi: 10.1148/radiology.164.2.3602406.

Kaneda, Y. *et al.* (1997) 'Experimental Study on External Tibial Rotation of the Knee', *The American Journal of Sports Medicine*, 25(6), pp. 796–800. doi: 10.1177/036354659702500611.

Kang, K.-T. *et al.* (2018) 'Comparison of Kinematics in Cruciate Retaining and Posterior Stabilized for Fixed and Rotating Platform Mobile-Bearing Total Knee Arthroplasty with respect to Different Posterior Tibial Slope.', *BioMed research international*, 2018, p. 5139074. doi: 10.1155/2018/5139074.

Kapandji, I. A. (1970) 'The Knee.', in Kapandji, I. A. (ed.) *The physiology of the Joints*. 2nd edn. Edinburgh: Churchill Livingstone, pp. 72–135.

Kapandji, I. A. (1971) 'The physiology of the joints, vol. 2: Lower Limb. By I. A. Kapandji, Paris. Second edition. 11 × 8½ in. Pp. 219. Illustrated. 1970. Edinburgh and London: E. & S. Livingstone Ltd. £2.75', *British Journal of Surgery*. Wiley, 58(5), pp. 403–403. doi: 10.1002/bjs.1800580528.

Karrholm, J., Brandsson, S. and Freeman, M. A. R. (2000) 'Tibiofemoral movement 4 : changes of axial tibial rotation caused by forced rotation at the weight-bearing knee studied by RSA', *Journal of Bone and Joint Surgery - British Volume*, 82(B), pp. 1201–1203. doi: 0301-620X/00/810715.

Karuppal, R. (2016) 'Kinematic alignment in total knee arthroplasty: Does it really matter?', *Journal of Orthopaedics*, 13(4), pp. A1–A3. doi: 10.1016/j.jor.2016.10.001.

Katz, M. A. *et al.* (2001) 'Determining femoral rotational alignment in total knee arthroplasty', *The Journal of Arthroplasty*, 16(3), pp. 301–305. doi: 10.1054/arth.2001.21456.

Kauffmann, C. *et al.* (2003) 'Computer-aided method for quantification of cartilage thickness and volume changes using MRI: Validation study using a synthetic model', *IEEE Transactions on Biomedical Engineering*. doi: 10.1109/TBME.2003.814539.

Kidoh, M. *et al.* (2014) 'Reduction of dental metallic artefacts in CT: Value of a newly developed algorithm for metal artefact reduction (O-MAR)', *Clinical Radiology*. doi: 10.1016/j.crad.2013.08.008.

Kinzel, G. L. and Gutkowski, L. J. (1983) 'Joint models, degrees of freedom, and anatomical motion measurement.', *Journal of biomechanical engineering*. doi: 10.1115/1.3138385.

Kinzel, V., Ledger, M. and Shakespeare, D. (2005) 'Can the epicondylar axis be defined accurately in total knee arthroplasty?', *Knee*. doi: 10.1016/j.knee.2004.09.003.

Koo, S. and Andriacchi, T. P. (2008) 'The knee joint center of rotation is predominantly on the lateral side during normal walking', *Journal of Biomechanics*, 41(6), pp. 1269–1273. doi: 10.1016/j.jbiomech.2008.01.013.

Kozanek, M. *et al.* (2009) 'Tibiofemoral kinematics and condylar motion during the stance phase of gait', *Journal of Biomechanics*. doi: 10.1016/j.jbiomech.2009.05.003.

Kroon, D.-J. (2016) 'Finite Iterative Closest Point'. MATLAB Central File Exchange.

Available at: www.mathworks.com/matlabcentral/fileexchange/24301-finite-iterative-closest-point.

Kurosawa, H. *et al.* (1985) 'Geometry and motion of the knee for implant and orthotic design', *Journal of Biomechanics*. doi: 10.1016/0021-9290(85)90663-3.

Kurtz, S. M. *et al.* (2009) 'Future Young Patient Demand for Primary and Revision Joint Replacement: National Projections from 2010 to 2030', *Clinical Orthopaedics and Related Research®*, 467(10), pp. 2606–2612. doi: 10.1007/s11999-009-0834-6.

LaPrade, R. F. (2007) 'The Anatomy of the Medial Part of the Knee', *The Journal of Bone and Joint Surgery (American)*, 89(9), p. 2000. doi: 10.2106/JBJS.F.01176.

Laskin, R. S. *et al.* (2000) 'Deep-dish congruent tibial component use in total knee arthroplasty: A randomized prospective study', in *Clinical Orthopaedics and Related Research*. doi: 10.1097/00003086-200011000-00006.

Last, R. J. (1950) 'THE POPLITEUS MUSCLE AND THE LATERAL MENISCUS', *The Journal of Bone and Joint Surgery. British volume*, 32-B(1), pp. 93–99. doi: 10.1302/0301-620X.32B1.93.

Lee, T. Y. and Chhem, R. K. (2010) 'Impact of new technologies on dose reduction in CT', *European Journal of Radiology*. doi: 10.1016/j.ejrad.2010.06.036.

Lewis, J. L. and Lew, W. D. (1978) 'A Method for Locating an Optimal "Fixed" Axis of Rotation for the Human Knee Joint', *Journal of Biomechanical Engineering*. doi: 10.1115/1.3426209.

Li, G., Wuerz, T. H. and DeFrate, L. E. (2004) 'Feasibility of Using Orthogonal Fluoroscopic Images to Measure In Vivo Joint Kinematics', *Journal of Biomechanical Engineering*, 126(2). doi: 10.1115/1.1691448.

Li, J. S. *et al.* (2013) 'Kinematic characteristics of the tibiofemoral joint during a step-up activity', *Gait and Posture*. doi: 10.1016/j.gaitpost.2013.03.004.

Li, N. *et al.* (2014) 'Posterior cruciate-retaining versus posterior stabilized total knee arthroplasty: A meta-analysis of randomized controlled trials', *Knee Surgery, Sports Traumatology, Arthroscopy*. doi: 10.1007/s00167-012-2275-0.

Lu, T. W. and O'Connor, J. J. (1999) 'Bone position estimation from skin marker co-ordinates using global optimisation with joint constraints', *Journal of Biomechanics*. doi: 10.1016/S0021-9290(98)00158-4.

Lucchetti, L. *et al.* (1998) 'Skin movement artefact assessment and compensation in the estimation of knee-joint kinematics', *Journal of Biomechanics*. doi: 10.1016/S0021-9290(98)00083-9.

Lustig, S. *et al.* (2008) 'Relationship between the surgical epicondylar axis and the articular surface of the distal femur: An anatomic study', *Knee Surgery, Sports*

Traumatology, Arthroscopy. doi: 10.1007/s00167-008-0551-9.

Lützner, J. *et al.* (2017) 'No difference in range of motion between ultracongruent and posterior stabilized design in total knee arthroplasty: a randomized controlled trial', *Knee Surgery, Sports Traumatology, Arthroscopy*, 25(11). doi: 10.1007/s00167-016-4331-7.

Mahfouz, M. *et al.* (2012) 'Three-dimensional morphology of the knee reveals ethnic differences', in *Clinical Orthopaedics and Related Research*. doi: 10.1007/s11999-011-2089-2.

Mahoney, O. M. *et al.* (2012) 'No functional advantage of a mobile bearing posterior stabilized TKA.', *Clinical Orthopaedics and Related Research*, 470(1), pp. 33–44. doi: 10.1007/s11999-011-2114-5.

Majeed, A. and Aylin, P. (2005) 'The ageing population of the United Kingdom and cardiovascular disease', *BMJ*, 331(7529), p. 1362. doi: 10.1136/bmj.331.7529.1362.

De Man, B. *et al.* (2000) 'Reduction of metal streak artifacts in x-ray computed tomography using a transmission maximum a posteriori algorithm', *IEEE Transactions on Nuclear Science*.

Maniar, R. (2006) 'Rationale for the posterior-stabilized rotating-platform knee', *Orthopedics*.

Manner, P. W. (2016) *Knee Replacement Implants*, *OrthoInfo*. Available at: https://orthoinfo.aaos.org/en/treatment/knee-replacement-implants/ (Accessed: 9 June 2019).

Maravi, P. *et al.* (2015) 'Role of MRI in Orthopedics', *Orthopaedic Journal of M.P. Chapter*, 21(2), pp. 74–77. Available at: http://ojmpc.com/index.php/OJMPC/article/download/31/25.

Marchand, P. and Marmet, L. (1983) 'Binomial smoothing filter: A way to avoid some pitfalls of least-squares polynomial smoothing', *Review of Scientific Instruments*, 54(8). doi: 10.1063/1.1137498.

Martini, F. H., Nath, J. L. and Bartholomew, E. F. (2018) *Fundamentals of Anatomy and Physiology*. 11th edn, *Learning*. 11th edn. Edited by S. Beauparlant. Pearson Education, Inc. doi: 612.

Maruyama, S. *et al.* (2004) 'Functional comparison of posterior cruciate-retaining versus posterior stabilized total knee arthroplasty', *Journal of Arthroplasty*. doi: 10.1016/j.arth.2003.09.010.

De Marzi, L. *et al.* (2013) 'Calibration of CT Hounsfield units for proton therapy treatment planning: Use of kilovoltage and megavoltage images and comparison of parameterized methods', *Physics in Medicine and Biology*. doi: 10.1088/0031-9155/58/12/4255.

Matsuda, S. *et al.* (2003) 'A comparison of rotational landmarks in the distal femur and the tibial shaft', *Clinical Orthopaedics and Related Research*. doi: 10.1097/01.blo.0000072904.36018.79.

Matsuda, S. *et al.* (2004) 'Anatomical analysis of the femoral condyle in normal and osteoarthritic knees', *Journal of Orthopaedic Research*. doi: 10.1016/S0736-0266(03)00134-7.

Matsumoto, H. *et al.* (2000) 'Axis location of tibial rotation and its change with flexion angle', *Clinical Orthopaedics and Related Research*. doi: 10.1097/00003086-200002000-00022.

Matziolis, G. *et al.* (2011) 'Kinematic analysis of the flexion axis for correct femoral component placement', *Knee Surgery, Sports Traumatology, Arthroscopy*. doi: 10.1007/s00167-011-1554-5.

Mazzoli, V. *et al.* (2017) 'Accelerated 4D self-gated MRI of tibiofemoral kinematics', *NMR in Biomedicine*. doi: 10.1002/nbm.3791.

McCollough, C. H. *et al.* (2012) 'Achieving routine submillisievert CT scanning: Report from the Summit on Management of Radiation Dose in CT', *Radiology*. doi: 10.1148/radiol.12112265.

Mehranian, A. *et al.* (2013) '3D prior image constrained projection completion for x-ray ct metal artifact reduction', *IEEE Transactions on Nuclear Science*. doi: 10.1109/TNS.2013.2275919.

Mensch, J. and Amstutz, H. (1975) 'Knee morphology as a guide to knee replacement.', *Clinical Orthopaedics and Related Research®*, 112, pp. 231–41. Available at: https://www.ncbi.nlm.nih.gov/m/pubmed/1192638/.

Mettler, F. A. *et al.* (2008) 'Medical radiation exposure in the U.S. in 2006: Preliminary results', in *Health Physics*. doi: 10.1097/01.HP.0000326333.42287.a2.

Meyer, E. *et al.* (2012) 'Frequency split metal artifact reduction (FSMAR) in computed tomography', *Medical Physics*. doi: 10.1118/1.3691902.

Miki, K. *et al.* (2016) 'Single-energy metal artefact reduction with CT for carbonion radiation therapy treatment planning', *British Journal of Radiology*. doi: 10.1259/bjr.20150988.

Mink, J. H., Levy, T. and Crues, J. V (2014) 'Tears of the anterior cruciate ligament and menisci of the knee: MR imaging evaluation.', *Radiology*. doi: 10.1148/radiology.167.3.3363138.

Mochizuki, T. *et al.* (2014) 'The clinical epicondylar axis is not the functional flexion axis of the human knee', *Journal of Orthopaedic Science*, 19(3), pp. 451–456. doi: 10.1007/s00776-014-0536-0.

Moller, T. and Trumbore, B. (1998) *Fast, minimum storage ray-triangle intersection*, *Doktorsavhandlingar vid Chalmers Tekniska Hogskola*.

Moore, D. C. *et al.* (2015) 'Computed Tomography Image-Based Kinematic Analysis: An Overview', in Neu, C. P. and Genin, G. M. (eds) *Handbook of Imaging in Biological Mechanics*. Florida: CRC Press, p. 556.

Moreland, J. R., Bassett, L. W. and Hanker, G. J. (1987) 'Radiographic analysis of the axial alignment of the lower extremity', *Journal of Bone and Joint Surgery - Series A*. doi: 10.2106/00004623-198769050-00016.

Morsbach, F. *et al.* (2013) 'Reduction of metal artifacts from hip prostheses on CT images of the pelvis: Value of iterative reconstructions', *Radiology*. doi: 10.1148/radiol.13122089.

Moskowitz, R. W. (1984) *Osteoarthritis: Diagnosis and Management*. 2nd, Illustr edn. Saunders.

Most, E. *et al.* (2004) 'Sensitivity of the knee joint kinematics calculation to selection of flexion axes', *Journal of Biomechanics*, 37(11), pp. 1743–1748. doi: 10.1016/j.jbiomech.2004.01.025.

Nakagawa, S. *et al.* (2000) 'Tibiofemoral movement 3: full flexion in the living knee studied by MRI', *The Journal of Bone and Joint Surgery*, 82(8), pp. 1199–1200. doi: 10.1302/0301-620X.82B8.10718.

Narkhede, H. P. (2013) 'Review of Image Segmentation Techniques', *International Journal of Science and Modern Engineering*, (18).

Nguyen, K. T. *et al.* (2016) 'Quantitative analysis of knee movement patterns through comparative visualization', in *Mathematics and Visualization*. doi: 10.1007/978-3-319-24523-2_12.

Noble, P. C. *et al.* (2005) 'Does total knee replacement restore normal knee function?', *Clinical orthopaedics and related research*, (431), pp. 157–65. Available at: http://www.ncbi.nlm.nih.gov/pubmed/15685070.

Noble, P. C. *et al.* (2006) 'The John Insall Award: Patient Expectations Affect Satisfaction with Total Knee Arthroplasty', *Clinical Orthopaedics and Related Research*, 452, pp. 35–43. doi: 10.1097/01.blo.0000238825.63648.1e.

Nordin, M. and Frankel, V. (1982) 'Biomechanics of the Knee', in Helfet, A. (ed.) *Disorders of the Knee*. 2nd edn. Cambridge: JB Lippincott, pp. 19–33.

Nowakowski, A. (2006) 'Das Transversalträger-Tibiaplateau (TTTP)', *Orthopädische Praxis*, 42(7), pp. 419–28.

Oxford Economics (2010) 'The Economic Costs of Arthritis for the UK Economy', (Final Report).

Pal, N. R. and Pal, S. K. (1993) 'A review on image segmentation techniques', *Pattern Recognition*, 26(9). doi: 10.1016/0031-3203(93)90135-J.

Pan, T. (2005) 'Comparison of helical and cine acquisitions for 4D-CT imaging with multislice CT', *Medical Physics*, 32(2). doi: 10.1118/1.1855013.

Patel, A. *et al.* (2015) 'The epidemiology of revision total knee and hip arthroplasty in England and Wales', *The Bone & Joint Journal*, 97-B(8), pp. 1076–1081. doi: 10.1302/0301-620X.97B8.35170.

Patel, V. V. *et al.* (2004) 'A three-dimensional MRI analysis of knee kinematics', *Journal of Orthopaedic Research*. doi: 10.1016/j.orthres.2003.08.015.

Paudel, M. R. *et al.* (2014) 'Clinical evaluation of normalized metal artifact reduction in kVCT using MVCT prior images (MVCT-NMAR) for radiation therapy treatment planning', *International Journal of Radiation Oncology Biology Physics*. doi: 10.1016/j.ijrobp.2014.02.040.

Pennock, G. R. and Clark, K. J. (1990) 'An anatomy-based coordinate system for the description of the kinematic displacements in the human knee', *Journal of Biomechanics*. doi: 10.1016/0021-9290(90)90378-G.

Pham, D. L. and Prince, J. L. (1999) 'An adaptive fuzzy C-means algorithm for image segmentation in the presence of intensity inhomogeneities', *Pattern Recognition Letters*. doi: 10.1016/S0167-8655(98)00121-4.

Piazza, S. J. and Cavanagh, P. R. (2000) 'Measurement of the screw-home motion of the knee is sensitive to errors in axis alignment', *Journal of Biomechanics*, 33(8), pp. 1029–1034. doi: 10.1016/S0021-9290(00)00056-7.

Pierrart, J. *et al.* (2014) 'New dynamic three-dimensional MRI technique for shoulder kinematic analysis', *Journal of Magnetic Resonance Imaging*. doi: 10.1002/jmri.24204.

Pinskerova, V. *et al.* (2004) 'Does the femur roll-back with flexion?', *Journal of Bone and Joint Surgery - Series B*. doi: 10.1302/0301-620X.86B6.14589.

Pinskerova, V. *et al.* (2009) 'The knee in full flexion: AN ANATOMICAL STUDY', *Journal of Bone and Joint Surgery - British Volume*, 91-B(6), pp. 830–834. doi: 10.1302/0301-620X.91B6.22319.

Post, Z. D. *et al.* (2010) 'Mobile-bearing total knee arthroplasty. Better than a fixed-bearing?', *Journal of Arthroplasty*. Elsevier Inc., 25(6), pp. 998–1003. doi: 10.1016/j.arth.2009.07.014.

Power, S. P. *et al.* (2016) 'Computed tomography and patient risk: Facts, perceptions and uncertainties', *World Journal of Radiology*. doi: 10.4329/wjr.v8.i12.902.

Preston, D. C. (2006) *Magnetic Resonance Imaging (MRI): Basics*. Available at:

https://case.edu/med/neurology/NR/MRI Basics.htm#:~:text=The most common MRI sequences,longer TE and TR times.

Ranawat, C. S. *et al.* (2004) 'In Vivo Kinematics for Fixed and Mobile-Bearing Posterior Stabilized Knee Prostheses', *Clinical Orthopaedics and Related Research*. doi: 10.1097/00003086-200401000-00030.

Ranawat, C. S., Luessenhop, C. P. and Rodriguez, J. A. (1997) 'The press-fit condylar modular total knee system. Four-to-six-year results with a posterior-cruciate-substituting design', *Journal of Bone and Joint Surgery - Series A*.

Randen, A. *et al.* (2008) 'Acute appendicitis: Meta-analysis of diagnostic performance of CT and graded compression US related to prevalence of disease', *Radiology*. doi: 10.1148/radiol.2483071652.

Reilly, R. and M. (2019) *Medical Imaging for Health Professionals: Technologies and Clinical Applications*. First. Hoboken, NJ: Wiley.

Reuleaux, F. (1875) *Lehrbuch der kinematik, Vol.1*. 1st edn. F. Vieweg. Available at: https://books.google.com.mt/books?id=MsdJAAAAMAAJ&source=gbs_book_other_versions.

Robb, J. (1994) *Estimates of radiation detriment in a UK population*. Chilton. Available at: https://inis.iaea.org/search/search.aspx?orig_q=source:%22ISBN 0 85951 385 0%22.

Robertson, P. L. *et al.* (2014) 'Anterior cruciate ligament tears: evaluation of multiple signs with MR imaging.', *Radiology*. doi: 10.1148/radiology.193.3.7972833.

Robertsson, O. *et al.* (2000) 'Patient satisfaction after knee arthroplasty: A report on 27,372 knees operated on between 1981 and 1995 in Sweden', *Acta Orthopaedica Scandinavica*, 71(3), pp. 262–267. doi: 10.1080/000164700317411852.

Roland, M., Hull, M. L. and Howell, S. M. (2010) 'Virtual Axis Finder: A New Method to Determine the Two Kinematic Axes of Rotation for the Tibio-Femoral Joint', *Journal of Biomechanical Engineering*, 132(1), p. 011009. doi: 10.1115/1.4000163.

Rosen, M. P. *et al.* (2000) 'Impact of abdominal CT on the management of patients presenting to the emergency department with acute abdominal pain', *American Journal of Roentgenology*. doi: 10.2214/ajr.174.5.1741391.

Rosen, M. P. *et al.* (2003) 'Value of abdominal CT in the emergency department for patients with abdominal pain', *European Radiology*.

Sandhya, P. H. and Kumar, S. (2017) 'A Survey on Fuzzy C-means Clustering Techniques', *International Journal of Engineering Development and Research (IJEDR)*, 5(4), pp. 1151–1155. Available at: https://ijedr.org/papers/IJEDR1704186.pdf.

Sando, T. *et al.* (2015) 'Ten-year results comparing posterior cruciate-retaining versus posterior cruciate-substituting total knee arthroplasty', *Journal of Arthroplasty*. doi: 10.1016/j.arth.2014.09.009.

Sankur, B. (2004) 'Survey over image thresholding techniques and quantitative performance evaluation', *Journal of Electronic Imaging*. doi: 10.1117/1.1631315.

Sathasivam, S. and Walker, P. S. (1997) 'A computer model with surface friction for the prediction of total knee kinematics', *Journal of Biomechanics*. doi: 10.1016/S0021-9290(96)00114-5.

Schmidt, R. *et al.* (2003) 'Fluoroscopic analyses of cruciate-retaining and Medial Pivot knee implants', in *Clinical Orthopaedics and Related Research*. doi: 10.1097/01.blo.0000063565.90853.a4.

Scott, W. N. (2018) *Surgery of the Knee*, *Insall & Scott Surgery of the Knee*. Elsevier. doi: 10.1016/B978-1-4377-1503-3.00078-0.

Sharkey, P. F. *et al.* (2014) 'Why Are Total Knee Arthroplasties Failing Today—Has Anything Changed After 10 Years?', *The Journal of Arthroplasty*, 29(9), pp. 1774–1778. doi: 10.1016/j.arth.2013.07.024.

Shaw, J. A. and Murray, D. G. (1974) 'The Longitudinal Axis of the Knee and the Role of the Cruciate Ligaments in Controlling Transverse Rotation', *The Journal of Bone & Joint Surgery*, 56(8), pp. 1603–1609. doi: 10.2106/00004623-197456080-00008.

Sheldon, S. (1994) *Orthopaedic Basic Science*. Edited by S. Sheldon. American Academy of Orthopaedics.

Shenoy, R., Pastides, P. S. and Nathwani, D. (2013) '(iii) Biomechanics of the knee and TKR', *Orthopaedics and Trauma*, 27(6), pp. 364–371. doi: 10.1016/j.mporth.2013.10.003.

Shiavi, R. *et al.* (1987a) 'Helical motion analysis of the knee-II. Kinematics of uninjured and injured knees during walking and pivoting', *Journal of Biomechanics*. doi: 10.1016/0021-9290(87)90032-7.

Shiavi, R. *et al.* (1987b) 'Helical motion analysis of the knee—I. Methodology for studying kinematics during locomotion', *Journal of Biomechanics*, 20(5), pp. 459–469. doi: 10.1016/0021-9290(87)90247-8.

Sikorski, J. M. (2008) 'Alignment in total knee replacement', *The Journal of Bone and Joint Surgery. British volume*, 90-B(9), pp. 1121–1127. doi: 10.1302/0301-620X.90B9.20793.

Van Sint Jan, S. *et al.* (2002) 'Registration of 6-DOFs electrogoniometry and CT medical imaging for 3D joint modeling', *Journal of Biomechanics*. doi: 10.1016/S0021-9290(02)00074-X.

Siu, D. *et al.* (1996) 'Femoral articular shape and geometry: A three-dimensional computerized analysis of the knee', *Journal of Arthroplasty*. doi: 10.1016/S0883-5403(05)80012-9.

Smidt, G. L. (1973) 'Biomechanical analysis of knee flexion and extension', *Journal of Biomechanics*, 6(1), pp. 79–92. doi: 10.1016/0021-9290(73)90040-7.

Smith, B. A., Livesay, G. A. and Woo, S. L. (1993) 'Biology and biomechanics of the anterior cruciate ligament.', *Clinics in sports medicine*, 12(4), pp. 637–70. doi: 10.1080/19397030902947041.

Soudan, K., Van Audekercke, R. and Martens, M. (1979) 'Methods, difficulties and inaccuracies in the study of human joint kinematics and pathokinematics by the instant axis concept. Example: The knee joint', *Journal of Biomechanics*, 12(1), pp. 27–33. doi: 10.1016/0021-9290(79)90006-X.

Steindler, A. (1955) *Kinesiology of the Human Body under Normal and Pathological Conditions.*, *Journal of Bone and Joint Surgery - British Volume*. Available at: https://journals.lww.com/jbjsjournal/Citation/1955/37060/Kinesiology_of_the_Human_Body_under_Normal_and.27.aspx.

Stiehl, J. B. *et al.* (1997) 'In Vivo Kinematic Analysis of a Mobile Bearing Total Knee Prosthesis', *Clinical Orthopaedics and Related Research*. doi: 10.1097/00003086-199712000-00010.

Strasser, H. (1917) *Lehrbuch der Muskel und Gelenkmechanik.* 3rd edn. Berlin: Springer Verlag.

Subburaj, K., Ravi, B. and Agarwal, M. (2010) 'Computer-aided methods for assessing lower limb deformities in orthopaedic surgery planning', *Computerized Medical Imaging and Graphics*. doi: 10.1016/j.compmedimag.2009.11.003.

Sun, Y., Teo, E. C. and Zhang, Q. H. (2006) 'Discussions of knee joint segmentation', in *ICBPE 2006 - Proceedings of the 2006 International Conference on Biomedical and Pharmaceutical Engineering*. doi: 10.1109/ICBPE.2006.348611.

Tanifuji, O. *et al.* (2013) 'Three-dimensional in vivo motion analysis of normal knees employing transepicondylar axis as an evaluation parameter', *Knee Surgery, Sports Traumatology, Arthroscopy*. doi: 10.1007/s00167-012-2010-x.

Tay, S. C. *et al.* (2007) 'Four-dimensional computed tomographic imaging in the wrist: Proof of feasibility in a cadaveric model', *Skeletal Radiology*. doi: 10.1007/s00256-007-0374-7.

The Mathworks Inc. (2018) 'MATLAB'. NAtick, Massachusettes. Available at: www.mathworks.com.

Thompson, W. O. *et al.* (1991) 'Tibial meniscal dynamics using three-dimensional reconstruction of magnetic resonance images', *The American Journal of Sports*

Medicine, 19(3), pp. 210–216. doi: 10.1177/036354659101900302.

Toshiba Medical Systems (2008) 'Dynamic Volume Imaging - Special Issue', *Toshiba Medical Systems Journal*. Available at: https://ch.medical.canon/wp-content/uploads/sites/33/2017/01/2008-VISIONS-Special-Dynamic-Volume-ImagingFINAL.pdf.

Toshiba Medical Systems (2012) *Product Data No. MPDCT0314EA*.

Tsujii, A. *et al.* (2018) 'Arthroscopic minimum saucerization and inferior-leaf meniscectomy for a horizontal tear of a complete discoid lateral meniscus: Report of two cases', *International Journal of Surgery Case Reports*. doi: 10.1016/j.ijscr.2018.11.027.

Udupa, J. K. and Saha, P. K. (2003) 'Fuzzy connectedness and image segmentation', in *Proceedings of the IEEE*. doi: 10.1109/JPROC.2003.817883.

Uecker, M. *et al.* (2010) 'Real-time MRI at a resolution of 20 ms', *NMR in Biomedicine*. doi: 10.1002/nbm.1585.

UNSCEAR (2000) *Sources and Effects of Ionizing Radiation, United Nations Scientific Committee on the Effects of Atomic Radiation UNSCEAR 2000 Report to the General Assembly, with Scientific Annexes*, *UNSCEAR 2000 Report*.

Vaishya, R., Agarwal, A. K. and Vijay, V. (2016) 'Extensor Mechanism Disruption after Total Knee Arthroplasty: A Case Series and Review of Literature', *Cureus*. doi: 10.7759/cureus.479.

Varadarajan, K. M. *et al.* (2009) 'Can in vitro systems capture the characteristic differences between the flexion-extension kinematics of the healthy and TKA knee?', *Medical Engineering and Physics*. doi: 10.1016/j.medengphy.2009.06.005.

Vedi, V. *et al.* (1999) 'Meniscal movement', *The Journal of Bone and Joint Surgery*, 81(1), pp. 37–41. doi: 10.1302/0301-620X.81B1.8928.

Veselko, M., Jenko, M. and Lipuscek, I. (1998) 'The use of the co-ordinate measuring machine for the study of three-dimensional biomechanics of the knee.', *Computers in biology and medicine*, 28(4), pp. 343–57. Available at: http://www.ncbi.nlm.nih.gov/pubmed/9805195.

Victor, J., Van Doninck, D., Labey, L., Van Glabbeek, F., *et al.* (2009) 'A common reference frame for describing rotation of the distal femur', *The Journal of Bone and Joint Surgery. British volume*, 91-B(5), pp. 683–690. doi: 10.1302/0301-620X.91B5.21827.

Victor, J., Van Doninck, D., Labey, L., Innocenti, B., *et al.* (2009) 'How precise can bony landmarks be determined on a CT scan of the knee?', *Knee*. doi: 10.1016/j.knee.2009.01.001.

Victor, J. (2009) 'Rotational alignment of the distal femur: A literature review', *Orthopaedics & Traumatology: Surgery & Research*, 95(5), pp. 365–372. doi: 10.1016/j.otsr.2009.04.011.

Waldman, S. D. and Campbell, R. S. D. (2011) *Imaging of Pain*. doi: 10.1016/C2009-0-39533-1.

Walker, P. S. *et al.* (2011) 'Reference axes for comparing the motion of knee replacements with the anatomic knee', *Knee*. doi: 10.1016/j.knee.2010.07.005.

Walker, P. S. and Erkiuan, M. J. (1975) 'The Role of the Menisci in Force Transmission Across the Knee', *Clinical Orthopaedics and Related Research*, 109, pp. 184–92. doi: 10.1097/00003086-197506000-00027.

Weber, W. and Weber, E. (1837) 'Ueber die Mechanik der menschlichen Gehwerkzeuge, nebst der Beschreibung eines Versuchs über das Herausfallen des Schenkelkopfs aus der Pfanne im luftverdünnten Raume', *Annalen der Physik und Chemie*, 116(1), pp. 1–13. doi: 10.1002/andp.18371160102.

Whittle, Michael (2012) *Whittle's gait analysis.* 5th edn. Edited by J. Richards, D. Levine, and Micheal Whittle. Churchill Livingstone.

Wilson, D. A. (2011) *Clinical Veterinary Advisor: The Horse*. doi: 10.1016/C2009-0-38641-9.

Woolf, A. D. and Pfleger, B. (2003) 'Burden of major musculoskeletal conditions.', *Bulletin of the World Health Organization*, 81(9), pp. 646–56. Available at: http://www.scirp.org/journal/doi.aspx?DOI=10.4236/abb.2012.324063.

Wu, G. *et al.* (2002) 'ISB recommendation on definitions of joint coordinate system of various joints for the reporting of human joint motion—part I: ankle, hip, and spine', *Journal of Biomechanics*. doi: 10.1016/S0021-9290(01)00222-6.

Wu, G. *et al.* (2005) 'ISB recommendation on definitions of joint coordinate systems of various joints for the reporting of human joint motioN, Part II: shoulder, elbow, wrist and hand', *Journal of Biomechanics*. doi: 10.1016/j.jbiomech.2004.05.042.

Wu, G. and Cavanagh, P. R. (1995) 'ISB recommendations for standardization in the reporting of kinematic data', *Journal of Biomechanics*. doi: 10.1016/0021-9290(95)00017-C.

Wylde, V. *et al.* (2008) 'Patient-reported outcomes after fixed- versus mobile-bearing total knee replacement', *The Journal of Bone and Joint Surgery. British volume*, 90-B(9), pp. 1172–1179. doi: 10.1302/0301-620X.90B9.21031.

Yamazaki, T. *et al.* (2007) '3D kinematics of normal knee using X-ray fluoroscopy and CT images', in *World Congress on Medical Physics and Biomedical Engineering 2006*. doi: 10.1007/978-3-540-36841-0_706.

Yao, J. *et al.* (2014) 'In vivo measurements of patellar tracking and finite helical axis using a static magnetic resonance based methodology', *Medical Engineering and Physics, doi: 10.1016/j.medengphy.2014.08.014*

Lothian NHS Board

South East Scotland Research
Ethics Committee 02

Waverley Gate
2-4 Waterloo Place
Edinburgh
EH1 3EG
Telephone 0131 536 9000

www.nhslothian.scot.nhs.uk

Date   28 April 2015
Your Ref
Our Ref

Enquiries to: Joyce Clearie
Extension: 35674
Direct Line: 0131 465 5674
Email: Joyce.Clearie@nhslothian.scot.nhs.uk

27 April 2015

Dr Leela Biant
Consultant Orthopaedic Surgeon
NHS Lothian
51 Little France Crescent
Edinburgh
EH16 4SA]

Dear Dr Biant

Study title:	**Randomised controlled trial of patient-specific instrumentation vs standard instrumentation in total knee arthroplasty**
REC reference:	**15/SS/0058**
IRAS project ID:	**177817**

Thank you for your letter of 26th April, responding to the Committee's request for further information on the above research and submitting revised documentation.

The further information has been considered on behalf of the Committee by the Chair.

We plan to publish your research summary wording for the above study on the HRA website, together with your contact details. Publication will be no earlier than three months from the date of this favourable opinion letter. The expectation is that this information will be published for all studies that receive an ethical opinion but should you wish to provide a substitute contact point, wish to make a request to defer, or require further information, please contact the REC Manager, Ms Joyce Clearie, joyce.clearie@nhslothian.scot.nhs.uk. Under very limited circumstances (e.g. for student research which has received an unfavourable opinion), it may be possible to grant an exemption to the publication of the study.

Confirmation of ethical opinion

On behalf of the Committee, I am pleased to confirm a favourable ethical opinion for the above research on the basis described in the application form, protocol and supporting documentation as revised, subject to the conditions specified below.

Conditions of the favourable opinion

Headquarters
Waverley Gate, 2-4 Waterloo Place, Edinburgh EH1 3EG

Chair Mr Brian Houston
Chief Executive Tim Davison
Lothian NHS Board is the common name of Lothian Health Board

NHS
Lothian

The favourable opinion is subject to the following conditions being met prior to the start of the study.

ADDITIONAL CONDITION SPECIFIED BY THE REC

- The PIS needs to be amended as still clearly states that the participants are only having a CT scan of their knee. Please see Page 3 under the Figure 5. Can this be corrected, please?

[Where additional conditions are specified by the REC:]
You should notify the REC in writing once all conditions have been met (except for site approvals from host organisations) and provide copies of any revised documentation with updated version numbers. The REC will acknowledge receipt and provide a final list of the approved documentation for the study, which can be made available to host organisations to facilitate their permission for the study. Failure to provide the final versions to the REC may cause delay in obtaining permissions.

Management permission or approval must be obtained from each host organisation prior to the start of the study at the site concerned.

Management permission ("R&D approval") should be sought from all NHS organisations involved in the study in accordance with NHS research governance arrangements.

Guidance on applying for NHS permission for research is available in the Integrated Research Application System or at http://www.rdforum.nhs.uk.

Where a NHS organisation's role in the study is limited to identifying and referring potential participants to research sites ("participant identification centre"), guidance should be sought from the R&D office on the information it requires to give permission for this activity.

For non-NHS sites, site management permission should be obtained in accordance with the procedures of the relevant host organisation.

Sponsors are not required to notify the Committee of approvals from host organisations

Registration of Clinical Trials

All clinical trials (defined as the first four categories on the IRAS filter page) must be registered on a publically accessible database. This should be before the first participant is recruited but no later than 6 weeks after recruitment of the first participant.
There is no requirement to separately notify the REC but you should do so at the earliest opportunity e.g. when submitting an amendment. We will audit the registration details as part of the annual progress reporting process.

To ensure transparency in research, we strongly recommend that all research is registered but for non-clinical trials this is not currently mandatory.

If a sponsor wishes to request a deferral for study registration within the required timeframe, they should contact hra.studyregistration@nhs.net. The expectation is that all clinical trials will be registered, however, in exceptional circumstances non registration may be permissible with prior agreement from NRES. Guidance on where to register is provided on the HRA website.

It is the responsibility of the sponsor to ensure that all the conditions are complied with before the start of the study or its initiation at a particular site (as applicable).

NHS
Lothian

Ethical review of research sites

NHS sites

The favourable opinion applies to all NHS sites taking part in the study, subject to management permission being obtained from the NHS/HSC R&D office prior to the start of the study (see "Conditions of the favourable opinion" below).

Non-NHS sites

The Committee has not yet completed any site-specific assessment (SSA) for the non-NHS research site(s) taking part in this study. The favourable opinion does not therefore apply to any non-NHS site at present. We will write to you again as soon as an SSA application(s) has been reviewed. In the meantime no study procedures should be initiated at non-NHS sites.

Approved documents

The final list of documents reviewed and approved by the Committee is as follows:

Document	Version	Date
Covering letter on headed paper [Covering letter]	1	09 March 2015
Covering letter on headed paper [Covering letter re PO]	2	03 April 2015
Covering letter on headed paper responding to REC FINC	3	26 April 2015
GP/consultant information sheets or letters [GP Letter]	1	09 March 2015
Participant consent form [Consent]	2	03 April 2015
Participant information sheet (PIS) [PIS]	3	26 April 2015
REC Application Form [REC_Form_13032015]		13 March 2015
Research protocol or project proposal [Study Protocol]	2	03 April 2015
Summary CV for Chief Investigator (CI) [CV CI]	1	09 March 2015
Validated questionnaire [CRF Booklet]	2	03 April 2015

Statement of compliance

The Committee is constituted in accordance with the Governance Arrangements for Research Ethics Committees and complies fully with the Standard Operating Procedures for Research Ethics Committees in the UK.

After ethical review

Reporting requirements

The attached document *"After ethical review – guidance for researchers"* gives detailed guidance on reporting requirements for studies with a favourable opinion, including:

- Notifying substantial amendments
- Adding new sites and investigators
- Notification of serious breaches of the protocol

NHS
Lothian

- Progress and safety reports
- Notifying the end of the study

The HRA website also provides guidance on these topics, which is updated in the light of changes in reporting requirements or procedures.

User Feedback

The Health Research Authority is continually striving to provide a high quality service to all applicants and sponsors. You are invited to give your view of the service you have received and the application procedure. If you wish to make your views known please use the feedback form available on the HRA website: http://www.hra.nhs.uk/about-the-hra/governance/quality-assurance/

HRA Training

We are pleased to welcome researchers and R&D staff at our training days – see details at http://www.hra.nhs.uk/hra-training/

15/SS/0058	Please quote this number on all correspondence

With the Committee's best wishes for the success of this project.

Yours sincerely

Chair

Email:joyce.clearie@nhslothian.scot.nhs.uk

Enclosures: "After ethical review – guidance for researchers" *[SL-AR2]*

Copy to: *Ms Susan Shepherd, NHS Lothian Research & Development Office*

ANNEX B: NHS ETHICAL APPROVAL – QEUH, GLASGOW

WoSRES
West of Scotland Research Ethics Service

NHS
Greater Glasgow and Clyde

Dr Philip Riches
106 Rottenrow East
Glasgow
G4 0NW

West of Scotland REC 3
West of Scotland Research Ethics Service
West Glasgow Ambulatory Care Hospital
(former Royal Hospital for Sick Children Yorkhill)
Dalnair Street
Glasgow G3 8SW
www.nhsggc.org.uk

Date	16TH December 2016
Your Ref	
Our Ref	
Direct line	0141 232 1805
E-mail	WOSREC3@ggc.scot.nhs.uk

Dear Dr Riches

Study title:	**4D imaging of fixed and mobile knee implants: are mobile bearings mobile?**
REC reference:	**16/WS/0182**
IRAS project ID:	**200771**

Thank you for responding to the request for additional conditions of the favourable opinion. I can confirm the REC has received the documents listed below and that these comply with the approval conditions detailed in our letter dated 04 October 2016.

One of the conditions of approval was that people had consented to be contacted about future research. However you confirmed that this was not the case but gave the following assurances:

We can assure the committee that participants will be current and active participants in related research and, as such, we are very confident that correspondence will highly appropriate. The potential pool of recruits will be outpatients and will be under routine clinical oversight following total knee arthroplasty. One person, Alistair McEwan, will be responsible for recruiting to both trials. The paperwork emphasises the fact that this project is completely unnecessary to the original TKA trial and there is no compulsion or obligation to take part. This is a standalone project and we are only recruiting from this pool of participants since we are interested in how their new knees articulate.

The above response is acceptable to the Committee.

Documents received

The documents received were as follows:

Document	Version	Date
Other [Letter of Changes]	1.0	28 October 2016
Participant consent form [Consent Form (Control)]	3.1	18 October 2016
Participant consent form [Consent Form (Participant)]	3.1	18 October 2016

Participant information sheet (PIS) [PIS (Control)]	3.1	18 October 2016
Participant information sheet (PIS) [PIS (Patient)]	3.1	18 October 2016
Research protocol or project proposal [Scanning Protocol]	1.7	18 October 2016

Approved documents

The final list of approved documentation for the study is therefore as follows:

Document	Version	Date
Evidence of Sponsor insurance or indemnity (non NHS Sponsors only) [Strathclyde Professional Indemnity]	UM113/12	18 July 2016
Letters of invitation to participant [Preliminary Contact Letter (Control participants)]	1.1	01 March 2016
Letters of invitation to participant [Preliminary Contact Letter (Patient Participants)]	1.1	01 March 2016
Other [Strathclyde Combined Liability]	Y016458QB E0116A/113	18 July 2016
Other [Letter of Changes]	1.0	28 October 2016
Participant consent form [Consent Form (Control)]	3.1	18 October 2016
Participant consent form [Consent Form (Participant)]	3.1	18 October 2016
Participant information sheet (PIS) [PIS (Control)]	3.1	18 October 2016
Participant information sheet (PIS) [PIS (Patient)]	3.1	18 October 2016
REC Application Form [REC_Form_07092016]		07 September 2016
Research protocol or project proposal [Scanning Protocol]	1.7	18 October 2016
Summary CV for Chief Investigator (CI) [Philip Riches CV]	1	
Summary CV for student [Andre Attard CV]	1	
Summary CV for supervisor (student research) [Philip Riches CV]	1	

You should ensure that the sponsor has a copy of the final documentation for the study. It is the sponsor's responsibility to ensure that the documentation is made available to R&D offices at all participating sites.

16/WS/0182	**Please quote this number on all correspondence**

Yours sincerely

[signature]

Liz Jamieson
REC Manager

Copy to: Ms Helen Baigrie, University of Strathclyde
Dr Maureen Travers, R&D – NHS Greater Glasgow and Clyde

ANNEX C: **S**

TUDY PARTICIPANT PRELIMINARY LETTERS

Dept. of Biomedical Engineering – University of Strathclyde
GCRF, Queen Elizabeth University Hospital
Preliminary Contact Letter (patient) - Ver 1.1 - 20160301

Date: _____

Address: _____

_____

_____

Dear _____,

The Department of Biomedical Engineering at the University of Strathclyde and the Orthopaedic Department at the Queen Elizabeth University Hospital (QEUH) are collaborating in a research study on the performance of total knee replacements (TKR). As part of this research project, we would like to recruit volunteers who have recently undergone a TKR surgery, to have their knee imaged during motion using dynamic CT. We are contacting you because you have been identified by Mr Frederic Picard, consultant orthopaedic surgeon, as someone who has undergone a TKR. Please note that the research group at the University of Strathclyde do not hold your contact details and this letter has been sent by his secretary on our behalf.

We are inviting you to consider whether you would like to volunteer for this project. In participating, you would be one of a patient group that will have their knee analysed using the dynamic CT scanner at the QEUH. We would like people with total knee replacements in this patient group because we are evaluating the articulation within the knee for different knee implants and comparing them to the articulation of healthy control knees. Furthermore, to our knowledge, this will be the first time that people will have their knee imaged with dynamic CT during motion, providing valuable scientific information on how the knee functions with and without TKRs.

The scan will involve a low-risk radiation dose. As a patient volunteer, this is an unnecessary risk for you. Your participation in this study is therefore entirely voluntary, and you will be free to withdraw at any time without giving any reason. Nevertheless, if you are interested in knowing more, please contact us, using our details below, and we will be delighted in providing you with a much more detailed information sheet.

Yours sincerely,

Dr Philip Riches
Work: 0141 548 5703
Mobile: 0797 327 9019
philip.riches@strath.ac.uk

Mr Andre Attard
Mobile: 07835266072
andre.attard@strath.ac.uk

REF UK TOP 20 RESEARCH-
INTENSIVE UNIVERSITY

THE UK UNIVERSITY OF THE
YEAR WINNER

THE UK ENTREPRENEURIAL
UNIVERSITY OF THE
YEAR WINNER

ANNEX D: STUDY PARTICIPANT INFORMATION SHEET

Dept. of Biomedical Engineering – University of Strathclyde
GCRF, Queen Elizabeth University Hospital
Participant Information Sheet (patient) - Ver 3.1 - 20161018

Participant Information Sheet

Imaging study for the kinematic modelling of a healthy versus TKR knees

You are being invited to take part in a research study. Before you decide whether or not to take part, it is important for you to understand why the research is being done and what it will involve. Please take time to read the following information carefully. Talk to others about the study if you wish. Contact us if there is anything that is not clear or if you would like more information. Take time to decide whether or not you wish to take part.

Why have I been invited to take part?

The Department of Biomedical Engineering at the University of Strathclyde and the Radiology Department at the Queen Elizabeth University Hospital (QEUH) are collaborating in a research study on the performance of total knee replacements (TKR). As part of this research project, we would like to recruit volunteers who have recently undergone a TKR surgery, to have their knee imaged during motion using dynamic (4D) CT. We are contacting you because you have been identified by Mr Frederic Picard, consultant orthopaedic surgeon, as someone who has undergone a TKR. We are inviting you to consider whether you would like to volunteer for this project. In participating, you would be one of a patient group that will have their knee analysed using the dynamic CT scanner at the QEUH. We would like people with total knee replacements in this patient group because we are evaluating the articulation within the knee for different knee implants and comparing them to the articulation of healthy control knees. Furthermore, to our knowledge, this will be the first time that people will have their knee imaged with 4D CT during motion, providing valuable scientific information on how the knee functions with and without TKRs.

What is the purpose of the study?

Total knee replacements are operations that are offered to patients who have severe arthritis pain that is affecting daily activities that is no longer controlled with painkillers. The operation will replace the worn joints with metal implants and a plastic spacer. Total knee replacements are successful operations in the vast majority of patients. However, a small minority of patients are not entirely satisfied with the outcome of their knee replacement. Researchers are studying whether the type of implant has an effect on the outcome. There are two main implant types used in total knee replacement (TKR) surgery: the mobile and the fixed bearing prosthesis. The fixed bearing prostheses may also be subdivided into high and low congruent implants which refer to how well the implant components fit together. It is thought that the mobile bearing prosthesis better replicates the natural knee however current studies are yet to show which implant type patients prefer. This study will investigate how these three implant types (mobile high congruency, fixed high congruency and fixed low congruency) articulate within the replaced knee of the TKR patient.

The primary objective of this study is to look at which of the three different knee implants is better at restoring natural function so that we know what to recommend in the future. In order to determine which is the better implant, this study aims to measure knee joint articulation by using state-of-the-art CT imaging techniques. This will allow the researchers to analyse and compare the articulation within a healthy knee to that of the three different knee implants mentioned above.

What implants will be analysed during this study?

There are a number of different knee implants on the market. The Golden Jubilee Hospital in Glasgow use the Columbus® Knee System range (Aesculap AG, Tuttlingen, Germany) as the standard implant. In this study we will be investigating three different implants from the Columbus® range, a high congruency bearing in mobile (HCM) and fixed (HCF) configurations and a low congruency in a fixed configuration (LCF). If you were chosen for this study, you have one of these three implants.

What exactly are the imaging techniques which will be used?

In this study, a 4D CT scanner, the Toshiba Aquilion™ One, will be used to get an anatomical view of the articulation of the knee. 4D CT scanners are similar to conventional CT scanners with the difference that these scanners allow the patient to perform specific movements rather than the conventional static scanning method. This gives the researchers the opportunity to analyse how the anatomy being imaged articulates, which will ultimately allow the researchers to analyse and compare the articulation within a healthy knee to that of the three different knee implants mentioned above.

Do I have to take part?

No, it is up to you to decide whether or not to take part. Discuss it with family and friends or speak to a member of the research team for more information. If you do decide to take part, you will be given this information sheet to keep and be asked to sign a consent form. If you decide to take part, you are still free to withdraw at any time and without giving a reason. Deciding not to take part or withdrawing from the study will not affect the healthcare that you receive, or your legal rights. If you decide not to take part in this study, you will not be disadvantaged and you will receive the same standard of care and practice.

What will happen if I take part?

You will be asked to attend a session during which the research scan will be carried out at the radiology department at the QEUH. The session should last no longer than one hour (hopefully less than 30 minutes). The 4D-CT scan, which will take approximately 15 minutes, is low dose as it only scans the knee and is only of sufficient detail to track movements in real time, rather than a full definition CT. Before the scan you will be given a thorough understanding of what you are expected to do, while giving you time to ask any questions which you might have. During the scan you will be asked to lay facing down while you flex both your knees from fully straight to around 60 degrees of flexion in approximately three seconds (refer to Figure 1 and Figure 2).

Page 2 of 5
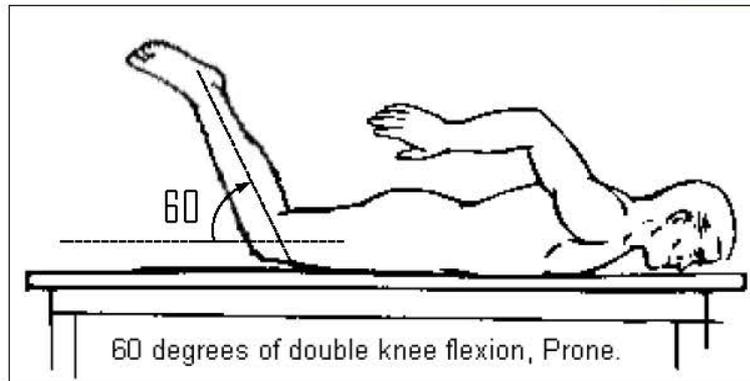
Figure 1: A diagram showing the range of motion which the participant is expected to perform during scanning.
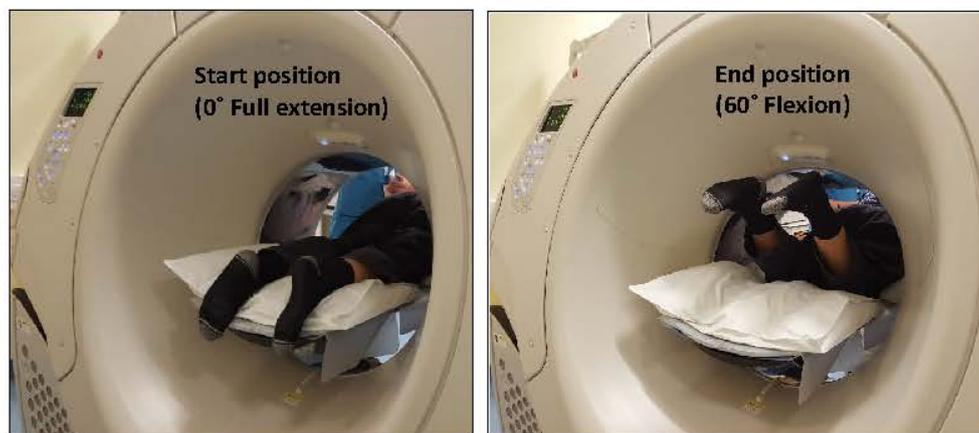
Figure 2: Photographs showing the participants' position and motion during the 4D CT scan.

What will happen to the collected data after it is captured?

Once the 4D CT scan is carried out the data will be completely anonymised and you will not be personally identifiable. The scans will be only reviewed by the research team. The research team is composed of biomedical engineers who are clinically and surgically unskilled, thus not being able to identify any kind of medical problems, if any, should they show on the resulting scans. They will only look at the motion of the bones within the knee. The anonymised images of the knee will be kept indefinitely, will hopefully be published, and used for further research and teaching purposes.

What are the possible benefits of taking part?

Your knee will be analysed very closely. We will have clear evidence of the articulation in your knee and how it compares to a healthy knee without a TKR. We hope that your help now will give us the information that will allow us to treat patients better in the future by being able to recommend the best treatment for them. However, there are no personal benefits in taking part.

Page 3 of 5

What are the possible disadvantages and risks of taking part?

The most important and only potential side effect of taking part in this study is the use of radiation. The amount of radiation used during the scan is 0.8mSv, which is equivalent to approximately 5 months of background radiation from natural sources such as cosmic rays. The fatal cancer risk is ~1 in 25,000, which can be classified as very low in comparison to the lifetime natural risk of cancer diagnosis which is 1 in 2 for people born in the UK after 1960. For clarification and comparative reasons, it is helpful to put this exposure in context. A range of other, standard radiological examinations using ionising radiation are listed, together with their associated effective doses and cancer risks in the table below [1,2]:

Examination	Effective dose (mSv)	Equivalent natural background exposure	Risk of developing fatal cancer
Chest X-ray	0.014	2 days	1 in 1,400,000
Pelvic X-ray	0.284	6 weeks	1 in 70,000
CT head	1.4	0.6 years	1 in 14, 000
Barium enema	2.2	1 year	1 in 9,000
CT chest-abdomen-pelvis	10	4 years	1 in 2,000
CT coronary angiography	2-30	1 year - 13 years	1 in 700 to 1 in 10,000

[1] HPA-CRCE-012, Frequency and collective dose for medical and dental X-ray examinations in the UK, 2008
[2] British Society of Cardiovascular Imaging, Survey of coronary CT angiography doses, 2014

The cancer risks quoted above must also be considered in context of the approximate 1 in 4 baseline risk of developing fatal cancer during the lifetime in the general population.

As a precautionary measure, we ask you to inform the research team if you had any scans (or were given any kind of radiation therapy) in the past, before consenting to this study, in order to check your eligibility for this study.

What if there is a problem?

If you have a concern about any aspect of this study please contact Dr. Philip Riches, Senior Lecturer, Department of Biomedical Engineering, University of Strathclyde, 0141 548 5703 who will do his best to answer your questions. If you wish to discuss this study with an Orthopaedic Surgeon not involved in the study, please contact Mr Kamal Deep at the Golden Jubilee National Hospital on 0800 616 267. The normal National Health Service complaints mechanisms will still be available to you (if appropriate).

Will my taking part in the study be kept confidential?

All the information we collect during the course of this study will be kept confidential and there are strict laws which safeguard your privacy at every stage.

Dept. of Biomedical Engineering – University of Strathclyde
GCRF, Queen Elizabeth University Hospital
Participant Information Sheet (patient) - Ver 3.1 - 20161018

What will happen to the results of the study?

The study will be written up as a scientific paper for publication in the public domain, so that other biomedical engineers, surgeons and hospitals can benefit from this knowledge in care of their patients. You will not be identifiable in any published results. If you would like to know the outcome of the study once it has been completed, kindly let us know and we will send you a summary of the results once they are available.

Who is organising the research?

This study is being organised by the Department of Biomedical Engineering at the University of Strathclyde in collaboration with the Queen Elizabeth University Hospital and the Golden Jubilee National Hospital.

Who has reviewed the study?

All research in the NHS is looked at by an independent group of people, called a Research Ethics Committee. They have given the study a favourable opinion. NHS management approval has also been obtained.

If you wish to make a complaint about the study, please contact NHS GG&C:

NHS Greater Glasgow and Clyde Complaints Team
Complaints Team
Glasgow Royal Infirmary
Castle Street
Glasgow
G4 0SF
Tel: 0141 211 5112

complaints@ggc.scot.nhs.uk

Thank you for taking the time to read this information sheet.

ANNEX E: STUDY CONSENT FORM

Dept. of Biomedical Engineering – University of Strathclyde
GCRF, Queen Elizabeth University Hospital
Consent Form (Patient) – Version 3.1 – 20161018

CONSENT FORM

Title of Project: 4D imaging of fixed and mobile knee implants

Please initial box

Participant ID:

1.   I confirm that I have read and understand the participant information sheet (version 3.1 dated 20161018) for the above study and have had the opportunity to consider the information and ask questions.

2.   I understand that my participation is voluntary and that I am free to withdraw at any time, without giving any reason, without my medical care or legal rights being affected.

3.   I understand that relevant sections of my medical notes and data collected during the study may be looked at by individuals from the research team, the Sponsor, NHS Greater Glasgow and Clyde and the University of Strathclyde, or other authorities, where it is relevant to my taking part in this research. I give permission for these individuals to have access to my records.

4.   I agree to my anonymised data being used in future studies and for teaching purposes.

5.   I agree to have my CT scan video recorded for documentation purposes. This data will be completely anonymised and I will not be personally identifiable.

6.   I am aware of the additional radiation involved with this CT scan.

7.   I agree to take part in the above study.

_____   _____   _____
Name of Participant   Date   Signature of participant

_____   _____   _____
Name of Researcher   Date   Signature of Researcher

When completed: 1 copy for participant; 1 copy (original) for researcher file; 1 copy for medical notes

Version: 3.1   Date: 18/10/2016

ANNEX F:RADIOLOGIST SCANNING PROTOCOL

Glasgow Clinical Research Imaging Facility	
4D Knee - GN16RH524	
4D Knee Scan	

Radiologist: Mark McCleery **Nurse:** Andre Attard and Alistair Ewen	

History	Pre and Post Op Knee Replacement- Controls and Patients
Patient Prep	• Confirm patient ID – EP-7 • Check pregnancy status – EP-8
Contra Indications	None
Patient Position/Centre	Feet first supine, knees bent over pad — **Centre:** Mid Patella at level of femoral condyles
IV Contrast	Non Contrast — **Injection:** Rate: — Cannula size:

Scan Technique:
- Practice leg movement with patient prior to scanning – both knees to move from flexion to full extension over 4.5 seconds. Use a metronome set to 60 bpm to help patient with timing.
- Feel where patient's femoral condoyle is on flexion and measure again on extension. Next half this distance. Ie 20mm measured = 10mm and remember this number.
- AP and Lateral Scout – cover above knee joint
- Place top of scan box to line up with the widest part of the femoral condyle of the knee you have measured previously.
- Alter start location by taking off 80mm + ½ of measured number (10mm)
- Ie if start location is 290 then new start location should be 200.
- Ensure scan FOV covers knee as it moves – may need LL
- Use full 160 mm Volume
- Turn on SEMAR if patient is post operative
- The scan will run continuously over 4.5 seconds, get the patient to start moving their legs in practiced motion. Start scan immediately before patient reaches flexion and scan until they have reached full extension and knee joint has locked.

Reconstructions:
- 4D volume 1mm/1mm – soft tissue standard (set up on protocol to auto reconstruct and transfer to PACS)

Images to PACS **(All set to Auto Send)**	• 4D volumes to 1mm/1mm • Soft Tissue Standard • Dose Report
Archiving	Anonymise patient to study ID and burn 4D volume to DVD for Andre
MPE DRL	
Local DRL	

Author	Owner	Revision	Active Date	Review date	Page
EMc	TH	1	22/02/2017	22/02/2018	1 of 1
This document is uncontrolled when printed. Check Revision BEFORE use!					

Open access   **Original article**

BMJ Open Quality

Health costs and efficiencies of patient-specific and single-use instrumentation in total knee arthroplasty: a randomised controlled trial

Andre Attard,[1] Gwenllian Fflur Tawy,[2] Michiel Simons,[3] Philip Riches,[1] Philip Rowe,[1] Leela C Biant[2]

[1]Biomedical Engineering, University of Strathclyde, Glasgow, UK
[2]Division of Cell Matrix Biology and Regenerative Medicine, University of Manchester, Manchester, UK
[3]Clinical Surgery, University of Edinburgh, Edinburgh, UK

Correspondence to
Dr Gwenllian Fflur Tawy; gwenllian.tawy@manchester.ac.uk

ABSTRACT

Aim To investigate whether patient-specific instrumentation (PSI) and single-use instrumentation (SUI) improve operating room efficiency in terms of time and cost to the healthcare provider over conventional/reusable instrumentation (CVR) when performing total knee arthroplasty (TKA).

Patients and methods Patients requiring TKA were randomised into one of four surgical groups: CVR, CVS (conventional/SUI), PSR (PSI/reusable) and PSS (PSI/SUI). All surgical procedures were video recorded to determine specific surgical time intervals. Other variables reported included the number of instrument trays used, missing equipment, direct instrument costs and the weight of the instruments the staff had to handle. Oxford Knee Score (OKS), estimated blood loss and lengths of hospital stay were also recorded as markers of patient experience.

Results PSR was significantly quicker in all the recorded time intervals, used less trays, experienced less missing equipment and resulted in lower blood loss and shorter hospital stays. SUI reported significantly slower operating room times and resulted in higher blood loss, but SUI was 88% lighter and 20% cheaper on average when compared with their reusable counterparts. Despite the economic advantages of PSI and SUI, the patients who reported greatest improvements in OKS were those allocated to the CVR group, but no clinically meaningful difference in OKS was found at any time point.

Conclusions PSI and SUI for TKA have the potential of reducing operating room times over conventional, reusable sets. This reduction will benefit theatre personnel ergonomically, while presenting the healthcare provider with potential cost-saving benefits in terms of reduced sterilisation costs and surgical times.

INTRODUCTION

Total knee arthroplasty (TKA) is currently the most effective and successful treatment for advanced osteoarthritis and its related pain in the knee.[1–3] In 2017, over 110 000 TKA procedures were performed in the UK.[4] Worldwide ageing populations and growing obesity rates are causing substantial increases in the volume of TKA procedures carried out annually.[5] One recent study predicted a growth in the procedure of 673% in the USA by 2030.[6]

The economic efficiency of TKA must be optimised for healthcare services to be able to respond to the growing demand in TKA without sacrificing the level of care provided to patients. This could be attained by reducing operative costs and times. Achieving these goals would allow for greater number of surgical cases to be completed daily without having to extend operating hours or increase the number of theatres used per day; both of which imply additional cost to the institution.

Over recent years, several orthopaedic manufacturers have introduced patient-specific instrumentation (PSI) and single-use instrumentation (SUI) for TKA. PSI is a bespoke surgical approach which aims to provide increased implant accuracy and surgical efficiency over conventional techniques.[7 8] PSI for TKA is designed using MRI or CT scans of the patient's preoperative knee.[7–9] Using the 3D image of the knee, a plan of the intended procedure can be created by the surgeon, which includes recommended implant size and alignment.[7 10] From the agreed plan, bespoke cutting blocks are created to guide the saw intraoperatively for accurate placement of the implant.[8] Given the detailed preoperative plan, PSI reduces the number of TKA instruments and intra-operative surgical steps. PSI could therefore reduce the length of each procedure and save on sterilisation costs of the reusable equipment.

Single-use instruments have the potential to further reduce the costs of sterilisation, as the instruments are disposed of postoperatively. Disposable instruments are commonly used in hospitals due to their appealing traits in favour of sterility, safety, efficiency and, when scaled sufficiently, cost.[11] TKA SUI is provided by the manufacturer in sealed

Open access
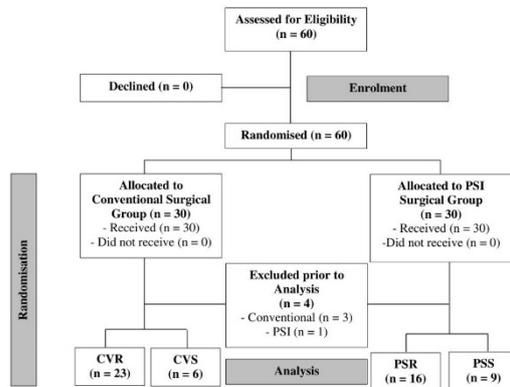
Figure 1 A Consolidated Standards of Reporting Trials (CONSORT) diagram of patient recruitment and involvement in this study. CVR, conventional/reusable; CVS, conventional/ single use; PSI, patient-specific instrumentation; PSR, patientspecific/reusable; PSS, patient specific/single use.

presterilised size-specific kits containing all the required tools. The published literatures on SUI have investigated their effect on surgical efficiency, institutional costs and their impact on risk of infections.[12–17]

However, current data on the use of both SUI and PSI in TKA are limited, with conflicting views on whether the technologies are appropriate and cost-effective for routine use.

The aim of this study was to perform a comparative investigation of the efficiency of conventional instrumentation, PSI and SUI. The research question was: Do PSI and SUI present improved efficiency in terms of time and cost savings to the institution over the conventional reusable instrumentation sets when performing TKA? The objective was to assess (1) instrument-related surgical efficiency, (2) instrument-related costs, and (3) whether patient-related outcomes were affected by the instrumentation used. We hypothesised that the use of PSI would improve surgical efficiency at the expense of increased cost, and that SUI would present similar efficiency while improving cost.

MATERIALS AND METHODS
Patient recruitment
A sample size calculation was used to predict group size, where the level of significance was 5% ($\alpha=0.05$) and the power was 80% ($\beta=0.2$).[18] The outcome variable used was the minimum clinically important difference in surgical time. Fifteen minutes was deemed clinically important, as this would allow for the addition of one extra TKA procedure a day. The SD for this variable used was 9 min, which was calculated from 50 consecutive conventional TKA operations carried out by the surgeon. Using these variables, it was determined that six patients were required per patient group.

Eligible patients were those diagnosed with osteoarthritis of the knee which was sufficiently symptomatic to require TKA. Patients were excluded if they showed signs of inflammatory arthritis, ligament problems, significant knee deformities, or if they required complex bone augmentation procedures. Written and verbal informed consent was provided by all patients.

The patients were randomised into four separate groups by block stratification (figure 1). The four instrument groups were: conventional/reusable (CVR), patient-specific/reusable (PSR), conventional/single-use (CVS) and patient-specific/single-use (PSS) instrumentation. Recruitment ended when at least six patients had undergone TKA in each surgical group.

This study is registered with ClinicalTrials.gov.

Surgical technique and instrumentation
One surgeon (LCB) performed all procedures between 2015 and 2016 at the Royal Infirmary of Edinburgh using a fixed-bearing prosthesis (GMK Sphere, Medacta International, Switzerland).

Conventional instrumentation
Patients randomised into the conventional group received standard care. Routine radiographs were taken of the preoperative knee during elective clinics and used to guide the operative plan. Bone cuts were performed using standard GMK Sphere instrumentation, using an intramedullary guidance rod for the femur and an extramedullary guidance rod for the tibia. The instruments were sterilised using an in-house standard autoclave procedure.

Patient-specific instrumentation
MyKnee PSI manufactured by Medacta International was used for this study protocol (Medacta International, Castel San Pietro, Switzerland). Patients randomised into the PSI group underwent a preoperative brief low radiation CT scan in addition to routine radiographs, as per the standardised MyKnee protocol. 3D plans of the preoperative knee showing the virtual positioning of the implant were uploaded onto an online case database so that the surgeon and technician could liaise on the operative plans. Bespoke cutting blocks were then designed, based on the plans to fit securely onto the osteophytes of the tibial and femoral bones (figure 2A). Once the plans were finalised, the PSI was created by 3D printing technology and shipped to the hospital. Intraoperatively, the cutting jigs were placed in their preplanned positions, checked by the surgeon and then pinned in place. The bone cuts were then performed according to the preoperative plan. Prosthetic fixation was performed using antibiotic laden cement. Reusable instruments were sterilised using an in-house standard autoclave procedure.

Single-use instrumentation
The SUI used for this study was the GMK Efficiency, designed specifically to implant the GMK Sphere TKA (Medacta International). Patients randomised into the
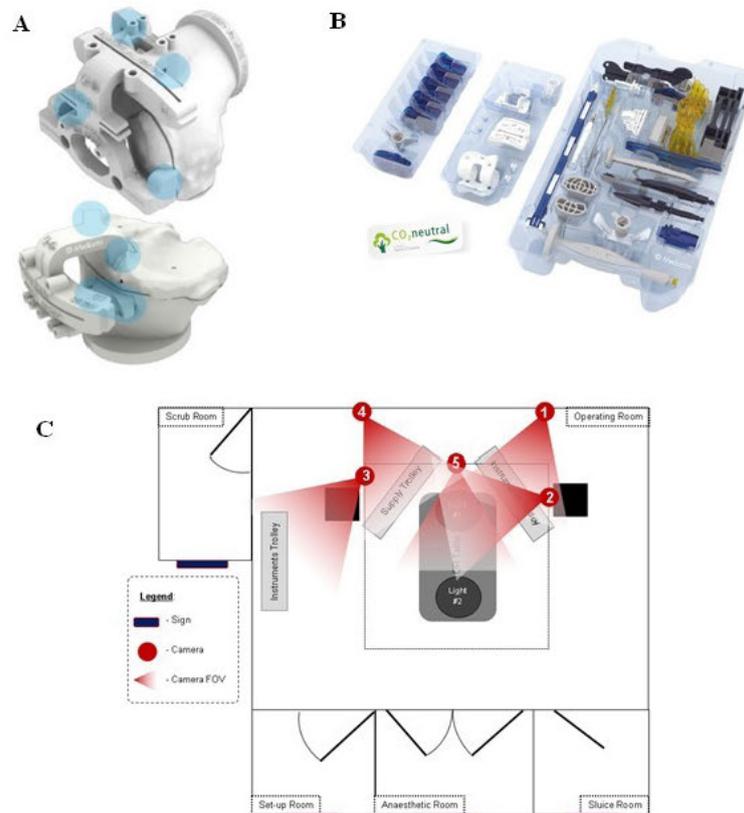
Figure 2 (A) MyKnee patient-specific cutting blocks secured onto the distal end of a femur (above) and proximal end of a tibia (below) using distinct anatomical landmarks (blue highlights). (B) The single-use GMK Efficiency instruments used for total knee arthroplasty (TKA). (C) Camera placement in theatre. FOV, field of view.

SUI group were not required to undergo any additional procedures. The SUI arrived in the hospital presterilised and in a presealed sterilised package (figure 2B).

Data collection

Intraoperatively, each surgery was video recorded using five cameras (figure 2C). Bespoke software synchronised the five recordings then extracted data on surgical time intervals and the number of trays opened per case (MATLAB Release 2016b, The MathWorks, Massachusetts, USA).

Complications, and the number of missing equipment reported per case, were documented intraoperatively by the surgeon. This information was recorded for the study by a member of the research team and then verified by the surgeon. Complications or delays experienced during surgeries were classified as 'instrument-related' or 'general'. The time spent waiting intraoperatively as a result of a general issue (verified by an orthopaedic surgeon) was deducted from the corresponding surgical interval, while instrument-related issues and delays were included in the analysis.

The time taken for the instruments to be taken for sterilisation and returned back to the theatre instrument stores was recorded using an in-house barcode tracking system. The weights of the conventional and SUI trays were averaged over three different instances throughout the length of the study.

Reusable instrument costs for the institution were calculated as the sterilisation cost (as quoted by the in-house sterilisation unit) for sterilising a single instrument tray. This price was subsequently multiplied by the average number of conventional trays used during the surgery. SUI prices were obtained from the company issuing the instruments, as the price the institution paid for each individual SUI set. The company also supplied the price for the patient-specific cutting jig and their corresponding 3D-printed bone models. CT scan cost was obtained from the institution radiology centre.

Additional variables were also reported to investigate the effect of PSI and SUI on patient outcome. The Oxford Knee Score (OKS) was completed by patients at preadmission clinics, then 6 weeks and 1 year following surgery. The OKS was scored by one member of the trial team and verified by another at a later date. The lengths of hospital stay for all patients were also reported. Finally, haematocrit levels were assessed at preadmission clinics and 24 hours following surgery. These variables were used to estimate blood loss during surgery (Equation 1).[19]

$$Estimated\ Actual\ Blood\ Loss\ = EBV$$
$$\times \left(\frac{Preoperative\ Haematocrit - Postoperative\ Haematocrit}{Mean\ Haematocrit} \right)$$

The estimated blood volume (EBV) was calculated by multiplying the patient weight (in kilograms) by a constant (mL/kg) which varied depending on body habitus.[19]

Patient and public involvement

Patients and members of the public were not involved in the design, recruitment or conduct of this study. There were lay members on the trial steering committee, however. The results of this study will be communicated to study participants on request.

RESULTS
Patient demographics

Sixty patients agreed to participate in this investigation. Of those, four were excluded from the analysis after randomisation, due to drained camera batteries which led to incomplete recordings (figure 1). There were no significant differences in patient demographics between groups (table 1).

Complications

Instrument-related issues occurred intraoperatively. In one case, a new tray was opened in a CVR procedure to replace a femoral extractor which showed remains of cement from previous use. In one CVS case, an SUI femoral extractor failed, and so a new reusable instrument tray was opened to replace it. In another CVS case, the tibia required recutting due to inaccuracies of SUI equipment. One complication arose in the PSR group, where the surgeon felt the tibial cutting jig was one size too small for the patient's knee, and so CVR instrumentation was used for the tibial cuts.

These complications were clearly the results of the original instrumentation trays containing inadequate equipment for the procedure, or missing crucial parts. Table 2 shows that for each conventional procedure carried out with reusable equipment, 1.48 parts were missing. This was lower when the PSI instrumentation was used (0.22).

In addition to instrument-related complications, three conventional instrumentation surgeries were delayed by approximately an hour each, and a further two surgeries were cancelled. Finally, one serious adverse event occurred in a CVR case when a sterilised instrument was found to be missing a filter, potentially affecting its sterility. This led to staff questioning whether the entire content of the tray was sterile, causing a delay of 20 min in initiating the procedure while a new sterile tray was sourced.

Time analysis

When comparing CVR and PSR surgical times, PSR instruments were quicker in all the surgical time intervals recorded (table 2). In particular, PSR total instrument time showed a statistically significant reduction of 9 min and 24 s over CVR (p=0.004). This was echoed in the procedure time (PT), which was 5 min shorter and borderline significant (p=0.054).

The single-use instruments used in conventional procedures took longer to set up in theatre than the conventional reusable instrumentation (table 1). The procedure was also longer, with differences near significance (p=0.054). Conversely, all variables which were recorded after set-up of the instruments were quicker with the SUI. 'Instrument Count Time' and 'Instrument Clean-up Time' were statistically significantly shorter when SUI was used. Findings were similar during PSI procedures. The only stage where SUI was significantly faster than reusable instrumentation was during packing of the instruments (p=0.041).

Weight analysis

The conventional and PSI instrumentation were shown to weigh similar amounts; however, the reusable instrumentation was significantly heavier than the SUI for both surgical approaches (table 3). On average, the differences

Table 1	Study group demographics				
	CVR	**CVS**	**PSR**	**PSS**	**Total**
n	23	6	18	9	56
Male/female*	10:13	3:3	11:7	5:4	29:27
Left/right knee*	13:10	4:2	9:9	6:3	32:24
Age (years)†	70.1 (35)	71.2 (24)	71.1 (39)	70.7 (21)	70.6 (40)
BMI (kg/m²)†	30.8 (15.2)	31 (21.51)	30.6 (17.52)	27.19 (14.66)	30.3 (21.92)

*Values are presented as ratios.
†Values are presented as mean (range).
BMI, body mass index; CVR, conventional/reusable; CVS, conventional/single use ; PSR, patient specific/reusable; PSS, patient specific/single use.

Table 2 Results for all instrumentation sets

Variables	CVR	CVS	PSR	PSS	P value CVR versus PSR	CVR versus CVS	PSR versus PSS
IDT*	00:02:29 (00:04:58)	00:03:54 (00:06:49)	00:01:14 (00:01:56)	00:07:50 (00:19:52)	**0.006†**	0.433†	**0.021‡**
IAT*	00:09:22 (00:13:31)	00:12:35 (00:06:59)	00:07:25 (00:12:31)	00:15:01 (00:21:03)	0.133‡	0.067‡	**0.013‡**
IST*	00:11:52 (00:17:55)	00:16:30 (00:10:41)	00:08:49 (00:23:26)	00:22:51 (00:36:29)	**0.022†**	**0.025‡**	**0.0005†**
SST*	00:30:10 (00:36:44)	00:34:51 (00:28:25)	00:25:43 (00:19:30)	00:31:54 (00:25:05)	0.054‡	0.258‡	**0.017‡**
PT*	01:03:10 (00:38:02)	01:05:28 (00:23:22)	00:56:10 (00:23:04)	00:58:46 (00:19:35)	0.054‡	0.57‡	0.814‡
ICT*	00:05:13 (00:09:14)	00:02:39 (00:03:35)	00:02:50 (00:04:18)	00:02:39 (00:05:02)	**0.002†**	**0.025†**	0.754‡
IPT*	00:03:37 (00:06:00)	00:02:24 (00:05:57)	00:03:14 (00:07:26)	00:01:39 (00:03:05)	0.18†	0.109‡	**0.041†**
ICuT*	00:09:15 (00:15:05)	00:05:03 (00:09:32)	00:06:04 (00:10:11)	00:04:18 (00:06:22)	**0.004‡**	**0.015‡**	0.117‡
TIT*	01:25:12 (00:28:12)	01:23:26 (00:48:03)	01:15:48 (00:41:34)	01:17:59 (00:23:28)	**0.004‡**	0.199†	0.585‡
IST*	74:16:29 (216:19:45)	N/A	85:11:48 (451:56:40)	N/A	0.536†	N/A	N/A
nTrays	3.74 (2)	N/A	2.89 (1)	N/A	**<0.0001†**	N/A	N/A
Missing equipment	1.48 (5)	N/A	0.22 (1)	N/A	**0.009†**	N/A	N/A
Blood loss (mL)	898.87 (1135.83)	936.82 (502.90)	785.24 (1784.97)	811.96 (1112.08)	0.358†	0.773‡	0.888‡
OKS (preoperative)	20.55 (29)	25 (11)	20.53 (25)	24.38 (14)	0.994‡	0.143‡	0.183‡
OKS (6 weeks)	32.44 (25)	30.33 (7)	33.07 (20)	25.8 (18)	0.782‡	0.608‡	**0.031‡**
OKS (1 year)	40.87 (17)	35.67 (22)	36.85 (19)	36.67 (28)	**0.05‡**	0.205‡	0.544†
Length of hospital stay	5 (11)	5.17 (5)	4.56 (7)	4.13 (3)	0.988†	0.507†	0.862†

Data expressed as mean (range).
nTrays denotes number of conventional instrument trays used per surgery.
Bold values denote statistical significance.
*Data presented in the format of (hours):(minutes):(seconds).
†Independent samples t-test.
‡Mann-Whitney test.
CVR, conventional/reusable; CVS, conventional/single use; IAT, instrument assembly time=scrub nurse started decanting first tray—scrub nurse finished decanting instruments; ICT, instrument count time=scrub nurse started counting instruments—scrub nurse finished counting instruments; ICuT, instrument clean-up time=scrub nurse started counting instruments—instrument trays closed and taken to sluice room; IDT, instrument decant time=instrument trays entered operating room—scrub nurse opened first tray; IPT, instrument packing time=scrub nurse started packing instruments—instrument trays closed and taken to sluice room; IST, instrument sterilisation time=time instruments were picked up by sterilisation unit (SU)—time instruments were dispatched from SU; IST, instrument set-up time=scrub nurse started assembling instruments—scrub nurse finished assembling instruments; N/A, not applicable; OKS, Oxford Knee Score; PSR, patient specific/reusable; PSS, patient specific/single use; PT, procedure time=knife to skin—closure with last clip; SST, surgical set-up time=scrub nurse performs first task—knife to skin; TIT, total instrument time=scrub nurse opened first tray—instrument trays closed and taken to sluice room.

Table 3 Instrument weights and costs per surgery for all four groups

Instrument type	Weight breakdown (kg)		Total mean weight (kg)	Cost breakdown (£)	Total cost (£)
CVR	Sphere femoral finishing tray	9.9	35.9	424.12*	424.12
	Sphere conventional tray	7.2			
	Sphere trial components	10.6			
	General instruments and accessories tray	8.2			
CVS	Conventional Efficiency instrument set	1.4	4.6	110.00	320.00
	General Efficiency instrument set	2.2		110.00	
	Efficiency femoral set	0.5		50.00	
	Efficiency insert set	0.5		50.00	
PSR	MyKnee instruments	12.5	33.7	327.73†	727.73
	Conventional MyKnee instrument set	10.1			
	Sphere trial components	10.6			
	MyKnee cutting blocks	0.5		250.00 (+150.00‡)	
PSS	General Efficiency instrument set	2.2	3.7	110.00	610.00
	Efficiency femoral set	0.5		50.00	
	Efficiency insert set	0.5		50.00	
	MyKnee cutting blocks	0.5		150.00	

*Sterilisation cost for a single tray × 3.74 trays.
†Sterilisation cost for a single tray × 2.89 trays.
‡Preoperative CT scan cost.
CVR, conventional/reusable; CVS, conventional/single use; PSR, patient specific/reusable; PSS, patient specific/single use.

between SUI and reusable equipment were approximately 30 kg. The mean number of trays used in conventional procedures using reusable equipment was 3.74 (table 3). This was one tray lower in PSI-guided procedures (2.89).

Cost analysis
The PSI variants were more costly than conventional instrumentation (table 3) due to the costs of a preoperative scan and manufacturing of the patient-specific cutting blocks.

Clinical outcomes
Patients who underwent TKA with reusable PSI were estimated to have lost the least amount of blood (table 2). Those allocated to the conventional group with SUI lost the greatest volume (936.82 mL). The PSI variants reported lower blood loss in patients than the conventional surgery, but this did not reach statistical significance.

Similar patterns were observed in the length of hospital stay for the patient groups (table 2). The patients who had lost the greatest EBV were also those who remained in hospital for longest (5 days). Those who were discharged earliest were in the PSS group. These patients left the hospital a day earlier than those undergoing conventional surgery (4.13 days).

OKS improved in all groups with each visit (table 2). Preoperatively, there were no statistically significant differences in the OKS between groups. Six weeks postoperatively, patients who had undergone the surgery with

PSI and reusable equipment had the best scores, whereas the PSI group who had been allocated to the SUI had the worst (p=0.031). One year postoperatively, these differences had narrowed. Patients who were allocated to the conventional group with reusable equipment had the greatest average OKS at 1 year. This score was significantly greater than that reported in patients in the PSI group allocated to the reusable equipment (p=0.05). The lowest average score at 1 year was reported in the conventional group who had undergone TKA with SUI.

According to a study by Beard and colleagues, a meaningful change in OKS at the group level is 9 points.[20] Additionally, the between-group minimal important difference for clinical trials was estimated to be 5 points. All groups in this study showed clinically meaningful improvement in their Oxford scores, but no group (when compared with another) showed a clinically meaningful difference in their Oxford score preoperatively, at 6 weeks, or at 1 year.

DISCUSSION
PSI and SUI are increasing in use in TKA to address the growing volume of patients undergoing TKA. These technologies aim to reduce surgical times, simplify the surgical process to improve TKA efficiency, and improve implantation accuracy and maintain or improve clinical outcomes. The main objective of this study was to assess instrument-related surgical efficiency with Medacta MyKnee and Efficiency instrumentation.

The simplest way to improve surgical efficiency is to reduce the length of each procedure. PSI should improve surgical efficiency, as it simplifies the surgical procedure by reducing the surgical steps required. Although some authors have reported a reduction in surgical times with PSI,[21–28] others have found no differences[29–31] or longer surgical times.[32] In this study, the shortest procedures on average were reported in the PSR group (table 2).

The PSI groups were discharged from hospital on average a day earlier than the conventional groups, representing an efficiency saving in operative time and inpatient stay.

Sterilisation delays directly affected surgeries as they led to long delays in initiating the procedures. Sterilisation times for the instruments turned out to be very unreliable, as can be noted from the ranges of instrument sterilisation time (IST) (table 2). Sterilisation-related issues are considered as one of the major pitfalls of reusable instrumentation, and this resonated in our study. Although each hospital has its own individual sterilisation arrangements, it is a familiar and common scenario that there can be breaches in the sterilisation wrapping around trays, cement on instruments and missing items from trays; all of which cause surgical delays. Using SUI reduces these risks, as sterilisation units are involved in the process to a much lesser extent.[15 33] Another factor which could be considered an additional risk of using reusable equipment is the transport of equipment off-site for sterilisation. This is commonplace for many hospitals, and can bring with it further complications and potential delays.[34] These complications could be reduced with the use of SUI.

Some surgeries were prolonged due to missing equipment in the instrument trays or incomplete sterilisation of certain equipment. These problems affect efficiency and add to the risk of surgical field contamination leading to infections, which are known to drastically affect patient recovery and institutional costs.

PSR showed a significant reduction in missing equipment compared with conventional reusable instruments. This may be associated with the fact that PSR uses fewer conventional trays.[24 32] This reduction in equipment reduces the likelihood of sterilisation-related problems arising during surgery. Quicker time intervals coupled with a reduction in trays and missing equipment correlate with an improved efficiency, while also reducing the risk of infection.[35]

When comparing efficiency of SUI with their corresponding reusable counterparts, the most prominent results identified a limitation in our study. Due to the fact that the SUI was relatively new to the surgeon and the theatre personnel, the results may have been affected by a learning curve. This may explain why CVS and PSS results do not agree with previous studies for SUI which reported notable time reductions during set-up time, operative time, clean-up time and turnover time.[13 14] In light of this, the results for CVS and PSS should be considered with caution. CVS and PSS both resulted in a significant increase in instrument set-up time and surgical set-up time. PT was also longer for both cases, although only by a narrow margin. On the contrary, clean-up times were significantly shorter, which ultimately compensated for the longer set-up times, leading to a marginally shorter total instrument time for CVS, while total instrument time for PSS was slightly longer. Clean-up times were predicted to be shorter as single-use instruments do not need to be placed in certain locations within the conventional trays, as they are disposed postoperatively. Moreover, CVS does not require any sterilisation resulting in significant cost saving while avoiding the intraoperative complications which arise with missing equipment and sterilisation issues. This results in significant turnarounds in terms of time and costs.

CVS was 87.2% lighter than CVR, and PSS was 89% lighter than PSR (table 3), making SUI very ergonomic and beneficial for the well-being of theatre personnel who have to repeatedly handle the trays. SUI is easier on the theatre personnel, which subsequently improves efficiency while also avoiding work-related injuries.

The second objective of this study was to investigate instrument-related costs. PSI was clearly more expensive than conventional instrumentation (table 3). This is mainly due to the cost of the preoperative CT scan and the manufacturing costs of the cutting jig. In this study we did not include costs saved as a result of shorter operating times, as they were not considered to be directly related instrument costs. Cendán and Good reported that even small deductions in surgical times (mean of 16 min) can open the opportunity for an increase in number of cases performed per day.[36] These values are consistent with the total instrument time reductions recorded for PSR in our study, which suggest that if operating room running costs were considered PSI costs have the possibility of approximating their conventional counterparts. However, the PSI patients left hospital on average a day earlier in our study which may offset the costs of the preoperative scan.

Alternatively, SUI offers a cheaper alternative, with CVS being 24.6% cheaper than CVR and PSS being 16.2% cheaper than PSR. This agrees with previous studies on the cost of SUI in TKA.[13 15] These benefits are an addition to the aforementioned advantages, since SUI is lighter and is unaffected by sterilisation delays. Use of SUI also reduces the cost of sterilisation. Further cost savings can be made in hospitals where equipment is usually transported off-site for sterilisation.[34]

Furthermore, it should be noted that a study performed on the SUI used in this study found that 435 L of water can be saved for each TKA surgery (otherwise used in sterilisation), thus reducing their environmental impact while further adding to their indirect cost savings.[37]

The third objective of this study was to investigate patient outcomes. The results reported in this study agree with previously published research that have concluded that PSI results in comparable outcomes to conventional TKA.[20 38 39] However, the PSI groups had lower blood loss and left hospital a day earlier on average. SUI resulted

in a slight increase in blood lost in comparison to their reusable counterparts, which is attributed to the longer PT (table 2). Those who were estimated to have lost the greatest volume of blood (CVS) were found to remain in hospital longest. Although differences were not statistically or clinically significant, they may be economically important, as earlier discharge of patients is a way to substantially save on TKA costs.

This study has limitations that should be acknowledged in light of the results obtained. First, we only investigated surgeries performed using instrumentation and prosthesis from a single manufacturer. Thus, it is unknown whether the results obtained in this study can be extrapolated to instrumentation produced by other manufacturers. Second, all the surgeries were performed by a single, high-volume surgeon who was accustomed to performing TKA surgeries using both CVR and PSR, but not using SUI. This may have influenced the results in terms of a reduction in time saved due to inexperience using specific single-use equipment. This was also noted with the theatre personnel who showed a clear learning curve when working with SUI. If the learning curve effects are surpassed, SUI has the potential of improving surgical efficiency and of presenting the healthcare provider with definite cost savings.[13-15 36 37] Finally, an uneven number of patients were randomised into the SUI and reusable groups. Due to a problem with dispatching the SUI at the beginning of the trial, patients were initially randomised into either the standard or the PSI group using reusable instrumentation. When the issue was resolved, the patients were randomised to one of the four intended groups, as originally planned. This was deemed necessary to ensure that those who would have been randomised into an SUI group did not have to wait longer than is necessary for their operation. A greater sample size for the SUI groups may have increased the reliability of the results.

This study formed one part of a larger investigation comparing the outcomes of conventional TKA to patient-specific TKA. This explains why we had access to data from significantly more patients in the non-SUI groups. Once we had completed collecting the data for this investigation, we deemed it appropriate to include all available results in the data analysis to improve the robustness of the research and to ensure we were being transparent about the data we had collected.

CONCLUSION

Surgical efficiency was significantly improved by PSI at the expense of increased cost. Surgical efficiency was not improved through use of SUI—nevertheless, instrument-related costs were cheaper and avoided sterilisation complications.

PSI presents the healthcare provider with potential cost savings should indirect instrument costs be considered. Conversely, SUI was less efficient due to learning curve effects.

REFERENCES

1. Dowsey MM, Nikpour M, Dieppe P, et al. Associations between pre-operative radiographic changes and outcomes after total knee joint replacement for osteoarthritis. Osteoarthritis Cartilage 2012;20:1095–102.
2. Klit J, Jacobsen S, Rosenlund S, et al. Total knee arthroplasty in younger patients evaluated by alternative outcome measures. J Arthroplasty 2014;29:912–7.
3. Lewis S, Price M, Dwyer KA, et al. Development of a scale to assess performance following primary total knee arthroplasty. Value in Health 2014;17:350–9.
4. National Joint Registry. National joint Registry: 13th annual report 2017. Available: http://www.njrcentre.org.uk/njrcentre/Portals/0/Documents/England/Reports/13th%20Annual%20Report/07950%20NJR%20Annual%20Report%202016%20ONLINE%20REPORT.pdf> [Accessed 19th Jun 2017].
5. Suri P, Morgenroth DC, Hunter DJ. Epidemiology of osteoarthritis and associated comorbidities. PM&R 2012;4:S10–S19.
6. Kurtz S, Ong K, Lau E, et al. Projections of primary and revision hip and knee arthroplasty in the United States from 2005 to 2030. J Bone Joint Surg Am 2007;89:780–5.
7. Abdel MP, Parratte S, Blanc G, et al. No benefit of patient-specific instrumentation in TKA on functional and gait outcomes: a randomized clinical trial. Clin Orthop Relat Res 2014;472:2468–76.
8. Rodrigues AST, Gutierres MAP. Patient-specific instrumentation in total knee arthroplasty. Should we adopt it? Revista Brasileira de Ortopedica 2016;52:242–50.
9. Okada Y, Teramoto A, Suzuki T, et al. Preoperative corrections are required for planning of patient-specific instrumentation in total knee arthroplasty. The Knee 2017;24:1492–7.
10. Chen JY, Chin PL, Tay DKJ, et al. Functional outcome and quality of life after patient-specific instrumentation in total knee arthroplasty. J Arthroplasty 2015;30:1724–8.
11. Haas SB, Carli A. Disposable instruments in total knee arthroplasty. Minim. Invasive Surg. Orthop. Cham: Springer International Publishing 2016:1349–56.
12. Mont MA, McElroy MJ, Johnson AJ, et al. Single-use instruments, cutting blocks, and trials increase efficiency in the operating room during total knee arthroplasty. The Journal of Arthroplasty 2013;28:1135–40.
13. Siegel GW, Patel NN, Milshteyn MA, et al. Cost analysis and surgical site infection rates in total knee arthroplasty comparing traditional vs. single-use instrumentation. J Arthroplasty 2015;30:2271–4.
14. Mont MA, Pivec R, Johnson AJ, et al. Single-use cutting blocks and trials lower costs in primary total knee arthroplasty. Surg Technol Int 2012;22:331–5.
15. Bonutti PM, Zywiel MG, Johnson AJ, et al. The use of disposable cutting blocks and trials for primary total knee arthroplasty. Techniques in Knee Surgery 2010;9:249–55.
16. Siddiqi A, Hardaker WM, Eachempati KK, et al. Advances in computer-aided technology for total knee arthroplasty. Orthopedics 2017;40:338–52.

17. DeHaan AM, Adams JR, DeHart ML, *et al*. Patient-specific versus conventional instrumentation for total knee arthroplasty: peri-operative and cost differences. *J Arthroplasty* 2014;29:2065–9.

18. Noordzij M, Tripepi G, Dekker FW, *et al*. Sample size calculations: basic principles and common pitfalls. *Nephrology Dialysis Transplantation* 2010;28:1388–93.

19. Gross JB. Estimating allowable blood loss. *Anesthesiology* 1983;58:277–80.

20. Beard DJ, Harris K, Dawson J, *et al*. Meaningful changes for the Oxford hip and knee scores after joint replacement surgery. *J Clin Epidemiol* 2015;68:73–9.

21. Abane L, Anract P, Boisgard S, *et al*. A comparison of patient-specific and conventional instrumentation for total knee arthroplasty: a multicentre randomised controlled trial. *Bone Joint J* 2015;97-B:56–63.

22. Barrack RL, Ruh EL, Williams BM, *et al*. Patient specific cutting blocks are currently of NO proven value. *The Journal of Bone and Joint Surgery. British volume* 2012;94-B(11_Supple_A):95–9.

23. Boonen B, Schotanus MGM, Kort NP. Preliminary experience with the patient-specific templating total knee arthroplasty. *Acta Orthop* 2012;83:387–93.

24. Chareancholvanich K, Narkbunnam R, Pornrattanamaneewong C. A prospective randomised controlled study of patient-specific cutting guides compared with conventional instrumentation in total knee replacement. *Bone Joint J* 2013;95-B:354–9.

25. Noble JW, Moore CA, Liu N. The value of Patient-Matched instrumentation in total knee arthroplasty. *The Journal of Arthroplasty* 2012;27:153–5.

26. Nunley RM, Ellison BS, Ruh EL, *et al*. Are patient-specific cutting blocks cost-effective for total knee arthroplasty? *Clin Orthop Relat Res* 2012;470:889–94.

27. Pfitzner T, Abdel MP, von Roth P, *et al*. Small improvements in mechanical axis alignment achieved with MRI versus CT-based patient-specific instruments in TKA: a randomized clinical trial. *Clin Orthop Relat Res* 2014;472:2913–22.

28. Pietsch M, Djahani O, Zweiger C, *et al*. Custom-fit minimally invasive total knee arthroplasty: effect on blood loss and early clinical outcomes. *Knee Surg Sports Traumatol Arthrosc* 2013;21:2234–40.

29. Barke S, Musanhu E, Busch C, *et al*. Patient-matched total knee arthroplasty : Does it offer any clinical advantages. *Acta Orthop Belg* 2013;79:307–11.

30. Barrett W, Hoeffel D, Dalury D, *et al*. In-vivo alignment comparing patient specific instrumentation with both conventional and computer assisted surgery (Cas) instrumentation in total knee arthroplasty. *J Arthroplasty* 2014;29:343–7.

31. Stronach BM, Pelt CE, Erickson J, *et al*. Patient-specific total knee arthroplasty required frequent Surgeon-directed changes. *Clin Orthop Relat Res* 2013;471:169–74.

32. Hamilton WG, Parks NL, Saxena A. Patient-specific instrumentation does not shorten surgical time: a prospective, randomized trial. *J Arthroplasty* 2013;28(8 Suppl):96–100.

33. Dell'Osso G, Celli F, Bottai V, *et al*. Single-use instrumentation technologies in knee arthroplasty: state of the art. *Surg Technol Int* 2016;28:243–6.

34. Dehnavieh R, Mirshekari N, Ghasemi S, *et al*. Health Technology assessment: Off-site sterilization. *Med J Islam Repub Iran* 2016;30.

35. Peersman G, Laskin R, Davis J, *et al*. Prolonged operative time correlates with increased infection rate after total knee arthroplasty. *HSS Jrnl* 2006;2:70–2.

36. Cendán JC, Good M. Interdisciplinary work flow assessment and redesign decreases operating room turnover time and allows for additional caseload. *Archives of Surgery* 2006;141:65–9.

37. Medacta & Solvay. Carbon footprint of single-use and reusable surgical instruments. Alpharetta, GA 2016;3.

38. Huijbregts HJTAM, Khan RJK, Sorensen E, *et al*. Patient-specific instrumentation does not improve radiographic alignment or clinical outcomes after total knee arthroplasty. *Acta Orthop* 2016;87:386–94.

39. Voleti PB, Hamula MJ, Baldwin KD, *et al*. Current data do not support routine use of patient-specific instrumentation in total knee arthroplasty. *J Arthroplasty* 2014;29:1709–12.

ANNEX H: RAW KINEMATIC DATA

C001 6 DoF Kinematics [Raw Data]

		Frame Number	1	2	3	4	5	6	7	8	9	10	11	12	13	14	Min	Max	Range
alpha (Flex/Ext angle)	Left	JCS	28.16881	20.89179	13.62798	6.889071	2.898417	-1.16451	-4.14206	-3.19068	-1.00911	0.738127	2.450016	8.624415	13.5779	14.10909	-4.14206	28.16881	32.31088
		TEA	29.87548	22.60279	15.34554	8.615079	4.581151	0.530964	-2.46313	-1.49621	0.623468	2.395461	4.090696	10.28167	15.27	15.76546	-2.46313	29.87548	32.33861
		GCA	28.37352	21.06635	13.77639	7.016225	3.018368	-1.05446	-4.03543	-3.08444	-0.89159	0.855995	2.57267	8.759395	13.72606	14.25866	-4.03543	28.37352	32.40895
		FEA	29.69966	22.38392	15.03833	8.20283	4.12271	-0.00487	-3.0502	-2.06749	0.102873	1.904415	3.639775	9.944721	14.98746	15.52743	-3.0502	29.69966	32.74986
	Right	JCS	24.65084	18.31065	13.49764	5.206958	2.01747	-2.01583	-4.03747	-4.19955	-2.29354	-0.04405	1.477871	6.104372	10.33021	12.45817	-4.19955	24.65084	28.85039
		TEA	26.11222	19.77334	14.97914	6.67139	3.502131	-0.55372	-2.59061	-2.76381	-0.82099	1.391964	2.92532	7.557109	11.80266	13.93019	-2.76381	26.11222	28.87603
		GCA	24.77773	18.42295	13.59412	5.29682	2.09559	-1.93252	-3.94939	-4.10703	-2.21467	0.051372	1.570158	6.199895	10.42446	12.55617	-4.10703	24.77773	28.88476
		FEA	28.99573	22.07854	16.79176	7.627236	4.189751	-0.2884	-2.54282	-2.76254	-0.55135	1.769195	3.476764	8.584369	13.29157	15.63686	-2.76254	28.99573	31.75827
beta (Ab/Adduction angle)	Left	JCS	4.978138	4.486889	4.092351	3.797548	3.030312	2.984644	2.637953	2.873844	2.212942	2.604021	2.47867	3.003515	3.744881	3.291381	2.212942	4.978138	2.765196
		TEA	1.887861	1.873557	1.997063	2.213086	2.040445	1.761075	1.936124	2.093917	1.258733	1.508209	1.287682	1.654235	1.373557	1.162881	1.162881	2.213086	1.050205
		GCA	7.028397	6.590001	6.214299	5.906417	5.117647	5.03963	4.662667	4.908822	4.269388	4.675468	4.562961	5.118564	5.866841	5.413138	4.269388	7.028397	2.759009
		FEA	-8.80077	-9.63193	-10.1399	-10.3351	-10.95	-10.7708	-10.9076	-10.7431	-11.5508	-11.2648	-11.4796	-11.1734	-10.4873	-10.9404	-11.5508	-8.80077	2.750035
	Right	JCS	3.824925	3.250692	3.579969	2.632855	2.966048	2.305939	1.931674	1.708083	2.508898	1.814665	2.105403	2.372208	3.090024	3.200844	1.708083	3.824925	2.116842
		TEA	-0.57731	-1.02551	-0.56583	-1.21967	-0.75236	-1.22536	-1.49906	-1.71415	-1.00815	-1.80951	-1.58826	-1.51581	-0.95364	-0.91272	-1.80951	-0.56583	1.243678
		GCA	5.881589	5.27072	5.555592	4.499602	4.780279	4.045901	3.631168	3.404283	4.244378	3.592169	3.910329	4.25271	5.028826	5.165057	3.404283	5.881589	2.477306
		FEA	-24.0251	-24.8827	-24.5273	-24.9367	-24.2371	-24.2977	-24.3166	-24.5069	-24.0506	-25.0912	-25.0189	-25.2841	-24.8853	-24.8731	-25.2841	-24.0251	1.258999
gamma (Int/External Rotation angle)	Left	JCS	-7.05156	-7.83526	-6.18583	-5.27506	-3.05714	-4.55493	1.838739	1.441033	0.449561	-1.67246	-6.89084	-3.74948	-4.92654	-4.53002	-7.83526	1.838739	9.673998
		TEA	-7.83526	-11.7737	-10.4229	-9.72881	-7.60869	-4.6801	-2.83384	-3.2198	-4.17647	-6.26784	-8.15119	-8.15119	-9.16465	-9.53823	-11.7737	-2.83384	8.939877
		GCA	-8.11905	-8.11905	-6.1997	-5.03856	-2.6742	-2.6742	2.475194	2.043889	-1.21111	-1.21111	-1.93161	-3.5775	-4.93854	-5.35228	-8.11905	2.475194	10.59424
		FEA	-3.47743	-6.03561	-6.19307	-6.96272	-5.73638	-3.7021	-2.55067	-2.71806	-3.19306	-4.88529	-5.12533	-5.00913	-4.94631	-5.2073	-6.96272	-2.55067	4.412051
	Right	JCS	-6.4691	-5.37773	-4.62094	-1.46884	2.707906	2.130684	7.011846	6.492943	6.620713	4.912128	2.967863	-1.73504	-1.25355	-2.42627	-6.4691	7.011846	13.48094
		TEA	-7.36787	-6.7569	-6.35362	-3.78126	0.185114	-2.130684	4.110276	3.581369	3.825445	2.256162	0.409416	1.379248	-3.2167	-2.33396	-7.36787	4.110276	11.47815
		GCA	-6.25093	-4.93308	-4.00738	-0.57692	3.703037	6.028716	8.191769	7.677392	7.749081	5.970513	3.978931	-4.88829	-0.53187	-1.77722	-6.25093	8.191769	14.4427
		FEA	-7.31956	-4.43959	-6.18059	-7.31956	-4.72925	-4.55493	-3.45499	-2.27291	-2.9625	-3.62162	-4.7903	-4.88829	-4.46086	-4.53002	-7.31956	-2.27291	5.046644
Q1 (Medio-Lateral Tibial displacement)	Left	JCS	8.058095	8.619139	8.8747	9.310516	9.802965	9.840519	9.929984	9.677492	10.34957	10.15604	10.11188	10.08478	9.427934	9.232469	8.058095	10.34957	2.291476
		TEA	6.465611	7.02322	7.249864	7.679881	8.158148	8.191463	8.280644	8.032932	8.698653	8.517085	8.474594	8.459402	7.814703	7.615588	6.465611	8.698653	2.233041
		GCA	3.749921	4.315465	4.608901	5.052311	5.563334	5.60644	5.696277	5.437526	6.117932	5.908741	5.862389	5.819689	5.146934	4.956248	3.749921	6.117932	2.368011
		FEA	12.84348	13.37016	13.33643	13.71424	14.06482	14.05997	14.14659	13.94191	14.55038	14.4765	14.44906	14.5411	14.00577	13.77379	12.84348	14.55038	1.706901
	Right	JCS	9.737526	10.38804	10.49045	11.05333	10.54011	10.86423	11.1449	11.04024	11.58224	10.95546	10.94927	10.45851	10.44327	10.36748	9.737526	11.58224	1.84471
		TEA	13.11668	13.72275	13.75697	14.29407	13.7658	14.06685	14.33206	14.20693	14.75332	14.16305	14.1595	13.70218	13.7207	13.65049	13.11668	14.75332	1.63664
		GCA	7.899843	8.576357	8.718646	9.296603	8.792183	9.129794	9.419519	9.326832	9.866252	9.218131	9.210384	8.700074	8.665082	8.586028	7.899843	9.866252	1.966409
		FEA	24.17393	24.50576	24.11928	24.49729	23.87621	24.03491	24.20465	23.95323	24.52676	24.16171	24.1745	23.92348	24.15033	24.11456	23.87621	24.52676	0.650543
Q2 (Antero-Posterior Tibial Drawer)	Left	JCS	22.00812	21.82325	20.7799	19.93239	19.0368	18.02507	17.02825	17.00485	17.69799	18.14255	19.13168	20.09481	20.89533	20.60796	17.00485	22.00812	5.003275
		TEA	16.94618	16.2174	14.71947	13.58109	12.52358	11.42718	10.38131	10.38268	11.06612	11.57253	12.59342	13.77841	14.83317	14.55222	10.38131	16.94618	6.564866
		GCA	14.68943	14.98619	14.53404	14.33023	13.85444	13.29612	12.64868	12.512	12.95398	13.20018	14.00039	14.32043	14.65539	14.32042	12.512	14.98619	2.474193
		FEA	9.23675	9.662531	9.419105	9.487594	9.188367	8.850198	8.372171	8.187804	8.47717	8.644679	9.351628	9.395363	9.546562	9.194076	8.187804	9.662531	1.474727
	Right	JCS	24.32268	23.36482	23.64522	20.97868	20.09405	19.2451	18.65153	18.9173	19.3846	19.5835	19.94156	20.90316	21.14072	22.38059	18.65153	24.32268	5.671154
		TEA	17.19323	15.92312	16.02069	13.21258	12.32932	11.49214	10.91877	11.17368	11.62878	11.79924	12.15408	13.13888	14.42583	14.7396	10.91877	17.19323	6.274466
		GCA	16.0847	15.71702	16.50565	14.84337	14.37712	14.08818	13.78839	14.07895	14.2665	14.15539	14.30269	14.65433	15.34258	15.36101	13.78839	16.50565	2.717262
		FEA	11.41944	11.26126	12.21691	10.95705	10.68322	10.60133	10.40239	10.67888	10.79371	10.52101	10.59414	10.71308	11.21424	11.13631	10.40239	12.21691	1.814518
Q3 (Tibial Distraction-Compression)	Left	JCS	24.11876	25.38542	26.12119	27.85112	28.62301	29.7447	30.73479	30.58868	29.73996	29.63467	29.17429	27.67948	26.64526	26.52405	24.11876	30.73479	6.616032
		TEA	28.98705	29.42832	29.27807	30.13241	30.36823	30.93846	31.51994	31.51398	30.95761	31.09506	30.84688	30.19844	29.80291	29.74119	28.98705	31.51994	2.532894
		GCA	20.82525	21.13125	20.99499	21.98992	22.3165	23.08443	23.81438	23.7668	23.02335	23.09848	22.77998	21.9096	21.47065	21.38541	20.82525	23.81438	2.989131
		FEA	21.34305	22.04971	21.34305	21.83137	21.96721	22.36422	22.85845	22.82049	22.50707	22.6646	22.4927	22.17517	21.97644	21.91785	21.34305	22.85845	1.515396
	Right	JCS	23.10841	24.32784	24.34973	27.11775	29.03393	29.52959	29.53291	29.31454	29.31018	28.53731	28.02016	26.9703	25.92813	25.32294	23.10841	29.53291	6.424496
		TEA	26.85829	27.26817	26.56668	28.1935	28.46696	28.9187	29.22959	28.98187	28.49628	28.83953	28.52725	28.15715	27.71309	27.41745	26.56668	29.22959	2.662912
		GCA	17.93704	18.24205	17.65195	19.42947	19.93332	20.64871	20.95755	20.72107	20.10343	20.31156	19.92758	19.38913	18.84062	18.49358	17.65195	20.95755	3.305592
		FEA	23.78316	24.01954	23.04074	24.42474	24.30395	24.79944	25.05485	24.77956	24.55974	24.79088	24.54392	24.21438	23.977	23.78325	23.04074	25.05485	2.014112

CO02 6 DoF Kinematics [Raw Data]

		Frame Number	1	2	3	4	5	6	7	8	9	10	11	12	13	14	15	16	17	18	Min	Max	Range
alpha (Flex/Ext angle)	Left	JCS	-3.03308	-1.48311	-1.82227	3.138677	6.811921	10.5274	14.99469	19.02424	23.37674	30.39483	34.89004	39.92822	44.55793	51.99511	58.16508	60.86916	60.08048	56.40841	-3.03308	60.86916	63.90223
		TEA	-0.67467	0.800847	0.350512	5.420556	9.030704	12.9914	17.6048	21.63091	26.14768	33.07221	37.58462	42.60004	47.22166	54.5575	60.60938	63.23799	62.43988	58.83657	-0.67467	63.23799	63.91266
		GCA	-2.04302	-0.52662	-0.93221	4.120765	7.775231	11.66711	16.25916	20.31276	24.8112	31.80711	36.34493	41.39753	46.05245	53.44987	59.54717	62.1883	61.38119	57.75743	-2.04302	62.1883	64.23132
		FEA	-2.2274	-0.6692	-1.03224	4.015119	7.723046	11.57318	16.17897	20.28932	24.82057	31.94766	36.56189	41.70659	46.45019	53.98172	60.17127	62.83409	62.0043	58.33653	-2.2274	62.83409	65.06149
	Right	JCS	1.540291	1.419731	1.44784	6.140392	9.885542	12.7085	16.89898	20.67894	24.35681	30.38606	35.32321	39.17007	46.04566	52.75028	59.15822	61.65884	60.23669	56.90623	1.419731	61.65884	60.23911
		TEA	3.967021	3.853858	3.879117	8.4986	12.17609	14.98127	19.10583	22.89418	26.5755	32.57325	37.46215	41.31063	48.07481	54.69244	61.02016	63.49	62.08481	58.79733	3.853858	63.49	59.63615
		GCA	1.872408	1.752131	1.780152	6.465791	10.20553	13.02454	17.20933	20.98299	24.65383	30.67121	35.59909	39.43343	46.30001	52.99459	59.39747	61.89149	60.46922	57.1427	1.752131	61.89149	60.13936
		FEA	2.358809	2.241438	2.268342	6.924702	10.63757	13.44821	17.60615	21.37732	25.04189	31.03347	35.93133	39.74643	46.55748	53.20059	59.56039	62.02942	60.61473	57.31376	2.241438	62.02942	59.78798
beta (Ab/Adduction angle)	Left	JCS	2.703702	2.377008	1.665091	2.759128	2.683563	4.57097	5.95918	6.368481	8.006028	9.023506	9.635078	10.39578	10.92074	11.00843	10.84598	10.67557	10.317	10.3413	1.665091	11.00843	9.343336
		TEA	2.285195	1.710826	1.063503	1.340062	0.677477	1.955111	2.63752	2.438214	3.428443	2.710315	2.908448	2.920684	3.175601	2.991943	2.076375	2.076141	1.770674	2.056454	0.677477	3.428443	2.750966
		GCA	5.084998	4.614511	3.937666	4.552622	4.117561	5.625547	6.555962	6.553554	7.73927	7.270258	7.59451	7.7127	8.032605	7.886723	7.457688	6.912106	6.616213	6.936012	3.937666	8.032605	4.094939
		FEA	9.199635	8.830798	8.128816	9.05854	8.830981	10.53618	11.6717	11.82377	13.14924	12.83128	13.20852	13.34369	13.6398	13.37893	12.78539	12.14977	11.88287	12.31869	8.128816	13.6398	5.510982
	Right	JCS	7.006191	7.056799	7.03526	6.916125	6.706634	6.858576	6.661764	7.231504	7.8014	8.389342	8.609475	9.658779	9.218999	9.162608	8.727541	9.079721	9.285886	9.361386	6.661764	9.658779	2.997015
		TEA	2.837809	2.813198	2.172692	1.569988	1.438109	1.082896	0.846179	1.354713	1.513286	1.438597	1.382775	2.293662	1.591512	1.259639	0.899964	1.259639	1.459741	1.539617	0.846179	2.837809	1.991629
		GCA	6.304525	6.355391	6.333792	6.20692	5.99466	6.146522	5.952771	6.52852	7.107192	7.715674	7.958179	9.028253	8.632628	8.627405	8.248106	8.623691	8.816418	8.861612	5.952771	9.028253	3.075481
		FEA	3.596117	3.652305	3.629475	3.302497	2.944381	2.994586	2.664244	3.131448	3.618696	4.108488	4.28326	5.319268	4.930563	3.342473	3.183944	5.046376	5.214134	5.209623	2.664244	5.319268	2.655024
gamma (Int/External Rotation angle)	Left	JCS	13.71062	14.9428	15.40287	12.51568	12.57146	11.73325	12.68675	15.70419	14.95134	15.825	15.75723	15.4402	15.44	16.45065	15.55194	16.45065	15.08181	14.74241	11.73325	16.45065	4.7174
		TEA	4.335081	5.584512	6.043526	3.241547	3.408208	2.714142	7.5329	8.916675	7.478393	8.220525	8.602891	8.852637	9.412165	11.40503	11.38587	11.5621	11.20049	10.32282	2.714142	11.5621	8.847961
		GCA	8.358828	9.531497	10.00985	6.939991	6.893898	5.960196	9.070867	9.808645	10.00796	10.02351	9.855082	10.00256	9.492563	11.38483	10.84598	10.79892	11.20049	9.935258	5.960196	11.38483	5.424639
		FEA	12.2344	13.2911	13.79274	10.34246	9.995986	8.745018	9.22116	11.08136	11.39383	10.90896	10.47173	9.794455	9.492563	10.1188	8.992426	8.70078	8.48513	8.256239	8.256239	13.79274	5.536503
	Right	JCS	6.009445	6.0112	5.99534	4.156372	1.668578	1.085296	0.320309	-0.59285	-0.60524	0.620345	2.011572	2.140087	2.427673	2.866823	2.651406	2.202375	2.187097	3.132728	-0.60524	6.01112	6.616358
		TEA	-0.60081	-0.60835	-0.62193	-2.09173	-4.25532	-4.57878	-4.93252	-5.06158	-5.45213	-3.13641	-1.14103	-0.52697	0.65995	1.999236	2.655024	2.545531	2.337633	2.829606	-5.45213	2.829606	8.281741
		GCA	5.886391	5.886569	5.87114	4.090341	1.649292	1.101294	0.388571	-0.44466	-0.47762	0.853831	2.302862	2.475769	2.836911	3.342473	3.183944	2.756064	2.729458	3.64666	-0.47762	5.886569	6.364185
		FEA	3.313166	3.307502	3.293462	1.74305	-0.50278	-0.89823	-1.37506	-1.76854	-2.02161	-0.09722	1.66558	2.085565	2.894493	3.835654	4.087159	3.816972	3.701238	4.407089	-2.02161	4.407089	6.428694
O1 (Medio-Lateral Tibial displacement)	Left	JCS	12.99313	13.08316	12.26943	12.53067	11.66737	11.5873	10.03961	9.758672	8.916675	8.220525	7.754454	7.379611	7.122166	6.29633	5.731458	5.377216	5.83453	6.130432	5.377216	13.08316	7.705944
		TEA	10.44062	10.52409	9.720999	9.993411	9.141112	9.069201	7.5329	6.428801	5.638734	5.736382	5.256603	4.866338	4.604257	3.75334	3.176415	2.806946	3.267814	3.576914	2.806946	10.52409	7.717146
		GCA	7.499438	7.601506	6.768267	7.009028	6.125561	6.030542	4.46197	3.495093	3.30451	2.601522	2.16058	1.814007	1.565061	0.785203	0.242426	-0.0839	0.366897	0.638606	-0.0839	7.601506	7.685408
		FEA	5.117988	5.24944	4.368574	4.55933	3.62662	3.495093	1.875533	1.480366	0.633768	-0.08592	-0.4655	-0.74304	-0.97124	-1.63883	-2.12765	-2.38583	-1.95093	-1.7383	-2.38583	5.24944	7.635265
	Right	JCS	11.25781	11.27357	11.21605	11.09183	10.87368	10.50701	10.53967	10.33246	9.125983	8.208878	8.208878	9.536693	8.073764	7.277849	6.918565	6.600384	6.384314	6.71127	6.384314	11.27357	4.889261
		TEA	7.790414	7.802155	7.572914	7.572914	5.638734	6.914394	6.937007	6.680694	5.638734	4.554256	4.512256	3.814805	4.511322	3.752638	3.453194	3.143723	2.924038	3.223224	2.924038	7.802155	4.878117
		GCA	9.505715	9.520844	9.33162	9.33162	9.107999	8.735182	8.551312	8.551312	7.526427	6.425392	6.425374	5.684196	6.306695	5.516644	5.166787	4.955884	4.633339	4.955884	4.633339	9.520844	4.887505
		FEA	16.44932	16.44533	16.47232	16.67782	16.56231	17.26492	17.42089	17.35375	16.44655	14.81138	14.59059	14.26494	13.0345	13.81992	14.2481	14.73221	14.43512	13.9347	13.0345	17.42089	4.386392
O2 (Antero-Posterior Tibial Drawer)	Left	JCS	17.64582	18.65007	17.798	20.5299	20.92575	22.37145	22.47013	22.58332	21.23983	21.89857	21.48437	21.4535	22.28021	22.7084	24.29459	23.89462	23.73469	23.5340	17.64582	24.29459	6.648762
		TEA	10.71741	11.54988	10.6884	13.16979	13.35483	14.77591	14.83704	14.92239	13.67702	14.37932	14.09029	14.23814	15.30223	16.16014	18.1547	17.97735	17.7494	17.25466	10.6884	18.15473	7.466329
		GCA	14.19044	14.87208	14.06866	15.90256	15.62643	16.48978	15.8986	15.40793	13.49786	13.2291	12.30784	11.76575	12.2403	12.11127	13.37634	12.87925	12.73808	12.67809	11.76575	16.48978	4.72403
		FEA	11.93715	12.67452	11.87846	13.83824	13.68753	14.21459	14.24459	13.88896	12.15846	12.22326	11.52232	11.23491	11.91569	12.20767	13.77565	13.40737	13.22366	12.98356	11.23491	14.65079	3.415885
	Right	JCS	23.02237	23.92381	21.02455	24.12173	25.35663	25.86121	26.70042	26.70042	26.7772	25.86776	26.15851	26.16879	25.40413	26.47234	26.99925	27.48365	27.19398	26.67298	21.00455	27.48365	6.459097
		TEA	12.2413	13.11568	10.26189	12.94326	13.90058	14.26223	14.89148	15.33414	14.90268	14.0822	14.5137	14.7281	15.3022	16.05255	17.29233	18.09416	17.62045	16.70868	10.26189	18.09416	7.832268
		GCA	16.44138	17.16113	14.46278	16.65272	16.17999	17.21142	17.35375	16.32628	16.32628	14.65422	14.41065	14.06424	12.80523	13.5656	13.96718	14.1545	14.45549	13.66536	12.80523	17.36117	4.555937
		FEA	16.44932	16.44533	16.47232	16.67782	16.56231	17.26492	17.42089	17.36954	16.44655	14.81138	14.59059	14.26494	13.0345	13.81992	14.2481	14.73221	14.43512	13.9347	13.0345	17.42089	4.386392
O3 (Tibial Distraction-Compression)	Left	JCS	34.55225	33.74285	34.68237	33.43596	32.99476	31.75722	31.0848	31.25254	30.83878	30.15765	29.20619	28.13597	27.28829	25.77077	23.89127	23.76288	24.16835	24.78015	23.76288	34.68237	10.91949
		TEA	30.37503	29.80144	30.68525	30.26668	30.45911	29.90874	30.03562	30.94513	31.41651	31.91941	31.77325	31.55443	31.44617	30.97706	29.80894	29.97803	30.32952	30.50211	29.80144	31.91941	2.117973
		GCA	23.22889	22.51642	23.42677	22.68665	22.67092	22.00419	22.06613	22.8584	23.3029	23.80204	23.72889	23.64707	23.7445	23.70917	23.01554	23.39206	23.63316	23.51941	22.00419	23.80204	1.797846
		FEA	24.19303	23.50448	24.44951	23.85128	23.99533	23.46662	23.78388	24.68823	25.28967	25.95406	25.96618	25.95162	26.09049	26.12572	25.46423	25.85008	26.05997	25.94505	23.46662	26.12572	2.659106
	Right	JCS	33.2848	32.33599	33.43628	33.43628	31.84584	31.57907	30.32806	29.95871	29.64461	30.0938	28.143	27.36008	25.85546	24.32354	22.87276	22.33723	22.58549	23.578	22.33723	33.43628	11.09905
		TEA	29.05844	28.04776	29.27505	29.36443	29.48006	29.85487	30.13746	30.66686	30.66686	31.63332	31.84439	31.84439	31.95228	31.67074	31.1536	31.2536	31.44447	31.24447	28.04776	31.95228	3.904512
		GCA	22.8215	21.86176	22.97737	22.64572	22.41932	22.58261	22.30444	22.70859	22.70859	23.37815	23.43382	23.56856	23.50713	23.44374	23.3869	23.44954	23.39784	23.65052	21.86176	23.65052	1.788759
		FEA	23.41433	22.44398	23.58582	23.27958	23.0743	23.24035	22.66471	23.001	23.36387	24.05872	24.07452	24.16719	24.17474	24.05332	23.96265	23.99601	23.93628	24.22001	22.44398	24.22001	1.776023

C003 6 DoF Kinematics [Raw Data]			1	2	3	4	5	6	7	8	MIN	MAX	RANGE
Frame Number			1	2	3	4	5	6	7	8	MIN	MAX	RANGE
alpha (Flex/Ext angle)	Left	JCS	12.98273	25.34298	35.70478	41.95909	48.3994	54.24916	60.91958	70.45062	12.98273	70.45062	57.46789
		TEA	13.89179	26.04994	36.23039	42.37252	48.74051	54.58806	61.23422	70.70433	13.89179	70.70433	56.81255
		GCA	12.78834	25.01291	35.25357	41.44215	47.85922	53.7404	60.42992	69.97677	12.78834	69.97677	57.18843
		FEA	12.93775	25.15189	35.39026	41.57409	47.97338	53.82775	60.49425	70.01253	12.93775	70.01253	57.07478
	Right	JCS	8.581588	20.83794	29.33855	34.67581	39.23545	46.09936	52.97009	63.68134	8.581588	63.68134	55.09975
		TEA	9.954282	22.05996	30.4692	35.78227	40.33318	47.1399	54.00732	64.71314	9.954282	64.71314	54.75885
		GCA	8.598264	20.72943	29.17274	34.51935	39.0957	45.93063	52.83144	63.58869	8.598264	63.58869	54.99042
		FEA	9.559978	21.66532	30.07483	35.38929	39.94125	46.74736	53.61543	64.32158	9.559978	64.32158	54.7616
beta (Ab/Adduction angle)	Left	JCS	10.90237	10.42636	10.32929	10.24237	9.72217	8.785681	8.027938	7.251217	7.251217	10.90237	3.651153
		TEA	1.332961	1.261032	1.824655	2.269912	2.397518	2.133007	2.224569	2.793176	1.261032	2.793176	1.532144
		GCA	6.073272	6.303603	6.945826	7.360049	7.393391	6.987784	6.857338	7.001897	6.073272	7.393391	1.320119
		FEA	5.743601	5.588358	5.931759	6.180538	6.057011	5.522368	5.263821	5.263355	5.263355	6.180538	0.917183
	Right	JCS	9.067253	8.996978	8.64622	7.962521	7.348553	7.113073	6.33019	5.300857	5.300857	9.067253	3.766395
		TEA	1.113393	1.264784	1.273297	0.898651	0.597536	0.910858	0.768463	0.893635	0.597536	1.273297	0.675761
		GCA	4.798528	5.534499	5.838555	5.600303	5.383729	5.766778	5.625143	5.61232	4.798528	5.838555	1.040026
		FEA	1.156922	1.352932	1.390246	1.032539	0.745023	1.076921	0.950898	1.096293	0.745023	1.390246	0.645223
gamma (Int/External Rotation angle)	Left	JCS	4.646504	4.626189	0.834731	1.567104	0.580505	-1.91376	-2.72325	-3.80505	-3.80505	4.646504	8.451553
		TEA	5.534316	7.533721	5.338931	6.969507	6.840876	5.056809	4.970679	4.743363	4.743363	7.533721	2.790358
		GCA	7.476978	8.429861	5.325348	6.404223	5.71041	3.420884	2.780533	1.814251	1.814251	8.429861	6.61561
		FEA	5.610196	6.675404	3.725173	4.922342	4.37048	2.226655	1.766205	1.079202	1.079202	6.675404	5.596202
	Right	JCS	2.854512	-2.33078	-4.2634	-5.2542	-5.51542	-5.6115	-5.57588	-4.97091	-5.6115	2.854512	8.466012
		TEA	3.060293	-0.44587	-1.25908	-1.57922	-1.29214	-0.61296	0.127055	1.664805	-1.57922	3.060293	4.63951
		GCA	6.241348	1.890838	0.426082	-0.3265	-0.41819	-0.31413	-0.15908	0.478103	-0.41819	6.241348	6.659541
		FEA	3.277713	-0.2424	-1.07069	-1.40249	-1.12662	-0.46607	0.253027	1.754693	-1.40249	3.277713	4.680208
Q1 (Medio-Lateral Tibial displacement)	Left	JCS	5.108887	5.180641	5.030957	4.448657	3.538747	4.141336	4.185168	4.954539	3.538747	5.180641	1.641894
		TEA	9.308473	9.603698	9.423719	8.804281	7.808891	8.363476	8.224372	8.874175	7.808891	9.603698	1.794808
		GCA	6.268987	6.465779	6.299144	5.696064	4.738326	5.314056	5.25553	5.958	4.738326	6.465779	1.727453
		FEA	6.70631	6.901009	6.734658	6.131926	5.174988	5.751167	5.694354	6.397943	5.174988	6.901009	1.726021
	Right	JCS	2.171578	0.913573	-0.05412	-0.5991	-0.67689	-1.43746	-1.93614	-2.29023	-2.29023	2.171578	4.461809
		TEA	7.75497	6.619657	5.768633	5.124483	5.071564	4.197193	3.603036	3.079973	3.079973	7.75497	4.674998
		GCA	5.392486	4.206298	3.306898	2.703868	2.640635	1.813453	1.258887	0.805889	0.805889	5.392486	4.586598
		FEA	7.011363	5.877402	5.027664	4.382421	4.329776	3.454151	2.858941	2.334015	2.334015	7.011363	4.677348
Q2 (Antero-Posterior Tibial Drawer)	Left	JCS	23.78669	25.47546	24.4097	25.09257	26.2553	27.00754	27.37396	28.87072	23.78669	28.87072	5.084024
		TEA	14.77974	16.24278	15.33484	16.25469	17.79287	19.01524	20.01167	22.5684	14.77974	22.5684	7.788664
		GCA	14.28304	14.25396	12.13172	12.3715	13.25734	13.91218	14.32928	16.19647	12.13172	16.19647	4.064741
		FEA	17.28544	17.65467	15.75476	16.07164	16.98608	17.62426	17.97782	19.67177	15.75476	19.67177	3.917004
	Right	JCS	22.48724	23.6026	23.43809	23.43287	24.14921	24.51254	25.18023	26.01578	22.48724	26.01578	3.52854
		TEA	12.00678	13.19833	13.41463	13.76249	14.86768	15.89744	17.39062	19.747	12.00678	19.747	7.740221
		GCA	13.41047	12.85984	11.83046	11.43127	11.89441	12.00384	12.61847	13.728	11.43127	13.728	2.296724
		FEA	12.47257	12.93413	12.63441	12.67142	13.512	14.1648	15.30073	17.15606	12.47257	17.15606	4.683495
Q3 (Tibial Distraction-Compression)	Left	JCS	28.61974	26.41265	25.27989	24.16456	22.39975	21.22094	19.42783	16.64616	16.64616	28.61974	11.97358
		TEA	28.09357	27.86647	28.34897	28.06711	27.06738	26.72022	25.72699	23.97637	23.97637	28.34897	4.372598
		GCA	20.58168	20.4632	21.29842	21.41752	20.95091	21.02448	20.64981	19.87581	19.87581	21.41752	1.541717
		FEA	22.75503	22.03014	22.29795	22.04325	21.17045	20.90529	20.12616	18.80923	18.80923	22.75503	3.945796
	Right	JCS	29.5586	27.18331	26.86268	25.44189	24.81099	23.12244	21.4187	18.88197	18.88197	29.5586	10.67664
		TEA	29.39756	29.17511	30.3121	29.7803	29.91404	29.22913	28.4851	27.27442	27.27442	30.3121	3.037683
		GCA	21.14415	20.70653	21.91841	21.53663	21.84173	21.57214	21.34384	21.11862	20.70653	21.91841	1.211883
		FEA	26.07266	25.79185	26.9751	26.50805	26.72523	26.212	25.6827	24.89311	24.89311	26.9751	2.081991

C004 6 DoF Kinematics [Raw Data]			1	2	3	4	5	6	7	8	9	Min	Max	Range
Frame Number			1	2	3	4	5	6	7	8	9	Min	Max	Range
alpha (Flex/Ext angle)	Left	JCS	24.46573	34.47206	41.30249	48.21495	58.51267	71.17565	75.51089	75.90187	75.98656	24.46573	75.98656	51.52084
		TEA	26.79359	36.7135	43.52702	50.3263	60.54536	73.09595	77.39603	77.77951	77.86726	26.79359	77.86726	51.07367
		GCA	25.28964	35.26837	42.08436	48.96505	59.2268	71.84958	76.16724	76.55409	76.64086	25.28964	76.64086	51.35121
		FEA	24.61521	34.55617	41.35499	48.19743	58.4172	71.00337	75.29634	75.67505	75.76694	24.61521	75.76694	51.15173
	Right	JCS	20.7879	30.71441	38.2927	45.74733	53.33813	62.29585	71.14097	71.65173	71.58472	20.7879	71.65173	50.86383
		TEA	23.37635	33.20127	40.61942	48.08051	55.58264	64.53671	73.28172	73.78829	73.72163	23.37635	73.78829	50.41194
		GCA	21.77463	31.67629	39.19883	46.6559	54.20733	63.1626	71.95233	72.4604	72.39348	21.77463	72.4604	50.68577
		FEA	21.87712	31.73455	39.23717	46.67678	54.23487	63.06645	71.88797	72.39793	72.33303	21.87712	72.39793	50.52081
beta (Ab/Adduction angle)	Left	JCS	6.996958	7.246054	8.107466	7.305856	7.77469	6.623845	7.090795	7.40289	7.143586	6.623845	8.107466	1.483621
		TEA	1.817084	1.25767	1.668486	0.505887	0.61714	-0.65988	-0.15543	0.162038	-0.09602	-0.65988	1.817084	2.476967
		GCA	5.515722	5.609026	6.392366	5.536532	5.972201	4.859857	5.359843	5.675393	5.416863	4.859857	6.392366	1.532509
		FEA	2.641499	2.493464	3.165537	2.243575	2.668348	1.686779	2.267001	2.590537	2.33389	1.686779	3.165537	1.478757
	Right	JCS	6.619658	6.763349	5.782634	6.750976	6.268732	8.175533	7.042253	6.986256	6.965169	5.782634	8.175533	2.392899
		TEA	1.927507	1.05951	-0.57754	-0.15401	-1.06862	0.490192	-0.80295	-0.86258	-0.88322	-1.06862	1.927507	2.996122
		GCA	5.514866	5.302133	4.078735	4.836422	4.173416	5.913761	4.670465	4.609806	4.589321	4.078735	5.913761	1.835026
		FEA	-2.28171	-2.76702	-4.03818	-3.19072	-3.62473	-1.44215	-2.07342	-2.09368	-2.11943	-4.03818	-1.44215	2.596031
gamma (Int/External Rotation angle)	Left	JCS	5.992212	4.930802	4.11748	3.64326	2.044429	0.298535	0.631153	-0.14959	-1.15397	-1.15397	5.992212	7.146178
		TEA	0.849591	0.765011	0.69104	1.015753	0.671403	0.523611	1.404701	0.67326	-0.32045	-0.32045	1.404701	1.725148
		GCA	4.958666	4.171237	3.558043	3.29607	2.020513	0.671741	1.137482	0.368867	-0.63318	-0.63318	4.958666	5.591841
		FEA	3.3083	3.044097	2.808284	2.938903	2.25587	1.623199	2.325517	1.578049	0.580445	0.580445	3.3083	2.727855
	Right	JCS	5.270486	2.245628	1.799517	0.539761	2.821373	0.14615	-0.5698	-0.59845	-0.59704	-0.59845	5.270486	5.868941
		TEA	-1.05197	-3.174	-2.82209	-3.21924	0.004381	-1.497	-1.0155	-0.97442	-0.98216	-3.21924	0.004381	3.223624
		GCA	3.092378	0.291452	0.058565	-0.96669	1.582787	-0.75286	-1.10761	-1.115	-1.11636	-1.11636	3.092378	4.208733
		FEA	0.825827	-0.60426	0.22486	0.249683	3.843063	2.687612	3.416328	3.468587	3.459475	-0.60426	3.843063	4.447321
Q1 (Medio-Lateral Tibial displacement)	Left	JCS	7.412539	6.235033	6.226403	6.30698	7.173061	7.962933	7.731737	7.831177	7.767362	6.226403	7.962933	1.73653
		TEA	9.814839	8.623016	8.585375	8.62548	9.473804	10.23321	9.949069	10.05923	10.00166	8.585375	10.23321	1.647831
		GCA	7.463663	6.2805	6.260406	6.324992	7.184057	7.96189	7.709776	7.813452	7.752105	6.260406	7.96189	1.701483
		FEA	7.591914	6.39836	6.357211	6.392423	7.238599	7.994316	7.703778	7.815236	7.758421	6.357211	7.994316	1.637105
	Right	JCS	13.49555	13.19861	12.05591	12.04614	10.31949	11.09775	9.134811	10.1019	10.08788	9.134811	13.49555	4.360742
		TEA	12.27824	11.97082	10.79421	10.79413	9.047497	9.793102	7.787075	8.756059	8.730727	7.787075	12.27824	4.491168
		GCA	10.39202	10.09241	8.94105	8.933749	7.201997	7.971924	5.997982	6.965551	6.948647	5.997982	10.39202	4.394042
		FEA	14.38586	14.05731	12.81252	12.83194	11.04511	11.72502	9.632317	10.60512	10.55703	9.632317	14.38586	4.753544
Q2 (Antero-Posterior Tibial Drawer)	Left	JCS	25.62787	27.2356	26.66279	27.25918	29.08169	30.16231	29.71686	30.14552	30.27813	25.62787	30.27813	4.650264
		TEA	13.32711	15.73323	15.98526	17.49096	21.00526	24.59389	25.06853	25.56647	25.72309	13.32711	25.72309	12.39598
		GCA	13.32434	14.51027	13.89235	14.61052	16.96989	19.27332	19.36701	19.84186	19.98802	13.32434	19.98802	6.663679
		FEA	12.98998	12.6409	10.99106	10.71416	11.69137	12.50314	12.16277	12.60411	12.74112	10.71416	12.98998	2.275825
	Right	JCS	25.45506	25.35967	25.58945	26.53324	27.35745	28.0893	28.75196	28.81395	28.49603	25.35967	28.81395	3.454278
		TEA	12.32331	13.05813	14.12838	16.24404	18.3741	20.92471	23.50767	23.69647	23.63358	12.32331	23.69647	11.37317
		GCA	14.00732	13.35587	13.38849	14.39335	15.46783	16.78887	18.28389	18.40612	18.08067	13.35587	18.40612	5.050249
		FEA	14.23026	12.84493	12.33879	12.82281	13.41072	14.1601	15.21207	15.30945	14.99068	12.33879	15.30945	2.970662
Q3 (Tibial Distraction-Compression)	Left	JCS	27.29119	24.14251	22.6482	20.29617	16.63826	13.91025	12.33255	11.75867	11.91461	11.75867	27.29119	15.53252
		TEA	31.47058	30.55318	30.58509	29.62713	27.79716	26.81851	25.64292	25.09681	25.24989	25.09681	31.47058	6.373768
		GCA	23.99896	23.06893	23.15802	22.36531	20.98102	20.84698	20.07621	19.56844	19.73717	19.56844	23.99896	4.430519
		FEA	15.74335	14.94727	15.31759	14.89928	14.38136	15.54862	15.27256	14.82989	15.00097	14.38136	15.74335	1.361989
	Right	JCS	26.66894	24.29183	22.36268	20.92796	19.26113	16.48272	14.33998	14.35877	14.37665	14.33998	26.66894	12.32896
		TEA	31.32123	31.5818	31.32731	31.54813	31.07884	29.92184	28.51698	28.71636	28.73604	28.51698	31.5818	3.064824
		GCA	22.89749	22.71066	22.38723	22.66432	22.56201	21.7929	21.23478	21.38609	21.39448	21.23478	22.89749	1.662707
		FEA	20.36958	20.25039	19.90299	20.32516	20.18889	19.80602	19.34493	19.63168	19.63469	19.34493	20.36958	1.02465

P001 6 DoF Kinematics [Raw Data]

Measurement	Side	Method	1	2	3	4	5	6	7	8	9	10	11	12	13	14	15	16	17	18	Min	Max	Range
alpha (Flex/Ext angle)	Left	JCS	15.94906	13.74495	9.238459	6.408653	9.225523	8.697898	10.33849	11.0228	13.27727	14.46822	16.22598	18.84542	21.98126	27.91628	32.38232	37.13637	44.24772	54.27692	6.408653	54.27692	47.86827
	Left	TEA	18.54133	16.2294	11.75959	8.922282	11.69036	11.16741	12.82131	13.45385	15.84748	16.9533	18.6211	21.27335	24.4702	30.39394	34.86994	39.61239	46.68469	56.56588	8.922282	56.56588	47.6436
	Left	GCA	17.15303	14.86946	10.36881	7.522796	10.32034	9.793638	11.44896	12.10289	14.45561	15.59586	17.30072	19.95073	23.13901	29.08691	33.57589	38.33811	45.4445	55.37948	7.522796	55.37948	47.85668
	Left	FEA	16.52578	14.23458	9.74021	6.895407	9.686736	9.16079	10.81622	11.46514	13.82847	14.96054	16.65658	19.30764	22.49876	28.44147	32.92784	37.68555	44.78369	54.70287	6.895407	54.70287	47.80746
	Right	JCS	20.93004	18.40793	15.98653	13.53458	12.1481	12.96726	14.69835	16.93433	18.81153	22.01189	22.23736	23.98737	27.06817	31.8833	38.91475	40.34197	45.55434	52.88212	12.1481	52.88212	40.73402
	Right	TEA	22.44159	20.04299	17.46999	15.04837	13.68461	14.43585	16.23604	18.42629	20.01189	22.01189	23.75607	23.8741	26.98407	33.49004	38.37084	40.34197	47.02986	54.32543	13.68461	54.32543	40.64083
	Right	GCA	20.79098	18.32919	15.82285	13.38226	12.0505	12.79048	14.56064	16.7769	17.15842	20.35874	22.10488	23.8741	26.98407	33.49004	36.77936	38.76718	45.44778	52.76943	12.00505	52.76943	40.76438
	Right	FEA	21.55594	19.05472	14.14968	12.76609	13.57167	13.57167	15.32027	17.55013	17.92849	21.12276	22.86658	24.62441	27.71647	32.54016	37.55402	39.5526	46.205	53.53515	12.76609	53.53515	40.76905
beta (Ab/Adduction angle)	Left	JCS	6.900991	5.754174	5.676854	5.380859	5.201862	5.19811	5.44619	5.063384	6.452669	5.824066	5.189918	5.715169	6.576732	7.106863	7.746583	8.263926	8.913491	8.613491	5.063384	8.913287	3.849903
	Left	TEA	3.980136	3.09157	3.539489	3.582107	3.069376	3.128037	3.181005	2.720733	3.839117	3.078238	2.24888	2.478924	2.99502	2.9086	3.112901	3.198867	3.269684	2.305371	2.24888	3.980136	1.731257
	Left	GCA	6.682805	5.702876	5.960492	5.874786	5.48778	5.523158	5.64884	5.216283	6.434172	5.718838	4.955956	5.28575	5.913971	6.011691	6.33309	6.521682	6.702971	5.804927	4.955956	6.702971	1.747015
	Left	FEA	6.201235	5.243722	5.547513	5.492352	5.07534	5.116296	5.22455	4.78523	5.979115	5.252486	4.473046	4.777882	5.377514	5.426448	5.715166	5.873238	6.017362	5.085096	4.473046	6.201235	1.728189
	Right	JCS	-0.57465	0.256612	-1.10655	-1.00787	-0.9013	-1.41433	-0.74355	-0.97933	-0.88061	-0.57395	-0.43626	-0.10263	0.407514	0.860493	0.024424	-0.0721	0.728136	0.921081	-1.41433	0.921081	2.335407
	Right	TEA	1.051321	2.192993	1.141203	1.539585	1.813275	1.205011	1.659851	1.150189	1.201481	1.106689	1.023049	1.131181	1.242233	1.06986	-0.41012	-0.76398	-0.81944	-1.54073	-1.54073	2.192993	3.733723
	Right	GCA	2.118541	2.118541	0.917003	1.172449	1.365837	0.802565	1.362204	0.982273	1.05617	1.150234	1.169559	1.38221	1.676197	1.784998	0.585834	0.343005	0.651927	0.305977	0.305977	2.118541	1.812564
	Right	FEA	1.120301	-0.59317	-1.89454	-1.73233	-1.58925	-2.12373	-1.7024	-1.49844	-1.79156	-1.47519	-1.47519	-1.08772	-0.64856	-0.30022	-1.23659	-1.37038	-0.68245	-0.59131	-2.12373	-0.30022	1.823519
gamma (Int/External Rotation angle)	Left	JCS	-1.48647	4.215819	5.584787	6.330914	7.190814	7.84596	7.58238	7.157771	6.529334	5.171998	4.118437	4.714982	4.318606	4.310827	4.926159	4.456948	4.711974	2.913448	2.913448	7.84596	4.932512
	Left	TEA	4.215819	-1.42029	-1.22687	-0.57719	0.381921	1.017515	0.815101	0.420602	-0.11858	-1.41528	-2.37765	-1.64157	-1.85482	-1.46026	-0.50257	-0.57057	0.348292	-0.40017	-2.37765	1.017515	3.395163
	Left	GCA	-2.3051	0.918045	1.310348	2.077256	2.919983	3.577842	3.305307	2.88146	2.240419	0.889729	-0.15373	0.455187	0.083433	0.164878	0.874875	0.534706	1.03374	-0.31796	-0.31796	3.577842	3.8958
	Left	FEA	-0.07054	0.344615	0.702221	1.449352	2.311972	2.966014	2.705423	2.286874	1.662948	0.322179	-0.70646	-0.0748	0.460669	-0.27794	0.479216	0.191862	0.77409	-0.45457	-0.70646	2.966014	3.672478
	Right	JCS	-0.62608	0.458671	0.521136	-0.18911	0.080476	0.528851	0.301119	0.22218	0.523474	0.439245	0.504009	0.460669	0.407514	1.182198	0.874875	0.534706	-1.19856	-2.77135	-2.77135	1.182198	3.953552
	Right	TEA	-6.76479	-6.72363	-6.56833	-7.17668	-6.84409	-6.43806	-6.73739	-6.90366	-6.61637	-6.80554	-6.7885	-6.87354	-6.20848	-7.78547	-8.13175	-9.53896	-8.47281	-9.78955	-9.78955	-6.20848	3.581071
	Right	GCA	-3.38395	-3.34112	-3.19429	-3.81479	-3.49159	-3.08063	-3.36841	-3.52631	-3.2379	-3.42423	-3.41016	-3.50112	-2.85441	-4.47998	-4.90079	-6.34431	-5.42875	-6.95723	-6.95723	-2.85441	4.102817
	Right	FEA	-0.9034	-0.97555	-0.94844	-1.69096	-1.43838	-0.98646	-1.18552	-1.23406	-0.92733	-0.96343	-0.87057	-0.88429	-0.1077	-1.54715	-1.79802	-3.1996	-2.08701	-3.47262	-3.47262	-0.1077	3.364924
Q1 (Medio-Lateral Tibial displacement)	Left	JCS	6.498551	6.377247	7.469023	6.779474	7.109355	7.244312	7.234599	7.527804	6.500903	7.456311	6.449848	6.41391	6.316806	6.175129	6.205764	6.651399	6.610191	7.240758	6.175129	7.527804	1.352675
	Left	TEA	8.642196	8.51207	9.605945	8.917776	9.245471	9.379908	9.372688	9.66408	8.639922	9.598197	8.587464	8.555763	8.467671	8.334652	8.36936	8.820883	8.783456	9.42752	8.334652	9.66408	1.329429
	Left	GCA	4.67452	4.568353	5.656529	4.96461	5.298242	5.43409	5.4201	5.716416	4.684809	5.635298	4.636159	4.592955	4.480388	4.323857	4.347504	4.783037	4.735342	5.342752	4.323857	5.716416	1.392559
	Left	FEA	4.883898	4.777453	5.865695	5.17382	5.507382	5.643214	5.629303	5.925561	4.894041	5.844621	4.845347	4.802276	4.689995	4.533737	4.557513	4.993233	4.945657	5.553493	4.533737	5.925561	1.391824
	Right	JCS	7.47079	7.458329	7.363708	6.623724	6.452973	6.367899	6.65477	6.64772	6.508796	6.587704	5.844621	7.531712	8.223437	8.622288	8.583502	9.190354	8.841764	9.466085	6.367899	9.466085	3.098186
	Right	TEA	3.753168	3.81867	3.759146	3.058547	2.950046	2.82123	3.052433	3.017032	2.958199	2.842773	2.871223	3.799028	4.426359	4.791285	4.733843	5.338744	5.04744	5.68692	2.82123	5.68692	2.865691
	Right	GCA	3.684645	3.73276	3.665408	2.956026	2.833642	2.714581	2.958199	2.929121	2.762743	2.802446	2.871223	3.773664	4.375556	4.748049	4.694767	5.300103	4.996023	5.632122	2.714581	5.632122	2.917542
	Right	FEA	7.024178	7.006559	6.909616	6.167028	5.992158	5.909978	6.200531	6.195357	6.05877	6.141016	7.147531	7.086096	7.782081	8.183177	8.145624	8.752605	8.400226	9.023544	5.909978	9.023544	3.113566
Q2 (Antero-Posterior Tibial Drawer)	Left	JCS	19.61989	19.59429	18.77383	18.63699	19.89881	19.60348	19.00004	19.54682	20.52471	19.9434	20.50532	20.69294	21.83252	22.56038	23.27735	23.90485	25.03935	27.87107	18.63699	27.87107	9.23408
	Left	TEA	11.69214	11.55457	10.76068	10.65447	11.84864	11.55885	11.86161	11.48031	12.5266	12.92604	12.45781	12.72513	13.99812	14.98507	15.95277	16.90754	18.5946	22.34995	10.65447	22.34995	11.69549
	Left	GCA	13.53962	13.65683	13.26185	13.40359	14.3704	14.12671	14.2725	13.84403	14.65077	14.95167	14.34082	14.33656	15.27289	15.63994	16.13575	16.58055	17.52204	20.26022	13.26185	20.26022	6.998369
	Left	FEA	13.61098	14.01968	14.17552	14.66187	15.29193	15.11266	15.05575	14.54547	15.06424	15.22041	14.40012	14.06263	14.5974	14.22041	14.16621	14.03478	14.15427	15.82685	13.61098	15.82685	2.215872
	Right	JCS	29.81357	29.83067	30.56539	30.69445	30.481	30.44381	30.16152	29.70239	30.24919	30.06993	30.32324	29.45794	29.59848	29.05649	29.44675	28.60917	29.0047	30.15727	28.60917	30.69445	2.085281
	Right	TEA	19.503	19.71802	20.55853	20.89988	20.80447	20.67734	20.29072	19.639	20.16961	19.78648	19.945	18.99116	19.02823	18.3591	18.60718	17.77114	18.2542	19.65315	17.77114	20.89988	3.128735
	Right	GCA	21.78037	22.43995	23.7677	24.53453	24.68812	24.42602	23.07207	22.66332	23.11614	22.14367	21.97364	20.6933	20.12349	18.51942	17.85168	16.62036	15.84504	16.62036	15.84504	24.68812	8.84308
	Right	FEA	24.03588	24.19136	25.04977	25.33396	25.20864	25.1503	24.73377	24.13612	24.66467	24.31434	24.34298	23.5546	23.10596	22.85242	23.10596	22.23935	22.56914	23.75235	22.23935	25.33396	3.094614
Q3 (Tibial Distraction-Compression)	Left	JCS	23.54483	23.33235	24.72463	24.57815	24.57815	24.70434	24.42692	24.16671	23.53699	23.4955	22.89676	22.58199	22.31944	21.69002	22.31944	20.87314	20.13207	18.93968	17.00961	25.74352	8.733906
	Left	TEA	24.35218	23.78424	24.44509	24.25389	24.25389	24.30167	24.29975	24.16743	23.84064	24.00125	23.75141	23.89628	24.09431	24.41837	24.28516	24.47351	24.0882	23.44571	23.44571	24.94168	1.49597
	Left	GCA	18.90765	18.39526	19.26954	19.0359	19.09133	19.16201	19.07355	18.8906	18.542	18.55914	18.20608	18.25633	18.39907	18.56538	18.37301	18.50568	18.16229	17.67224	17.67224	19.9717	2.299462
	Left	FEA	11.94582	11.43887	12.38044	12.20909	12.20909	12.28833	12.17286	11.97433	11.6081	11.62019	11.23751	11.28781	11.46318	11.72556	11.66174	11.97972	11.99247	12.17686	11.23751	13.13968	1.902168
	Right	JCS	29.73688	29.35235	29.68943	29.80243	29.80243	30.12632	30.21477	29.93192	30.11438	29.75604	29.6924	29.11078	29.09608	28.76979	28.08161	28.53892	26.5716	24.93528	24.93528	30.21477	5.279493
	Right	TEA	25.5364	24.63412	24.45702	24.36211	23.84653	24.34004	24.76615	24.94119	25.19333	25.48567	25.75007	25.55815	26.18965	26.91772	27.2797	28.19057	27.65404	28.19057	23.84653	28.19057	4.344038
	Right	GCA	15.56896	14.85258	14.84301	14.94961	14.55086	14.95751	15.24789	15.23103	15.47286	15.55306	15.72251	15.41882	15.91851	16.47704	16.75989	17.62987	17.20042	17.38535	14.55086	17.62987	3.07901
	Right	FEA	26.65005	25.99647	26.06387	26.16633	25.7744	26.17921	26.45098	26.40488	26.619	26.60532	26.54576	26.36906	26.71621	26.96464	26.85622	26.39781	26.39781	25.64208	25.64208	27.57303	1.930958

P002 6 DoF Kinematics [Raw Data]

Measurement	Side	Method	1	2	3	4	5	6	7	8	9	10	11	12	13	14	15	16	17	18	Min	Max	Range
alpha (Flex/Ext angle)	Left	JCS	23.21219	20.9859	18.6389	15.38131	13.5477	14.14849	15.47216	18.54212	22.74954	24.94364	28.86663	32.01224	33.80586	36.53086	39.60456	43.20797	46.94756	50.19068	13.5477	50.19068	36.64298
	Left	TEA	25.25178	23.03549	20.7111	17.45865	15.55489	16.17151	17.50797	20.61989	24.80872	26.99495	30.87342	33.99756	35.77602	38.48524	41.52112	45.09794	48.78745	51.98953	15.55489	51.98953	36.43465
	Left	GCA	24.06137	21.84063	19.50699	16.25052	14.37078	14.9821	16.31486	19.41374	23.6113	25.80112	29.69573	32.82733	34.61077	37.32494	40.37217	43.9562	47.65859	50.86973	14.37078	50.86973	36.49894
	Left	FEA	25.1504	22.90557	20.55404	17.26283	15.31314	15.94341	17.30174	20.46255	24.70122	26.91393	30.84709	34.014	35.81827	38.56072	41.65208	45.27481	49.05489	52.35289	15.31314	52.35289	37.03975
	Right	JCS	30.24538	26.94938	23.49824	21.06496	20.08234	20.39871	22.88702	24.18271	28.0909	30.10438	33.88706	37.23967	39.13534	41.71293	44.50098	47.83834	52.70615	55.48553	20.08234	55.48553	35.40319
	Right	TEA	31.59618	28.31069	24.84951	22.51844	21.45177	21.77868	24.30712	25.5612	29.45246	31.46085	35.24287	38.59427	40.52129	43.06884	45.85233	49.19728	54.0606	56.85409	21.45177	56.85409	35.40232
	Right	GCA	30.72942	27.43934	23.98061	21.61149	20.57533	20.89844	23.41342	24.6796	28.58142	30.5922	34.37576	37.72873	39.64733	42.20449	44.99013	48.33411	53.19983	55.99069	20.57533	55.99069	35.41536
	Right	FEA	30.56826	27.26705	23.80444	21.38388	20.38425	20.70301	23.20718	24.49611	28.41186	30.42916	34.2255	37.5845	39.50488	42.07186	44.86465	48.2169	53.09286	55.89164	20.38425	55.89164	35.50739
beta (Ab/Adduction angle)	Left	JCS	6.687336	6.552238	6.559512	6.266176	5.306258	5.536372	5.80624	6.614626	6.8821	7.057003	6.958583	7.075499	7.097576	7.257126	7.063444	7.158797	6.657785	6.087912	5.306258	7.257126	1.950867
	Left	TEA	1.78029	1.820959	2.020731	2.008202	1.215788	1.390852	1.542076	2.083752	2.010294	2.017619	1.639156	1.54883	1.460198	1.461866	1.106257	1.032963	0.382751	-0.29525	-0.29525	2.083752	2.379004
	Left	GCA	3.959287	3.93821	4.069747	3.956223	3.102192	3.297483	3.491916	4.129995	4.177122	4.242801	3.959936	3.938815	3.886418	3.938745	3.633354	3.610044	3.000877	2.349669	2.349669	4.242801	1.893131
	Left	FEA	-9.34448	-9.3023	-9.08297	-9.0373	-9.77868	-9.62149	-9.50445	-9.01881	-9.11551	-9.09657	-9.41432	-9.41862	-9.44356	-9.32466	-9.51953	-9.36533	-9.73631	-10.1364	-10.1364	-9.01881	1.117566
	Right	JCS	-1.71286	-1.68788	-1.97916	-0.48973	-1.8371	-1.65934	-0.94784	-1.61411	-1.63916	-1.63506	-1.49753	-1.38709	-0.86903	-1.2024	-1.16661	-0.94185	-0.84204	-0.5501	-1.97916	-0.48973	1.489433
	Right	TEA	-0.64861	-0.40131	-0.46368	1.180371	-0.10137	0.055847	0.605331	-0.14427	-0.42928	-0.56141	-0.68357	-0.80629	-0.42211	-0.93574	-1.09651	-1.10768	-1.3502	-1.25281	-1.3502	1.180371	2.530575
	Right	GCA	-0.05377	0.119563	-0.0225	0.259804	0.258804	0.424803	1.566483	0.313232	0.117495	0.030441	-0.00898	-0.06079	0.362923	-0.099961	-0.20652	-0.15578	-0.31412	-0.17174	-0.31412	1.566483	1.880606
	Right	FEA	4.00309	4.108934	3.881831	5.403603	4.066411	4.241094	4.922185	4.235802	4.131791	4.084706	4.106963	4.094761	4.534723	4.085529	3.985849	4.030881	3.838764	3.948207	3.838764	5.403603	1.56484
gamma (Int/External Rotation angle)	Left	JCS	6.084142	6.194169	7.909578	6.98417	8.495274	9.037288	8.798826	9.230938	8.102408	7.943448	6.098921	5.97353	5.819193	5.919341	4.090578	4.061872	4.360157	2.906714	2.906714	9.230938	6.324224
	Left	TEA	1.630574	1.553571	3.078902	1.903911	3.283694	3.868445	3.726593	4.392427	3.608837	3.639305	2.14979	2.321852	2.34211	2.713695	1.200098	1.550828	2.253477	1.157667	1.157667	4.392427	3.23476
	Left	GCA	3.185575	3.191872	4.802253	3.740858	5.182806	5.747459	5.560889	6.119178	5.181114	5.127645	3.483269	3.526513	3.471767	3.727208	2.0804	2.271449	2.806141	1.562855	1.562855	6.119178	4.556323
	Left	FEA	1.808344	1.297971	2.369662	0.5619	1.569382	2.274355	2.392378	3.665527	3.699906	4.157443	3.424564	4.201816	4.564447	5.452367	4.513014	5.52506	6.90073	6.376605	0.5619	6.90073	6.338829
	Right	JCS	14.6723	14.38659	14.16405	13.17278	13.25761	13.90508	13.98496	14.14814	14.49252	14.62751	14.97552	15.32181	16.6651	15.6457	15.95582	16.20187	16.40362	16.67934	13.17278	16.67934	3.506564
	Right	TEA	10.76902	10.55103	10.41281	9.488555	9.603378	10.24133	10.25	10.37918	10.63209	10.72692	11.0126	11.31807	12.64468	11.60888	11.91073	12.15971	12.39	12.69542	9.488555	12.69542	3.206869
	Right	GCA	12.04177	11.85578	11.74662	10.83971	10.96101	11.59689	11.58814	11.70747	11.9262	12.00106	12.24494	12.50886	13.80976	12.73789	12.99781	13.19301	13.3389	13.59269	10.83971	13.80976	2.97005
	Right	FEA	13.1002	13.14588	13.27513	12.71957	12.71957	13.3343	13.15749	13.1888	13.13641	13.06933	13.06426	13.06426	14.2253	12.96676	13.02262	12.97285	12.76327	12.53226	12.52326	14.2253	1.693463
δ1 (Medio-Lateral Tibial displacement)	Left	JCS	5.743935	5.748251	6.049535	6.52398	6.099749	5.943398	6.410627	6.254011	6.060415	6.132483	5.73947	5.813079	5.853528	5.815024	6.232166	6.349757	6.071521	6.305808	5.73947	6.52398	0.784509
	Left	TEA	5.52634	5.519166	5.819255	6.314598	5.871142	5.718052	6.200188	6.026644	5.843221	5.930207	5.519804	5.614255	5.665389	5.632007	6.045251	6.162592	5.88715	6.116011	5.519166	6.314598	0.795432
	Left	GCA	3.64573	3.643753	3.944382	4.430273	3.995513	3.840948	4.316342	4.150454	3.962429	4.042668	3.640131	3.725155	3.771456	3.735757	4.150765	4.268218	3.991513	4.222828	3.640131	4.430273	0.790142
	Left	FEA	10.21348	10.16507	10.46088	11.03121	10.51877	10.37738	10.913	10.67872	10.5318	10.67231	10.19951	10.36875	10.45822	10.44322	10.84248	10.95892	10.6935	10.90289	10.16507	11.03121	0.866132
	Right	JCS	4.386643	4.331986	4.308412	4.345738	3.338941	3.28191	3.417169	3.310576	3.428264	3.424854	3.450436	3.342248	3.546637	4.280014	4.258282	4.141691	4.049586	4.112157	3.28191	4.386643	1.104733
	Right	TEA	1.074834	1.045949	1.011637	1.08788	0.086904	0.017061	0.137002	0.03376	0.105437	0.113268	0.117108	0.054549	0.262251	0.997819	0.976413	0.908334	0.843646	0.893053	0.017061	1.08788	1.070818
	Right	GCA	1.609932	1.580728	1.546549	1.622309	0.621262	0.551578	0.671708	0.568425	0.640672	0.648363	0.652472	0.589349	0.797009	1.53255	1.511114	1.442461	1.377432	1.427003	0.551578	1.622309	1.070732
	Right	FEA	-1.18413	-1.19045	-1.23416	-1.12384	-2.11972	-2.20078	-2.09425	-2.19456	-2.16317	-2.1455	-2.1607	-2.1833	-1.9727	-1.25321	-1.25633	-1.28193	-1.32261	-1.28473	-2.20078	-1.12384	1.07694
δ2 (Antero-Posterior Tibial Drawer)	Left	JCS	21.42054	20.97184	20.75585	22.3387	18.70294	19.14868	19.79767	20.55676	22.12582	22.19595	22.76571	23.72544	23.9709	24.98262	25.40987	26.42422	27.21775	27.58496	18.70294	27.58496	8.882018
	Left	TEA	10.67396	10.35895	10.31443	9.6313	8.667124	9.065272	9.593654	10.12981	11.4039	11.3652	11.94595	12.59125	12.8015	13.7618	14.16467	15.19106	16.0518	16.52357	8.667124	16.52357	7.856446
	Left	GCA	11.31454	11.24298	11.4464	11.09285	10.33969	10.67245	11.05608	11.26804	12.09696	11.81162	11.98009	12.27362	12.28131	12.94651	13.0154	13.65465	14.11571	14.24112	10.33969	14.24112	3.901434
	Left	FEA	10.85683	10.90655	11.24045	11.07052	10.41398	10.71503	11.02674	11.0697	11.65901	11.25779	11.21529	11.34588	11.26541	11.78811	11.71697	12.18504	12.49589	12.51485	10.41398	12.51485	2.10087
	Right	JCS	31.30559	30.76106	31.68174	30.65765	31.00789	30.81604	31.17591	30.6958	31.72809	31.19101	31.2161	30.51859	30.53264	30.71331	30.84143	30.70393	31.51089	32.14942	30.51859	32.14942	1.630836
	Right	TEA	17.53615	17.23809	18.46367	17.73367	18.1465	17.93238	18.04961	17.42183	18.12175	17.43551	17.24812	16.39227	16.36437	16.47639	16.58385	16.45043	17.35382	18.12423	16.36437	18.46367	2.099303
	Right	GCA	18.2283	18.2249	19.75564	19.21378	19.73193	19.48393	19.37981	18.64944	19.00365	18.1381	17.60036	16.44323	16.23283	16.11171	15.95769	15.52233	15.98865	16.49816	15.52233	19.75564	4.233309
	Right	FEA	21.73614	21.50372	22.78592	22.04293	22.50071	22.27443	22.35373	21.72663	22.36296	21.63576	21.34492	20.39279	20.29184	20.31307	20.30236	20.02492	20.69325	21.30418	20.02492	22.78592	2.761004
δ3 (Tibial Distraction-Compression)	Left	JCS	30.33593	30.60367	31.00315	32.33877	32.74098	32.56896	32.39293	31.11827	30.04715	29.99996	28.76571	28.49984	28.44231	27.65505	27.03812	26.01156	25.41236	25.00918	25.00918	32.74098	7.731796
	Left	TEA	27.40841	27.20929	27.14035	27.84955	27.84707	27.7795	27.89883	27.26048	27.02671	27.46633	27.01996	27.41921	27.76305	27.76218	27.5398	27.6176	27.48821	27.76518	27.01996	27.89883	0.878871
	Left	GCA	21.24481	21.09778	21.09375	21.88877	21.93456	21.85982	21.92554	21.20741	20.88431	21.27016	20.77656	21.15325	21.48831	21.2861	21.36179	21.15883	21.37712	21.72427	20.77656	21.93456	1.158006
	Left	FEA	19.46493	19.2884	19.31033	20.17173	20.15238	20.03568	20.20572	19.46864	19.15031	19.58806	19.08446	19.53062	19.91026	19.74434	19.9901	19.88621	20.13685	20.62351	19.08446	20.62351	1.539042
	Right	JCS	33.33713	33.81133	34.53221	34.78586	34.89497	35.11561	34.50862	34.31512	33.79088	33.39605	33.16944	32.1563	31.86563	31.52437	31.32221	30.19409	30.191	28.6701	28.6701	35.11561	6.445512
	Right	TEA	28.88056	28.53108	28.3659	28.07418	27.9399	28.24744	28.2474	28.37252	28.79936	28.92615	29.67294	29.54547	29.76305	30.07711	30.60677	30.36266	30.191	30.80918	27.9399	30.80918	2.869273
	Right	GCA	24.0188	23.7384	23.68942	23.45557	23.37567	23.66822	23.58367	23.66506	24.00123	24.0749	24.75489	24.57792	24.77416	25.07495	25.092	25.38164	25.28524	25.96246	23.37567	25.96246	2.586793
	Right	FEA	27.87868	27.80411	27.95832	27.88136	27.88939	28.17458	27.96674	27.96468	28.06978	28.01282	28.44462	28.03243	28.08108	28.13106	28.4512	27.96037	27.46749	27.90755	27.46749	28.4512	0.983718

P003 6 DoF Kinematics [Raw Data]

Measurement	Side	Method	1	2	3	4	5	6	7	8	9	10	11	12	13	14	15	16	17	18	Min	Max	Range
alpha (Flex/Ext angle)	Left	JCS	25.77618	23.43399	22.08357	20.41394	21.92292	23.30658	26.08217	29.44599	30.43945	31.6157	33.38096	37.07332	39.14343	44.81505	49.82741	54.39046	60.49772	65.92565	20.41394	65.92565	45.51171
		TEA	25.94753	23.58531	22.22563	20.5759	22.06203	23.45064	26.27564	29.63979	30.6335	31.81606	33.58133	37.28146	39.36142	45.05654	50.06536	54.67489	60.7586	66.1914	20.5759	66.1914	45.61551
		GCA	25.3517	23.0284	21.68747	19.98224	21.53071	22.91042	25.63241	29.00691	30.00271	31.17569	32.94486	36.63725	38.70281	44.36555	49.38522	53.92635	60.05024	65.47867	19.98224	65.47867	45.49643
		FEA	25.56688	23.22557	21.87531	20.20617	21.71467	23.0983	25.8718	29.23481	30.22811	31.40369	33.16875	36.86002	38.92884	44.59685	49.60904	54.16407	60.27357	65.69902	20.20617	65.69902	45.49286
	Right	JCS	14.35726	14.0418	10.35627	9.339448	10.66453	9.966814	11.24856	14.53207	17.05862	18.41131	20.73232	24.02305	28.22844	32.5885	39.19056	43.2409	49.93488	55.60301	9.339448	55.60301	46.26356
		TEA	16.77402	16.48182	12.80909	11.83807	13.13802	12.53452	13.79075	16.94931	19.61352	20.78899	21.8763	26.44746	30.65724	34.92853	41.40311	45.40535	52.03716	57.6532	11.83807	57.6532	45.81514
		GCA	15.47784	15.1731	11.48931	10.49302	11.80785	11.1543	12.42541	15.65306	18.24683	19.51687	21.53669	25.15247	29.3567	33.67579	40.21348	44.23645	50.89039	56.52317	10.49302	56.52317	46.03015
		FEA	15.20743	14.8922	11.21895	10.20692	11.52701	10.83534	12.11031	15.38152	17.88082	19.24604	21.53669	24.8026	28.9555	33.28974	39.86956	43.89137	50.52423	56.14932	10.20692	56.14932	45.9424
beta (Ab/Adduction angle)	Left	JCS	-1.5237	-0.80963	-0.44963	-1.9093	-0.29576	-0.43519	-2.51748	-2.03863	-1.93133	-2.0422	-1.86409	-1.81691	-1.97236	-2.27854	-1.96796	-2.87492	-2.2251	-2.27544	-2.87492	-0.29576	2.579155
		TEA	-4.67655	-4.00915	-3.6736	-5.16075	-3.52254	-3.63716	-5.66363	-5.10781	-4.97574	-5.05602	-4.82974	-4.67265	-4.76116	-4.86553	-4.35586	-5.06454	-4.1297	-3.90786	-5.66363	-3.52254	2.141094
		GCA	-1.29591	-0.52313	-0.12947	-1.54718	0.028352	-0.14562	-2.29711	-1.90375	-1.82179	-1.96263	-1.82967	-1.87687	-2.0851	-2.53496	-2.3495	-3.36751	-2.86186	-3.03415	-3.36751	0.028352	3.395866
		FEA	-0.772	-0.05641	0.303895	-1.15597	0.45777	0.318073	-1.76607	-1.29184	-1.18639	-1.29975	-1.12595	-1.09007	-1.25317	-1.58509	-1.30292	-2.24015	-1.63714	-1.73469	-2.24015	0.45777	2.697921
	Right	JCS	5.726309	5.873776	5.602696	5.841836	5.787406	6.41732	6.361244	5.747549	7.097395	5.827984	6.725003	6.826138	7.327577	7.07461	6.521752	6.419197	6.352741	6.154978	5.602696	7.327577	1.724881
		TEA	1.589234	1.776144	1.991616	2.364854	2.133567	2.850899	2.624733	1.5878	2.606148	1.178645	1.78651	1.500654	1.530914	0.826742	-0.34081	-0.77788	-1.31913	-1.8382	-1.8382	2.850899	4.689097
		GCA	3.373106	3.539574	3.499351	3.803111	3.664073	4.337146	4.199769	3.383366	4.579646	3.233366	3.996604	3.917771	4.202775	3.744103	2.916528	2.668463	2.402546	2.077655	2.077655	4.579646	2.501991
		FEA	-3.36642	-3.22082	-3.49339	-3.24809	-3.30999	-2.67675	-2.73791	-3.34403	-1.96831	-3.21649	-2.27187	-2.07808	-1.41647	-1.45365	-1.58641	-1.37844	-0.84837	-0.46397	-3.49339	-0.46397	3.029422
gamma (Int/External Rotation angle)	Left	JCS	-0.94346	-1.06086	-1.10225	-1.08747	-1.08022	-0.97044	-1.26012	-1.5895	-1.8794	-0.57211	-0.05262	-0.96448	-2.22242	-2.26663	-1.8904	-1.96884	-0.99584	-0.55316	-2.26663	-0.05262	2.214013
		TEA	0.260644	0.012035	-0.10561	-0.18353	-0.0928	0.094861	-0.03724	-0.18451	-0.42149	0.948415	1.559849	0.835945	-0.31938	-0.09585	0.497453	0.604846	1.793953	2.404364	-0.42149	2.404364	2.825852
		GCA	-2.39094	-2.49752	-2.53171	-2.50751	-2.50877	-2.40641	-2.70958	-3.049	-3.34093	-2.0357	-1.51783	-2.42887	-3.68384	-3.71014	-3.3057	-3.35044	-2.31636	-1.80758	-3.71014	-1.51783	2.192313
		FEA	-0.99606	-1.08269	-1.10632	-1.06958	-1.08218	-0.99059	-1.31675	-1.69012	-1.99295	-0.70094	-0.20425	-1.16334	-2.44742	-2.56167	-2.24487	-2.37531	-1.46741	-1.07828	-2.56167	-0.20425	2.357411
	Right	JCS	5.161319	5.314324	6.702119	6.847724	6.782425	6.855888	7.927879	5.871945	5.205012	3.438286	2.839564	0.851315	0.162948	-0.30215	-1.3614	-0.9139	-0.67875	-0.25368	-1.3614	7.927879	9.289275
		TEA	-2.27603	-2.14632	-1.00637	-0.92524	-0.90731	-0.88178	0.272847	-1.55279	-2.03455	-3.68782	-4.09487	-5.78825	-6.06955	-6.07586	-6.38023	-5.43702	-4.335	-3.13714	-6.38023	0.272847	6.653076
		GCA	1.646245	1.785743	3.031135	3.18802	3.122131	3.16702	4.28704	2.364021	1.799625	0.098633	-0.39509	-2.22114	-2.68899	-2.90671	-3.5638	-2.85576	-2.16992	-1.34725	-3.5638	4.28704	7.850843
		FEA	5.526473	5.629488	6.433487	6.4182	6.562662	6.525882	7.80069	6.264763	5.996361	4.443662	4.208416	2.732494	2.689152	2.87946	2.777306	3.785515	4.895081	6.002568	2.689152	7.80069	5.111538
Q1 (Medio-Lateral Tibial displacement)	Left	JCS	8.646221	8.56883	9.554725	9.79811	9.49769	8.696417	8.040218	7.959195	7.238868	7.905923	6.103375	5.902499	4.77849	3.484064	2.354804	1.610008	0.754024	0.180144	0.180149	9.79811	9.617961
		TEA	7.24429	7.11453	8.080537	8.308135	7.991537	7.274124	6.610408	6.58225	5.889237	6.558964	4.711154	4.467281	3.295088	1.932948	0.735902	-0.06233	-1.01307	-1.61591	-1.61591	8.308135	9.924046
		GCA	4.372331	4.307367	5.297983	5.545115	5.248533	4.427359	3.772945	3.679376	2.952566	3.618987	1.827181	1.636509	0.529934	-0.75442	-1.8676	-2.59971	-3.43321	-4.00021	-4.00021	5.545115	9.545323
		FEA	5.6923	5.626359	6.616603	6.86344	6.566557	5.746948	5.092393	4.999811	4.273512	4.93998	3.147332	2.955857	1.842383	0.562762	-0.55168	-1.28479	-2.12005	-2.6876	-2.6876	6.86344	9.551036
	Right	JCS	10.60573	10.6027	11.49609	11.52758	11.27985	11.10919	11.39546	11.77328	10.21037	10.0831	9.859946	8.949417	8.674691	8.191512	7.50879	7.012203	6.589118	6.240019	6.240019	11.77328	5.533258
		TEA	9.169262	9.177248	10.06196	10.07771	9.831945	9.665613	9.953636	10.33679	8.769334	8.652328	8.422047	7.524015	7.262559	6.785292	6.111693	5.608516	5.168029	4.827856	4.827856	10.33679	5.508929
		GCA	8.637331	8.641918	9.529307	9.549912	9.303539	9.135872	9.423355	9.804861	8.23881	8.11864	7.890556	6.988671	6.723123	6.244034	5.567622	5.066477	4.631355	4.28843	4.28843	9.804861	5.51643
		FEA	14.03527	14.08139	14.93605	14.89736	14.6584	14.50704	14.80113	15.20272	13.61956	13.53804	13.2831	12.42831	12.21276	11.75594	11.1139	10.58792	10.08724	9.777949	9.777949	15.20272	5.424774
Q2 (Antero-Posterior Tibial Drawer)	Left	JCS	30.75092	30.47278	31.90548	32.16811	32.42455	32.11386	31.45834	31.97433	31.15745	30.32655	29.31124	29.30419	28.52871	29.33946	29.79009	30.48029	31.03622	33.18845	28.52871	33.18845	4.659744
		TEA	20.29609	20.37657	22.02359	22.57722	22.5672	22.13538	22.03538	20.987	20.0329	19.0471	18.30133	17.35304	16.35724	16.63888	16.7151	17.18193	17.52548	19.62518	16.35724	22.57722	6.219978
		GCA	18.70134	19.07165	20.88885	21.60931	21.45962	20.75283	20.96734	18.96479	17.89162	16.76377	15.82736	14.47178	13.24433	12.92636	12.51553	12.51993	12.35498	14.0432	12.35498	21.60931	9.254328
		FEA	22.12694	22.23397	23.89634	24.44602	24.44529	23.8969	22.78789	22.78001	21.8114	20.8061	20.04147	19.03952	18.00419	18.17655	18.15311	18.48354	18.68215	20.63528	18.00419	24.44602	6.441835
	Right	JCS	23.71576	24.01031	23.41833	23.31982	22.56372	23.15364	22.60529	23.11419	23.62372	24.53721	24.96259	25.88295	26.22674	26.37579	26.82327	26.61846	26.96283	27.47224	22.56372	27.47224	4.908516
		TEA	15.06118	15.37274	14.73449	14.63594	13.88329	14.51961	13.97517	14.47057	15.10453	15.96739	16.50352	17.55669	18.15094	18.56899	19.52514	19.7079	20.76381	21.99311	13.88329	21.99311	8.109821
		GCA	16.03877	16.37467	16.17221	16.1875	15.2831	15.96948	15.27871	15.42301	15.7107	16.46714	16.69975	17.35519	17.4174	17.31178	17.48047	17.15586	17.4552	18.03275	15.27871	18.03275	2.754036
		FEA	15.50161	15.82946	15.62458	15.63474	14.7344	15.40241	14.71522	14.88505	15.14299	15.94032	16.15598	16.81581	16.86809	16.78257	16.99154	16.70681	17.02212	17.61972	14.71522	17.61972	2.904499
Q3 (Tibial Distraction-Compression)	Left	JCS	41.08435	40.61969	39.94494	40.26545	39.16687	40.48428	40.24918	40.3149	41.14353	41.60819	40.82006	40.19989	39.82129	39.09771	36.81083	35.72148	34.38056	32.2066	32.2066	41.60819	9.401587
		TEA	32.46785	31.62711	30.79399	30.76019	29.99628	31.49401	31.59922	32.31208	33.29903	34.0229	33.50619	33.63924	32.81054	33.07632	32.90084	32.79084	32.91594	32.02532	29.99628	34.0229	4.026618
		GCA	25.81905	24.92236	24.01335	23.94135	23.21756	24.79607	24.99993	25.82066	26.87448	27.59548	27.23139	27.52009	27.65698	27.45242	27.62525	27.84853	27.84883	28.0471	23.21756	28.45883	5.24127
		FEA	31.83912	31.06376	30.20805	30.2414	29.4167	30.93105	31.02122	31.62515	32.62325	33.26294	32.79525	32.81385	32.81054	32.15332	31.8781	31.69344	31.67087	30.67393	29.4167	33.26294	3.846239
	Right	JCS	28.54348	28.86288	29.79723	29.59181	29.42005	29.51293	29.27031	28.52731	27.42371	27.41425	26.26543	25.56551	24.81434	24.1989	23.41556	23.01777	21.70262	21.79048	21.70262	29.79723	8.094617
		TEA	30.30356	30.55193	30.82647	30.42695	30.54023	30.47157	30.53006	30.43302	29.72892	29.89232	29.17699	28.97385	28.9594	29.03518	29.20503	29.35944	28.89253	29.59823	28.89253	30.82647	1.933935
		GCA	23.29085	23.56182	23.96998	23.62672	23.65653	23.65447	23.62385	23.36299	22.64324	22.7665	22.01472	21.79798	21.75737	21.84909	22.14254	22.42617	22.25229	23.29126	21.75737	23.96998	2.21261
		FEA	24.80899	25.07631	25.61705	25.27947	25.27024	25.23622	25.23241	25.01377	24.06206	24.19875	23.38422	23.04308	22.92272	22.9341	23.18894	23.32511	23.05418	25.61705	22.92272	25.61705	2.694336

P004 6 DoF Kinematics [Raw Data]

Measurement	Side	System	1	2	3	4	5	6	7	8	9	10	11	12	13	14	15	16	17	18	MIN	MAX	RANGE
alpha (Flex/Ext angle)	Left	JCS	0.242761	1.236419	2.785465	4.113217	8.447862	12.92085	18.25358	21.5402	25.91155	30.97699	35.8667	41.85179	50.16065	58.40587	62.04167	62.77412	59.22488	54.95555	0.242761	62.77412	62.53136
	Left	TEA	2.798561	3.804391	5.305096	6.809555	11.12632	15.65649	21.17735	24.60037	29.13738	34.26802	39.23578	45.40295	53.96009	62.28705	66.09937	66.5781	63.15918	58.74912	2.798561	66.5781	63.77954
	Right	GCA	1.712087	2.718456	4.232553	5.709426	10.04305	14.57745	20.09117	23.51084	28.04779	33.18385	38.15371	44.3258	52.90007	61.23378	65.08653	65.50203	62.11657	57.68337	1.712087	65.50203	63.78995
	Right	FEA	0.207097	1.216246	2.727944	4.22417	8.5601	13.10167	18.63695	22.07249	26.62779	31.76111	36.72764	42.91163	51.50558	59.82359	63.7165	64.04875	60.71869	56.26425	0.207097	64.04875	63.84166
	Left	JCS	14.88372	14.90034	16.31857	20.40156	22.2564	27.19355	31.58974	35.71362	39.99541	41.22725	46.22178	53.1865	61.51976	68.25775	72.33257	72.34422	69.7704	66.48222	14.88372	72.34422	57.4605
	Left	TEA	15.38468	15.40153	16.84338	21.00934	22.90133	27.93557	32.38696	36.59914	41.02417	42.26961	47.44075	54.46674	62.86293	69.68717	73.508	73.87431	71.29644	68.00483	15.38468	73.87431	58.48963
	Right	GCA	14.91017	14.9268	16.35555	20.4837	22.35647	27.3388	31.75315	35.92041	40.2794	41.51567	46.60341	53.58687	61.94168	68.72012	72.7851	72.85872	70.28514	66.99889	14.91017	72.85872	57.94855
	Right	FEA	16.06773	16.08383	17.49237	21.5747	23.41813	28.31729	32.66879	36.76222	41.00283	42.22239	47.14637	54.0418	62.29973	68.95701	73.00984	72.9652	70.41301	67.15127	16.06773	73.00984	56.94211
beta (Ab/Adduction angle)	Left	JCS	-5.63599	-5.45277	-5.48174	-4.49995	-4.058	-3.27248	-1.81955	-0.84041	0.389994	1.240195	2.13072	3.65792	5.883184	7.379244	8.986859	7.47158	7.809245	6.432069	-5.63599	8.986859	14.62285
	Left	TEA	-1.79646	-1.82855	-2.18807	-1.51543	-2.02846	-2.24925	-2.01746	-1.79303	-1.55902	-1.83408	-2.00789	-1.74892	-1.17832	-1.15735	-0.15578	-1.76588	-0.86824	-1.5027	-2.24925	-0.15578	2.093473
	Right	GCA	1.955403	1.966272	1.668914	2.400403	2.042991	1.960381	2.324793	2.611333	2.903485	2.660501	2.483448	2.691466	3.106365	2.884255	3.744972	2.117288	3.142685	2.653015	1.668914	3.744972	2.076058
	Right	FEA	4.670495	4.662149	4.334381	5.03418	4.57432	4.368954	4.563623	4.734282	4.861089	4.416589	4.031112	3.963902	3.972545	3.33772	4.002706	2.356047	3.551398	3.284399	2.356047	5.03418	2.678133
	Left	JCS	7.220175	7.206139	7.200243	8.394153	8.577781	8.835485	8.065592	8.63218	10.2564	10.07938	11.74677	10.8653	10.2635	10.54913	10.06697	11.36672	11.55637	11.88756	7.200243	11.88756	4.687318
	Left	TEA	12.64272	12.62863	12.61648	13.77348	13.93114	14.09198	13.2085	13.6291	15.07856	14.84668	16.26594	14.98526	13.82605	13.60347	12.79528	14.08951	14.48741	15.0787	12.61648	16.26594	3.649466
	Right	GCA	10.04572	10.03155	10.01392	11.16428	11.32342	11.50192	10.64492	11.1156	12.62605	12.41403	13.97237	12.80525	11.87811	11.87482	11.2951	12.5073	12.81356	13.2894	10.01392	13.92731	3.913457
	Right	FEA	3.259185	3.244675	3.199023	4.291839	4.4365	4.611635	3.794406	4.339165	5.964038	5.791596	7.497491	6.722981	6.328545	6.841912	6.522383	7.821872	7.906598	8.114357	3.199023	8.114357	4.915335
gamma (Int/External Rotation angle)	Left	JCS	12.785	13.30601	13.10182	13.1932	10.65593	10.62533	10.3786	10.90842	11.09009	11.85479	12.81155	12.56726	12.38959	11.72343	10.04527	10.52776	11.30434	11.63215	10.04527	13.30601	3.260741
	Left	TEA	0.493535	0.95036	0.651168	-2.22613	-2.05166	-2.19919	-2.47732	-1.90998	-1.61273	-0.62392	0.643379	0.903948	1.637603	2.095306	0.978578	1.573942	1.799869	1.506891	-2.47732	2.095306	4.57263
	Right	GCA	2.973811	3.364387	2.964573	-0.01378	-0.14093	-0.61609	-1.3062	-1	-1.05389	-0.46653	0.41098	0.190299	0.270527	0.121979	-1.2613	-0.69522	-0.23528	-0.21274	-1.3062	3.364387	4.670586
	Right	FEA	1.903104	2.246016	1.775661	-1.27245	-1.59484	-2.26581	-3.181	-3.00603	-3.22274	-2.80136	-2.06673	-2.44002	-2.52119	-2.76472	-4.17445	-3.60554	-3.12935	-3.06534	-4.17445	2.246016	6.420466
	Left	JCS	1.151067	1.190928	1.099908	0.457583	0.625004	1.001643	1.809744	1.498361	2.056373	2.506968	2.414826	1.754244	2.015954	1.254855	1.022136	1.422576	0.988511	1.799198	0.457583	2.506968	2.049386
	Left	TEA	0.966303	1.004565	0.776285	-0.26325	-0.2751	-0.37027	0.033383	-0.65668	-0.49329	-0.1468	-0.68051	-1.86877	-2.16908	-3.33151	-3.76306	-3.38916	-3.69842	-2.71591	-3.76306	1.004565	4.76762
	Right	GCA	0.709267	0.748316	0.586465	-0.26064	-0.18467	-0.04669	0.559506	0.06023	0.424061	0.824117	0.518133	-0.39174	-0.38843	-1.32768	-1.64464	-1.25716	-1.63861	-0.7538	-1.64464	0.824117	2.468757
	Right	FEA	-0.51857	-0.47753	-0.46988	-0.82482	-0.52395	0.213841	1.349226	1.346463	2.226476	2.769643	3.053581	2.905545	3.757583	3.450592	3.475234	3.883704	3.287375	3.884505	-0.82482	3.884505	4.709325
O1 (Medio-Lateral Tibial displacement)	Left	JCS	13.87211	13.84366	13.9932	13.23948	12.45435	12.6424	12.17826	11.7159	11.55617	11.11266	10.94061	10.2129	8.982116	8.896966	8.802246	9.206833	8.86541	9.315596	8.802246	13.9932	5.190956
	Left	TEA	13.51086																		13.51086	18.65725	5.146139
	Right	GCA	16.10106																		15.20738	20.30605	5.098665
	Right	FEA	22.75448																		17.659621	22.75448	5.094859
	Left	JCS	39.75134																		36.81936	39.81588	2.99652
	Left	TEA	37.86095																		34.42317	37.86095	3.437782
	Right	GCA	28.88883																		25.66314	28.88883	3.225692
	Right	FEA	28.61774																		26.03289	28.61774	2.584849
O2 (Antero-Posterior Tibial Drawer)	Left	JCS	32.77871																		17.58717	32.77871	15.19154
	Left	TEA	31.57289																		27.71988	31.76791	4.048031
	Right	GCA	24.12124																		21.59762	24.1871	2.589485
	Right	FEA	10.45142																		6.954752	10.45441	3.496667
	Left	JCS	24.2922																		13.50335	24.39108	10.88773
	Left	TEA	17.97878																		17.5825	23.75919	6.176695
	Right	GCA	13.21348																		12.73578	19.03201	6.296232
	Right	FEA	18.64425																		18.30764	24.62653	6.318891

P005 6 DoF Kinematics [Raw Data]

		Frame Number	1	2	3	4	5	6	7	8	9	10	11	12	13	14	15	16	17	18	MIN	MAX	RANGE
alpha (Flex/Ext angle)	Left	JCS	34.09518	30.7129	28.87087	24.17906	21.92029	18.89664	15.78924	13.84081	12.19389	11.92496	13.93829	17.66758	21.28066	22.99058	24.32869	26.93725	29.74575	33.98938	11.92496	34.09518	22.17021
		TEA	35.1482	29.9209	29.9209	25.2158	22.94835	19.97198	16.84081	14.88718	13.24271	12.9657	15.00452	18.74209	22.30175	23.96761	25.32921	27.98965	30.78044	35.02555	12.9657	35.1482	22.1825
		GCA	34.11628	30.73891	28.90158	24.21338	21.95534	18.95526	15.84323	13.89545	12.25144	11.97987	14.00016	17.72764	21.31411	23.00291	24.34768	26.97288	29.76735	34.00058	11.97987	34.11628	22.13641
		FEA	35.40174	32.01546	30.1745	25.47042	23.20336	20.22158	17.09203	15.13836	13.4933	13.21679	15.25422	18.99165	22.55731	24.22901	25.58854	28.24261	31.03721	35.28482	13.21679	35.40174	22.18495
	Right	JCS	38.73202	34.49799	31.95342	31.18593	28.74149	26.74893	24.06856	22.41607	20.87574	21.96647	25.15055	26.93873	27.59044	30.59872	31.91683	32.75032	34.59139	35.61229	20.87574	38.73202	17.85628
		TEA	40.38804	36.14024	33.58146	32.83636	30.43014	25.69683	28.37547	24.07006	22.52169	23.67779	26.90568	28.62983	29.27641	32.3033	33.59951	34.43424	36.29161	37.28284	22.52169	40.38804	17.86635
		GCA	38.93842	34.7121	32.17128	31.4043	28.96404	26.97264	24.29531	22.64658	21.10738	22.022	25.38311	27.16465	27.81503	30.81758	32.13328	32.95505	34.80101	35.3822	21.10738	38.93842	17.83104
		FEA	39.75923	35.5038	32.93638	32.22274	29.85789	27.74647	25.07219	23.45891	21.9038	23.09439	26.36989	28.05449	28.69853	31.7549	33.02742	33.86538	35.75418	36.69389	21.9038	39.75923	17.85542
beta (Ab/Adduction angle)	Left	JCS	3.907603	3.816123	3.723849	3.450088	3.265106	4.209224	3.666182	3.528783	3.520883	3.391667	3.850744	4.140652	3.11807	2.017016	2.499473	3.890666	3.19604	2.745322	2.017016	4.209224	2.192208
		TEA	-4.21362	-4.3355	-4.17977	-4.41056	-4.50285	-3.41724	-3.79104	-3.81133	-3.82499	-3.49604	-3.49604	-4.24768	-4.62133	-5.79525	-5.37427	-4.06665	-4.84029	-5.35315	-5.79525	-3.41724	2.378006
		GCA	1.428325	1.277988	1.392035	1.092752	0.945575	1.945707	1.467057	1.373309	1.404223	1.281549	1.692943	1.901783	0.809918	-0.32069	0.139882	1.492121	0.761338	0.267002	-0.32069	1.945707	2.2664
		FEA	-4.19033	-4.32881	-4.20012	-4.43597	-4.53392	-3.46815	-3.85699	-3.88656	-3.79681	-3.90926	-3.57072	-3.47861	-4.66094	-5.82673	-5.39103	-4.07848	-4.83841	-5.35315	-5.82673	-3.46815	2.358577
	Right	JCS	3.449423	3.086995	2.784929	3.269719	3.96713	2.778092	2.784649	3.154132	2.991586	4.006844	4.919284	3.929304	3.865869	4.383429	3.985726	4.050554	4.548456	3.829999	2.778092	4.919284	2.141192
		TEA	-3.92822	-4.14202	-4.33556	-3.81589	-2.99832	-4.07756	-3.91249	-3.43877	-3.49819	-2.55842	-1.84743	-2.93882	-3.03811	-2.67555	-3.13435	-3.10657	-2.68541	-3.4424	-4.33556	-1.84743	2.488134
		GCA	-1.29044	0.909753	0.602415	1.086457	1.784096	0.598179	0.613087	0.990079	0.836156	1.845134	2.743767	1.748978	1.684315	2.19986	1.803166	1.869227	2.371483	1.656411	0.598179	2.743767	2.145587
		FEA	4.576565	4.672542	4.64244	5.2057	6.154169	5.176593	5.454378	5.986447	5.975871	6.879344	7.469185	6.302323	6.172324	6.374546	5.840373	5.816646	6.115602	5.291879	4.576565	7.469185	2.89262
gamma (Int/External Rotation angle)	Left	JCS	4.699941	4.994429	6.287913	6.93136	6.159169	8.19908	7.997121	8.20411	8.565672	9.860074	9.749	8.42545	7.566431	6.348419	6.002404	6.666326	5.999145	7.935598	4.699941	9.860074	5.160134
		TEA	3.888983	3.705797	4.741227	4.733879	5.693075	5.401151	4.678049	4.63324	4.78562	5.069501	6.302956	5.353863	4.973383	3.983219	3.822353	3.784968	4.57369	4.13925	3.705797	6.302956	2.597159
		GCA	4.205589	4.354709	5.569876	6.017557	7.193138	7.182527	6.749001	6.882	7.182148	7.490604	8.541436	7.249813	6.5347	5.386086	5.094921	4.801335	5.318344	4.467819	4.205589	8.541436	4.335847
		FEA	4.170056	3.987807	5.023258	5.01485	5.972855	5.678288	4.952103	4.90489	5.054965	5.338476	6.574662	5.629844	5.252779	4.264179	4.10377	4.066715	4.855974	4.420848	3.987807	6.574662	2.586855
	Right	JCS	15.81869	16.07306	16.26525	17.21464	16.54432	16.54593	16.89182	16.37196	15.60314	15.06465	15.54905	16.11399	15.66747	15.51357	15.32544	15.39204	15.14638	14.40293	14.40293	17.21464	2.811713
		TEA	14.07798	13.79181	13.66448	14.52038	13.55274	13.31029	12.62968	12.62968	11.68459	11.2737	12.13012	12.90502	12.53652	12.74994	12.72369	12.89413	12.88036	12.26468	11.27377	14.52038	3.246618
		GCA	16.14628	16.24034	16.3357	16.49238	16.49238	16.41815	16.07986	16.07986	15.25299	14.75546	15.36033	15.99338	15.57169	15.53243	15.39454	15.49288	15.31733	14.61257	14.61257	17.25587	2.643297
		FEA	9.573937	9.930074	10.20041	11.17053	10.57999	10.67283	11.13642	11.13642	10.00242	9.39722	9.720284	10.22119	9.749	9.477465	9.25013	9.290033	8.986073	8.223804	8.223804	11.17053	2.946723
Q1 (Medio-Lateral Tibial displacement)	Left	JCS	-0.34355	-0.314	-0.88545	-0.85813	-1.27031	-1.16218	-1.51009	-1.42903	-1.60569	-1.63669	-1.3492	-0.94359	-1.61875	0.116994	0.051424	-0.28916	0.049911	1.034346	-1.63669	1.034346	2.671032
		TEA	6.608362	6.652688	6.001768	6.034687	5.638981	5.690662	5.283851	5.367674	5.108162	5.117656	5.424837	5.895012	5.312287	7.057214	6.990583	6.666326	6.9867	7.935598	5.108162	7.935598	2.827436
		GCA	3.544686	3.577137	2.990072	3.018489	2.609549	2.706584	2.347097	2.428696	2.235753	2.212715	2.504071	2.922371	2.265386	4.002931	3.937152	3.599774	3.935173	4.912623	2.212715	4.912623	2.699908
		FEA	6.687938	6.732846	6.078794	6.111935	5.716877	5.766334	5.357202	5.441134	5.178357	5.189446	5.497404	5.970123	5.391041	7.136329	7.069656	6.746043	7.06568	8.013178	5.178357	8.013178	2.834821
	Right	JCS	3.617215	3.595179	3.579299	3.095491	2.226655	2.584833	1.7481	1.49677	1.271009	0.958266	0.788844	0.958452	1.176537	3.034503	2.508167	2.517228	2.382511	3.206513	0.788844	3.617215	2.82837
		TEA	7.616694	7.578399	7.521703	7.012754	6.120625	6.451083	5.577655	5.293768	5.02147	4.718442	4.600473	4.818777	5.042748	6.960054	6.412569	6.443152	6.329527	7.156857	4.600473	7.616694	3.016221
		GCA	4.866115	4.837699	4.805801	4.312126	3.434149	3.781449	2.930316	2.66621	2.422186	2.113255	1.964025	2.152743	2.373138	4.254391	3.719755	3.737263	3.610823	4.43613	1.964405	4.866115	2.902089
		FEA	3.830861	3.861633	3.861633	3.408081	2.567277	2.958815	1.954096	1.784341	1.459907	1.459907	1.228563	1.339566	1.550567	3.33712	2.836235	2.819395	2.659294	3.479292	1.228563	3.861633	2.835764
Q2 (Antero-Posterior Tibial Drawer)	Left	JCS	26.47861	26.62551	26.62551	26.37011	26.06093	25.61126	26.13465	26.3586	26.34502	26.88524	26.6416	26.51393	25.86286	25.11015	25.53366	25.74444	25.76859	26.12188	25.11015	27.00439	1.894237
		TEA	16.81778	17.1433	17.1354	17.1354	16.9728	16.7609	17.51359	17.90948	18.03936	18.60686	18.18829	17.7524	16.82042	15.93622	16.28569	16.37943	16.25767	16.44961	15.93622	18.60686	2.670642
		GCA	15.58558	16.6675	16.60739	17.20744	17.3322	17.49324	18.65597	19.2941	19.63722	20.23541	19.55876	18.64716	17.25889	16.1652	16.33691	16.07304	15.59527	15.2417	15.24147	20.23541	4.993943
		FEA	17.79445	18.27	17.86945	17.63783	17.3677	17.00727	17.60668	17.90865	17.9559	18.51171	18.19088	17.93746	17.18586	16.3874	16.80034	17.01842	17.03125	17.42235	16.3874	18.51171	2.124314
	Right	JCS	29.46589	30.14546	30.22643	30.88148	31.34678	31.38054	31.76596	31.31864	30.974	30.77686	31.35326	31.00504	30.54972	30.32508	29.465	29.07111	29.53072	28.46865	28.46865	31.76596	3.297303
		TEA	19.47245	19.90893	19.86779	20.48643	20.88823	20.84875	21.19158	20.74684	20.39233	20.22306	20.83768	20.50722	20.06959	19.95027	19.12839	18.78113	19.32226	18.31686	18.31686	21.19158	2.874716
		GCA	20.12038	21.15414	21.47138	21.47138	22.91315	23.16116	23.61116	22.93234	23.44487	23.1147	23.31402	22.76585	22.24011	21.70286	20.71292	20.24075	20.52927	19.38046	19.38046	23.85071	4.470252
		FEA	26.34283	26.82782	26.79569	27.43586	27.85002	27.76801	27.768	27.60802	27.21802	27.0902	27.78476	27.45248	27.0176	26.92311	26.0009	25.73811	26.28669	25.24206	25.24206	28.0782	2.83614
Q3 (Tibial Distraction-Compression)	Left	JCS	32.93405	32.12125	32.69898	33.70705	34.50789	34.72205	34.77994	35.32295	34.99722	35.39461	34.97598	34.5711	34.98036	34.98926	34.54728	34.19062	33.60082	32.52757	32.52757	35.39461	2.867041
		TEA	31.34871	30.9343	30.10462	30.3167	30.68736	30.35312	30.10666	30.10666	29.86766	29.84233	29.75927	30.01035	31.01547	31.62724	31.37461	31.35082	31.33985	31.1775	29.49242	31.62724	2.134826
		GCA	23.81212	23.37663	22.59581	22.82911	23.26602	22.99314	22.93234	22.93234	22.39856	22.7688	22.58506	22.67807	22.63397	23.03014	23.77586	23.77672	23.72138	23.49471	22.39856	24.03014	1.631584
		FEA	33.92591	33.55431	32.74762	32.99989	38.38373	33.06532	32.81297	32.81297	32.19393	33.53985	32.46599	32.72072	33.71469	34.3177	34.05702	34.01678	33.97484	33.75338	32.19393	34.3177	2.123764
	Right	JCS	24.24905	24.36834	23.74567	23.74567	24.15064	24.41463	24.75817	24.74448	24.82277	24.60612	23.91948	24.22286	24.32436	24.28047	24.20629	24.58095	24.1633	24.75131	23.74567	24.82277	1.077101
		TEA	27.74628	27.0399	26.51222	25.67959	25.14191	25.14191	25.50252	24.72407	24.48247	24.41506	24.29682	25.02653	25.2999	26.0717	26.23081	26.78055	26.67871	27.61865	24.29682	27.74628	3.449464
		GCA	19.88291	19.3153	18.883	18.15325	17.86981	17.87572	17.72361	17.81559	17.67956	17.59558	17.34122	17.91161	18.1191	18.59644	18.70905	19.21531	19.07935	19.86737	17.34122	19.88291	2.541691
		FEA	26.24498	26.05065	25.83297	25.15304	25.05136	25.24459	25.31879	25.50252	25.48208	25.29476	24.79554	25.31887	25.47601	25.57276	25.66372	26.10712	25.79527	26.5076	24.79554	26.5076	1.71205

P0066 DoF Kinematics [Raw Data]

		Frame Number	1	2	3	4	5	6	7	8	9	10	11	12	13	14	15	16	17	18	MIN	MAX	RANGE
alpha (Flex/Ext angle)	Left	JCS	21.38086	21.30832	21.21837	18.74858	19.80912	19.4203	19.17257	18.59924	20.46836	22.07457	22.26697	25.13304	28.13216	32.21167	36.33736	40.38818	46.4009	49.91974	18.59924	49.91974	31.3205
		TEA	23.23431	23.15733	23.00259	20.62161	21.58659	21.22488	21.05669	20.47473	22.27387	23.92051	24.08617	26.89594	29.87632	33.93728	38.02492	42.02584	47.95932	51.42706	20.47473	51.42706	30.95233
		GCA	22.16627	22.09346	21.99596	19.54572	20.59015	20.20606	19.96977	19.39722	21.25097	22.85655	23.04516	25.89502	28.88106	32.94149	37.04531	41.07415	47.05505	50.55815	19.39722	50.55815	31.16093
		FEA	22.29037	22.21704	22.10407	19.6949	20.70325	20.32925	20.11952	19.54824	21.36884	22.97327	23.15464	25.9742	28.93393	32.94939	37.00148	40.98037	46.88904	50.3636	19.54824	50.3636	30.81536
	Right	JCS	11.37361	11.36412	11.2995	9.535532	9.895272	6.602781	9.659495	13.61362	12.69037	11.58456	11.51828	13.32892	19.21673	23.04646	25.2741	27.5247	32.56637	35.9452	6.602781	35.9452	29.34242
		TEA	12.73766	12.72629	12.6627	10.88791	11.2498	7.99662	11.01334	14.99059	14.06659	12.96648	12.83822	14.65921	20.52172	24.32354	26.54248	28.85247	33.91797	37.28317	7.99662	37.28317	29.28655
		GCA	12.01679	12.00593	11.942	10.16882	10.53035	7.260849	10.29391	14.26877	13.34391	12.24104	12.12935	13.94819	19.8156	23.61764	25.83423	28.14312	33.21104	36.57335	7.260849	36.57335	29.3125
		FEA	12.49235	12.48448	12.41903	10.66596	11.0235	7.700149	10.78853	14.71962	13.79766	12.68783	12.6746	14.47479	20.37948	24.22991	26.46348	28.66592	33.68941	37.07991	7.700149	37.07991	29.37976
beta (Ab/Adduction angle)	Left	JCS	10.18123	10.09387	9.00823	9.998111	8.663551	9.033552	10.25101	10.00945	9.227115	10.19421	9.78291	9.362753	9.637239	10.24375	10.55896	10.61347	10.54154	10.21923	8.663551	10.61347	1.949919
		TEA	6.105244	6.022352	4.944041	6.082794	4.685209	5.07842	6.308802	6.103456	5.207549	6.077362	5.655564	5.074332	5.190513	5.601047	5.742268	5.6502	5.406083	5.008791	4.685209	6.308802	1.623593
		GCA	8.405618	8.318781	7.233817	8.24309	6.899836	7.27296	8.492412	8.255709	7.458249	8.413794	8.001221	7.564274	7.825975	8.423029	8.738015	8.801429	8.7593	8.463519	6.899836	8.801429	1.901593
		FEA	0.274089	0.188334	-0.89505	0.158332	-1.20533	-0.82498	0.398895	0.174087	-0.65872	0.272743	-0.1422	-0.60481	-0.34862	0.276062	0.659862	0.830516	1.018988	0.89422	-1.20533	1.018988	2.224321
	Right	JCS	0.802515	0.755358	0.79971	0.473513	0.534094	1.417534	0.512411	1.180941	1.138984	1.254132	-0.29629	-0.0088	-0.5978	-1.35424	-1.61869	0.095758	0.882144	0.476997	-1.61869	1.417534	3.036226
		TEA	-0.12892	-0.17566	-0.14874	-0.38358	-0.33762	0.679634	-0.34974	0.160238	0.154801	0.313892	-1.23263	-1.01735	-1.83266	-2.72928	-3.07263	-1.43683	-0.81591	-1.3242	-3.07263	0.679634	3.752266
		GCA	2.291522	2.244662	2.270888	2.01552	2.065853	3.040232	2.050886	2.603283	2.589024	2.736779	1.422654	1.649848	0.649848	-0.23308	-0.57352	1.061343	1.66599	1.136179	-0.57352	3.040232	3.613749
		FEA	2.004368	1.956913	1.979036	1.611978	1.68506	2.451547	1.655178	2.458399	2.385443	2.462941	0.911162	1.259795	0.861407	0.220919	0.020604	1.796596	2.712484	2.386552	0.020604	2.712484	2.69188
gamma (Int/External Rotation angle)	Left	JCS	-0.07144	-0.11171	-0.11516	1.67227	0.044249	0.085238	0.231471	0.201652	-0.40623	-0.40062	0.383467	-2.79797	-3.89391	-4.26217	-5.69537	-6.47433	-7.13821	-7.95452	-7.95452	1.67227	9.626785
		TEA	-3.52546	-3.57036	-3.57396	-1.96556	-3.51217	-3.50021	-3.37879	-3.44653	-3.9194	-3.80476	-3.00423	-5.9717	-6.83921	-6.88498	-7.97714	-8.40887	-8.54015	-9.03707	-9.03707	-1.96556	7.071506
		GCA	-0.48548	-0.52793	-0.53312	1.17646	-0.41722	-0.38866	-0.25152	-0.29879	-0.84778	-0.79292	-0.00238	-3.09309	-4.09385	-4.33167	-5.63223	-6.28119	-6.75414	-7.46091	-7.46091	1.17646	8.637373
		FEA	-1.3332	-1.38595	-1.40502	-0.04093	-1.48777	-1.51321	-1.40926	-1.53706	-1.82491	-1.54295	-0.72569	-3.41201	-3.98821	-3.64941	-4.37054	-4.45677	-4.11139	-4.35159	-4.45677	-0.04093	4.41584
	Right	JCS	2.332198	2.317971	2.331797	2.254238	2.321466	1.751906	2.248273	1.267628	0.13725	-1.16082	-0.36597	-0.57519	-0.95504	-0.31415	-0.79609	0.99121	0.508737	1.548527	-1.16082	2.332198	3.493016
		TEA	0.036835	0.022448	0.035229	-0.04678	-0.29879	-0.84778	-1.29482	-2.1361	-2.83779	-2.89958	-3.45276	-2.71564	-2.42673	-2.25221	-1.82491	-0.94012	-0.45206	-0.15208	-3.45276	0.036835	3.489599
		GCA	0.659688	0.645762	0.661241	0.630706	0.688224	0.208257	0.62137	-0.46228	-1.56946	-2.83938	-2.04125	-2.29676	-2.42673	-2.25221	-2.77633	-1.02879	-0.5889	-0.59126	-2.83938	0.688224	3.527602
		FEA	4.296223	4.281938	4.297147	4.255247	4.315333	3.809663	4.246834	3.183498	2.073389	0.799174	1.345707	1.212544	1.364518	0.820082	1.364518	1.905355	2.542527	2.834368	0.799174	4.315333	3.516158
Q1 (Medio-Lateral Tibial displacement)	Left	JCS	2.837833	2.995355	3.362085	3.3035	4.152862	4.193628	2.860886	3.845872	3.513078	2.818677	2.954463	2.24856	2.61229	1.955376	1.945563	1.384321	1.238364	1.473379	1.238364	4.193628	2.955264
		TEA	3.554836	3.714664	4.058012	4.02191	4.861297	4.909507	3.581983	4.586657	4.213757	3.588575	3.704287	3.015404	3.399718	2.762371	2.765269	2.221571	2.077078	2.317359	2.077078	4.909507	2.83243
		GCA	3.048518	3.207364	3.560673	3.514993	4.358629	4.403668	3.073921	4.070208	3.714393	3.059723	3.183987	2.487853	2.863399	2.217716	2.215199	1.664028	1.518911	1.756948	1.518911	4.403668	2.884758
		FEA	6.541812	6.707062	6.995448	7.012195	7.828133	7.893842	6.578584	7.629536	7.16236	6.699889	6.768412	6.11954	6.55224	5.960887	5.993662	5.491207	5.350152	5.602816	5.350152	7.893842	2.54369
	Right	JCS	1.87355	1.876282	1.793994	1.75417	1.738721	1.883043	1.734364	2.3309	1.645832	1.88448	1.960453	2.144465	2.092338	2.535287	3.264845	3.679656	4.362368	5.62252	1.645832	5.62252	3.976688
		TEA	2.503382	2.506126	2.414644	2.369531	2.352773	2.500376	2.349126	2.964952	2.282248	2.523503	2.603792	2.793831	2.742891	3.189421	3.922096	4.342192	5.031381	6.28152	2.282248	6.28152	3.999272
		GCA	-0.31804	-0.31534	-0.37137	-0.39609	-0.4078	-0.27284	-0.41418	0.12726	-0.56456	-0.33336	-0.26972	-0.10292	-0.15843	0.274287	0.994943	1.39466	2.058875	3.347625	-0.56456	3.347625	3.912186
		FEA	2.733353	2.736067	2.667251	2.635178	2.621646	2.761163	2.61625	3.18452	2.495988	2.730814	2.800462	2.975642	2.921778	3.359478	4.084468	4.491535	5.164757	6.439582	2.495988	6.439582	3.943594
Q2 (Antero-Posterior Tibial Drawer)	Left	JCS	23.78618	23.68435	24.38217	24.17117	23.66588	23.74426	23.55449	22.00269	22.56836	23.96171	23.95429	24.36309	24.85506	25.70588	25.76319	25.94641	26.19148	26.62539	22.00269	26.62539	4.622704
		TEA	17.44841	17.34348	17.98294	17.68359	17.19797	17.1046	17.0046	15.55056	16.15821	17.70384	17.68179	18.26716	18.98005	20.15269	20.57047	21.13625	21.98069	22.78525	15.55056	22.78525	7.234693
		GCA	14.92715	14.82984	15.51794	15.44274	14.8776	13.98387	14.80796	13.3003	13.75166	15.08793	15.06439	15.36145	15.76321	16.52786	16.55038	16.7487	17.09631	17.63739	13.3003	17.63739	4.337087
		FEA	13.53762	13.44446	14.13489	14.2135	13.57828	12.71019	13.5545	12.08196	12.41572	13.65432	13.61877	13.74351	13.96979	14.50164	14.29814	14.28427	14.34366	14.73264	12.08196	14.73264	2.650683
	Right	JCS	30.28095	30.27381	31.99292	31.01427	31.16061	30.16626	31.07239	31.39831	29.5294	28.45714	28.58398	27.50382	29.1322	28.13723	27.18813	26.71909	27.3371	25.45838	25.45838	31.99292	6.534545
		TEA	21.81577	21.80822	23.49771	22.57071	22.70005	21.87501	22.62282	22.8751	21.04919	20.02593	20.13738	19.03017	20.5341	19.53166	18.60972	18.21623	18.97476	17.21349	17.21349	23.49771	6.284222
		GCA	21.70988	21.70366	23.4165	22.68167	22.77479	22.2806	22.72137	22.52804	20.79089	19.87713	20.00259	18.68948	19.57377	18.15765	16.99039	16.34313	16.57184	14.46466	14.46466	23.4165	8.951842
		FEA	15.76313	15.75802	17.46033	16.76386	16.84665	16.42072	16.7995	16.53931	14.82228	13.92855	14.09182	12.75183	13.59527	12.2069	11.0698	10.41952	10.73017	8.725324	8.725324	17.46033	8.73501
Q3 (Tibial Distraction-Compression)	Left	JCS	18.97218	19.06934	18.31757	19.55946	19.21092	19.7689	19.584	20.7617	19.27319	20.0068	19.48948	19.13688	18.56406	17.63753	16.9641	16.58515	15.35332	14.48068	14.48068	20.7617	6.281027
		TEA	22.55174	22.65571	21.90514	22.81791	22.7003	23.23791	23.06147	24.11619	22.8347	23.67322	23.13904	22.93695	22.95509	22.39253	22.16006	22.1373	21.43191	20.85423	20.85423	24.11619	3.261956
		GCA	16.46702	16.55815	15.77993	16.6462	16.48201	16.99818	16.91084	17.87562	16.65149	17.6102	17.1224	17.19619	17.11448	17.08388	16.82277	16.814	16.50183	14.63151	15.77993	17.87562	2.095687
		FEA	13.70429	13.81855	13.1085	13.87982	13.89731	14.40531	14.09169	15.19729	13.98567	14.86953	14.41307	14.48024	14.5392	14.27914	14.42804	14.77518	14.74738	14.63151	13.1085	15.19729	2.088795
	Right	JCS	26.1649	26.17354	24.86084	25.30758	24.97114	26.97636	25.17397	25.37043	26.47412	27.42625	27.95322	28.14753	25.71976	25.2891	25.47362	25.68537	24.97311	24.42257	24.42257	28.14753	3.724955
		TEA	24.15125	24.15947	22.7947	22.98828	22.70454	24.19337	22.87207	23.69149	24.67958	25.48133	26.02266	26.53036	25.02471	25.25509	25.83975	26.41611	26.50775	26.57677	22.70454	26.57677	3.872238
		GCA	18.14513	18.15132	16.81027	16.99229	16.70988	18.25583	16.87789	17.68892	18.6833	19.47116	19.95303	20.44601	18.96644	19.19417	19.77271	20.43757	20.69194	20.79879	16.70988	20.79879	4.088907
		FEA	16.95161	16.95831	15.59622	15.60997	15.36246	16.54874	15.50692	16.71187	17.6225	18.29909	18.8234	19.50839	18.66139	19.33392	20.1628	20.98906	21.70716	22.16164	15.36246	22.16164	6.799175

ANNEX I: MATLAB PARENT SCRIPT (`SKM.M`)

Strathclyde Knee Modelling (SKM) Software v.2.3

4D CT volume segmentation, registration and kinematic data analysis

Copyright© 2016 Andre Attard, University of Strathclyde.

Start with a clean slate (and start timer)

```matlab
clear;
close all;
clc;
imtool close all;

% Start timer
tic0 = tic;
```

Initialise data structure array to save all data

```matlab
data = struct();

% Update log
data.log = cell(1,2);
data = logIt(data, 'Strathclyde Knee Modelling software (v2.3)\n',...
                                                '*Keywords');
data = logIt(data, strcat('Kindly refer to these messages to view the',...
                    ' progress\nof the code execution.\n'), '-Errors');
```

Get 4DCT filenames, sort DICOM files and generate GUI

```matlab
data = sortDICOM(data);

% Create data structure fields
data = createDataStruct(data);

% Create GUI
data = createPlots(data);

% Input participant and session details and save in |data| structure. This
% will be used to anonymously label saved results.
```

Volume pre-processing

```matlab
% Measure Time Elapsed
data.timer.initialisingTime = secs2hms(toc(tic0));
data = logIt(data, sprintf('Time for initialisation: %s\n\n', ...
```

```matlab
                                    secs2hms(toc(tic0))), 'Strings');

% Clear any unnecessary variables
clear prompt default tic0 cmap;

%  Read, permute, threshold, identify bones, (register), find ROIs and
%  model them
for i = 1:length(data.fileList)
    % Update log
    data = logIt(data, sprintf('Segmentation for Frame %d initiated.\n',...
                                                i), 'Keywords');

    % Start timer for each time phase
    eval(sprintf('tic%d = tic;', i));


    % Update log
    data = logIt(data, 'Extracting raw data ... ', 'Comments', 0);


    % Read DICOM data
    data.raw{i} = dicomread(data.fileList(i).name);


    % Remove singleton dimension
    data.raw{i} = squeeze(data.raw{i});


    % Rotate matrix and save as RAW
    % !!To make an interactive rotation module by showing A-P M-L on image
    % and allowing the user to select where is what (similar to Mimics)!!
    data.raw{i} = flip(data.raw{i}, 3);


    % Compute a 3D affine transformation matrix to scale raw data to real
    % size dimensions. Each voxel will be 1mm x 1mm x 1mm in real world
    % dimensions
    tform = affine3d([data.voxScale(1)      0               0       0; ...
                        0           data.voxScale(2)         0       0; ...
                        0               0           data.voxScale(3) 0; ...
                        0               0               0           1]);
    %data.mask{i} = imwarp(data.mask{i}, tform);
    data.raw{i} = imwarp(data.raw{i}, tform);
    data.size{i} = size(data.raw{i});


    % Update log
    data = logIt(data, 'Complete\n', 'Comments');


    % Clear raw field data (required for memory management).
    clear tform;
```

GUI setup

```
% Visualise GUI panels
data.Plots{1,4}.Visible = 'on';
data.Plots{1,5}.Visible = 'on';
```

Segmentation module

Volume Pre-processing

Divided raw volume into two parts, the healthy and replaced knee, and determine which of the three possible combinations of knees is occurring in the data being analysed. This will affect which loops in the following segmentation algorithm are used.

```
data = preProcMod(data, i);

% Adjust loop according to mode identified in |preProcMod|
switch getappdata(0, 'mode')
    case 1 % 2 Healthy Knees
        % Extract healthy knees bone masks (1)
        m = 1;
        n = 1;
    case 2 % 1 Healthy & 1 Replaced Knee
        % Frame 1: Extract healthy knee bone mask (1) and Replaced knee
        %          implant mask (2) and bone mask (3).
        if i == 1
            m = 1;
            n = 3;
        % Remaining Frames: Extract healthy knee bone mask (1) and replaced
        %                   knee implant mask (2) only
        else
            m = 1;
            n = 2;
        end
    case 3 % 2 Replaced Knees
        % Frame 1: Extract Replaced knees implant mask (2) and bone mask (3)
        if i == 1
            m = 2;
            n = 3;
        % Remaining Frames: Extract implant masks (2) only.
        else
            m = 2;
            n = 2;
        end
end

% Loop segmentation process form |SKMv2_2| N times (healthy knee,
% implant vs soft-tissue, and bone).
```

```matlab
    for counter = m:n
        % Fuzzy C-means segmentation, segments N-dimensional grayscale
        % images into c-classes using a memory efficient implementation of
        % the FCM clustering algorithm. The computational efficiency is
        % acheived by using the histogram of the image intensities during
        % the clustering process instead of the raw image.
        data = segModule(data, i, counter);
```

Set orientation of mask.

This is done in order to make sure that the knee model is always facing the same direction. Otherwise, some parts of the code will not work correctly due to dependency on the axis limits - which will vary if the model has different orientations for each patient.

```matlab
        % Run orientation module
        data = orientMask(data, i, counter);

        % Subtract implant from bone mask (to aid manual segmentation)
        if counter == 3
            for cc = 1:length(data.temp{3,1}.subMask)
                data.mask{i}(data.temp{3,1}.subMask{cc,1} == 1) = 0;
            end

            % Generate patch
            % axes(data.Plots{1,2});
            data.patches{1,i} = PATCH_3Darray(data.mask{i}, ...
                                                    [0.65 0.65 0.65]);
            data.patches{1,i}.AmbientStrength = 0.3;
            data.patches{1,i}.DiffuseStrength = 0.3;
            data.patches{1,i}.SpecularStrength = 0.3;
            data.patches{1,i}.SpecularExponent = 5;
            data.patches{1,i}.SpecularColorReflectance = 0.3;
            data.patches{1,i}.FaceLighting = 'gouraud';
            data.patches{1,i}.BackFaceLighting = 'lit';
            title(sprintf('Segmented mask for Frame %d of %d', i, ...
                                        length(data.fileList)));
            view(-100,40);

            % Add lighting
            data.Plots{1,6} = camlight('left');
            data.Plots{2,6} = camlight('right');
            data.Plots{1,6}.Style = 'infinite';
            data.Plots{2,6}.Style = 'infinite';

            % Hide patch
            data.patches{1,i}.Visible = 'off';
        end
```

Crop mask to ROI (Remove unwanted regions)

```matlab
% Run cropping module
data = cropModule(data, i);
```

Remove remaining small unwanted volumes

```matlab
% Run module to remove patella and any remaining small voxels
data = deleteModule(data, i, counter);
```

Isolate disconnected volumes (bone(s)) into individual subMasks

```matlab
data = isolateMasks(data, i);
```

Manually segment connected bones that remain in mask

For the case that bones are very close to each other, such that they were not identified as separate bodies by the segmentation method, this module takes the user through a slice by slice manual segmentation

```matlab
% *Ask user if he wants to perform Manual Segmentation.*
% This is an intensive task which is only required if the bones are
% connected by a small amount of voxels. Here if the number of masks
% is equal to 4 (i.e. 2 femurs + 2 tibias) the user
% is informed that manual segmentation should not be required.
if data.nVolumes{i} == 4
    choice = questdlg({'There are already the required 4 bones',...
        ' in the mask. Are you sure you want to further manually',...
        ' segment the mask?'}, ...
        'Manual segmentation confirmation.', 'No');
    switch choice
        case 'No'
        case 'Yes'
            % Run module to manually separate remaining attached
            % bones
            data = manualSeg(data, i);
    end
    clear choice
else
    % Run module to manually separate remaining attached bones
    data = manualSeg(data, i);
end
```

Remove the disconnected components in the masks

```matlab
        % Run module to remove any remaining small voxels (as a result of
        % manual segmentation)
        data = deleteModule(data, i, counter);
```

Isolate remaining bones into subMasks

```matlab
        data = isolateMasks(data, i);
```

Final check to make sure all 4 bones are isolated

```matlab
        marker = 0;
        while marker == 0
            if data.nVolumes{i} ~= 4
                choice = questdlg({'There should be 4 seperate bones in',...
                    ' the mask. It is highly suggested to retry manual',...
                    ' segmentation in order to segment ALL FOUR',...
                    ' individual bones. Do you want to perform further',...
                    ' manual segmention of the individual masks?'}, ...
                    'Manual segmentation confirmation.', 'Yes');
                switch choice
                    case 'Yes'
                        % Run module to manually seperate remaining
                        % attached bones
                        data = manualSeg(data, i);
                        % Run module to remove any remaining small voxels
                        % (as a result of manual segmentation)
                        data = deleteModule(data, i, counter);
                        % Isolate remaining bones into |subMasks|
                        data = isolateMasks(data, i);
                    case 'No'
                        marker = 1;
                end
                clear choice
            elseif data.nVolumes{i} == 4
                choice = questdlg({'There are already the required 4',...
                    ' volumes in the mask. Are you sure you want to',...
                    ' perform further manual segmentation of the',...
                    ' individual masks?'}, ...
                    'Manual segmentation confirmation.', 'No');
                switch choice
                    case 'Yes'
                        % Run module to manually seperate remaining
                        % attached bones
                        data = manualSeg(data, i);
                        % Run module to remove any remaining small voxels
                        % (as a result of manual segmentation)
```

```
                        data = deleteModule(data, i, counter);
                        % Isolate remaining bones into |subMasks|
                        data = isolateMasks(data, i);
                    case 'No'
                        marker = 1;
                end
                clear choice
            end
        end
```

Post-process volume

Clear `nVolumes`, `nMasks`, `subMask`, etc.... leave data array as if it is in pre-seg stage - except if both knees are segments, in that case, join the mask and adjust the data substructures to match.

```
        data = postProcMod(data, i, counter);
    end
```

Volume identification and mask Labelling

This is required for the registration of the other volumes. When the volumes are labelled, any of the bones can be selected depending on laterality of bones.

```
    data = boneLabel(data, i);
```

Visualise segmentation

```
    data = visFrame(data, i);
```

Sorting of masks

Sort the masks by laterality of bone and kind of bone. The subscripts of the corresponding masks are saved in fields `LBonesIdx`, `RBonesIdx`, `femurIdx`, and `tibiaIdx` in the `data` structure.

```
    data = sortMasks(data, i);

    % Measure time elapsed to segment bone in this frame
    eval(sprintf('data.timer.segmentation%d = secs2hms(toc(tic%d));',i,i));
    time = eval(sprintf('secs2hms(toc(tic%d))', i));
    data = logIt(data, sprintf('Time to Segment Frame %d: %s\n\n', i, ...
                time), 'Strings');
```

```matlab
    % Clear obsolete variables
    eval(sprintf('clear time marker tic%d choice counter m n', i));
end
```

Play all saved frames once at 3fps

Create temp axes

```matlab
tempAxes = axes('Parent', data.Plots{1,4}, 'Color', ...
        [0.94 0.94 0.94], 'Units', 'normalized', 'DataAspectRatio', ...
        [1 1 1], 'Visible', 'off', 'Position', [0.025 0.025 0.95 0.95], ...
        'Box', 'on', 'LineWidth', 2, 'XLim', ...
        [0 data.info{1,1}.Rows*data.voxScale(1)], 'YLim', ...
        [0 data.info{1,1}.Columns*data.voxScale(2)], 'ZLim', ...
        [0 data.info{1,1}.NumberOfFrames*data.voxScale(3)]);
movie(tempAxes, data.movie, 1, length(data.fileList));
cla;
delete(tempAxes);
clear tempAxes
```

Femur and Tibia Registration Module

```matlab
% Initialise GUI - Pending until end of code development. Use https://uk.mat
% hworks.com/matlabcentral/answers/71078-command-window-output-to-gui#answe
% r_82310 to update Command Window commands in a GUI static text box.

% *Registration of bone masks (Transforming i=2:end bones onto i=1)*
% In this section the registration of the femur bone masks at i=2:end are
% registered onto femur mask at i=1. This registration is performed in
% order to obtain the transformation matrices of the movement that is
% occuring between frames. The aim is to transform the masks corresponding
% to the lateral side of the femur being registered from i=2:end onto the
% corresponding femur at i=1 to remove the relative movement and thus have
% all the movement occurring around a static femur

% Get 3d coordinates of segmented voxels in subMasks and use these 3d
% coordinates to generate a bone point cloud. The point clouds will be used
% in the subsequent step to register the bones.
data = mask2pc(data);

% Perform rigid ICP registration of femoral bones using |fminsearch|
% optimiser
data = regFemur(data);

% Transform the 3D coordinates of all the bones stored in |pts3D| using
% the transformation matrices obtained from the femoral registration.
% Also generate the corresponding |pointCloud| and store them in the
% |data| struct.
data = tformBones(data);
```

```
% Create boundary mesh structures of the bones in the new positions
data = createMeshes(data, 'bonePts', 0);


% Perform rigid ICP registration of tibial bones using |fminsearch|
% optimiser - This is required to be able to transform the coordinate
% system ROIs and axes from frame 1 to the rest.
data = regTibia(data);


% Transform the replaced knee bones onto the rest of the frames using the
% registration transformation matrices obtained above.
data = replaceImplants(data);
```

STL implementation for locating ROIs lying in the extremities

Registration of STL models onto bone pointClouds (for i = 1:end)

```
% Import, sort and label STL generic bone models (Femurs & Tibias)
data = importSTL(data);


% Perform rigid ICP registration using |fminsearch| optimiser
data = regSTL(data);


% Transform the 3D STL coordinates stored in |data.stlModels{1,i}.vertices|
% using the transformation matrices obtained from the registration. Also
% generate the corresponding |pointCloud| and store them in the |data|
% struct.
data = transformSTL(data);


% Visualise STL to CT registration result.
data = showSTL(data);
```

Coordinate System ROIs identification and definition modules

```
% Locate the Centre of Femur head by best fitting a sphere into a
% cropped point cloud of the medial-proximal portion of the femur.
data = femHeadCentre(data);


% Locate the centre of the ankle.
data = ankleCentre(data);


% Define tibial ROIs
data = tibROI(data);


% Define tibial CS using defined tibial ROIs
data = tibAxes(data);


% Define femoral ROIs for JCS axis coordinate system
data = femROI(data);
```

```
% Define Geometric Centre Axis (GCA)
data = GCA(data);


% Define femur axes using JCS method, and TEA and GCA axes.
data = femAxes(data, 'GCA');


% Define Trans-Epicondylar Axis (TEA)
data = TEA(data);


% Define femur axes using JCS method, and TEA and GCA axes.
data = femAxes(data, 'JCS', 'TEA');
```

Contact Point Analysis

This function locates the tibiofemoral contact points (based on the shortest euclidean distances) for each knee in all frames.

```
% Locate Tibio-femoral contact points
data = contactAnalysis(data);


% Visualise Contact point analysis results
data = showCP(data);
```

Functional FEA identification module

```
% Identify and visualise the functional flexion-extension axis (FEA).
data = optimFEA(data);
data = showFEA(data);


% Define femur axes using JCS method, and TEA and GCA axes.
data = femAxes(data, 'FEA');
data = showAxes(data);


% Visualise zDisplacement of FEaxis with progressing flexion
data = zFFA(data);
```

6 DOF Kinematics calculations and visualisation

```
% Kinematics extraction module
data = kinematics(data);
data = showKinematics(data);
```

Centre-of-Rotation (Axial) identification

Run Centre of Rotation analysis module

```
data = centRot(data);


% Visualise CoRs
data = showCoR(data);
```

- 467 -

Data Export to MS Excel

Extract all data to MS Excel

```
data = exportData(data);
```